Osamu Oda

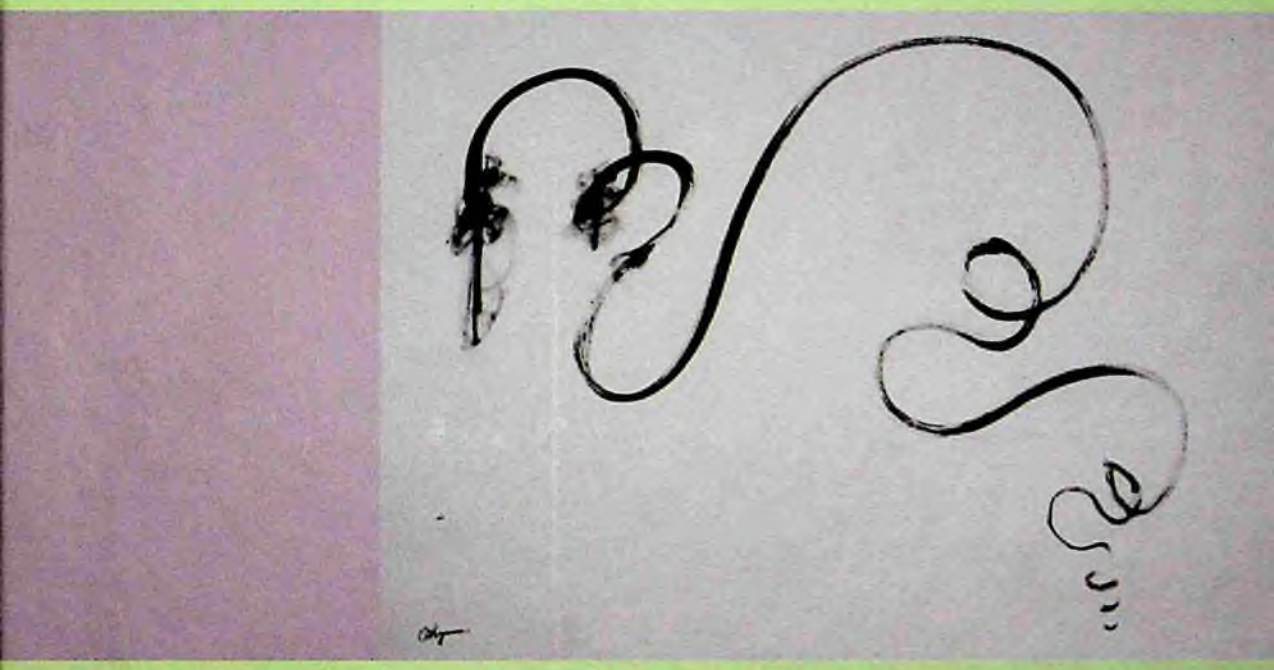

Compound Semiconductor Bulk Materials and Characterizations

Compound Semiconductor Bulk Materials and Characterizations

Compound Semiconductor Bulk Materials and Characterizations

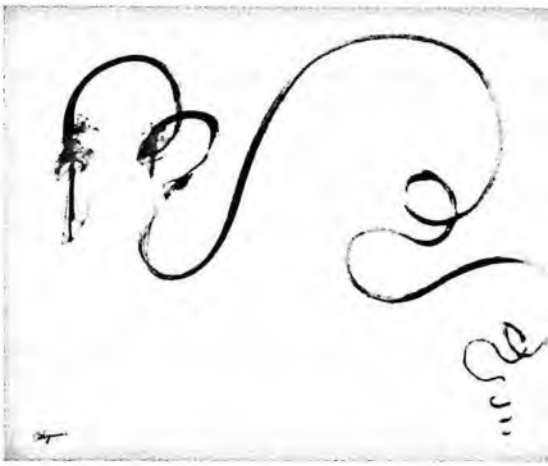

Osamu Oda

Aichi Science & Technology Foundation, Japan

World Scientific

NEW JERSEY · LONDON · SINGAPORE · BEIJING · SHANGHAI · HONG KONG · TAIPEI · CHENNAI

Published by

World Scientific Publishing Co. Pte. Ltd.

5 Toh Tuck Link, Singapore 596224

USA office: 27 Warren Street, Suite 401-402, Hackensack, NJ 07601

UK office: 57 Shelton Street, Covent Garden, London WC2H 9HE

British Library Cataloguing-in-Publication Data

A catalogue record for this book is available from the British Library.

COMPOUND SEMICONDUCTOR BULK MATERIALS AND CHARACTERIZATIONS

ISBN-13 978-981-02-1728-0

ISBN-10 981-02-1728-5

Printed in Singapore by World Scientific Printers (S) Pte Ltd

PREFACE

Compound semiconductor materials are becoming more important year by year as the basic materials for electronic and optical applications. It has already become clear that Si is the most indispensable material for the present prosperity in the electronic and information/communication industry. It is used in ICs for computers which are the main products in the present electronic industry. The silicon industry is now extensively developed in many fields mainly for micro processing units (MPUs) and memories for computers and for power devices for switching power supplies and for control units for hybrid automobiles.

Compound semiconductors are attractive since they have different properties from those of elementary semiconductors such as Si and Ge. Because of their possibilities, much research has been devoted to developing these compound semiconductors such as III-V materials, II-VI materials, IV-IV materials, nitrides, SiC, chalcopyrite and other materials. In order to realize various applications using these materials, it is indispensable to grow high quality single crystals.

Main applications of compound semiconductors are infrared and visible LEDs based on the photoemission characteristics. For these applications, conductive GaP and GaAs substrates are industrially produced and widely used. GaAs substrates are also used for infrared and visible light LDs. GaP is mainly grown by the LEC method and conductive GaAs is mainly grown by horizontal boat methods. High quality GaAs crystals have been recently grown by the VB/VGF methods. Conductive GaP and GaAs for LEDs and LDs have become a big market and have led the compound semiconductor industry.

Semi-insulating (SI) GaAs has been developed worldwide in the 80's in the expectation that it would find application in high speed super-computers. In fact, GaAs electronic device and ICs have been extensively explored for application in the high frequency field exceeding 10 GHz. SI-GaAs however could not find its application in this field. This was because large computers can be water-cooled so that silicon devices could compete with GaAs. The main application of GaAs was HEMTs for satellite broadcasting where high frequency devices of 10 GHz were required, but its take-up was less than expected for computer applications. In this period, many manufacturers have been disappointed and it seemed that no large application can be found for SI-GaAs.

The turning point for SI-GaAs was for cellular phones which need low power consumption devices at high frequency but only at 800 MHz, which was much less than people expected for GaAs. When this application was required, the GaAs technology community could react quickly since the technology was already matured for higher level computer applications. The production of GaAs devices started simultaneously with the rise of the cellular phone business. Because of this unexpected success, SI-GaAs became the third main industrial material.

Another application of compound semiconductors is InP based optical devices, laser and detectors for quartz fiber communications. The development of an information society based on the Internet accelerated the development of InP materials and devices. The development of InP started early in the 70's and it was a long time before the FTTH (fiber to the home) system was recently networked in individual homes.

Other III-V materials such as InAs, InSb, GaSb do not have the applications for a large market. They can be used as far infrared detectors, Hall sensors, but the consumption is still small compared with others. They however have other potentialities as high frequency devices and thermovoltaic devices.

Applications are rather difficult to find for II-VI materials because of the difficulty in crystal growth and conductivity type control because of the specific self-compensation problem. Industrially, polycrystalline ZnSe is used as window material for high power lasers and CdTe is used as substrate for far-infrared detectors in the wavelength range of 10 μm. The development of ZnSe was prominent and short wavelength LDs and LEDs have actually been made. Technologically, the application of ZnSe was nearly ready for the real industrialization but was in vain because of the quick development of GaN LDs and LEDs. This however does not deny the future challenging possibility of ZnSe.

Other II-VI materials such as CdS, CdSe, ZnS and ZnTe have long been studied but except the application of CdS for photodetectors, important applications have not yet been found.

As new materials, GaN based epitaxial layers are now important for shortwave length LEDs and LDs. These epitaxial layers are firstly grown on sapphire substrates, but SiC has been developed as a substrate for these applications. Since there is a large lattice mismatching for these devices, GaN substrates are strongly desired and various crystal growth methods are now under investigation. SiC crystal growth was mainly developed for its application as substrate for GaN epitaxial growth, but SiC crystal itself is now widely desired for power devices, mainly for automobile and switching applications.

For growing these compound semiconductor crystals, a variety of methods have been studied and developed. In the early days, melt growth methods such as horizontal boat methods (HB/HGF/HZM methods) and the liquid encapsulated Czochralski (LEC) method were predominant. Vertical boat growth methods (VB/VGF methods) which were not applied for a long period for industrial production have however been reconsidered and are now going to reach the stage of industrial production. Not only melt growth methods but also vapor phase growth methods is becoming more widely used in industry. New methods of crystal growth are still being developed and each in turn can be considered as the new method. In this sense, the crystal growth method is not yet fully established and there is always a possibility of new methods to replace the present one. For this to happen, the new method has to be able to have better cost performance with the ability to grow better quality crystals. The reader may find some clue for this new method in the various past trials described in this book.

In this way, several compound semiconductors have found industrial applications and in fact they are industrially produced. The scale of total material production in the

world now exceeds 900 million dollars and is steadily increasing. It is therefore clear that the field of compound semiconductors will become a large business, which has come after Si by compensating for what Si can not do, such as light emitting, high-power and high-frequency devices. The above market scale is only for bulk and epitaxial materials. It should be noted that the market scale of devices using these compound semiconductors is at least ten times more, and that of final systems are at least one hundred times more than that of materials. This means that these compound semiconductor materials support and contribute to the market scale of 90 billion dollars as a new industry.

It however should be noted that this increasing prosperity of compound semiconductors did not arise suddenly in a short period of research and development. In fact, the study of most of them started more than 50 years ago. Many researchers devoted most of their lives in research and development of compound semiconductor materials, by dreaming and believing in the realization of useful devices based on these materials even at the time when there was no evidence and proof for their future success. And finally, we are now convinced that their belief was true and the existence of these materials has proved of value in this society. We should not forget the efforts of these pioneering scientists and engineers. This success could not be achieved without their convinced belief and effort.

In this book, I summarize and update most of their fundamental work in a way that young students, engineers and scientists can be in touch with how these materials have been developed against what kind of obstacles and how they were overcome, and what are even now to be overcome. I have tried to construct this book in such a way that everybody will be able to grasp the essence of bulk compound semiconductor materials as quickly as possible.

For this purpose, in Part 1, fundamentals are written in such a way that the basics will be covered without special knowledge. In Part 1, physical properties, bulk crystal growth methods, principles of bulk crystal growth, defects, characterization methods and applications are covered. Those who are familiar with these subjects can skip Part 1 depending on their knowledge. Part 1 however can be used as a reference to the terminology which appears in Part 2 and 3 where each compound semiconductor material is discussed in detail. In Part 2, III-V compound semiconductors and in Part 3, II-VI compound semiconductors are reviewed. In each chapter, as many references as possible are reviewed so that all efforts in each material are covered. I hope that this book will help the further development of compound semiconductor materials not only in developed countries but also in others which are developing rapidly.

This book took a long time to write because I was engaged in a company affiliation for the research and development and most of my time was spent on practical industrial development. I however believe that the experience in industry will help me to arrange the book's content, focusing on the real priorities in the development of bulk compound semiconductor materials. I would like to thank very much everyone in Japan Energy Corporation where the author spent twenty years in the field of bulk crystal growth and characterization activities. I am especially grateful to ex-directors T. Ogawa, I. Tsuboya, Y. Koga, K. Aiki, I. Kyono and T. Ohtake for their encouragement and useful

discussion and Drs. K. Hirata, A. Onozuka, K. Kainosho, R. Hirano, K. Sato, S. Asahi and M. Uchida and Messrs T. Fukui, K. Katagiri, T. Fukui, M. Ohoka, D. Kusumi, H. Yamamoto, M. Seiwa, M. Oyake, H. Sawatari, S. Katsura, K. Matsumoto, H. Okazaki, K. Kohiro, T. Inoue, G. Kano, Y. Seki, M. Mori, H. Shimakura, H. Momoi, K. Urata, S. Yaegashi, T. Imaizumi, A. Noda, A. Arakawa, M. Ohta and Ms. Y. Matsuda for their collaboration, and Drs. M. Ohmori, H. Araki, J. Takahashi, K. Suga, U. Nakata, H. Kurita, M. Taniguchi, Y. Taniguchi for the helpful discussions I had with them. I would like to express my appreciation for all scientists who made helpful suggestions and with whom I had good discussions in a kindhearted manner with a warm friendship. They are Professors G. Müller at University Erlangen-Nüernberg, D.C. Look at Wright State University, P. Rudolph at IKZ (Institut für Kristallzuchtung), S. Porowski at High Pressure Research Center, B.H.T. Chai at University of Central Florida, H.J. Scheel at Ecole Polytechnique Federal Lausanne, S. Nakamura at University of California, T. Fukuda, M. Isshiki, T. Yao and S. Uda at Tokoku University, T. Ogawa at Gakushuin University, M. Umeno at Chubu University, T. Sasaki and H. Asahi at Osaka University, H. Hasegawa at Hokkaido University, F. Hasegawa at Tsukuba University, T. Egawa at Nagoya Instutut of Technology, T. Taguchi and K. Tadatomo at Yamaguchi University, M. Tajima at Institute Space Astron. Sci., Y. Nanishi at Ritsumeikan University, A. Yoshikawa at Chiba University, A. Yoshida and A. Wakahara at Toyohashi University, K. Hiramatsu at Mie University, M. Kasuga and T. Matsumoto at Yamanashi University, K. Kishino at Sophia University, M. Yamada at Kyoto Institute of Technology, O. Wada at Kobe University, K. Terashima at Shonan Institute of Technology and Drs. D.J. Stirland and M.R. Brozel at GEC Marconi, C.J. Miner at Bell-Northern Research, R. Fornari at MASPEC, D. Bliss at AFRL/Hanscom AFB, V. D. Mattera at ATT Bell Lab. R. Triboulet at CNRS Meudon, E. Molva and B. Daudin at Centre de l'Energie Nucleaires de Grenoble, G. Jacob at Inpact, J.P. Faurie at Lumilog, M. Huber at Thomson-CSF, J.H. Maurice at AFOSR/AFOARD, S. Watanabe at Lumiled, K. Matsumoto at Taiyo Nippon Sanso, A. Ishibashi and N. Nakayama at Sony, M. Abe at Hoya Advanced Semiconductor Technology, T. Sekiguchi at NRIM, U. Makita and Y. Sugiyama, K. Arai, H. Okumura at Electrotechnical Lab. (presently AIST), S. Miyazawa at NTT (presently Waseda University), K. Hoshikawa at NTT (Presently Shinshu University), S. Shinoyama at NTT (presently NEL Crystal), K. Itoh at NEC, D. Ueda and U. Ban at Matsushita Electric Industries, K. Moriya at Mitsui Mining & Smelting, N. Ohtani at Nippon Steel, M. Isemura and M. Hata at Sumitomo Chemical, K. Uehara at Kobe Steel, R. Ohno at Acrorad and M. Tanaka and M. Imaeda at NGK Insulators. I also would like to thank very much for those with whom I was able to have fruitful discussions during JAMS and SEMI activities for compound semiconductor material standardization. They are S. Okubo, M. Kashiwa, Y. Otoki, S. Kuma at Hitachi Cable, K. Ushio, T. Kikuta, J. Kikawa, Y. Ito and S. Yoshida at Furukawa Electrics, Y. Kadota, A. Tanaka and Y. Masa at Sumitomo Metal Mining, Y. Sano at Oki Electric Industry, K. Yamada and T. Takahashi at Shin-Etsu Semiconductors, T. Sato at Showa Denko, K. Fujita and M. Tatsumi at Sumitomo Electric Industries, H. Goto, M. Kitsunai and Y. Katsuno at Mitsubishi Chemicals, R. Toba, K. Iwasaki and N. Narita at Dowa Mining and K. Kashima at Toshiba Ceramics.

I want to acknowledge Dr. F.S. Skeffington for his careful and thorough review of the manuscript and Ms. M. Ng at World Scientific Corporation for awaiting with patience the completion of this book, and understanding its value. Finally, I wish especially to thank my wife Mikiko and my daughter Tomoko for their encouragement during the writing of this book.

Osamu Oda

Nagoya, Japan
October 2006

CONTENTS

PART 1

FUNDAMENTALS

1. PHYSICAL PROPERTIES
2. CRYSTAL GROWTH METHODS
3. PRINCIPLES OF CRYSTAL GROWTH
4. DEFECTS
5. CHARACTERIZATION
6. APPLICATIONS

1. PHYSICAL PROPERTIES

1.1 INTRODUCTION

Compound semiconductors which consist of various elements have widely ranging physical properties. They have therefore many possible applications. The physical properties which may vary, include bandgaps, crystal lattice structures, electron and hole mobilities, optical properties, thermal conductivity, and so on. By selecting appropriate compound semiconductor materials, it becomes possible to realize various devices which can not be achieved using the main elemental semiconductor material, silicon. It is therefore important to understand the physical properties of compound semiconductors and to know how to select appropriate materials for desired applications. Explanation of these properties can be found in speciality books.[1-9]

1.2 COMPOUND SEMICONDUCTORS

Among many compounds which consist of more than two elements, some show semiconductor properties. Some typical semiconductors are shown in Table 1.1. Compounds which show semiconductor properties have the following features according to Wilson's model.[10]

(i) The conductivity of the semiconductor is electronic. Ionic conductivity is excluded.

(ii) Conductivity is largely increased as a function of temperature.

(iii) Conductivity is very dependent on the kind of impurities and their concentrations.

Elemental semiconductors such as Si and Ge have covalent tetrahedral bonds because of sp_3 hybrid orbitals. Compound semiconductors also have tetrahedral bonds but they include not only covalent bonds but also ionic bonds. This is because compounds are formed from different elements which have different electronegativity. Table 1.2 shows the electronegativity of each element calculated by Pauling's law.[11] Electonegativity indicates the strength with which atoms attract electrons. The difference of electronegativity of constituent elements is therefore an indication of the ionicity strength as shown in Table 1.3.[12,13] When the ionicity is strong, constituent elements

Table 1.1 Various Semiconductor Materials

Elemental	Si, Ge
II-VI compound	CdS, CdSe, CdTe, ZnS, ZnSe, ZnTe
	$Hg_{1-x}Cd_xTe$, $Cd_{1-x}Zn_xTe$
III-V compound	GaP, GaAs, GaSb, InP, InAs, InSb
IV-IV compound	PbS, PbSe, PbTe, $Pb_{1-x}Sn_xTe$, $Pb_{1-x}Sn_xSe$
IV-IV compound	SiC, $Si_{1-x}Ge_x$
V-VI compound	Bi_2Te_3
Chalcopyrite	$AgGaS_2$, $AgGaSe_2$, $CuInS_2$, $CuInSe_2$, $ZnGeP_2$, $CdGeP_2$

Table 1.2 Electronegativity

Li	Be	B		C	N	O	F
1.0	1.5	2.0		2.5	3.0	3.5	4.0
Na	Mg	Al		Si	P	S	Cl
0.9	1.2	1.5		1.8	2.1	2.5	3.0
K	Ca	Sc	Ti~ Ga	Ge	As	Se	Br
0.8	1.0	1.3	1.7±10.2	1.8	2.0	2.4	2.8
Rb	Sr	Y	Zr~In	Sn	Sb	Te	I
0.8	1.0	1.2	1.9±10.3	1.8	1.9	2.1	2.5
Cs	Ba	La~Lu	Hf~Tl	Pb	Bi	Po	At
0.7	0.9	1.1	1.9±0.4	1.8	1.9	2.0	2.2
Fr	Ra	Ac	Th				
0.7	0.9	1.1	1.3				

are strongly attracted.

Compound semiconductor materials can be predicted by a simple rule. When the total number of valence electrons of constituent elements are divided by the number of elements comprising the compound and when this ratio gives four, the compound has a tendency to be semiconducting. In Fig. 1.1, this simple rule is shown. III-V, II-VI and I-III-VI_2 materials in fact obey this simple rule.[14]

Compound semiconductors can be more strictly predicted by the Mooser-Person law.[15-16] Materials which show semiconducting properties have to obey the following laws.

(i) In the case of elemental semiconductors, the constituent atom has eight electrons including electrons which form covalent bonds and these electrons produce s, p orbital closed shells.

Table 1.3 Ionicity of Various Semiconductors

Compound		Difference of Electronegativity	Ionicity (%)
II-VII	KCl	2.2	71
	KBr	2.0	64
	KI	1.7	53
II-VI	CdS	1.0	22
	CdSe	0.9	19
	CdTe	0.6	11
	ZnS	1.0	22
	ZnSe	0.9	19
	ZnO	2.0	64
III-V	InP	0.6	11
	InAs	0.5	9
	InSb	0.3	6
	GaAs	0.5	9
IV	Ge	0.0	
IV-VI	PbS	0.9	19
	PbSe	0.8	17
	PbTe	0.5	9

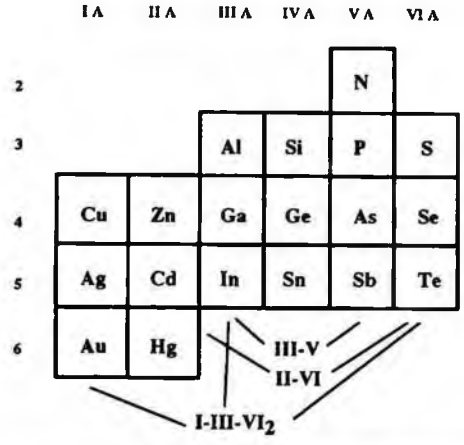

Fig. 1.1 Periodic table for compound semiconductors (reprinted from Ref. 14 with permission, copyright 1979 Elsevier)

Table 1.4 Mooser and Pearson's Law

Substance	ne	na	b	Substance	ne	na	b
Si	4	1	4	SiC	8	2	4
CdS	8	1	0	PbS	8	1	0
InSb	8	1	0	$CuInSe_2$	16	2	0
In_2Te_3	24	3	0				

(ii) For compound semiconductors, the condition (i) is applied to each constituent atom.

Elements from IV group to VII group satisfy the first condition (i) and following the second condition (ii), compound semiconductors include these elements. This is represented by the following equation.

$$n_e/n_a + b = 8 \qquad (1.1)$$

Here, for the compound in question, n_e is the number of valence electrons per molecule and n_a is the number of group IV to VII atoms per molecule. b is the average number of covalent bonds formed by one of these atoms with other atoms of groups IV to VII. Several examples of Mooser-Pearson's law[16] are shown in Table 1.4. The other prediction of semiconductor materials is also discussed by Pamplin.[17] In fact, from these estimations, III-V and II-VI materials were predicted as promising compound semiconductor materials and they have been developed from the earliest times.

1.3 CRYSTAL STRUCTURE

Fundamentals of crystal structures are well explained in many books.[18-20] Semiconducting materials basically have the structures explained below depending on the nature of bonding. As explained above, semiconducting materials have tetrahedral bonds and

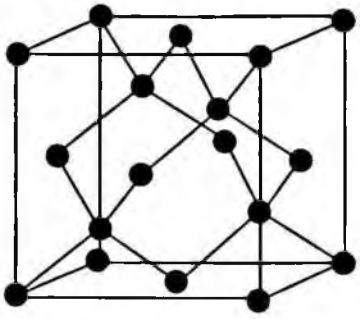

Fig. 1.2 Diamond lattice structure.

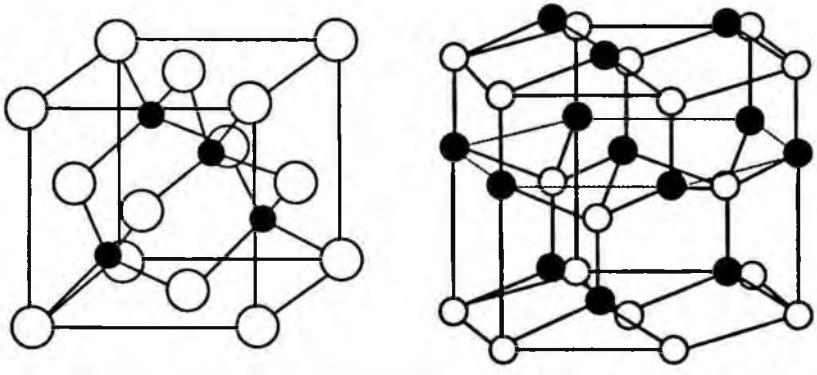

Fig. 1.3 (s) Zincblende lattice structure and (b)Wurtzite lattice structure. (○) A atom, (●) B atom.

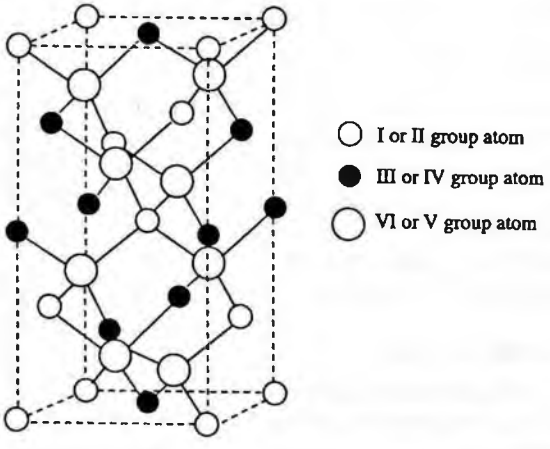

Fig. 1.4 Chalcopyrite lattice structure.

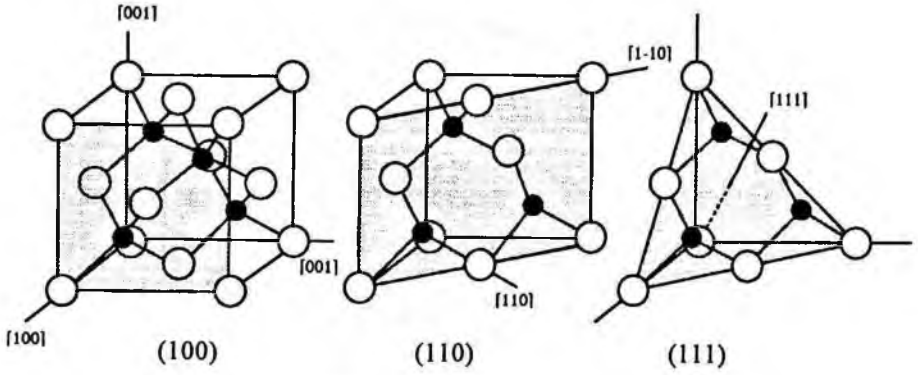

Fig. 1.5 Miller indices for low-index planes.

therefore form cubic or hexagonal structures.

Elemental semiconductors such as Si and Ge have diamond structures as shown in Fig. 1.2. Each atom has tetrahedral bondings with each other due to sp^3 hybrid orbitals. This structure is formed with two face centered cubic lattices with the origin point deviating at the position (1/4, 1/4, 1/4). Each atom has four nearest neighbor atoms thus satisfying sp^3 hybrid orbitals to obtain eight outer shell electrons.

Many compound semiconductors such as GaAs, InP, GaP and CdTe have zincblende structures as shown in Fig. 1.3 (a). This structure is very similar to the diamond structure. A atoms form a face centered cubic lattice while B atoms form another face centered cubic lattice with the deviation of (1/4,1/4,1/4). A atoms are therefore surrounded by four nearest neighbor B atoms. This is the same for B atoms. Each atom has tetrahedral bonds with four other different atoms.

The modification of zincblende structure is the wurzite structure as shown in Fig. 1.3 (b). In this structure, A atoms form a hexagonal lattice and B atoms form another hexagonal structure with the deviation of (3/8)c. In this structure, A atoms are surrounded by four nearest neighbor B atoms thus form tetrahedral bondings as in the case of zincblende structures. When an atomic plane of the zincblend structure is rotated 180 degrees along [111] axes, it corresponds to the wurzite structure. Compound semiconductors with larger ionicity have a tendency to take this wurzite structure.

Fig. 1.4 is a chalcopyrite structure in which cation sites in the zincblend structure are alternately occupied by I and III group elements in the case of I-III-VI_2 structures and by II and IV group elements in the case of II-IV-V_2 structures.

Crystal faces and orientations are defined by Miller indices as shown in Fig. 1.5. Since in the case of zincblende structure, (111) plane (A face) and (-1-1-1) plane (B face) are not identical, there is a difference of etching characteristics.

1.4 BAND STRUCTURES, BANDGAPS AND LATTICE CONSTANTS

When atoms are close enough to form crystals, electron orbitals overlap and each electron has different energy levels due to the Pauli law. These band structures can be

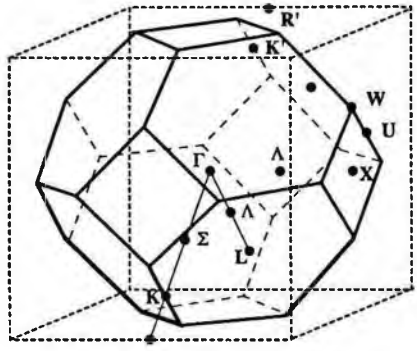

Fig. 1.6 Brillouin zone.

obtained by solving the Schrödinger equation under periodic potentials due to crystal periodicity. There are various approaches to solving the Schrödinger equation such as linear combination of atomic orbitals, tight binding approximation, pseudopotential method, $\mathbf{k} \cdot \mathbf{p}$ perturbation method and the orthogonalized plane wave method. To show electron energies, it is sufficient to represent the energy as a function of wave number k. Wave number space for a unit cell is called the first Brillouin zone.[21] Fig. 1.6 shows the first Brillouin zone for zinc blend structure. Fig. 1.7 shows examples of band structures for typical semiconductor materials.[22]

In semiconductors, electrons are forbidden to have a certain range of energies and they are called band gaps. Compound semiconductors are categorized to two types as direct and indirect transition materials.[23] In direct transition materials, as shown in Fig. 1.8 (a) electrons can be excited from the valence band to the conduction band without any phonon generation. In indirect transition materials, as shown in Fig. 1.8 (b), elec-

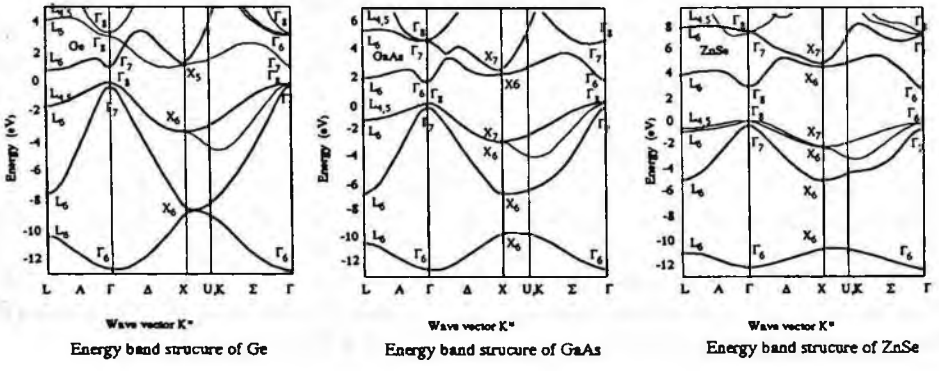

Fig. 1.7 Energy band structures (reprinted from Ref. 22 with permission, copyright 1983 American Physical Society)

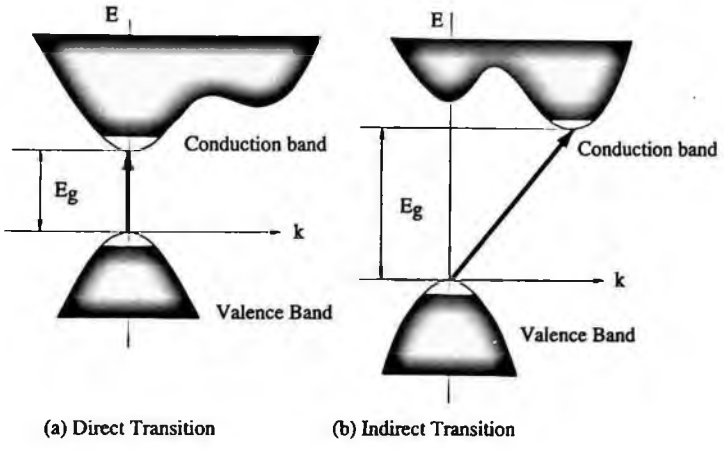

Fig. 1.8 Direct and indirect transitions.

trons are recombined via holes with phonon interactions.

The lattice constant is systematically changed. It becomes smaller when the compounds consist of smaller diameter atoms, and becomes larger when the compounds consist of larger diameter atoms. In Fig. 1.9 (a), the relationship between the molecular weight and the melting point is shown. When the molecular weight becomes larger, the melting point becomes lower. This is because when the molecular weight becomes larger, the lattice constant becomes larger and the binding force becomes smaller. Even for similar molecular weights, the melting point becomes higher with the progression

Table 1.5. Main Semiconductors and their Lattice Constant, Bandgap and Transition Type

	Material	Crystal structure	Lattice constant (Å)	Bandgap (eV)	Transition type
IV	Si	Diamond	5.4309	1.107	indirect
	Ge	Diamond	5.6575	0.66	indirect
	GaP	Zincblende	5.451	2.261	indirect
III-V	GaAs	Zincblende	5.654	1.435	direct
	GaSb	Zincblende	6.095	0.72	direct
	InP	Zincblende	5.869	1.351	direct
	InAs	Zincblende	6.058	0.35	direct
	InSb	Zincblende	6.479	0.180	direct
	ZnS	Zincblende	5.409	3.66	direct
	ZnSe	Zincblende	5.668	2.67	direct
II-VI	ZnTe	Zincblende	6.103	2.26	direct
	CdS	Wurzite	a=4.137 c=6.716	2.38	direct
	CdSe	Wurzite	a=4.299 c=7.015	1.74	direct
	CdTe	Zincblende	6.481	1.44	direct

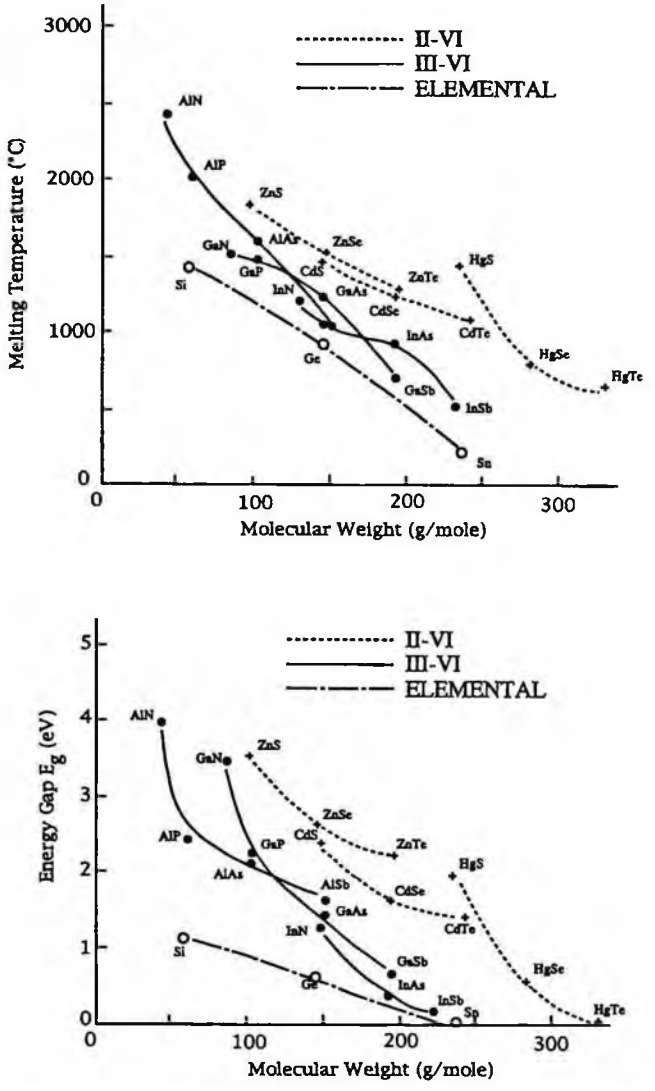

Fig. 1.9 Melting point and energy gap as a function of molecular weight (reprinted from Ref. 14 with permission, copyright 1979 Elsevier)

of II-VI compound > III-VI compound > Si, Ge. This is because the binding force becomes larger when the ionicity becomes larger. Fig. 1.9 (b) shows the relationship between the bandgap and the molecular weight. The bandgap becomes larger as the binding energy becomes larger.[14]

Fig. 1.10 shows the relationship between the lattice constants and the band gaps for III-V materials and their mixed crystals.[24, 25] In Fig. 1.10(b), direct and indirect regions

(a)

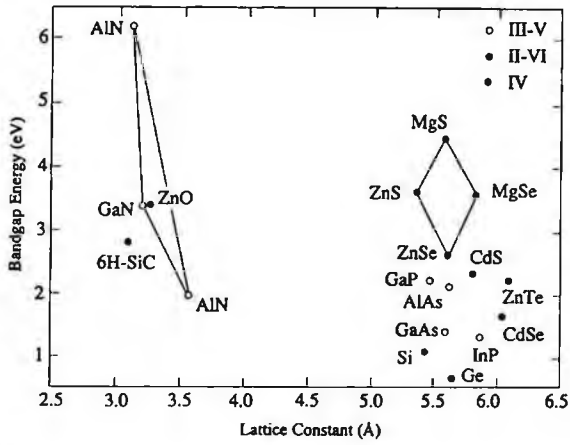

(b)

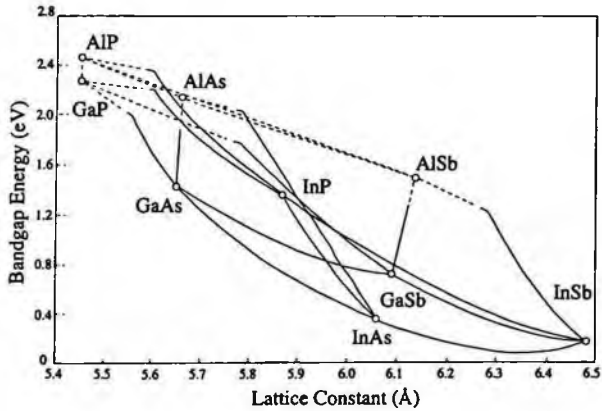

Fig. 1.10 Relationship between bandgap energy and lattice constant of various materials. (a) II-VI, III-V and IV group materials (from Ref. 24 with permission), (b) III-V materials (solid line: direct, dotted line: indirect) (from Ref. 25 with permission).

are also indicated. In Table 1.5, lattice constants, bandgaps and transition types are summarized for the main semiconductor materials. Stronger ionicity gives strong bonds thus gives larger band gaps.

1.5 OPTICAL PROPERTIES

In the case of direct transition type semiconductors, in the k (momentum) space, the top of the valence band and the bottom of the conduction band are at the same energy axis. For this type of semiconductor, if carriers are injected by application of a forward bias to a p-n junction or if light falls on it whose energy is higher than the bandgap Eg, by the process referred to in Fig. 1.8, the light with the wavelength of λ_0 corresponding to E_g can be emitted with high efficiency.[26]

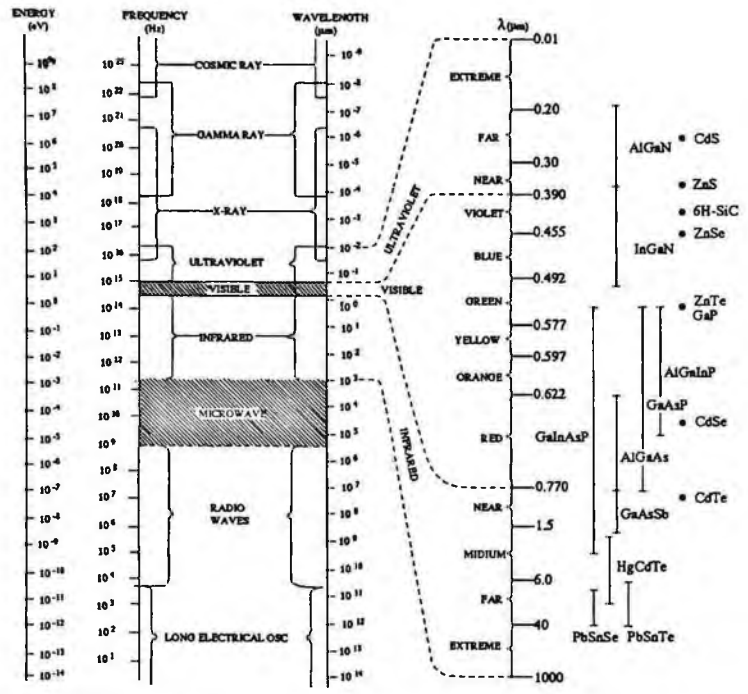

Fig. 1.11 Chart of electromagnetic spectra (left side from Ref. 27 with permission) with various materials (right side).

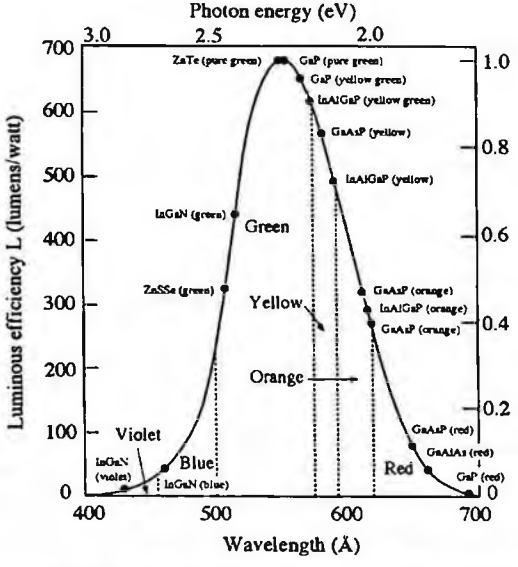

Fig. 1.12 Eye sensitivity as a function of wavelength and various materials.

$$\lambda_0\ (\mu m) = 1.239/\ E_g\ (eV) \qquad (1.2)$$

In the case of indirect semiconductors as Si, Ge and GaP, there is a k-space difference between electrons and holes, so that electrons need the change of momentum for recombination as shown in Fig. 1.8. Because of this change, most of energy is emitted as heat (lattice vibration-phonon) and light emission efficiency is low.

Fig. 1.11 shows the relationship between the bandgap energy, frequency and the wavelength. Fig. 1.12 shows the sensitivity of the eye as a function of wavelength. It is seen that many compound semiconductor materials exist for the wide range of wavelength from ultraviolet to far infrared. By applying these optical properties various LEDs and LDs can be made.

1.6 ELECTRICAL PROPERTIES

1.6.1 Carrier Concentration

Carrier concentrations in semiconductors are determined as a thermal equilibrium between thermal excitation of electrons, ionization of impurities and ionization of defect levels.

(1) Intrinsic semiconductors

Electron concentration and hole concentration in semiconductors can be represented as follows according to the Boltzmann statistics.

$$n = N_c \exp\left(-\frac{E_c - E_F}{kT}\right) \qquad (1.3)$$

$$\text{where} \quad N_c = 2\left(\frac{2\pi m_e^* kT}{h^2}\right)$$

$$p = N_v \exp\left(-\frac{E_f - E_v}{kT}\right) \qquad (1.4)$$

$$\text{where} \quad N_v = 2\left(\frac{2\pi m_h^* kT}{h^2}\right)$$

Here, n is the electron concentration, p the hole concentration, N_c the effective density of states in the conduction band, N_v the effective density of states in the valence band, E_F the Fermi energy, E_c the energy level of donor, E_v the energy level of acceptor, me* the density-of-state effective mass of electrons, mh* the density-of-state effective mass of holes, h the Planck constant, k the Boltzmann constant, T the absolute temperature.

The product of n and p is represented as follows.

$$np = n_i^2 = N_C N_v \exp(-E_g / kT) \qquad (1.5)$$

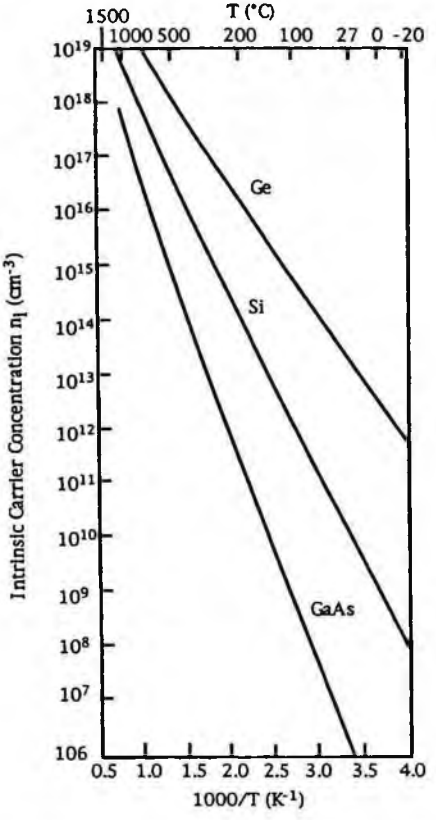

Fig. 1.13 Intrinsic carrier concentration as a function of reciprocal temperature (reprinted from Ref. 28 with permission, copyright 1970 American Institue of Physics).

Here, $E_g = E_c - E_v$ is the energy bandgap.

In the case of intrinsic materials where impurities are negligible, n=p due to the neutral condition. Therefore,

$$n = p = \sqrt{N_C N_v}\ \exp(-E_g / kT) \qquad (1.6)$$

In Fig. 1.13, intrinsic carrier concentration, n_i, is shown as a function of reciprocal temperature.[28] Because of larger bandgap of GaAs than Si and Ge, GaAs has lower intrinsic carrier concentrations and therefore can be made semi-insulating.

(2) Donors and acceptors

In reality, in semiconductor materials, there are always some impurities and defects and some of them are ionized and affect carrier concentrations. Impurities which have more valence electrons than substituted host constituent atoms and can be thermally

ionized act as donors. They offer electrons in the conduction band. Impurities which have fewer valence electrons than substituted host constituent atoms and can be thermally ionized act as acceptors. They attract electrons thus leaving holes in the valence band. The concentrations of ionized donors and acceptors are represented as follows. Various point defects can also act as donors and acceptors depending on their structures. Their detailed characteristics are discussed in Chapter 4.

(3) Fermi level and Schokley diagram

The position of the Fermi level is important to characterize the electrical properties of compound semiconductors. The Fermi level is determined as a function of the concentrations of various defects such as donors, acceptors and deep levels. It can be determined graphically by the Schokley diagram developed for conductive Si.[29] The Schokley diagram can be applied also for compound semiconductors, even for those which are semi-insulating due to deep levels.[30]

The concentrations of carriers and ionized shallow donors and acceptors and ionized deep donors and acceptors can be represented as follows.

$$n = N_c \exp\left(-\frac{E_c - E_F}{kT}\right) \tag{1.7}$$

$$N_a^- = \frac{N_a}{1+0.5 \exp\left(\frac{E_a - E_F}{kT}\right)} \tag{1.8}$$

$$N_{aa}^- = \frac{N_{aa}}{1+0.5 \exp\left(\frac{E_{aa} - E_F}{kT}\right)} \tag{1.9}$$

$$p = N_v \exp\left(-\frac{E_f - E_v}{kT}\right) \tag{1.10}$$

$$N_d^+ = \frac{N_d}{1+2 \exp\left(\frac{E_F - E_d}{kT}\right)} \tag{1.11}$$

$$N_{dd}^+ = \frac{N_{dd}}{1+2 \exp\left(\frac{E_F - E_{dd}}{kT}\right)} \tag{1.12}$$

Here, the nomenclatures are as follows. E_a is the ionization energy of shallow acceptor, N_a the concentration of shallow acceptor, E_{aa} the ionization energy of deep acceptor, N_{aa} the concentration of deep acceptor, E_d the ionization energy of shal-

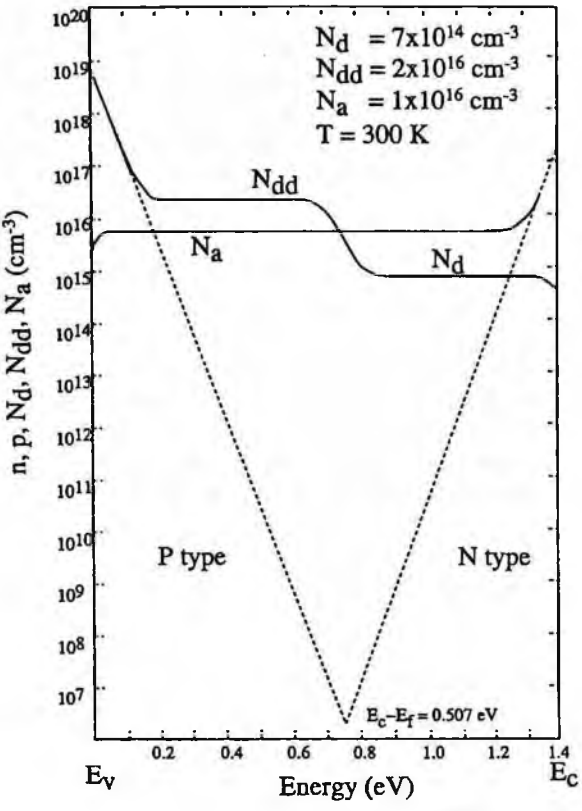

Fig. 1.14 Schockley diagram for semi-insulating GaAs where the deep donor is EL2.

low donor, N_d the concentration of shallow donor, E_{dd} the ionization energy of deep donor and N_{dd} the concentration of deep donor.

These carriers and ionized species must satisfy the following neutral conditions.

$$n + N_a^- + N_{aa}^- = p + N_d^+ + N_{dd}^+ \qquad (1.13)$$

Eqs. 1.7-1.13 can not be solved analytically, but they can be solved graphically by the Schokley diagram and/or by the iteration method. Fig. 1.14 shows an example of the Schockley diagram for undoped semi-insulating GaAs. It can be seen that the Fermi level is determined by the cross point between the positive charge line and the negative charge line. This Schokley diagram is important for the consideration of the resistivity depending on the defect concentrations. Several examples will be shown in the case of semi-insulating GaAs and InP in Chapters 8 and 10, respectively.

Table 1.6 Effective Mass and Mobility for Various Semiconductors

Material		Effective Mass			Mobility	
		m_e^*	$m_p h^*$	$m_p l^*$	μ_e	μ_h
IV	Si	0.26	0.55	0.24	1350	475
	Ge	0.56	0.37	-	3800	1900
III-V	GaP	0.12	0.86	0.14	200	120
	GaAs	0.065	0.45	0.082	8500	420
	GaSb	0.049	0.33	0.056	7700	1400
	InP	0.077	0.56	0.12	6060	150
	InAs	0.027	0.41	0.024	33000	460
	InSb	0.0135	0.438	0.016	78000	1700
II-VI	ZnS	0.28	1.4		140	5
	ZnSe	0.17	~0.7		530	28
	ZnTe	0.122	0.42	0.17	340	110
	CdS	0.171	~5		350	15
	CdSe	0.112	>1.0		650	
	CdTe	0.0963	0.62	0.092	1050	80

1.6.2 Mobility

Mobility is defined as the proportional constant between velocity v and electric field E as the following equation.

$$v = \mu E \tag{1.14}$$

Mobility takes a constant value under a low electric field lower than several kV/cm and this mobility is referred to as low field mobility. Low field mobility is represented by

$$\mu = \frac{q\tau}{m^*} \tag{1.15}$$

Here, τ is the momentum relaxation time, m* the effective mass of carriers and q the elementary charge. Mobilities of electrons and holes are thus inversely proportional to the effective mass m* and the mobility becomes fast if the m* is small. Since effective mass is determined by the curvature of the band, the material whose band curvature is smaller can be selected for larger mobility. Table 1.6 shows the effective mass and the mobility of various compound semiconductors. It is seen that the mobility of direct transition crystals is larger. For example, in the case of GaAs, the electron mobility is six times larger than Si at room temperature. This is one of the reason why GaAs is used for high frequency devices such as MESFETs, HEMTs and so on.

Relaxation time of scattering and therefore the mobility is determined by the overlapping of various scattering mechanisms. Table 1.7 shows various scattering mechanisms.[31]

In periodical potential in the crystals, carriers transport basically without any scattering thus giving the largest mobility. In reality, carriers are scattered by various mechanisms. Scattering mechanisms are basically classified into two main scattering processes. One is due to lattice vibration and the other is due to impuri-

Table 1.7 Various Scattering Mechanisms

Lattice Scattering	Acoustic Phonon	Deformation Potential Scattering
		Piezoelectric Scattering
	Optical Phonon	Polar Optical Scattering
		Nonpolar Optical Scattering
Impurity and Defect Scattering	Ionized Impurity Scattering	
	Neutral Impurity Scattering	
	Defect Scattering	
	Alloy Scattering	

ties and/or defects. When temperature is increased, lattice vibration increases. Lattice vibrations are classified into two modes, acoustic mode with very low frequencies and optical mode with high frequencies. When the lattice is deformed in crystals with certain ionicities, dipoles are formed and thus carriers are scattered strongly due to this electric field. There are thus four main lattice scattering mechanisms and they have following features.

(1) Optical phonon scattering

Depending on crystal ionicity, there are nonpolar optical phonon scattering and polar optical phonon scattering. For elemental semiconductors such as Si and Ge, in which only covalent bonding is predominant, polar optical phonon scattering does not exist.

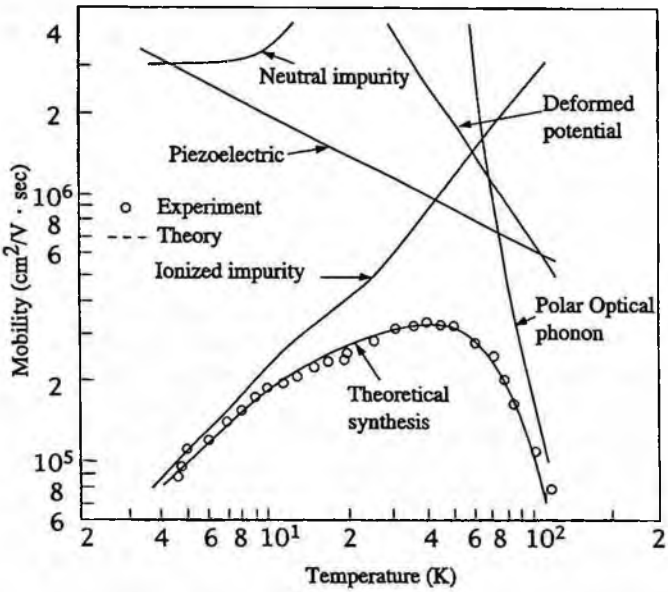

Fig. 1.15 Mobilities under various scattering mechanisms (reprinted from Ref. 31 with permission, copyright 1998 American Institue of Physics).

For compound semiconductors, nonpolar optical phonon scattering is predominant at higher temperatures.

$$\mu = \left(\frac{m^*}{m_0}\right)^{-\frac{3}{2}} T^{\frac{1}{2}} \left\{ \exp\left(\frac{\theta}{T}\right) - 1 \right\} \tag{1.16}$$

(2) Acoustic phonon scattering

Nonpolar acoustic scattering is called deformation potential scattering. This is because deformation of lattice waves changes the band edge and originates a deformation potential and becomes the origin of scattering. Polar acoustic scattering is called piezoelectric scattering and predominates for low temperatures and for II-VI materials.

(3) Impurity scattering

When impurities are ionized, carriers are strongly scattered by Coulomb potential. Since thermal velocity of carriers is increased as temperature rises, ionized impurity scattering becomes negligible at higher temperatures. Ionized impurity scattering is represented as follows.

$$\mu = \left(\frac{m^*}{m_0}\right)^{-\frac{1}{2}} T^{\frac{3}{2}} \tag{1.17}$$

When defects are ionized, the scattering effect is similar to that in the case of impurities.

When impurities are neutral, carriers are scattered only when they impinge on impurities. The scattering effect is very small and there is temperature dependence. The mobility in this case is represented as follows.

$$\mu = m^* \tag{1.18}$$

Fig. 1.15 shows the temperature dependence of the mobility of GaAs analyzed by Wolfe et al.[31, 32] It can be seen that at higher temperatures, nonpolar optical scattering is predominant and at lower temperatures, ionized impurity scattering is predominant.

When various scattering takes place, total relaxation time τ is represented as

$$\frac{1}{\tau} = \Sigma \frac{1}{\tau_i} \tag{1.19}$$

from various relaxation time τ_i due to each scattering mechanism. The total mobility can be represented as

$$\mu = \Sigma \frac{1}{\mu_i} \tag{1.20}$$

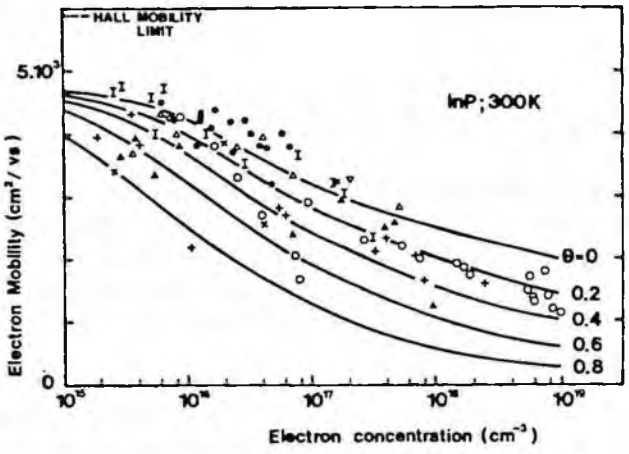

(a)

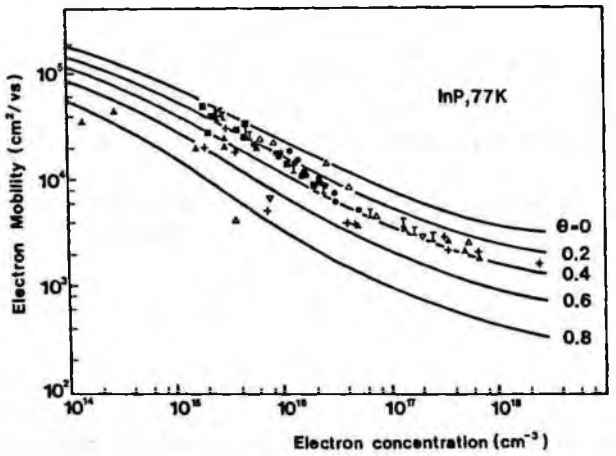

(b)

Fig. 1.16 Theoretical (solid lines) and experimental values of mobility at 300 K (a) and 77 K (b) as a function of electron concentration in n-type InP for various compensation ratios (reprinted from Ref. 33 with permission, copyright 1980 American Institue of Physics).

The relationship between carrier concentration and mobility is calculated in several cases. In Fig. 1.16, an example for InP is shown. When the material is conductive, most shallow donors and acceptors are ionized. The carrier concentration n is therefore approximately equal to $N_d - N_a$. Compensation ratio θ is defined as N_a/N_d. Therefore, from the calculated figure, N_d and N_a can be calculated when mobility and the carrier concentration are known.

The effect of impurities is also negligible even at room temperature. Fig. 1.16 shows the electron mobility as a function of impurity concentration for the case of InP. If the impurity concentration exceeds $1x10^{17}\,cm^{-3}$, electron mobility becomes less than 4000 $cm^2/V \cdot sec$ in the case of InP. When the impurity concentration becomes higher than $10^{17}\,cm^{-3}$, the mobility between 77K and room temperature remains nearly constant. From the compensation ratio and the carrier concentration, the concentration of donors and acceptors can be represented as follows.

$$N_d = \frac{n}{1-\theta} \tag{1.21}$$

$$N_a = \frac{\theta}{1-\theta} n \tag{1.22}$$

Fig. 1.17(a) shows the temperature dependence of electron mobilities of III-V compound semiconductors compared with Si and Ge. In the case of Si and Ge, since the purity of Si and Ge is of the order of $10^{12}\,cm^{-3}$, there is no impurity scattering even at low temperatures and the electron mobilities rise as the temperature falls. In the case of III-V crystals, there is a peak at around 100 K and at tempera-

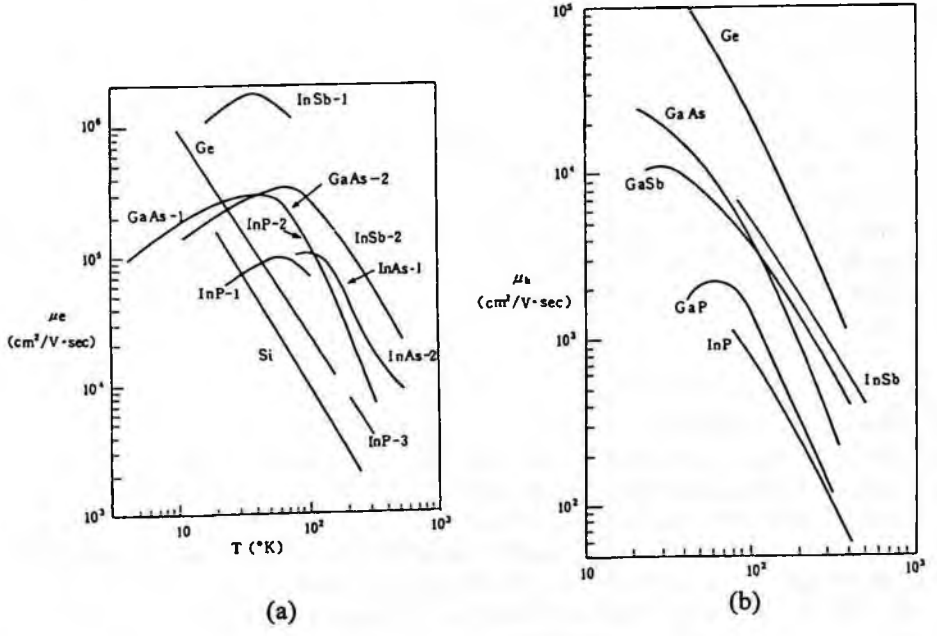

Fig. 1.17 Temperature dependence of (a) electron mobilities (from Ref. 34 with permission) and hole mobilities (reprinted from Ref. 35 with permission, copyright 1975 Elsevier).

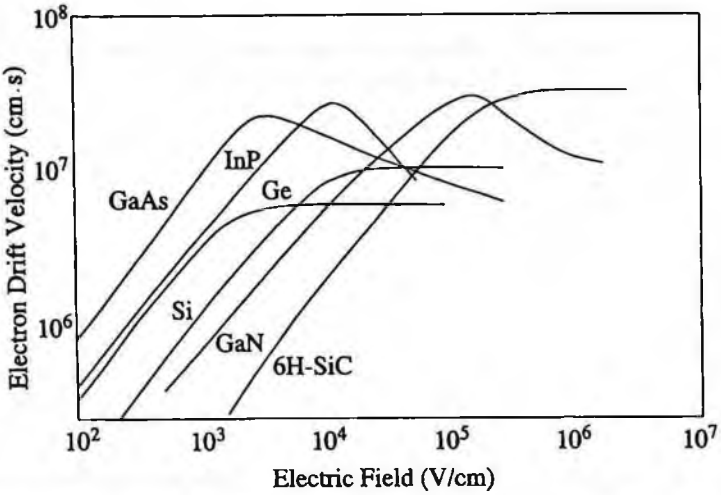

Fig. 1.18 Electron drift velocities as a function of electric field (from Ref. 36 with permission. InP data are from Ref. 37 with permission, copyright 1972 American Physical Society).

tures lower than this point the mobility falls. This is because electron scattering becomes predominant due to impurities and defects. Fig. 1.17(b) shows the case of hole mobilities and the same tendency can be seen.

1.6.3 High Field Properties

In high frequency devices, the electric field is stronger due to micro fine structure processing. Under such a high electric field, the electron drift velocity of Si is saturated at a lower velocity. In the case of compound semiconductors such as GaAs and InP, the drift velocity shows a maximum and then decreases and becomes saturated. This is because electrons at Γ point are accelerated and scattered to higher energy L point. From Fig. 1.18, it can be seen that GaAs, InP, GaN and SiC are promising materials for high speed devices.

1.7 OTHER PROPERTIES

1.7.1 General Properties

In Table 1.8, various properties such as melting point, thermal conductivity, linear expansion coefficient, elastic moduli and dielectric constant are summarized.

GaAs and InP have less thermal conductivity than Si, so in devices such as power FETs, LDs and Gunn diodes which generte large amounts of heat, the thickness must be made 30-100 μm so as to minimize the thermal resistance.

Fig. 1.19 shows the hardness as a function of interatomic distance.[38] The lower the interatomic distance, the more fragile the material.

Table 1.9 shows the etching solutions for various semiconductor materials.[39] To obtain flat etching faces, a combination of oxidizing agent and acid is used. These etching

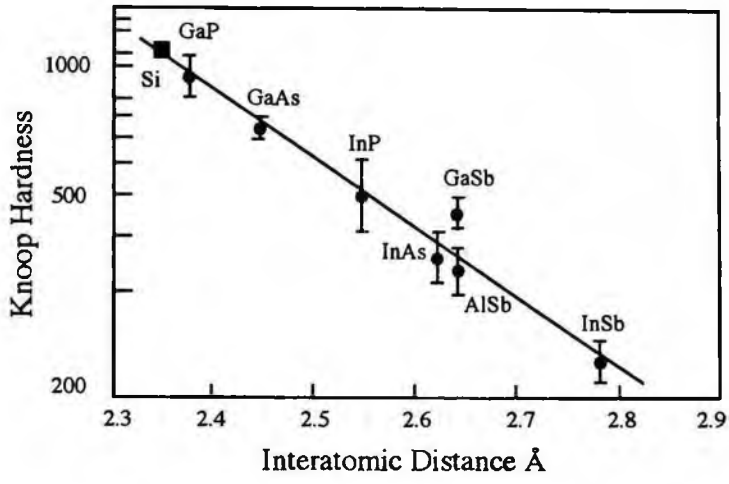

Fig. 1.19 Hardness as a function of interatomic distance.[32]

procedures are very important when applied to wafers produced from grown bulk single crystals. The chemistry of etching properties is discussed in detail by Faust. [39]

1.7.2 Stacking Fault Energy

A stacking fault is a plane defect where the stacking of single crystal planes is misordered. This means that in the case of a zincblende structure, ABCABC stacking is misordered as AB/ABCA. In the case of a wurzite structure, ABABAB stacking is

Table 1.8 Physical Properties of Various Semiconductors

Material	Melting Point (°C)	Thermal Conductivity (W/cm·K)	Linear Expansion Coefficient (10^{-6}/K)	Elastic Moduli (10^{11}dyne/cm^2) C_{11}	C_{12}	C_{44}	Dielectric Constant
IV							
Si	1,410	1.4	2.6	16.57	6.39	7.96	11.9
Ge	937	0.61	5.75	12.89	4.83	6.71	16.2
GaP	1,467	1.1	5.3	14.12	6.253	7.047	11.11
III-V							
GaAs	1,238	0.54	6.0	11.88	5.38	5.98	13.18
GaSb	712	0.33	6.7	8.849	4.037	4.325	15.69
InP	1,070	0.7	4.5	10.22	5.76	4.60	12.56
InAs	943	0.26	5.19	8.329	4.526	3.959	15.15
InSb	525	0.18	5.04	6.75	3.47	3.16	17.9
II-VI							
ZnS	1,830	0.27	6.7	10.46	6.53	4.48	8.3
ZnSe	1,515	0.19	7.7	8.10	4.88	4.41	9.1
ZnTe	1,238	0.18	8.3	7.13	4.07	3.12	10.1
CdS	1,475	0.27	6.5 (//), 5.0(⊥)	8.43	5.21	1.49	10.33(//), 9.35(⊥)
CdSe	1,350	0.09	4.4	7.49	4.61	1.32	10.65(//), 9.70(⊥)
CdTe	1,090	0.06	4.70-4.90	5.33	3.65	2.04	10.3

Table 1.9 Various Etchants

AlSb	$3HNO_3$:2HF:$5CH_3COOH$	metallic luster
	$2H_2O_2$:HF	flat surface (after water boiling
GaP	HNO_3:2HCl:$2H_2O$	(111) both surface flat
	1%Br_2:CH_3OH	flat surface
	$5HNO_3$:3HF:$3CH_3COOH$	etch pit
GaAs	HNO_3:2HCl:$2H_2O$	(111), (-1-1-1) surface determination
	HNO_3:$9H_2O$	determination of pn interface
	H_2O_2:5NaOH(5%)	etch pits
	1-2%Br_2:CH_3OH	flat surface
	1cc HF:2cc H_2O:8mg$AgNO_3$:1g CrO_3	etch pits on (111), (-1-1-1), (100), (110) surfaces
	H_2O_2:3-8H_2SO_4:H_2O	flat surfaces
GaSb	$2HNO_3$:HF:CH_3COOH	flat surface with etch pits on (111)
	HNO_3:HF:H_2O	etch pits on (111)
InP	1% Br_2:CH_3OH	flat surface
	HCl:0.4N-$FeCl_2$	etch pits on (111), (-1-1-1), (100)
InAs	HCl	flat surface
	$3HNO_3$:HF:$2H_2O$	pn junction interface
	HNO_3:HCl:H_2O	etch pits
InSb	I_2:CH_3OH	flat surface
	HNO_3:2HF:CH_3COOH	flat surface with etch pits on (111)
	HF:H_2O_2:$8H_2O$:	both side etch pits
	HNO_3:HCl:H_2O	etch pits

misordered as AB/CABA. The formation energy of this defect is very critical to the formation of twins. When this energy is small, twins are easily formed.

The stacking fault energy (SFE) has been estimated by Gottschalk et al.,[40] Jordan et al.,[41] Takeuchi et al.[42] and others. The various data are summarized by Takeuchi et al. as

Table 1.10 Stacking Fault Energy of Various Materials

Material	Structure	γ (mJ/m^2)
GaP	zincblende	41 ± 4
GaAs	zincblende	55 ± 5
GaSb	zincblende	53 ± 7
InP	zincblende	17 ± 3
InAs	zincblende	30 ± 3
InSb	zincblende	38 ± 4
ZnS	zincblende	<6
ZnSe	zincblende	13.2 ± 1.5
		12.6 ± 0.4
ZnTe	zincblende	16 ± 4
ZnO	wurzite	>43
CdS	wurzite	8.5 ± 2.1
		14 ± 4
CdSe	wurzite	14 ± 5
CdTe	zincblende	10.1 ± 1.4
		9.7 ± 1.7

See the references for each data in Ref. 42.

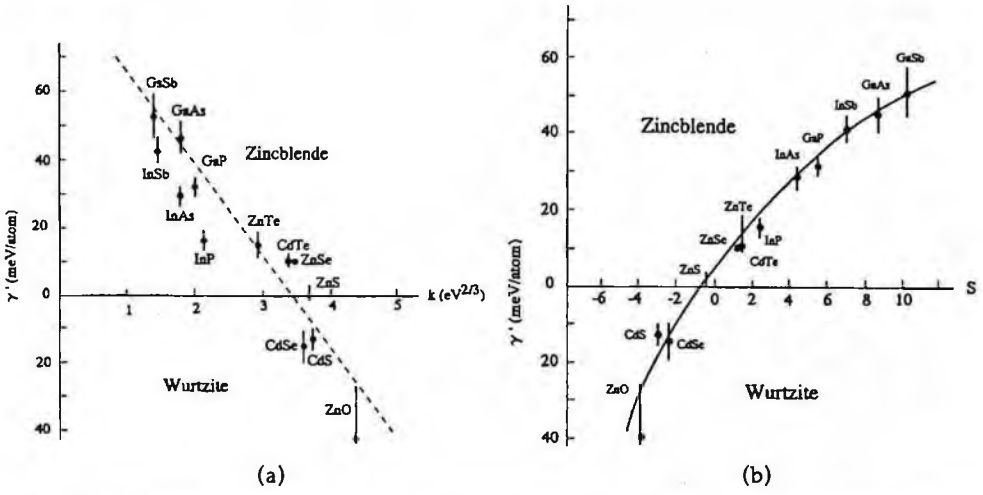

Fig. 1.20 (a) Reduced stacking fault energy as a function of k value. (b) Reduced stacking fault energy as a function of charge redistribution index s (reprinted from Ref. 42 with permission, copyright 1984 Taylor & Francis).

in Table 1.10. They have analyzed these data as the relationship between the reduced SFE (the energy per atom in the fault plane) and the k value or the s value as shown Fig. 1.20. Here, the k value is the proportional constant between the ionicity energy gap C and the covalent energy gap E_h, expressed as $C = kE_h^{1/3}$, and the s value is the charge redistribution index defined by Phillips and Van Vechten.[43] It was found that there is a strong correlation between the reduced stacking fault energy γ' and k and s as shown in Fig. 1.20. This relationship is explained by the contribution of the ionicity and the electrostatic energy to the SFE.

1.7.3 Critical Resolved Shear Stress

Critical resolved shear stress (CRSS) is the stress above which dislocations can be moved. When this value is small, dislocations can be easily generated. Table 1.11 shows the critical resolved shear stress for various compound semiconductors.[40] It can be predicted that the dislocation density may be higher for lower CRSS.

The thermal stress during crystal growth must be less than the CRSS in order to obtain dislocation free crystals.

Kirchener et al.[44] have systematically analyzed all known critical resolved shear stress (τ_c) data as a function of temperature (Fig. 1.21(a)). They found that the τ_c/G vs kT/Gb^3 curve shows a master curve and there is a universal relationship (Fig. 1.21(b)) even among various materials even with different structures. Here. G is the shear modulus $G = (C_{11}-C_{12}+C_{44})/3$ and b is the Burger's vector.

Table 1.11 Critical Resolved Shear Stress of Various Materials (N/mm^2)

GaSb	GaAs	InSb	GaP	InAs	InP
15.8	1.9	5	4	0.8	1.8

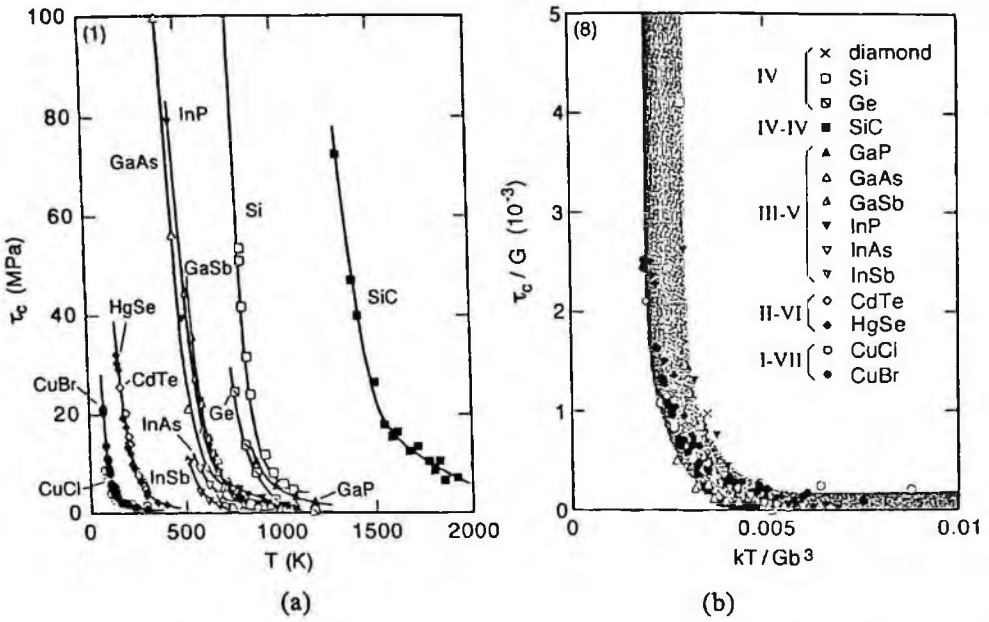

Fig. 1.21 (a) Temperature dependence of critical resolved shear stress (τ_c) and (b) τ_c against kT/Gb^3. All data fall into the shaded band (reprinted from Ref. 44 with permission, copyright 1983 Elsevier).

REFERENCES

1. *Physics and Chemistry of II-VI Compounds*, eds. by M. Aven and J. S. Prener (North-Holland, Amsterdam 1967)
2. B. Ray, *II-VI Compounds* (Pergamon Press, Oxford, 1969)
3. J. L. Pankove, *Optical Processes in Semiconductors* (Dover, New York, 1971)
4. R. H. Bube, *Photoconductivity of Solids* (R. E. Krieger, New York, 1978)
5. K. Zanio, *Semiconductors and Semimetals Vol. 13* (Academic Press, New York, 1978)
6. S. M. Sze, *Physics of Semiconductor Devices* (John Wiley & Sons, New York, 1981).
7. *Recent Compound Semiconductor Handbook (in japanese)*, ed. by T. Ikoma (Science Forum, Tokyo, 1982).
8. *Landolt-Börnstein, Vol. 17 Semiconductors*, ed. O. Madelung (Springer-Verlag, Berlin, 1982).
9. H. Hartmann, R. Mach and B. Selle, *in Currents Topics in Materials Science, Vol. 9* ed. E. Kaldis (North-Holland, Amsterdam, 1982)
10. A.H. Wilson, *Proc. Roy. Soc.* **A133** (1931) 458.
11. L. Pauling, *The nature of the Chemical Bond* (Cornell University Press, New York, 1960)
12. J.C. Phillips, *Bonds and Bands in Semiconductors* (Academic Press, New York, 1973).
13. J.C. Phillips, *Rev. Modern Phys.* **42** (1979) 317.
14. C.J. Nuese, in *Crystal Growth: A Tutorial Approach*, eds. W. Bradsley, D.T.J. Hurle and J.B. Mullin (North-Holland, Amsterdam, 1979) p. 353.
15. E. Mooser and W. B. Pearson, *J. Electron.* **1** (1956) 629.
16. E. Mooser and W. B. Pearson, *J. Chem. Phys.* **26** (1957) 893.
17. B.R. Pamplin, *J. Phys. Chem. Solids* **25** (1964) 675.

18. F.C. Phillips, *An Introduction to Crystallography* (Wiley, 3rd ed. 1963).
19. C. Kittel, *Introduction to Solid State Physics, 5th ed.* (John Wiley & Sons, New York 1976).
20. R.W.G. Wyckoff, *Crystal Structures, 2nd ed.* (Interscience, 1963)
21. L. Brillouin, *Wave Propagation in Periodic Structures* (Dover, New York, 2nd ed., 1963).
22. J. R. Chelikowsky and M. L. Cohen, *Phys. Rev.* **B14** (1971) 556.
23. H.C. Casey, Jr. and F.A. Trumbore, *Mater. Sci. Engineer.* 6 (1970) 69.
24. Data presented in a pamphlet of Cambridge Chemical Company.
25. Y. Nannichi, *J. Mater. Sci. Soc. Jpn. (in japanese)* **10** (1973) 160.
26. Y. Okuno, *Light Emitting Diodes (in japanese)* (Sangyo Tosho, Tokyo, 1993).
27. S. M. Sze, *Physics of Semiconductor Devices* (John Wiley & Sons, New York, 1981) p. 683.
28. C.D. Thurmond, *J. Electrochem. Soc.* **122** (1975) 1133.
29. W. Schockley, *Electrons and Holes in Semicondcutors* (D. Van Nostrand, Princeton, N.J., 1950)
30. S. Martin and G. Jacob, *Acta Electronica* **25** (1983) 123.
31. C.M. Wolfe, G.E. Stillman and W.T. Lindley, *J. Appl. Phys.* **41** (1970) 5585.
32. G.E. Stillman and C.M. Wolfe, *Thin Solid Films* **31** (1976) 69.
33. W. Walukiewicz, J. Lagowski, L. Jastrzebski, P. Rava, M. Lichtenstieger, C.H. Gatos and H.C. Gatos *J. Appl. Phys.* **51** (1980) 2659.
34. S. Gonda and M, Kawashima, in *Recent Compound Semiconductor Handbook (in japanese)*, ed. by T. Ikoma (Science Forum, Tokyo, 1982) p. 22.
35. J.D. Wiley, in *Semiconductors and Semimetals Vol. 10* (Academic Press, New York, 1975) p. 91.
36. K. Arai and S. Yoshida, *Fundamentals and Applications of SiC Devices (in japanese)* (Ohmsha, Tokyo, 2003).
37. L.D. Nielsen, *Phys. Rev. Lett.* A **38** (1972) 221.
38. M. Ura, from the text for a lecture in Scientec Co. (1980).
39. J. W. Fuast, *Compund Semiconductors, Vol.1 Preparation of III-V Compounds*, eds. by R. K. Willardson and H. L. Goering (Reinhold, New York, 1962) p. 445.
40. H. Gottshalk, G. Patzer and H. Alexander, *phys. stat. sol.* (a) **45** (1978) 207.
41. A. S. Jordan, R. Von A. R. Neida and J. W. Nielsen, *J. Appl. Phys.* **52** (1981) 3331.
42. S. Takeuchi, K. Suzuki and K. Maeda, *Phil. Mag.* A **50** (1984) 171, http;//www.tandf.co.uk./journals.
43. J. C. Phillips and J. A. Van Vechten, *Phys. Rev. Lett.* **23** (1969) 1115.
44. H.O.K. Kirchner and T. Suzuki, *Acta Mater.* **46** (1998) 305.

2. CRYSTAL GROWTH METHODS

2.1 INTRODUCTION

For growing single crystals, many kinds of crystal growth methods have been developed for various materials such as metals, oxides and semiconductors. These various methods have been reviewed by several authors.[1-13] Crystal growth methods which have been applied to compound semiconductor materials are summarized in Table 2.1. For most compound semiconductor materials, melt growth methods are the main methods of industrial manufacture. This is because they are appropriate to grow large single crystals quickly. In the case of solution growth methods and vapor phase growth methods, growth rates are rather lower compared to melt growth methods and they are in general limited to growing compound semiconductor materials which are difficult to grow by the melt growth method from the viewpoint of physical properties such as high melting temperature and/or high decomposition vapor pressure. In this chapter, crystal growth methods applied to compound semiconductor materials are reviewed. Beginning in Chapter 7, the crystal growth method applied to each of various materials is described in more detail .

2.2 MELT GROWTH METHODS

2.2.1 Horizontal Boat Growth Methods

Crystals can be grown using boat type containers in sealed ampoules and in many cases, the growth is performed under controlled vapor pressure of the constituent element. These methods are called boat-growth methods. This crystal growth is performed in horizontal and vertical arrangements.

(1) Horizontal Gradient Freezing (HGF) method

The HGF method is based on a directional solidification of the melt by decreasing the melt temperature as shown in Fig. 2.1(a). The precise arrangement is found in Ref. 14. The simple gradient freezing growth in a vertical configuration was first performed by Tamman.[15] In the HGF method, the material in a boat crucible is sealed in an ampoule and melted at a temperature higher than the melting point. The temperature of the ampoule is then cooled as seen in the figure. In this method, the ampoule is not moved and the temperature distribution is changed as the crystal can be grown from the seed end. This method is mainly used for the industrial production of conductive GaAs (Sec. 8.3.1).

(2) Horizontal Bridgman (HB) method

Bridgman[16] and Stockbager[17] invented a method to grow crystals by moving the crucible instead of changing the temperature profile. The horizontal arrangement on the basis of this method was applied to grow GaAs[18] and CdTe[19] crystals. Thereafter, this

Table 2.1 Various Crystal Growth Methods

Growth Method	Materials
Melt Growth Methods	
Boat Growth Methods	
Horizontal Bridgman (HB)	GaAs, CdTe
Horizontal Gradient Freezing (HGF)	GaAs, CdTe
Horizontal Zone Melting (HZM)	GaAs, InSb
Vertical Bridgman (VB)	GaAs, CdTe, GaSb, InP
Liquid Encapsulated Vertical Bridgman (LE-VB)	GaP, GaAs
Vertical Gradient (VGF)	GaAs, CdTe, ZnTe, GaP, InP
Liquid Encapsulated Vertical Gradient Freezing (LE-VGF)	CdTe, GaAs
Vertical Zone Melting (VZM) (or Ingot-sealed zone melting)	CdTe, GaAs
Liquid Encapsulated VZM (LE-VZM)	GaAs
Pulling Methods	
Czochralski (CZ)	GaSb, InSb
Liquid Encapsulated Czochralski (LEC)	GaAs, GaP, GaSb, InP, InAs
Liquid Encapsulated Kyropoulus (LEK)	GaAs, InP
Floating Zone (FZ)	GaAs, GaSb
Liquid Encapsulated Floating Zone (EFZ)	GaAs
Other Methods	
Shaped Crystal Growth Method	
Stepanov	Si, GaSb
Edged-Defined Film-Fed Growth (EFG)	Si, InSb, GaAs
Inverted Stepanov	Si
Shaped Melt Lowering (SML)	GaAs, GaSb
Heat-Exchange Method (HEM)	GaAs, CdTe
Solution Growth Method	
Simple Solution Growth Method	Various materials
Pressure-Controlled Solution Growth (PC-SG)	GaN
Temperature Gradient Zone Melting (TG-ZM) (or Travelling Solvent Method (TSM))	GaP, ZnTe
Travelling Heater Method (THM)	GaSb, GaP, CdTe, InSb, ZnSe
Solute Solution Diffusion (SSD) Method (or Temperature Solvent Growth (TSV))	GaP, InP
Solvent Evaporation (SE)	CdTe, ZnSe, ZnTe
Temperature Difference Method Control Vapor Pressure (TDM-CVP)	GaP, GaAs, ZnSe, ZnTe
Hydrothermal Synthesis	CdS, ZnS
Vapor Phase Growth Method	
Direct Synthesis (DS)	Various materials
Physical Vapor Transport (PVT)	SiC, CdTe, ZnS, ZnSe, ZnTe
Sublimation Travelling Heater Method (STHM)	CdTe, ZnSe, ZnTe
Chemical Vapor Transport (CVT)	ZnSe, ZnS, ZnTe, CdS, CdTe

method was developed for the industrial production of compound semiconductor materials. The HB method is used mainly for the industrial production of conductive GaAs (Sec. 8.3.1). As shown in Fig. 2.1(b), compound semiconductor raw material is set in a quartz boat and sealed in a quartz ampoule with the volatile constituent element. At the

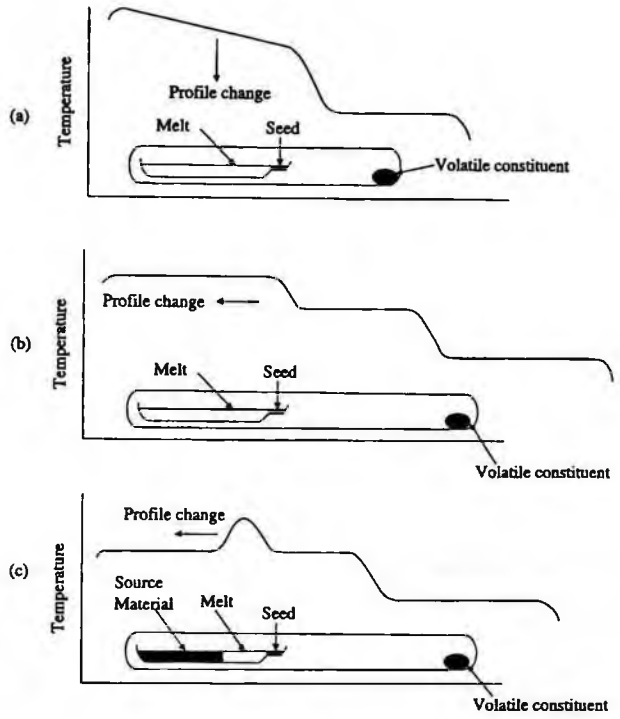

Fig. 2.1 Horizontal boat growth methods. (a) Horizontal Gradient Freezing (HGF), (b) Horizontal Bridgman and (HB) and (c) Horizontal Zone Melting (HZM) methods (from Ref. 14 with permission).

top of the boat, a seed crystal is set for single crystal growth. The ampule is then moved slowly in a furnace with the appropriate temperature distribution. In many cases, the vapor of the dissociative constituent of the crystal is pressurized during crystal growth to prevent decomposition. The principle of this method is reviewed by Rudolph and Kiessling.[19] Parsey and Thiel[20] have developed a sophisticated HB furnace arrangement for precise temperature profile control using a multi-zone furnace.

(3) Horizontal Zone Melting (HZM) method

Zone melting was first invented by Pfann[21, 22] for material purification. As explained in Chapter 3, the material can be purified after zone passing due to the distribution coefficient of impurities. This method is called zone refining (ZR) when it is mainly used for purification and is called zone leveling (ZL) when it is used to dope impurities homogeneously.

The horizontal arrangement of this method is called the Horizontal Zone Melting (HZM) method. In this method, the melt zone is moved from the seed part as seen in (Fig.2.1(c)). This method is industrially used for GaAs crystal growth under arsenic vapor pressure control (Sec. 8.3.1).

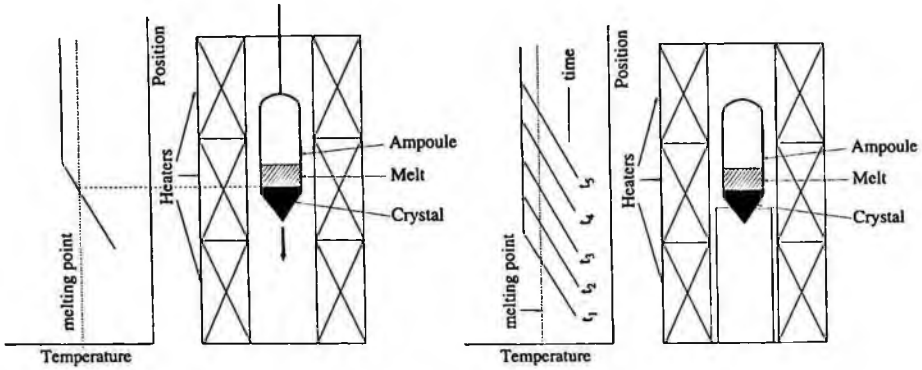

Fig. 2.2 Vertical boat growth methods. (a) Vertical Bridgman (VB) and (b)Vertical Gradient Freezing (VGF) methods.

2.2.2 Vertical Boat Growth Methods

In the vertical configuration as seen in Fig. 2.2, crystals are grown as in the initial invention by Tamman[15] for changing the temperature profile and those by Bridgman[16] and Stockbarger[17] for moving the crucible or the furnace. The former method is called the vertical gradient freezing (VGF) method and the latter the vertical Bridgman (VB) method. In the case of most compound semiconductors, liquid encapsulant such as B_2O_3 is used for preventing the decomposition of the charge materials, and then they are called Liquid Encapsulant VB (LE-VB)[23] and Liquid Encapsulant VGF (LE-VGF). They are old crystal growth methods for growing metal and oxide single crystals, but are also applied for various compound semiconductors. The application of these methods to compound semiconductors is reviewed in Refs. 24-31.

The VB/VGF methods have the following advantages.

(i) Low dislocation density can be achieved due to the low axial temperature gradient during crystal growth.

(ii) No necessity for crystal diameter control

(iii) Round shaped crystals can be obtained while only D-shaped crystals are obtained in HB/HGF/HZM methods

(iv) Uniformity across wafers is good compared with the HB/HGF/HZM methods, because wafers can be cut perpendicular the crystal axis.

(v) High cost performance because of low cost crystal growers

The VB/VGF methods however have the following disadvantages.

(i) Low growth rate due to low heat dissipation

(ii) Low single crystal yield because the seeding can not be observed.

(1) Vertical Bridgman (VB) method

In this method, the material is set in an appropriate crucible as shown in Fig. 2.2(a) and

cooled in an appropriate temperature distribution. In many cases, single crystal seeds are set in the bottom of the crucible. In the case of compound semiconductors, one of the constituents is usually volatile. The crucible is therefore set in a quartz ampoule and the constituent element is set in the bottom of the closed ampoule to heat in such a way that vaporization is prevented during crystal growth.

In the case of the VB method, when a large diameter ampoule with a large amount of charge is lowered in the furnace, the temperature distribution in the furnace is changed since the heat capacity of the ampoule is too large. For the growth of low dislocation density crystals, it is necessary to grow crystals under a lower temperature gradient, extremely low, less than 5 °C/cm. It is therefore not desirable for the temperature profile to change during crystal growth. This therefore is a disadvantage of the VB method.

Ostrogorsky et al. have developed the Submerged Heater Method (SHM). [32, 33] In this method, the temperature difference and the distance between the growth interface and the submerged heater are held constant so that crystal growth can be performed without significant convection and the segregation of impurities can be kept constant.

(2) Vertical Gradient Freezing (VGF) method

The VGF method was first applied for the growth of GaAs by Chang et al.[34] in a pyrolytic boron nitride crucible without using seed crystals. In the VGF method, instead of lowering the crucible, the temperature profile is changed for growing crystals (Fig. 2.2(b)). The advantages of this method compared with the VB method are as follows.

(i) When a crucible with a large load is not moved, the temperature profile can be well controlled during crystal growth.

(ii) Since the crucible is not moved, the height of the furnace can be lower than in the VB method.

(iii) There is no mechanical vibration since the ampoule is fixed in a constant position in the furnace.

The VGF method has however a disadvantage that the growth rate rises when the temperature profile is lowered at a constant rate. The growth rate comes unlimited when the maximum temperature in the furnace becomes close to the melting point. In the case of the VGF method, it is therefore necessary to control very precisely the rate of temperature decrease using a multi-zone furnace.

A more sophisticated VGF method, in which temperature distribution can be more precisely controlled has been invented. Potard[35] developed a VGF method combined with a dilatometry, by which it is possible to measure the solidified fraction during crystal growth.

(3) Vertical Zone Melting (VZM) method

This method was formerly used to grow compound semiconductor crystals and it is also called the "sealed-ingot zone melting method", in which compound semiconductor materials are sealed in ampoules and are zone melted in a vertical configuration[36, 37] as shown in Fig. 2.3. When an encapsulant such as B_2O_3 is used, it is called Liquid Encapsulant VZM (LE-VZM) method as applied in the crystal growth of GaAs.[38]

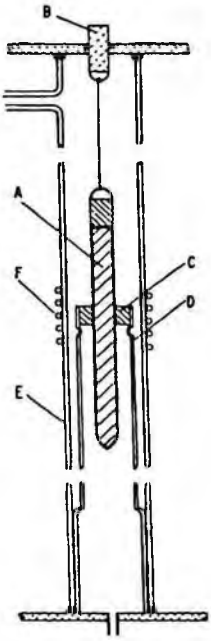

Fig. 2.3 Vertical zone-melting method. A: quartz enveloped ingot, B: shaft to variable speed drive mechanism, C: graphite suscepter, D: quartz suscepter holder, E: quartz for protection from atmosphere, F: induction coil (reprinted from Ref. 37 with permission of The Electrochemical Society).

2.2.3 Pulling Methods

(1) Czochralski (CZ) method

The CZ method which was first invented by Czochralski[39] is a crystal growth method mainly used for industrial production of silicon. As shown in Fig. 2.4 (a), a single crystal seed attached to a pulling rod is dipped in the melt in a crucible which is rotated and by raising and rotating the pulling rod, single crystals are grown. The fundamentals of this method are reviewed in detail.[40, 41]

This method has the advantage that it allows a high growth rate and the growth of large diameter crystals. In fact, in the case of silicon, 300 mm diameter single crystals of considerable length can be grown by this method. This method is however applicable only to a limited number of compound semiconductor materials whose decomposition pressure is very low or negligible. GaSb and InSb crystals can be grown by this method as explained in Chapters 9 and 12.

There are various modifications of the CZ method. Gremmelmeier[42] has used a modified CZ method for growing GaAs, in a sealed system with magnetic coupling for rotation and pulling. Arsenic vapor pressure was applied in the ampoule to prevent the decomposition of GaAs. In order to prevent impurity segregation, the floating crucible[43] method has been developed.

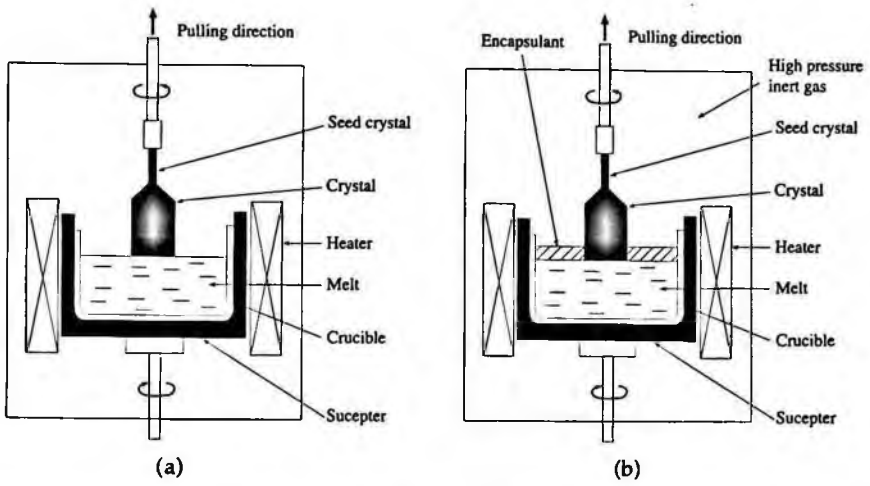

Fig. 2.4 Crystal pulling methods. (a) Czochralski (CZ) and (b) Liquid Encapsulated Czochralski (LEC) methods.

(2) Liquid Encapsulated Czochralski (LEC) method

First invented by Metz et al.[44] and Mullin et al.[45, 46] to apply the Czochralski method to the crystal growth of dissociative compound semiconductor materials, there is the Liquid Encapsulating Czochralski (LEC) method. In this method, a glass material, mainly B_2O_3, is used to encapsulate the melt as shown in Fig. 2.4 (b). Inert gas such as argon or nitrogen at high pressure up to 100 atm is applied in the furnace so as to prevent the decomposition of the compound semiconductor material melt. The application of inert gas at high pressure prevents the volatile constituent from forming a gas bubble in the B_2O_3 encapsulant and floating to the surface of the encapsulant B_2O_3 and being removed from the encapsulant. Since the crystal growth is performed under high pressure conditions, high pressure vessels are needed for the LEC method.

This is one of the most successful crystal growth methods and is industrially applied to the production of the most important III-V compound single crystals such as GaAs, GaP, InP and InAs.

The disadvantage of this method is in the fact that the axial temperature gradient is rather greater than in boat growth methods, so that it is difficult to reduce the dislocation densities. To counter this disadvantage, various modifications have been developed such as vapor pressure-control (Sec. 2.5.2), application of magnetic field (Sec. 3.4), full encapsulation (Fig. 8.8) and so on.

(3) Kyropolous and Liquid Encapsulated Kyropolous (LEK) methods

Instead of growing crystals by pulling up the seed crystal, the seed crystal is dipped in the melt and slightly raised up just for growing the initial part of the crystal. The melt

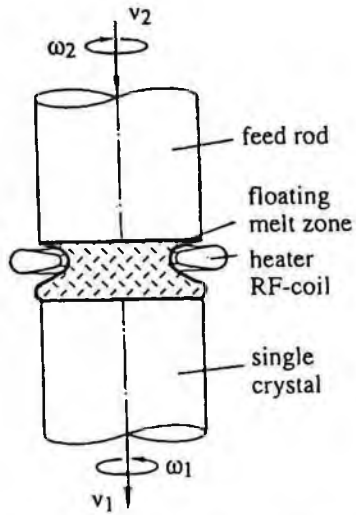

Fig. 2.5 Principle of the Floating Zone (FZ) method with RF coil in needle-eye configuration (reprinted from Ref. 11 with permission).

itself is then crystallized in the crucible[47]. When an encapsulant such as B_2O_3 is used, it is called the Liquid Encapsulant Kyropolous (LEK) method.[48]

2.2.4 Floating Zone (FZ) Method

This method was developed for growing high purity Si single crystals.[49, 50] As shown in Fig. 2.5, part of the polycrystal feed rod is melted by a zone heater and this melted zone can be held as it is because of the capillary force of the melt without touching any container materials. Since the melt is not in contact with any furnace material, high purity crystal can be grown without the incorporation of impurities from the furnace material.

This method has been applied for the growth of GaAs without encapsulant[51] and with encapsulant[52-54]. When an encapsulant is used, it is called the Encapsulated Floating Zone (EFZ) method.

2.2.5 Other Methods

(1) Shaped Crystal Growth Method

Stepanov et al.[55, 56] first applied a pulling method to grow crystals of various shapes such as sheets, tubes and rods directly from melts using wetting dies. This method is called the Stepanov method. When non-wetting dies such as graphite, tungsten and molybdenum are used, it is called the Edge-Defined Film-Fed Growth (EFG) method (Fig. 2.6) and was used to grow Si, Ge and sapphire ribbon crystals.[57-59] When an encapsulant such as B_2O_3 is used, this method is called the Liquid Encapsulated Stepanov (LES) method.[60] The LES method has been applied for the crystal growth of compound semiconductors such as GaAs.[61, 62]

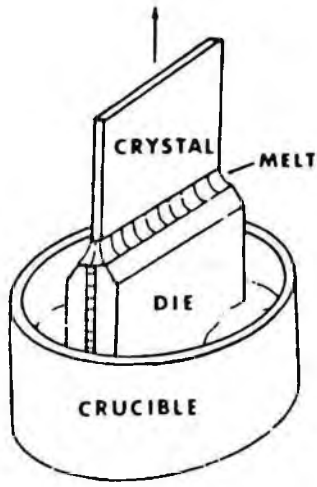

Fig. 2.6 Edge-Defined Film-Fed Growth (EFG) method (reprinted from Ref. 60 with permission, copyright 1975 TMS).

In the inverted Stepanov method, the crystal is grown downward from a die attached to the melt.[63] The modified method which is called Shaped Melt Lowering (SML) has been used for growing GaSb crystals.[64]

(2) Heat Exchange Method (HEM)

In this method, a heat exchange via liquid helium is performed at the bottom of the crucible as shown in Fig. 2.7 in order to dissipate the latent heat of growth of crystals in a crucible. This method was first developed for growing oxide crystals[65-68] and was developed to grow polycrystalline Si crystals for solar cell applications. This method was also applied for growing compound semiconductors.

2.3 SOLUTION GROWTH METHODS

2.3.1 Simple Solution Growth Method

The solution growth (SG) method is based on crystal growth from a solvent which contains the constituents. The solvent may be one of the constituents itself or some other element or compound may be used. This method is also called the flux method[69-71] and has been developed mainly for growing a variety of oxide crystals.

The solution is heated above the melting point and is cooled to crystallize the compound semiconductor materials. Since this method is based on the precipitation of the compound from the solvent, it has the following disadvantages.

(i) During crystal growth, the composition of the solution is significantly changed because of the difference of the composition between the grown crystal and the solution.

(ii) Because of this significant change of the solution composition, supercooling

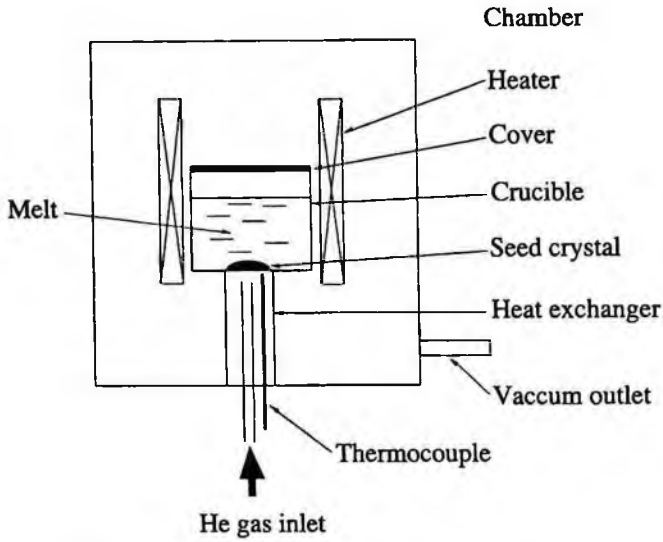

Fig. 2.7 Heat Exchange Method (HEM).

happens easily as described in Sec. 3.6.

(iii) To prevent tsupercooling, the growth rate has to be very low.

The solution growth method has however several advantages. Since the crystal is grown from a solution, impurities with a segregation coefficient, k, less than unity can be left in the solution so that the purification can be achieved during crystal growth. This method can be applied under low pressures even for the crystal growth of compound semiconductors whose decomposition vapor pressure is very high. Because of these advantages, the solution growth method has been applied to many binary, ternary and mixed-crystal compound semiconductor materials[69] but most of them were limited to research purposes.

This method is however promising for compound semiconductors like nitrides which are difficult to grow by conventional methods. In order to avoid the above mentioned disadvantages of this method, the pressure-controlled SG (PC-SG) method has been invented.[72-75]

2.3.2 Traveling Heater Method (THM)

Pfann[21] has proposed a growth method in which the melted zone is located under a temperature gradient and the melted zone is moved in order to grow crystals at the lower temperature region as shown in Fig. 2.8 (a). This method which is called the Temperature Gradient Zone Melting (TGZM) method has been theoretically examined by Tiller[76] and later it was called the Travelling Solvent Method (TSM).[77]

Instead of this method, the traveling heater method (THM), where the heater or the ampoule is moved as shown in Fig. 2.8 (b) has been developed. In a closed quartz ampoule, a solution zone whose composition is rich with a constituent element of the compound is first made and the zone is moved from bottom to top in order that the

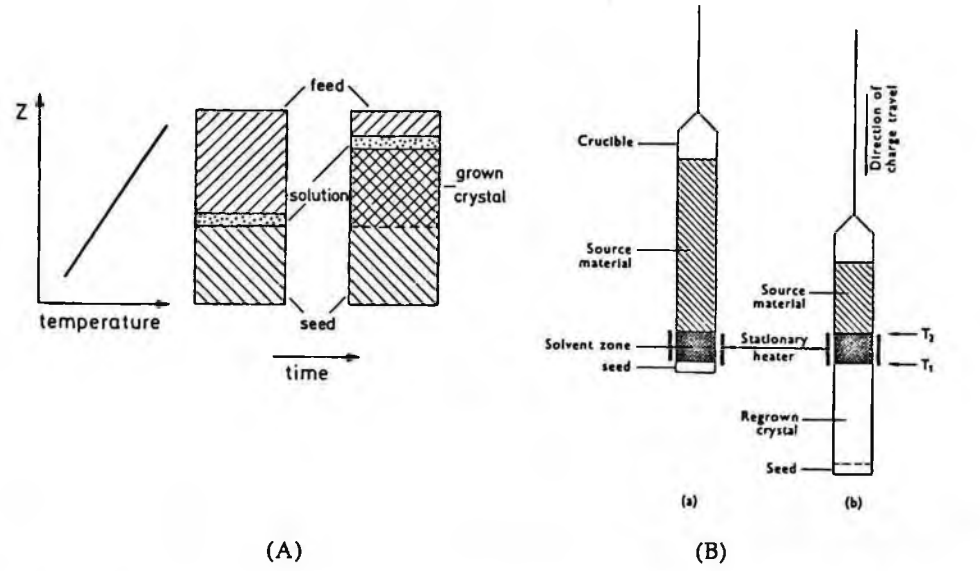

Fig. 2.8 (A) Traveling Solvent Method (TSM) or Temperature Gradient Zone Melting (TGZM) method (reprinted from Ref. 4 with permission of Springer Science and Bysiness Media). The zone moves in the direction of the arrow driven by the concentration difference ΔC established across the zone by the temperature gradient. (B) Traveling Heater Method (THM). (a) Before growth, (b) during crystal growth. (reprinted from Ref. 78 with permission of Springer Science and Bysiness Media)

source material is dissolved in the solution and crystallized to the bottom of the solution zone. Since the melting point of the solution is lower than the melting point of the compound, low temperature crystal growth can be achieved. The advantage of this method compared with the TSM is that crystal growth can be performed at a constant temperature. The crystal growth rate is however limited because of the slower diffusion coefficients of the constituent elements in the solution. This method in principle allows of the growth of high purity crystals so that it is used where the application requires very high purity material.

The THM was first proposed by Broader and Wolff[77] for growing GaP crystals from a Ga solution. Since then this method has been applied to other III-V materials and II-VI materials as explained in detail after Chapter 7. This method is reviewed in detail by Wolff and Mlavsky[78] and Benz et al.[4] Theoretical studied of the temperature distribution and mass transportation have been carried out by many authors.[79-81]

2.3.3 Solute Solution Diffusion (SSD) Method

This method was first applied to the growth of GaP crystals[82, 83] and was reviewed and renamed as the Temperature Gradient Solution (TGS) growth method by Gillessen et al.[5] The method is based on dissolving the constituent whose vapor pressure is high in

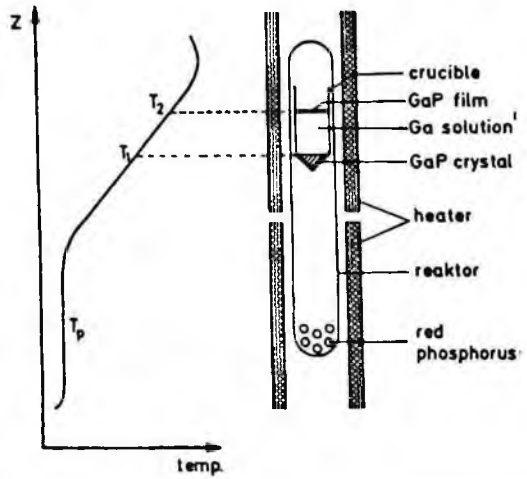

Fig. 2.9 Solute Solution Diffusion (SSD) method first applied for GaP single crystal growth (reprinted from Ref. 83 with permission, copyright 1973 IEEE).

the melt of the other constituent and the compound material is crystallized from the bottom of the crucible as shown in Fig. 2.9. Since crystal growth can be performed at low temperatures, high purification can be achieved. This method has been applied to various materials and was proved that it is effective in improving the purity. The crystal growth rate is however limited as in the case of THM because of the low diffusion coefficients of the constituent element in the solution. This method was applied not only for GaP (Chapter 7) but also for InP (Chapter 10), mainly for high purity polycrystal synthesis.

2.3.4 Solvent Evaporation (SE) Method

This method is based on the evaporation of solvent causing the solute concentration to increase above the solubility and crystal growth occurs. This method was first suggested in Ref. 84 and was applied to the growth of CdTe.[85-87] The advantage of this method is that crystal growth can be performed without decreasing the temperature which has the possibility of overcoming the constitutional supercooling problem Fig. 2.10 shows a furnace configuration. The evaporated solvent from the upper crucible is deposited at the bottom of the ampoule, as shown in the figure, by reducing the temperature of the lower furnace.

2.3.5 Temperature Difference Method under Controlled Vapor Pressure (TDM-CVP)

Nishizawa et al.[88] have developed the TDM-CVP method for GaAs crystal growth, by which stoichiometric crystal growth can be performed under controlled vapor pressure. This method is then applied to crystal growth not only of GaAs,[89, 90] but also of GaP,[90, 91]

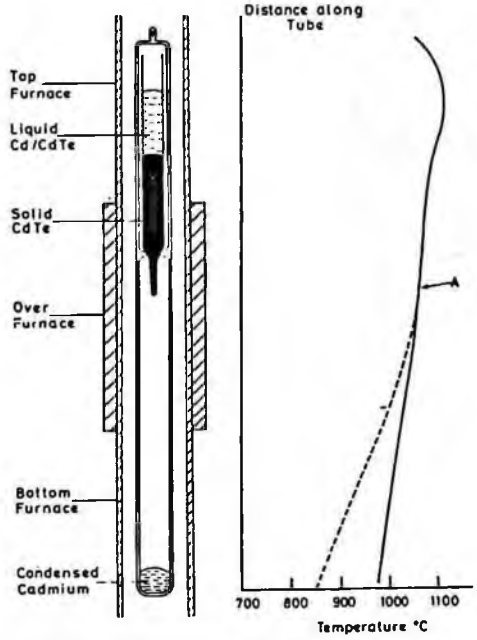

Fig. 2.10 Schematic diagram of the Solvent Evaporation (SE) method and associated furnace profile. During growth, the lower furnace temperature is reduced so that the profile "hinges" about point A (reprinted from Ref. 87 with permission, copyright 1985 Elsevier).

ZnSe[92-96] and ZnTe.[97] This method is reviewed by Nishizawa et al.[98]

In Fig. 2.11, a typical furnace configuration for this method is shown. The metal solvent is held in the upper crucible and the temperature of the upper region T_1 is maintained ΔT higher than the temperature of the lower region T_2. The source on the surface of the melt is dissolved in the solvent and diffuses towards the lower region and recrystallizes at the bottom of the crucible. The growth temperature can be kept constant since the solute is constantly supplied from the source material.

2.3.6 Hydrothermal Synthesis Method

This method is industrially applied in the large scale production of quartz. The principle of this method is the precipitation of quartz from a NaOH aqeous solution. In order to achieve an appropriate solubility of quartz in water, temperature and pressure are increased in an autoclave as shown in Fig. 5.12. The application of this method to various oxide materials is reviewed by Demianets.[99] The advantage of this method is in its large scale production ability and the low production cost. This method has not been studied so extensively for compound semiconductors but is reported for the growth of some crystals[100, 101] which are difficult to grow by conventional methods.

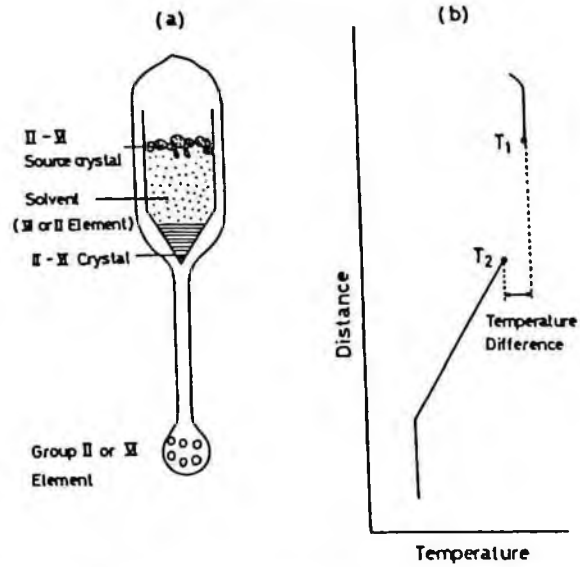

Fig. 2.11 Temperature Difference Method under Optimum Control Vapor Pressure (TDM-CVP). Schematic diagram of (a) the growth system and (b) the temperature distribution of furnace (reprinted from Ref. 93 with permission, copyright 1985 American Institue of Physics).

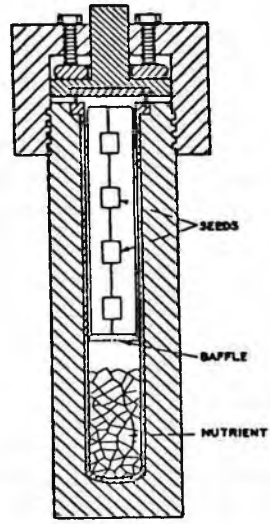

Fig. 2.12 Hydrothermal synthesis method in an autoclave (reprinted from Ref. 3 with permission, copyright 1979 Elsevier).

2.4 VAPOR PHASE GROWTH METHOD

The vapor phase growth method is industrially applied in the crystal growth of CdTe and SiC which have high sublimation pressures. This method is also promising for ZnSe, ZnS whose sublimation pressure is rather higher. There are three methods, the

direct synthesis (DS) method, the physical vapor transport (PVT) and the chemical vapor transport (CVT) methods.

2.4.1 Direct Synthesis (DS) Method

In early vapor phase growth studies, the material was prepared directly from its constituents and the reacted compound was deposited in the lower temperature region in order to grow crystals. An example of this method is shown for ZnS crystal growth,[102] where ZnS was prepared by the direct reaction of Zn vapor with a carrier gas, H_2S. This method was applied to crystal growth of various materials in older times, but only small crystals could be obtained.

2.4.2 Physical Vapor Transport (PVT) Method

This method is applicable for compound materials whose sublimation pressure is high. The compound is sublimed in an open tube with a carrier gas or in a closed tube. This method is reviewed by Kaldis[103] and Kaldis and Piechtka.[104]

(1) Open tube method

In this method, the source material is set in an open tube at a higher temperature region and the material is vaporized and transported to the lower temperature region.[105] There are a variety of open tube methods and some of them are explained from Chapter 7 on for various compound semiconductor materials.

(2) Closed tube method

In this method, the source material is set in an closed tube at a higher temperature region and the material is vaporized and transported to the lower temperature region. The method known as the Kremheller method[106] was first applied by Czyzak et al.[107] and Greene et al.[108] for compound semiconductors. This method was then developed as the Piper-Polish method (self-sealing method) as shown in Fig. 2.13.[109] In the Piper-Polish method, the tube itself is not sealed and during heating impurities can be evacuated from the source material. The vaporized compound is then deposited between the wall of the ampoule and the ampoule sealing tube, and the ampoule is thus self-closed. After the ampoule is closed, the source materials are transported to the lower temperature region and crystals are grown.

In order for this method to be successful, it is necessary that the grown compound has a high binding energy so that the source material can be evaporated as a compound molecule without significant dissociation of the vaporized material and for this purpose, the vapor pressure of the constituent atoms is controlled.[110, 111]

In the above PVT method, when grown crystals contact the ampoule wall, because of the thermal stress during cooling, dislocations are generated and cracking occurs.[112] The ampoule wall also induces non-controlled nucleation during crystal growth which results in polycrystallization. To counter these problems, the "free growth" or "contactless" method has been invented and developed[113-119] where the seed substrate is separated from the ampoule by a clearance.[116] In this free-growth method, molten metal

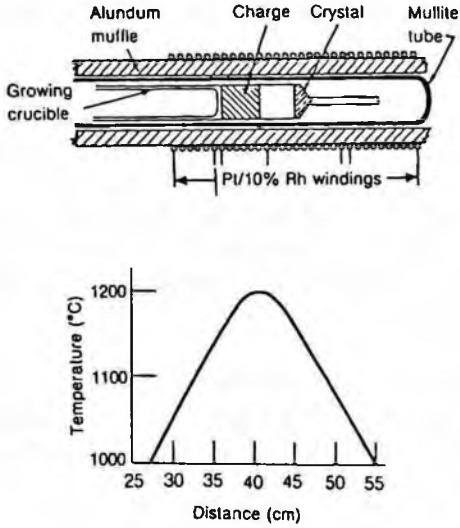

Fig. 2.13 Self closed tube vapor phase growth (Piper-Polish) method (reprinted from Ref. 109 with permission, copyright 1961 American Institue of Physics).

such as tin can be used to control the temperature distribution during crystal growth.

The partial pressure of the constituent element affects the growth rate. Prior[110] first studied PVT crystal growth while controlleing the vapor pressure of the constituent elements. Igaki et al.[120] studied systematically the effect of the vapor pressure on the growth rate of CdTe.

As a modification of the PVT method, Sublimation THM (STHM) as shown in Fig. 2.14 was first applied to the growth of CdTe and ZnTe by Triboulet.[121] This method utilizes the vapor phase instead of a solution zone for solution THM.

2.4.3 Chemical Vapor Transport (CVT) Method

To reduce the growth temperature, a transport medium such as iodine is used for vapor phase growth, which is then referred to as the chemical vapor transport (CVT) method. This method was first applied for compound materials by Shäfer[122-124] but the principle was known as the method of van Arkel-de Boer for preparing certain metals by thermal decomposition of their halides on a hot wire.[125] The CVT method is reviewed by Nitscheet al.[126, 127] and Ray.[125]

A typical example for ZnS_xSe_{1-x} crystal growth is shown in Fig. 2.15.[128] In a quartz ampule, the source material, the transport medium, iodine and a seed crystal are sealed as shown in the figure. When the ampoule is heated under the temperature distribution as shown in the figure in the case of the crystal growth of ZnSe, ZnSe is dissociated at the surface of the source material as

$$ZnSe \rightarrow Zn + (1/2)\, Se_2 \qquad (2.1)$$

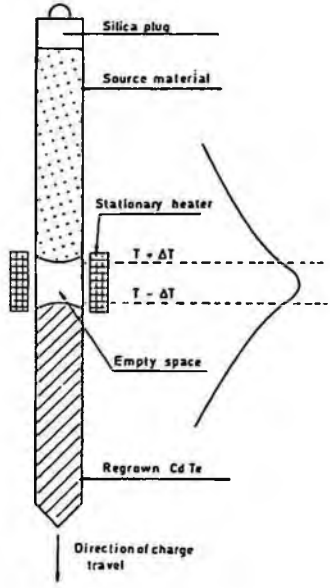

Fig. 2.14 Sublimation Travelling Heater Method (STHM) (from Ref. 121 with permission).

Dissociated Zn reacts with iodine to form ZnI_2 as

$$Zn + I_2 \rightarrow ZnI_2. \qquad (2.2)$$

ZnI_2 vapor diffuses to the lower temperature part where ZnSe is deposited by the fol-

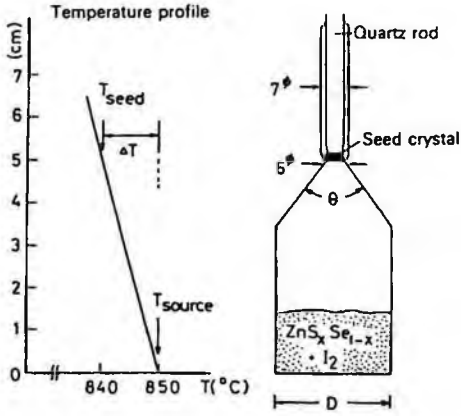

Fig. 2.15 A typical example of Chemical Vapor Transport (CVT) method for the case of ZnS_xSe_{1-x} crystal growth. Schematic illustration of the growth ampoule and the temperature profile of the furnace at the growth position (reprinted from Ref. 128 with permission, copyright 1979 Elsevier).

lowing reaction.

$$ZnI_2 + (1/2)\,Se_2 \rightarrow Zn\,Se + (1/2)Se_2 + I_2 \qquad (2.3)$$

Since crystals can be grown at lower temperatures, this method is effective in growing single crystals free from twins caused by the phase transition. The disadvantage is that iodine is incorporated in the crystal.

The transport rate can be expressed as[129]

$$\tau = -\frac{D(P_2^{T_2} - P_1^{T_1})\,A}{RTL}. \qquad (2.4)$$

Here, P_2 and P_1 are the pressure of ZnI_2 at the source temperature (T_1) and at the growth temperature (T_2). D is the diffusion coefficient, R the gas constant, T the average temperature and A the cross section of the growth ampoule.

2.4.4 Solid Phase Reaction (Solid State Recrystallization)

This method is based on recrystallization via grain growth in the solid state. When crystals with small grains are annealed below the melting point, grain growth occurs and a single grain becomes a large grain with the single phase. The principle of this method is reviewed by Aust[130] and the method was applied for crystal growth of ZnSe.[131, 132]

2.5 MODIFICATION OF CRYSTAL GROWTH METHODS

The above mentioned methods are the fundamental methods for crystal growth. In reality, several modifications can be applied for more effective crystal growth.

2.5.1 In-Situ Synthesis

In most compound semiconductors, the pre-synthesized material is used for growing crystals. For some materials, it is however possible to synthesize the material from the constituent elements directly in the crystal growth furnace. The examples are GaAs, GaSb, InSb, InAs and ZnTe. In the case of InP, polycrystal starting material can be synthesized by a phosphorus injection method (Sec. 10.3)

2.5.2 Vapor Pressure Control

Since most compound semiconductor materials have a volatile constituent, control of vapor pressure during crystal growth is one of the key issues for crystal growth. In the case of HB/HGF and VB/VGF methods and PVT methods, it is easy to control the vapor pressure of the volatile constituents because in sealed ampoules, the constituent element is held in the reservoir region and is heated to apply the desired pressure.

For Czochralski and LEC methods, various vapor pressure control methods have been developed. Some examples are as shown in Fig. 2.16. There are closed CZ methods,[42, 133–135] the vapor-pressure-controlled Czochralski CZ (PCZ) method[136, 137] and vapor pressure controlled LEC (VLEC) methods.[11] VLEC methods have various terms

(a)

1. Upper flange
2. Inner chamber
3. Seal
4. Crucible
5. Upper shaft
6. GaAs
7. Groove
8. Spring
9. Optical window
10. As pressure controlling furnace
11. Heater
12. Lower shaft
13. B203
17. Outer chamber

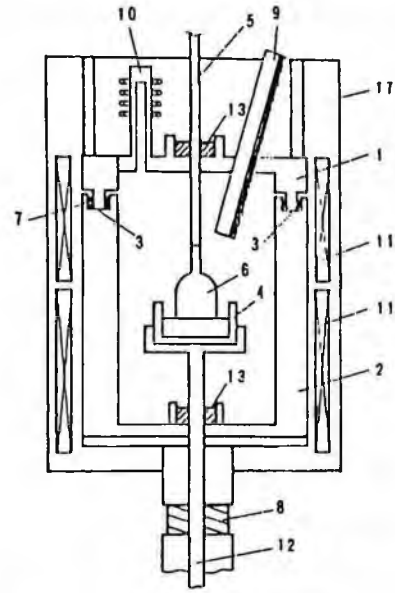

(b)

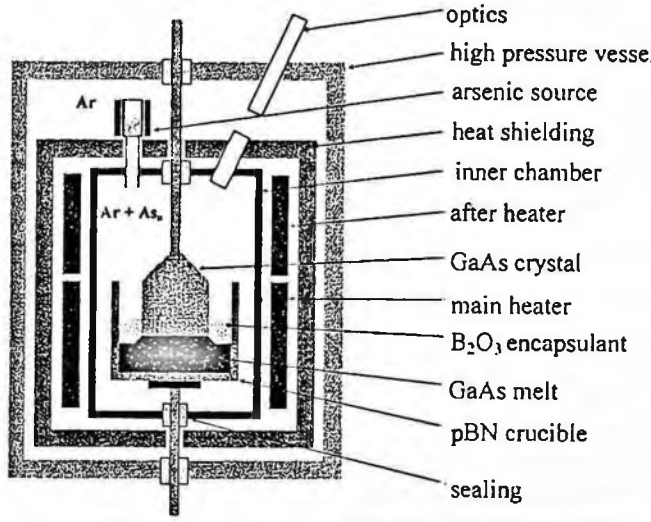

Fig. 2.16 Vapor pressure control methods. (a) Vapor Pressure controlled Czochralski (PCZ) method (from Ref. 137 with permission) and (b) Vapor-pressure-controlled LEC method (VLEC) method (this is also called VCZ or PC-LEC method) (reprinted from Ref. 147 with permission, copyright 2001 Elsevier).

applied to them such as arsenic ambient controlled LEC (As-LEC),[138, 139] vapor pressure controlled Chochralski (VCZ)[140, 141] and pressure controlled LEC (PC-LEC).[142, 143] As a

simple vapor pressure application method, the thermal baffle LEC (TB-LEC) method[144, 145] was also employed.

The problem in controlling the vapor pressure in CZ and LEC methods is how to seal the vaporized constituent atoms from the system. Various methods have been proposed and applied.

(i) Magnetic transport of sealed ampoule[42]
(ii) Molten metal sealing[133]
(iii) Closed crucible[134]
(iv) B_2O_3 sealing[135-141]
(v) Mechanical sealing[142, 143]
(vi) Thermal baffling[144, 145]

In most cases, the vapor pressure of the volatile constituent is controlled by heating the reservoir of the volatile constituent. The vapor pressure controlled methods were reviewed by Rudolph et al.[146, 147] and the details of these developments are mentioned after Chapter 9.

2.5.3 Magnetic Field Application

The application of a magnetic field is effective in controlling externally the convection in the melt and thus to control the crystal growth conditions. The principle of the application of a magnetic field is explained in Sec. 3.4. The magnetic field can be applied horizontally and vertically. The application has been investigated extensively for LEC methods and some studies have been performed for the vertical Bridgman and Kyropolus methods. The effectiveness of the application of a magnetic field is clearly demonstrated in the case of silicon crystals mainly for controlling oxygen concentrations. For compound semiconductors, the effectiveness to improve the quality of crystals has been extensively studied.

2.5.4 Accelerated Crucible Rotation Technique (ACRT)

This technique is a method in which the crucible is rotated under acceleration force in order to control fluid, thermal and mass flows for appropriate crystal growth. The method was used for flux growth methods from about 1960 and was clearly named as ACRT by Scheel and Schultz-Dubis.[148] The method was experimentally[149] and theoretically[150] developed in 1972. Since then this method was studied extensively for the flux method and it has been applied to zone refining, Bridgman methods and also to crystal pulling methods for semiconductor materials.[151-156] The theoretical aspect of this method is also reviewed by Capper et al.[157] and Brice et al.[158]

REFERENCES

1. J.B. Mullin, in *Crystal Growth and Characterization*, eds. R. Ueda and J.B. Mullin (North-Holland, Amsterdam, 1975) p. 75.
2. H. C. Gatos, in *Crystal Growth: A Tutorial Approach*, eds. by W. Bardsley and D. T. J. Hurle (North-Holland, Amsterdam, 1979) p.1.
3. D. T. J. Hurle, in *Crystal Growth: A Tutorial Approach*, eds. by W. Bardsley and D. T. J. Hurle (North-Holland, Amsterdam, 1979) p. 91.
4. K-W. Benz and E. Bauser, in *Crystals: Growth, Properties and Applications, Vol.3 III-V Semicon*

ductors (Springer-Verlag, Berlin, 1980) p. 1.
5. K. Gillessen, A. J. Marshall and J. Hesse, in *Crystals: Growth, Properties and Applications, Vol.3 III-V Semiconductors* (Springer-Verlag, Berlin, 1980) p. 49.
6. *Crystal Growth*, ed. B.R. Pamplin (Pergamon Press, Oxford, 1980)
7. J. B. Mullin, in *Crystal Growth of Electronic Materials*, eds. by E. Kaldis (Elsevier Science, Amsterdam, 1985) p. 269.
8. R. Fornari, *Mater. Sci. Engineer.* **B9** (1991) 9.
9. M. Isshiki, in *Widegap II-VI Compounds for Opto-electronic Applications*, ed. H.E. Ruda (Chapman & Hall, 1992) p. 3.
10. *Handbook of Crystal Growth, Vol.2 Bulk Crystal Growth*, ed. D.T.J. Hurle, (Elsevier Sci. Amsterdam, 1996).
11. G. Müller, *Mater. Sci. Forum* **276-277** (1998) 87.
12. *Book on Crystal Growth Technology*, ed. H.J. Scheel (John Wiley & Sons, New York, 2004)
13. J.B. Mullin, *J. Appl. Phys.* **264** (2004) 578.
14. S. Mizuniwa, M. Kashiwa, T. Kurihara and S. Okubo, *Hitachi Cable Rev.* **7** (1988) 51.
15. G. Tamman, *Lehrbuch der Metallographie*, ed. L. Voss (Leipzig und Hamburg, 1914), *Metallography* (The Chemical Catalogue, New York, 1925) p. 26.
16. P.W. Bridgman, *Proc, Am. Acad. Sci.* **60** (1925) 305.
17. D.C. Stockbarger, *J. Opt. Soc. Am.* **27** (1937) 416, Rev. Sci. Instrum. 7 (1963) 113.
18. T. Suzuki, S. Akai and K. Kohe, in *Semiconductor Research Vol. 12 (in japanese)*, ed. J. Nishizawa (Kogyo Chousakai, Tokyo, 1976) p. 87.
19. P. Rudolph and F.M. Kiessling, *Cryst. Res. Technol.* **23** (1988) 1207.
20. J.M. Parsey, Jr. and F.A. Thiel, *J. Crystal Growth* **73** (1985) 211.
21. W.G. Pfann, J. Metals **September** (1955) 961, *Trans. Met. Soc. AIME* **203** (1955) 961.
22. W.G. Pfann, *Zone Melting, 2nd ed.* (Wiley, New York, 1966) and W.G. Pfann, in *Crystal Growth and Characterization*, eds. R. Ueda and J.B. Mullin (North-Holland, Amsterdam, 1975) p. 53.
23. K. Hoshikawa, H. Nakanishi, H. Kohda and M. Sasaura, J. *Crystal Growth* **94** (1989) 643.
24. A.G. Fischer, in *Crystal Growth*, ed. B.R. Pamplin (Pergamon Press, 1980) p. 521.
25. W. A. Gault, E.M. Monberg and J.E Clemans, *J. Crystal Growth* **74** (1986) 491.
26. J. E Clemans, W.A. Gault and E.M. Monberg, *AT&T Tech. J.* **65** (1986) 86.
27. A. Horowitz and Y.S. Horowitz, *Mater. Res. Bull.* **21** (1986) 1123.
28. E.D. Bourret, in *F. Weinberg Int. Symp. Solid. Process* (US, 1990) p. 362.
29. K. Hoshikawa, in *Semiconductor Research Vol. 35*, ed. J. Nishizawa (in japanese) (Kogyo Chouakai, Tokyo, 1991) p. 3.
30. E. Monberg, in *Handbook of Crystal Growth, Vol. 2 Bulk Crystal Growth*, ed. D.T.J. Hurle (Elsevier Sci., Amsterdam, 1996) p. 52.
31. T. Asahi, K. Kainosho, K. Kohiro, A. Noda, K. Sato and O. Oda, in *Book on Crystal Growth Technology*, eds. H.J. Scheel and T. Fukuda (John Wiley & Sons, New York, 1979) p. 323.
32. A.G. Ostrogorsky, *J. Crystal Growth* **104** (1990) 233.
33. A.G. Ostrogorsky and G. Müller, *J. Crystal Growth* **137** (1994) 64.
34. C.E. Chang, V.F. S. Yip and W.R. Wilcox, *J. Crystal Growth* **22** (1974) 247.
35. C. Potard, J. *Crystal Growth* **54** (1981) 558.
36. F.K. Heumann, *J. Electrochem. Soc.* **109** (1962) 345.
37. M.R. Lorenz and R.E. Halsted, *J. Electrochem. Soc.* **110** (1963) 343.
38. E.M. Swiggard, *J. Crystal Growth* **94** (1989) 556.
39. J. Czochralski, *Z. Phys. Chem.* **91** (1918) 219.
40. J. R. Carruthers and A. F. Witt, in *Crystal Growth and Characterization*, eds. R. Ueda and J.B. Mullin (North-Holland, Amsterdam, 1975) p. 107.
41. D.T.J. Hurle and B. Cockayne, in *Handbook of Crystal Growth, Vol.2 Bulk Crystal Growth*, ed. D.T.J. Hurle (Elsevier Sci., Amsterdam, 1996) p. 100.
42. R. Gremmelmeier, *Z. Naturforsch.* **11a** (1956) 511.

43. W.F. Leverton, *J. Appl. Phys.* **29** (1958) 1241.
44. E. P. A. Metz, R. C. Miller, and R. Mazelsky, *J. Appl. Phys.* **33** (1962) 2016.
45. J.B. Mullin, B.W. Straughan and W.S. Brickell, *J. Phys. Chem. Solids* **26** (1965) 782.
46. J.B. Mulin, R.J. Heritage, C.H. Holliday and B.W. Straughan, *J. Crystal Growth* **3/4** (1968) 281.
47. S. Kyropoulous, *Z. Anorg. Chem.* **154** (1926) 308.
48. G. Jacob, *J. Crystal Growth* **58** (1982) 455.
49. J. Bohm, A. Lüdge and W. Schröder, in *Handbook of Crystal Growth, Vol.2 Bulk Crystal Growth*, ed. D.T.J. Hurle (Elsevier Sci., Amsterdam, 1996) p. 215.
50. W. Keller, *J. Crystal Growth* **36** (1976) 215.
51. J.M. Whelan and G.H. Wheatley, *J. Phys. Chem. Solids* **6** (1958) 169.
52. E.M. Swiggard, *J. Electrochem. Soc.* **114** (1967) 976.
53. E.S. Johnson and W.P. Allred, *Bull. Am. Phys. Soc.* **17** (1972) 1185.
54. E.S. Johonson, *J. Crystal Growth* **30** (1975) 249.
55. A.V. Stepanov, *Soviet Phys.-Tech. Phys.* **4** (1959) 339.
56. A.L. Shakh-Budagov and A.V. Stepanov, *Soviet Phys.-Tech. Phys.* **4** (1959) 349.
57. S.V. Tsivinski, Yu.I. Koptev and A.V. Stepanov, *Soviet Phys.-Solid State* **7** (1965) 449.
58. H.E. Labelle, Jr and A.I. Mlavsky, *Mater. Res. Bull.* **6** (1971) 571.
59. G.H. Schwuttke, T.F. Ciszek, K.H. Yang and A. Kran, *IBM J. Res. Develop.* **2** (1978) 335.
60. J.C. Swartz, T. Surek and B. Chalmers, *J. Electron. Mater.* **4** (1975) 255.
61. T.A. Gould and A.M. Stewart, *J. Crystal Growth* **76** (1986) 323.
62. T. Fujii, M. Eguchi and T. Fukuda, *J. Crystal Growth* **87** (1988) 573.
63. K.M. Kim, S. Berkman, H.E. Temple and G.W. Cullen, *J. Crystal Growth* **50** (1980) 212.
64. S. Miyazawa, *J. Crystal Growth* **60** (1982) 331.
65. F. Schmid and D. Viechnicki, *J. Am. Ceram. Soc.* **53** (1970) 528.
66. F. Schmid and C.P. Khattak, *Laser Focus/ Electro-Optics* **19** (1983) 147.
67. C.P. Khattak and F. Schmid, in *Advances in Optical Materials*, ed. by S. Musikant, Proc. SPIE **505** (1984) 4.
68. J.L. Caslavsky, in *Crystal Growth Electronic Materials*, ed. K. Kaldis (Elsevier Sci., Amsterdam, 1985) p. 113.
69. R.H. Deltch, in *Crystal Growth*, ed. B.R. Pamplin (Pergamon, 1980) p. 427.
70. W. Tolksdorf, in *Crystal Growth of Electronic Materials*, ed. E. Kaldis (Elsevier Sci., Amsterdam, 1985) p. 175.
71. R.A. Laudise, in *The Art and Science of Growing Crystals*, ed. J.J. Gilman (John Wiley & Sons, New York, 1963) p.252.
72. T. Inoue, Y. Seki, O. Oda, S. Kurai, Y. Yamada and T. Taguchi, *Jpn. J. Appl. Phys.* **39** (2000) 2394.
73. O. Oda, T. Inoue, Y. Seki, A. Wakahara, A. Yoshida, S. Kurai, Y. Yamada and T. Taguchi, *IEICE Trans. Electron.* **E83-C** (2000) 639.
74. T. Inoue, Y. Seki, O. Oda, S. Kurai, Y. Yamada and T. Taguchi, *Jpn. J. Appl. Phys.* **229** (2001) 35.
75. T. Inoue, Y. Seki, O. Oda, S. Kurai, Y. Yamada and T. Taguchi, *phys. stat. sol.* (b) **223** (2001) 15.
76. W.A. Tiller, *J. Appl. Phys.* **34** (1963) 2757, 2763.
77. J.D. Broader and G.A. Wolff, *J. Electrochem. Soc.* **110** (1963) 1150.
78. G.A. Wolff and A.I. Mlavsky, in *Crystal Growth, Theory and Techniques*, ed. C.H.L. Goodman (Plenum, New York, 1974) p. 193.
79. R. O. Bell, *J. Electrochem. Soc.* **121** (1974) 1366.
80. T. Boeck and P Rudolph, *J. Crystal Growth* **79** (1986) 105.
81. P. Rudolph, T. Boeck and P. Schmidt, *Cryst. Res. Technol.* **31** (1996) 221.
82. G. Poiblaud and G. Jacob, *Mater. Res. Bull.* **8** (1973) 845.
83. K. Kaneko, M. Ayabe, M. Dosen, K. Morizane, S. Usui and N. Watanabe, *Proc. IEEE* **61** (1973) 884.
84. D. Elwell and H.J. Scheel, *Crystal Growth from High Temperature Solutions* (Academic Press, London, 1975).

85. B. Lunn and V. Bettridge, *Rev. Phys. Appl.* **12** (1977) 151.
86. J. B. Mullin, C. A. Jones, B. W. Straughan and A. Royle, *J. Crystal Growth* **59** (1982) 35.
87. A. W. Vere, V. Steward, C. A. Jones, D. J. Williams and N. Shaw, *J. Crystal Growth* 72 (1985) 97.
88. J. Nishizawa, S. Shinozaki, and K. Ishida, *J. Appl. Phys.* 44 (1973) 1638.
89. J. Nishizawa, H. Otsuka, S. Yamakoshi, and K. Ishida, *Jpn. J. Appl. Phys.* **13** (1974) 46.
90. J. Nishizawa, Y.Okuno and H.Tadano, *J. Crystal Growth* **31** (1975) 215.
91. J. Nishizawa and Y. Okuno, *IEEE Trans. Electron Devices* **ED-22** (1975) 716.
92. J. Nishizawa, K. Itoh, Y. Okuno, F. Sakurai, M. Koike, and T. Teshima, *Proc. IEEE Inter. Electron Devices Meet.* (Washington DC, 1983) p. 311.
93. J. Nishizawa, K. Ito, Y. Okuno and F. Sakurai, *J. Appl. Phys.* **57** (1985) 2210.
94. J. Nishizawa, R. Suzuki and Y. Okuno, *J. Crystal Growth* **59** (1986) 2256.
95. J. Nishizawa and K. Suto, *Rep. Tech. Group Electron. Mater., IEE Jpn.* **EFM-88-28** (1988) 45.
96. F. Sakurai, H. Fujishiro, K. Suto and J. Nishizawa, *J. Crystal Growth* **112** (1991) 153.
97. T. Maruyanam T. Kanbe and Y. Okuno, *Jpn. J. Appl. Phys.* **27** (1988) 1538.
98. J. Nishizawa, Y. Okuno and K. Suto, in *Semiconductor Technologies* (Ohmsha and North-Holland, Tokyo, 1986) p. 17.
99. L.N. Demianets, *Prog. Crystal Growth Character.* **21** (1990) 299.
100. Q. Nie, Q. Yuan, W. Chen and Z. Xu, *J. Crystal Growth* **265** (2004) 420.
101. A. Kremheller, A.K. Levine and G. Gashurov, *J. Electrochem. Soc.* **107** (1960) 12.
102. R. Frerichs, *Phys. Rev.* **72** (1947) 594.
103. E. Kaldis, in *Crystal Growth; Theory and Techniques Vol.1*, ed. C.H.L. Goodman (Plenum, London, 1974) p. 49.
104. E. Kaldis and M. Piechotka, in *Handbook of Crystal Growth, Vol.2 Bulk Crystal Growth*, ed. D.T.J. Hurle (Elsevier Sci., Amsterdam, 1996) p. 614.
105. I. Teramoto, *Phil. Mag.* **8** (1963) 357.
106. A. Kremheller, *J. Electrochem. Soc.* **107** (1960) 422.
107. S.J. Czyzak, D.G. Craig, C.E. McCain and D.C. Reynolds, *J. Appl. Phys.* **23** (1952) 932.
108. L.C. Greene, D.C. Reynolds, S.J. Czyzak and W.M. Baker, *J. Chem. Phys.* **29** (1958) 1375.
109. W.W. Piper and S.J. Polich, *J. Appl. Phys.* **32** (1961) 1278.
110. A.C. Prior, *J. Electrochem. Soc.* **108** (1961) 82.
111. P. Hoschl and C. Konak, *Czech J. Phys.* **13** (1963) 850.
112. M. Hemmat and M. Weinstein, *J. Electrochem. Soc.* **114** (1967) 851.
113. E.V. Markov and A.A. Davidov, *Izv. Akad. Nauk SSSR, Neorg. Mater.* **7** (1971) 575.
114. E.V. Markov and A.A. Davidov, *Izv. Akad. Nauk SSSR, Neorg. Mater.* **11** (1975) 1755.
115. E.V. Markov and A.A. Davydov, *Inorg. Mater.* **11** (1975) 1504.
116. B.M. Bulakl, V.I.Kozlovsky, N.K. Moiseeva, A.S. Nasibov, G.S. Pekar and P.V. Reznikov, *Krist. Tech.* **15** (1980) 995.
117. B.M. Bulakh, *J. Crystal Growth* 7 (1970) 196.
118. A.A. Davydov, V.N. Ermolov, S.V. Neustroev and L.P. Pavlova, *Inorg. Mater.* **28** (1992) 32.
119. K. Grasza, *J. Crystal Growth* **128** (1993) 609.
120. K. Igaki, N. Ohashi and K. Mochizuki, *Jpn. J. Appl. Phys.* **15** (1976) 1429.
121. R. Triboulet, *Rev. Phys. Appl.* **12** (1977) 123.
122. H. Schäfer, H. Jacob and K. Etzel, *Z. Anorg. Chem.* **286** (1956) 27, 42.
123. H. Schäfer, H. Jacob and K. Etzel, *Z. Anorg. Chem.* **290** (1957) 279.
124. H. Schäfer, H. Jacob and K. Etzel, *Z. Anorg. Chem.* **291** (1957) 221, 294.
125. B. Ray, *II-VI Compounds* (Pergamon Press, Oxford, 1969).
126. R. Nitsche, *Phys. Chem. Solids* **17** (1960) 163.
127. R. Nitsche, H.U. Bolsterli and M. Lichensteiger, *J. Phys. Chem. Solids* **21** (1961) 199.
128. S. Fujita, T. Mimoto and T. Noguchi, *J. Crystal Growth* **47** (1979) 326.
129. G. Mandel, *J. Phys. Chem. Solids* **23** (1962) 587, **4** (1956) 165.
130. K.T. Aust, *J. Crystal Growth* **13/14** (1972) 57.

131. K. Terashima, M. Kawachi and M. Takena, *J. Crystal Growth* **102** (1990) 387.
132. K. Terashima, M. Kawachi and I. Tanigawa, *Oyo Buturi (Monthly Publ. Jpn. Soc. Appl. Phys.) (in japanese)* **61** (1992) 821.
133. J.L. Richards, *J. Appl. Phys.* **34** (1957) 289.
134. A. Steinmann and U. Zimmerli, *J. Phys. Chem. Solids Suppl.* (1967) 81.
135. P. C. Leung and W. P. Allred, *J. Crystal Growth* **19** (1973) 356.
136. K. Tomizawa, K. Sassa, Y. Shimanuki and J. Nishizawa, *J. Electrochm. Soc.* **131** (1984) 2394.
137. K. Tomizawa, K. Sassa, Y. Shimanuki and J. Nishizawa, *Inst. Phys. Conf. Ser.* **91** (1988) 435.
138. S. Ozawa, H. Miyairi, M. Nakajima and T. Fukuda, *Inst. Phys. Conf. Ser.* **79** (1986) 25.
139. S. Ozawa, H. Miyairi, J. Kobayashi and T. Fukuda, *J. Crystal Growth* **85** (1987) 553.
140. K. Tada, M. Tatsumi, M. Nakagawa, T. Kawase and S. Akai, *Inst. Phys. Conf. Ser.* **91** (1987) 439.
141. M. Tatsumi, T. Kawase and K. Tada, in *Non-Stroichiometry in Semiconductors*, Eds. K.J. Bachmann, H.L. Hwang and C. Schwab (Elsevier Sci., Amsterdam, 1992) p. 107.
142. K. Kohiro, K. Kainosho, O. Oda, *J. Electron. Mater.* **20** (1991) 1013.
143. K. Kohiro, M. Ohta and O. Oda, *J. Crystal Growth* **158** (1996) 197.
144. R. Hirano, T. Kanazawa and M. Nakamura, in *Proc. 4th Int. Conf. on InP and Related Materials* (Newport, 1992) p. 546.
145. R. Hirano and M. Uchida, *J. Electron. Mater.* **25** (1996) 347.
146. P. Rudolph, M. Neubert, S. Arulkumaran and M. Seifert, *Cryst. Res. Technol.* **32** (1997) 35.
147. M. Neubert and P. Rudolph, *Prog. Crystal Growth Character. Mater.* **43** (2001) 119.
148. H.J. Scheel and E.O. Schultz-Dubis, *J. Crystal Growth* **8** (1971) 304.
149. H.J. Scheel, *J. Crystal Growth* **13/14** (1972) 560.
150. E.O. Schulz-Dubois, *J. Crystal Growth* **12** (1972) 81.
151. D. Mateika, *J. Crystal Growth* **13/14** (1972) 698.
152. B.R. Pamplin, *J. Crystal Growth* **26** (1974) 239.
153. B.R. Pamplin, *J. Phys* **C3/9/36** (1975) C3-35.
154. F.V. Wald and R.O. Bell, *J. Crystal Growth* **30** (1975) 29.
155. T.L. Chu, M. Gill and R.K. Smeltzer, *J. Crystal Growth* **33** (1976) 53.
156. P. Capper, J.J. Gosney and C.L. Jones, J. *Crystal Growth* **70** (1984) 356.
157. P. Capper, J.J. Gosney, C.L. Jones and E.J. Pearce, *J. Electron. Mater.* **15** (1986) 361.
158. J.C. Brice, P. Capper, C.L. Jones and J.J.G. Gosney, *Prog. Crystal Growth Character. Mater.* **13** (1986) 197.

3. PRINCIPLES OF CRYSTAL GROWTH

3.1 INTRODUCTION

Before undertaking crystal growth work, it is important to have an understanding of the basic principles of the various methods. It is at least necessary to understand phase diagrams, the concept of stoichiometry, the theory of convection, the relationship between temperature distribution and thermal stress in grown crystals, segregation and supercooling, the effect of the application of magnetic fields and crystal diameter control. This fundamental knowledge helps to grow crystals effectively, especially when we encounter difficulties. Most of these principles can be found in Refs. 1-14 in more detail, but in this chapter, the essence is summarized in such a way that researchers and engineers can consult them quickly for their crystal growth work. When more details are required, the readers can find them in the above mentioned references.

3.2 PHASE DIAGRAM

Since compound semiconductors consist of more than two elements, it is important to understand the phase diagram. The principle of the phase diagram is explained well in speciality books.[15-19] Fig. 3.1(a) and (b) shows typical phase diagrams, the composition-temperature (X-T) diagram and the pressure-temperature (P-T) diagram of GaAs.[19, 20] In Fig. 3.1(a), a constant temperature line is drawn. This constant temperature line is also shown in Fig. 3.1(b). At the same temperature, there are two points for vapor-liquid-solid (V-L-S) phase equilibrium, one at the arsenic rich side (point A) and one at the gallium-rich side (point B). Experimentally obtained phase diagrams for various materials can be found in Refs. 15 and 16. From these phase diagrams, we can predict crystal growth conditions, such as the growth temperature, decomposition pressure of the constituent, the possibility of constitutional supercooling and so on. Phase diagrams can also be calculated based on thermodynamics.[21]

From Fig. 3.1(b), it is seen that the vapor pressure of arsenic rises when the temperature falls for arsenic-rich material. This fact is often overlooked in crystal growth. Since the vapor pressure rises during the cooling process from that at the melting point, it happens that the solidified melt including the arsenic rich material explodes during cooling because the arsenic vapor pressure in the solidified melt is greatly increased during cooling. The same explosion takes place for other materials such as CdTe, ZnSe and others. It is therefore important to preview the phenomena which will take place not only for crystal growth but also for the cooling process from the phase diagram.

The stoichiometry of compound semiconductors is very important both for the growth behavior of the crystals and for their properties which depend on intrinsic defects due to non-stoichiometry. Most compound semiconductors have non-stoichiometric regions as shown in Fig. 3.1(a). In many cases, the congruent point deviates from the stoichiometric composition. It is therefore necessary to find an appropriate

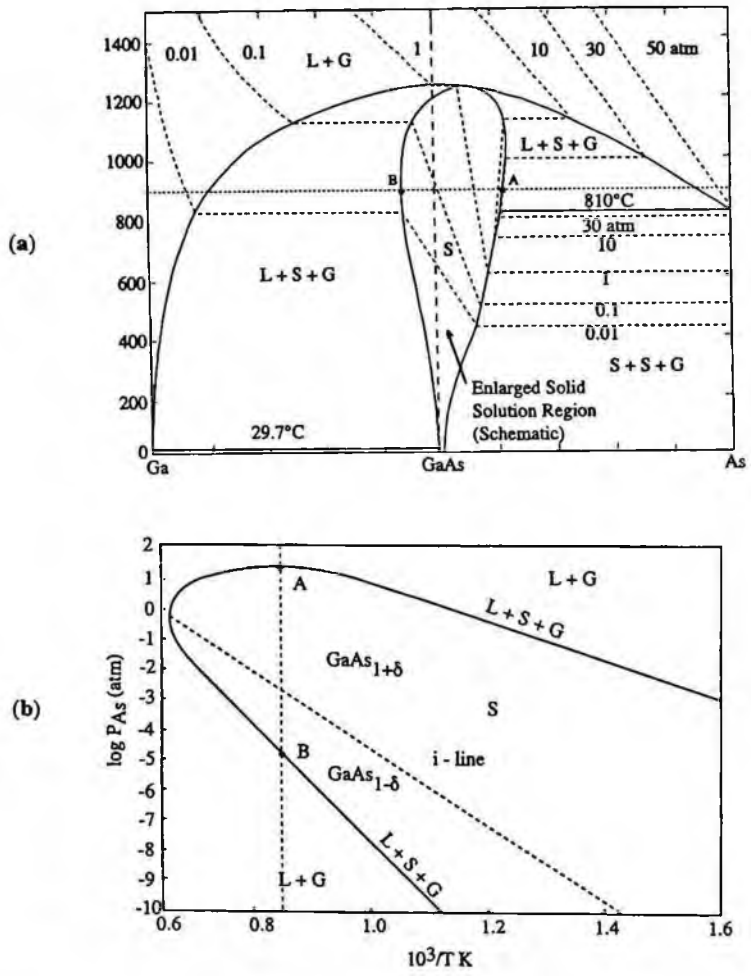

Fig. 3.1 Phase diagrams for GaAs. (a) Composition-temperature (X-T) diagram (reprinted from Ref. 19 with permission, copyright 1991 Elsevier) and (b) pressure-temperature (P-T) diagram (from Ref 20 with permission).

melt composition to control the composition of the crystals grown. The melt composition thus affects the composition of the crystals grown, and their defect structures. Recently, precise phase diagrams for this non-stoichiometric region have been calculated based on the thermodynamics of various defects.[22] These precise phase diagrams make it easy to predict defect structures in grown crystals. Precise stoichiometry can be determined by X-ray diffraction measurement and by coulometric titration analysis as explained in Chapter 5.

The melt composition is also important to consider whether constitutional supercooling will take place. If the melt composition deviates greatly from the stoichiomet-

ric composition, constitutional supercooling takes place and it becomes difficult to grow single crystals under conventional conditions. This is explained in detail in Sec. 3.6.2.

3.3 CONVECTION

3.3.1 Gas Convection

Gas convection in the crystal growth furnace affects the temperature fluctuation in the melt and the temperature distribution in the growing crystal. The strength of the convection of an ideal gas is represented by the Rayleigh number as

$$R_a = \frac{\Delta T}{T} \frac{g d^3}{K_0 \nu_0} p^2 \qquad (3.1)$$

Here, ν_0 is the kinematic viscosity, K_0 the thermal diffusivity, d the depth of the convection cell, g the acceleration due to gravity, ΔT the vertical temperature difference across the gas cell, p the gas pressure.[13]

As R_a increases so does gas convection. As seen from Eq. 3.1, R_a is proportional to the temperature difference between the melt surface and the radiation shield in the furnace, the cube of the height between the melt surface and the radiation shield and the square of the gas pressure. In a high pressure furnace, it is known that gas convection is very active due to the high pressure of atmospheric gas. From Eq. 3.1, it is seen that a reduction in gas convection can be achieved by minimizing the space surrounding the material, for instance by using a thermal baffle or something equivalent to reduce the distance d and by reducing the pressure of atmospheric gas. This typical example can be seen in the case of InP single crystal growth. A thermal baffle for the pressure controlled LEC method was largely effective in reducing the temperature fluctuation in the melt, by minimizing gas convection.[23]

3.3.2 Melt Convection

In the melt, different types of convection can occur and their possibility can be theoretically calculated as follows. They are discussed by various authors.[6, 8, 14, 24-26]

(1) Buoyancy-driven convection

Buoyancy-driven convection, which is also called natural convection, takes place due to a gradient of density in the melt generated by the gravity field. This density gradient is due to the temperature gradient arising from the removal of the latent heat and to the solute concentration due to segregation.

Buoyancy-driven convection due to the temperature gradient is called thermal convection and the driving force can be expressed in dimensionless form by normalizing the Navier-Stokes flow equations. When the temperature gradient upwards and the flow are parallel to the gravitational field, the driving force is expressed by a non-dimensional number, the Rayleigh number, as

$$R_a = \frac{g \alpha \delta T_v h^3}{k\nu} \tag{3.2}$$

where α is the thermal expansion coefficient, ΔT_v the vertical temperature difference, h the vertical height, k the thermal diffusivity and ν the kinematic viscosity.

When the temperature gradient is horizontal and the flow is perpendicular to the gravitational field, the driving force is expressed by a non-dimensional number, the Grashof number.

$$G_r = \frac{g \alpha \Delta T_H \ell^3}{\nu^2} \tag{3.3}$$

where ΔT_H is the horizontal temperature gradient and ℓ the horizontal length.

The Rayleigh and Grashof numbers are related by a non-dimensional number, the Prandtl number P_r which expresses the ratio of viscosity to thermal energy dissipation in the melt as follows.

$$R_a = G_r P_r; \qquad P_r = \nu / k . \tag{3.4}$$

The Rayleigh and Grashof numbers show the degree of thermal convection for vertical flow and horizontal flow and when these values exceed the critical value, convection becomes unstable and the flow is changed from a quiescent, steady state to unsteady, turbulent states. The Prandtl number is a physical constant and is an important factor for predicting melt flow behavior. It is known that metals and semiconductors have low Prandtl numbers and oxides have high Prandtl numbers.

When the density gradient is caused by the solute concentration due to segregation, this natural convection is called solutal convection and the driving force can be expressed by the solutal Rayleigh number.[26]

$$R_a^D = \frac{g \beta \Delta C \delta_D^3}{\nu D} \tag{3.5}$$

where β is the solutal expansion coefficient of the liquid, ΔC the concentration difference due to segregation, δ_D the diffusion boundary thickness and D the liquid diffusion coefficient.

(2) Surface tension driven convection

Convection flows are also driven by surface tension gradients.[7, 12, 27-32] These flows are independent of gravitational force. Surface tension gradient convection is induced by temperature difference and composition difference. The former convection is known as thermo-capillary flow and the driving force can be expressed by a dimensionless Marangoni number as

$$Ma_T = \left(\frac{d\sigma}{dT}\right) \frac{\Delta T d}{\rho \nu \kappa} \qquad (3.6)$$

where ΔT is the vertical temperature gradient and σ the surface tension. The latter convection is called Marangoni flow and the driving force can be expressed by a solutal Marangoni number, Ma_s.

The comparison between buoyancy-driven flow and surface tension-driven flow can be determined by the dynamic Bond number

$$B_o = g \rho \alpha d^2/(\partial\sigma/\partial T) = Ra / Ma_T \qquad (3.7)$$

Since the driving force for buoyancy convection, Ra, is proportional to h^3 and that for Marangoni convection to h^2, the preference is strongly related to the melt height. Since the Bond number is proportional to d^2g, it can be easily known that buoyant-driven effect is dominant for large systems on earth while the thermo-capillary effect becomes dominant for small systems and/or in low gravity. Low Prandtl number material such as semiconductor materials tend to be influenced by thermocapillary convection since the critical Marangoni number is low. The Marangoni number is a function of the temperature dependence of surface tension. Tegetmeier et al.[33] deduced a formula for $d\sigma/dT$, and showed some data for various semiconductor materials .

Marangoni convection must be considered for FZ, CZ and other containerless methods, but is negligible for container methods such as VB/VGF methods.

(3) Forced convection

In order to control natural convection, forced convection by rotation of the growing crystal and of the crucible is imposed.[34]

- crystal rotation

Flow around crystal rotation can be represented by the Reynolds number as

$$R_e = \pi \Omega d^2 \nu^{-1} \qquad (3.8)$$

where Ω is the crystal rotation rate and d the crystal diameter. When this number exceeds the critical Reynolds number, the flow around the crystal becomes turbulent. In order to compensate for thermal convection by crystal rotation, two driving forces must be comparable with respect to viscosity.[35] This is represented as

$$Gr = Re^2 \qquad (3.9)$$

From this relationship, the crystal diameter and the rotation rate where thermal convection can be counteracted by crystal rotation is represented as

$$d = (g \alpha \Delta T R^3 \pi^{-1/2})^{1/4} \Omega^{-1/2} \qquad (3.10)$$

Here, R is the crucible radius. From this equation, an appropriate crystal rotation condition can be predicted.

The validity of Eq. 3.10 is different depending on the direction of convection. Eq. 3.10 is valid when the direction of natural convection and forced convection are parallel, while it is modified as

$$G_r = R_{e_r}^{2.5} \qquad (3.11)$$

when the direction of natural convection and forced convection are perpendicular. Further modification of this relationship is discussed by Miller et al.,[36] Kobayashi[37] and Miyazawa.[38]

- crucible rotation

Crucible rotation is performed in order to average the non-axisymmetry of the temperature distribution and also for controlling the global flow. The flow intensity is represented by a Reynolds number as

$$R_{e_m} = \pi \, \Omega \, d^2 \, \nu^{-1} \qquad (3.12)$$

Here, Ω is the rotation rate of the melt. It is known that a steady liquid motion in a rotating fluid becomes only two-dimensional with respect to coordinate axes rotating with the crucible, according to the Tylor-Proudman theorem. This two-dimensional motion appears as a set of spiral streamlines rising and falling along cylindrical surfaces with the rotation axis to a stationary observer. Near the top and tail surfaces, the Tylor-Proudman theorem breaks down because of the viscosity effect. In these regions, the Ekamn shear layers cause inward and outward rotating flow motions to occur.

For the case of Czochralski growth, flow modes are summarized as a function of crystal rotation and crucible rotation as shown in Fig. 3.2. When crystal and crucible are rotated in the same direction, which is called iso-rotation mode, the outer melt rotates with the crucible as a "solid body" and the inner melt rotates at an angular velocity between those of crystal and crucible, in a spiral motion according to the Taylor-Proudman theorem, where the melt moves towards the faster rotating surface. When the crystal and the crucible are rotated in opposite directions, which is called counter-rotation mode, a third region is formed near the solid-liquid interface, the region which is isolated from the outer melt and is controlled only by crystal rotation. Flow in the lower region is governed by the Taylor-Proudman theorem. In this mode, the flow near the solid-liquid interface can be isolated from the thermal convection.

(4) Mixed convection

In real crystal growth, all the above convections interfere with each other. Based on these principles, melt flows in various crystal growth methods such as Czochralski methods, LEC methods, VB/VGF methods, and FZ methods are studied both experimentally and theoretically. These studies show that melt flow is very complex in reality and instabilities must be considered as will be discussed below.

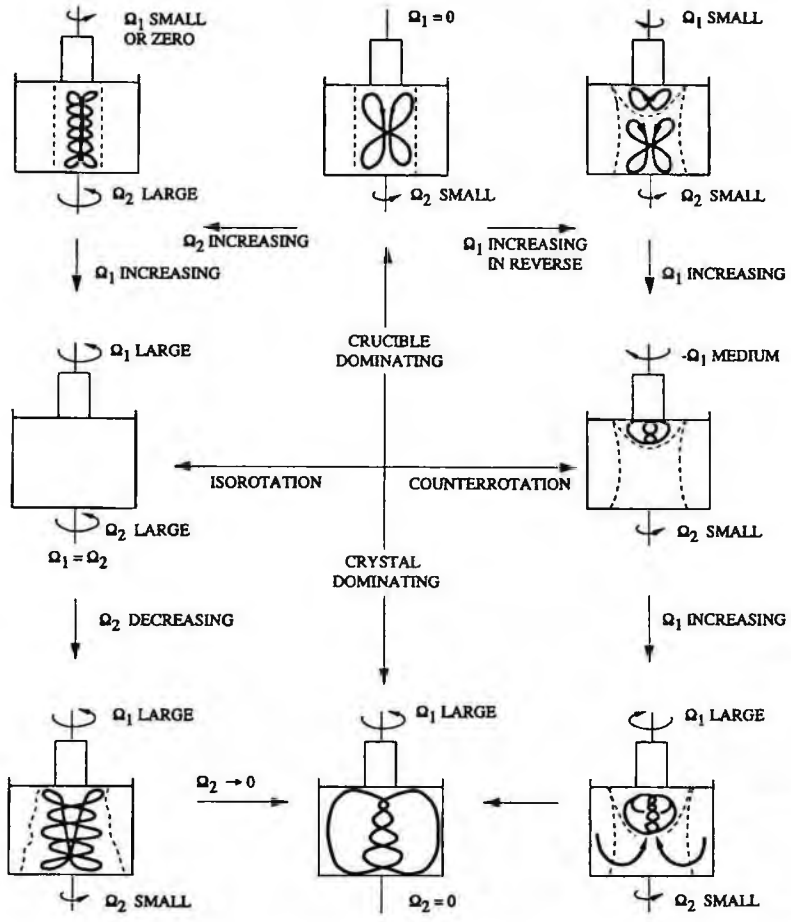

Fig. 3.2 Melt flow depending on crucible and crystal rotations (reprinted from Ref. 5 with permission, copyright 1979 Elsevier).

3.3.3 Instability of Melt Convection

As mentioned above, melt convection is governed by various driving forces, such as buoyancy, surface tension, and external forces, whose intensities can be represented by dimensionless numbers such as the Rayleigh number (R_a), the Marangoni number (M_a) and the Reynolds number (R_e), respectively. When these numbers exceed the critical value for each, the melt flow becomes unsteady and any further increase of these numbers results in the flow becoming chaotic and turbulent. The instabilities caused by these driving forces have been discussed by various authors.[14, 39-43]

Müller et al.[40] have investigated the instability of natural convection as a function of the aspect ratio and two Raleigh numbers for various growth configurations, theoreti-

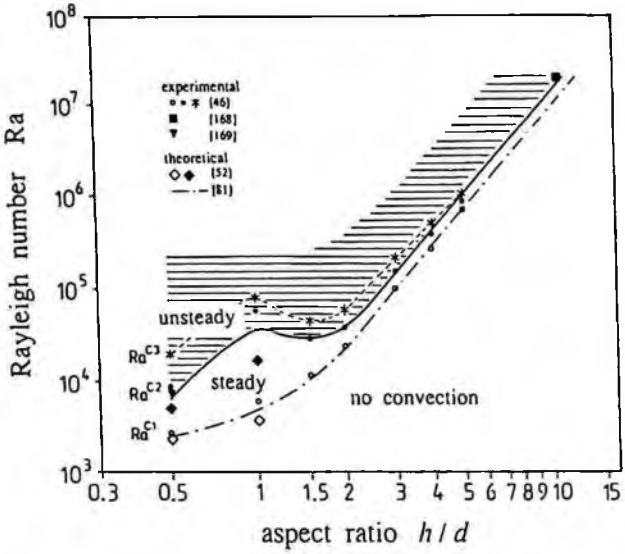

Fig. 3.3 Rayleigh number as a function of the aspect ratio(reprinted from Ref. 14 with permission of Springer Science and Bysiness Media). The sources of experimental and theoretical data are shown in Ref. 14.

cally and experimentally. Fig. 3.3 shows how the melt is destabilized as a function of aspect ratio. Here, the critical Rayleigh number for the onset of convection is determined as a Rayleigh number where the Nusselt number, N_u (the ratio of the total convective and conductive heat flux to the conductive heat flux) is unity. It can be shown that the flow becomes unsteady and time-dependent as a function of aspect ratio. Müller et al.[14, 41, 42] also analyzed the instabilities in various crystal growth configurations by considering two Rayleigh numbers, the conventional Rayleigh number, R_a and the wall Rayleigh number, Ra_w.

Ristorcelli and Lumley[43] discussed the instabilities of various modes of convection as applied to Czochralski crystal melt. In this paper, various critical dimensionless numbers for melt instabilities are summarized. The melt instability from crystal rotation is predicted to occur when the Reynolds number exceeds Re_c = 5-8 x 10^4. The vertical buoyancy instability will occur when the critical Grashof number, Gr_c = 10^7 - 10^8. For horizontal buoyancy flow, the instabilities occur above critical Rayleigh numbers Rac (transition to two-dimensional flow), Rac_1 (transition to three-dimensional flow) and Rac_0 (time dependent flow). They are of the order of 10^3 for low Prandtl number melts. For Marangoni flow, the critical Marangoni number is Ma_c = 10^4 but for precise analysis the Richardson number is used.

3.3.4 Fluid Flow and Crystal/Melt Interface Shape

It is known that the quality of grown crystals depends on the crystal/melt interface. The

crystal/melt interface affects the thermal stress of grown crystals and the segregation behavior of impurities and dopants. It is therefore desirable that the interface shape be as flat as possible.

The crystal/melt interface is determined by the fluid flow mode which is related to various types of convection discussed in Sec. 3.3.2. There are several models for the determination of the crystal/melt interface shape.

(i) From the analysis of the hydrodynamics in oxide melts, Takagi et al.[44] postulates that for a flat shape, a certain critical Reynolds number must be attained.

(ii) When natural convection and forced convection are equal, a flat interface shape results. This can be formulated as $Gr = Re^2$ as Eq. 3.9.[35]

(iii) Natural convection and forced convection must be equal for a flat interface but the relationship between Gr and Re can be expressed as $Gr/Re^{2.5} = 0.1$.[45]

(iv) The flat interface shape is determined from the relationship between the Taylor (Ta) and Rossby (Ro) numbers.[39]

Simulation experiments observing the interface shape have been performed by various authors.[39, 46-49]

Since the solid-liquid (S-L) interface during crystal growth is one of the very important factors in the growth of high quality single crystals, it is very useful to analyze the fluid flow in the melt to deduce the S-L interface shape. Indeed, numerical algorithms for studying the S-L interface have been derived for various crystal growth methods, such as CZ[50] and boat-growth methods.[51-53] Koai et al.[54] examined theoretically the influence of the crucible assembly on the interface shape for the vertical Bridgman GaAs crystal growth.

3.4 MAGNETIC FIELD APPLICATION

Thermal convection arises from temperature gradients and gravity during crystal growth as discussed in Sec. 3.3.2. This thermal convection gives rise to instability of the growth interface, resulting in micro-segregation of impurities and defect nuclei, thus becoming the main reason for deterioration of crystal quality. The stirring effect due to thermal convection causes the crucible material to dissolve into the melt and results in macro-segregation.

The application of a magnetic field is effective in controlling thermal convection. This was first investigated to control the temperature fluctuation in Ga melt[55] and it was applied to the horizontal boat growth of InSb[56, 57] and was found to be effective in the suppression of micro segregation due to the interface instability. It is also found that the application of a magnetic field is effective in suppressing the stirring effect in Si and GaAs. This method has been therefore extensively studied experimentally and theoretically. These studies are reviewed by Hurle,[58] Hoshi et al.,[59, 60] Langlois[61] and Fukuda and Terashima.[62]

In a viscous fluid, the Rayleigh number, Ra, is used to estimate the intensity of thermal convection. Ra is expressed as a ratio of buoyancy which drives thermal convection and the viscous force which suppresses it.

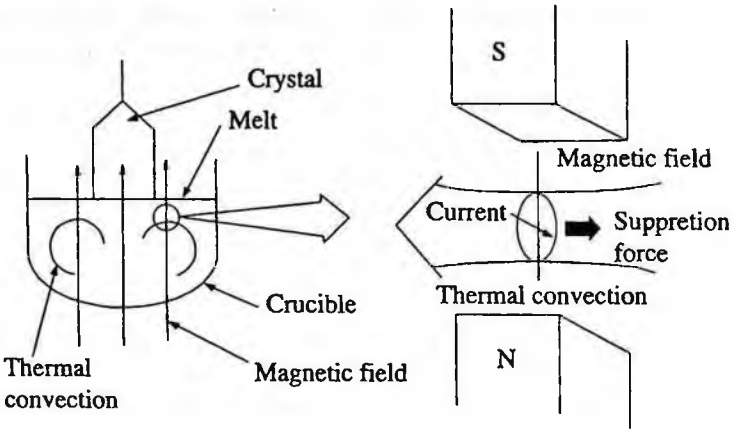

Fig. 3.4 Suppression of thermal convection by the Lorenz force due to the application of a magnetic field (from Ref. 63 with permission)

$$Ra = \frac{\text{buoyancy}}{\text{viscous force}} = \frac{\rho g \alpha v \beta d^2/\kappa}{\rho v v/d^2} = \frac{g \alpha \beta d^4}{\kappa v} \qquad (3.13)$$

Here, g is the acceleration due to gravity, ρ the fluid density, α the volume expansion coefficient, κ the thermal diffusion coefficient, ν the dynamic viscous coefficient, v the thermal convection speed, d the depth of fluid and β the temperature gradient applied to the direction of depth. In the case of Si and GaAs, it is known that the Ra number is of the order of 10^5-10^7, thus the buoyancy force is much larger than the viscous force, and the thermal convection flow is strongly turbulent. On the other hand, the melt of semiconductor materials such as Si and GaAs has good electrical conductivity. Since electrical current can flow in the melt, the application of a magnetic field can suppress the thermal convection because of Lorenz effect[63, 64] (Fig. 3.4).

When the velocity of thermal convection is v , the uniform application of a magnetic field, H, generates an electric field $\mu v H$. Here, μ is the permittivity. Due to the induced electric field, a current $\sigma \mu v H$ flows. Here, σ is the electrical conductivity. The magnetic field reacts to this current flow and forms an electromagnetic force. This force reaches a maximum when the thermal convection and the magnetic fields are perpendicular.

In the case of Czochralski crystal growth, this force lines up opposite to thermal convection so that it acts as the suppression force for thermal convection. Since this force acts similar to the conventional viscous force, it is referred to as the magnetic viscous force[65] and is expressed as

$$\text{magnetic viscous force} = \sigma \mu^2 v H^2 \qquad (3.14)$$

The intensity of this magnetic viscous force is expressed as the Q value,[64] which is the ratio to the conventional viscous force.

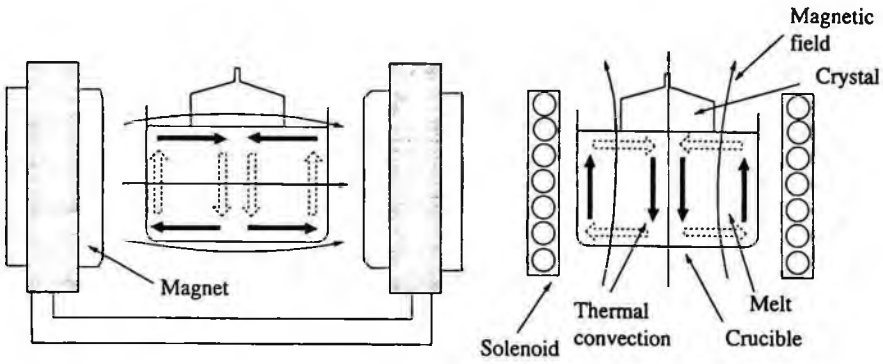

Fig. 3.5 (a) Horizontal magnetic field application[66] and (b) vertical magnetic field application for CZ crystal growth[67] (From Ref. 63 with permission).

$$Q = \frac{\text{magnetic viscous force}}{\text{conventional force}} = \frac{\sigma\mu^2 H^2}{\rho\upsilon/d^2} \qquad (3.15)$$

This Q value is normally very high, the order of 10^4-10^5 for semiconductor materials so that the application of a magnetic field is very effective in suppressing thermal convection.

There are two methods of applying magnetic fields, one transverse using magnets[66] (Fig. 3.5(a)), and the other axial (vertical) using solenoid coils[67] (Fig. 3.5(b)) or superconducting magnets.[68] The effect of magnetic fields has been investigated theoretically in various simulation studies. It is argued that the magnetic field has an effect in putting the segregation coefficient to unity.[69, 70] The effectiveness of different magnetic field applications is also discussed.[71]

The fact that the application of a magnetic field is effective in suppressing thermal convection has been shown in many cases.[57, 58, 71-73] The direct effect is shown to be the suppression of temperature fluctuations in semiconductor melts as shown in Fig. 3.6.[74] Due to the suppression of thermal convection, various consequent effects on crystal quality are experimentally and theoretically reported.

(i) Suppression of impurity growth striations [67, 73-75]

(ii) Reduction of microscopic defects[76]

(iii) Reduction of impurities derived from crucible materials[59, 77]

(iv) Homogenization of impurity concentration along the crystal axis due to the control of segregation coefficients[78]

(v) Control of native defects[79]

The other factors such as temperature gradient, rotation conditions and others also control thermal convection but the application of a magnetic field brings a new factor and it gives more freedom to crystal growth conditions.

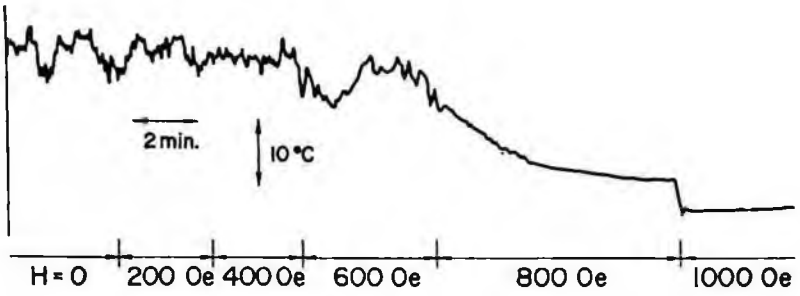

Fig. 3.6 Suppression of temperature fluctuation in GaAs melt by the application of a magnetic field (from Ref. 74 with permission).

3.5 TEMPERATURE DISTRIBUTION AND THERMAL STRESS

Since dislocations are mainly formed during crystal growth due to thermal stress generated in the growing crystal under the thermal conditions applying in each case as pointed out by Jordan et al.,[80] it is important to analyze the temperature distribution and the thermal stress in the crystal for predicting the distribution of dislocations. The temperature distributions under various crystal growth conditions can be obtained by computer simulation using various finite element methods. A typical example is seen in the analysis by Derby et al.[81-84] From the temperature distribution, the thermal stress is calculated and the dislocation densities and distributions are predicted under a certain hypothesis for correlating the dislocation densities and the thermal stresses. Some examples are for CZ,[85] LEC[86] and VB.[87] The results of these analyses will give helpful suggestions to crystal growers designing crystal growth conditions to minimize the occurrence of dislocations.

These computer simulations are based firstly on the analysis of the temperature distribution by solving the heat conduction equation which is typically represented for a cylindrical coordinate system as follows.

$$\frac{\partial T}{\partial z} = \kappa \left(\frac{\partial^2 T}{\partial r} + \frac{1}{r} \frac{\partial T}{\partial r} + \frac{\partial^2 T}{\partial z^2} \right) \tag{3.16}$$

Here, k is the thermal diffusivity. Under appropriate boundary conditions, the above heat conduction equation is solved to obtain the temperature distribution in growing crystals. For quasi-steady state (QSS) conditions, Jordan et al.[80] represented the temperature distribution by using Bessel functions.

Thermal stresses in the crystal can then be calculated from a classical thermoelastic theory as follows.

$$\sigma_r = \frac{\alpha E}{1-\nu}\left(\frac{1}{r_0^2}\int_0^{r_0} Tr\,dr - \frac{1}{r^2}\int_0^{r} Tr\,dr\right) \tag{3.17}$$

$$\sigma_\theta = \frac{\alpha E}{1-n}\left(\frac{1}{r_0^2}\int_0^{r_0} Tr\,dr + \frac{1}{r^2}\int_0^{r} Tr\,dr - T\right) \tag{3.18}$$

$$\sigma_z = \frac{\alpha E}{1-n}\left(\frac{2}{r_0^2}\int_0^{r_0} Tr\,dr - T\right) \tag{3.19}$$

Here, E, ν and α are Young's modulus, Poisson's ratio and the linear thermal expansion coefficient respectively.

From these thermal stresses, dislocation densities are calculated under various assumptions. There are several models for predicting dislocation densities. Jordan et al.[80] proposed a critical resolved shear stress model in which the dislocation density is assumed to be linear to the difference between the critical resolved shear stress (CRSS) and thermoelastic stress. From Schmid's law, it is known that dislocation gliding occurs when the resolved shear stress, σ_{CRSS}, exceeds the critical resolved shear stress. In this model, the dislocation density can be assumed to be proportional to σ_{CRSS} and can be expressed as

$$d_\perp \propto \sigma_{tot} \equiv 4\left|\sigma_I\right| + 2\left(\left|\sigma_{II}\right| + \left|\sigma_{III}\right| + \left|\sigma_{IV}\right| + \left|\sigma_V\right|\right) \tag{3.20}$$

where

$$\sigma_I = \frac{-\sqrt{6}}{6}\left(\sigma_r - \sigma_\theta\right)\cos(2\phi) \tag{3.21}$$

$$\sigma_{II} = \frac{\sqrt{6}}{6}\left[\left(\sigma_\psi - \sigma_\theta\right) - \left(\sigma_\rho - \sigma_\theta\right) \times \frac{2}{\sqrt{2}}\sin\phi\,\sin\left(\phi + \pi/4\right)\right] \tag{3.22}$$

$$\sigma_{III} = \frac{\sqrt{6}}{6}\left[\left(\sigma_\psi - \sigma_\theta\right) - \left(\sigma_\rho - \sigma_\theta\right) \times \frac{2}{\sqrt{2}}\sin\phi\,\sin\left(\phi - \pi/4\right)\right] \tag{3.23}$$

$$\sigma_{IV} = \frac{-\sqrt{6}}{6}\left[\left(\sigma_\psi - \sigma_\theta\right) - \left(\sigma_\rho - \sigma_\theta\right) \times \frac{2}{\sqrt{2}}\cos\phi\,\cos\left(\phi + \pi/4\right)\right] \tag{3.24}$$

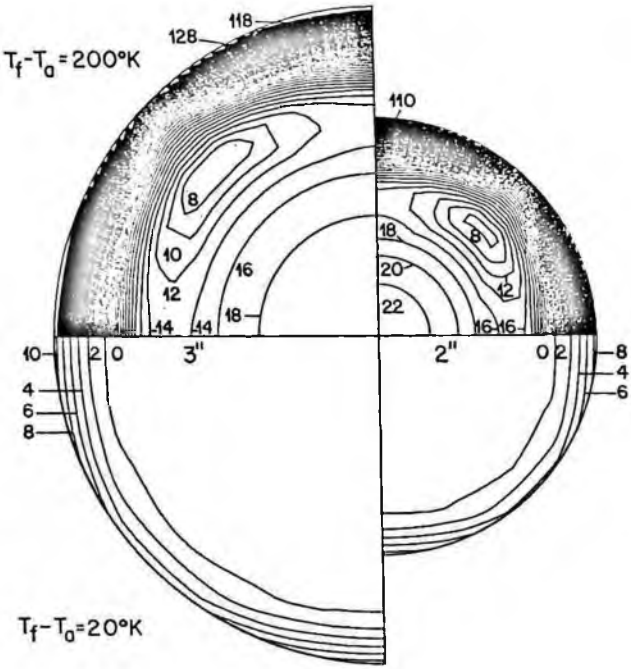

Fig. 3.7 Dependence of dislocation density distribution on diameter at the top end of LEC pulled <100> GaAs boules. The top and bottom halves represent high temperature gradient and low temperature gradient respectively (reprinted from Ref. 80 with permission, copyright 1984 Elsevier).

$$\sigma_V = \frac{-\sqrt{6}}{6}\left[\left(\sigma_\psi - \sigma_\theta\right) + \left(\sigma_\rho - \sigma_\theta\right) \times \frac{2}{\sqrt{2}} \cos\phi \sin\left(\phi - \pi/4\right)\right] \qquad (3.25)$$

In Fig. 3.7, typical dislocation density distributions are shown for the case of LEC growth. It is known that the calculated dislocation densities are similar to the experimental ones, showing the same four fold symmetry.

For more precise prediction of dislocation densities, it is necessary to consider a dynamic dislocation multiplication based on the Haasen model.[88, 89] Müller and Völk[90] and Maroudas and Brown[91] have applied the Haasen model to predicting the dislocation densities in InP crystals grown by the LEC method. Tsui et al.[92] have applied this method to predicting the dislocation densities in GaAs grown by the VB method. In the Haasen model, the plastic shear strain rate $\dot{\varepsilon}^{pl}$ is represented as follows.

$$\dot{\varepsilon}^{pl} = NV_0 b\left(\tau_a - D\sqrt{N}\right)^m \exp\left(-Q/kT\right) \qquad (3.26)$$

where D is a strain hardening factor, b the Burgers vector, N the density of moving dislocations, τ_a the applied stress, Q the Pierls potential, k the Boltzman's constant, V_0

the pre-exponential factor, T the absolute temperature and m a material constant. The total shear strain rate $\dot{\varepsilon}$ is given by

$$\dot{\varepsilon} = \dot{\varepsilon}^{el} + \dot{\varepsilon}^{pl} = \dot{\tau} / G + \dot{\varepsilon}^{pl} \qquad (3.27)$$

which is used in the Haasen model. The dislocation density can be calculated using a dislocation multiplication equation and stress rate equation as described in detail in Ref. 90-92.

Computer simulation was applied not only to predicting dislocation distributions but also to developing a crystal growth method by which dislocation density can be reduced. Kelly et al.[93-95] developed a method which is called the heat flux control system (HFCS) in which the hot zone configuration is designed in such a way that the heat flux can be controlled so as to decrease the dislocation density. The effect of impurity hardening is also considered by computer simulation[96-98] under the assumption that the CRSS is increased by impurity hardening.

For practical crystal growth, it is convenient to have a simpler equation to predict under what conditions, one can obtain the desired dislocation level. The following predictions are applicable to this purpose.

Temperature gradient and thermal stress are related by simple equations. Tsivinsky[99] deduced the following equation.

$$\tau_{CRSS} > \tau_{max} = (1/2)\, D \cdot \alpha \cdot G \cdot VT \qquad (3.28)$$

Here, τ_{CRSS} is the critical resolved shear stress, D the crystal diameter, α the thermal expansion coefficient, G the shear modulus, VT the temperature gradient.

As shown in Ref. 100, Katagiri also deduced a similar equation which is expressed as

$$\left[\frac{dT}{dz}\right]_{max} \leq 1.8 \times 10^{-5} \frac{\tau_{CRSS}}{\alpha h^{1/2} R^{3/2}} \left(1 - \frac{1}{2} hR\right). \qquad (3.29)$$

Here, α is the thermal conductivity of the crystal, h the cooling constant of Newton's law, R the crystal radius and dT/dz the axial temperature gradient in the crystal. This calculation has been compared with the experimental results for InP crystal growth to determine the constants in Eq. 3.29. The axial temperature gradient required for dislocation free crystals is then plotted as a function of crystal diameter as shown in Fig. 3.8. From this figure, it is easily seen that dislocation-free crystals can be obtained very easily when the crystal diameter is less than about 1 cm under the conventional axial temperature gradient. It is also known that for realizing dislocation-free crystals, very small temperature gradients are required such as 2-4 °C/cm and less than 2 °C/cm for 50 mm and 75 mm diameter crystals, respectively. These calculations are not strictly accurate, but are very practical for predicting to what extent we need to improve the temperature environment for a desired dislocation density level.

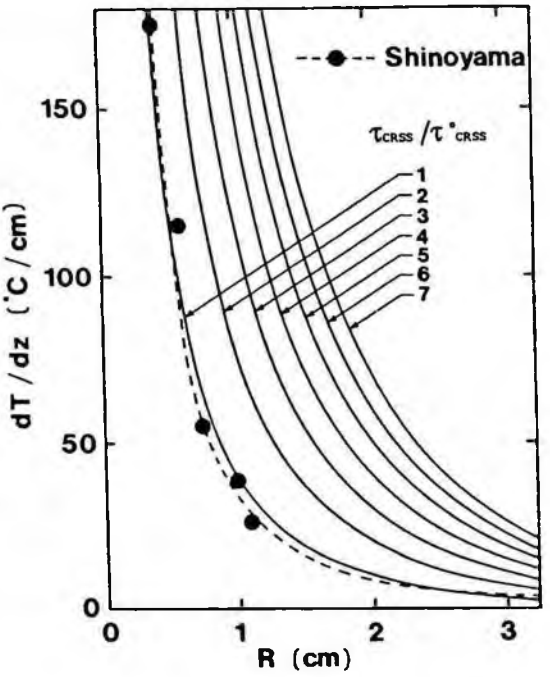

Fig. 3.8 Relationship between the axial temperature gradient (dT/dz) and the critical diameter (R) for dislocation-free InP crystals grown by the LEC method, calculated according to eq. 3.29. The calculation was made varying the critical resolved shear stress τ_{CRSS}. Black points are the data by Shinoyama and the dotted line is the empirical law of Shinoyama (reprinted from Ref. 100 with permission, copyright 1990 Elsevier).

3.6 SEGREGATION AND SUPERCOOLING

3.6.1 Segregation

In crystal growth, it is necessary to dope with impurities to control the conductivity type and the resistivity of the crystals grown. N-type materials are doped with shallow donor impurities and p-type materials are doped with shallow acceptor impurities. Impurities are also doped to reduce dislocation densities by the effect of impurity hardening. Isoelectronic impurities which will not affect the electrical properties are also doped to reduce dislocation densities. A typical example is In-doping for semi-insulating GaAs (Sec. 8.3.2).

When impurities are doped in the melt and the crystal is grown, the segregation of impurities occurs.[5, 10, 101-103] The equilibrium segregation coefficient (called also distribution coefficient), the ratio between the concentration of the impurity in the solid and the liquid, k_0 can be represented as

$$k_0 = C_{S_0} / C_{L_0} \qquad (3.30)$$

where Cs_0 and C_{L_0} are the equilibrium impurity concentrations in the solid and the liquid respectively as seen in schematic equilibrium phase diagrams in Fig. 3.9. De-

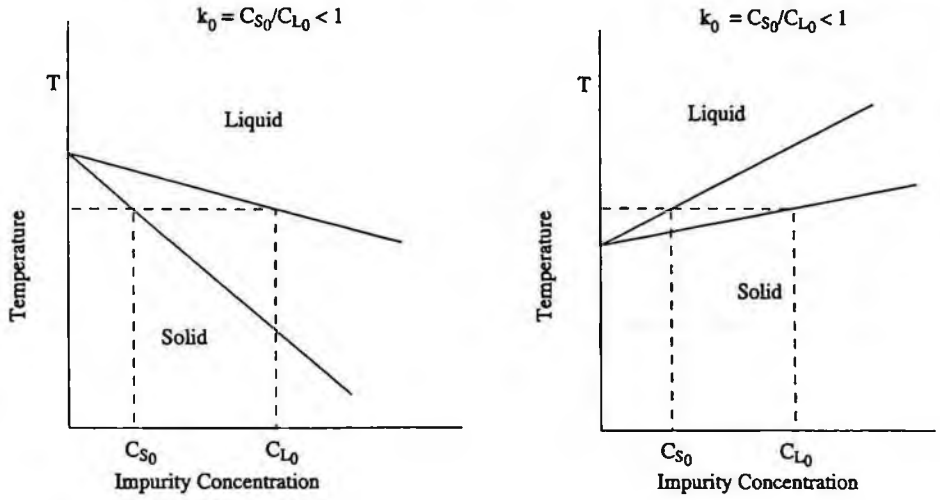

Fig. 3.9 Segregation coefficient for different phase diagram.

pending on the phase diagram shape, k_0 becomes >1 or <1.

In order to dope impurities quantitatively, we need to know the segregation coefficients for each impurity to determine the quantity to charge in the starting material. It is however noted that in real crystal growth, we must consider the effective segregation coefficients, different from the equilibrium ones because of growth conditions, such as growth rate, rotation speed, temperature distribution and so on.

In real crystal growth, when the diffusion of impurities in the melt is slow, they accumulate at the solid-liquid (S/L) interface and the impurity concentration has a distribution in the boundary layer as shown in Fig. 3.10. This interface segregation coefficient k* is defined as

$$k^* = C_s/C_B \tag{3.31}$$

which is similar to the equilibrium segregation coefficient. Here, C_s is the impurity concentration in the grown crystal and C_B is that in the liquid just at the S/L interface.

This segregation coefficient however can not be experimentally measured. The effective segregation coefficient k_e is defined as

$$k_e = C_s/C_L. \tag{3.32}$$

Here, C_L is the impurity concentration in liquid in equilibrium. The effective segregation coefficient can be determined by analyzing the impurity concentration in the solid and in the liquid. When the melt is well stirred, the value of k_e approaches to k* and k_0 when the equilibrium condition is satisfied at the interface.

The effect of various growth conditions on k_e has been analyzed, accounting for the diffusion process at the solid-liquid interface. The k_e is expressed by the following equation due to Burton, Prim and Slichter.[104]

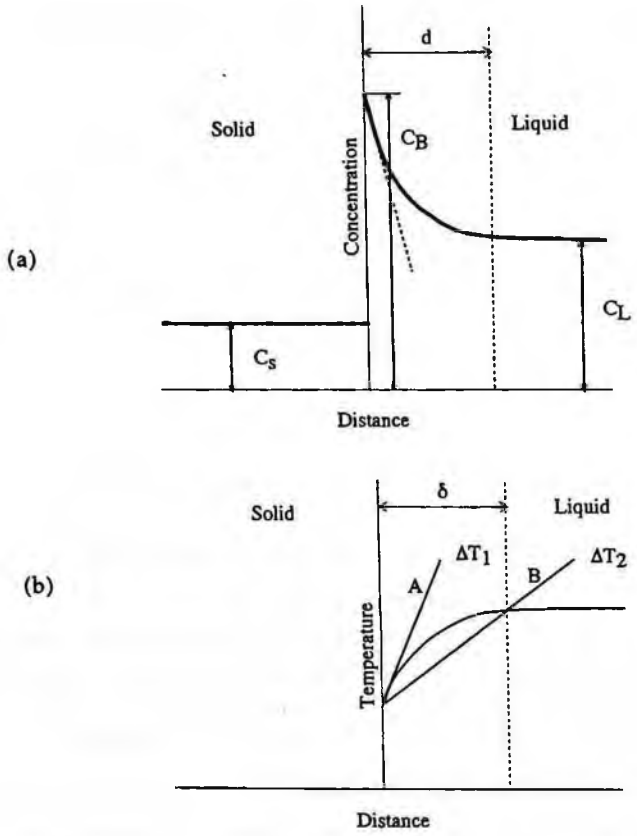

Fig. 3.10 (a) Solute concentration distribution at the solid/liquid interface and (b) temperature distributions.

$$k_e = \frac{C_S}{C_L} = \frac{k_0}{k_0 + (1 - k_0)\exp(-V\delta/D_L)} \qquad (3.33)$$

Here, V is the growth rate, δ the thickness of the boundary layer and D_L the diffusion coefficient of impurity in the liquid. The thickness of the boundary layer is expressed as

$$\delta = 1.60\, D_L^{1/3} \nu^{1/6} \omega^{-\frac{1}{2}} \qquad (3.34)$$

where, ν is the viscosity of the liquid and ω the angular velocity of the crystal.

The impurity concentration in grown crystal is represented by Pfann[105] as

$$C = k_e C_0 (1-g)^{k_e - 1} \qquad (3.35)$$

Here, C_0 is the initial impurity concentration and g the fraction solidified. The effective segregation coefficient is then determined by analyzing the impurity concentrations in the grown crystal as a function of growth axis and k_e is calculated from Eq. 3.35. Further detailed theories for segregation coefficients and the effect of convection are discussed by several authors.[106-109]

3.6.2 Constitutional Supercooling

When the melting point is slightly changed during crystal growth because of the segregation of dopant impurities or of constituent elements, constitutional super cooling occurs.[110]

As shown in Fig. 3.10, because of segregation a concentration distribution at the solid-liquid interface occurs. In the case of impurity doping, the equilibrium segregation coefficient is expressed as shown in Fig. 3.9 and Eq. 3.30. In the case of binary compound semiconductors, the equilibrium segregation coefficient k_0 is defined as shown in Fig. 3.11. In the case of ternary mixed compound semiconductors, the equilibrium segregation coefficient is defined as shown in Fig. 3.12.

In each case, there is a change of composition in the melt during crystal growth, thus changing the melting point as shown in Fig. 3.10 (b). If the temperature gradient ΔT_1 in the melt is sufficiently large, as shown in line A in Fig. 3.10 (b), then the melt temperature is higher than the melting point in the melt at any point therefore no irregular solidification in the melt takes place. If the temperature gradient ΔT_2 in the melt is small as shown as line B, then the melt temperature near the solid/liquid interface becomes lower than the melting point in the melt, causing rapid solidification at the interface region. This is called constitutional supercooling and steady crystal growth becomes difficult, leading to polycrystallization and/or twin formation.

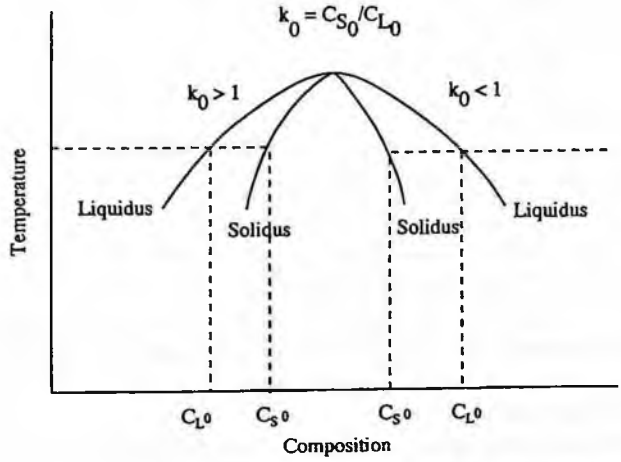

Fig. 3.11 Segregation coefficient due to non-stoichiometry.

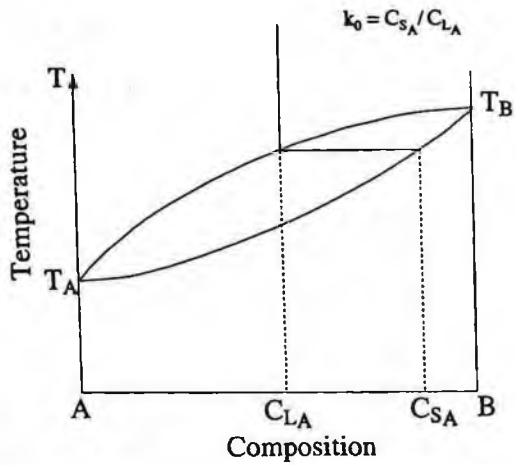

Fig. 3.12 Segregation coefficient for the case of mixed crystals

Constitutional supercooling occurs in the following cases.

(i) High impurity doping for conductivity control or reduction of dislocations.

When doping is higher than the middle of 10^{18} cm^{-3} as in the case of Si doping in GaAs or Zn or S doping in InP, it is known that polycrystallization easily occurs under normal crystal growth conditions. High concentration doping of In to GaAs is also a typical example of this case.

(ii) Crystal growth from non-stoichiometric melt

When the melt composition deviates greatly from the stoichiometric composition, polycrystallization occurs due to constitutional supercooling. For GaAs crystal growth, it is known that polycrystallization takes place when the crystal is grown from a very Ga-rich melt exceeding a melt composition of Ga/(Ga+As) of 0.46 (Sec. 8. 3.2 (1)).

(iii) Crystal growth of ternary mixed compound semiconductors

It is well known that the growth of mixed compound crystals such as InGaAs, InGaP is difficult and this is explained by the phase diagram as shown in Fig. 3.12. In most phase diagrams of mixed compounds, the segregation coefficient becomes large for desired compositions due to the deviation of the solidus line from the liquidus line. This induces supercooling and it makes it difficult to grow mixed crystals.

(iv) Crystal growth from solution

Crystal growth methods such as THM or solvent evaporation are based on growth in solution. In such cases, the melt composition deviates greatly from the stoichiometric composition, therefore crystal growth can not be achieved with the same growth rate as that by melt growth methods. In most solution growth methods, the growth rate must be much lower, more than one order of magnitude compared with melt growth methods to prevent constitutional supercooling.

Since the concentration distribution at the solid-liquid interface is expressed by the BPS (Burton, Prim and Slichter[104]) equations as Eqs. 3.33 and 3.34, it can be seen from these equations how supercooling may be avoided.

(i) Decreasing the crystal growth rate

The decrease of V leads to the semi-exponential decrease of the effective segregation coefficient. This is therefore a very effective method if it is allowed.

(ii) Decreasing the solute concentration

An absolute decrease in the solute concentration reduces the range in which the melting point can change. This is allowed in the case of binary compounds from stoichiometric compositions.

(iii) Increasing the rotation rate

This changes the thickness of the boundary layer, d, by forced convection but the effectiveness is not so great since d is changed as a function of $\Omega^{-1/2}$ as Eq. 3.34.

(iv) Increasing the temperature gradient

When the temperature gradient is increased from ΔT_2 to ΔT_1, supercooling is avoided as shown in Fig. 3.10 (b). This can be applied only when it is allowed from the viewpoint of crystal qualities. As explained Sec. 3.5, a big temperature gradient leads to high dislocation densities.

Supercooling can thus be avoided but the selection of which of the above mentioned methods to use must be determined depending on each case.

3.7 DIAMETER CONTROL SYSTEM

In the case of CZ and LEC methods, it is essential to have diameter control because the growing crystal is in the free state and the diameter fluctuates. This does not occur in the case of container growth methods such as HB, HGF, VB, VGF, where the diameter of growing crystals is determined by the crucible inner diameter.

Diameter control in the CZ or LEC methods are necessary from two points of view. It is desirable to control the diameter in order to increase the material yield. When the diameter fluctuates, there is excess material loss in obtaining the same diameter wafers. Secondly, from the point of view of dislocation generation, it is desirable to control the diameter to reduce unnecessary thermal stress due to the fluctuation of the crystal shape and to avoid polycrystallization.

Automatic diameter control (ADC) was developed for crystal growth of Si, Ge and oxides by the CZ method.[111-117] The difficulty of diameter control of compound semiconductors was pointed out by Nygren for the case of GaP LEC crystal growth.[117] This difficulty concerning several compound semiconductors is due to the high pressure atmosphere and the existence of encapsulant material which greatly changes the thermal environments compared with the case of elemental semiconductors and oxides. The development of diameter control has been reviewed by Hurle.[118-120]

Various methods, as follows, have been used for crystal diameter control for various crystals.

- manual diameter control in GaP LEC growth[117]
- bright ring meniscus reflection[121]
- usage of choracle[122]
- X-ray observation of the growth interface[123, 124]
- direct observation of the diameter by X-ray transmission[125]
- infrared radiation sensing[111]

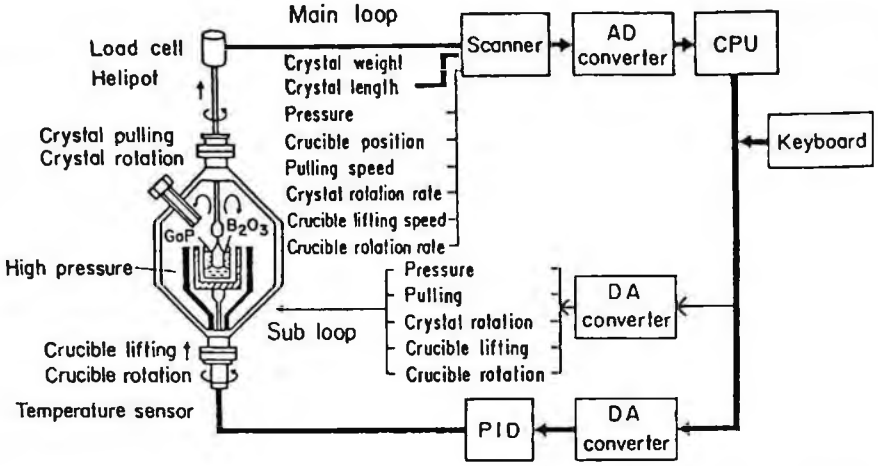

Fig. 3.13 Block diagram of a computer-assisted diameter control system for the LEC method (from Ref. 24 with permission).

- infrared bright ring detection[112, 113, 116, 126]
- pull rate control[127]
- crystal weighing method[115, 128-130]
- crucible/melt weighing method[131-134]
- cooling plot method[135]

Among these various methods, the crystal weighing method with a computer control system which is referred to as automatic diameter control (ADC) has become predominant for crystal growth of compound semiconductors. In ADC, a sensitive weight sensor called a load cell is used to detect the weight of growing crystal and the diameter is calculated from the time derivative of the measured weight. The calculated diameter is compared with the reference diameter and the deviation is regulated by controlling the growth temperature.

The weight of growing crystal is expressed[136-138] as

$$W(t) = M_0 + \int_0^t \rho_s g\pi R^2 V_z dt + \rho_l g\pi R^2 H + 2\pi R\gamma_{st} \qquad (3.36)$$

Here, the first term M_0 is initial weight including the seed holder and the seed crystal. The second term is the crystal weight, where ρ_s is the density of crystal, g the gravitational acceleration, R the crystal radius, V_z the growth velocity. The third term is the hydrostatic head of the meniscus where ρ_l is the density of the melt, H the meniscus height. The fourth term is the surface tension, where γ_{st} is the surface tension acting vertically downward. The derivative of the measured weight dW(t)/dt is proportional to the diameter square R^2. The radius of the growing crystal thus calculated is com-

pared with the desired diameter and to correct the deviation, the heater temperature is increased or decreased depending on the sign of the deviation. When the real diameter is larger than the desired one, the heater temperature is increased to reduce the diameter. When the real diameter is less than the desired one, the heater temperature is reduced to increase the diameter. For this temperature regulation, a form of control such as PID is applied so as to improve the response. In reality, the regulation is very difficult, especially because the melt height is reduced as the crystal is grown and the response changes as a function of the melt height. To overcome this time delay due to changing responsivity, various techniques have been attempted. In several cases, the advance control method is known to be effective for good regulation.

For weight sensors, two types of sensors are used, one is a strain gauge sensor and the other is a differential transfer system. The resolution of the sensor must be sufficient in relation to the total weight of grown crystals. In many cases, the differential transfer system is used.

Fig. 3.13 shows an example of an automatic diameter control (ADC) system based on a computer control system.[124] The weight sensor signal via an A/D converter is input to a computer where the diameter of growing crystal is calculated and the signal for controlling the heater is fed back after data processing.[124, 139] Other examples of diameter control are described by Riedling[140] and Magnanini et al.[141]

REFERENCES

1. *Compound Semiconductors, Vol.1, Preparation of III-V compounds*, ed. R. K. Willardson and H. L. Goering (Reinhold, New York, 1962).
2. R. F. Sekerka, in *Crystal Growth: an Instroduction*, ed. P. Hartman (North-Holland, Amsterdam, 1973) p. 403.
3. J.B. Mullin, in *Crystal Growth and Characterization*, eds. R. Ueda and J. B. Mullin (North Holland, Amsterdam, 1975) p. 61.
4. J.B. Mullin, in *Crystal Growth and Characterization*, eds. R. Ueda and J. B. Mullin (North Holland, Amsterdam, 1975) p. 75.
5. J. R. Carruthers and A. F. Witt, in *Crystal Growth and Characterization*, eds. R. Ueda and J. R. Mullin (North-Holland, Amsterdam, 1975) p. 107.
6. J. R. Carruthers, in *Crystal Growth, a Tutorial Approach*, ed. W. Bardsley, T. T. J. Hurle and J. B. Mullin (North-Holland, Amsterdam, 1977) p. 157.
7. F. Rosenberger, *Fundamentals of Crystal Growth I* (Springer-Verlag, Berlin, 1979).
8. L.F. Donaghey, *Crystal Growth*, ed. B. R. Pamplin, (Pergamon Press, Oxford, 1980) p. 65.
9. C.D. Brandle, *Crystal Growth*, ed. B. R. Pamplin, (Pergamon Press, Oxford, 1980) p. 275.
10. J.S. Shah, *Crystal Growth*, ed. B. R. Pamplin, (Pergamon Press, Oxford, 1980) p. 301.
11. D. T. J. Hurle, Adv. Colloid Interface Sci. 15 (1981) 101.
12. D. T. J. Hurle, in *Crystal Growth of Electronic Materials*, ed. E. Kaldis (Elsevier Sci., Amsterdam, 1985) p. 3, p. 11.
13. J. B. Mullin, in *Crystal Growth of Electronic Materials*, ed. E. Kaldis (Elsevier Sci., Amsterdam, 1985) p. 269.
14. G. Müller, in *Crystals: Growth, Properties and Applications*, ed. H. C. Freyhardt (Springer Verlarg, Berlin, 1988) p. 1.
15. K. Weiser, in *Compound Semiconductors, Vol.1, Preparation of III-V compounds*, ed. R. K. Willardson and H. L. Goering (Reinhold, New York, 1962) p. 471.
16. J. C. Woolley, in *Compound Semiconductors, Vol.1, Preparation of III-V compounds*, ed. R. K. Willardson and H. L. Goering (Reinhold, New York, 1962) p. 3.

17. W. B. White, in *Crystal Growth: A Tutorial Approach*, ed. W. Bardsley, D. T. J. Hurle and J. B. Mullin (North Holland, Amsterdam, 1979) p. 17.
18. F. Rosenberger, *Fundamentals of Crystal Growth I* (Springer-Verlag, Berlin, 1979) p. 66, p. 145.
19. H. Wenzl, A. Dahlen, A. Fattach, S. Petersen, K. Mika and D. Henkel, *J. Crystal Growth* **109** (19791) 191.
20. S. Akai, N. Kitou, K. Fujita and Y. Nishida, *Proc. 14th Simposium, Stoiciometry of Compound Crystals (in japanese)* (Electric and Communication Institute, Tohoku University, 1977) p. 1-2-1.
21. M. Tmar, A. Gabriel, C. Chatllion and I. Ansara, *J. Crystal Growth* **69** (1984) 421.
22. H. Wenzl, A. Dalhen, A. Fattah, S. Petersen, K. Mika and D. Henkel, *J. Crystal Growth* **109** (1991) 191.
23. K. Kohiro, M. Ohta and O. Oda, *J. Crystal Growth* **158** (1996) 197.
24. F. Rosenberger and G. Müller, *J. Crystal Growth* **65** (1983) 91.
25. D.T.J. Hurle, *J. Crystal Growth* **65** (1983) 124.
26. J. R. Carruthers, *J. Crystal Growth* **32** (1976) 13.
27. L. E. Scriven, C. V. Steernlig, *J. Fluid Mech.* **19** (1964) 321.
28. D. A. Nield, *J. Fluid Mech.* **19** (1964) 341.
29. K. A. Smith, *J. Fluid Mech.* **24** (1966) 401.
30. D. Schwabe, *PCH Physico-Chemical Hydrodynamics* **2** (1981) 263.
31. D. Schwabe, in *Crystals, Growth, Properties and Applications*, ed. by H. J. Freyhardt (Springer-Verlag, Berlin, 1988) p. 75.
32. F. Rosenberger, *Fundamentals of Crystal Growth I* (Springer-Verlag, Berlin, 1979) p. 387.
33. A. Tegetmeier, A. Cröll and K. W. Benz, *J. Crystal Growth* **141** (1994) 451.
34. J. R. Carruthers and K. Nassau, *J. Appl. Phys.* 39 (1968) 5205.
35. J. R. Carruthers, *J. Crystal Growth* **32** (1976) 212.
36. D.C. Miller, A.J. Valentino and I.K. Shick, JJ. *Crystal Growth* **44** (1978) 121.
37. H. Kobayashi, *J. Crystal Growth* **53** (1981) 339.
38. M. Miyazawa, *J. Crystal Growth* **53** (1981) 636.
39. C. D. Brandle, *J. Crystal Growth* **57** (1982) 65.
40. G. Müller, G. Neumann and W. Weber, *J. Crystal Growth* **70** (1984) 78.
41. G. Müller, G. Neumann and H. Matz, *J. Crystal Growth* **84** (1987) 36.
42. G. Müller, *J. Crystal Growth* **128** (1993) 26.
43. J. R. Ristorcelli and J. L. Lumley, *J. Crystal Growth* **116** (1992) 447.
44. K. Takagi, T. Fukuzawa and M. Ishii, *J. Crystal Growth* **32** (1976) 89.
45. Y. Mori, *Trans. ASME* **83C** (1961) 479.
46. M. Berkowski, K. Iliev, V. Nikolov, P. Peshev and W. Piekarczyk, *J. Crystal Growth* **83** (1987) 507.
47. A. Hirata, M. Tachibana, Y. Okano and T. Fukuda, *J. Crystal Growth* **128** (1987) 195.
48. M. Watanabe, M. Eguchi, K. Kakimoto, H. Ono, S. Kimura and T. Hibiya, *J. Crystal Growth* **151** (1995) 285.
49. T.A. Campbell and J.N. Koster, *J. Crystal Growth* **140** (1994) 414.
50. H. Kopetsch, *J. Crystal Growth* **88** (1988) 71.
51. J. J. Derby and R. A. Brown, *J. Crystal Growth* **87** (1988) 251.
52. K. Oda, T. Saito, J. Nishihama and T. Ishihara, *J. Crystal Growth* **97** (1989) 186.
53. K. Oda, T. Saito, J. Nishihama, T. Ishihara and M. Sato, *J. Crystal Growth* **129** (1993) 30.
54. K. Koai, K. Sonnenberg and H. Wenzl, *J. Crystal Growth* **137** (1995) 59.
55. D. T. J. Hurle, *Phil. Mag.* **13** (1966) 305.
56. H. A. Chedzey and D. T. J. Hurle, *Nature* **210** (1966) 933.
57. H. P. Utech and M. C. Flemings, *J. Appl. Phys.* **37** (1966) 2021
58. D. T. J. Hurle, *Crystal Growth*, ed. H. S. Peiser (Pergamon Press, Oxford, 1967) p. 659.
59. K. Hoshi, N. Isawa and N. Suzuki, *Nikkei Electronics (in japanese)* **September** (1980) 154.
60. K. Hoshi, N. Isawa and N. Suzuki, in *Semiconductor Research Vol. 20 (in japanese)*, ed. J.

Nishizawa (Kogyo Chosakai, Tokyo, 1983) p. 253.
61. W. E. Langlois, *Physicochem. Hydrodyn.* **2** (1981) 245.
62. T. Fukuda and K. Terashima, *Oyo Buturi (Monthly Publ. Jpn. Soc. Appl. Phys.) (in japanese)* **53** (1984) 42 .
63. Y. Hirata, *Kinzoku (Metal) (in japanese)* **56** (1986) 30.
64. S. Chandrasekhar, Phil. Mag. Series 7, **43** (1952) 501.
65. T. G. Cowling, *Magnetohydrodynamics* (Interscience, Now York, 1963).
66. A. F. Witt, C.J. Herman and H. C. Gatos, *J. Mater. Sci.* **5** (1970) 822.
67. K. Hoshikawa, *Jpn. J. Appl. Phys.* **21** (1982) L545.
68. K. Terashima and T. Fukuda, *J. Crystal Growth* **63** (1983), 423.
69. D. T. J. Hurle and R. W. Series, *J. Crystal Growth* **73** (1985) 1.
70. S. Kobayashi, *J. Crystal Growth* **75** (1986) 301.
71. K. Hoshikawa, H. Kohda, H. Hirata and H. Nakanishi, *Jpn. J. Appl. Phys.* **19** (1980) L33.
72. H. Hirata and N. Inoue, *Jpn. J. Appl. Phys.* **23** (1984) L527.
73. J. Osaka and K. Hoshikawa, in *Semi-Insulating III-V Materials*, eds. D. C. Look and J. S. Balkemore (Shiva, Nantwich, 1984) p. 127.
74. J. Osaka, H. Kohda, T. Kobayashi and K. Hoshikawa, *Jpn. J. Appl. Phys.* **23** (1984) L195.
75. K. Hoshikawa, H. Kohda and H. Hirata, *Jpn. J. Appl. Phys.* **23** (1984) L38.
76. H. Kohda, K. Yamada, H. Nakanishi and T. Kobayashi, J. Osaka and K. Hoshikawa, *J. Crystal Growth* **71** (1985) 813.
77. K. Hoshikawa, H. Hirata, H. Nakanishi and K. Ikuta, *Proc. 4th Intern. Symp. on Silicon Materials, Science and Technology, Volume on Semiconductor Silicon*, eds. H. R. Huff, R. Kriegler and Y. Takeiski, (Electrochem. Soc., Tokyo, 1981) p. 101.
78. H. Hirata and N. Inoue, *Jpn. J. Appl. Phys.* **24** (1985) 139.
79. R. Terashima, T. Katsumata, F. Orito, T.Kikuta and T. Fukuda, *Jpn. J. Appl. Phys.* **22** (1983) L 401.
80. A. S. Jordan, R. Caruso and A.R. Von Neida, *Bell Syst. Tech. J.* **59** (1980) 593, *J. Crystal Growth* **70** (1984) 555.
81. J.J. Derby, R.A. Brown, F.T. Geyling, A.S. Jordan and G.A. Nikolokopoulou, *J. Electrochem. Soc.* **132** (1985) 470.
82. J.J. Derby and R.A. Brown, *J. Crystal Growth* **75** (1986) 605.
83. J.J. Derby and R.A. Brown, *J. Crystal Growth* **83** (1987) 137.
84. J.J. Derby and R. A. Brown, *J. Crystal Growth* **87** (1988) 251.
85. N. Kobayashi and T. Iwaki, *J. Crystal Growth* **73** (1985) 96.
86. C. Schvezov, I. V. Samarraasekera and F. Weinberg, *J. Crystal Growth* **84** (1987) 219.
87. A. S. Jordan, E. M. Monberg and J.E. Clemans, *J. Crystal Growth* **128** (1993) 444.
88. P. Haasen, *Z. Phys.* **167** (1962) 461.
89. H. Alexander and P. Haasen, *Solid State Phys.* **22** (1968) 27.
90. J. Völkl and G. Müller, *J. Crystal Growth* **97** (1989) 136.
91. D. Maroudas and R. A. Brown, *J. Crystal Growth* **108** (1991) 399.
92. C. T. Tsai, M. W. Yao and A. Chait, *J. Crystal Growth* **125** (1992) 69.
93. K. W. Kelly, K. Koai and S. Motakef, *J. Crystal Growth* **113** (1991) 254.
94. K. W. Kelly, S. Motakef and K. Koai, *J. Crystal Growth* **113** (1991) 265.
95. S. Motakef, K. W. Kelly and K. Koai, *J. Crystal Growth* **113** (1991) 279.
96. N. Miyazaki, H. Uchida, T. Munakata and T. Fukuda, *JSME Int. J.* **A37** (1994) 124.
97. A. S. Jordan and J. M. Parsey, Jr., *J. Crystal Growth* **79** (1986) 280.
98. S. McGuigan, B. W. Swanson and R. N. Thomas, *J. Crystal Growth* **94** (1989) 75.
99. S. V. Tsivinskii, *Inzh. Fiz. Zh.* **5** (1962) 59.
100. O. Oda, K. Katagiri, K. Shinohara, S. Katsura, T. Takahashi, K. Kainosho, K. Kohiro and R. Hirano, in *Semiconductors and Semimetals Vol.31* (Academic Press, New York, 1990) p. 93.
101. W.A. Tiller, K.A. Jackson, J.W. Rutter and B. Chalmers, *Acta. Met.* **1** (1953) 428.
102. W.A. Tiller, in *The Art and Science of Growing Crystals*, ed. J. J. Gilman (John Wiley & Sons,

New York, 1963) p. 276.
103. F. Rosenberger, in *Fundamentals of Crystal Growth I* (Springer-Verlag, Berlin, 1979) p. 395.
104. J. A. Burton, R. C. Prim and W. P. Slichter, *J. Chem. Phys.* **21** (1953) 1987.
105. W. G. Pfann, *Trans. Am. Inst. Mining. Met. Engeer.* **194** (1952) 747.
106. D.T.J. Hurle and E. Jakeman, *J. Crystal Growth* **5** (1969) 227.
107. F. Rosenberger and G. Müller, *J. Crystal Growth* **65** (1983) 91.
108. P.M. Adornato and R.A. Brown, *J. Crystal Growth* **89** (1987) 155.
109. A.G. Ostrogorsky and G. Müller, *J. Crystal Growthh* **121** (1992) 587.
110. D.T.J. Hurle, *Solid-State Electron.* **3** (1961) 37.
111. E.J. Patzner, R.G. Dessauer and M.R. Poponiak, *Semicon. Products and Solid State Technol.* **October** (1967) 24.
112. K. E. Domey, *Solid State Technol.* **October** (1971) 41.
113. U. Gross and R. Kersten, *J. Crystal Growth* **15** (1972) 85.
114. T. V K. J. Gärtner, K. F. Rittinghaus ann A. Seeger, *J. Crystal Growth* **13/14** (1972) 619.
115. W. Bardsley, G. W. Green, C. H. Holliday and D. T. J. Hurle, *J. Crystal Growth* **16** (1972) 277.
116. D. F. O'Kane, T. W. Kwap, L. Guiltz adn A. L. Bednowitz, *J. Crystal Growth* **13/14** (1972) 624.
117. S. F. Nygren, JJ. *Crystal Growth* **19** (1973) 21.
118. D.T.J. Hurle, *J. Crystal Growth* **42** (1977) 473.
119. D. T. J. Hurle, *J. Crystal Growth* **85** (1987) 1.
120. D. T. J. Hurle, *J. Crystal Growth* **128** (1993) 15.
121. T. G. Digges, Jr., R. H. Hopkins adn R. C. Seidensticker, *J. Crystal Growth* **29** (1975) 326.
122. R. M. Ware and M. Whittaker, in *Abstracts of the 5th Int. Conf. Crystal Growth* (Boston, 1978) p. 132.
123. H.J.A. Van Dijk, J. Goorissenm U. Gross, R. Kersten and J. Pistorius, *Acta Electronica* **17** (1974) 45.
124. H. J. Van Dijk, C. M. G. Jochem, G. J. Scholl and P. van der Werf, *J. Crystal Growth* **21**(1974) 310.
125. S. Ozawa and T. Fukuda, *J. Crystal Growth* **76** (1986) 323.
126. H. Blumberg and K. Th. Wilke, *Kristal und Technik* **9** (1974) 447.
127. U. Ekhult and T. Carlberg, *J. Crystal Growth* **76** (1986) 317.
128. T. Fukuda, S.Washizuka, Y. Kokubun, J. Ushizawa and M. Watanabe, in *Proc. Gallium Arsenide and Related Compounds* (1981) p. 43.
129. S. Washizuka, J. Ushizawa, Y. Kokubun, M. Watanabe and T. Fukuda, *Oyo Buturi (Monthly Publ. Jpn. Soc. Appl. Phys.) (in japanese)* **52** (1983) 515.
130. R. C. Reinert and M. A. Yatsko, *J. Crystal Growth* **21** (1974) 283.
131. T. R. Kyle and G. Zydzik, *Mater. Res. Bull.* **8** (1973) 443.
132. A. E. Zinnes, B. E. Nevis and C. D. Brandle, *J. Crystal Growth* **19** (1973) 187.
133. A. J. Valentino and C. D. Brandle, *J. Crystal Growth* **26** (1974) 1.
134. T. Satoh, J. Inui and H. Iwamoto, Fujitsu Sci. Technol. **March** (1976) 93.
135. Z. Burstein and M. Azulay, *Mater. Res. Bull.* **19** (1984) 49.
136. W. Bardsley, B. Cockayne, G. W. Green, D. T. J. Hurle, G. J. Joyce, J. M. Roslington, P. T. Tufton, H. C. Webber and M. Healey, *J. Crystal Growth* **24/25** (1974) 369.
137. W. Bardsley, D.T.J. Hurle and G.C. Joyce, *J. Crystal Growth* **40** (1977) 13.
138. W. Bardsley, D.T.J. Hurle, G.C. Joyce and G.C. Wilson, *J. Crystal Growth* **40** (1977) 21.
139. K. Terashima, H. Nakajima and T. Fukuda, in *Proc. 3rd Conf. Semi-Insulating III-V Materials*, eds. S. Makram-Ebeid adn B. Tuck (Shiva, Nantwich, 1982) p. 397.
140. K. Riedling, *J. Crystal Growth* **89** (1988) 435.
141. R. Magnanini, M. Curti, L. Zanotti, C. Paorici and T. Gorog, *Acta Physica Hungarica* **70** (1991) 231.

4. DEFECTS

4.1 INTRODUCTION

Defects in crystals are categorized in principle into four types such as point defects, line defects and plain defects and other defects such as precipitates, inclusions and voids as shown in Table 4.1. Line defects, plain defects and other defects (precipitates/ inclusions/voids) are basically undesirable and for bulk crystal growth they are preferably eliminated. Point defects exist thermodynamically and it is important to know how to control them in order to obtain appropriate properties. Some point defects act as important species in realizing the desired properties. Precise defect science is explained by various authors.[1-6]

4.2 POINT DEFECTS

Point defects are important in compound semiconductors because they dominate the electrical and optical properties. Point defects are defects which are formed as irregularities of atom arrangements in lattice sites. Compared with elemental semiconductors, compound semiconductors have more kinds of point defects because they have at least two constituents.

4.2.1 Various Point Defects

For a compound semiconductor MX where M is a constituent with positive electronegativity and X is a constituent with negative electronegativity, there are six elemental point defects as follows

Vacancy of M atom V_M
Vacancy of X atom V_X

Table 4.1 Various Defects

Point Defect	Vacancy
	Interstitial atom
	Antisite Atom
	Complex Defect
Line Defect	Edge Dislocation
	Screw Dislocation
	Mixed Dislocation
	Lineage and Low Angle Grain Boundary
Plain Defect	Stacking Fault Defect
	Twin and Microtwin
Other Defect	Precipitate
	Inclusion
	Voids

Interstitial M atom	M_i
Interstitial X atom	X_i
Antisite defect of M atom	M_X
Antisite defect of X atom	X_M

Vacancies are point defects due to the absence of atoms at the lattice site. Interstitials are atoms which are located at the interstitial site deviated from the proper lattice site. Antisite defects are atoms which are located at the lattice site for another constituent atom. The nomenclature for these defects are based on that by Kröger et al. [4,5]

In real crystals, some point defects are predominant over others depending on the difference of the formation energies of these point defects. Typical combinations of these defects are as follows.

(i) Schottky defects
M vacancies V_M and X vacancies V_X are predominant. When $[V_M]=[V_X]$, the stoichiometry can be preserved.
(ii) Frenkel defects on M sublattice
M vacancies V_M and M interstitial atoms M_i are predominant. When $[V_M]=[M_i]$, the stoichiometry can be preserved
(iii) Frenkel defects on X sublattice
X vacancies V_X and X interstitial atoms X_i are predominant. When $[V_X]=[X_i]$, the stoichiometry can be preserved.
(iv) Substitutional Disorder

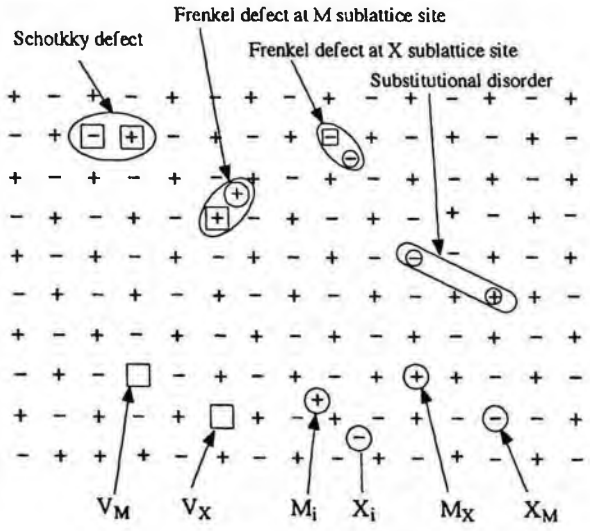

Fig. 4.1 Schematic diagram for various point defects. +: cation, -: anion.

M antisite defects M_X and X antisite defects X_M are predominant. When $[M_X]=[X_M]$, the stoichiometry can be preserved.

(v) Interstitial Disorder

M interstitial defects M_i and X interstitial defects X_i are predominant. When $[M_i]=[X_i]$, the stoichiometry can be preserved. This type of combination is rare in reality .

In Fig. 4.1, these elementary point defects are shown schematically. It should be noted that even stoichiometric compounds have point defects which are determined by thermodynamics. Stoichiometry can be maintained when the numbers of defects which are opposite in composition are equal as mentioned above. In addition to these elementary point defects, there are many types of complex defects, such as those with impurities. In real compound semiconductors, non-stoichiometric forms are found and the concentrations of various defects are determined by the following thermodynamics.

4.2.2 Thermodynamics of Point Defects

(1) Elementary point defect concentrations

For five combinations of elementary point defects, the concentrations obey the mass action law as follows.

$$[V_M][V_X] = K_S = C_S \exp(-G_S/RT) \tag{4.1}$$

$$[V_M][M_i] = K_F = C_F \exp(-G_F/RT) \tag{4.2}$$

$$[V_X][X_i] = K_F = C_F \exp(-G_S/RT) \tag{4.3}$$

$$[M_X][X_M] = K_A = C_A \exp(-G_A/RT) \tag{4.4}$$

$$[M_i][X_i] = K_I = C_I \exp(-G_I/RT) \tag{4.5}$$

Here, the constant K is the reaction constant and C the pre-exponential and G the defect formation Gibbs free energy.

There are six variables, $[V_M]$, $[V_X]$, $[M_i]$, $[X_i]$, $[M_X]$, $[X_M]$ while only five equations (Eqs. 4.1- 4.5). To calculate all the variables, we need one more equation which represents the stoichiometry.

$$[V_M] + [X_i] + [X_M] = [V_X] + [M_i] + [M_X] \tag{4.6}$$

From these six equations (Eqs. 4.1 - 4.6), all concentrations of point defects can be calculated when the reaction constant and the Gibbs free energies are known.

(2) Ionization of point defects

In real crystals, elementary defects are ionized according to the energy levels they occupy. The ionization obeys the Fermi-Dirac distribution law. They are represented as

follows when only single ionization is considered

$$V_M = V_M^- + e^+ + E_1 \qquad \frac{p[V_M^-]}{[V_M]} = K_1 \qquad (4.7)$$

$$V_X = V_X^+ + e^- + E_2 \qquad \frac{n[V_X^+]}{[V_X]} = K_2 \qquad (4.8)$$

$$M_i = M_i^+ + e^- + E_3 \qquad \frac{n[M_i^+]}{[M_i]} = K_3 \qquad (4.9)$$

$$X_i = X_i^+ + e^+ + E_4 \qquad \frac{p[X_i^+]}{[X_i]} = K_4 \qquad (4.10)$$

$$M_X = M_X^- + e^+ + E_5 \qquad \frac{p[M_X^-]}{[M_X]} = K_5 \qquad (4.11)$$

$$X_M = X_M^+ + e^- + E_6 \qquad \frac{n[X_M^+]}{[X_M]} = K_6 \qquad (4.12)$$

The equilibrium constant K_i is related to the ionization energy as

$$K_i = A_i \exp(-E_i/RT) \qquad (4.13)$$

The concentrations of free electrons and free holes are determined by the reaction of the rupture of chemical bonding by thermal vibration which is represented as follows.

$$\text{chemical bond} = e^- + e^+ + E_g \qquad n \cdot p = K_i = C_i \exp(-E_g/kT) \qquad (4.14)$$

Here, n and p are the density of electrons and holes, K_i the reaction constant, C_i the term concerned with the activity coefficient and E_g the bandgap. Since a crystal must be electrically neutral, we have the following neutral condition.

$$[V_M^-] + [X_i^-] + [X_i^-] + n = [V_X^+] + [M_i^+] + [X_M^+] + p \qquad (4.15)$$

For stoichiometric crystals, we have the following mass balance equation.

$$[M_i] + [M_i^+] + [M_X] + [M_X^-] - [V_M] - [V_M^-] =$$

$$[X_i] + [X_i^-] + [X_M] + [X_M^+] - [V_X] - [V_X^+] \qquad (4.16)$$

From six neutral defect equations, six ionized defect equations, the free carrier equation, the neutral condition and the mass balance equation, all 14 variables can be calculated.

(3) Non-stoichiometry

In the real crystal, stoichiometry is not easily held because of the dissociation of a constituent element which is volatile. This non-stoichiometry is due to the reaction between solid crystal and the vapor phase. These reactions can be represented as follows.

$$M_g = M_M + V_x \tag{4.17}$$

$$M_g = M_i \tag{4.18}$$

$$1/2(X_2)_g = M_M + V_M \tag{4.19}$$

$$1/2(X_2)_g = X_i \tag{4.20}$$

$$2M_g = M_x + M_M \tag{4.21}$$

$$(X_2)_g = X_X + X_M \tag{4.22}$$

The concentrations of point defects which can be created due to the reaction with the vapor phase can be represented as follows under the condition that $[M_M] = [X_X] = 1$.

$$[V_X] = K_r\, p_M \tag{4.23}$$

$$[M_i] = K_R\, p_M \tag{4.24}$$

$$[M_X] = K'_R p_M^2 \tag{4.25}$$

$$[V_M] = K_{ox}\, p_{X_2}^{1/2} \tag{4.26}$$

$$[X_i] = K_{Ox}\, p_{X_2}^{1/2} \tag{4.27}$$

$$[X_M] = K'_{OX}\, p_{X_2} \tag{4.28}$$

As the above equations, the concentrations of all elemental point defects can be represented by the partial vapor pressures of the constituents. The partial vapor pressures are however mutually related as follows.

$$(MX)_s = M_g + 1/2(X_2)_g \qquad p_M \Sigma\, p_{X_2}^{1/2} = K_p \tag{4.29}$$

It should therefore be noted that the concentrations of all elemental point defects can be represented by only one partial vapor pressure, conventionally by a partial vapor pressure of the most volatile constituent. Using one of equations (Eqs. 4.21-4.26) instead of the mass balance equation for stoichiometry, all concentrations of elemental point defects can be deduced.

(4) Brouwer plot

As mentioned above, all concentrations of elemental point defects can be deduced from basic equations. The analytical solution of all these equations is however complicated since most equations are represented as products while the neutral condition equation is the sum of the defect concentrations. Brouwer[7] has proposed a simple graphical solution to these equations.

For a typical case of the Frenkel disorder of the constituent of M, the Brouwer plot can be shown as in Fig. 4.2. In the figure, it is easily seen that when the partial vapor pressure of M is low, metal vacancies are predominant and the crystal is p-type (I region) while when the partial vapor pressure of M is high, metal interstitials are predominant and the crystal is n-type (II region). When the partial vapor pressure of M is in the medium region, the stoichiometry of the crystal can be preserved.

4.2.3 Diffusion Constants

Point defects each have a diffusion coefficient. These diffusion coefficients have been studied by many authors and some of them are summarized in Fig. 4.3.

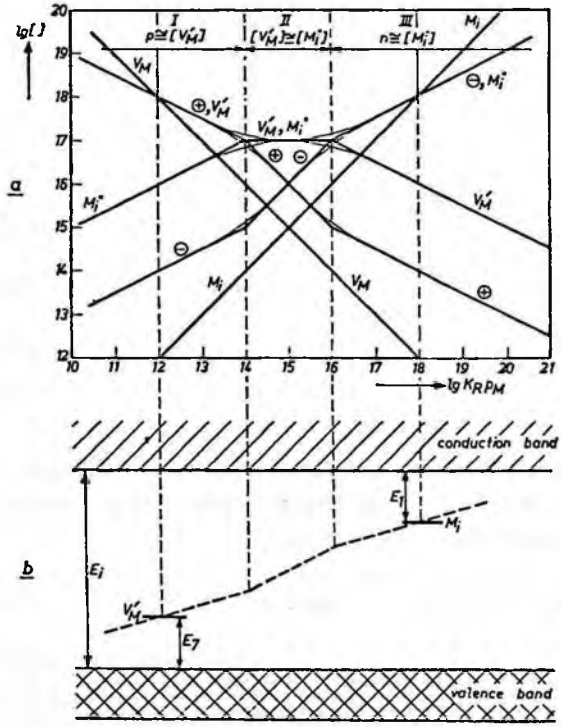

Fig. 4.2 An example of Brouer plot. (a) Concentrations of defects in a crystal of composition of MX with Frenkel disorder. (b) The position of the Fermi level relative to the bands (reprinted from Ref. 4 with permission, copyright 1956 Elsevier).

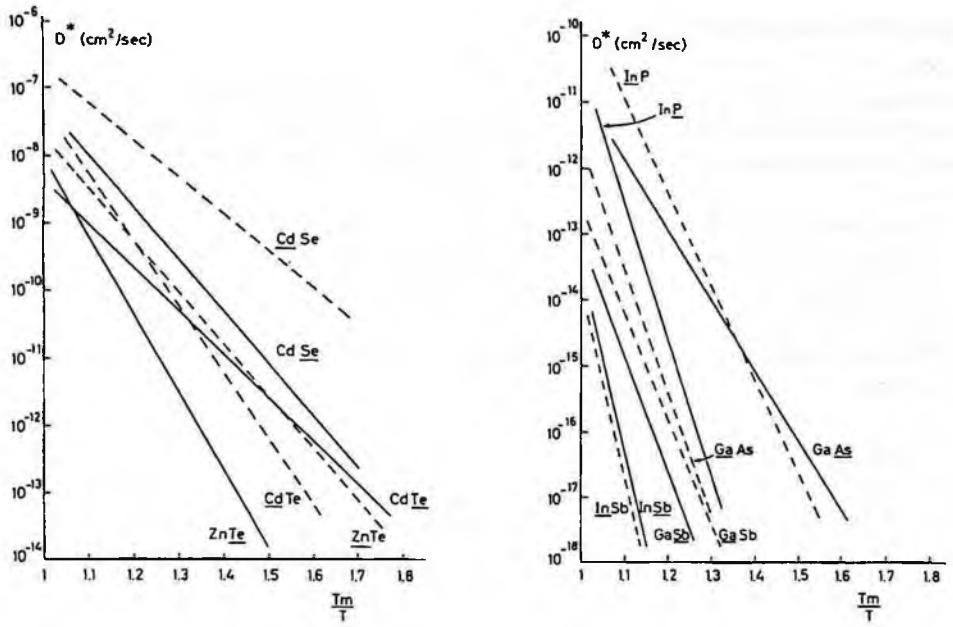

Fig. 4.3 Self-diffusion coefficients of the underlined elements for (a) II-VI compounds (from Ref. 8 with permission) and (b) III-V compounds versus the reciprocal reduced temperature (data from Ref. 9 with permission of Springer Science and Bysiness Media).

Diffusion constants are basically represented as follows.

$$D = D\exp\left(-\frac{Q}{kT}\right) = \left[a_0^2 \nu \exp\left(\frac{\Delta S_v + \Delta S_m}{kT}\right)\right] \exp\left(\frac{-\Delta H_v - \Delta H_m}{kT}\right) \quad (4.30)$$

Here, $\left[a_0^2 \nu \exp\left(\frac{\Delta S_v + \Delta S_m}{kT}\right)\right]$ is the frequency factor, $Q = \Delta H_v + \Delta H_m$ is the activation enthalpy. Q is also known as the diffusion activation energy. Here, ΔS_v and ΔH_v are the entropy and enthalpy for vacancies respectively, and ΔH_v and ΔH_m are the entropy and enthalpy for atoms to jump to a vacancy site, respectively. a_0 is the lattice constant and ν the jump frequency.

Eq. 4.3 shows Arrhenius plots of the diffusion coefficients for II-VI and III-V compound materials. The pre-exponential coefficient, D_0, is a constant and the exponential factor shows the reciprocal temperature dependence. Theoretical calculations on diffusion phenomena are described in speciality books.[10-12]

4.2.4 Non-stoichiometry

In Sec. 4.2.2, the thermodynamical calculation of point defects is described. Since compound semiconductor materials consist of more than two elements, they easily deviate from the stoichiometric composition as explained in Sec. 3.2 and this non-stoichiometry can be represented in the phase diagrams based on the thermodynamical calculations.[13-15]

These deviations influence various properties of compound semiconductors.

(i) Electrical properties and the self compensation mechanism

(ii) Optical properties such as photoluminescence

(iii) Formation of precipitates and inclusions

The stoichiometry control of compound semiconductors is reviewed by Nishizawa.[16-18]

4.2.5 Self Compensation

In the case of II-VI compounds, their conductivity type is difficult to control. Except for CdTe, other compounds show only one conductivity type, n-type for CdS, CdSe, ZnS, ZnSe and p-type for ZnTe. This phenomenon is known as self-compensation and is explained by various models[4, 19-40] as reviewed in Refs. 41 and 42.

(1) Compensation by point defect formation

In the case of compounds of higher ionicity, when impurities are doped for conductivity control, point defects which have opposite charges are formed in order to keep elec-

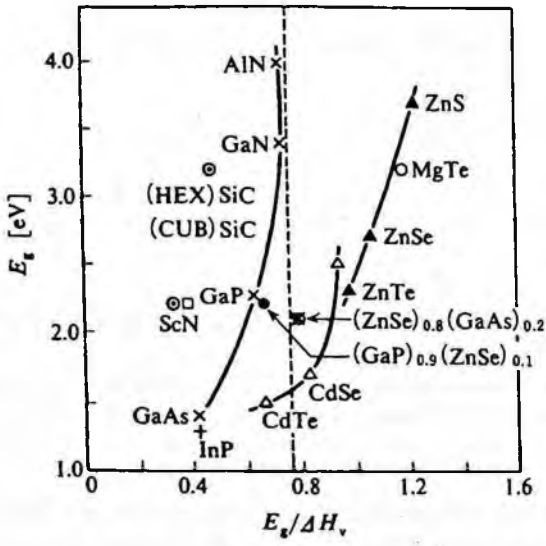

Fig. 4.4 Bandgap energies and enthalpies for vacancy formation (from Ref. 21 with permission).

Table 4.2 Measure of Self Compensation

Material	Q_1^{min}	R_M/R_N
KCl	2.12×10^8	-
ZnO	-	1.98
ZnS	-	1.26
ZnSe	-	1.15
ZnTe	3.09×10^2	0.99
CdS	-	1.42
CdSe	-	1.30
CdTe (n-type)	3.23×10	1.12
CdTe (p-type)	8.70×10^2	1.12
GaAs (p-type)	1.70×10^{-3}	-

trical neutrality.[4, 5, 19-22] When the energy E_1 which is emitted due to the recombination of electrons and holes by impurity doping is greater than the defect formation energy, E_2, impurity doping induces defect formation. E_1 is related to the bandgap and E_2 is related to the crystal ionicity. Self-compensation occurs easily when the bandgap is large and the ionicity is large. Mandel et al.[19, 20] explained this self-compensation by the value of Q_1^{min} which is related to the ratio of vacancies to impurities (Table 4.2). He also used the tetrahedral radius ratio R_M/R_N. When the radius of the II element is larger than that of the VI element, the compound becomes n-type and when it is smaller, it becomes p-type.

Fig. 4.4 shows the relationship between the bandgap and vacancy formation enthalpy, ΔH_v. When $E_g/\Delta H_v$ is
greater, with greater bandgap and greater ionicity, the effect of self compensation becomes greater. A similar explanation was offered by Kumimoto et al.[23]

Nishizawa et al.[24] explained self-compensation from the viewpoint of the vapor pressure of the constituents. They explained the electrical conductivity type by the deviation from stoichiometry. When the vapor pressure of the VI element is higher than that of the II element, the compound shows n-type conductivity while when it is lower, the compound shows p-type. This is because when the vapor pressure of the VI element is higher, VI site vacancies are easily formed so that it shows n-type and when the vapor pressure of the II element is higher, II site vacancies are easily formed so that it shows p-type.

It is not only elementary point defects but also complex defects such as vacancy-impurity defects that are considered to be the origin of self-compensation.[25-28]

(2) Lattice relaxation

The incorporation of dopants causes the lattice to relax and breaks the surrounding bonds, giving rise to compensating defects.[29-31] Such a relaxation may lead to the formation of bistable impurity centers.

(3) Solubility limit

It is also pointed out that there is a solubility limit for doped impurities.[32-35] The solubil-

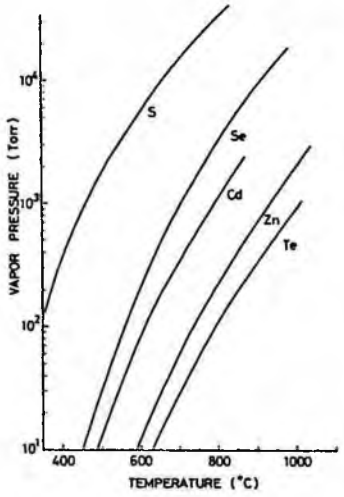

Fig. 4.5 Vapor pressures of constituent elements for II-VI materials (from Ref. 24 with permission).

ity of various dopants have therefore been theoretically studied. The solubility may depend on the position of the Fermi level, that is, the doping level.

(4) Impurity effect

Neumark[32] explained the difficulty of the control of conductivity type in II-VI compounds from the viewpoint of impurities, He paid attention to amphoteric impurities such as I group elements Li or Na. These impurities act as acceptors when they are located on the II site and act as donors when they are located at interstitial sites. Neumark calculated the chemical equilibrium equations for both cases and predicted the effective carrier concentrations and the conductivity type. He showed even though these impurities are highly doped, they amphoterically act as donors and acceptors and therefore do not increase the effective carrier concentrations.

Pfister[36] and Pautrat et al.[37,38] showed that in telluride compounds such as ZnSe and ZnTe, large amounts of impurities are gettered in Te precipitates while they are diffused out to the matrix at lower annealing temperatures at which Te precipitates disappear. These diffused-out impurities make it difficult to control the conductivity.

Igaki[39] showed that the self compensation of ZnSe is due to acceptor impurities . It was found that when ZnSe is heat treated in molten Zn metal, residual acceptor impurities could be diffused out to the Zn melt. Low resistive ZnSe could be obtained by heat treatment under pressure control.

For some dopants, it is also pointed out that they form relatively deep levels in the bandgap.[40]

4.2.6 Defect Control

Defect control technology is one of the main points in the preparation of compound semiconductors because point defects dominate the electrical and optical properties of compound semiconductors.[43-45] Point defects are determined not only during crystal growth but also during the cooling process after crystal growth. In several materials such as GaAs and InP, a thermal annealing process after crystal growth is positively applied in order to control point defects.

During crystal growth, the concentration of point defects is thermodynamically determined at each temperature under the corresponding overpressure. Just below the melting point, the concentration of each point defect is the highest but during cooling the point defect concentration changes.

4.3 DISLOCATIONS

4.3.1 Fundamentals of Dislocations

The main defects in crystals are dislocations. Dislocations are a kind of line defect and are mainly classified into two types, edge dislocations and screw dislocations[46] as shown in Fig. 4.6. Dislocations are defects due to atomic plane distortions and are characterized by Burgers vectors.[46-48] In the case of edge dislocations, the Burgers vector is normal to the dislocation line, while in the case of screw dislocations, the Burgers vector is parallel to the dislocation line. In reality, most dislocations are mixed, consisting of edge dislocations and screw dislocations. In the case of compound semiconductors, there are three types of dislocations, α, β and screw dislocations as shown in Fig. 4.7.[49, 50]

Dislocations are conventionally measured by etching procedures and in this case, the dislocation density is known as the Etch Pit Density (EPD). For each material, there are appropriate etchants as described from Chapter 7 on.

The dislocation movement of various compound semiconductors has been measured in various ways[49-50] and some of them are summarized in Fig. 4.8.[49]

4.3.2 Thermal Stress and Dislocations

Dislocations are the defects formed due to thermal non-equilibrium and can be eliminated if the appropriate conditions exist. They are mainly formed during crystal growth or during the cooling process and depend on the thermal stress in the crystal which is dependent on the crystal growth atmosphere. Many investigations have been performed to predict the thermal stress in the crystal by computer simulations as explained in Sec. 3.5.

In the case of silicon, dislocation free crystals are obtained even for large diameters. In the case of compound semiconductors, it is rather difficult to obtain dislocation free crystals and this is attributed to be the critical resolved shear stress as explained in Sec. 1.7.3 and Sec. 3.8. As shown in Fig. 3.8 for the case of InP, dislocation free crystals can be obtained theoretically if the conditions are satisfied.[53] In fact, for the case of InP, when the crystal diameter is small, dislocation free single crystals are obtained.

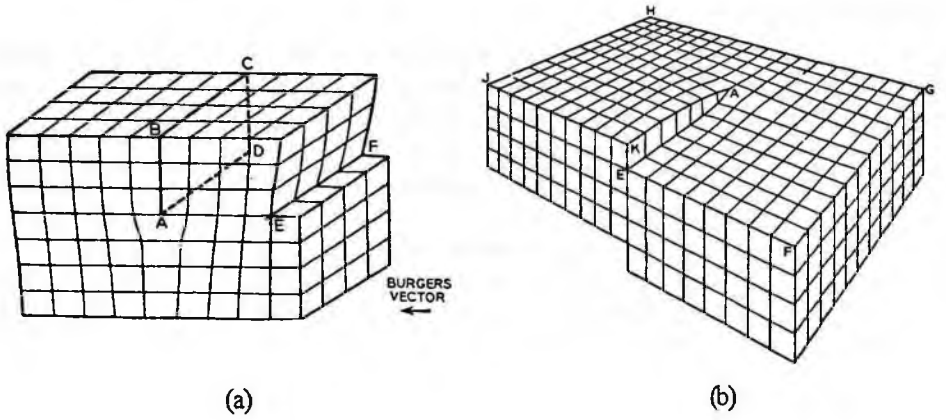

Fig. 4.6 Edge dislocation (a) and screw dislocation (b).

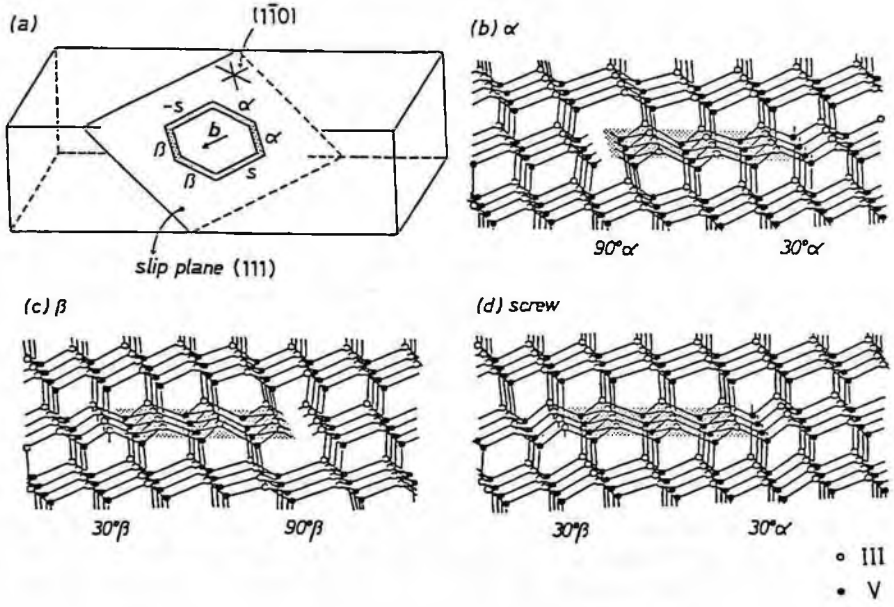

Fig. 4.7 Various dislocations: (a) a dislocation loop on a slip plane, and atomic arrangements at the core of (b) α dislocations, (c) β dislocations and (d) screw dislocations in a III-V (II-VI) compound. The shared regions denote an intrinsic stacking fault. Open circles correspond to group III (II) atoms and solid circles correspond to group V (VI) group atoms (reprinted from Ref. 49 with permission, copyright 1982 Elsevier).

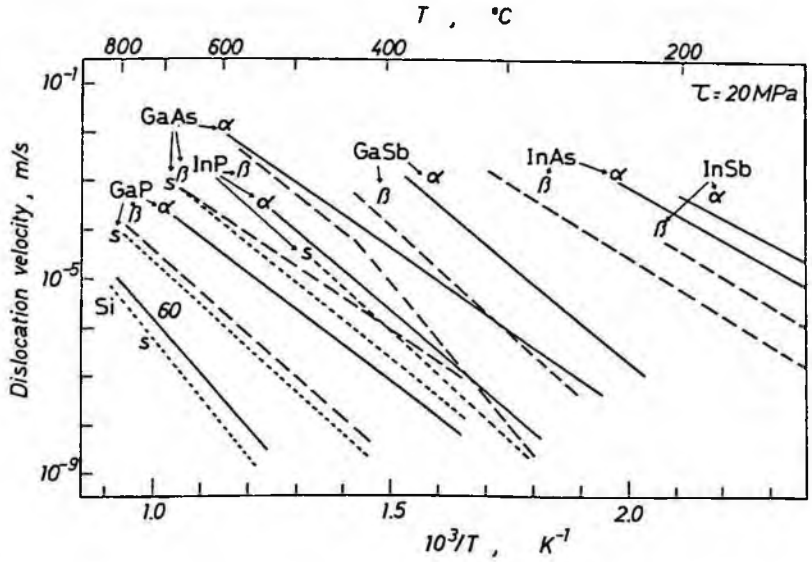

Fig. 4.8 Velocities of α, β and screw dislocations under a shear stress of 20 MPa in a series of undoped III-V compounds plotted against the reciprocal of temperature. Data for 60° and screw dislocations in high-purity Si are also shown (reprinted from Ref. 49 with permission, copyright 1982 Elsevier).

In order to realize low dislocation crystals, it is therefore desirable to grow crystals under a lower temperature gradient.

4.3.3 Necking

Necking was first applied to the CZ crystal growth of silicon by Dash.[54-56] In this method, the diameter of the seeded crystal is made smaller to the level of several millimeters by increasing the pulling rate and the dislocation density is decreased in the region after this necking procedure. The necking method is indispensable for growing dislocation-free (DF) Si single crystals. This method was also applied to LEC crystal growth of compound semiconductors such as GaAs[57, 58] and InP,[59] and was found effective in growing DF crystals. This effect was however limited to small diameter crystals.

4.3.4 Impurity Hardening

Dislocation densities can be reduced when appropriate impurities are doped. This is widely known for various compound semiconductor materials as the impurity hardening effect. Typical examples are shown in Fig. 4.9 for the case of GaAs and InP. This dislocation reduction may occur due to the dislocation pinning around impurity atoms whose atomic radius is different from host atoms.[60, 61] The principle of impurity hardening is believed to be due to the decrease of critical resolved shear stress (CRSS). Dislo-

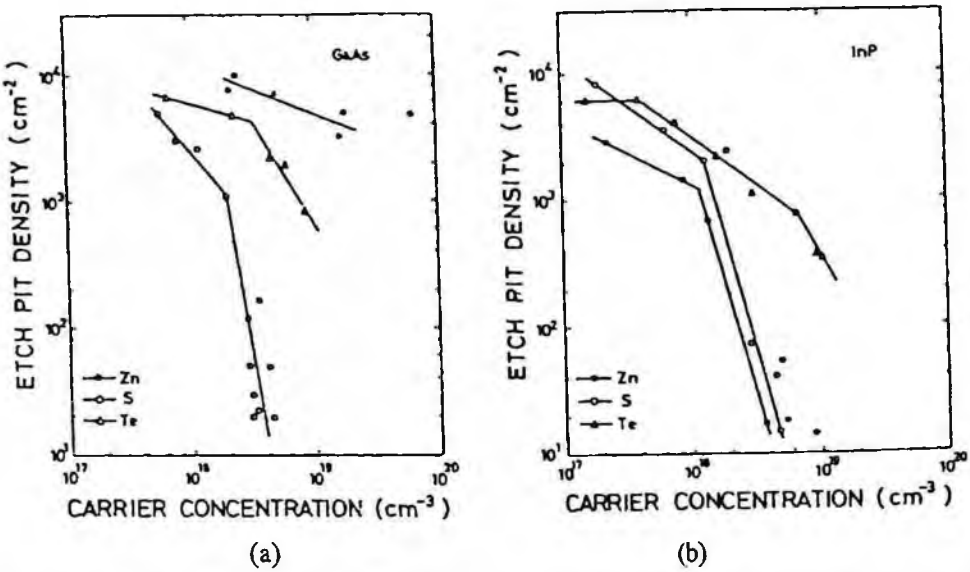

Fig. 4.9 Impurity effect on the EPD of GaAs crystals (a) and InP crystals (b) (reprinted from Ref. 60 with permission, copyright 1978 American Institue of Physics).

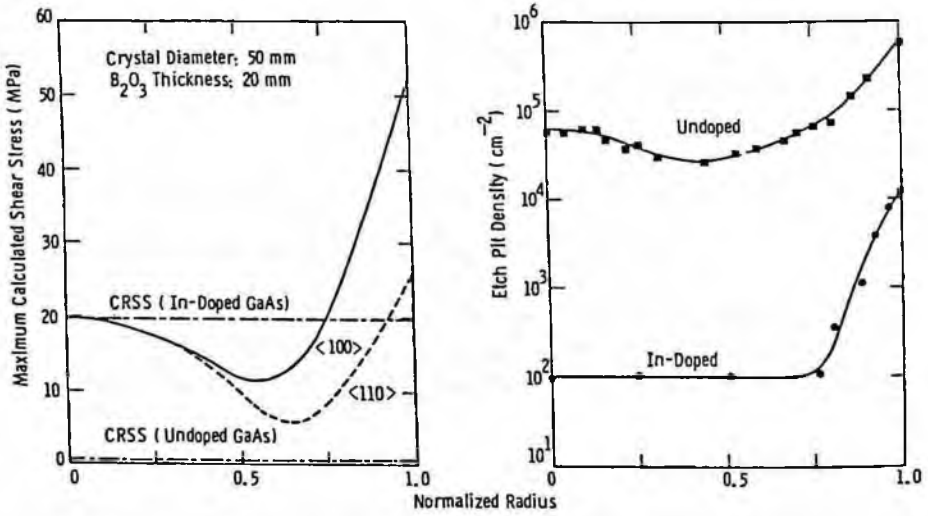

Fig. 4.10 Comparison of the maximum radial shear stress and measured etch pit density (EPD) in undoped and In-doped LEC GaAs crystals (reprinted from Ref. 64 with permission, copyright 1986 American Institue of Physics).

cation reduction by impurity hardening in InP has been theoretically analyzed by Jordan et al.[62] based on the quasi-steady state (QSS) heat transfer/thermal stress model as

explained in Sec. 3.5.

The mechanism of dislocation reduction in GaAs by In doping has been explained by the solute hardening model[63-65] as shown in Fig. 4.10 and the yield stress of In-doped GaAs has been measured.[66-68] There is some discrepancy in measured data but Guruswamy et al.[68] claimed that the CRSS increase by In-doping is sufficient to explain the dislocation reduction.

4.3.5 Lineages and Low Angle Grain Boundaries

Lineage is a defect of agglomeration of dislocations which are gathered as lines as shown in Fig. 15.36 for the case of CdTe. Lineages seem to occur when dislocations can easily move in a low dislocation density atmosphere when they can move without colliding. They are also formed even when the dislocation density is high if the density is so high that their tangling occurs easily. In any case, lineages are formed in small index planes and orientations since when dislocations agglomerate under these conditions, the total energy reaches a minimum. When the density of dislocations is increased and when these dislocations are aligned, it makes small angle grain boundaries[69] as shown in Fig. 4.11.

4.4 STACKING FAULT DEFECTS AND TWINS

Twins are plane defects which are made as shown in Fig. 4.12. There are several types of twins[60] but 60° rotation twins are known to be predominant in III-V materials. The ease of twin formation depends on the stacking fault energy of each material. As shown in Fig. 1.24, various compound materials have specific stacking fault energies. It is

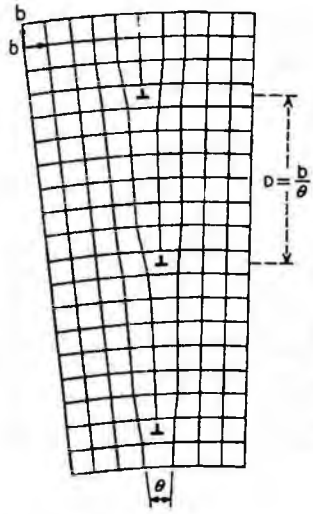

Fig. 4.11 Schematic representation of a tilt boundary composed of edge dislocations (reprinted from Ref. 69 with permission, copyright 1955 Elsevier).

known that crystals with lower stacking fault energies are normally difficult to grow without twins. Twin formation is however dependent on the crystal growth conditions and when the conditions are optimized, crystals can be grown without twins. In practice, the ease of twin formation is in the following order depending on the stacking fault energy[70] as explained in Sec. 1.7.2.

$$\text{CdTe, ZnSe} > \text{InP} > \text{GaAs, GaP} \tag{4.30}$$

The following have been considred as factors which affect twin formation.
(i) water content in the encapsulant B_2O_3[53]
(ii) seed orientation[53, 71, 72, 77]
(iii) conical growth angle[72, 73]
(iv) interface shape[72, 73]
(v) crucible and crystal rotation conditions[53]

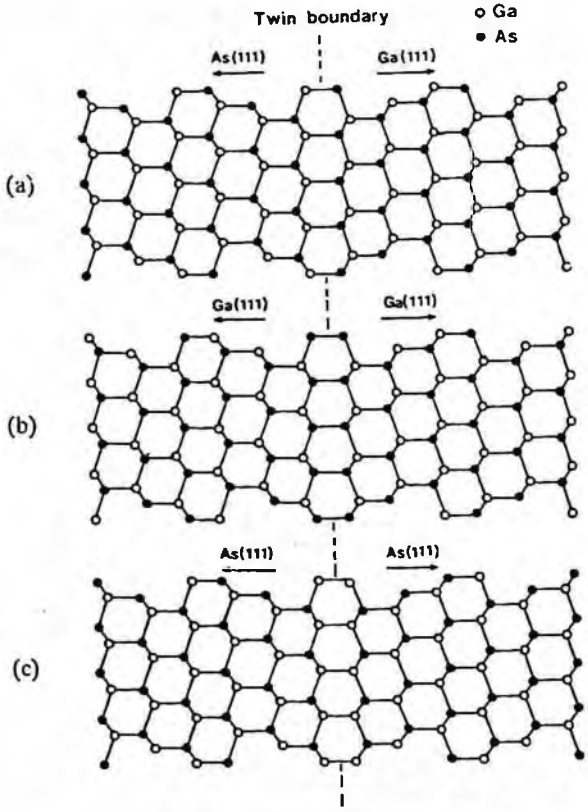

Fig. 4.12 Structure models of (a) 60° rotation twin, (b) inversion twin with As-As bonds at the twin boundary, and (c) inversion twin with Ga-Ga bonds at the twin boundary (reprinted from Ref. 80 with permission, copyright 1992 Elsevier).

(vi) melt composition/non-stoichiometry[53]
(vii) axial temperature gradient[53, 74]
(viii) temperature fluctuation[53, 75-77]
(ix) presence of scum[78]
(x) growth angle and crystal shape[63, 79]
(xi) facet growth[75]
(xii) growth rate[53]

Since it is known that twinning tends to occur during shoulder formation in CZ/LEC growth, twinning can be avoided by using large seed crystals or by growing with smaller or larger cone angles.

Twinning is a phenomenon which stems from an atomic plane stacking disorder as shown in Fig. 4.12 (a). Since twinning is thus only due to an atomic plane disorder during crystal growth, a small fluctuation of all the above factors can lead to twinning. These very sensitive factors have to be well controlled in industrial production.

The mechanism of twin formation has been discussed by various authors. It was first doubted that twin formation is like deformation twinning as in the case of metals but this assumption was denied by Billig and others.[81-83]

Hurle[84, 85] has discussed its mechanism for LEC crystal growth. According to his mechanism, twinning occurs when atomic steps in the solid-liquid interface are anchored to the three phase boundary among the solid-liquid, solid-gas, and liquid-gas as shown in Fig. 4.13. The free energy change due to the absorption of steps can be represented as

$$\gamma_e \, h = h \, (\sigma_{SG} - \sigma_{SL} \cos \nu - \sigma_{LG} \cos \Theta_L^0) / \sin \nu \qquad (4.31)$$

where Θ_L^0 is the contact angle of the meniscus to the crystal surface, ν the angle depicted in Fig. 4.13 and σ_{SG}, σ_{SL} and σ_{LG} the interfacial energies (L = liquid, S= solid and G = gas).

The maximum and the minimum of ν are given as

$$\gamma \sin \nu_{max} = \sigma_{SG} - \sigma_{SL} \cos \nu_{max} - \sigma_{LG} \cos \Theta_L \qquad (4.32)$$

and

$$\nu_{min} = \phi^0 - \cos \Theta_L \, . \qquad (4.33)$$

Here, ϕ^0 is the wetting angle given by the following equation.

$$\sigma_{SL} + \sigma_{LG} \cos \phi^0 = \sigma_{SG} \qquad (4.34)$$

Neglecting the torque terms in Eq. (4.31),

$$\sigma_{SL} \cos \upsilon = \sigma_{SG} - \sigma_{LG} \cos \Theta_L \qquad (4.35)$$

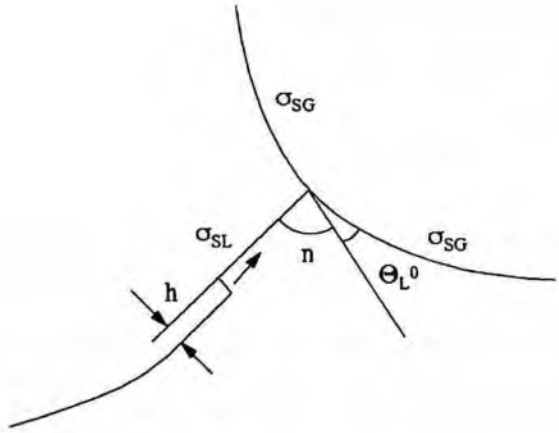

Fig. 4.13 Representation of the three phase boundary (TPB) having a facetted solid-liquid interface (reprinted from Ref. 85 with permission, copyright 1995 Elsevier)

A large value of v requires a small value of $(\sigma_{SG} - \sigma_{LG} \cos \Theta_L) / \sigma_{SL}$. Eliminating $\cos \Theta_L$ using Eq. 4.34, this criterion becomes

$$(\sigma_{SG} - \sigma_{SL})^2 / (\sigma_{LG}^2 - \sigma_{SL}^2)^2 \qquad (4.36)$$

When the value of Eq. 4.36 is smaller, the probability of the occurence of twins is supposed to become greater. Table 4.3 shows the calculated value for various semiconductor materials.[85]

The above mentioned twinning mechanism can explain the experimental results. It is known that in the case of Ge and Si, twinning occurrence is very rare while in the case of GaAs and InP, especially in the case of InP, twinning is well known to easily happen. Most twinning factors also can be explained by the above mechanism.[85]

From these considerations, it is concluded that the following procedures are effective in avoiding twin formation.

(i) Reduction of temperature fluctuation

(ii) Promotion of grown-out at well defined growth angles

Table 4.3 Parameter Related with Twinning Occurrence

Material	$(\sigma_{SG} - \sigma_{SL})^2 / (\sigma_{LG}^2 - \sigma_{SL}^2)^2$
Ge	0.87
Si	0.93
InSb	0.51
GaAs (CZ)	0.64
GaAs (LEC)	0.58
InP (CZ)	0.63
InP (LEC)	0.42

(iii) Growth from a melt in excess of one constituent
(iv) Elimination of surface-active solutes

4.5 FACETS AND STRIATIONS

Heterogeneous incorporation of impurities in grown crystals occurs in the form of striations.[86] Striations are due to variations in the segregation of impurities and/or that of the constituent composition. Striations therefore occur due to variations in growth conditions such as the growth rate, the rotation speed and the melt composition.[87-89] In considering striations, not only the perpendicular macroscopic crystal growth but also the lateral microscopic growth have to be considered. Unsteady buoyancy convection in the melt during crystal growth also gives rise to irregular striations. The origin of unsteady buoyancy convection is discussed in Sec. 6.3.3. Striations can be revealed mainly by appropriate etching and by scanning electron microscopic observation as explained in Sec. 5.4.4.

Striations can be classified into six types, three as non-rotational striations (types 1-3) and three as rotational striations (types 4-6) as shown in Fig. 4.14, from the study of the crystal growth of InSb.[90] Non-rotational striations stem from growth rate variations due to the temperature fluctuation or variation of the pulling rate. Rotational striations are due to crucible or crystal rotations and they are rather more pronounced than non-rotational striations so that they can be observed even at lower impurity concentration. Explanation of each type of striation can be seen in Ref. 90.

To avoid striations, the following procedures are effective in practical crystal growth.

(i) Reduction of impurity doping concentrations by growth under low temperature gradients.

(ii) Reduction of temperature fluctuations by improving the furnace configuration (Sec. 10.3.3) and/or by the application of a magnetic field (Sec. 4.4).

(iii) Reduction of mechanical variation of rotations and pulling speed.

Other methods for avoiding striations, such as the reduction of gravity by growing crystals in space and the use of Coriolis force as applied in a centrifuge have been studied.[91, 92]

4.6 PRECIPITATES, INCLUSIONS AND VOIDS

There are two types of precipitates. One is due to non-stoichiometry and the other is due to impurities. These precipitates are undesirable because they locally change the properties of semiconductors. They are also undesirable in the production of high quality polished substrates, because they are dropped off and leave pits on the mirror-polished surfaces.

In most compound semiconductors, departure from the stoichiometric composition is inevitable. This makes it possible for the material to generate precipitates. If the congruent point of the phase diagram departs from the stoichiometric composition, the excess constituent atoms will form precipitates depending on the thermal history. Examples of this are often seen in the case of GaAs, CdTe and other crystals as explained

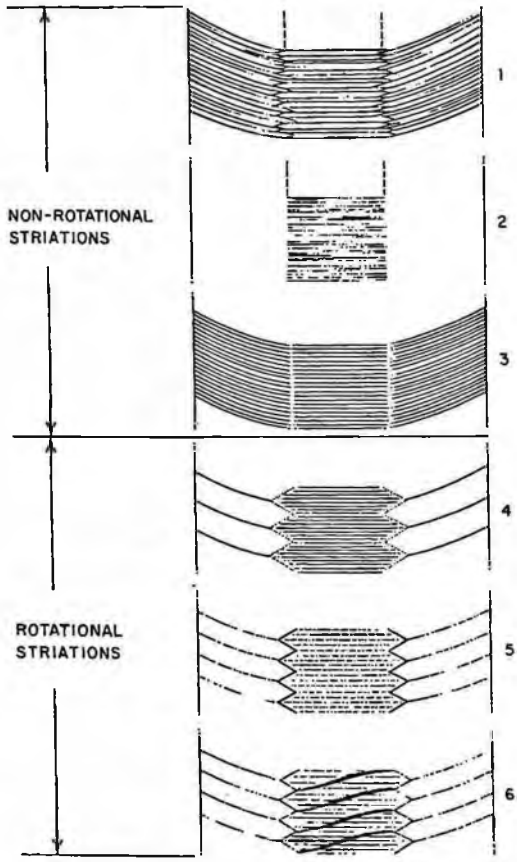

Fig. 4.14 Schematic diagram of impurity striations encountered in InSb single crystals (reprinted from Ref. 90 with permission of The Electrochemical Society)

from Chapter 7 on.

Impurities also form precipitates. If the solid solubility of the impurities is low, they can easily form precipitates. These impurities are in many cases transition metals whose solubility limit is small and which are used as dopants in the preparation of semi-insulating materials.

REFERENCES

1. C. Wagner, *Thermodynamics of Alloys* (Addison-Wesley, Cambridge, 1952).
2. F. Seitz, *Imperfections in Nearly Perfect Crystals* (John Wiley & Sons, New York, 1952).
3. K. Hauffe, *Reaktionen in und an Festen Stoffen* (Springer Verlag, Berlin, 1955).
4. F.A. Kröger and H.J. Vink, in *Solid State Physics Vol. 3*, eds. F. Seiz and D. Turnbull (Academic Press, New York, 1956) p. 307.
5. F.A. Kröger, *The Chemistry of Imperfect Crystals* (North Holland, Amsterdam, 2nd ed. 1974)
6. R.A. Swalin, *Thermodynamics of Solids* (John Wiley & Sons, New York, 1962)
7. G. Brouwer, *Philips Res. Rep.* 9 (1954) 366.
8. M.M. Hennenberg and D.A. Stevenson, *phys. stat. sol.* (b) **48** (1971) 255.

9. E.C. Casey, in *Atomic Diffusion in Semiconductors*, ed. D. Shaw (Plenum, New York, 1973) p. 351.
10. J. Crank, *The Mathmatics of Diffusion* (Oxford University Press, London, 1956)
11. P.G. Shewmon, *Diffusion in Solids* (McGraw-Hill, London, 1981).
12. *Atomic Diffusion in Semiconductors*, ed. D. Shaw (Plenum, London, 1988).
13. R.M. Logan and D.T. L. Hurle, *J. Phys. Chem. Solids* **32** (1971) 1739.
14. D.T.H. Hurle, *J. Phys. Chem. Solids* **40** (1979) 613.
15. H. Wenzl, A. Dalhen, A. Fattah, S. Petersen, K. Mika and D. Henkel, *J. Crystal Growth* **109** (1991) 191.
16. J. Nishizawa, *J. Crystal Growth* **99** (1990) 1
17. J. Nishizawa, *Non-Stoichiometry in Semiconductors*, eds. K.J. Backmann, H.L. Hwang and C. Shcwab (North-Holland, Amsteradm, 1992) p. 95.
18. J. Nishizawa and Y. Oyama, *Mater. Sci. Engineer.* **R12** (1994) 273.
19. G. Mandel, *Phys. Rev.* **134** (1964) A1073.
20. G. Mandel, F. Morehead and P.R. Wagner, *Phys. Rev.* **136** (1964) A826.
21. J.P. Dismukes, *RCA Review* **31** (1971) 1717.
22. Y. Marfaing, *Prog. Crystal Growth Character.* 4 (1981) 317, *Rev. Phys. Appl.* **12** (1977) 211.
23. H. Kukimoto, in *Growth and Optical Properties of Wide-Gap II-VI Low-Dimensional Semiconductors*, ed. T.C. McGill, (Plenum, New York, 1989) p. 119.
24. Nishizawa, Y. Okuno and K. Suto, in *Semiconductor Technologies* (Ohmsha and North-Holland, Tokyo, 1986) p. 17.
25. Y. Marfaing, *J. Crystal Growth* **161** (1996) 205.
26. T. Ido, A. Heurtel, R. Triboulet and Y. Marfaing, *J. Chem. Solids* **48** (1987) 781.
27. D.B. Laks, C.G. Van de Walle, G.F. Neumark and S.T. Pantelides, *Appl. Phys. Lett.* **63** (1993) 1375.
28. L. Shceerback, P. Feichouk, P. Fochouk and P. Panchouk, *J. Crystal Growth* **161** (1996) 219.
29. D.J. Chadi, *Appl. Phys. Lett.* **59** (1991) 3589.
30. D.J. Chadi, *Phys. Rev. Lett.* **72** (1994) 534.
31. C.H. Park and D.J. Chadi, *Phys. Rev. Lett.* **75** (1995) 1134.
32. G. F. Neumark, *J. Appl. Phys.* **57** (1985) 3383.
33. G.F. Neumark, *Phys. Rev. Lett.* **62** (1989) 1800.
34. W. Faschinger, S. Ferreira and H. Sitter, *J. Crystal Growth* **151** (1995) 267.
35. W. Faschinger, *J. Crystal Growth* **159** (1996) 221.
36. J.C. Pfister, *Rev. Phys. Appl.* **15** (1980) 707.
37. J.L. Pautrat, N. Magnea and J.P. Faurie, *J. Crystal Growth* **53** (1982) 8668.
38. J.L. Pautrat, J.M. Francou, N. Magnea, E. Molva and K. Saminadayar, *J. Crystal Growth* **72** (1985) 194.
39. K. Igaki, *Solid Physics (in japanese)* **17** (1982) 97.
40. N. Bhargava, *J. Crystal Growth* **59** (1982) 15.
41. N.V. Agrinskaya and T.V. Mashovets, *Semiconductors* **28** (1994) 843.
42. U.V. Desnica, *Vacuum* **50** (1998) 463.
43. K. Sumino, *Mater. Sci. Technol.* **11** (1995) 667.
44. K. Wada, *Appl. Phys. Sci.* **85** (1995) 246.
45. Y.Y. Loginov, P.D. Brown and C.J. Humphreys, *Mat. Res. Soc. Symp. Proc.* **373** (1995) 529.
46. W.T. Read Jr., *Dislocations in Crystals* (McGraw-Hill, New York, 1953).
47. J. Weertman and J.R. Weertman, *Elementary Dislocation Theory* (Macmillan, 1964).
48. J.P. Hirth and L. Lothe, *Theory of Dislocations* (John Wiley & Sons, New York, 1982)
49. K. Sumino, *Handbook of Semiconductors; Completely Revised Edition*, ed. by T.S. Moss (Elsever Sci., Amsterdam, 1994) p. 73.
50. I. Yonenaga, *J. Phys. III France* 7 (1997) 1435.
51. H. Siethoff, *Phil. Mag. Lett.* 66 (1992) 1.
52. S. Gurusway, K.T. Faber and J.P. Hirth, in *Semiconductors and Semimetals Vol.37*, eds. R.K. Willardson and A.C. Beer (Academic Press, New York, 1992) p. 189.

53. O. Oda, K. Katagiri, K. Shinohara, S. Katsura, T. Takahashi, K. Kainosho, K. Kohiro and R. Hirano, in *Semiconductors and Semimetals Vol. 31*, eds. R.K. Willardson and A.C. Beer (Academic Press, New York, 1990) p. 93.
54. W.C. Dash, *J. Appl. Phys.* **29** (1958) 736.
55. W.C. Dash, *J. Appl. Phys.* **30** (1959) 459.
56. W. C. Dash, in *Growth and Perfection of Crystals*, eds. R. M. Doremus, B. W. Roberts and D. Turnbull (Wiley, New York, 1958) p. 361.
57. A. Steinemann and U. Zimmerli, J. *Phys. Chem. Solid. Suppl.* **1** (1967) 81.
58. B. C. Grabmaier and J. G. Grabmaier, *J. Crystal Growth* **13/14** (1972) 635.
59. S. Shinoyama, C. Uemura, A. Yamamoto and S. Tohno, *Jpn. J. Appl. Phys.* **19** (1980) L331.
60. M. Seki , H. Watanabe and J. Matsui, *J. Appl. Phys.* **49** (1978) 822.
61. T. Kamejima, J. Matsui, Y. Seki and H. Watanabe, *J. Appl. Phys.* **50** (1979) 3312.
62. A.S. Jordan, G.T. Brown, B. Cockayne, D. Brasen and W.A. Bonner, *J. Appl. Phys.* **58** (1985) 4383.
63. H. Ehrenreich and J.P. Hirth, *Appl. Phys. Lett.* **46** (1985) 668.
64. S. McGuigan, R.N. Thomas, D.L. Barrett and B.W. Swanson, *Appl. Phys. Lett.* **48** (1986) 1377.
65. S. McGuigan, B.W. Swanson and R.N. Thomas, *J. Crystal Growth* **94** (1989) 75.
66. M.G. Tabache, E.D. Bourret and A.G. Elliot, *Appl. Phys. Lett.* **49** (1986) 289.
67. H.M. Hobgood, S. McGuigan, J.A. Spitznagel and R.N. Thomas, *Appl. Phys. Lett.* **48** (1986) 1654.
68. S. Guruswamy, J.P. Hirth, K.T. Faber, *J. Appl. Phys.* **60** (1986) 4136.
69. R.G. Shulman, in *Semiconductors*, ed. N.B. Hannay (Maruzen, 1959) p. 482.
70. H. Gottschalk, G. Patzner and H. Alexander, *phys. stat. sol. (a)* **45** (1978) 207.
71. K.F. Hulm and J.B. Mullin, *Solid State Electron.* **5** (1962) 211.
72. W.A. Bonner, *J. Crystal Growth* **54** (1981) 21.
73. A.N. Buzynin, V.A. Abtinov, V.V. Osino and V.M. Tatarintsev, *Izv. Akad. Nauk SSSR, Ser. Fiz.* **52** (1988) 1889.
74. G.W. Iseler, *J. Crystal Growth* **54** (1981) 16.
75. M. Shibata, Y. Sasaki, T. Inada and S. Kuma, *J. Crystal Growth* **102** (1990) 557.
76. A. Steinemann and U. Zimmeerli, *Solid-State Electron.* **6** (1963) 597.
77. J.P. Tower, R. Tobin, P.J. Pearah and R.M. Ware, J*J. Crystal Growth* **114** (1991) 665.
78. K. Matsumoto, in *Bulk Crystal Growth Technology* (Gordon and Breach, New York, 1989) p. 169.
79. S. Shinoyama and C. Uemura, *J. Mater. Sci. Soc. Jpn. (in japanese)* **21** (1985) 273.
80. T. P. Chen, F. R. Chen, Y. C. Cyuang, Y. D. Guo, J. G. Peng, T. S. Huang and L. J. Chen, *J. Crystal Growth* **118** (1992) 109.
81. E. Billig, *J. Inst. Metals* **83** (1954/5) 53.
82. A.T. Churchman, G.A. Greach and J. Winton, *Proc. Roy. Soc. A* **238** (1956) 194.
83. G.T. Brown, B. Cockayne and W.R. McEwan, *J. Mater. Sci.* **15** (1980) 1469.
84. D.T.J. Hurle, *Sir Charles Frank 80th Birthday Tribute*, eds. R.G. Chambers, J. Enderby, A. Keller, A.R. Lang and J.W. Steeds (Hilger, Bristol, 1991) p. 188.
85. D. T. J. Hurle, *J. Crystal Growth* **147** (1995) 239.
86. F. Rosenberger, in *Fundamentals of Crystal Growth I* (Springer-Verlag, Berlin, 1979) Chapter 6.
87. K. Morizane, A.F. Wit and H.C. Gatos, *J. Electrochem. Soc.* **114** (1967) 738.
88. K.M. Kim, A.F. Witt and H.C. Gatos, *J. Electrochem. Soc.* **119** (1972) 1218.
89. A.F. Witt, M. Lichtensteiger and H.C. Gatos, *J. Electrochem. Soc.* **120** (1973) 119.
90. A.F. Witt and H.C. Gatos, *J. Electrochem. Soc.* **113** (1966) 808.
91. G. Müller, *J. Crystal Growth* **99** (1990) 1242.
92. G. Müller, G. Neumann and W. Weber, *J. Crystal Growth* **119** (1992) 8.

5. CHARACTERIZATION

5.1 INTRODUCTION

In producing high quality bulk compound semiconductor materials, appropriate crystal characterization is indispensable. It is therefore necessary for material scientists to have knowledge of various characterization techniques and to have the ability to select the appropriate ones. In many cases, characterization takes a long time. It is therefore important to select the most effective characterization method depending on the material to be developed. In Table 5.1, various characterization methods are summarized and in Ref. 1, most of them are explained. It should be also noted that characterization methods are rapidly developed year by year and that it is important to be always acquainted with new methods. In several international conferences,[2] these developments can be followed.

5.2 X-RAY DIFFRACTION

5.2.1 Orientation Determination

The most common X-ray diffraction method for the determination of crystal orientation is the Laue method.[3, 4] This method however is used only in the first stage of the crystal growth experiments. Once the conditions for growing a crystal of a certain orientation are determined, it becomes important to determine the precise crystal orientation to an accuracy of 0.01 degrees.

The cut-off plane diffraction method[5] is applied for this precise measurement. This method is based on a diffractometer but the reflection angle against an arbitrary zero angle is measured for two orientations 180 degrees apart and the deviation angle can be calculated from the two values. The same measurement is performed for the orthogonal direction and from two deviation angles, the precise orientation of the grown crystal is determined. The precise measurement of orientation is industrially performed for all crystals as a routine procedure because the orientation is crucial for the quality of epitaxial layers.

5.2.2 Multiple Crystal X-ray Diffraction

Various multiple crystal X-ray diffraction methods are often used for evaluating the crystallinity of grown crystals.

Double crystal X-ray diffraction (DCXD)[6] (Fig. 5.1) is an effective way to examine the crystallinity in the first stage of bulk material development. The incident X-ray is first reflected by the first reference crystal and the reflected X-ray is directed on to the sample crystal and the reflected X-ray intensity is measured as a function of the incident angle. The basis of this method is in that wavelength dispersion and angle dispersion can be largely reduced because X-ray diffraction occurs only when plane of reflection in the reference crystal and that in the sample crystal are parallel.

Table 5.1 Various Characterization Methods

Technique	Method	Characterization
X-ray diffraction		
	Cutoff plane measurement	Precise determination of crystal orientation
	Double crystal X-ray diffraction	Crystallinity
	Five crystal X-ray diffraction	Crystallinity
	Transmission X-ray topography (Lang method)	Defects in bulk crystals
	Reflection X-ray topography (Berg-Barret method)	Defects in surface region
	Bond method	Precise determination of lattice constant
Electron beam irradiation		
	Transmission electron Microscope	Dislocations, precipitates Microscopic defects
	EBIC	Defects in bulk crystals
Optical characterization		
	Photoluminescence	Recombination centers
	Chatodoluminescence	Recombination centers
	IR transmission microscopy	IR-non-transparent defects
	IR scattering tomography	Microscopic defects
Electrical characterization		
	Hall measurement	Electrical properties
	C-V measurement	Carrier profile
	DLTS	Deep levels
	ICTS	Deep levels
	TSC	Deep levels
	Three guard electrode method	Non-uniformity of electrical properties
Composition analysis		
	SSMS	Purity
	SIMS	Purity
	GDMS	Purity
	FT-IR	Light element analysis
	Coulometric titration	Non-stoichiometry

The most sophisticated but easily applicable method is the five crystal X-ray diffraction method[7] in which a monochromator consisting of four Ge crystals is used to obtain a monochronized X-ray beam as shown in Fig. 5.2. By the -/- arrangement between the b crystal and the c crystal, a monochronized X-ray beam with 5 arcsec and 12 arcsec full width of the half maximum (FWHM) can be obtained respectively for (440) and (220) Ge crystals. In this method, it is not necessary to use the first reference crystal which is the same as the sample crystal as in the case of the double crystal X-ray diffraction. Secondly, since the monochronized X-ray beam is aligned by the a and d crystals as an incident beam, it is not necessary to align all the crystals for appropriate diffraction to occur. The five crystal X-ray diffraction (Fig.5.2) is therefore the most

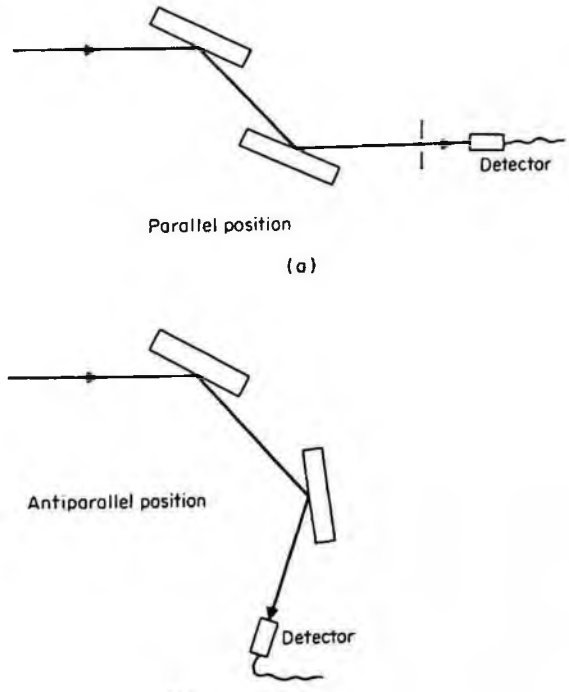

Fig. 5.1 Two geometries for double crystal X-ray diffraction. (a) parallel arrangement and (b) antiparallel arrangement (from Ref. 6 with perimssion, copyrright 1975 McGraw-Hill).

simple and precise method for measuring the rocking curve.

The FWHM of the rocking curve is a useful parameter for evaluating the crystallinity. The FWHM can be calculated theoretically as

$$\theta = \sqrt{\frac{\cos\theta_1}{\cos\theta_2}}\,\frac{3\sqrt{2\,|\psi_h|}}{2\sin 2\Theta} \qquad (5.1)$$

here, Θ is the Bragg angle, θ_1 the incident angle to the crystal surface and θ_2 the output angle and

$$|\psi_h| = \frac{1}{\pi}\left(\frac{e^2}{mc^2}\right)\frac{\lambda^2\,|F_h|}{v}. \qquad (5.2)$$

Here, $|F_h|$ is the structure factor, λ the wavelength, v the cell volume, e the unit charge, m the electron mass and c the speed of light.

In practice, the FWHM is expressed as

$$\Delta\theta^2 = \sqrt{\Delta\theta_i^2} \quad (i = 1, 2, 3\ldots) \qquad (5.3)$$

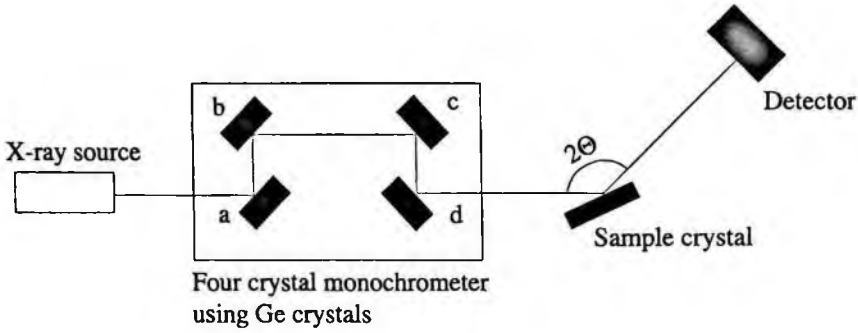

Fig. 5.2 Five-crystal X-ray diffraction system.

in which the FWHM of all reference crystals is superimposed.

It also should be noted that the irradiation area affects the FWHM so that the same irradiation area must be used to compare the crystallinity in various samples.

When the sample crystal is a perfect crystal with good crystallinity, the FWHM is very close to the theoretical value. When the sample has cell structures because of high dislocation density even though it is a single crystal from Laue diffraction, the FWHM becomes very large because diffraction from each cell occurs as a function of the scanning angle.

It therefore should be noted that to develop high quality compound semiconductor materials, it is essential to evaluate the FWHM, and that the FWHM must be close to the theoretical value. Normally below 20 arcsec is a significant criterion for high quality materials.

5.2.3 X-ray Diffraction Topography

By scanning the sample and the film together as shown in Fig. 5.3, a two dimensional X-ray diffraction pattern can be obtained[8,9] and this method is known as X-ray diffraction topography. There are two configurations as shown in Fig. 5.3, one is based on the transmission of X-rays, the Lang method (Fig. 5.3(a)) and the other is based on the reflection of X-rays, the Berg-Barret method (Fig. 5.3(b)). Each method has its own advantages.

(1) Lang method

The Lang method is mainly used to examine dislocation distributions. Most compound semiconductor materials have a relatively high absorption coefficient for X-rays. In the case of the transmission method, it is therefore necessary for the sample to have a long X-ray exposure time. In this sense, the Lang method is not convenient for routine material evaluation. The Lang method is therefore used to examine the material in the first stage of its development.

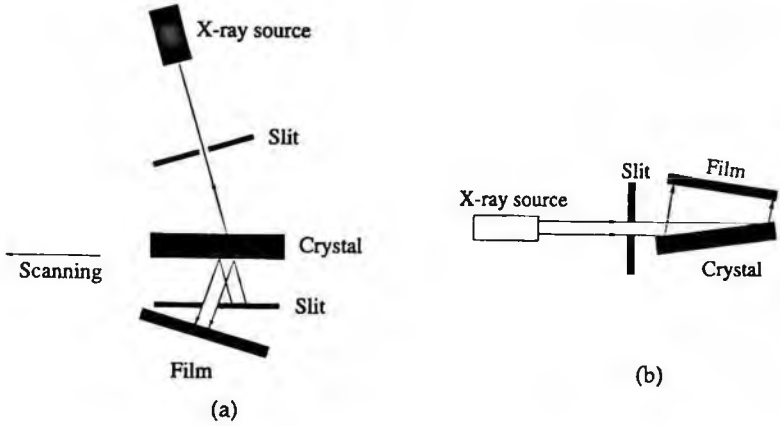

Fig. 5.3 X-ray topographic diffraction arrangement. (a) Lang method and (b) Berg-Barret method.

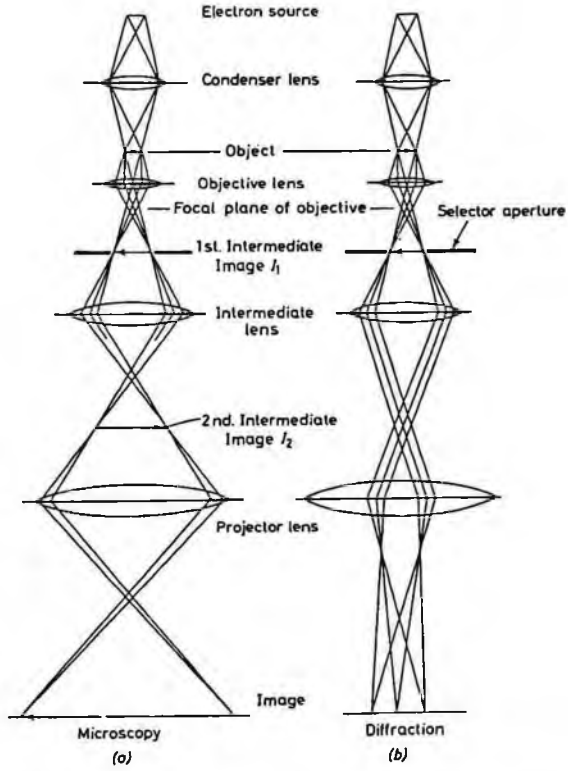

Fig. 5.4 Ray paths in the electron microscope. (a) Under microscopy conditions and (b) diffraction conditions (reprinted from Ref. 12 with permission, copyright 1965 Elsevier).

(2) Berg-Barret method

Since this method is based on the reflection of X-rays,[10, 11] it is easy to obtain figures with a short exposure time. The information is however limited to the surface regions, thus this method is convenient for examining the surface defect distribution. This method is therefore used to examine residual defects in polished wafers.

5.3 ELECTRON IRRADIATION

5.3.1 Transmission Electron Microscopy (TEM)

Using electron transmission,[12, 13] defects in the material can be observed at high resolution. Fig. 5.4 shows a typical arrangement for transmission electron microscopy. For this observation, it is necessary to prepare a very thin sample so that electrons can pass through the sample. For this, the ion milling method is used. This method is used for examining and identifying very small microscopic defects. A typical example is the case of the investigation of arsenic precipitates in GaAs. Fig. 5.5 shows an arsenic precipitate observed by TEM. It is also possible to know the composition of this precipitate by energy dispersive X-ray (EDX) micro analysis as shown in the figure.[14]

5.3.2 Electron Beam Induced Current (EBIC)

This method is based on the electron beam induced current which flows in a Schottky

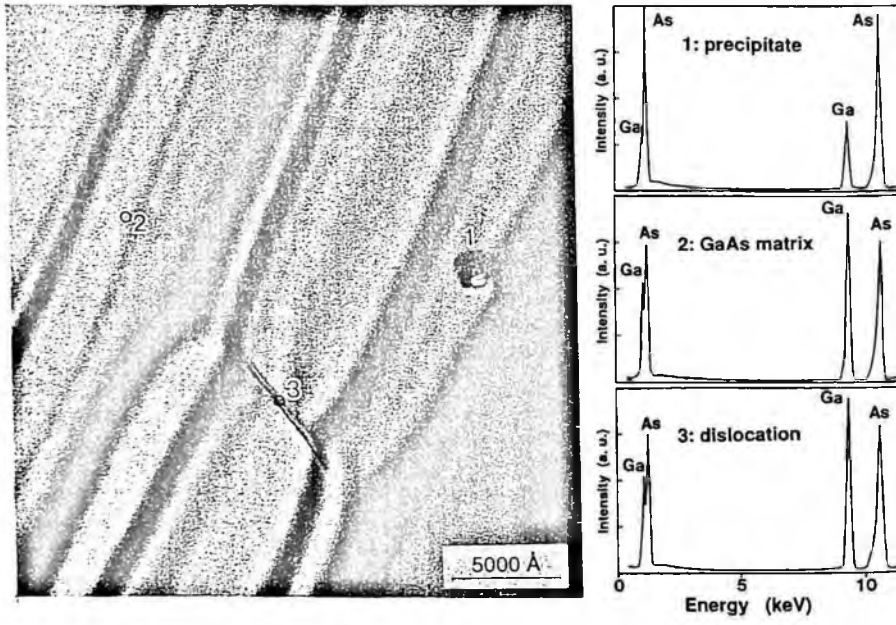

Fig. 5.5 TEM micrograph with an arsenic precipitate in GaAs. EDX spectra measured for selected areas are shown (1: arsenic precipitate, 2: GaAs matrix, 3: dislocation) (reprinted from Ref. 14 with permission, copyright 1990 Elsevier).

configuration.[15] On the surface of a sample to be measured, a very thin plane electrode is deposited. The thickness of the electrode film must be sufficiently thin for the irradiated electron beam to penetrate it. Since electrons with high energy of more than 20 keV generate electron-hole pairs, these excited electrons and holes can be made to flow via Schottky diodes as shown in Fig. 5.6. It is known that the resolution is better for EBIC than for cathodoluminescence (Sec. 5.4.2).

5.4 OPTICAL CHARACTERIZATION

Most optical characterization techniques tend to be based on simple methods and they are frequently used in the development of compound semiconductor materials.

5.4.1 Photoluminescence (PL)

Photoluminescence characterization has been used very frequently for assessing the quality of compound semiconductors. The principle and characterization examples are explained in Refs. 17-21. A typical basic photoluminescence measurement is performed by an arrangement as shown in Fig. 5.7.[20] To perform a photoluminescence measurement, it is necessary to irradiate the sample with light of a wavelength whose energy is larger than the band gap of the material. Thus, lasers such as He-Ne lasers, Ar lasers and He-Cd lasers are used depending on the band gap of the materials to be examined. As a result, electron-hole pairs are generated between the valence band and the conduction band and they recombine by the various processes shown in Fig. 5.8. During these recombinations, luminescence is observed for each process except in the case of non-radiative recombinations. To observe the luminescence, appropriate photodetectors must be selected choosing from InAs detectors, Ge detectors and GaAs detectors.

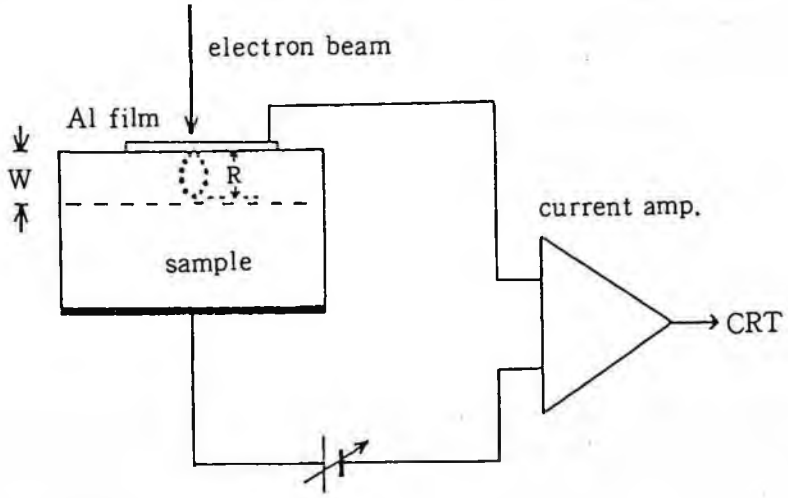

Fig. 5.6 Electron Beam Induced Current (EBIC) measurement (from Ref. 16 with permission).

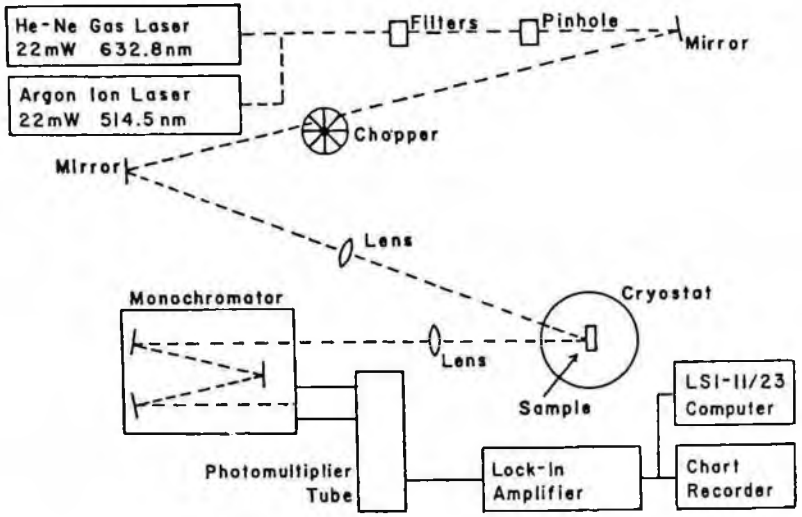

Fig. 5.7 Block diagram of a photoluminescence spectrum measurement system (reprinted from Ref. 22 with permission, copyright 1985 American Institue of Physics).

Principally, basic photoluminescence peaxplained in Table 5.2 are observed. These peaks are categorized in three regions.

(1) Edge emissions

These are based on transitions between free electrons and free holes (Fig. 5.8(a)), those of free excitons (Fig. 5.8(b, c), those of excitons bound with donors or acceptors (Fig. 5.8(d-f)), and those between free electrons and holes bound with shallow acceptors

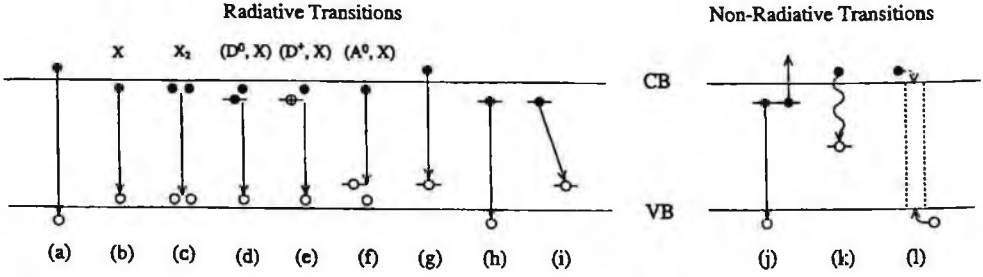

Fig. 5.8 Various transitions in photoluminescence. (a) intraband transition, (b) free exciton, (c) exciton molecule, (d) neutral donor and exciton, (e) ionized donor bound exciton, (f) neutral acceptor bound exciton, (g) free electron to hole captured at an acceptor, (h) electron captured at a donor to free hole, (i) donor-acceptor pair, (i) Auger transition, (k) phonon emission, (l) pipe transition.

Table 5.2 Various Emissions for Photoluminescence

Emissions	Transitions	Nomenclature
Edge Emissions	Direct transition	
	Free excitons	X
	Exciton impact	X-X
	Exciton molecules	X_2
	Exciton bound to neutral acceptors	(A^0, X) or I_1
	Exciton bound to neutral donors	(D^0, X) or I_2
	Exciton bound to ionized acceptors	(A^-, X)
	Exciton bound to ionized donors	(D^+, X) or I_3
	Electrons - shallow acceptors	
	Holes-shallow donors	
Donor-Acceptor Pairs	Shallow donor to shallow accepter	(D, A)
Deep Levels	Deep donors, deep acceptors	

(Fig. 5.8(g)) or between free holes and electrons bound with donors (Fig. 5.8(h)).

The energy for interband transition (Fig. 5.8(a)) is simply the bandgap energy. The observation of this transition is however very rare.

The exciton transition energy (Fig. 5.8(b) can be represented as

$$h\nu = E_g - E_x \tag{5.4}$$

Here, E_x is the binding energy of excitons and is represented as follows.

$$E_x = - m_r^* q^4/2h^2\varepsilon^2 n^2 \tag{5.5}$$

Here, n is an integer $\geqq 1$ indicating the various exciton states and m_r^* is the reduced mass represented as

$$\frac{1}{m_r^*} = \frac{1}{m_e^*} + \frac{1}{m_h^*} \tag{5.6}$$

where m_e^* and m_h^* are electron and hole effective masses, respectively. Depending on the orbit number, n, distinct sharp lines can be observed when the material is very pure.

When the density of excitons is increased by increasing the excitation intensity, exciton impact occurs with emission energy of

$$h\nu_{X\text{-}X} = E_g - 2E_x \tag{5.7}$$

When two excitons are bound as a molecule, it is called a exciton molecule. When one of these excitons diminishes with recombination, it emits light with the following energy,

$$h\nu_m = E_g - E_x - E_m \tag{5.8}$$

where E_m is the binding energy of two excitons and is 0.33 E_x.

Phonon replica lines for exciton transitions can be observed for the following energies, when the recombination includes lattice vibrations.

$$h\nu_{LO} = E_g - E_x - nh\omega_{LO} \tag{5.9}$$

Bound exciton lines can be observed for the following energies, depending on the binding energies for bound excitons. There are several bound excitons, with neutral donors or accepters, and with ionized donors and acceptors, as shown in Fig. 8.10.

$$h\nu_{BX} = E_g - E_x - E_{BX} \tag{5.10}$$

(2) Donor-Acceptor (D-A) pair emissions

These are based on the transitions between acceptors and donors. These emissions are observed when impurities are at higher concentrations. These emissions are therefore used as an indicator of the purity of materials. The energies for D-A pair transition can be represented as follows.

$$h\nu_{DA} = E_g - (E_d + E_a) + \frac{e^2}{\varepsilon R} \tag{5.11}$$

Here, R is the distance between the donor and the acceptor to which the neighboring carriers are bound. Since the distance R has a distribution, the D-A pair emission has various wavelength so that the D-A pair transition shows rather broad emission lines.

When the level of donors and acceptors is shallow, D-A emission can be observed only at low temperatures so that this emission is not interesting for applications but is important to determine precisely the levels of shallow donors and acceptors. When the level of donors or acceptors is deeper, D-A emission can be observed at room temperature and is important for applications to LEDs.

(3) Deep level emissions

Via various deep levels, excited electrons and holes recombine resulting in lower intensity of edge emissions and DA pair emissions. Photoluminescence is a semi-quantitative method for evaluating material quality. In principle, for undoped pure materials, good quality material shows highly resolved free exciton peaks. It should be also noted that when the number of deep level defects is low, highly resolved photoluminescence is observed.

(4) Non-recombination transitions

Except for the above mentioned radiative recombination transitions which can be observed as light emissions, there are non-recombination transitions as shown in Fig. 5.8 (j-l). They are Auger transitions, phonon emissions and recombinations through defects or inclusions. These transitions decrease the total radiative recombinations. When the total photoluminescence intensity is weak, it must be considered that the material includes these non-recombination centers.

5.4.2 Scanning photoluminescence (SPL)

Recently, room temperature scanning photoluminescence has been developed whose space resolution is raised 3 μm.[23-28] An example of the configuration of scanning photoluminescence is shown in Fig. 5.9. Since a high speed Si photodetector is used for the

detection of luminescence, short duration light irradiation is possible and this high speed irradiation avoids the light irradiation decay. This is the reason why photoluminescence mapping with good resolution has become possible. A PL topograph system has also been developed for examining defect propagation from substrate to epitaxial layers, as demonstrated for InGaAsP/InP.[27]

5.4.3 Cathodoluminescence (CL)

Cathodoluminescence is a luminescence which occurs when the material is irradiated by high energy electron irradiation.[15, 29-31] As shown in Fig. 5.10, an electron beam is scanned in a scanning electron microscope and luminescence light is gathered by a mirror and detected by a detector such as a photomultiplier. The electrical signal is then input to a CRT display which is tuned. By this configuration, microscopic luminescence non-uniformity can be observed with high resolution. Cathodoluminescence is a simple method to observe the optical uniformity of compound semiconductor materials with better resolution than PL.

The advantage of CL is in that the beam can be focused to 10 nm easily and can be scanned to obtain two-dimensional non-uniformity. When the accelerating voltage is changed, information depending on the depth can be obtained. Since the electron energy is high, wide bandgap materials can be easily characterized.

5.4.4 IR Transmission Micrography

Since most compound semiconductor materials have bandgaps below which IR light is transmitted, the material can be observed as it is transparent by this method, and this

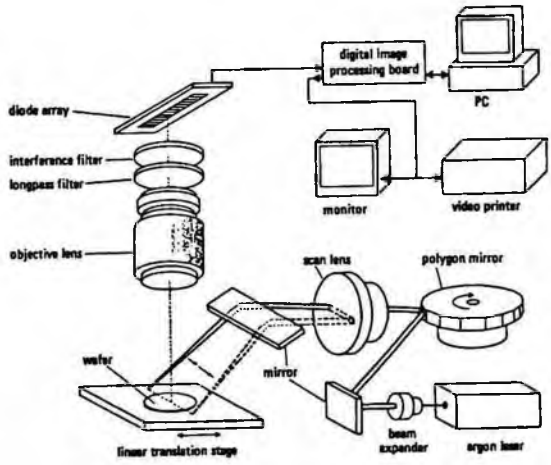

Fig. 5.9 Schematic diagram of a photoluminescence scanner (from Ref. 28 with permission).

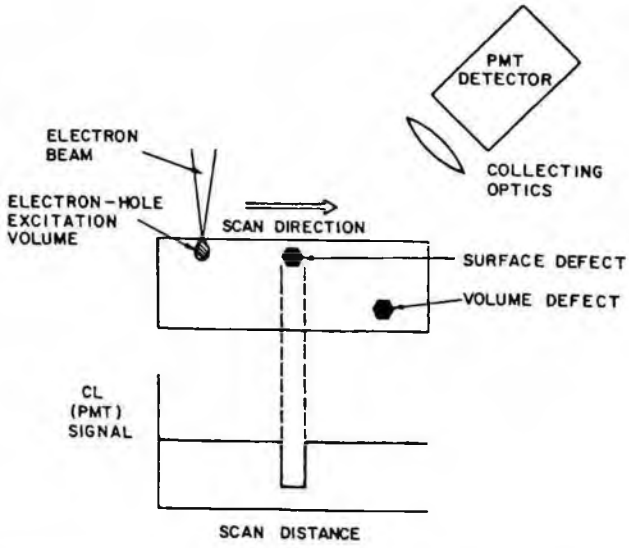

Fig. 5.10 Principle of cathodoluminescence (reprinted from Ref. 31 with permission, copyright 1979 American Institue of Physics).

has been used to evaluate crystal qualities.[32-37] Fig. 5.11 shows a typical IR transmission microscope configuration. This method is an effective method to observe precipitates which are not transparent to infrared light. Since it can be focused as a normal microscope, it is easy to observe precipitate distribution in depth. By using crossed Nicoles to polarize the incident and to analyze transmitted light, it is also possible to observe stresses in materials, due to the stress-induced birefringence depending on the photoelastic properties of the material. In fact, it has been proved by Bond and Andrus[32] and Jenkins et al.[33] that the stress field due to dislocations can be observed. Various observation examples for GaP, GaAs and InP have been shown by Elliott et al.[34,35] and Cao and Witt.[36] Carlson and Witt[37] have developed an IR transmission system to observe striations in grown crystals from the microscopic measurement of free charge carriers.

5.4.5 IR Scattering Tomography

As mentioned above, most semiconductor materials are transparent to infrared light. When the scattered infrared light can be observed, it is known that high resolution observation becomes possible. This is because the observation is based on the Tyndall phenomenon,[38,39] allowing extreme resolution (down to several hundred Å) far beyond the conventional resolution of the level of the light wavelength.[40,41] From the viewpoint of diffraction, this method is similar to the small-angle X-ray scattering and the scattering intensity is dependent on $\sin\theta / \lambda$ where 2θ is the diffraction angle and λ is the wavelength of the incident light. Since the wavelength of infrared light is 10^4 times longer than that of X-rays, 90 angle light scattering is possible, where the reflection of

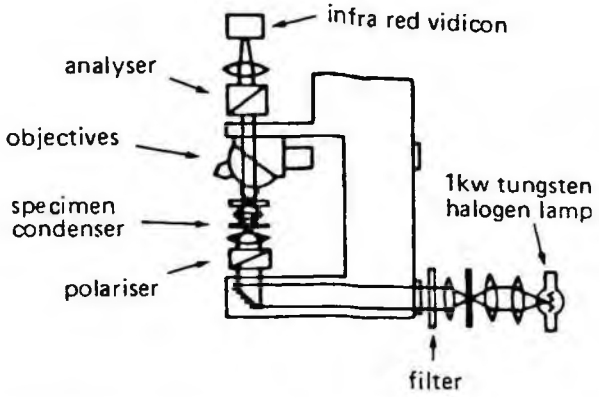

Fig. 5.11 Typical infrared microscope (from Ref. 35 with permission).

the incident light is small so that this method is very effective to observe small scatterers. It should also be noted that in the case of X-ray observation, it is necessary to prepare a very thin sample for the X-rays to penetrate, while in this method, very thick samples can be easily observed which are transparent to the incident light. Since infrared light is scattered only by free electrons and electrons weakly bound to impurities, it is very sensitive to free electron perturbations due to dislocations and micro-precipitates.[42]

It was however difficult to observe these scattered lights since the intensity of the scattered light was too weak to observe with the naked eye. In order to detect this very weak scattered light, a CCD camera was used and computer analysis of the data was developed to construct scattered light images[43, 44] as shown in Fig. 5.12. Using this newly developed system, the observation of scattered light has become possible and three dimensional observation, i.e. tomographic observation has become possible. There are various application examples of this method for GaP, GaAs, InP, CdTe.[45-52]

5.4.6 Laser Scattering

Inelastic laser light scattering is very effective for detecting various particles on the polished surface. When the particle is irradiated by a laser beam, the intensity of the scattered light depends on; (1) the size of the particle with respect to the laser wavelength, (2) the state of polarization, (3) the particle shape and (4) the particle index of refraction with respect to the surrounding medium. As explained by Takami,[53] various surface inspection systems have been developed and they are industrially applied for commercial polished wafers.

5.5 ELECTRICAL PROPERTIES

5.5.1 Hall Measurement

Hall measurement is a method based on the Hall effect for measuring resistivity and

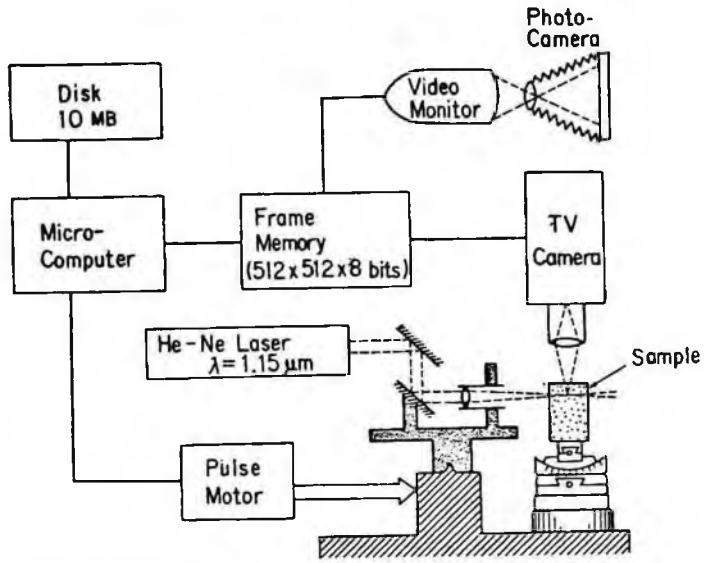

Fig. 5.12 Schematic drawing of infrared light scattering tomography (from Ref. 43 with permission)

mobility. This measurement is normally performed by the Van der Pauw method.[54,55] On the four corner of a square sample, ohmic electrodes are made as shown in Fig. 5.13[55] and the resistivity is measured according to the following equations.

$$R_1 = \frac{V_{CD}}{I_{AB}} \tag{5.12}$$

$$R_2 = \frac{V_{DA}}{I_{BC}} \tag{5.13}$$

$$\rho = \frac{\pi d}{\ln 2} \cdot \frac{R_1 + R_2}{2} \cdot f\left(\frac{R_1}{R_2}\right) \tag{5.14}$$

Here, R_1 is the resistance calculated when the current, I_{AB}, is passed between A and B and the voltage, V_{CD}, between C and D is measured. R_2 is the resistance calculated when the current, I_{BC}, is passed between B and C and the voltage, V_{DA}, between D and A is measured. From these resistances, the material resistivity, ρ, is calculated as Eq. 5.14. Here, d is the sample thickness and f is the correction factor.[56] When $R_1/R_2 < 1.5$, one can consider that $f = 1$.

A magnetic field is then applied and the Hall coefficient R_H is measured.

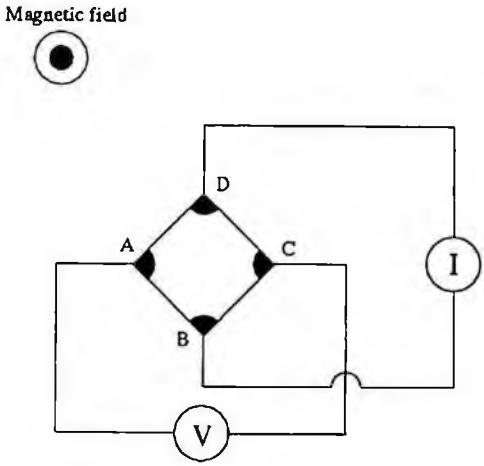

Fig. 5.13 Sample configuration for Hall measurement (reprinted from Ref. 55 with permission, copyright 1994 Elsevier).

$$R_3 = \frac{V_{AC}}{I_{BD}} \tag{5.15}$$

$$R_H = \frac{d}{B} \cdot \Delta R_3 \tag{5.16}$$

R_3 is the resistance calculated when the current I_{BD} is passed between B and D and the voltage, V_{AC}, between A and C is measured. Here, B is the magnetic field and ΔR_3 the difference of R_3 before and after application of the magnetic field. The Hall mobility, μ_H and carrier concentration, n, can then calculated as follows.

$$\mu_H = \frac{R_H}{\rho} \tag{5.17}$$

$$n = \frac{1}{e\mu_H \rho} \tag{5.18}$$

Here, e is the elementary charge.

Hall measurement is now possible even for semi-insulating materials by using a system with high impedance.[57] For this measurement, it is necessary to pay attention to the precision of the magnetic field value and temperature. For precise measurement, it is necessary to prepare an appropriate sample shape[1] but in routine measurement, it was shown by a round-robin test[55] that a simple rectangular sample shape as shown in Fig. 5.13 is sufficient. It was pointed out that the temperature correction is a significant matter especially for semi-insulating materials such as GaAs.

5.5.2 C-V Measurement

Using a Schottky electrode or a pn junction, it is possible to measure the capacitance per unit area from the following equations.

$$C = \sqrt{\frac{\varepsilon_s \varepsilon N_d}{2(V_d - V_0)}} \tag{5.19}$$

Here, N_d is the concentration of ionized donors, V_d the diffusion voltage, V_0 the applied voltage, ε the vacuum permittivity and ε_s the relative permittivity of the semiconductor. According to this equation, the value of V_d can be obtained from the plot of $1/C^2$ and V and from the value of C, the value of N_d can be obtained. When the capacitance is measured by imposing a small AC voltage with a high frequency of about 1 MHz on the DC voltage, the carrier concentration can be obtained assuming that N_d is due to shallow donors. The basic method has been described in Ref. 58 and various modifications[59-63] have been developed in order to achieve a simple and rapid measurement. This method is used for the confirmation of the Hall measurement. It is also effective to measure the carrier concentration depth profile from the surface. The measurement can be performed by using metal electrodes deposited on a polished sample. As a depth profiling method, an etching solution is used to measure the carrier concentration by etching the sample surface, using a mercury contact electrode.

5.5.3 Transient Spectroscopies

The behavior of deep levels in semiconductors is explained by Shockley-Read-Hall (SHD) statistics.[64-67] The behavior of deep levels is summarized by Milnes.[68] Various methods have been developed to evaluate deep levels, as reviewed in Refs. 69-72.

(1) Deep Level Transient Spectroscopy (DLTS)

Transient spectroscopy methods as shown in Table 5.3 are useful techniques to examine deep levels in semiconductors. Among various methods, DLTS and ICTS methods are the most practical and they are very often used for compound semiconductor material characterization. This transient spectroscopy is based on the capacitance change, C(t), of a Schottky or a p-n junction as a function of time, expressed as in the following equation.

$$C(t) = C_\infty \left\{1 - \frac{N}{2} \exp\left(-\frac{t}{\tau}\right)\right\} \tag{5.20}$$

Here, C_∞, is the capacitance at $t = \infty$, τ the time constant, $N=N_T/(N_D+N_T)$ where N_T is the trap density and N_D the carrier density.

In DLTS,[73] when a forward pulse is superimposed on a constant reverse bias, a difference of junction capacitance is observed as shown in Fig. 5.14. When the temperature is scanned from a lower temperature to a higher temperature, the time constant for the variation of the junction constant is changed. When the capacitance difference at t_1

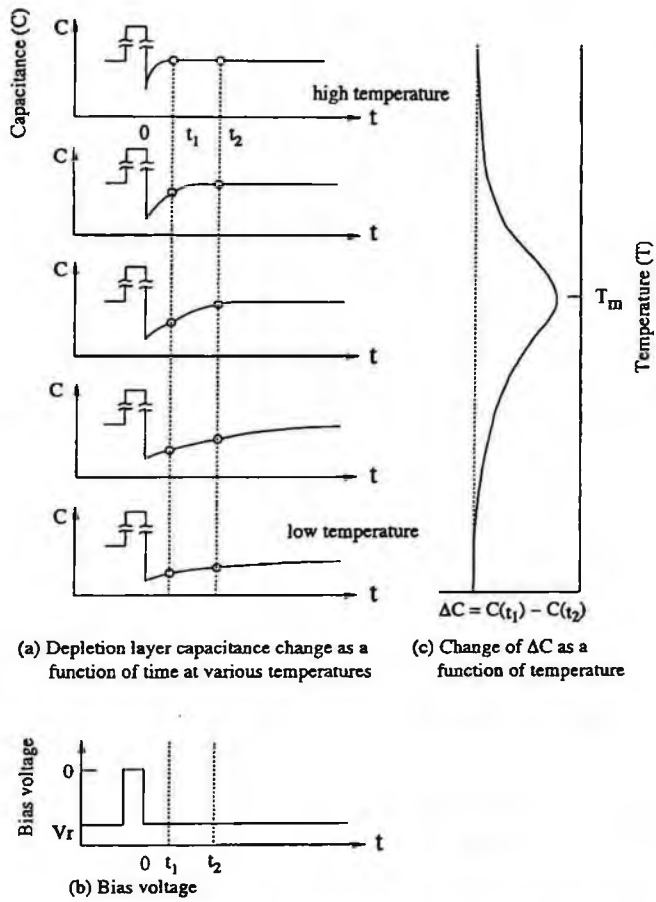

(a) Depletion layer capacitance change as a function of time at various temperatures

(b) Bias voltage

(c) Change of ΔC as a function of temperature

Fig. 5.14 Principle of DLTS method (reprinted from Ref. 73 with permission, copyright 1974 American Institue of Physics).

and t_2 is plotted as a function of temperature, the capacitance difference has a maximum at a certain temperature. The DLTS signal, S(T) is can be represented as,

$$S(T) = C(t_1) - C(t_2) \tag{5.21}$$

$$= C_\infty (N/2) \left\{ \exp\left(-\frac{t_1}{\tau}\right) - \exp\left(-\frac{t_2}{\tau}\right) \right\} \tag{5.22}$$

$$\Delta C = S(T) \exp\left(-\frac{t_1}{\tau_m}\right) \left\{ \exp\left(-\frac{\Delta t}{\tau_m}\right) - 1 \right\} \tag{5.23}$$

Here, $\Delta t = t_2 - t_1$. The time constant τ_m where the DLTS signal reaches a maximum can

Table 5.3 Various Transient Spectroscopic Methods

Method		Ref.
Electrical	DLTS (Deep Level Transient Spectroscopy)	73
	ICTS (Isothermal Capacitance Transient Spectroscopy)	74
	DLFS (Deep Level Fourier Spectroscopy)	80
Optical	ODLTS (Optical DLTS)	81
	DLOS (Deep Level Optical Spectroscopy)	82
	PICTS (Photo Induced Current Transient Spectroscopy)	83, 84
Thermal	TSC (Thermal Stimulated Current)	75-79
	TSCAP (Thermal Stimulated Capacitance)	76, 77, 85

be obtained as follows.

$$\frac{dS(t)}{dt} = 0 \tag{5.24}$$

$$\tau_m = \frac{(t_1 - t_2)}{\ln (t_1/t_2)} \tag{5.25}$$

ΔC thus can then be obtained as follows by inserting τ_m in Eq. 5.23.

$$\Delta C = S(T) \exp\left(-\frac{t_1}{\tau_m}\right)\left\{\exp\left(-\frac{\Delta t}{\tau_m}\right) - 1\right\} \tag{5.26}$$

From the value of ΔC, the trap density N_T can be obtained and by plotting $\ln (T^2\tau)$ versus T^{-1}, the activation energy of the trap can be obtained.

(2) Isothermal Current Transient Spectroscopy (ICTS)

Using ICTS,[74] it is possible to measure deep levels without scanning the temperature. When Eq. 5.20 is differentiated and multiplied by t,

$$t\frac{dC(t)}{dt} = \frac{C|N_t}{2\tau}\exp\left(-\frac{t}{\tau}\right) \tag{5.27}$$

At $t = \tau$, this function becomes

$$\frac{C N_t}{(2e)} = \frac{\Delta C}{e} \tag{5.28}$$

Therefore, when Eq .5.27 is calculated and plotted, without temperature scanning, the

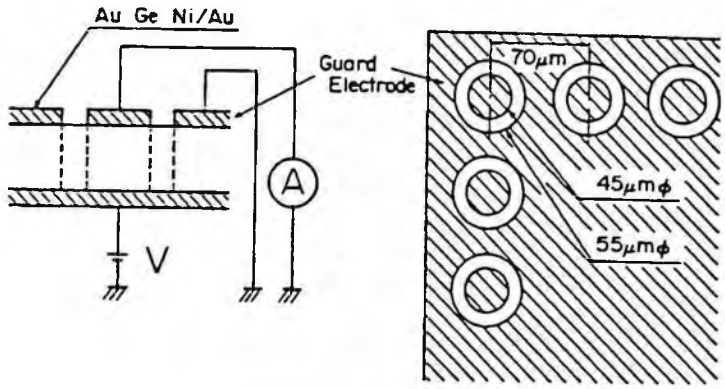

Fig. 5.15 Electrode arrangement of the three-electrode guard method (reprinted from Ref. 86 with permission, copyright 1985 American Institue of Physics).

time constant is obtained from the peak time, ΔC at the peak height and the trap density N_t. The advantage of ICTS is that no temperature scan is necessary but the disadvantage is that the peak position must be predicted prior to the measurement.

(3) Thermal Stimulated Current (TSC)

For high-resistive and semi-insulating materials, the TSC method[75-79] is an effective one. The TSC method is based on the carrier release from deep levels as a function of temperature. Before measurement, the sample is cooled and light-irradiated in order to capture carriers in deep levels. On increasing the temperature, the current due to released carriers is analyzed as a function of temperature. The equation for obtaining the energy of a deep level is given as follows.

$$\frac{T_m^4}{\beta} \propto \exp\left(\frac{E_c - E_t}{kT_m}\right) \tag{5.29}$$

Here, T_m is the peak temperature, E_c the energy of the bottom of the conduction band, E_t the energy of the deep level and β is the rate of temperature rise.

(4) Other Methods

Apart from the above methods, there are various modified methods[80-85] as shown in Table 5.3 for investigating the deep levels in semiconductors. DLTS and ICTS can be used only for conductive materials, while TSC and PITS methods can be used even for semi-insulating materials.

5.5.4 Three Guard Electrode Method

This method was developed to measure the uniformity of the resistivity over the wafer. A plain Ohmic contact electrode is made on the back side of the wafer and round electrodes covered with a protecting electrode are made on top of the wafer (Fig. 5.15).[86] The protecting electrode is earthed in a way that the leakage current will not affect the measurement. Since the electrodes are of diameter 45 μm at intervals of 70 μm, resistivity mapping of high resolution can be obtained. It is well known that the non-uniformity of the resistivity corresponds quite well to the crystallinity and affects the device performance in the case of semi-insulating GaAs as explained in Chapter 8.

5.6 IMPURITY AND COMPOSITION ANALYSIS

5.6.1 Solid Source Mass Spectroscopy (SSMS)

In SSMS,[87] ions generated from a sample by vacuum discharge are accelerated through slits and dispersed at a certain velocity. Out of the slit, ions are selected in a magnetic field depending on the m/Q, where m is the mass and Q the charge. Therefore, each element can be detected quantitatively from its intensity. For the mass spectroscopy, a Mattauch-Herzog type double convergence mass spectrometer is generally used.

5.6.2 Secondary Ion Mass Spectroscopy (SIMS) and Ion Micro Analyzer (IMA)

In this method,[88] the sample is sputtered by primary ions with energies of 1-10 keV and the emitted secondary ions are analyzed by a mass spectrometer. This method is also called IMA (Ion Microprove Analysis) when the ion beam diameter is sufficiently small to have the ability to scan. This method is useful to evaluate the depth profile of impurities.

5.6.3 Glow Discharge Mass Spectroscopy (GDMS)

GDMS[89] is the most recent analysis method which gives most reliable quantitative analysis results. The detection limit of GDMS is low compared with other methods. A typical analysis example for CdTe is shown in Table 15.9.

5.6.4 Fourier Transform Infrared (FT-IR) Spectroscopy

FT-IR is based on obtaining a transmitted light spectrum by the Fourier transformation of interferograms through a two light beam interferometer.[90] The method has an advantage that no slit is necessary for light dispersion and that all wavelengths can be measured simultaneously. Because of these advantages, high-resolution spectra can be obtained quickly

FT-IR is thus an effective analysis method for impurities which give infrared absorption depending on the vibration mode. The most typical useful example of FT-IR analysis is the case of carbon in GaAs. The infrared absorption due to localized vibration is measured by FT-IR and from the intensity, the carbon concentration is determined as explained in Sec. 8.5.1.

5.6.5 Chemical Analysis

The physical and optical analysis methods as mentioned above are effective in analyzing the main impurities in materials. It is however necessary to analyze these impurities quantitatively and/or becomes necessary to calibrate the above analysis methods.

Among the main chemical analysis methods, the following methods are well known.

(i) Induced coupled plasma spectroscopy (ICPS)[91]

(ii) Flameless atomic absorption spectroscopy (FAAS)[92, 93]

(iii) Nuclear activation analysis (NAA)

5.6.6 Stoichiometry Analysis

Since compound semiconductor materials consist of more than two elements, there is always a possibility that they will deviate from stoichiometry. The deviation is however very small and it is difficult to analyze this non-stoichiometry.

(1) X-ray diffraction method

For precise measurement of lattice constants, X-ray diffraction is applied and from the precise lattice constant measurement, stoichiometry can be analyzed.[94, 95]

(2) Coulometric titration method

The other effective method for stoichiometry measurement is the coulometric titration method, in which the specimen is dissolved in a specific solution and the rest of the solution is analyzed by coulometric titration.[96-98] This method was first established by Gardels and Corwell[96] to determine the stoichiometry of various inorganic compounds. This method has been applied to GaAs, InP and CdTe[99-101] and was found very effective in analyzing the stoichiometry quantitatively.

REFERENCES

1. W.R. Runyan, *Semiconductor Measurements and Instrumentation* (MaGraw-Hill, Tokyo, 1975)
2. As these conferences, there are two conferences, The International Workshop on Expert Evaluation and Control of Comound Semiconductor Materials and Technologies (EXMATEC) and The Interna tional Conference on Defect Recognition and Image Processing in Semiconductors (DRIP) which are held biennially.
3. *Characterization of Crystal Growth Defects by X-ray Methods*, eds. B.K. Tanner and D.K. Bowen (Plenum Press, London, 1980).
4. B.D. Cullity, *Elements of X-ray Diffraction* (Addison-Wesley, Cambridge, 1956)
5. T. Kikuchi, *Rigaku-Denki J.* **19** (19818) 24.
6. W.R. Runyan, in *Semiconductor Measurements and Instrumentation* (MaGraw-Hill, Tokyo, 1975) p. 255.
7. http://www.bruker.axs.de
8. G.A. Rozgoni and D.C. Miller, in *Crystal Growth: A Turorial Approach*, eds. W. Bardsley, D.T.J. Hurle and J.B. Mullin (North-Holland, Amsterdam, 1979) p. 307.
9. R. Koehler, *Appl. Phys.* **A58** (1994) 149.
10. C.S. Barrett, *Trans. AIME* **161** (1945) 15.
11. K. Koura and S. Kikuta, *X-ray Diffraction Technology (in japanese)* (Tokyo University, Tokyo, 1979).
12. P. B. Hirsch, A. Howie, R. B. Nicholson, D. W. Pashley and M. J. Whelan, *Electron Microscopy of*

Thin Crystals (Butterworths, London, 1965)
13. R.D. Heidenreivh, *Fundamentals of Transmission Electron Microscopy* (Interscience, New York, 1964).
14. H. Yamamoto, H. Shimakura, G. Kano, M. Seiwa, H. Nakata and O. Oda, in *Defect Control in Semiconductors*, ed. K. Sumino (North-Holland, Amsterdam, 1990) p. 1273.
15. D. B. Holt and D. C. Joy, *SEM Microcharacterization of Semiconductors* (Academic Press, New York, 1989) p. 3.
16. Y. Tokumaru, H. Okushi and Y. Okada, *Rep. Tech. Group Electron. Mater.* **EFM84-9** (1984) p. 73.
17. P.J. Dean, in *Junction Electroluminescence Applied Solid State Science Vol.1*, eds. R. Wolfe and C.J. Kriessman (Academic Press, New York, 1969) p. 1.
18. J. I. Pankove, *Optical Processes in Semiconductors* (Dover, New York, 1971) p. 12 and p. 107.
19. H. Hartmann, R. Mach and B. Selle, in *Wide Gap II-VI Compounds as Electronic Materials, Current Topics in Materials Science Vol.9*, ed. E. Kaldis, (North-Holland, Amsterdam, 1982) p. 89.
20. P. J. Dean, *Prog. Crystal Growth Character.* **5** (1982) 89.
21. H.B. Bebb and E.W. Williams, in *Semiconductors and Semimetals Vol. 8* (Academic Press, New York, 1975) p. 181.
22. N.G. Giles-Taylor, R.N. Bicknell, D.K. Blanks, T.H. Myers and J.F. Schetzina, J. Vac. Sci. Technol. **A3** (1975) 76.
23. H.J. Hovel and D. Guidotti, *IEEE Trans. Electron Devices* **ED-32** (1985) 2331.
24. S.K. Krawczyk, M. Garricues and H. Bouredocen, *J. Appl. Phys.* **60** (1986) 392.
25. M. Erman, G. Gillardin, J. le Bris, M. Renaud and E. Tomzik, *J. Crystal Growth* **96** (1989) 469.
26. G.E. Carver, *Semicond. Sci. Technol.* **7** (1992) A53.
27. B. Sartorius, D. Franke and M. Schlak, *J. Crystal Growth* **83** (1987) 238.
28. Th. Vetter and A. Winnacker, *J. Mater. Res.* **6** (1991) 1055.
29. B.G. Yacobi and D.B. Holt, *J. Appl. Phys.* **59** (1986) R1.
30. B.G. Yacobi and D.B. Holt, *Cathodoluminescence Microscopy of Inorganic Solids* (Plenum, New York, 1990).
31. A.K. Chin, H. Temkin and R.J. Roedel, *Appl. Phys. Lett.* **34** (1979) 476.
32. W.L. Bond and J. Andrus, *Phys. Rev.* **101** (1956) 1211.
33. D.A. Jenkins, T.S. Plaskett and P. Chaudhari, *Phil. Mag.* A **39** (1979) 237.
34. C.R. Elliott and J.C. Regnault, *Inst. Phys. Conf. Ser.* **60** (1981) 365.
35. C.R. Elliott, J.C. Regnault and B.T. Meggitt, *Proc. SPIE* **368** (1982) 96.
36. X.Z. Cao and A.F. Witt, *J. Crystal Growth* **91** (1988) 239, 652.
37. D.J. Carlson and A.F. Witt, *J. Crystal Growth* **108** (1991) 508, 112; ibid. **108** (1991) 255, 838.
38. L. Rayleigh, Phil. Mag. **xli** (1871), 107, 274., ibid. **xliv** (1897) 28.
39. G. Mie, *Ann. der Physik* (4) **25** (1906) 377
40. R. W. Wood, *Physical Optics* (Mac-Millan, New York, 1911) p. 641.
41. M. Born and E. Wolf, *Principle of Optics* (Pergamon Press, Oxford, 1970) p. 633.
42. T. Ogawa, in *Materials Science Monographs No. 31*, ed. J. P.Fillard (Elsevier Sci., Amsterdam, 1985) p. 1.
43. K. Moriya, and T. Ogawa, *Jpn. J. Appl. Phys.* **22** (1983) L207.
44. T. Ogawa and N. Nango, *Rev. Sci. Instrum.* **57** (1986) 1135.
45. C. Kuma, Y. Otoki and K. Kurata, in *Materials Science Monographs Vol. 31*, ed. J.P. Fillard (Elsevier Sci., Amsterdam, 1985) p. 19.
46. K. Moriya, *Materials Science Monographs Vol. 31*, ed. J.P. Fillard (Elsevier Sci., Amsterdam, 1985) p. 27.
47. T. Ogawa, *Jpn. J. Appl. Phys.* **25** (1986) L 316.
48. T. Ogawa, *Jpn. J. Appl. Phys.* **25** (1986) L 916.
49. K. Moriya, *Oyo Buturi (Monthly Publ. Jpn. Soc. Appl. Phys.) (in japanese)* **55** (1986) 542.
50. J, P. Fillard, P. Gall, A. Baroudi, *Jpn. J. Appl Phys.* **26** (1987) L1255.

51. T. Ogawa, *J. Crystal Growth* 96 (1989) 777.
52. J.P. Fillard, P.C. Montgomery, P. Gall, M Castagne and J. Bonnafe, *J. Crystal Growth* **103** (1990) 109.
53. K. Takami, *Mater. Sci. Engineer.* **B44** (1997) 181.
54. L.J. Van der Pauw, *Philips Res. Rept.* **13** (1958) 1.
55. S. Yoshida, Y. Itoh, M. Kashiwa, T. Inoue, K. Katsuno, K. Hajime, T. Otaki, T. Sato, R. Nakai and M. Matsui, *III-Vs Review* 7 (1994) 47.
56. G. Kusumoto, *Oyo Buturi (Monthly Publ. Jpn. Soc. Appl. Phys.) (in japanese)* **42** (1973) 756.
57. T. Obokata, A. Yahata, K. Ishida and T. Fukuda, *Oyo Buturi (Monthly Publ. Jpn. Soc. Appl. Phys.) (in japanese)* **54** (1984) 1212.
58. J. Hilibrand and R. D. Gold, *RCA Review* **21** (1960) 245.
59. G. W. Reutlinger, S. J. Regas, D. J. Sidor and B. Schwartz, *Solid State Electron.* **12** (1969) 31.
60. J. A. Copeland, *IEEE Trans. Electron. Devices* **DE-16** (1969) 445.
61. P. J. Baxandall, D. J. Colliver and A. F. Fray, *J. Phys. E* **4** (1971) 213.
62. T. Sukegawa and M. Ogita, *Rev. Sci. Instrum.* **50** (1979) 41.
63. F. Jelinek and J. Karlovsky, *TESLA Electronics* **3** (1983) 78.
64.W. Shockley and W. T. Jr., Read, *Phys. Rev.* **87** (1952) 835.
65. W. Shockley, *Proc. IRE* **46** (1958) 973.
66. R. N. Hall, *Proc. Inst. Electr. Engineer.* **106B Suppl. 17** (1959) 923.
67. C. T. Sah, R. N. Noyce and W. Schockley, *Proc. IRE* **45** (1957) 1228.
68. A. G. Milnes, *Deep Impurities in Semiconductors* (John Wiley & Sons, New York, 1973).
69. T. Ikoma, in *Semiconductor Research Vol. 12*, ed. J. Nishizawa (Kogyo Chousakai, Tokyo, 1976) p. 173.
70. T. Ikoma and T. Okumura, *J. IECE Jpn.* **64** (1981) 59, 195, 279.
71. T. Okumura, in *Recent Compound Semiconductor Handbook (in japanese)*, ed. T. Ikoma (Science Forum, Tokyo, 1982) p. 249.
72. F. Hasegawa, in *Defect Characterization Technology (in japanese)*, eds. T. Ikoma and F. Hasegawa (Science Forum, Tokyo, 1985) p. 146.
73. D.V. Lang, *J. Appl. Phys.* **45** (1974) 3023.
74. H. Okushi and Y. Tokumau, *Jpn. J. Appl. Phys.* **Suppl. 20-1** (1981) 261.
75. L.R. Weisberg and H. Schada, *J. Appl. Phys.* **39** (1968) 5149.
76. C. T. Sah, W. W. Chan, H. S. Fu and J. W. Walker, *Appl. Phys. Lett.* **20** (1972) 193.
77. M. G. Buehler, *Solid-State Electron.* **15** (1972) 69.
78. G. M. Sessler, in *Electrics* (Springer Verlag, Berlin, 1980) Chapters 2 and 3.
79. P. Braunlich, in *Thermally Stimulated Relaxation in Solids* (Springer Verlag, Berlin, 1979) Chaps. 2-4.
80. K. Ikeda and H. Takaoka, *Jpn. J. Appl. Phys.* **21** (1982) 462.
81. A. Mitonneau, G.M. Martin and A. Mircea, *Inst. Phys. Conf. Ser.* **33a** (1977) 73.
82. A. Chantre, G. Vincent and D. Bois, *Phys. Rev.* **B23** (1981) 5335.
83. Ch. Hurtes, M. Boulou, A. Mitonneau and D. Bois, *Appl. Phys. Lett.* **32** (1978) 821.
84. R. D. Fairman, F. J. Morin and J. R. Oliver, *Inst. Phys. Conf. Ser. 45 (1979) 134.*
85. J.C. Carballes and J. Lebailly, *Solid State Commun.* **6** (1968) 167.
86. T. Matsumura, T. Obokata and T. Fukuda, *J. Appl. Phys.* **57** (1985) 1182.
87. S. Aoki and G. Sokuyama, *Electronic Material Engineering (in japanese)* (Association of Electron ics, Tokyo, 1982)
88. E. Izumi, Y. Kato, M. Yano, Y. Arima, K. Iwamoto, K. Tamura, *Proc. 8th Symp. ISIAT '84* (Tokyo, 1984) p. 541.
89. Nano Sci. Co., http://www.nanoscience.co.jp/a3_1.html
90. P. Griffiths, *Chemical Infrared Fourier Transform Spectroscopy* (John Wiley & Sons, New York, 1975).
91. P.W.J.M. Bowmas, *Inductively Coupled Plasma Emission Spectroscopy* (John Wiley & Sons, New

York, 1987).
92. *Trace Analysis Vol.2 High Purity Metals and Semiconductors (in japanese)*, eds. K. Tada and A. Mizuike (Sangyou Tosho, 1973).
93. S. Nakajima and R. Obara, *Oyo Buturi (Monthly Publ. Jpn. Soc. Appl. Phys.) (in japanese)* **43** (1974) 422.
94. I. Fujimoto, *Jpn. J. Appl. Phys.* **23** (1984) L287.
95. T. Matsuzaki, Y. Tomotake, F. Yajima and T. Okano, *Jpn. J. Appl. Phys.* **25** (1986) 291.
96. M.C. Gardels and J.C. Corwell, *Anal. Chem.* **38** (1966) 774.
97. M.H. Yang, M.L. Lee, J.J. Shen and H.L. Hwang, *Mater. Sci. Engineer.* **B12** (1992) 253.
98. M.H. Yang, M.L. Lee and H.L. Hwang, *Non-Stoichiometry in Semiconductors* (Elsevier Sci., Amsterdam, 1992) p.15.
99. O. Oda, H. Yamamoto, M. Seiwa, G. Kano, T. Inoue, M. Mori, H. Shimakura and M. Oyake, *Semicond. Sci. Technol.* **7** (1992) A215.
100. K. Kainosho, O. Oda, G. Hirt and G. Müller, *Mat. Res. Soc. Symp. Proc.* **325** (1994) 101.
101. H. Ouyang, M.L. Peng, Y.M. Lin, M.H. Yang and H.L. Hwang, *J. Crystal Growth* **72** (1985) 232.

6. APPLICATIONS

6.1 INTRODUCTION

Compound semiconductor materials have many fields of application as explained below. They are used in more fields than Si devices even though the amount is less than Si for each field. The reason why compound semiconductors have more applications is due to their physical properties which are different from Si. They thus end up covering a very wide range of fields, including displays,[1] optical communication,[2] microwave communication,[3] solar cells,[4] radiation detectors,[5] sensors[6] and so on. This wide range of applications which already exist and are indispensable to human beings' lives convinces us that the development of compound semiconductors is an important factor for the prosperity of human life and economic and social development. This is much more so because for compound semiconductor materials, there are more possibilities that new materials with new properties can be developed. In this chapter, existing industrial applications and future applications are reviewed. All applications are briefly summarized in Table 6.1.

6.2 PHOTONIC DEVICES

The main applications of compound semiconductors are photonic devices which are based on the advantage that compound semiconductor materials have a range of bandgaps. Photonic devices are categorized as light emitting devices such as laser diodes (LDs) and light emitting diodes (LEDs) and photodetectors. All these applications now establish a market scale of more than five billion dollars a year. Photonic devices also have a future as optoelectronic integrated circuits and optical computers.

6.2.1 Laser diodes

Laser diodes are diodes based on double hetero pn junction structures by which carriers are confined and light is emitted by carrier recombination and by stimulated emission.[7] Laser diodes were first proposed by Baisov in 1961.[8] Kroemer proposed the double hetero (DH) pn junction structures for laser diodes.[9] Hereafter, various lasing experiments were tried and room temperature continuous oscillation was finally realized by Hayashi and Panish for AlGaAs/GaAs laser diodes in 1970.[10] The review of DH lasers are found in Ref. 11.

A typical DH structure for a GaAs based laser diode is as shown in Fig. 6.1(a). Carriers are confined between n-GaAlAs and p-GaAlAs due to the bandgap difference between GaAs and GaAlAs. Carriers are recombined efficiently in the GaAs layer as in Fig. 6.1(b) and the emitted light itself is also confined because of the difference of refractive index as shown Fig. 6.1(c). Lasing happens when stimulated emission occurs. As seen in Fig. 6.2 (a), when electrons recombines with holes, light is spontaneously emitted. When light is absorbed, electrons are excited and electron and hole pairs

Table 6.1 Applications of Compound Semiconductors

Devices	Materials	Applications
Photonic devices		
Laser Diodes (LDs)		
Far Infrared LDs	PbSnTe/PbTe	Gas analysis
IR LDs	InGaAsP/InP	Fiber communications
Visible Light LDs		
Red LDs	AlGaAs/GaAs	CD players
	InGaAlP/GaAs	DVDs
Ultraviolet LDs	InGaN/sapphire	DVDs
Light Emitting Diodes (LEDs)		
IR LEDs	InGaAsP/InP	Fiber communications
	GaAlAs/GaAs	Detectors
Red LEDs	AlGaAs/GaAs	
	GaAsP/GaAs	
	GaP(Zn, O)	
Orange LEDs	GaAsP/GaP	
Green LEDs	GaP(N)	Displays
	GaP	
Blue LEDs	InGaN/sapphire	
	ZnSe/GaAs	
	ZnSe/ZnSe	
White LEDs	InGaN/sapphire	Displays, Lighting
	ZnSe/ZnSe	Displays
Ultraviolet LEDs	AlGaN/sapphire	Sterilization
Photodetectors		
Far IR	HgCdTe/CdTe	Nightvision
Middle IR	InSb	Thermoviewer
IR	InGaAs/InP	Fiber communications
Visible Light	AlGaAs/GaAs	Fiber communications
Electronic Devices		
MESFET	GaAs	Cellular phones
HEMT	AlGaAs/GaAs	Cellular phones
		Satellite broadcasting
	InGaAs/InP	Anticollision sensors
HBT	InGaAs/InP	Cellular Phones
JFET	GaAs, InP	Cellular Phones
Gunn Diodes	GaAs, InP	Anticollision sensors
Solar Cells		
	GaAs-base	Satellite
	CdTe-base	Terrestrial power generation
	InP-base	Satellite
	chalcopyrite-base	Terrestrial power generation
Radiation detectors		
	CdTe	Medical instruments
	GaAs	Astronology
Magnetic Sensors		
Hall Sensors	InSb, InAs	Motor speed sensors
Magnetic Resistance Devices	InSb	Contactless sensors

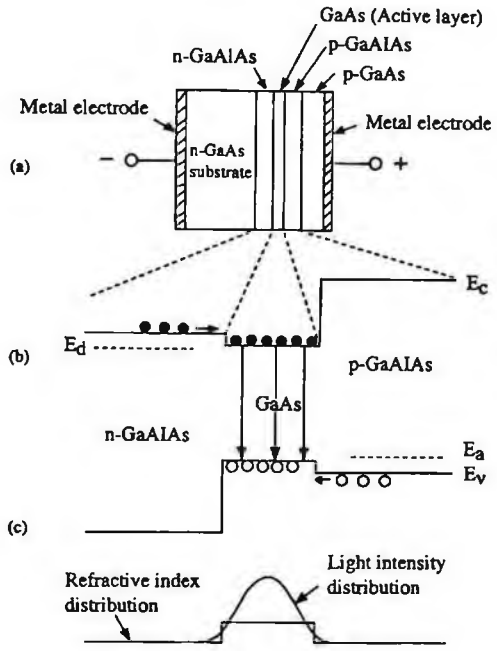

Fig. 6.1 GaAs based double hetero structure laser diode. (a) Laser structure, (b) band diagram, (c) distributions of refractive index and light intensity.

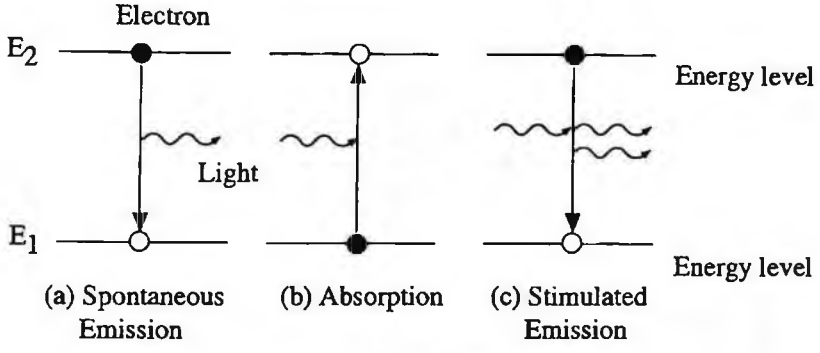

Fig. 6.2 Energy levels and photoabsorption, photoemission.

are generated (Fig. 6.2 (b)). When this excitation exceeds spontaneous recombination, stimulated emission as shown in Fig. 6.2(c) occurs.

The intensity of emitted light as a function of injected current is as shown in Fig. 6.3. When the current is low, spontaneous emission is predominant and this type of emission occurs in LEDs. When the current exceeds the threshold, lasing occurs.

There are three types of laser diodes depending on the wavelength, infrared LDs,

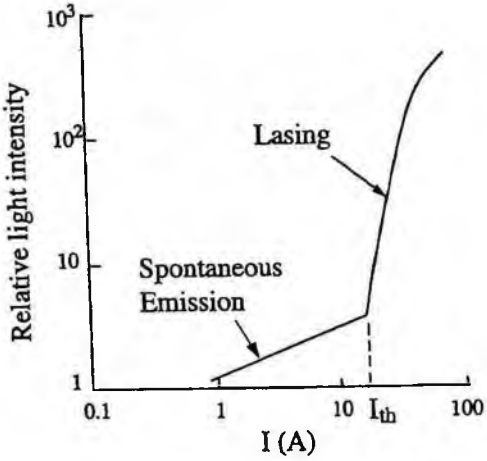

Fig. 6.3 Threshold current (I_{th}) for lasing.

visible LDs and long wavelength LDs.[11] In Fig. 6.4, the possible wavelengths for various materials are shown. For these laser diodes, conductive GaAs, InP, GaSb substrates are used for the epitaxial growth of mixed compound semiconductor materials as summarized in Table 6.1.

Infrared laser diodes based on InGaAsP/InP in the wavelength of 1.2-1.6 μm are mainly used for long distance optical fiber communications.[12, 13] Infrared laser diodes based on InGaAsP/GaAs in the wavelength of 0.7-0.8 μm are mainly for CD players

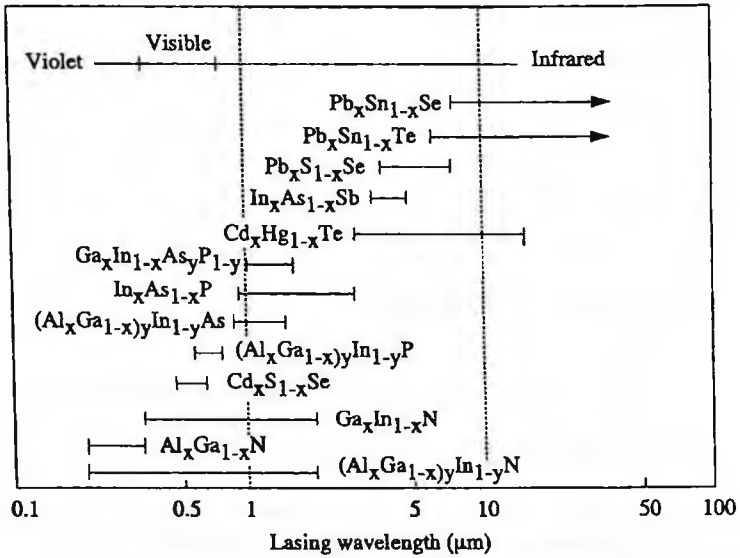

Fig. 6.4 Possible lasing wavelength for various materials.

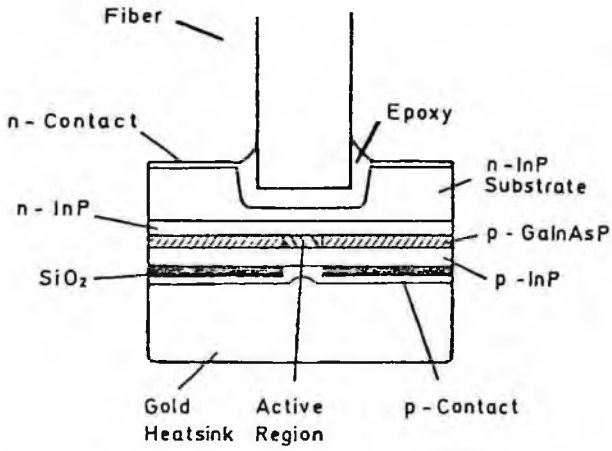

Fig. 6.5 Infrared InP based LED (reprinted from Ref.37 with permission, copyright 1977 IEEE).

and laser printers and partly for optical fiber communications.[14, 15] Visible light laser diodes based on GaAlAs/GaAs and InGaAlP/GaAs in the wavelength of 0.5-0.7 μm have been developed as light sources for CD players, DVD players, laser printers and optical disk memories.[16-21] Shorter wavelength lasers based on InGaN/sapphire have recently been developed as light sources for high density DVD players.[22-24] ZnSe lasers have also been developed for short wavelengths.[25, 26] Long wavelength laser diodes in the wavelength of about 2-10 μm are under development,[27, 28] aiming at gas analyzers and atmosphere contamination detectors. Various lasers based on AlGaInSb/GaSb and PbSnSeTe/PbTe are under development.[29]

6.2.2 Light Emitting Diodes (LEDs)

There are various types of LEDs as shown in Table 6.1. These LEDs are summarized in Refs. 7 and 30-35. Most of them have been developed for visible wavelengths and are used for displays and functional applications and some of them have been developed for infrared wavelengths for fiber communications.

(1) Infrared LEDs

Quartz fiber communications mainly use infrared laser diodes and detectors. For very short distance communications, it is necessary to use low cost light emitting devices. Infrared LEDs[36] based on GaAs for the 0.8-0.9 mm wavelength range and those based on InP for 1.3 mm wavelength[37, 38] are used for local fiber communications. Fig. 6.5 shows an InP based infrared LED which is applicable for the wavelength of 1.3 mm. The performance requirements for fiber communication are brightness and high response rate. Increased brightness is obtained by applying double hetero structures and high response rate is obtained by high impurity concentrations which decrease the car-

Table 6.2 Various Light Emitting Diodes (LEDs)

Material		Growth		Wave	Transition
Emitting layer	Substrate	method	Color	length (nm)	type
InGaAsP	InP	LPE(DH)	IR	1300	direct
GaAs(Si)	GaAs	LPE	IR	940	direct
GaAs(Zn)	GaAs	diffusion	IR	900	direct
$Al_{0.35}Ga_{0.65}As$(Si)	GaAs	LPE(SH)	IR	880	direct
GaAs	GaAs	LPE(DH)	IR	870	direct
$Al_{0.03}Ga_{0.97}As$	GaAs	LPE(DH)	IR	850	direct
$Al_{0.15}Ga_{0.85}As$	GaAs	LPE(DH)	IR	780	direct
GaP(Zn,O)	GaP	LPE	red	700	indirect
$Ga_{0.65}Al_{0.35}As$	GaAs	LPE(SH)	red	660	direct
$Ga_{0.65}Al_{0.35}As$	GaAs	LPE(DH)	red	660	direct
$GaAs_{0.6}P_{0.4}$	GaAs	VPE+diffusion	red	650	direct
$GaAs_{0.45}P_{0.55}$(N)	GaP	VPE+diffusion	red	650	direct
$GaAs_{0.35}P_{0.65}$(N)	GaP	VPE+diffusion	orange	630	indirect
InAlGaP	GaAs	MOCVD	orange	620	direct
$GaAs_{0.25}P_{0.75}$(N)	GaP	VPE+diffusion	orange	610	indirect
InAlGaP	GaAs	MOCVD	yellow	590	direct
$GaAs_{0.15}P_{0.85}$(N)	GaP	VPE+diffusion	yellow	588	indirect
$GaAs_{0.10}P_{0.90}$(N)	GaP	VPE+diffusion	yellow	583	indirect
GaP(N)	GaP	VPE+diffusion	yellow	590	indirect
InAlGaP	GaAs	MOCVD	yellow-green	573	direct
GaP(N)	GaP	LPE	yellow green	565	indirect
GaP	GaP	LPE	green	555	indirect
ZnTe	ZnTe	diffusion	green	555	direct
InGaN	sapphire	MOCVD	green	525	direct
ZnSSe	GaAs	MBE	green	513	direct
InGaN	sapphire	MOCVD	blue	460	direct
SiC	SiC	LPE	blue	480	indirect
ZnSe	ZnSe	diffusion	blue	480	direct
ZnS	ZnS	MOCVD	blue	460	direct
InGaN	sapphire	MOCVD	violet	400	direct
AlGaN	sapphire	MOCVD	ultraviolet	405	direct
AlGaInN	sapphire	MOCVD	ultraviolet	330	direct

LPE: Liquid Phase Epitaxy, VPE: Vapor Phase Epitaxy, MOCVD: Metal Organic Chemical Vapor Deposition, SH: Single Hetero, DH: Double Hetero

rier life time.[39]

(2) Visible LEDs

Visible LEDs between red and green are made industrially using two main compound semiconductor materials, GaP, GaAs. This is one reason why these two materials are the most important materials in compound semiconductors. GaN based LEDs are made industrially for short-wavelength LEDs following these two materials. Zn based materials such as ZnSe, ZnTe and ZnO are promising for short-wavelength LEDs and are under investigation.

- *Red LEDs*

Red LEDs are produced in various systems. GaP doped with Zn and O can emit red light due to recombination between Zn and O[30] as shown in Fig. 6.6(a).

$Ga_{1-x}As_xP$ epitaxial layers are grown on GaAs substrates by hydride chemical vapor deposition for red LEDs. Typical LED structure is shown in Fig. 6.6 (b). Since there is a large lattice mismatching between the epitaxial layer and the substrate, it is necessary to grow a thick composition gradient layer on the substrate before growing p-n layers.[31]

GaAlAs epitaxial layers are grown on GaAs substrates by liquid phase epitaxy.[40] Typical LED structure is shown in Fig. 6.6 (c). In the case of GaAlAs, high quality epitaxial layers can be grown on the substrate since it has a lattice matching with GaAs substrates. Two types of p-n junctions result and high efficiency LEDs can be made using double hetero structures.

- *Yellow and orange LEDs*

The bandgap of GaAsP can be changed from red wavelength to yellow wavelength in the range of direct transition.[31] Growing epitaxial layers of desired composition on GaP substrates, yellow and orange LEDs can be fabricated as shown in Fig. 6.7(a). To prevent the lattice mismatch between GaP substrates and the active layers, the composition gradient layer is grown between them.

InAlGaP layers can be grown on GaAs substrates by the MOCVD method (Fig.

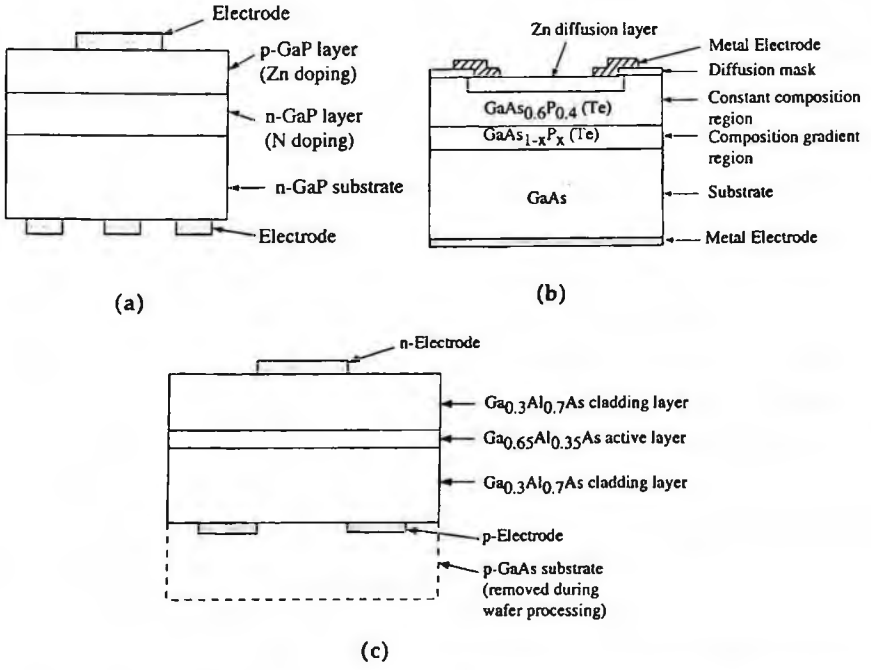

Fig. 6.6 Red LEDs based on (a) GaAs (Zn-O), (b) GaAsP and (c) DH-GaAlAs.

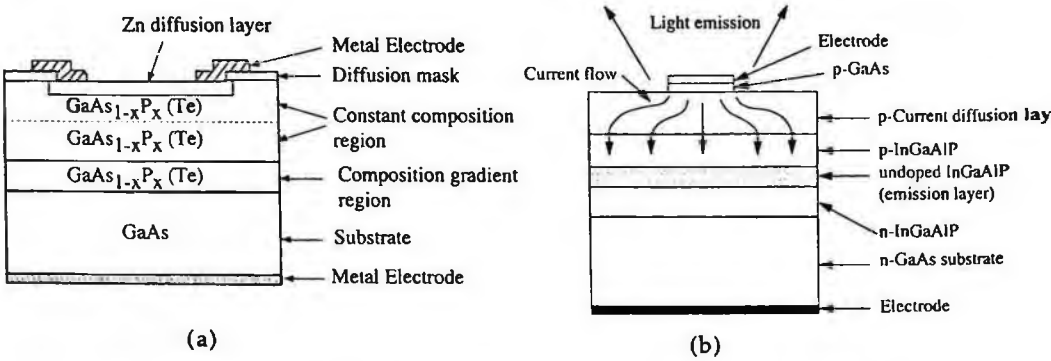

Fig. 6.7 Yellow and orange LEDs based on (a) GaAsP and (b) InAlGaP.

6.7(b)). Since InAlGaP has good lattice matching with GaAs, high quality double hetero structures can be grown, and thus high luminosity LEDs can be produced.[41-44]

- *Green LEDs*

GaP has a bandgap of 2.26 eV which corresponds to the wavelength of 555 nm, pure green light. GaP is therefore used for green LEDs (Fig. 6.8(a)). When N is doped in GaP, it makes isoelectronic levels and direct transitions can be realized between the valence band and N levels. This is the reason why N doped GaP has strong luminosity. Since N level is slightly lower than the bottom of the conduction band, the wavelength of emitted light becomes yellow green, slightly longer than that expected for GaP.[45, 46]

Pure green GaP LEDs have been produced by liquid phase epitaxy.[47] The epitaxial growth has been performed by the temperature difference method by controlled vapor pressure (TDM-CVP). Since GaP itself is an indirect transition material, the luminosity itself is very weak. Besides this, red emission is predominant in GaP due to complex

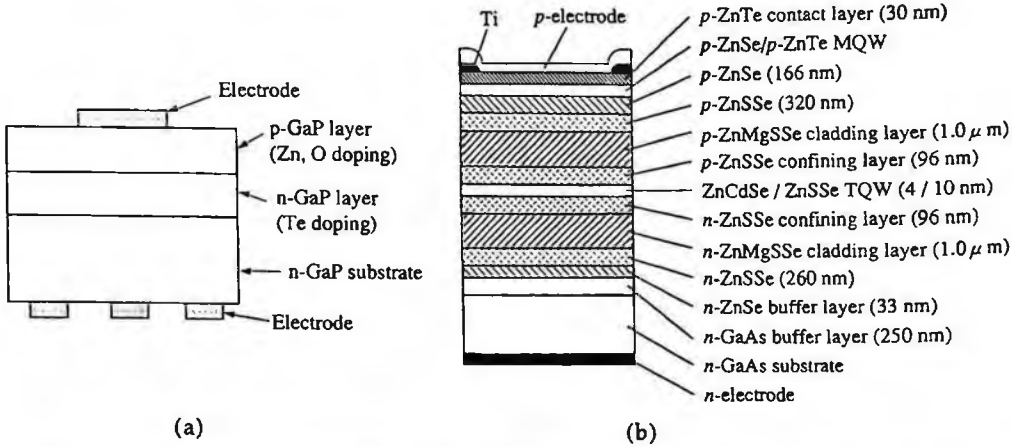

Fig. 6.8 Yellow green LEDs based on (a) N-doped GaP and (b) blue-green LEDs with ZnCdSe/ZnSSe/ZnMgSSe on GaAs (from Ref. 51 with permission).

defects. In liquid phase epitaxy, this red emission is suppressed by purification and pure green emission can be achieved.[48] The luminosity is however lower than N-doped yellow-green GaP LEDs.

Another attempt at achieving pure green LEDs uses ZnTe material. ZnTe has a bandgap of 2.26 eV which corresponds to pure green light 555 nm and ZnTe is a direct bandgap material. ZnTe is therefore a promising material for pure green LEDs. ZnTe has however two main problems. One is in that high quality material cannot be obtained. Secondly, pn junctions can not be realized due to the self-compensation problem. Sato et al. however first showed that a pn junction can be reproducibly made using high quality ZnTe single crystals and showed LED emission in preliminary results.[49, 50]

ZnSe has been studied for blue-green LEDs, based on ZnSe based epitaxial layers on GaAs substrates[51,52] as shown in Fig. 6.8 (b). As explained in Sec. 4.2.5, the difficulty of pn junction formation because of the self-compensation phenomenon is the obstacle for this LED. The other obstacle is that it is difficult to obtain high quality bulk single crystals of ZnSe. There are reports that high efficiency, long lifetime LEDs based on the homo-epitaxial growth of ZnSe to ZeSe substrates can be prepared by vapor phase growth.[53, 54]

Blue-green LEDs have recently been realized based on GaN materials. These LEDs were developed by the extension to longer wavelengths of blue LEDs based on GaN as explained below. To obtain blue-green, the In content in the InGaN active layer is increased from blue (x = 0.2) to pure green (x = 0.4). This increase of the In content makes it difficult to fabricate InGaN layers due to the phase separation in the InGaN phase. This phase separation problem is well resolved in commercial LEDs.[55-57]

- *Blue and violet LEDs*

For full color displays, three primary colors, red, green, blue are necessary. Red and green LEDs already existed but blue LEDs have only recently been achieved. Several materials have been investigated for blue LEDs.

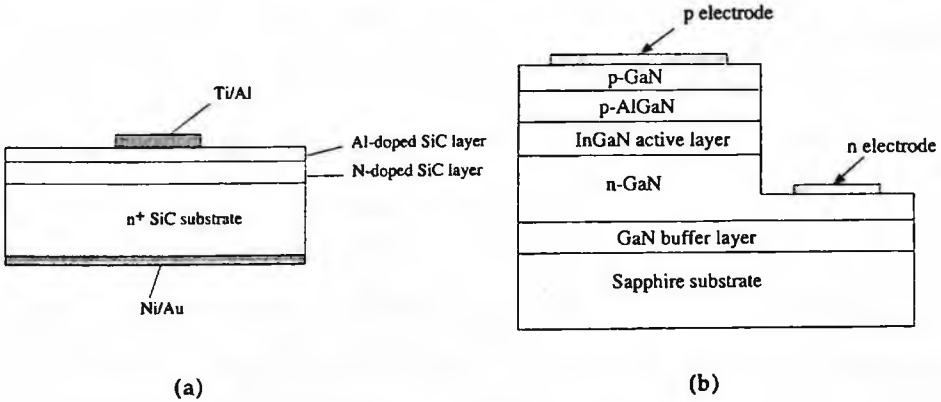

Fig. 6.9 Blue LED based on (a) SiC and (b) GaN.

Blue LEDs based on SiC have been explored for a long period. SiC has a bandgap of 2.93 eV and is a promising material for blue LEDs.[58] SiC crystals have been grown by the Lely method and large diameter substrates have been reported. Blue light emission has been reported using the homoepitaxial pn junction as shown in Fig. 6.9(a).

Blue LEDs have been industrially achieved based on InGaN layers grown by MOCVD on sapphire substrates (Fig. 6.9(b)). In this system, highly efficient blue LEDs can be produced even though there is a large lattice mismatching between epitaxial layers and substrates.[59-64] The mechanism of this high efficiency is still under question but it may be related to the existence of In which promotes carrier localization. By reducing the In content, it is also possible to produce violet LEDs.[65]

- White LEDs

White light LEDs are promising devices not only for backlighting of cellular phone screens and automobile panels but also for illumination lighting replacing incadescent lights and fluorescent lights. In order to achieve brightness exceeding the present lighting devices, various white light LED structures have been proposed[66-68] as shown in Fig. 6.10. A simple way is to use three RGB LEDs as shown in Fig. 6.10(a) but this is too costly.

The first white light LEDs were realized applying blue light LEDs to excite yellow phosphors[68] as shown in Fig. 6.10 (b). The combination of blue light and yellow light makes white light. This configuration however does not give satisfactory chromaticity. In order to achieve better chromaticity, various phosphors have been investigated.

The other structure is to apply ultraviolet LEDs to excite three color (RGB) phosphors in order to achieve white light emission of satisfactory chromaticity (Fig. 6.10 (c)). This structure has been proposed in a Japanese national project named " The lighting toward the 21st century" [69] and reported white light LEDs.[70]

Matsubara et al.[71-73] have developed phosphor-free white light LEDs using ZnSe LEDs which emit blue light. In this structure, yellow light is emitted from the ZnSe substrate due to excitation by the blue light. This is because ZnSe substrate material emits yellow light due to native defects in the substrate material. Blue light from the LED structure and yellow light from the substrate causes white light to be emitted.

Another structure is based on quantum dots and rare earth metal doped structures (Fig. 6.10(d)). Damilano et al.[74] showed that white light emission can be achieved from a structure involving various sizes of quantum dots. The application of quantum dots for white light emission is very practical since good white light needs the integration of light of various wavelengths. This need compensates for the difficulty of the control of quantum dot size. The fact that various sizes of quantum dots are spontaneously made helps by producing light of various wavelengths. The other advantage of quantum dot LEDs is that no phosphor is necessary since the quantum dots can emit all colors by being of all different sizes. The chromaticity of the quantum dot LED is however very limited since the colors are not all pure. To counter this disadvantage, the doping of rare earth metals is effective. In fact, Steckl et al.[75] have shown that white light LEDs can be made from quantum wells doped with rare earth metals. Rare-earth metals have been doped as emitters in quantum dots and it was shown that RGB and white light

emissions can be achieved.[76]

(3) Ultraviolet (UV) LEDs

Ultraviolet LEDs are important not only as light sources for white light LEDs but also for various applications such as gas decomposers, deodorizers, bill detectors and so on. Near UV (NUV) LEDs have been developed using InGaN based emitting layers[77] as in the case of blue LEDs, while ultraviolet LEDs have been studied using Al(In)GaN based emitting layers instead of InGaN based emitting layers[78-80] as shown in Fig.

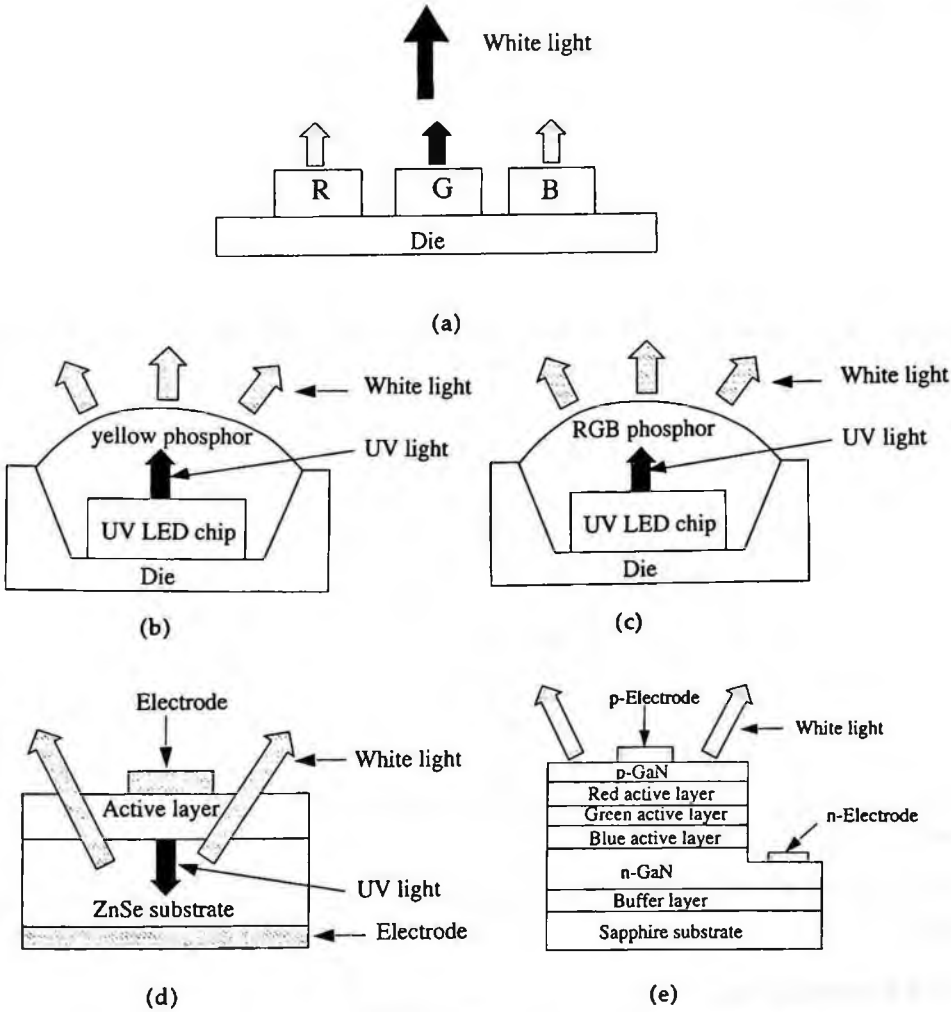

Fig. 6.10 White LED structures. (a) Three RGB LEDs, (b) blue LED with yellow phosphor, (c) ultraviolet LED with three color phosphors, (d) ZnSe LED without phosphor, (e) three RGB active layer LED without phosphor.

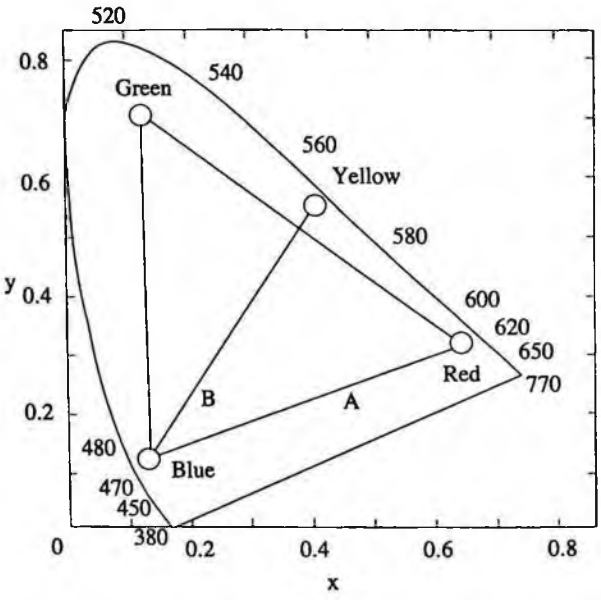

Fig. 6.11 CIE Chromaticity coordinates (x, y) diagram. White light can be made from three colors (A) or from two colors (blue and yellow) (B).

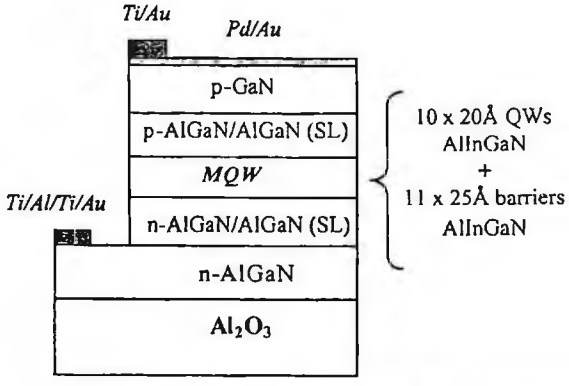

Fig. 6.12 Ultraviolet LED structure with quaternary MQW active layer (from Ref. 80 with permission)

6.12(a). Various structures are now under investigation in order to increase the intensity.[81]

6.2.3 Photodetectors

When light is absorbed in semiconductor materials, electron-hole pairs are generated. This occurs as intrinsic transitions from the valence band to the conduction band or as extrinsic transitions via impurity levels. A general photodetector has basically three

processes: (1) carrier generation by incident light, (2) carrier transport and/or multiplication, and (3) interaction of current with the external circuit to provide the output signal. In order to take out generated carriers as external current, there are several structures such as photoconductor cells, photodiodes (pin photodiodes, Avalanche photodiodes) and phototransistors. In Fig. 6.13, the detectability and the detection bandwidth of various photodetectors are summarized. The detectivity D* is defined as,

$$D^* = \frac{A^{\frac{1}{2}} B^{\frac{1}{2}}}{NEP} \qquad (6.1)$$

here, A is the detector area, B the bandwidth and NEP the noise equivalence power. There are several reviews of photodetectors.[82-88]

Various materials have been used as photodetectors such as HgCdTe and CdTe[89] for far-infrared detectors, lead compounds (PbS, PbSe, PbTe, PbSnTe)[90] and InSb for infrared detectors,[91, 92] and GaAs[93, 94] and InP[95, 96] are used for infrared detectors for optical communications. For ultraviolet (UV) detectors, various materials such as SiC, GaN and AlN are under development.[97-99] Using AlGaAs/GaAs quantum wells, it is also possible to produce far-infrared detectors, known as quantum well infrared detectors (QWIP).[100]

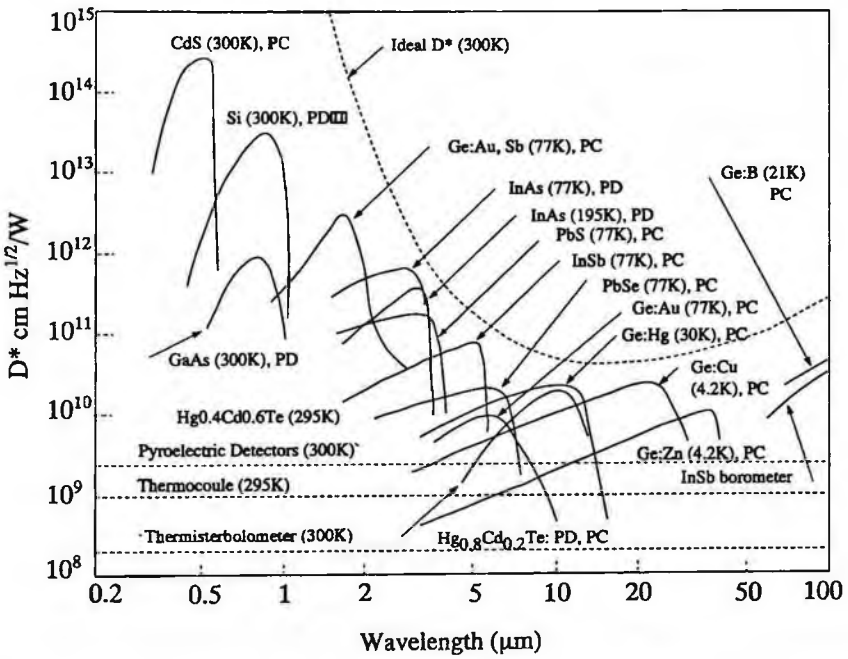

Fig. 6.13 Detectivity for various photodetectors (PC: photoconductor and PD: photodiode) (from Ref. 88 with permission).

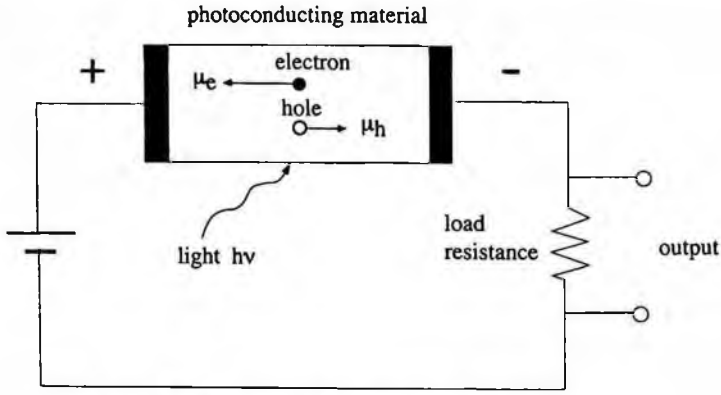

Fig. 6.14 photoconductive cell operation.

(1) Photoconductor cells

Photoconductors are based on the photoconductive effect.[101] Carriers generated by light absorption are transported in semiconductors and the generated current is simply detected as seen in Fig. 6.14. The photoconductivity due to light irradiation is represented as follows.

$$\Delta\sigma = e(\mu_e \Delta n + \mu_h \Delta p) \qquad (6.2)$$

Here, $\Delta\sigma$ is the photoconductivity, Δn and Δp are electrons and holes generated by light irradiation. Materials which have high photoconductivity compared with the conductance in the dark are appropriate for photoconductors.

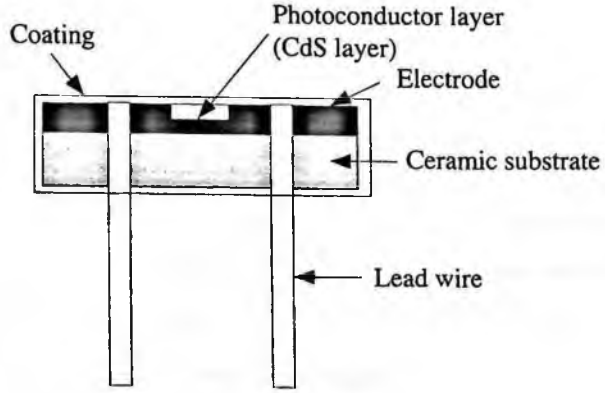

Fig. 6.15 Schematic diagram of a CdS photoconductor.

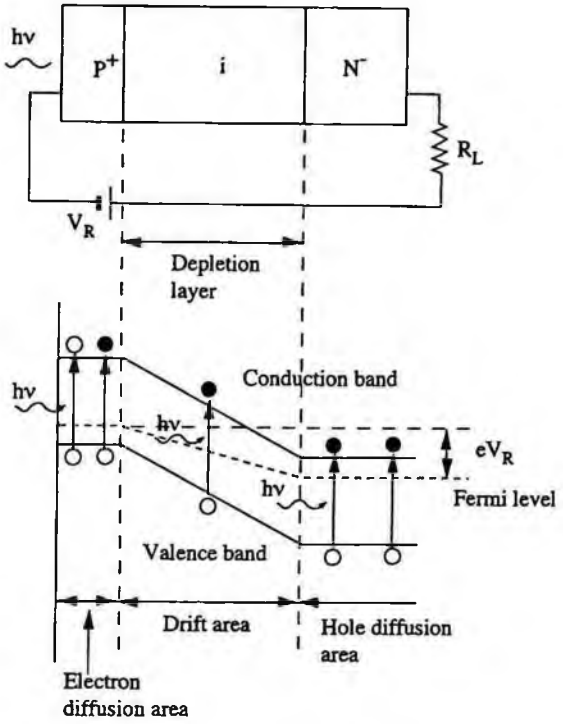

Fig. 6.16 Operation of pin-photodiode.

Photoconductors including CdS photocells for visible light detectors (Fig. 6.15), and CdSe, PbS, PbSe and InSb photocells for infrared detectors have been made. HgCdTe, PbSnTe are used for far infrared detectors. Fig. 6.15 shows a CdS photocell which is used as a camera photometer and automatic luminance control system.

(2) Photodiodes (PDs)

Photodiodes are based on a pn junction structure under reverse bias.[102] When light is absorbed in the junction area, electrons and holes generated in the depletion region are transported to both electrodes due to the high electric field in the depletion region. Apart from simple pn-PDs, there are two other more sensitive photodiodes, pin-PDs and Avalanche PDs.

- pin-PDs

In the case of pin PDs, an i-layer with low carrier concentration and a thin p^+ layer are formed on an n^+ substrate as seen in Fig. 6.16. When the reverse bias is applied between the cathode and the anode, the depletion region is expanded in the i-layer and a high electric field is formed in the i-layer. When light strikes the surface, the anode side, it is absorbed exponentially as a function of depth. Excited carriers in the depletion re-

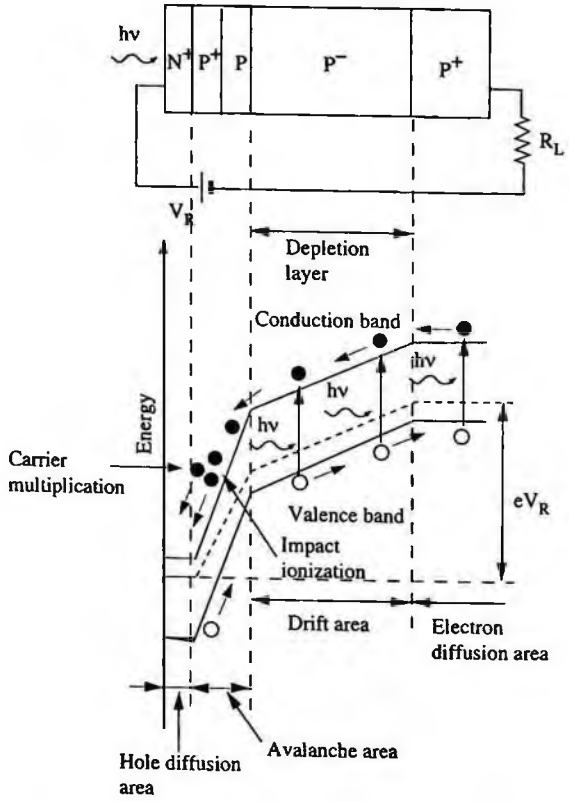

Fig. 6.17 Operation of avalanche photodiode.

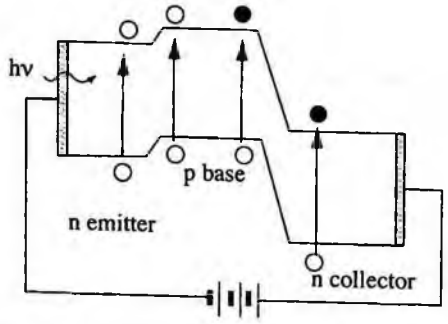

Fig. 6.18 Phototransistor operation.

gion are transported to both electrodes with high saturated drift velocity (Fig. 6.16). Since the electric field is much higher in the i-layer than in the n-layer for conventional pn-PDs, the photoresponse of pin-PDs is fast and the cutoff frequency is of the order of several 10 kHz. Carriers in the p^+ layer and n^+ substrate are transported by diffusion so that their velocity is small and the recombination of carriers occurs easily so that the photosensitivity deteriorates. From this point of view, the thickness of these layers must be well designed. Various photodiodes based on GaAs, GaAsP, InGaAs(P),[103] InAs, HgCdTe and PbSnTe have been realized.

- Avalanche PDs

In the case of Avalanche photodiodes (APDs), a low doping p-layer is formed in the pn junction as shown in Fig. 6.17 and a very high electric field can appear in this layer.[102, 104] When carriers generated by light irradiation are injected into this layer, they are amplified by impact ionization. This is called the Avalanche effect. This multiplication factor M is represented by the following Miller's empirical equation,

$$M = \frac{1}{1 - (V/V_B)^n} \qquad (n = 2 - 6) \qquad (6.3)$$

where V is the bias voltage and V_B the breakdown voltage.

APDs thus have a high multiplification factor up to M = 1000 and are very sensitive so that they are low noise and high speed detectors with cutoff frequencies of several GHz. However, their performance is very sensitive to temperature so that precise temperature control is required. Avalanche photodiodes are made not only with Si and Ge but also with compound semiconductors, such as GaAs, InP, InGaAs(P) and GaAlSb.

(3) Phototransistors

Phototransistors are based on p-n-p or n-p-n transistors in which the base region is used as the light active region without the electrode. The emitter is forward biased and the collector is reverse biased. In the case of the n-p-n structure, holes generated by light irradiation gather in the base while electrons generated by light irradiation flow from the base to the emitter and to the collector. The base energy level is therefore more positively biased and because of this forward bias, electrons are injected from the emitter to the base as shown in Fig. 6.18. Therefore. the photocurrent is multiplied due to this forward biasing. The multiplication is about $10\text{-}10^3$ but the photoresponse is low because carriers are transported by diffusion.

Phototransistors are made with Si and even with compound semiconductors.[105] They are applied in fire alarm sensors, crime prevention sensors, mark readers and writing-pens.

6.3 ELECTRONIC DEVICES

Electronic devices using compound semiconductor materials are mainly based on semi-insulating GaAs and InP, but recently GaN and SiC materials have been exten-

sively investigated. The fundamentals of electronic devices can be seen in Refs. 106-108. As shown in Fig. 1.22, GaAs has higher saturated electron velocities compared with Si. High frequency devices can thus be developed using GaAs substrates and they are widely used in many fields. GaAs devices were first developed for military applications in the US, but they are now used for many civil applications. Successful examples of them are cellular phones and satellite broadcasting applications. InP is another candidate for electronic devices. As shown in Fig. 1.22, InP has a high saturated electron velocity and therefore is believed to be more promising than GaAs for electronic devices. These high frequency devices are promising for anticollision automotive radars.[109]

Recently, a demand has developed for electronic devices for automobiles to handle high powers for hybrid, electric and fuel cell cars. As seen in Table 6.3, wide band gap compound semiconductors, especially SiC and GaN are promising materials for these high power devices.[110, 111]

Device structures are classified as shown in Table 6.4. Details of these devices are reviewed in various publications. In this chapter, they are briefly explained from the viewpoint of material development.

6.3.1 Metal-Semiconductor Field Effect Transistor (MESFET)

MESFET as reviewed by Sze[112] was first proposed by Mead.[113] MESFET (metal field effect transistor) is based on the Schottky diode gate[114] as shown in Fig. 6.19. Three electrodes, source, gate and drain are formed on a conductive layer (an active layer) which is formed by ion implantation or epitaxial growth. A current is passed through the source and the drain and is controlled by applying a voltage to the gate electrode. The gate is based on a Schottky diode, and by applying a negative bias, the depletion

Table 6.3 Electronic Device Performances of Various Materials (from Ref. 110 with permission)

	Si	GaAs	4H-SiC	6H-SiC	3C-SiC	GaN	Diamond
Bandgap (eV)	1.11	1.43	3.02	2.86	2.20	3.39	5.47
Thermal conductivity (W/cm•K)	1.51	0.54	4.9	4.9	4.9	1.3	20.9
Electron mobility (cm^2/V•sec)	1500	8500	1000	460	800	900	1800
Hole mobility (cm^2/V•sec)	450	420	120	10	70	400	1600
Saturated drift velocity $x10^7$ (cm/sec)	1	2	2.7	2.0	2.0	2.7	2.7
Breakdown field (10^5 V/cm)	3	6.5	35	28	12	26	56
Figure of merit							
Johnson' index	1	19	990	400	730	550	2500
Key's index	1	0.52	5.8	5.0	5.8	1.5	32
$1/R_{on}$	1	53	890	260	490	340	3900
f_{max}	1	14	13	4.9	8.0	9.1	50

Table 6.4 Various Electronic Devices

FET	MESFET	GaAs, InP
	MISFET	InP, SiC
	JFET	GaAs, AlGaAs/GaAs, SiC
	HEMT	AlGaAs/GaAs, AlGaN/GaN
BT	HBT	AlGaAs/GaAs/AlGaAs
SIT		GaAs/GaAs
BED	Gunn diode	GaAs,InP

FET: Field Effect Transistor, MESFET: Metal-Semiconductor Feiled Effect Transistor, JFET: Junction Field Effect Transistor, MISFET: Metal-Insulator-Semiconductor Field Effect Transistor, HEMT: High Electron Mobility Transistor, BT: Bipolar Transistor, HBT: Hetero Bipolar Transistor, SIT: Static Induction Transistor, BED: Bulk Effect Device, GD: Gunn diode

layer is expanded so that the source-drain current is controlled. In the case of GaAs, Schottky electrodes can be easily formed and this is one of the main reasons why GaAs electronic devices have been widely developed.[114] Since undoped semi-insulating GaAs can be used, isolation between MESFETs is easy only requiring the substrate material. This is very advantageous compared to Si in which pn junctions are necessary for device isolation. This is one of the reason why GaAs ICs are believed to be promising from the viewpoint of low power dissipation.

In the case of InP, Schottky electrodes can not be formed easily. This is the reason why the development of InP electronic devices has been slow compared with GaAs. The reason why it is difficult in the case of InP may be because the native oxides such as In_2O_3 and P_2O_5 are not stable while the native oxides such as Ga_2O_3 and As_2O_5 are stable. The achievement of a stable InP Schottky electrode would therefore be highly desirable and one monolayer of stable oxide has shown promise.[115]

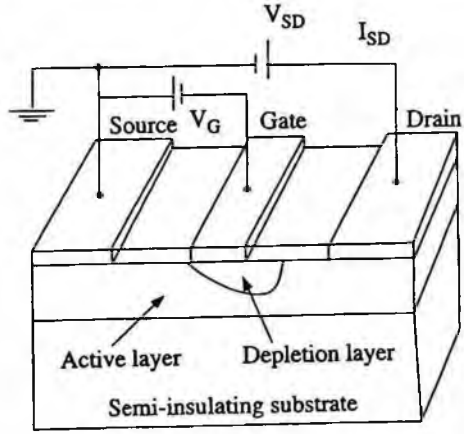

Fig. 6.19 Metal-Semiconductor Field Effect Transistor (MESFET)

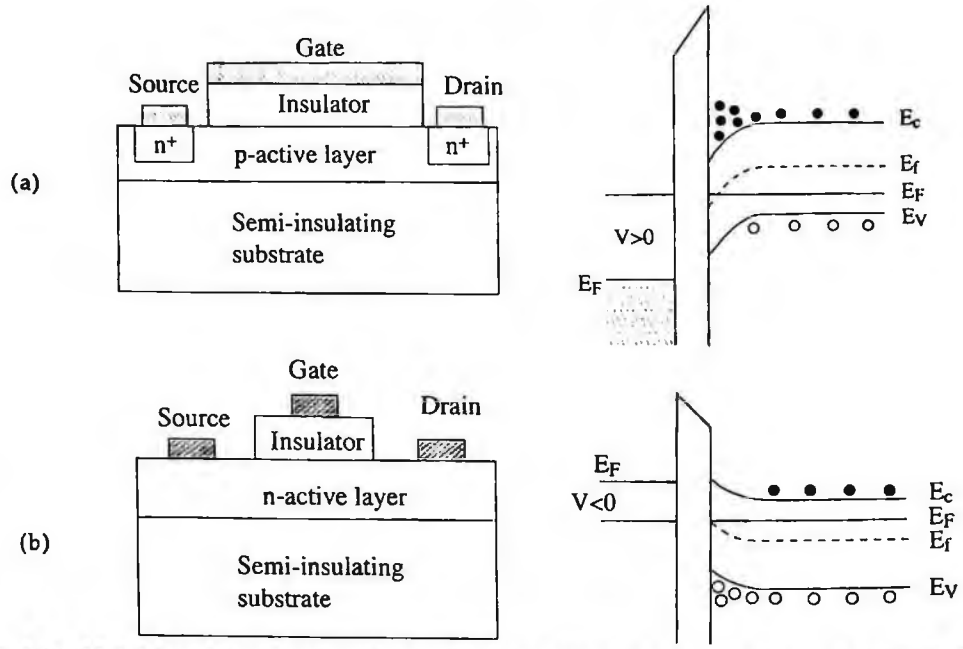

Fig. 6.20. Metal-Insulator-Semiconductor FET (MISFET). (a) inversion type MISFET, (b) depletion type MISFET.

6.3.2 IGFET (Insulating Gate FET)/MISFET(Metal-Insulator-Semiconductor FET)/MOSFET(Metal-Oxide-Semiconductor FET)

The first IGFET using GaAs was reported by Becke and White.[116] IGFETs are also known as MISFETs and MOSFETs. These devices are based on a gate which is formed by a metal-insulator-semiconductor structure as shown in Fig. 6.20. There are two types devices, the inversion type and the depletion type. As shown in Fig. 6.20 (a), when a positive voltage is applied to the gate, minority carrier electrons accumulate at the surface of the p-substrate and an n-channel is formed. The current through this n-channel can be controlled by the gate voltage. This is called the inversion-type device and is normally-off since when the gate is not biased, no n-channel is formed and no current flows.

The depletion type device is as shown in Fig. 6.20 (b). The gate is formed on an n-type substrate. When no bias voltage is applied at the gate, current flows through the n-substrate between the source and drain. This current is controlled by expanding the depletion layer under the gate by applying a negative gate bias. This is a normally-on type device since current flows through the source and the drain when no gate bias is applied. The structure is similar to MESFETs but the source-drain current is controlled by the depletion layer formed under the insulating layer.

The advantage of these devices is in the fact that depletion and accumulation type devices can be made so that complementary devices for integrated circuits (ICs) become possible, but it is difficult to find good insulating layers.

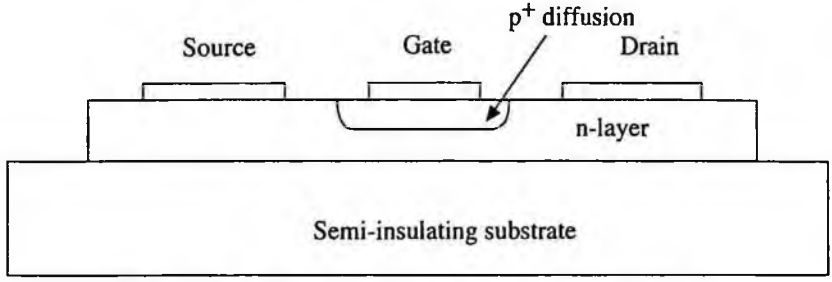

Fig. 6.21 Junction Field Effect Transistor (JFET).

In the case of GaAs, because of the high concentration of interface levels, the inversion type device can not be realized. The depletion type device however has been shown to be possible[117] since the Fermi level can be changed in the range where there are not many interface levels. In the case of InP, inversion type devices can be made much more easily than with GaAs since the positions of interface levels are close to the conduction band.[118]

6.3.3 Junction Field Effect Transistor (JFET)

The operation of JFETs was first proposed by Schockley[119] and analyzed by Decay and Ross.[120] The operation of GaAs based JFET was then analyzed by Lehovec and Zuleeg.[121] This device is based on a pn structure as the gate as shown in Fig. 6.21. The current through the active layer is controlled by applying the bias voltage to the gate and varying the depletion layer in the pn junction. JEFTs based on GaAs have been reported.[122] Planer type JFETs[123] and hetero junction type JFETs[124] have been reported. The advantage of the JFET is that both normally-on type and normally-off type devices can be made so that complementary circuits can be made for ICs, and that high transconductance (g_m) and high saturation current can be obtained. In fact, JFET ICs have been developed using GaAs substrates.[125]

6.3.4 High Electron Mobility Transistor (HEMT)

The HEMT was invented by Mimura et al.[126] based on the application of nAlGaAs/undoped GaAs modulation doped layer[127] as the active layer of FET. When an undoped active layer (GaAs) is covered by a larger bandgap highly n-doped layer (AlGaAs) as shown in Fig. 6.22, carriers in the highly n-doped layer are injected into the undoped layer and without doping the undoped layer a two dimensional electron gas (2DEG) with high carrier concentration can be formed which acts as the active layer. Since high carrier concentration can be achieved, high electron mobility can be obtained without impurity scattering. Because of this 2DEG, high mobility transistors can be made.

The first HEMT was made using AlGaAs/GaAs layers on GaAs substrates and was developed using higher mobility InGaAs/InP layers on InP substrates. The highest cut-off frequency reported is in excess of 500 GHz.[128]

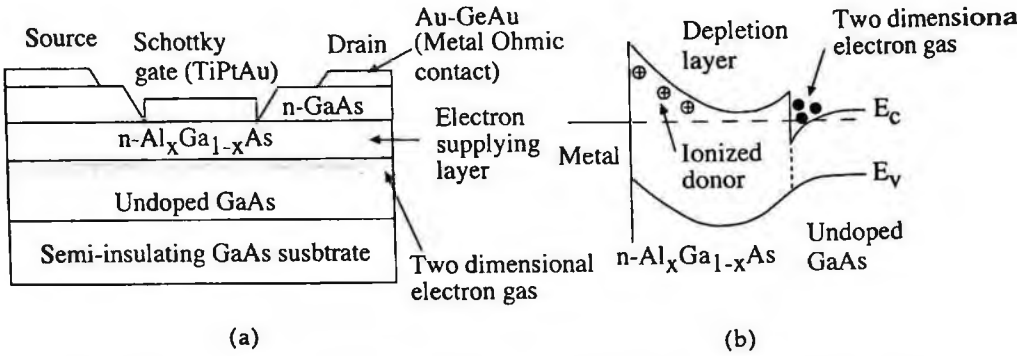

Fig. 6.22 (a) Structure of depletion-HEMT, (b) band diagram of depletion-HEMT

6.3.5 Hetero Bipolar Transistor (HBT)

This is a bipolar transistor in which a wide bandgap material is used as the emitter. The operation analysis of this device was first performed by Kromer.[129] The advantages of this structure are as follows.

(i) The reverse injection of minority carriers from the base to the emitter is small so that high emitter injection efficiency and high current gain are obtained.

(ii) Even though the base concentration is made high, high current gain is obtained with low base resistance so that a high speed transistor with high current gain is achieved. In the 80's, supported by the development of MBE and MOCVD, various HBTs have been extensively studied.

In Fig. 6.23, a typical HBT, with n-AlGaAs emitter, p$^+$ GaAs base and n$^+$-GaAs collector is shown [130]. In the HBT, electron carriers flows from the emitter through the base to the collector, and this collector current (I_C) is controlled by the base current (I_B). The HBT is thus a current driven device which is different from the FET where the source-drain current is controlled by the gate voltage, that is a voltage driven device. HBTs have the following advantages.

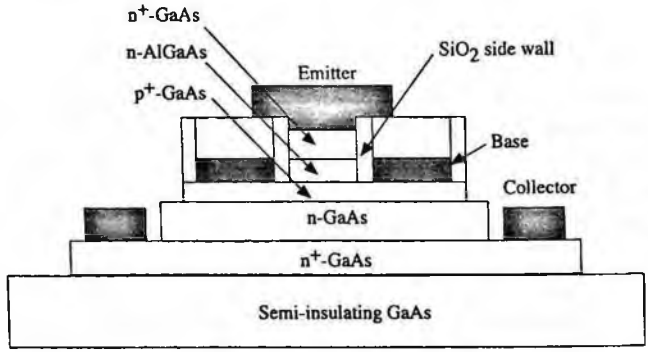

Fig. 6.23 Schematic structure of hetero bipolar transistor (HBT).

(i) While FETs need two power supplies, negative one and positive one, HBTs can be operated by only one power supply.

(ii) Current can be made to flow perpendicularly to the surface of the substrate so that the current per surface area can be made large and the area of transistors can be made small.

(iii) Signal deviation is small so that it is appropriate for cellular phone communication over CDMA networks.

HBTs have been also developed not only using AlGaAs/GaAs layers on GaAs substrates but also using InGaAs/InP layers on InP substrates. The highest cutoff frequency reported so far came close to 1 THz.[130]

6.3.6 Gunn Diodes

Gunn[131] first found that when a bias is applied at two Ohmic contacts either side of n-GaAs, it oscillates with high frequency when the electric field exceeds a threshold value. This is called Gunn effect and it was explained by Kroemer[132] as a RWH (Ridley-Watkins-Hilsum) mechanism.

GaA has two conduction valleys, L valley and U valley as seen in Fig. 1.10. Electrons at the L valley have higher mobility, having small effective mass, than those at the U valley where electrons have larger effective mass. When the electric field is increased, electrons at the L valley move to the U Valley so that the mobility is decreased. Mean drift velocity as a function of the electric field is therefore shown as Fig. 6.24. It is seen that between E_1 and E_2, there is a negative resistance.

Because of this negative resistance, a high field dipole domain is generated in the GaAs as shown in Fig. 6.25, where electrons accumulate at the cathode side and holes accumulate at the anode side because the electric field is high and the mobility is low in the domain. When this domain reaches the anode, since there is no low mobility area, a heavy current flows and then a new domain is generated at the cathode and moves from the cathode to the anode. Because of this domain transfer, high frequency oscillation occurs. The frequency, f, is represented as follows,

$$f = v/L \qquad (6.4)$$

where v is the mean drift velocity of the domain and L is the thickness of GaAs bulk material. The Gunn effect is observed for GaAs, InP, CdTe and GaAsP and Gunn diodes based on InP which oscillate at 500 GHz have been reported.[133]

6.3.7 Integrated Circuits (ICs)

The above fundamental devices are integrated as digital ICs[134] for computer applications, as MMICs[135] for wireless communications especially for cellular phones and as OEICs[136] for high speed fiber communications.

Following the report of a GaAs MESFET,[113] the operation frequency has been improved up to microwave range[114] and even logic devices based on Gunn devices have been studied.[137, 138] The first logic device using GaAs MESFETs was reported from

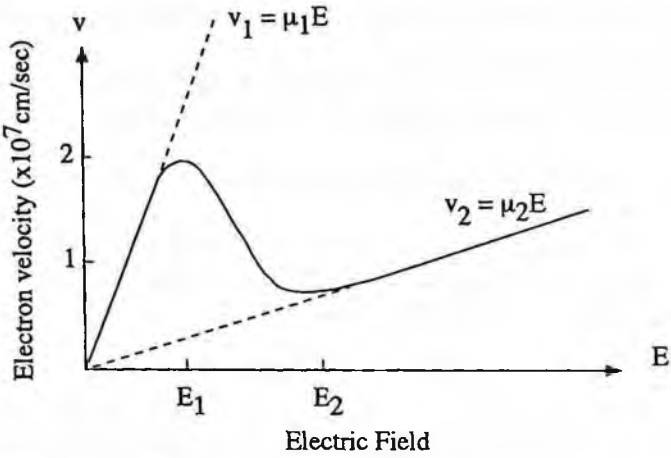

Fig. 6.24 Dependence of the velocity of conducting electrons of n-type GaAs on the electric field.

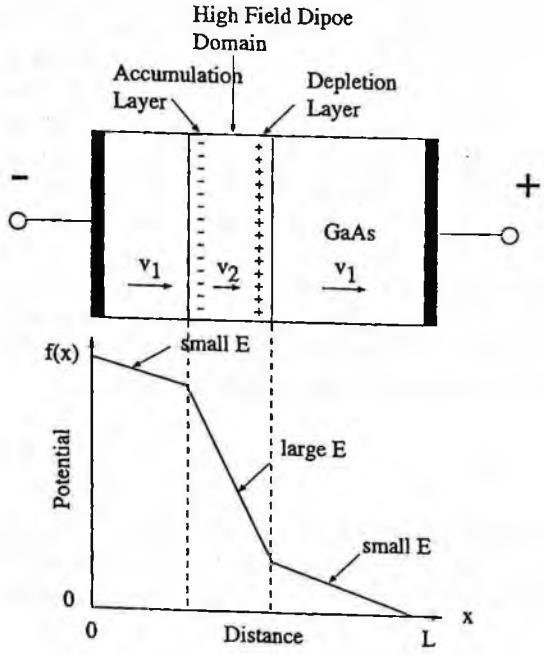

Fig. 6.25 Operation of the Gunn diode.

HP[139] and since then GaAs logic ICs have been developed extensively. The concept of Optoelectronic Integrated Circuits (OEICs) was proposed by Somekh[140] and the first OEIC was reported by Ury et al.[141] The combination of high frequency devices with

optoelectronic devices has been extensively studied to develop small-scale ICs for fiber communication systems. These OEICs have been developed mainly based on GaAs substrates for short wavelength (0.8-0.9 μm) and on InP substrates for long wavelength (1-1.6 μm) applications. Various OEICs are reviewed in Refs. 136, 142 and 143. GaAs ICs are now important for high-speed local, point-to-point and local-area network (LAN) communications.[144]

6.3.8 Power Devices

For power devices based on SiC substrates, various structures such as SBDs, JFETs, MOSFETs and SITs have been extensively studied.[110, 111, 145] AlGaN/GaN HEMTs using SiC substrates or Si substrates are also under development for power devices.[146, 147] These high power devices with higher frequencies and high break down voltages are promising for automobile applications and for low power consumption switching devices.

6.4 SOLAR CELLS

Solar energy, based on the nuclear fusion in the sun, is an eternal, environmentally friendly and clean form of energy which is expected to reduce the consumption of fossil fuels which generate CO_2 gas destroying the earth's environment. Si based solar cells such as single crystal Si, polycrystal Si and amorphous Si are made industrially. Compound semiconductor solar cells are however promising from the viewpoint of energy conversion efficiency and radiation resistivity. The principle and various solar cells are reviewed in Refs. 148-150.

As shown in Fig. 6.26, compound semiconductors have higher absorption coefficients because most of them are direct transition so that the thickness of the solar cell can be smaller than Si which is indirect transition. This is the main reason why compound semiconductors are promising for solar cells.

Typical solar cells are based on the photovoltaic effect which occurs at the pn junction as shown in Fig. 6.27. When the solar cell is irradiated with light, electron-hole pairs are generated. When the pn junction is short-circuited as shown in Fig. 6.27 (a), electrons flow to the n region and holes flow to the p region due to the electric field in the depletion region at the pn junction. The photocurrent, I_L, thus flows out in the external circuit without any external electric field. This photocurrent is known as the short-circuit photocurrent.

When the pn junction is open-circuited as shown in Fig. 6.27 (b), electrons accumulate in the n region forming the negative space charge, and holes accumulate in the p region forming the positive space charge. Because of this space charge, the Fermi level of the n region is raised with respect to that of the p region, and the energy difference V_{OC}, which is called the open photovoltage, is formed. V_{OC} depends on the light irradiation intensity and the maximum is the diffusion voltage of the pn junction where the bottom of the conduction band of the n region equals to that of the p region.[152]

The I-V characteristics of the above pn junction are as shown in Fig. 6.28. Without light, it shows conventional diode characteristics as seen as the dark current. When

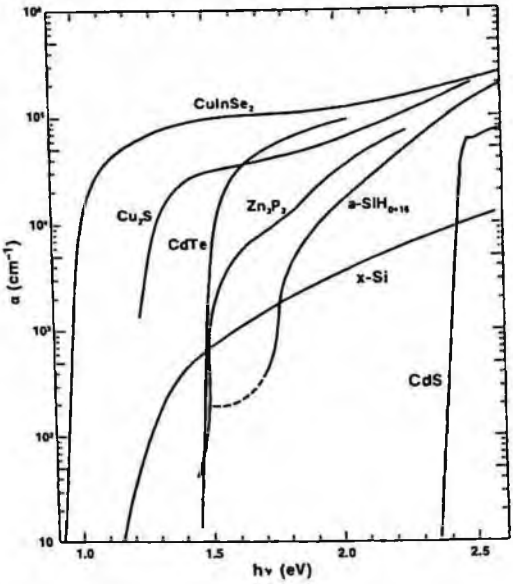

Fig. 6.26 Optical absorption coefficients for some highly absorbing compound semiconductors. Also shown are the absorption coefficients for amorphous and crystalline silicon (reprinted from Ref. 151 with permission, copyright 1982 IEEE).

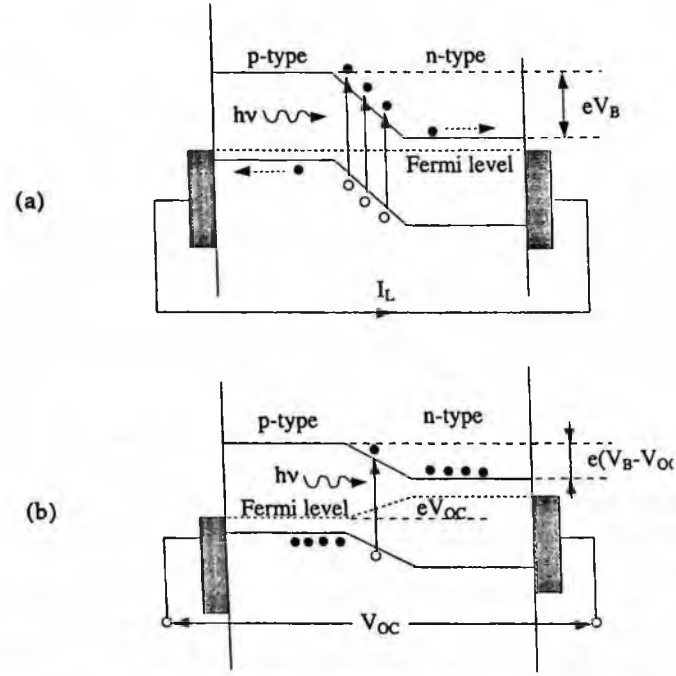

Fig. 6.27 Photovoltaic effect of the pn junction. (a) short-circuited photocurrent state, (b) open-circuited photovoltaic state.

irradiated with light, the I-V characteristics are deviated to the negative current side with I_L, the short-circuit photocurrent. This is the maximum current that can be generated. When the circuit is opened, the maximum open photovoltage, V_{oc}, is obtained without any current flow.

When a load resistance is put in the circuit, the I-V relationship is represented as follows.

$$I = I_s [\exp (eV/kT) - 1] - I_L \tag{3.5}$$

Here, IL is the photocurrent which flows reversely to the dark current, I_s [exp (eV/kT) – 1]. Here, Is is the saturation current. When I = 0, this equation gives the open circuit voltage as

$$V_{oc} = \frac{kT}{e} \ln \left[1 + \frac{I_L}{I_s} \right] \tag{3.6}$$

When V = 0, this equation gives the short-circuit current I_L.

In real solar cell operation with a load resistance, R, the current and the voltage are determined at the cross point between the I-V curve and V = – IR line. Power is consumed by the resistance with $P = RI^2$. To maximize power generation, the load resistance must be selected so that the product P = IV becomes maximum (Fig. 6.28).

Solar energy has an irradiation spectrum as shown in Fig. 6.29.[154] It has a peak at about 0.4 μm and has a long tail to longer wavelength. In order to absorb as much solar

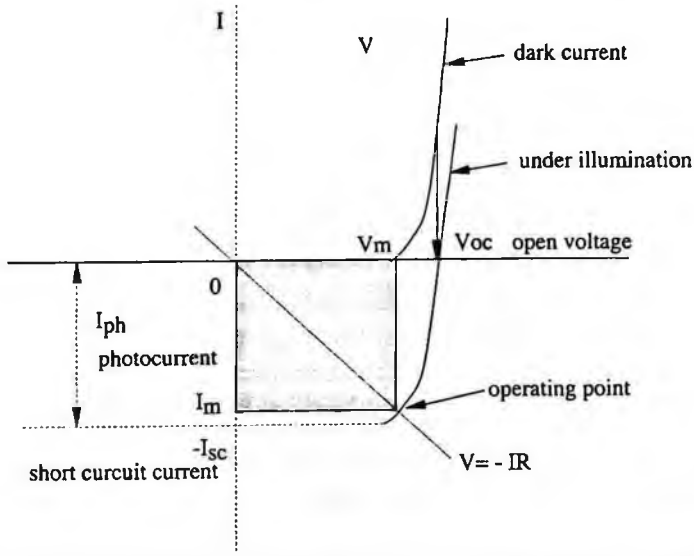

Fig. 6.28 I-V characteristics of a solar cell without light illumination and with light illumination.

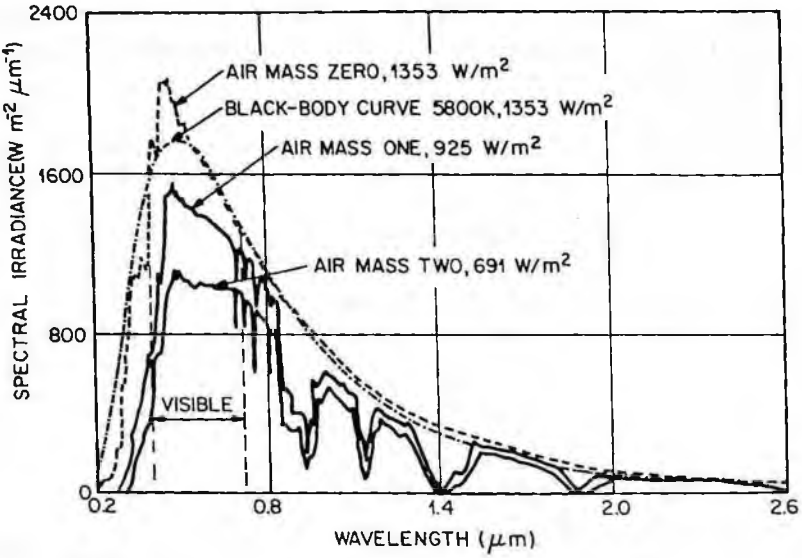

Fig. 6.29 Four curves related to solar spectral irradiance.[154]

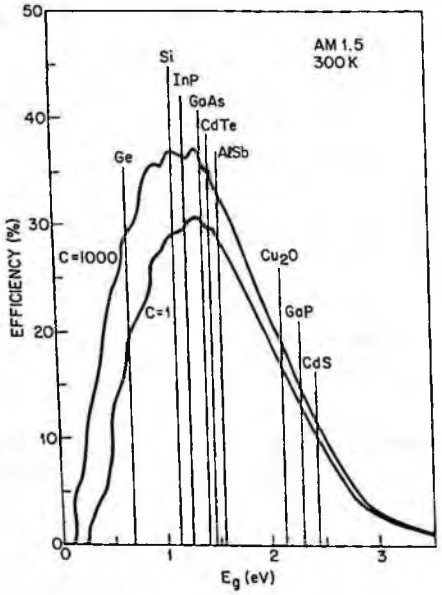

Fig. 6.30 Ideal solar-cell efficiency at 300K for 1 sun and for 1000 sun concentration.[155]

energy as possible, solar cell material must have an appropriate bandgap. It is noted that if the bandgap is too small, energy larger than the bandgap is lost as phonons and converted to heat. If the bandgap is too large, light with energy less than the bandgap is transmitted. It is thus known that there is an optimum bandgap for a solar cell to obtain the greatest energy conversion.

Fig. 6.30 shows the ideal conversion efficiency for various solar cell materials.[155] It is seen that the greatest conversion efficiency can be obtained with a bandgap around 1.4-1.7 eV.[156] CdTe, GaAs and InP are materials with high conversion efficiencies. It is also important that the material be of direct transition type so that the light can be effectively absorbed. In indirect transition materials, light is absorbed by giving energy to phonons and the energy conversion is thus reduced.

6.5 FUNCTIONAL DEVICES

Apart form the above mentioned devices, there are other devices which are classified as functional devices. They are radiation detectors, Hall devices and magnetoresistance devices.

6.5.1 Radiation Detectors

Radiation detectors include there are ionization chambers, Geiger-Muller counters, scintillation counters, proportional counters and semiconductor detectors. Regarding semiconductor detectors, various reviews are published.[5, 157-163]

When semiconductors are irradiated by, e.g., X-rays and γ-rays, electron-hole pairs are formed due to the excitation of electrons from the valence band to the conduction band. The energy for the formation of one electron-hole pair is referred to as the W value. In the case of semiconductor materials, W values are much lower than those for the ionization of gases (~30 eV). Semiconductor detectors are therefore more sensitive radiation detectors than ionization chambers. For one radiation photon, therefore many electron-hole pairs can be formed compared with other detectors. This is the reason why semiconductor detectors can be used for high energy resolution detectors. For several semiconductor detector materials, the W value is known to be represented as

$$W = 1.95\ E_g + 1.4\ eV \qquad (6.7)$$

against the energy bandgap, E_g, at room temperature[164] as shown in Fig. 6.31.

This photoelectric effect, namely the excitation of electrons from the valence band to the conduction band, depends approximately on Z^4, where Z is the atomic number. The higher the atomic number of the material, the higher the photoelectric effect against the Compton effect as shown in Fig. 6.32. Radiation stopping power is therefore proportional to the average atomic number by four. Higher Z material therefore needs less thickness to detect the same radiation energy, thus making it easier to realize detectors of small size .

Electrons and holes which are generated in semiconductor materials are transported to electrodes under the electric field. This transport velocity is represented as μE and because of the transport of both carriers, charges can be induced at the electrodes.

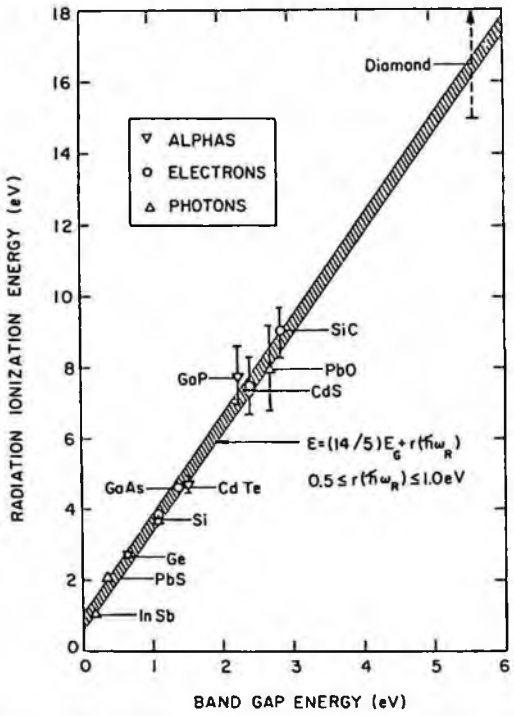

Fig. 6.31 Relationship between the bandgap energy and the average energy for electron-hole pair formation (reprinted from Ref. 164 with permission, copyright 1968 American Institue of Physics).

Table 6.5 Performances of Radiation Detector Materials

	E (eV)	Z	e(eV)	m (cm/V·s)		μτE (cm)	
				electron	hole	electron	hole
Si (300K)	1. 12	14	3. 61	1 350	480	200	200
Ge (77K)	0.74	32	2.98	3.6×10^4	4.2×10^4	200	200
SiC	2.2	14-6					
GaAs (300K)	1. 4	31-33	4. 2	8 600	400	0.086	0.004
						-0. 86	-0.04
GaP	2.25	31-15	7.8	300	100		
CdS	2.42	48-16	6.3	300	50		
ZnTe	2.26	30-52		340	100		
CdSe	1.75	48-34	5.8	720	75	29	3.0
CdTe (300K)	1. 47	48-52	4. 43	1100	100	0.5	0.025
InSb	0.17	49-51	1.2	78000	750		
GaSb	0.67	31-51		4000	1400		
InAs	0.36	49-33		33000	460		
InP	1.27	49-15		4600	150		
AlSb	1.52	13-51	5.055*	200(1200)*	550(700*)		
HgI_2 (300K)	2.13	80-53	4. 2	100	4	1	0.1

* theoretical value

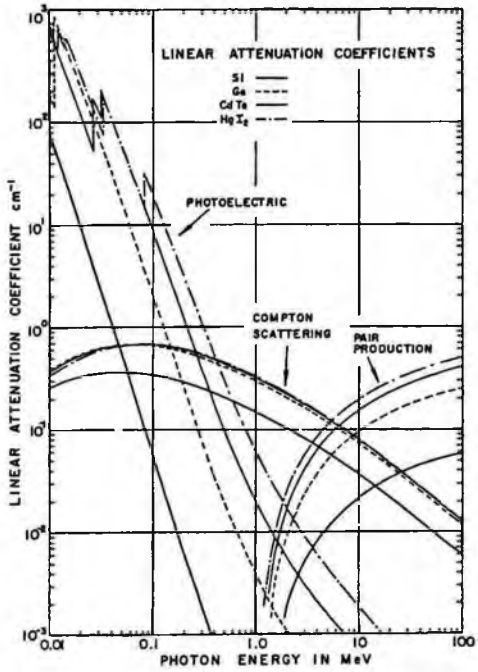

Fig. 6.32 Linear attenuation coefficients for photoelectric absorption, Compton scattering and pair production in Si, Ge, CdTe and HgI_2 (reprinted from Ref. 165 with permission, copyright 1973 IEEE).

These charges are amplified and analyzed by pulse height analyzers and the measurement of energy can be achieved. In reality, due to carrier trapping and recombination in materials because of impurities and defects, transporting carriers decay with lifetime τ. The product $\mu\tau E$, the mean free path that carriers can travel in the material, is therefore an important parameter indicating the energy resolution performance of detector materials.

Semiconductor detectors have thus the following features.

(i) Higher energy resolution

(ii) High detection efficiency

(iii) Smaller size

As shown in Table 6.5 summarized from Refs. 157-163, various compound semiconductor materials are believed to be good candidates for radiation detectors because they have higher atomic numbers and higher stopping powers. Some of them are explained in Chapter 7 and following. In practice, CdTe radiation detectors have been developed and they are mainly used in medical application fields. CdTe radiation detectors are also good candidates for radiation dosimetry and spectrometry.

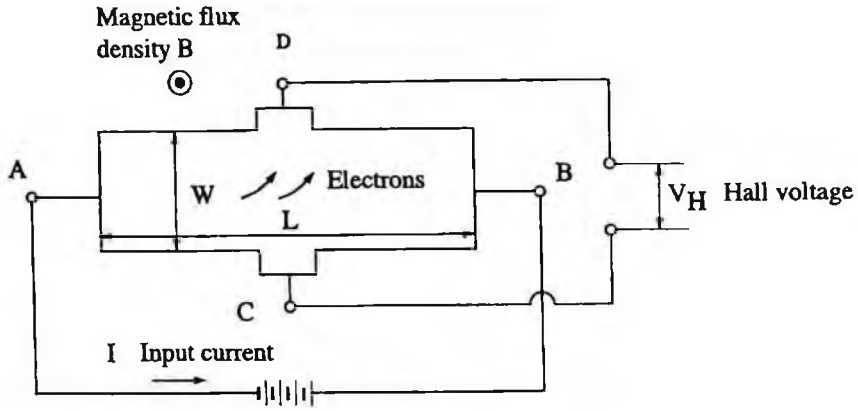

Fig. 6.33 Principle of the operation of the Hall sensor

6.5.2 Magnetic sensors

When electrons move in semiconductor materials, a magnetic field will induce a Lorenz force and the trajectory of the electrons will be changed. The greater the mobility, the higher the output due to this magnetic field. As magnetic sensor materials, compound semiconductor materials with high mobilities such as InAs, InSb and GaAs are mainly applied. Magnetic sensors include Hall devices and magnetic resistance devices. These magnetic sensors are reviewed in Refs. 6 and 165-167.

(1) Hall sensors

In Fig. 6.33, the principle of the Hall sensor based on the Hall effect[168] is demonstrated. A Hall sensor is formed from four electrodes. When a current flows through one pair of electrodes, a voltage V_H appears between the other pair of electrodes under the application of a magnetic field perpendicular to the Hall device. The Hall voltage is represented as follows.

$$V_H = R_H IB/d, \quad R_H = 1/qn \qquad (6.8)$$

Here, V_H is the Hall voltage, I the current, B the magnetic flux density, d the thickness of the Hall device, q the electronic charge and n the carrier concentration.

Table 6.6 summarizes typical Hall device performances.[169] InSb has a high mobility so that the operating voltage of Hall devices is low. GaAs has a larger bandgap so that its temperature dependence is low and the magnetic resistance effect at higher magnetic fields is negligible, giving a good linearity.[170]

(2) Magnetic resistance devices

A magnetic resistance device is formed from a rectangular shape with two electrodes.

Table 6.6 Various Hall Device Materials

	Hall mobolity μ_H ($cm^2/V \cdot sec$)	Bandgap Eg (eV)	Melting point (°C)	Electron concentration (cm^{-3})
InSb(single crystal)	70,000	0.17	530	undoped
InSb	20,000-30,000	0.17	530	$-2x10^{16}$
InAs(single crystal)	28,000	0.36	945	undoped
InAs(polycrystal)	20,000	0.36	945	$\sim 2x10^{16}$
GaAs(epitaxial)	4,500	1.4	1,237	$\sim 2x10^{16}$
GaAs(ion implantation)	3,000	1.4	1,237	$\sim 3x10^{17}$
GaSb (single crystal)	3,000	1.0	706	undoped
InP (single crystal)	4,000	1.26	1,062	undoped
InSb-GaSb (mixed crystal)	~6,000	0.2-0.36	-	-
Si	1,400	1.08	1,410	undoped

It is based on the resistance change due to the magnetic fleld. When electrons flow in the material, the Lorenz force deflects the trajectory of these electrons. This change causes change in resistance and it makes a magnetic sensitive device. For this application, InSb is mainly used.[171] These magnetic resistance devices are used for non contact

REFERENCES

1. M.W. Hodap, in *Semiconductors and Semimetals Vol. 48*, eds. R.K. Willardson and A.C. Beer (Academic Press, New York, 1997) p. 227.
2. K. Onabe, *Jpn. J. Appl. Phys.* **21** (1982) 791.
3. *Ultra High Speed Compound Semicondcutor Devices*, eds. T. Sugano and M. Ohmori (Baifukan, Tokyo, 1986)
4. T. Surek, *J. Crystal Growth* **275** (2005) 292.
5. M. Cuzin, *Nucl. Instrum. Methods* **A253** (1987) 407.
6. J. Heremans, D.L. Partin, C.M. Thrush and L. Green, *Semicon. Sci. Technol.* **8** (1993) S424.
7. S.M. Sze, *Physisc of Semiconductor Devices* (John Wiley & Sons, New York, 1981) p. 681.
8. N.G. Basov, O.N. Krokhin and U.M. Popov, *Phys. JETP* **13** (1961) 1320.
9. H. Kroemer, *Proc. IEEE* **52** (1963) 1782.
10. I. Hayashi and M. B. Panish, *J. Appl. Phys.* **41** (970) 150.
11. H.C. Casey, Jr. and M.B. Panish, *Heterostructure Lasers* (Academic Press, New York, 1978).
12. M.E. Lines, *J. Appl. Phys.* **55** (1984) 4058.
13. J.J. Hsieh, J.A. Rossi and J.P. Donnelly, *Appl. Phys. Lett.* **28** (1976),707.
14. K. Mito, in *Optoelectronics Material Manual* (in japanese) (Optronics, Tokyo, 1986) p. 281.
15. M. Hirao and M. Nakamura, *Oyo Buturi (Monthly Publ. Jpn. Soc. Appl. Phys.) (in japanese)* **12** (1980) 1207.
16. H. Wada and S. Fujiwara, in *Optoelectronics Material Manual (in japanese)* (Optronics, Tokyo, 1986) p. 288.
17. K. Kishino, A. Kikuchi, Y. Kaneko and I. Nomura, *Appl. Phys. Lett.* **58** (1991) 1822.
18. K. Itaya, M. Ishikawa, K. Nitta, M. Oajima and G. Hatakoshi, *Jpn. J. Appl. Phys.* **30** (1991) L590.
19. D.P. Bour, D.W. Treat, R.L. Thornton, R.D. Bringans , T.L. Paoli, R.S. Geels and D.W. Welch *IEEE Photonics Tech. Lett.* **4** (1992) 1081.
20. D.P. Bour, D.W. Treat, R.L. Thornton, T.L. Paoli, R.D. Bringans and B.S. Krusor, *Appl. Phys. Lett.* **60** (1992) 1927.
21. K. Kishino, *Oyo Buturi (Monthly Publ. Jpn. Soc. Appl. Phys.) (in japanese)* **74** (2005) 1477.
22. S. Nakamura and G. Fasol, *The blue Laser Diode* (Springer-Verlag, Berlin and Heidelberg, 1997)
23. S. Nakamura, M. Senoh, S. Nagahama, N. Iwasa, T. Yamada, T. Matsushita, H. Kiyoku, Y.

Sugimoto, T. Kozaki, H. Umemoto, M. Sano and K. Chocho, *Jpn. J. Appl. Phys.* **36** (1997) L1568.
24. S. Nakamura, M. Senoh, S. Nagahama, N. Iwasa, T. Yamada, T. Matsushita, Y. Sugimoto and H. Kiyoku, *Jpn. J. Appl. Phys.* **36** (1997) L1059.
25. H. Okuyama, K. Nakano, T. Miyajima and K. Akimoto, *Jpn. J. Appl. Phys.* **30** (1991) L1620.
26. E. Kato, H. Noguchi, M. Nagai, H. Okuyama, S. Kijima and A. Ishibashi, *Electron. Lett.* **34** (1998) 282.
27. K. Kobayashi,in *Optoelectronics Material Manual* (in japanese) (Optronics, Tokyo, 1986) p. 296.
28. K. Horikoshi and N. Kobayashi, *Oyo Buturi (Monthly Publ. Jpn. Soc. Appl. Phys.) (in japanese)* **12** (1980) 1214.
29. Y. Horikoshi, in *Semiconductors and Semimetals Vol. 22*, eds. R.K. Willardson and A.C. Beer (Academic Press, New York, 1985) p. 93.
30. H.C. Casey, Jr. and F.A. Trumbore, *Mater. Sci. Engineer.* **6** (1970) 69.
31. A.A. Bergh and P.J. Dean, Proc. IEEE, **60** (1972) 156.
32. M.H. Pilkuhn, in *Device Physics Vol. 4*, ed. C. Hilsum, (North-Holland, Amsterdam, 1981) p. 539.
33. H. Yonezu, *Optoelectronics Material Manual (in japanese)* (Optronics, Tokyo, 1986) p. 300.
34. T. Kawabata, *Optoelectronics Material Manual (in japanese)* (Optronics, Tokyo, 1986) p. 345.
35. Y. Okuno, *Light Emitting Diodes (in japanese)* (Sangyo Tosho, Tokyo, 1993).
36. H. Nomura, *Electronic Materials (in japanese)* **November** (1983), 67.
37. R.C. Goodfellow, A.C. Carter, I. Griffith and R.R. Bradley, *IEEE Trans. Electron. Devices* ED-26 (1979) 1215.
38. M. Hirotani, T.E. Sale, J. Woodhead, J.S. Roberts, P.N. Robson, T. Saak and T. Kato, *J. Crystal Growth* **170** (1997) 390.
39. J. Blondelle, H. De Neve, P. Domeester, P. Van Daele, G. Borghs and R. Beats, *Electron. Lett.* **30** (1994) 1787.
40. S. Ishimatsu and Y. Okuno, *Optoelectronics* **4** (1989) 21.
41. C.P. Kuo, R.M. Fletcher, T.D. Osentowski, M.C. Lardizabal, M.G. Craford and V.M. Robbins, Appl. Phys. Lett. 57 (1990) 2937.
42. H. Sugawara, K. Itaya, M. Ishikawa and G. Hatakoshi, *Jpn. J. Appl. Phys.* **31** (1992) 2446.
43. M.R. Krames, M. Ochiai-Holcomb, G.E. Hofler, C. Carter-Comen, E.I. Chen, P. Grillot, N.F. Gardner, H. Chui, J-W. Huang, S.A. Stockma, I-H. Tan, F.A. Kish, M.G. Craford, T-S. Tan, C. Kocot, M. Jueschen, J. Posselt, B.P. Loh, G. Sasser and D. Collins, *Appl. Phys. Lett.* **75** (1999) 2365.
44. F.A. Kish, F.M. Steranka, d.C. DeFevere, D.A. Vanderwater, K.G. Park, C.P. Kuo, T.D. Osentowski, M.J. Peanasky, J.G. Yu, R.M. Fletcher, D.A. Steigerwald , M.G. Craford and V.M. Robbins, *Appl. Phys. Lett.* **64** (1994) 2839.
45. R.A. Logan, H.G. White and W. Wiegmann, *Appl. Phys. Lett.* **13** (1968) 139.
46. T. Takahashi, *Monthly Display (in japanese)* **2** (1996) 43.
47. J. Nishizawa and Y. Okuno, *IEEE Trans. Electron Devices* **ED-22** (1975) 716.
48. J. Nishizawa, Y. Okuno, M. Koike and F. Sakurai, *Jpn. J. Appl. Phys.* **19 suppl. 19-1** (1980) 377.
49. K. Sato, T. Asahi, M. Hanafusa, A. Noda, A. Arakawa, M. Ucidha, O. Oda, Y. Yamada and T. Taguchi, *phys. stat. sol. (a)* **180** (2000) 267.
50. O. Oda, K. Sato, T. Asahi, A. Arakawa and M. Uchida, *Monthly Display (in japanese)* **2** (1996) 34.
51. N. Nakayama, S. Kijima, S. Itoh, T. Ohata, A. Ishibashi and Y. Mori, *Opt. Rev.* **2** (1995) 167.
52. N. Nakayama, *Monthly Display (in japanese)* **June** (1996) 33.
53. D.B. Eason, Z. Yu, W.C. Hughes, C. Boney, J.W. Cook, Jr., J.F. Schetzina, D.R. Black, G. Cantwell and W.C. Harsch, *J. Vac. Sci, Technol.* **B13** (1995) 1566.
54. W.C. Harsch, G. Cantwell and J.F. Schetzina, *phys. stat. sol. (b)* **187** (1995) 467.
55. S. Nakamura, T. Mukai and M. Senoh, *Appl. Phys. Lett.* **64** (1994) 1687.
56. S. Nakamura, M. Senoh, N. Iwasa and S. Nagahama, *Jpn. J. Appl. Phys.* **34** (1995) L797.
57. T. Mukai, M. Yamada and S. Nakamura, *Jpn. J. Appl. Phys.* **38** (1999) 3976.
58. K. Koga and T. Yamaguvhi, *J. Jpn. Assoc. Crystal Growth* **17** (1990) 32.

59. J.L. Pankove, E.A. Miller, D. Richman and R.B. Zettterstrom, *Appl. Phys. Lett.* **19** (1971) 63.
60. S. Nakamura, T. Mukai and M. Senoh, *Appl. Phys. Lett.* **64** (1994) 1687.
61. S. Nakamura, M. Senoh, N. Iwasa and S. Nagahama, *Jpn. J. Appl. Phys.* **34** (1995) L797.
62. S. Nakamura, M. Senoh and T. Mukai, *Appl. Phys. Lett.* **62** (1993) 2390.
63. S. Nakamura, M. Senoh, N. Iwasa and S. Nagahama, *Appl. Phys. Lett.* **67** (1995) 1868.
64. T. Mukai, M. Yamada and S. Nakamura, *Jpn. J. Appl. Phys.* **38** (1999) 3976.
65. S. Nakamura, *Microelectron. J.* **25** (1994) 651.
66. M. Hashimoto, I. Akasaki and N. Sawaki, in *Proc.3rd Int. Display Research Conf.* (Kobe, 1983)
67. K. Bando, Y. Noguchi, K. Sakano and Y. Shimizu, in *Tech. Digest. Phosphor Res. Soc. 264th Meeting (in japanese)* (Nov. 29, 1996) p. 5.
68. S. Nakamura and G. Fasol, *The Blue Laser Diode* (Springer-Verlag, Berlin and Heidelberg, 1997) p. 252.
69. T. Taguchi, *J. IEICE Jpn.* **J84-C** (2001) 1040.
70. K. Tadatomo, H. Okagawa, T. Jyoichi, M. Kato, M. Harada and T. Taguchi, *Mitsubishi Cable Industries Bull.* **99** (2002) 35.
71. H. Matsubara, F. Nakanishi, H. Doi, K. Katayama, A. Saegusa, T. Mitsui, T. Takebe and S. Nishine, *SEI Tech. Rev.* **155** (1999) 93.
72. K. Katayama, H. Matsubara, F. Nakanishi, T. Nakamura, H. Doi, A. Saegusa, T. Mitsui, T. Matsuoka, M. Irikura, T. Takebe, S. Nishine and T. Shirakawa, *J. Crystal Growth* **214/215** (2000) 1064.
73. T. Nakamura, 162 Comittee, 40th Meeting (2004) p. 13.
74. B. Damilano, N. Grandjean, F. Semond, J. Massiers and M. Leroux, *Appl. Phys. Lett.* **75** (1999) 962.
75. A.J. Steckl and J.M. Zavada, *MRS Bulletin* **September** (1999) 33.
76. Y. Hori, T. Andreev, X. Bliquard, E. Monroy, D. Jalabert, Le Si dang, M. Tanaka, O. Oda and B. Daudin, *phys. stat. sol. (c)* **2** (2005) 2373.
77. K. Tadatomo, H. Okagawa, Y. Ohuchi, T. Tsunekawa, Y. Imada, M. Kato and T. Taguchi, *Jpn. J. Appl. Phys.* **40** (2001) L583.
78. T. Nishida and N. Kobayashi, *phys. stat. sol. (a)* **176** (1999) 45.
79. A. Kinoshita, H. Hirayama, M. Ainoya, A. Hirata and Y. Aoyagi, *Appl. Phys. Lett.* **77** (2000) 175.
80. M.A. Khan, V. Adivarahan, J.P. Zhang, C. Chen, E. Kuokstis, A. Chitnis, M. Shatalov, J.W. Yang and G. Simin, *Jpn. J. Appl. Phys.* **40** (2001) L1308.
81. Various stuctures are found in *J. Jpn. Assoc. Crystal Growth* **29** (2002).
82. L.K. Anderson, M. DiDomenico, Jr. and M.B. Fisher, in *Advances in Microwaves, Vol. 5*, ed. L. Young, (Academic Press, New Tork, 1970) p. 1.
83. H. Melchior, in *Laser Handbook, Vol. 1* (North-Holland, Amsterdam, 1972) p. 725.
84. H. Melchior, Phys. Today **November** (1977) 32.
85. *Infrared Detector II, Semiconductors and Semimetals Vol. 12*, eds. R.K. Willardson and A.C. Beer (Academic Press, New York, 1977)
86. P.W. Kruse, in *Optical and Infrared Detectors*, ed. by R. J. Keyes (Springer Verlag, Berlin, 1977)
87 .S.M. Sze, *Physisc of Semiconductor Devices* (John Wiley & Sons, 1981) p.743.
88. A. Kurahashi, *Optoelectronics Material Manual (in japanese)* (Optronics, Tokyo, 1986) p. 307.
89. M.B. Reine, A.K. Sood and T.J. Tredwell, in *Semiconductors and Semimetals Vol. 18*, eds. R.K. Willardson and A.C. Beer (Academic Press, New York, 1981) p. 201.
90. *Semiconductors and Semimetals Vol. 5*, eds. R.K. Willardson and A.C. Beer (Academic Press, New York, 1970).
91. Y.K. Su, U.H. Liaw, T-P. Sun and G-S Chen, *J. Appl. Phys.* **81** (1997) 739.
92. Catalog of Hamamatsu Photonics Co., http://www.hpk.co.jp.
93. F. Capasso, *Laser Focus/Electro-Optics* **20** (1984) 84.
94. Y. Horikoshi, A. Fischer and K. Ploog, *Appl. Phys. Lett.* **45** (1984) 919.
95. Y. Matsushima, Y. Noda, Y. Kushiro, K. Sakai, S. Akiba and K. Utaka, in *Tech. Digest 4th Int.*

Conf. Integ. Opt. Fiber Comm. (Tokyo, 1983) p. 226.
96. H. Terauchi, A. Yamaguchi, N. Yamabayashi, H. Nishizawa, Y. Kuhara, M. Kuroda and N. Iguchi, *Sumitomo Electrics (in japanese)* **127** (1985) 106.
97. M. Razeghi and A. Rogalski, *J. Appl. Phys.* 79 (1996) 7433.
98. Y.A. Goldberg, *Semicon. Sci. Technol.* **14** (1999) R41.
99. D.M. Brown, E.T. Downey, M. Ghezzo, J.W. Kretchmer, R.J. Saia, Y.S. Liu, J.A. Edmond, G. Gati, J.M. Pimbley and W.E. Schneider, *IEEE Trans Electron. Devices* **40** (1993) 325.
100. D.D. Coon, R.P.G. Karunasiri and L.Z. Liu, *Appl. Phys. Lett.* **47** (1985) 289.
101. M. Wada, in *Semiconductor Engineering* (Tomokura, Tokyo, 1966) p. 170.
102. S.M. Sze, *Physisc of Semiconductor Devices* (John Wiley & Sons, New York, 1981) p. 743.
103. Y. Matsushima, *Functional Devices (Kinou Zairyou) (in japanese)* **April** (1984) 34.
104. G.E. Stillman and C.M. Wolfe, in *Infrared Detector II*, in *Semiconductors and Semimetals Vol. 12*, eds. R.K. Willardson and A.C. Beer (Academic Press, New York, 1977) p. 291.
105. P.D. Wright, R.J. Nelson and T. Cella, *Appl. Phys. Lett.* **37** (1980) 192.
106. S.M. Sze, *Physisc of Semiconductor Devices* (John Wiley & Sons, New York, 1981) p. 61, p. 243.
107. J. Baliga, *IEEE Trans. Electron. Devces* **43** (1996) 1717.
108. M.J. Kelly, *Microelectron. J.* **24** (1993) 723.
109. K. Fujimura, in *MWE'95 Microwave Workshop Digest* (1995) p. 225.
110. K. Arai and S. Yoshida, *Fundamentals and Applications of SiC Devices (in japanese)* (Ohmsha, Tokyo, 2003).
111. P.L. Dreike, D.M. Fleetwood, D.B. King, D.C. Sprauer and T.E. Zipperian, *IEEE Trans. Compon. Pack. Manuf. Technol. A* **17** (1994) 594.
112. S.M. Sze, *Physisc of Semiconductor Devices* (John Wiley & Sons, New York, 1981) p. 312
113. C.A. Mead, *Proc. IEEE* **54** (1966) 307.
114. P. Greling, *IEEE Trans.* **MTT-32** (1984) 1144.
115. H. Sawatari and O. Oda, *J. Appl. Phys.* **72** (1992) 5004.
116. H.W. Becke and J.P. White, *Electronics* **June** (1967) 82.
117. T. Sugano, F. Koshiga, K. Yamasaki and S. Takahashi, *IEEE Trans Electron. Devices* **ED-27** (1980) 449.
118. T. Ito and K. Ohata, *IEEE Trans. Electron. Devices* **ED-82** (1982) 44 .
119. W. Schockley, *Proc. IRE* **40** (1952) 1365.
120. G.C. Decay and I.M. Ross, *Proc. IRE* **41** (1953) 970.
121. R. Lehovec and R. Zuleeg, *Solid State Electron.* **13** (1970) 1415.
122. J.K. Notthoff and R. Zuleeg, in *IEDM Tech. Dig.* (1975) p. 624.
123. T. Onuma and T. Sugawa, in *Proc. Int. Symp. GaAs Related Mater.* (1981) p.4 13.
124. H. Morkoc, S.G. Bandy, R. Sankaran, G.A. Antypas and R.L. Bell, *IEEE Trans. Electron. Devices* **ED-25** (1978) 619.
125. R. Zuleeg, J.K. Notthoff and G.L. Troeger, *IEEE Electron. Dev. Lett.* **EDL-5** (1984) 21.
126. T. Mimura, S. Hiyamizu, T. Fujii and K. Nanbu, *Jpn. J. Appl. Phys.* **19** (1980) L225.
127. R. Dingle, H.L. Störmer, A.G. Gossard and W. Wiegmann, *Appl. Phys. Lett.* **33** (1978) 665.
128. K. Shinohara, Y. Yamashita, A. Endoh, K. Hikosaka, T. Matusi, T. Mimura and S. Hiyamizu, *Jpn. J. Appl. Phys.* **41** (2002) L437.
129. H. Kroemer, *Proc. IRE* **45** (1957) 1535.
130. M. Dahlstroml, M. Urteaga, S. Krishnan, N. Parthasarathy and M.J. W. Rodwell, in *Proc. 14th Int. Conf. on InP and Related Materials* (Stockholm, 2002) p. 47.
131. J.B. Gunn, *Solid State Commun.* **52** (1963) 88.
132. H. Kroemer, *Proc. IRE* **52** (1964) 1736.
133. H. Eisele and R. Kamoua, *IEEE Trans. Microwave Theory Tech.* **52** (2004) 2371.
134. H. Yanazawa, in *IEEE GaAs IC Symp.* (1990) p. 7.
135. M.R. Stiglitz and L.D. Resnick, *Microwave J.* **January** (1989) 33.
136. O. Wada, T. Sakurai and T. Nakagami, *IEEE J. Quantum Electron.* **QE-22** (1986) 805.

137. T. Isobe, S. Yanagisawa and T. Nakamura, in *Proc. 8th Conf. Solid State Devices* (Tokyo, 1976) p. 135.
138. S. Hasuo, T. Nakamura, G. Goto, K. Kazetani, H. Ishiwatari, H. Suzuki and T. Isobe, in *Proc. 5th Cornell Eng. Conf.* (1975) p. 185.
139. R. Vab Tuyl and C.A. Liechti, in *ISSCC Dig. Tech. Papers* (1974) p. 114.
140. S. Somekh and A. Yariv, in *Proc. Conf. Int. Telemetry* (Los Angels, 1972) p. 407.
141. I. Ury, K.Y. Lau, N. Bar-Chain and A. Yariv, *Appl. Phys. Lett.* **41** (1982) 126.
142. T.L. Koch and U. Koren, *IEE Proc. J.* **138** (1991) 139.
143. T. Otsuji, *Oyo Buturi (Monthly Publ. Jpn. Soc. Appl. Phys.) (in japanese)* **71** (2002) 1352.
144. R.M. Hickling and M.D. Warklick, *EDN* **January** (1990) 119.
145. J.H. Edgar, *J. Mater. Res.* **7** (1992) 235.
146. T. Kikkawa, T. Igarashi, H. Haematsu, T. Tanaka and Y. Otoki, in *5th Conf. Nitride Semicon. Tech. Dig.* (2003) p. 469.
147. M. Hikita, M. Yanagihara, K. Nakazawa, H. Ueno, Y. Hirose, T. Ueda, Y. Uemoto, T. Tanaka, D. Ueda and T. Egawa, in *IEDM Tech. Dig.* (2004) p. 803.
148. S.M. Sze, *Physisc of Semiconductor Devices* (John Wiley & Sons, 1981) p. 790.
149. T. Inoguchi, *Optoelectronics Material Manual (in japanese)* (Optronics, Tokyo, 1986) p. 317.
150. J.C.C Fan, *Solar Energy Materials* 23(1991), 129.
151. A. Herman, L. Febick, K. Zweibel and R. Hardy, in *Proc. 16th IEEE PV Specialists Conference* (1982), 840.
152. H.J. Hovel, Solar Cells, in *Semiconductors and Semimetals Vol. 14*, eds. R.K. Willardson and A.C. Beer (Academic Press, New York, 1979).
153. K.J. Bachmann, *Current Topics of Material Science Vol.3; Material Aspects of Solar Cells* (North-Holland, Amsterdam), 1979).
154. M.P. Thekaekara, in *Suppl. Proc. 20th Annu. Meet. Inst. Environ. Sci.* (1974) p. 21.
155. *Principal Conclusions of the American Physical Society Study Group on Solar Photovoltaic Energy Conversion*, American Physical Socierty, New York, 1979.
156. J.J. Loferski, *J. Appl. Phys.* **27** (1956) 777.
157. G. F. Knoll, *Radiation Detection and Measurement* (John Wiley & Sons, New York, 1979)
158. G. T. Ewan, *Nucl. Instrum.& Methods* **162** (1979) 75.
159. *Semiconductors for Room Temperature Nuclear Detector Applications*, Semicon. Semimet., Vol. 43, eds. T.E. Schlesinger and R.B. James, (Academic Press, New York, 1995).
160. C. Scharager, P. Sifert, A. Holtzer and M. Schieber, *IEEE Trans. Nucl. Sci.* **NS-27(1)** (1980) 276.
161. E. Sakai, *Nucl. Instrum. Methods* **196** (1982) 132.
162. *Nuclear Radiation Detector Materials*, eds. E.E. Haller et al. (North-Holland, New York, 1983).
163. S. F. Kozlov, R. Stuck, M. Mage-Ali and P. Siffert, *IEEE Trans. Nucl. Sci.* **NS-22** (1975) 160.
164. C.A. Klein, *J. Appl. Phys.* **39** (1968) 2029.
165. H.L. Malm, T.W. Raudorf, M. Maritni and K.R. Zanio, *IEEE Trans. Nucl. Sci.* **NS-20** (1973) 500.
166. J.P. Jan, *Solid-State Physics*, ed. F. Seitz and D. Turnbull (Academic Press, New York, 1957).
167. H. Weiss, *Structure and Application of Galvanomagnetic Device* (Peragamon Press, 1969).
168. E.H. Hall, Phil. Mag. **5** (1980) 301.
169. Res. Rep. Compound Semicon. Dev. I, 57-M-190 (Jpn. Technol. Trans. Assoc.)
170. Y. Sugiyama, *Rep. Electrotech. Lab.* **54** (1990) 65.
171. K. Nishimura, H. Goto, S. Yamada, H. Geka, A. Okamoto and I Shibasaki, in *Proc. 21st Sencor Symp.* (2004) p. 337.

PART 2

III-V Materials

7. GaP
8. GaAs
9. GaSb
10. InAs
11. InP
12. InSb

7. GaP

7.1 INTRODUCTION

GaP is one of the compound semiconductor materials which has a large market share and whose developement began a long time ago and has been extensively studied. The reason why GaP was first developed was because it had a possibility for light emitting diodes (LEDs). Since GaP has a comparatively large bandgap (2.26 eV), it is possible to make LEDs of various colors such as red, yellow and green by controlling the dopants.[1]

7.2 PHYSICAL PROPERTIES

The physical properties of GaP[2] are summarized in Table 7.1. The melting point of GaP is rather high at 1467 °C and the dissociation pressure of P at the melting point is as high as 39 ± 7 atm. GaP has a wide bandgap as wide as 2.26 eV so that it is used as LED material for various colors. Even though GaP is an indirect transition material, LEDs have been realized by appropriate doping.

Fig. 7.1 shows the phase diagram of GaP.[3] Jordan et al.[4] have calculated thermodynamically the densities of Ga vacancies and P vacancies as a function of vapor pressure and temperature and obtained the precise phase diagram as shown in Fig. 7.2.

The band structure of GaP[5] is as shown in Fig. 7.3. GaP has a zincblende structure and its conduction band has its minimum at X1 [100] similar to silicon and its valence band has its maximum at Γ16 [000].[5] Since GaP is an indirect transition semiconductor, recombination between electrons and holes is accompanied by phonon generation.

7.3 CRYSTAL GROWTH

Since GaP is dissociable at high temperatures as shown in Fig. 7.1, it has been difficult to grow single crystals. Preliminary work on crystal growth of GaP is summarized by Miller.[6] Industrially, GaP polycrystals are synthesized by the HB method and single

Table 7.1. Physical Properties of GaP

Crystal Structure	zincblende
Lattice Constant	5.4495 Å
Density	4.1297 g/cm^3
Melting Point	1467 °C
Linear Expansion Coefficient	5.3-5.81 x10^{-6}/deg
Thermal Conductivity	1.1 W/cm·K
Dielectric Constant	11.1
Refractive index	2.529
Bandgap at Room Temperature	2.261 eV
Intrinsic Carrier Concentration	5X10^{15} cm^{-3}
Electron Mobility	200 cm^2/V·sec
Hole Mobility	120 cm^2/V·sec
Intrinsic Resistivity	2x10^{16} Ω·cm

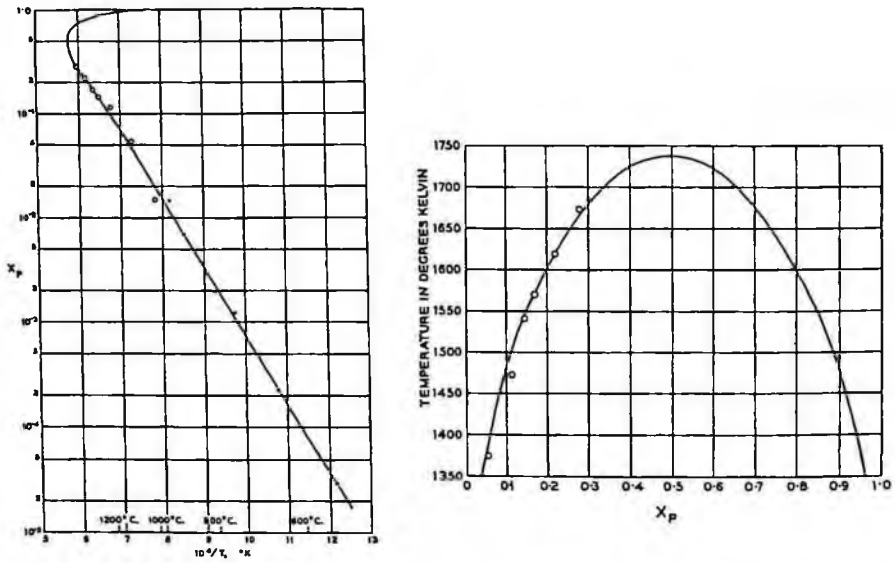

Fig. 7.1 Phase diagram of GaP (reprinted from Ref. 3 with permission, copyright 1965 Elsevier).

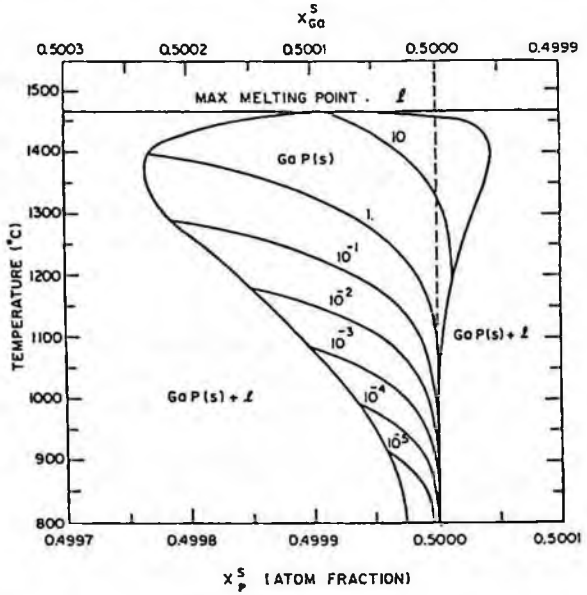

Fig. 7.2 The solid composition of GaP as a function of temperature for fixed values of P_{P_2}. Each isobar is identified on top by its P_{P_2} in units of atm. The envelope curve to the isobars is the solidus boundary of GaP (reprinted from Ref. 4 with permission, copyright 1974 American Institue of Physics).

crystals are grown by the LEC method. In order to reduce dislocation densities, VGF or VB methods have also been used. Some reviews[7-9] have summarized the development of GaP crystal growth.

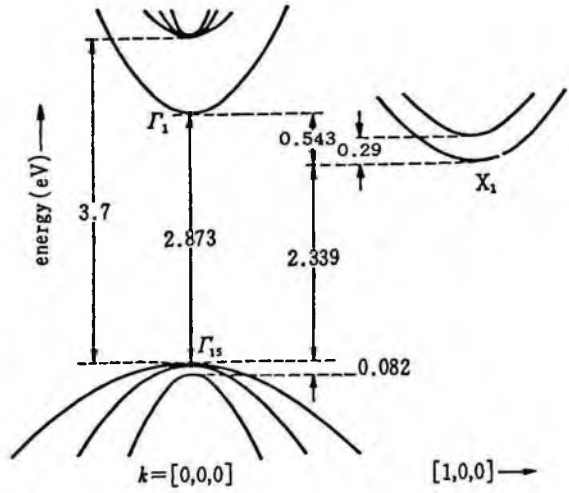

Fig. 7.3 Band structure of GaP (1.6K) (from Ref. 5 with permission).

7.3.1 Polycrystal Synthesis

In earlier times, GaP powders were grown by the reaction of $Ga+PCl_3$ or $GaPO_4+H_2$. The vapor growth (VG) method based on the reaction of $Ga+P+GaI_3$[10] and the solution growth (SG) method based on the reaction of Ga+P or $Ga+PH_3$[11] were then developed. The VG method has the advantage that the yield is high and the process quantity is large, but the disadvantage is the low growth rate and the necessity to seal the ampoule. By the SG method, Ga solution saturated by GaP is cooled down from 1100-1200 °C and GaP crystals are grown. The quality of grown crystals is high but the growth yield is low.

The melt growth method has been developed by Fischer[12] and Matsumoto.[7] Fischer has synthesized GaP crystals of about 80 g using a two zone furnace and reacting the Ga melt with phosphorus vapor in a high pressure demountable chamber.

In the method described in Ref. 7, the synthesis is performed in an apparatus as shown in Fig. 7.4. The apparatus is set in a high pressure furnace and the inert gas is controlled in such a way that the inner pressure P_1 is higher than the outer pressure P_2. Ga and B_2O_3 in the crucible are melted and the Ga melt temperature is raised to 1500 °C. Phosphorus is heated to about 590 °C in order to convert Ga to GaP by the reaction between Ga and the phosphorus vapor.

Industrially, GaP is synthesized using a high pressure horizontal Bridgman (HB) furnace as shown in Fig. 7.5. In the HB furnace, Ga in a boat and red phosphorus ingot are sealed in a quartz ampoule. Ga is heated up to 1200 °C and phosphorus is heated to 400 °C. Phosphorus vapor is dissolved in the molten Ga. When the ampule is moved, GaP is deposited in the Ga melt in the colder region and polycrystal GaP is grown.

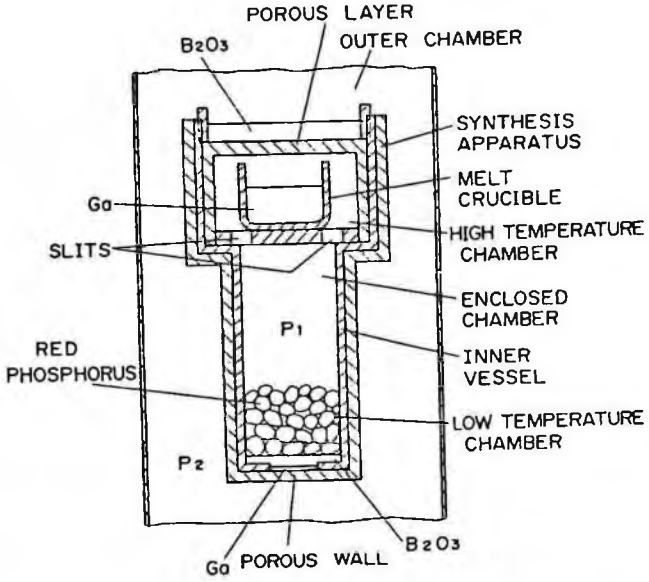

Fig. 7.4 Vertical section of an apparatus for synthesizing GaP polycrystals (reprinted from Fig. 5.2 at p. 138 in Ref. 7 with permission).

7.3.2 Single Crystal Growth

For GaP, several crystal growth methods have been investigated as shown in Table 7.2.[12-32] In the early days, the solution growth method was studied extensively. In industrial production, the liquid encapsulating Czochralski (LEC) method is mainly used for reasons of cost performance and productivity.

(1) Melt growth

- Liquid Encapsulated Czochralski (LEC) method

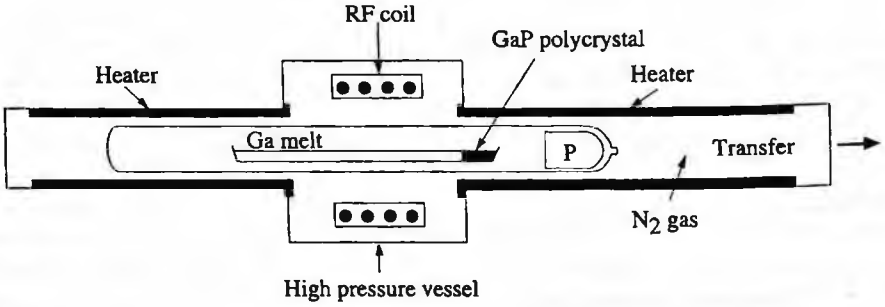

Fig. 7.5 Polycrystal synthesis furnace for GaP (from Ref. 9 with permission).

Table 7.2 Various Crystal Growth of GaP

Method	Results	Authors	Year	Ref.
THM	First application of the THM to compound semiconductors	Broder et al.	1963	34
LEC	First application of the LEC method to GaP	Bass et al.	1968	13
LEC	First application of the LEC method to GaP	Mullin et al.	1968	14
VGF	Growth by the soft ampoule method	Fischer	1970	12
LEC	Growth with doping of S, Se, Te and Zn	Nygren et al.	1971	15
LEC	Study of defects in LEC crystals	Rozgonyi	1972	16
LEC	Growth from non-stoichiometric melts	von Neida	1972	17
LEC	Use of flat-bottom crucibles and after-heaters	Nygren	1973	19
LE-VGF	First application of B_2O_3 encapsulant to VGF	Blum et al.	1973	28
SSD	Frist concept of SSD growth	Poiblaud et al.	1973	33
SSD	First application of the SSD method to compound semiconductors	Kaneko et al.	1973	30
LEC	Observation of growth by X-ray imaging	Pruett et al.	1974	20
SSD	Improvement of SSD for increasing the growth rate	Gillessen et al.	1976 1977	31, 32
LEC	Dislocation-free crystal growth by necking	Roksnoer et al.	1977	21
LEC	Diameter control by choracle	Ware et al.	1978	22
LEC	Effect of diameter control on thermal stress	Watanabe et al.	1978	23
LEC	Automatic computer control of diameter	Fukuda et al.	1981	24
LEC	Improvement of temperature distribution	Watanabe et al.	1983	25
LEC	Automatic computer control of diameter	Washizuka et al.	1983	26
VGF	Growth with seeding under phosphorus pressure control	Gault et al.	1986	27
LE-VB	52 mm diameter dislocation free crystals	Okada et al.	2000	29

LEC: Liquid Encapsulated Czochralski, VGF: Vertical Gradient Freezing, LE-VGF: Liquid Encapsulated VGF, LE-VB: Liquid Encapsulated Vertical Bridgman, SSD: Synthesis by the Solute Diffusion, THM: Travelling Heater Method

For the industrial growth of GaP crystals, the LEC method (Sec. 2.2.3(2)) is mainly used. Using a LEC furnace as shown in Fig. 2.4, GaP polycrystals are placed in a crucible with the encapsulant B_2O_3. Inert gas such as nitrogen or argon is introduced into the furnace up to 70 atm above the dissociation pressure of GaP. The crucible is then heated to melt the GaP polycrystals and the seed crystal is dipped to grow GaP single crystals.

The advantage of the LEC method is its high growth rate with the capacity to grow large diameter crystals. The purity of crystals can be improved because of the gettering effect of B_2O_3. In the case of GaP, because phosphorus diffuses out through B_2O_3, it makes B_2O_3 opaque and changes the heat balance at the liquid-solid interface. In order to overcome this problem, it is essential to optimize the crystal growth conditions such as the inert gas pressure, the temperature gradient, the water content of B_2O_3 and the thickness of B_2O_3.

When the crucible was heated by RF heaters, the axial temperature gradient in B_2O_3 was in the level of 500 °C/cm which was too high to grow crystals without fracturing.[17] However, after applying a resistive heater system, the temperature gradient in B_2O_3 was reduced to 100-250 °C/cm and large diameter crystals could be grown reproduc-

ibly.[7] It is also reported that dislocation-free crystals can be grown by optimizing the growth conditions, mainly controlling the radial temperature distribution by using the bottom heater.[25]

In the case of GaP, it is known that diameter control is very difficult because of the low viscosity of GaP at the melting point. To control the diameter, various methods such as the preprogramming method,[17] X-ray imaging method,18 weighing method[19, 20] and the coracle method[22] have been investigated. The coracle method is very effective in growing <111> crystals but can not be applied for growing <100> crystals because twinning occurs very easily.

The computer control system has been developed for growing single crystals up to 62 mm by closed loop control using a weighing method.[24] After applying this method, crystal growth under lower temperature gradients became possible.

- High Pressure Vertical Gradient Freezing (HP-VGF) method

Fischer[12] and Gault et al.[27] have grown GaP single crystals by the HP-VGF method. In Fig. 7.6, the HP-VGF furnace configuration and the crucible arrangement are shown. By this HP-VB method, <111> oriented GaP single crystals with a diameter of 50 mm and with a weight of 1300 g (Fig. 7.7) can be grown. Growth has been achieved under axial temperature gradients of as low as 8 °C/cm and the dislocation density of grown crystals can be down to the region of 800 - 2000 cm^{-2}.

- Liquid Encapsulated Vertical Bridgman (LE-VB) and Vertical Gradient Freezing (VGF) methods

Blum et al. first applied B_2O_3 as an encapsulant for the growth of GaP by the VGF method[28] and found that the dislocation density could be reduced to the region of 10^3 cm^{-2}.

Okada et al.[29] examined the growth of GaP by the LE-VB method. They have grown S-doped 52 mm diameter GaP single crystals and shown that the dislocation density can be reduced to less than 10^2 cm^{-2}. The advantage of the LE-VB method is that ampoule sealing is not necessary for each growth process.

(2) Solution growth

- Solute Solution Diffusion (SSD) method

In order to grow high purity GaP, a solution growth method which is referred to as the SSD method (Sec. 2.3.3) was first reported.[30] This method has been applied also by Gillessen et al.[31, 32] The same principle has been invented simultaneously by Poiblaud and Jacob[33] for the growth of GaP. This method is based on growth in a solution in which the solution composition is controlled by the phosphorus vapor supplied by heating the phosphorus reservoir as shown in Fig. 2.9. This method has the advantage of being able to grow high purity GaP crystals but the growth rate is low.

- Travelling Heater Method (THM)

The THM has been applied to the growth of GaP by Broder and Wolff.[34] The travelling

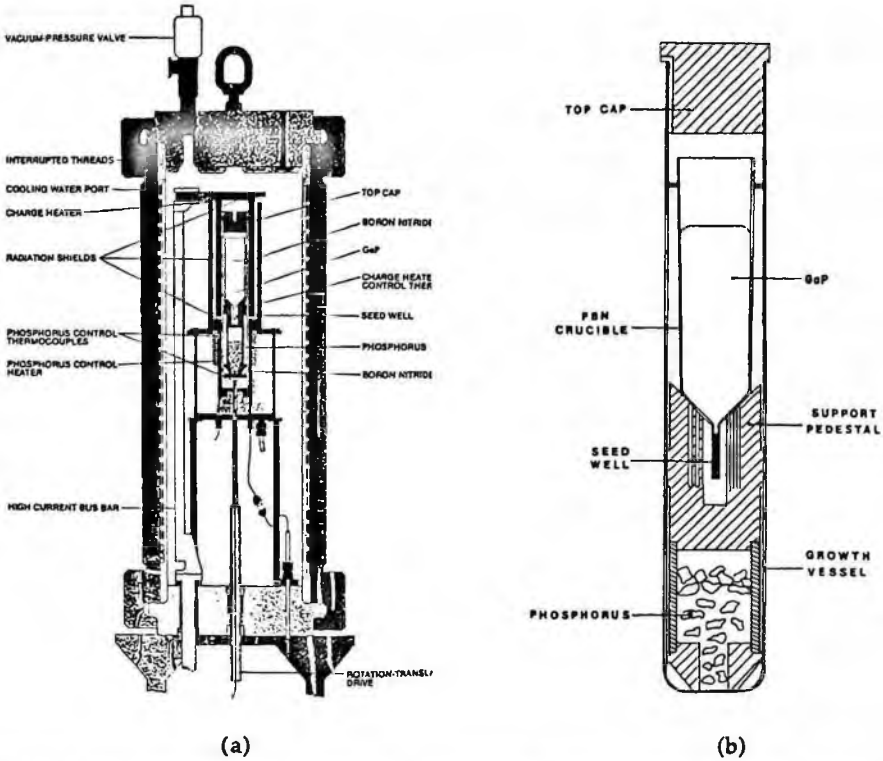

(a) (b)

Fig. 7.6 (a) Cross sectional view of a high-pressure VGF furnace and (b) the growth vessel and contents (reprinted from Ref. 27 with permission, copyright 1986 Elsevier).

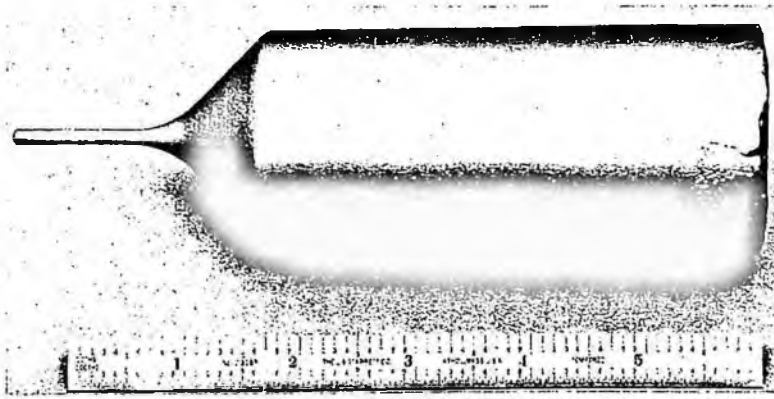

Fig. 7.7 <111> seeded 50 mm diameter GaP single crystal grown by the HP-VGF method (reprinted from Ref. 27 with permission, copyright 1986 Elsevier).

heater zone is heated by a RF coil to about 1100 °C and single crystals with a diameter of about 60 mm and a length of 25 mm have been grown.

7.3.3 Reduction of Dislocation Densities

Since the dislocation density affects the light emission efficiency of LEDs, especially for yellow-green LEDs,[35] it is important to reduce it. In order to decrease the dislocation density, the following methods have been applied.

(1) Necking

As mentioned in Sec. 4.3.3, necking is a procedure effective in growing dislocation-free crystals. In the case of GaP, Roksnoer et al. have applied this necking procedure and were able to obtain dislocation-free crystals.[21] It was however shown that dislocations are newly generated from the shoulder part of the growing crystal and they propagate into the crystal and the density increases as high as 10^5 cm^{-2} level.

(2) Growth from non-stoichiometric melt

GaP crystals have been grown from a phosphorus rich melt (up to 36 at%). A lower growth temperature could be used and the PL quantum efficiency was improved.[17] There was however the problem of the formation of Ga inclusions and a deceased growth rate.

(3) Impurity hardening

Matsumoto[7] reported that silicon doping was effective not only in reducing defects such as D-pits (Dislocation pits) but also S-pits (Saucer pits). It is also found that the EPD in epitaxial layers on Si-doped substrates is the same as that in the substrate. The impurity hardening method has the disadvantage that the melt is contaminated, preventing crystal growth and that light adsorption in the crystal deteriorates because of the impurity .

(4) Reduction of temperature gradient

Among various techniques for the reduction of dislocation densities, crystal growth under low temperature gradient with diameter control is industrially applied.[23] As predicted by the Tsivinsky equation as explained in Sec. 3.5, the reduction of axial temperature gradient is effective in reducing dislocation densities. In practice, Watanabe et al.[36] showed that the dislocation densities could be reduced as a function of the axial temperature gradient as shown in Fig. 7.8.

When the axial temperature gradient is reduced, diameter control becomes difficult because the radial growth rate rises. In order to grow low EPD crystals, crystal diameter control becomes very important. Watanabe et al.[23, 36] developed a computer controlled system (Fig. 3.13) which can be applied even under a low temperature gradient.

(5) VGF/VB method

The application of VGF/VB methods is an alternative method to reduce dislocation

densities. Since the temperature gradient can be greatly lowered compared with the LEC method, crystals with low dislocation densities can be obtained. As explained above, these methods have been proven effective in reducing dislocation densities and other defects, and are useful for growing larger diameter single crystals with low dislocation densities.[28, 29]

(6) Effect of Stoichiometry

Nishizawa et al.[37] have studied the effect of phosphorus over pressure on the dislocation density of GaP in the TDM-CVP method (Sec. 2.3.5). It was shown that under the appropriate overpressure, the dislocation density could be minimized.

7.4 CHARACTERIZATION

7.4.1 Purity

An example of the purity of LEC GaP is shown in Table 7.3.[7] Even though a silica crucible is used, the contamination of Si is as low as 0.03 ppmw. This is explained by the oxidation of impurities such as C, Si, B, Al, Mg, Ca which have higher formation free energies than that of B_2O_3. It is also suggested that the addition of Ga_2O_3 is effective in reducing impurities by oxidizing those whose oxide formation free energies are larger than that of Ga_2O_3.

7.4.2 Defects

(1) Dislocations and micro-defects

The relationship between the efficiency of radiative recombination and the lattice defect density has been studied.[35, 38, 39] As shown in Fig. 7.9, GaP has a large amount of dislocations in the 10^5 cm^{-2} range and micro-defects in the 10^6 - 10^7 cm^{-2} range, which impair the luminosity of green LEDs.

Dislocation densities of GaP are determined by counting the number of D-pits (dislocation-pits) which can be revealed by RC etchant (8 ml H_2O + 10 mg $AgNO_3$ + 6ml HNO_3 + 4 ml HF for 3 min. at 65 °C).[40-44] It is also known that B-pits (background pits) are revealed by RC etching.[25] The origin of B-pits is not clear but it is known that when substrates with high B-pit densities are used for LPE epitaxial growth, the density of pits on LPE layers is greatly increased.

Si-doped GaP single crystals show lower defect densities [7]. Not only the density of dislocations but also the density of S-pits (explained below) and small pits with cones were lowered. Using optical elasticity measurement, the residual stress in crystals with varying diameter was analyzed.[36, 44]

(2) Other defects

S-pit (saucer-shaped pits or shallow pits) can be revealed by RC etchant. Rozgonyi et al.[45] found that there is a correlation between the spatial inhomogeneities in the photoluminescence efficiency and the local variation of S-pit densities. It is therefore important to reduce not only dislocations but also micro-defects such as S-pits.[29, 40-43]

The origin of S-pits are considered to be as follows.

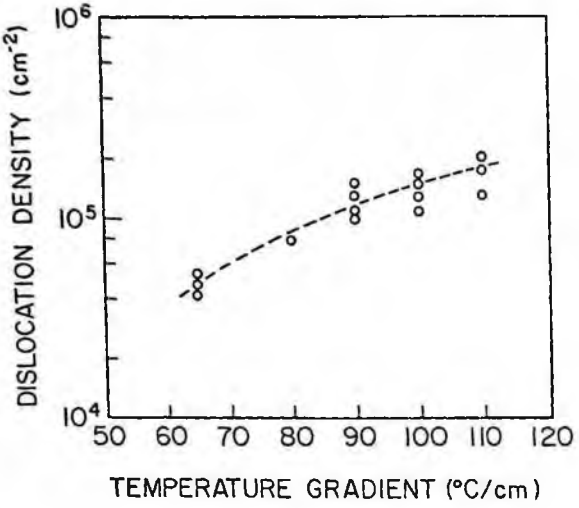

Fig. 7.8 Relationship between the axial temperature gradient and dislocation density (from Ref. 36 with permission).

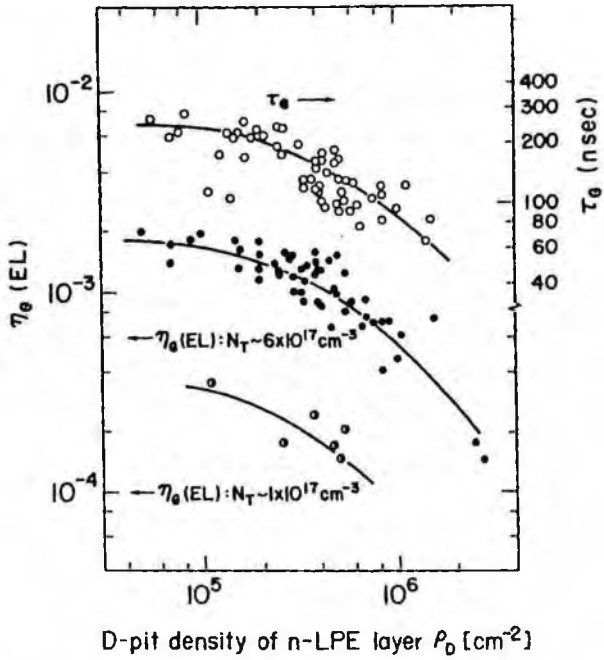

Fig. 7.9 Dependence of green LED quantum efficiency and minority carrier lifetime on the dislocation density of LPE layers(reprinted from Ref.39 with permission, copyright 1977 IEEE).

Table 7.3 Purity of LEC GaP

ppmw.

B	Al	Si	Mg	K	Ca	Fe	Cu	F	Cl	As	Zn	S	Te
0.4	0.008	0.03	ND	0.08	0.01	ND	ND	<0.006	0.03	0.02	<0.07	<0.03	<0.13

(i) Precipitated impurities such as O, S, Ga_2O_3, Ga_2S_3
(ii) Impurity-native defect complex
(iii) Dislocation loops decorated with impurities
(iv) Non-stoichiometric defects such as V_{Ga}

Okada et al.[29] have studied the origin of S-pits by analyzing dislocation-free LE-VB-grown crystals and concluded that they are vacancy-type Frank dislocation loops which surrounding stacking faults accompanied by P precipitates. It was also found that these S-pit defects can be eliminated by heat treatment due to the out-diffusion of originally formed Ga vacancies.[46]

(3) Striations

There are two types of striations, rotational and unrotational, as explained in Sec. 4.5. It is known that in an asymmetric thermal environment, remelt striations are generated. Iizuka[41] has reported the micro-defect distribution due to striations. These striations can be eliminated by making the thermal environment symmetrical, reducing temperature fluctuations and optimizing crystal and crucible rotations.

(4) Point defects

Jansen and Sankey[47] have calculated the formation energy of point defects in GaP by an ab initio pseudo-atomic method and shown the concentration of point defects as a function of stoichiometry.

(5) Deep levels

Deep levels have been measured by deep level transient spectroscopy (DLTS)[48-51] and some data are summarized in Figs 7. 10 . In Fig. 7.10 (a), the level indicated as Zn-O is a complex level made from Zn_{Ga} and O_P which is used for red light emission in LEDs. Oxygen which does not bind with Zn becomes an isolated deep donor. Since its capture cross section is three orders of magnitude smaller than that of the Zn-O complex, it does not impair the emission efficiency. The hole trap indicated HG in Fig. 7.10 (b) is known to be the level due to Cu incorporation, and traps HB and HP are due to defects formed by the degradation of red light emission LEDs.

7.4.3 Electrical Properties

(1) Carrier concentration and mobility

In Fig. 7.11, Hall mobilities at 300 K of undoped and Te-doped LEC grown GaP are shown.[7] These data are as high as those reported by Hara and Akasaki[52] on epitaxial layers, by Taylor et al.[10] on crystals by the VG method and by Nygren et al. on LEC crystals.[15]

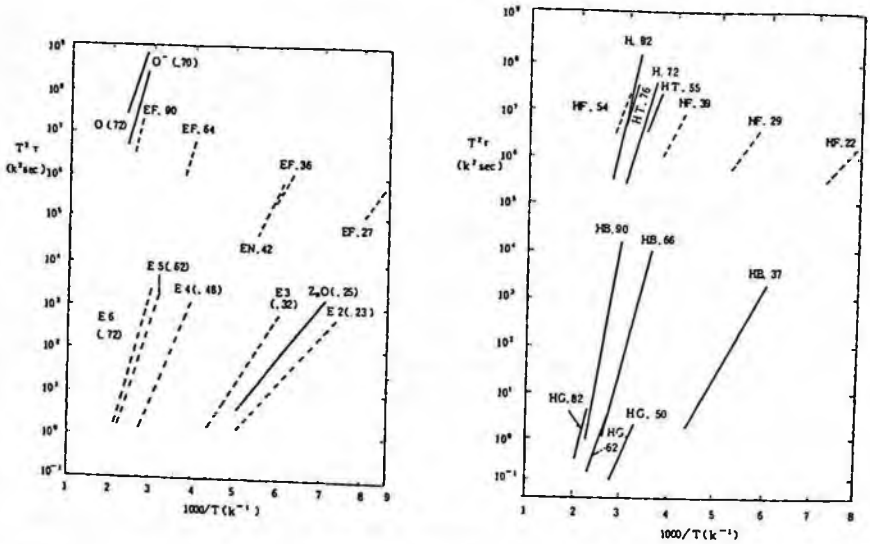

(a) (b)

Fig. 7.10 Deep levels in GaP measured by DLTS (from Ref. 50 with permission). (a) Electron traps and (b) hole traps. The references for each item of data are found in Ref. 50.

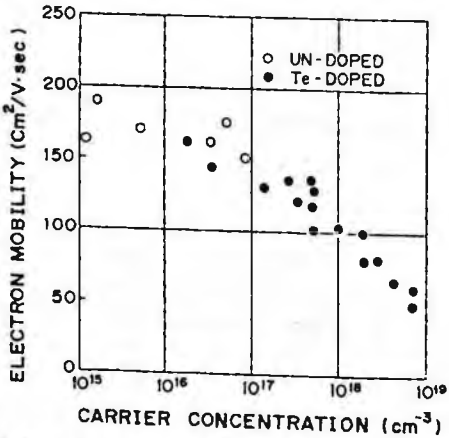

Fig. 7.11 Electron Hall mobility vs. electron concentration in undoped and Te-doped GaP (reprinted from Fig. 5.5 at p. 144 in Ref. 7 with permission).

Table 7.4. Distribution Coefficients of Various Dopants

Dopant	Distribution Coefficient	Solubility
O		$7X10^{16}$ (1,144 °C)
S	0.23	
Se	0.16	
Si	0.6	
Sn		$1.63x10^{19}$ (1,085 °C max)
Te	0.012	
Zn	0.096	$4.3x10^{20}$ (1,350 °C max)

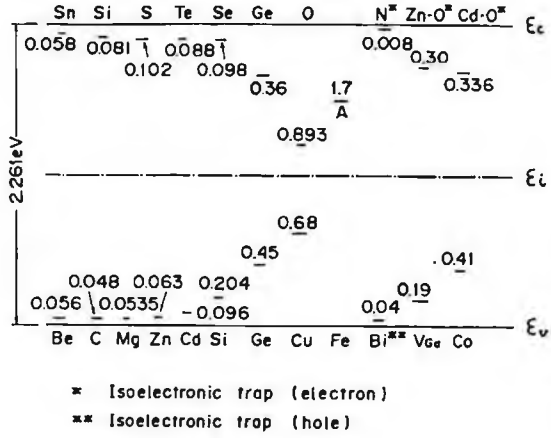

Fig. 7.12 Energy levels of impurities of GaP (reprinted from Fig. 5.7 at p. 145 in Ref. 7 with permission).

(2) Dopant and doping control

Donors and acceptors in GaP have energy levels as shown in Fig. 7.12. These data were obtained for GaP crystals grown by the SG, VPE and LPE methods.[1] Among them, Si is an amphoteric impurity and gives two levels at 0.081 eV as donor and 0.204 eV as acceptors. Ge also acts as an amphoteric impurity.

The distribution coefficients and the solubilities of various dopants are reported as shown in Table 7.4.[7, 15] In the case of doping with impurities such as Si, B, Al and O, mutual reaction must be considered because the melt is in touch with quartz and B_2O_3. The relationship of Si and the residual oxygen is analyzed based on that calculated for GaAs.[53] The relationship between B and Si was also experimentally examined and it was found that the results obey the theoretical relationship $N_B^4 \propto N_{Si}^3$.

(3) High resistive GaP

O and Fe form deep levels so that by doping them, semi-insulating GaP can be obtained.[7] High resistive GaP has been reported to have been prepared by the control of crystal growth conditions and by wafer annealing. Oda et al.[54] reported that GaP can be made to be semi-insulating after wafer annealing.

7.4.4 Optical Properties

GaP is an indirect transition semiconductor so that emissions by various lattice defects and impurities are predominant. The physics of emission centers and optical transitions are studied fundamentally by photoluminescence.[5, 55, 56]

(1) Edge emission

The edge emission spectrum at low temperature is as shown in Fig. 7.13.[57] Near the

absorption edge, three sharp lines, A, B, C and their phonon replica lines can be seen. The A line at 2.3177 eV is attributed to the allowed transition from the antiparallel state (J=1) of electron spin and hole spin. The B line at 2.3168 eV is due to the forbidden transition from the parallel state (J=2) of electron and hole spins. The C line at 2.310 eV is due to the recombination of excitons with a binding energy of 19 meV and has been proven to be due to neutral sulphur impurity.

(2) Isoelectronic trap emission

The A and B lines in Fig. 7.13 are known to be due to excitons bound with nitrogen atoms replacing P lattice sites.[58] Nitrogen atoms located at P lattice sites have greater electron negativity than P so that they capture electrons and by these negative charges, holes are trapped forming excitons with a binding energy of 11 meV. Impurities which act similarly to nitrogen are known as isoelectronic traps.[59]

Bi gives rise to isoelectronic traps, locating at P lattice sites. The A line of Bi is at 2.232 eV and the B line at 2.7 meV lower than A line. Bi has lower electron negativity than N so that holes are captured by Bi and electrons are trapped due to the positive charge.[60]

When the concentration of N is increased, many absorption and emission lines which converge to the A line are as shown in Fig. 7.14.[61] These lines are named NN1, NN2 from the longer wavelength side. The closest N-N pair captures excitons most strongly. When the distance between N-N pairs becomes greater, the binding energy of excitons becomes weaker. When the distance becomes infinite, it is the same as an

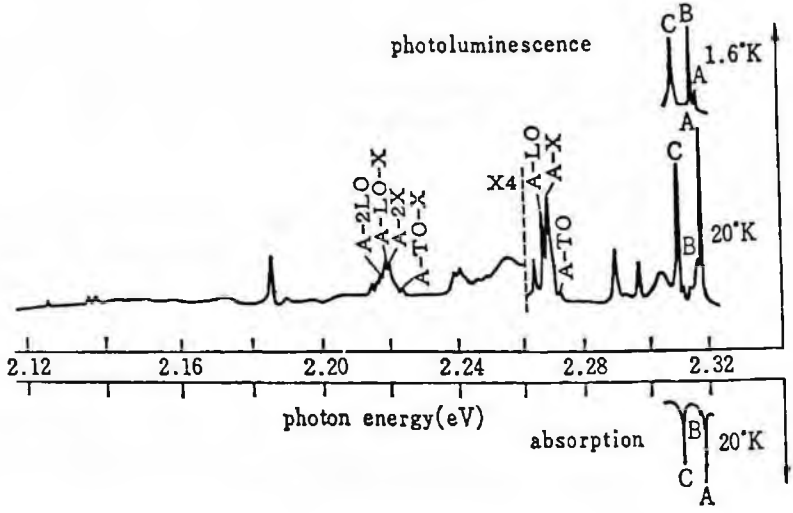

Fig. 7.13 Photoluminescence and absorption spectra near the absorption edge (reprinted from Ref. 57 with permission, copyright 1963 American Physical Society).

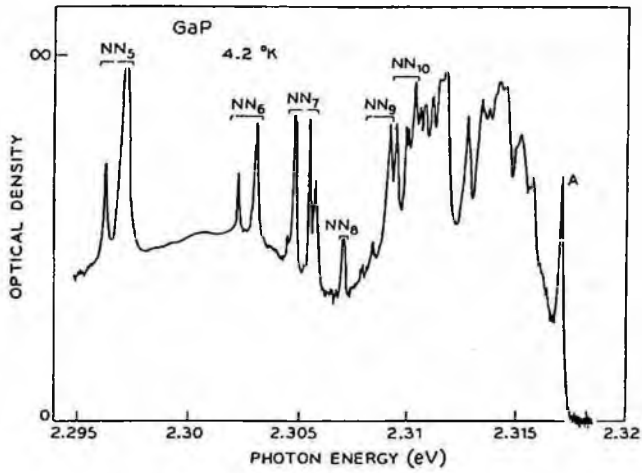

Fig. 7.14 NN luminescence spectrum from a GaP crystal containing nitrogen of about 5×10^{16} cm^{-3} (reprinted from Ref. 61 with permission, copyright 1966 American Physical Society).

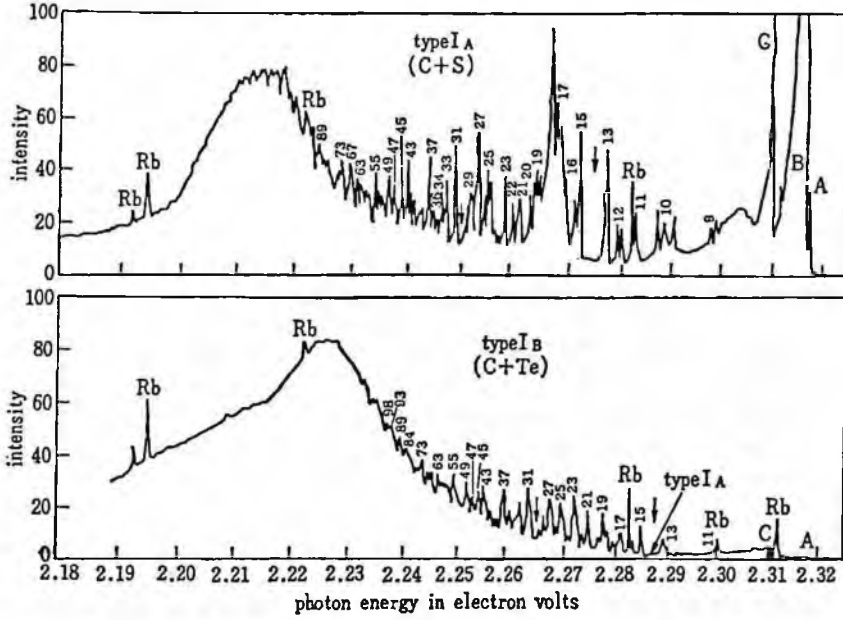

Fig. 7.15 Photoluminescence spectra from C-S and C-Te donor-acceptor pairs (1.6K) (reprinted from Ref. 62 with permission, copyright 1965 American Physical Society).

exciton bound by one N atom. Therefore, excitons captured by the closest N-N pair are called NN1 and the second nearest N-N pair are called NN2 and so on.

(3) Donor-Acceptor (D-A) pair emission

Unintentionally doped GaP shows many varied lines in the shorter wavelength region as shown in Fig. 7.15. GaP has S as donor and C as acceptor impurities. Donor-acceptor pair emission energy is given as Eq. 5-11 in Sec. 5.4.1(2). The distance between donors and acceptors, R, can only have allowed values since impurities are located at lattice sites. Therefore D-A pair emissions show many lines as shown in Fig. 7.15.[62] There is a difference of emission line structures in the case of C-S pairs where C and S are located at P lattice sites and in the case of S-Zn pairs where S located at the P lattice site and Zn at the Ga lattice site. Fig. 7.16 shows the emission energies as a function of the distance of D-A pairs, for the case of C-O, Zn-O and Cd-O. It is clearly seen that the theoretical calculation results agree with the experimental results.[63]

(4) Exciton emission bound to impurity pair

GaP doped with Zn acceptor and O donor shows an intense red emission. This emission is due to excitons, which are trapped by the Zn-O impurity pair. The Zn-O impurity pair is neutral from a long distance but since the binding energy of O is large, it acts as an electron trap at close range. Holes are captured by the charge of electrons trapped by O and thus Zn-O acts as a complex isoelectronic trap for excitons.[64, 65]

Similar emission is also observed in the case of GaP doped with Cd and O as shown in Fig. 7.17. Spectrum I is due to excitons trapped by complex Zn-O impurity pairs and Cd-O impurity pairs. Spectrum II is due to DA pair emission between electrons trapped by Zn-O or Cd-O impurity pairs and holes trapped by isolated acceptors.

7.5 APPLICATIONS

GaP is mainly used as a substrate for LEDs with colors from red to green as explained in Chapter 6. As shown in Table 6.2, various epitaxial layers are grown on GaP substrates.[1, 66] Since GaP has a wide bandgap, it becomes possible to make effective materials for LEDs of various colors by doping appropriate impurities as shown in Fig. 7.18. The structure of these LEDs is explained in Chapter 6. Since GaP is an indirect transition semiconductor, it is necessary to dope appropriate impurities in order to increase the emission efficiency.

Infrared LEDs are based on the recombination between electrons trapped at isolated oxygen donors and free holes as shown in Fig. 7.18. For red LEDs, Zn-O pairs are used for exciton recombination. The emission center is based on Zn which replaces the Ga lattice site and the neighboring O which replaces the lattice site of phosphorus. The Zn-O pair is neutral but the oxygen potential is large so that it can trap electrons to form excitons. This type of center is knwon as an isoelectronic trap. For yellow emissions and orange emissions, GaAsP grown on GaP is used. The emission wavelength can be controlled by changing the composition of GaAsP. To increase the emission efficiency,

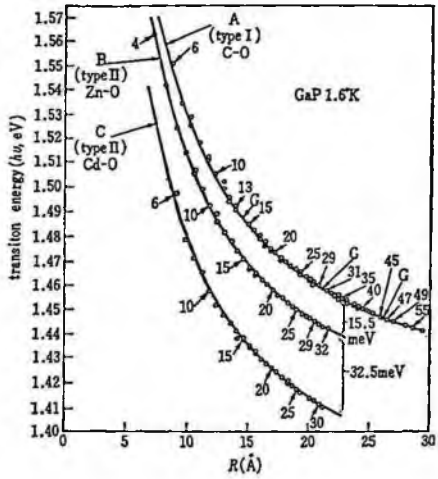

Fig. 7.16 The energies of discrete, infrared pair no-phonon lines observed in GaP (1.6K) doped with O donors and C, Zn or Cd acceptors, plotted against the pair separations, r (reprinted from Ref. 63 with permission, copyright 1968 American Physical Society).

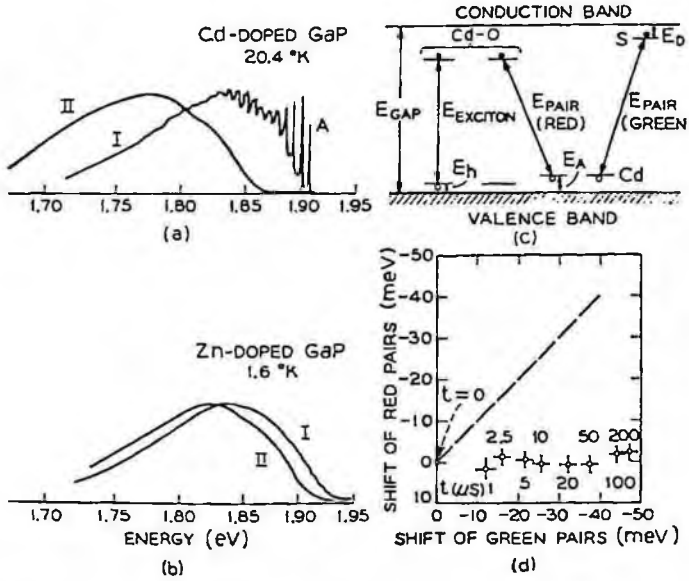

Fig. 7.17 (a) Curve I (Cd-O) exciton luminescence, Curve II (Cd-O)-Cd pair luminescence in Cd-doped GaP at 20.4°K. (b) Curve I (Zn-O) exciton luminescence, Curve II (Zn-O)-Zn pair luminescence in Zn-doped GaP at 1.6°K. Further details of the figure can be seen in Ref. 64 (reprinted from Ref. 64 with permission, copyright 1968 American Physical Society).

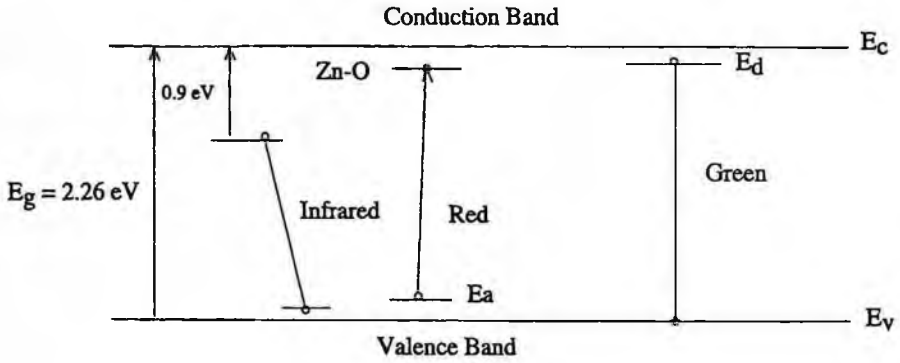

Fig. 7.18 Various levels for LED emission of GaP (from Ref. 9 with permission).

N is added as iso-electronic traps to improve the luminosity.

There are two types of emission mechanisms for yellow-green LEDs. One is the emission due to the recombination between electrons trapped at Te donors and free holes. The other is the emission due to N atoms at phosphorus lattice sites which trap electrons because the electronegativity of phosphorus is high. The excitons thus formed at N atoms recombine.[67, 68] The emission peak is near the maximal eye sensitivity 5500 Å and high-efficiency LEDs have been developed.[39, 69]

Nishizawa et al. have developed the temperature difference method by controlled vapor pressure (TDM-CVP) to grow GaP layers with controlled stoichiometry. Using these GaP layers, pure green LEDs with an emission wavelength of 555 nm have been realized.[70-75]

REFERENCES

1. H.C. Casey, Jr. and F.A. Trumbore, *Mater. Sci. Engineer.* **6** (1970) 69.
2. *Landolt-Börnstein, Vol. 17 Semiconductors*, ed. O. Madelung (Springer-Verlag, Berlin, 1982) p. 185.
3. C.D. Thurmond, *J. Phys. Chem. Solids* **26** (1965) 785.
4. A. S. Jordan, R. Caruso, A. R. Von Neida and M. E. Weiner, *J. Appl. Phys.* **45** (1974) 3472.
5. A. Kasami, in *Semiconductor Research Vol. 12*, ed. J. Nishizawa (in japanese) (Kogyo Chousakai, Tokyo, 1976) p. 211.
6. J.F. Miller, *Compound Semiconductors, Vol.1. Preparation of III-V Compounds*, eds. R.K. Willardson and H.L. Goering (Reinhold, New York, 1962) p. 194.
7. K. Matsumoto, in *Bulk Crystal Growth Technology* (Gordon and Breach, Amsterdam, 1989) p. 135.
8. M. Watanabe, *J. Mater. Sci. Soc. (in japanese)* **21** (1985) 290.
9. M. Kubota, *Optoelectronics Material Manual (in japanese)* (Optronics, Tokyo, 1986) p. 487.
10. R. C. Taylor, J. F. Woods, and M. R. Lorenz, *J. Appl. Phys.* **39** (1968) 5404.
11. C. M. Ringel, *J. Electrochem. Soc.* **118** (1971) 609.
12. A. G. Fischer, *J. Electrochem. Soc.* **117** (1970) 41C.
13. S. J. Bass and P. E. Oliver, *J. Crystal Growth* **3** (1968) 286.
14. J.B. Mullin, R.J. Heritage, C.H. Holliday and B.W. Straughan, *J. Crystal Growth* **3/4** (1968) 281.
15. S. F. Nygren, C.M. Ringel and H.W. Verleur, *J. Electrochem. Soc.* **118** (1971) 306.

16. G.A. Rozgonyi, A.R. von Neida, T. Iizuka and S.E. Haszko, *J. Appl. Phys.* **43** (1972) 3141.
17. A.R. von Neida, L.J. Oster and J.W. Nielsen, *J. Crystal Growth* **13/14** (1972) 647.
18. W. Bardsley, D. T. J. Hurle and G. C. Joyce, *J. Crystal Growth***40** (1977) 13.
19. S. F. Nygren, *J. Crystal Growth* **19** (1973) 21.
20. H. D. Pruett and S. Y. Lien, *J. Electrochem. Soc.* **121** (1974) 822.
21. P.J. Roksnoer, J.M.P.L. Huijbregts, W.M. Van de Wijgert and A.J.R. de Kock, *J. Crystal Growth* **40** (1977) 6.
22. R. M. Ware and M. Whittaker, in *Abstr. 5th Int. Conf. Crystal Growth* (1978) p. 132.
23. M. Watanabe, M. Nakajima and K. Hirahara, *Toshiba Rev. (in japanese)* **33**(1978) 830 .
24. T. Fukuda, S. Washizuka, Y. Kokubun, J. Ushizawa and M. Watanabe, *Inst. Phys. Conf. Ser.* **63**(1981) 43.
25. M. Watanabe, T. Fujii, J. Ushizawa and S. Washizuka, in *Extended Abstr. 15th Conf. Solid State Dev. Mater.* (Tokyo, 1983) p. 161.
26. S. Washizuka, J. Ushizawa, Y. Kokubun, M. Watanabe and T. Fukuda, *Oyo Buturi (Monthly Publ. Jpn. Soc. Appl. Phys.) (in japanese)* **52** (1983) 515.
27. W. A. Gault, E.M. Monberg and J.E Clemans, *J. Crystal Growth* **74** (1986) 491.
28. S.E. Blum and R.J. Chicotak, *J. Electrochem. Soc.* **120** (1973) 588.
29. H. Okada, T. Kawanaka and S. Ohmoto, *J. Appl. Phys.* **86** (1999) 3015.
30. K. Kaneko, M. Ayabe, M. Dosen, K. Morizane, S. Usui and N. Watanabe, *Proc. IEEE* **61** (1973) 884.
31. K. Gillessen and A.J. Marshall, *J. Crystal Growth* **32** (1976) 216.
32. K. Gillessen and A.J. Marshall, *J. Crystal Growth* **33** (1977) 356.
33. G. Poiblaud and G. Jacob, *Mater. Res. Bull.* **8** (1973) 845.
34. J.D. Broder and G.A. Wolff, *J. Electrochem. Soc.* **110** (1963) 1150.
35. M. Naito, H. Abe, Y. Iizuka, T. Beppe and A. Kasami, *Toshiba Rev. (in japanese)* **33** (1978) S33.
36. M. Watanabe, J. Ushizawa, S. Washizuka and Y. Kokubun, *Jpn. J. Appl. Phys.* **22** (1983) Suppl. 22-1, 427.
37. J. Nishizawa, Y. Okuno and K. Suto, in *Semiconductor Technologies* (Ohmsha and North-Holland, Tokyo, 1986) p. 17.
38. W.A. Brantley, O.G. Lorimor, P.D. Dapkus, S.E. Haszko and R.H. Saul, *J. Appl. Phys.* **46** (1975) 2629.
39. T. Beppe, M. Iwamoto, M. Naito and A. Kasami, *IEEE Trans. Electron Devices* **ED-24** (1977) 951.
40. J. L. Richard and Crocker, *J. Appl. Phys.* **31** (1960) 611.
41. T. Iizuka, *J. Electrochem. Soc.* **118** (1971) 1190.
42. F. Kuhn-Kuhnefeld, *Inst. Phys. Conf. Ser.* **339** (1977) 158.
43. G.A. Rozgonyi and T. Iizuka, *J. Electrochem. Soc.* **120** (1973) 673.
44. H. Kotake, K. Hirahara and M. Watanabe, *JJ. Crystal Growth* **50** (1980) 743.
45. A. Rozgonyi and M.A. Afromowitz, *Appl. Phys. Lett.* **19** (1971) 153.
46. H. Okada, T. Kawanaka and S. Ohmoto, *J. Appl. Phys.* **88** (2000) 6943.
47. R.W. Jansen and O.F. Sankey, *Phys. Rev. B* **39** (1989) 3192.
48. J. M. Dishman, D. F. Daly and W. P. Knox, *J. Appl. Phys.* **43** (1972) 4693.
49. A. Mircea and D. Bois, Inst. Phys. Conf. Ser. **46** (1979) 82.
50. T. Okumura, in *New Compound Semiconductor Handbook*, ed. T. Ikoma (Science Forum, Tokyo, 1982) p. 249.
51. K. Zdansky, J. Zavadil, D. Nohavica and S. Kugler, *J. Appl. Phys.* **83** (1998) 7678.
52. T. Hara and I. Akasaki, *J. Appl. Phys.* **39** (1968) 285 .
53. S. Akai, K. Fujita, M. Sasaki and K. Tada, in *Proc. Int. Symp. GaAs and Related Compounds* (Japan, 1981) p. 13.
54. O. Oda, H. Yamamoto, K. Kainosho, T. Imaizumi and H. Okazaki, *Inst. Phys. Conf. Ser.* **135** (1993) 285.
55. P.J. Dean, in *Junction Electroluminescence Applied Solid State Science Vol.1*, eds. R. Wolfe and

C.J. Kriessman, (Academic Press, New York, 1969) p.1.
56. A.A. Bergh and P.J. Dean, *Proc. IEEE* **60** (1972) 156.
57. D.G. Thomas, M. Gershenzon and J.J. Hopfield, *Phys. Rev.* **131** (1963) 2397.
58. D.G. Thomas, J.J. Hopfield and C.J. Frosch, *Phys. Rev. Lett.* **168** (1968) 857.
59. J.J. Hopfield, D.G. Thomas and R.T. Lynch, *Phys. Rev. Lett.* **15** (1966) 312.
60. F.A. Trumbore, M. Garehenzon and D.G. Thomson, *Appl. Phys. Lett.* 9 (1966) 4.
61. D.G. Thomas and J.J. Hopfield, *Phys. Rev.* **150** (1966) 680.
62. D.G. Thomas, M. Gershenzon and F.A. Trumbore, *Phys. Rev.* **133** (1964) A269.
63. P.J. Dean, G.H. Henry and C.J. Frosch, *Phys. Rev.* **168** (1968) 812.
64. C.H. Henry, P.J. Dean and J.D. Cuthbert, *Phys. Rev.* **166** (1968) 754.
65. T.N. Morgan, B. Welker and R.N. Bhargava, *Phys. Rev.* **166** (1968) 751.
66. Y. Okuno, *Light Emitting Diodes* (in japanese) (Sangyo Tosho, Tokyo, 1993).
67. R.A. Logan, H.G. White and W. Wiegmann, *Appl. Phys. Lett.* **13** (1968) 139.
68. R.A. Faulkner, *Phys. Rev.* **173** (1968) 991.
69. T. Takahashi, *Monthly Display (in japanese)* **2** (1996) 43.
70. J. Nishizawa and Y. Okuno, *IEEE Trans. Electron Devices* **ED-22** (1975) 716.
71. J. Nishizawa, Y.Okuno and H.Tadano, *J. Crystal Growth* **31** (1975) 215.
72. J. Nishizawa, Y. Okuno, M. Koike and S. Sakurai, *Jpn. J. Appl. Phys.* **19** (1980) 377.
73. J. Nishizawa, K. Itoh, Y. Okuno, M. Koike and T. Teshima, in *Proc. IEEE Int. Electron Devices Meeting (IEDM)* (1983) p. 311.
74. K. Suto and J. Nishizawa, *J. Appl. Phys.* **67** (1990) 459.
75. K. Suto, D. Iwamoto, J. Nishizawa and N. Chubachi, *J. Electrochem. Soc.* **140** (1993) 2682.

8. GaAs

8.1 INTRODUCTION

GaAs is one of the most important compound semiconductor materials because it is used not only for infrared LDs and infrared and red LEDs[1] but also used for high frequency electronic devices[2] which competes with Si in high frequency and low power operations as described in Chapter 6. The applications of variously doped GaAs are summarized in Table 8.1. The consumption of GaAs substrates is increasing year by year for these optoelectronic and electronic devices[3] and now exceeds about three hundred million dollars per year.

Industrially, conductive GaAs is produced mainly by the HB and HGF methods and semi-insulating GaAs is produced mainly by the LEC method. Production by the VB/VGF methods is however increasing because higher quality crystals can be grown.

Because of the importance of GaAs and because of the interesting physical properties, GaAs is the compound semiconductor material of all compound semiconductors about which the largest number of studies among various compound semiconductors has been performed so far. There are various reviews on GaAs.[4-9]

8.2 PHYSICAL PROPERTIES

The details of the physical properties of GaAs can be found in the literature.[10] The main properties are summarized in Table 8.2. As seen from the table, GaAs has a lattice constant with which that of AlGaAs mixed crystal can be matched. To this matching, GaAs owes its importance as a material for AlGaAs based LEDs and LDs. GaAs emerged also as the main substrate for GaAsP based visible light lasers. GaAsP does not lattice-match with GaAs but composition gradient layers are used to grow epitaxial layers on GaAs.

The other very important physical property is that semi-insulating GaAs can be obtained which is very appropriate for electronic devices. The semi-insulating properties can be obtained by Cr-doping or in the undoped state by in-situ synthesis LEC growth. The semi-insulating properties of GaAs permit the isolation of electronic devices so that GaAs is a good material for IC applications since each device can be isolated without any p-n junctions such as are required in the case of Si. This isolation property

Table 8.1 Applications of GaAs

Material	Dopant	Applications
Conductive GaAs	Si doped	LDs, LEDs
	Zn doped	
Semi-Insulating GaAs	Cr doped	High-frequency MESFET
	undoped	Cellular phones
		Satellite Communications
		Digital ICs

opened for GaAs the possibility that the integration scale might be increased more than with silicon though it has not been achieved because of the side-gating effect, a problem which must be solved in the future. The fact that the electron mobility of GaAs is greater than that of Si makes GaAs a promising material for high frequency devices. In fact, high-frequency MESFETs in the region of 1-12 GHz have been used industrially, overtaking Si devices. GaAs is also a very important substrate for AlGaAs/InGaAs and AlGaAs/InGaP based very high frequency devices with cutoff frequencies up to several hundreds of GHz.

GaAs has the disadvantage that it is a semiconductor material with two constituents, one of which, arsenic, has a dissociation pressure of about 1 atm. at the melting point. Because of this fact, GaAs can create many native and complex defects so that material control is much more difficult than with elemental semiconductors.

The X-T diagram[11-15] and P-T diagrams[12] have been studied extensively and are determined as shown in Fig. 3.1. The i-line, at which the stoichiometric composition can be obtained is also precisely determined.[16] The vapor pressure for obtaining the stoichiometric composition is expressed as follows

$$P_{opt}(\text{torr}) = 2.6 \times 10^6 \times \exp(-1.05/kT_g) \qquad (8.1)$$

from the study on the quality of LPE GaAs.

In order to understand the formation of defects, it is important to know exactly the solidus lines of GaAs. Various authors have examined the solidus lines.[17-19] There was controversy as to whether the congruent point is at the As-rich or the Ga-rich side. It is however established from the study of the origin of precipitates observed in GaAs[20] that the congruent point is at the As-rich side. The precise composition of the solidus lines are not yet well determined but the congruent point is estimated deviated not less than several 10^{18} cm^{-3} from coulometric titration analysis.

Other properties such as the stacking fault energy,[21, 22] surface tension[23, 24] and viscosity[25, 26] of molten GaAs have also been studied.

Table 8.2 Physical Properties of GaAs

Crystal Structure	zincblend
Lattice Constant	5.6419Å
Density	5.316 g/cm^3
Melting Point	1238 °C
Linear Expansion Coefficient	5.93x10^{-6} /deg
Thermal Conductivity	0.455 W/cm·K
Dielectric Constant	10.9
Refractive index	3.655
Bandgap at Room Temperature	1.428 eV
Optical Transition Type	direct
Intrinsic Carrier Concentration	1.8x10^6 cm^{-3}
Electron Mobility	8,500 cm^2/V·sec
Hole Mobility	420 cm^2/V·sec
Intrinsic Resistivity	3.8x10^8 Ω·cm

8.3 CRYSTAL GROWTH

Conductive GaAs bulk material is industrially grown by the horizontal boat growth methods such as HGF, HB and HZM methods. Even semi-insulating (SI) GaAs with Cr-doping has been industrially grown by the boat growth methods. However, after it was found that undoped SI GaAs is mainly grown by the LEC method through in-situ synthesis, the LEC method became the main method for growing SI GaAs. Recently, VB/VGF crystals are replacing these HB and LEC crystals because of their superior qualities. These crystal growth methods have been extensively reviewed in the literature.[27-31]

Table 8.3 Crystal Growth of GaAs by Horizontal Boat Growth Methods

Method	Result	Author	Year	Ref.
HB	3T-HB method for controlling Si and O	Shimoda et al.	1969	41
HB	Use of pBN boat and liner for undoped SI crystal growth	Swiggard et al.	1977	62
HB	Cr-O doped SI crystals, four level model	Fujita et al.	1980	60
HB	Cr-O doped SI crystals and various analysis	Bonnafe et al.	1981	61
HB	Doping with Si, B and O	Akai et al.	1981	35
HB	Gettering of Si by oxygen	Martin et al.	1982	36
HB	Effect of arsenic vapor pressure	Parsey et al.	1982	53, 54
HB	3T-HB growth method	Akai et al.	1983	42-44
HGF	Growth of dislocation free crystals	Mo et al.	1983	45
HGF	Growth rate control for Cr-doped SI crystal growth	Orito et al.	1984	46
HB	Oxygen distribution in semi-insulating GaAs	Shikano et al.	1985	37
HB	50 mm diameter undoped SI crystals and variouscharacterizations	Burke et al.	1986	63-65
HB	Low In doped low EPD crystals	Inoue et al.	1985	55
HB	Correlation between thermodynamic conditions and dislocation densities	Stourac et al .	1987	38
HB	Thermodynamical analysis of the Ga-As-Si-O system	Leitner et al.	1987	39
HB, HGF	Comparizon of HB and HGF methods	Hruban et al.	1987	47
HB	In-doping with Cr for Low EPD semi-insulating GaAs	Fujita et al.	1987	58, 59
HZM	Si-doped crystal 600 mm in length	Mizutani et al	1990	50
HZM	Cr-doped semi-insulating crystal with diameter from 75-100 mm	Mizuniwa et al.	1991-1992	51-52
HB	HB method without arsenic zone	Chen et al.	1989	40
HB	Dislocation reduction by M2T-HB method	Lie et al.	1991	56
HB	50 mm in diameter with 600 mm in EPD< 400 cm^{-2}	Inoue et al.	1991	57
HGF	Effect of As vapor pressure on the site distribution of silicon	Fujii et al.	1992-1993	48-49
HB	Use of pBN boat and B_2O_3 encapsulation for undoped SI crystals with 50ϕ mm x400 mm	Ishihara et al	1994	66
HB	50 mm diameter <100> single crystals	Murata et al.	1994	67

HB: Horizontal Bridgeman, HGF: Horizontal Gradient Freezing, HZM: Horizontal Zone Melting

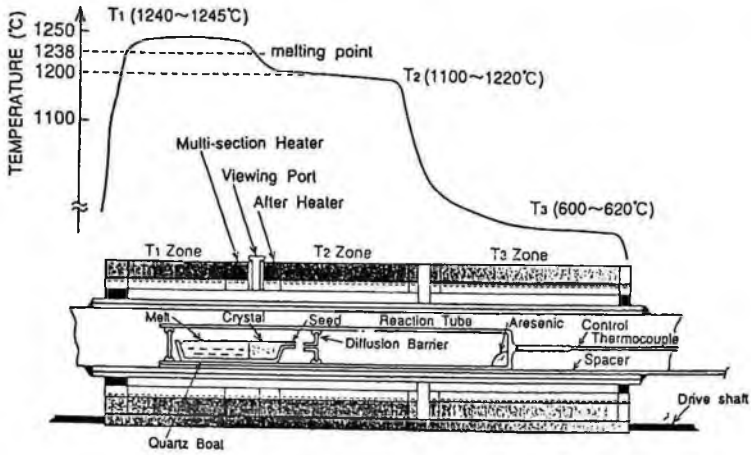

Fig. 8.1 Cross-sectional view of 3T-HB growth assembly (from Ref. 55 with permission).

8.3.1 Horizontal Boat Growth Methods

Conductive GaAs crystals are industrially grown by the HGF, HB and HGF methods. Since crystals are grown using boat containers, they are referred to as boat growth methods. In these methods, several configurations are used as shown in Fig. 2.1. In principle, the boat containing the GaAs melt is moved along the furnace in the case of the HB method while the temperature of the furnace is lowered in the case of the VGF method.

The HB and HGF method are reviewed by various authors.[32-34] In Table 8.3,[35-67] various studies on these HB and HGF crystal growth methods are summarized.

(1) Si contamination/doping

Since in both methods, contamination with silicon occurs from quartz boats and ampoules and with oxygen from the reaction of Ga, the control of this contamination is one of the key parameters of these methods. Si is also a dopant for n-type conductive material. In fact, Si incorporation has been extensively studied by various authors.[32, 35-40] Stourac[38] discussed the thermodynamic conditions of growth and the correlation with dislocation density and impurity content. Thermodynamic analysis of Ga-As-Si-O has been studied by Leitner and Moravec[39] and the solubility of oxygen was reported.

(2) Various configurations

In order to prevent Si contamination, the three temperature zone horizontal Bridgman (3T-HB) method (Fig. 8.1) has been developed.[29, 41-44] In this method, the medium temperature zone is controlled in order to control the vapor pressure of gallium suboxide (Ga_2O). Chen et al.[40] modified the 3T-HB method to the M2T-HB method which is simpler than the 3T-HB method.

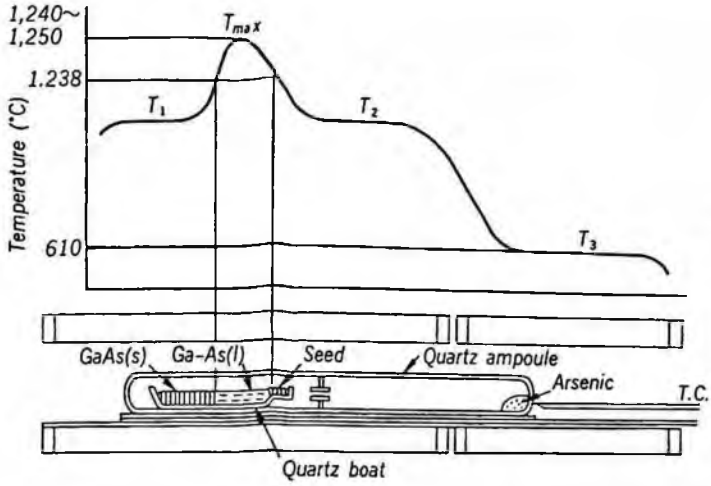

Fig. 8.2 Schematic drawing of HZM apparatus (from Ref. 51 with permission).

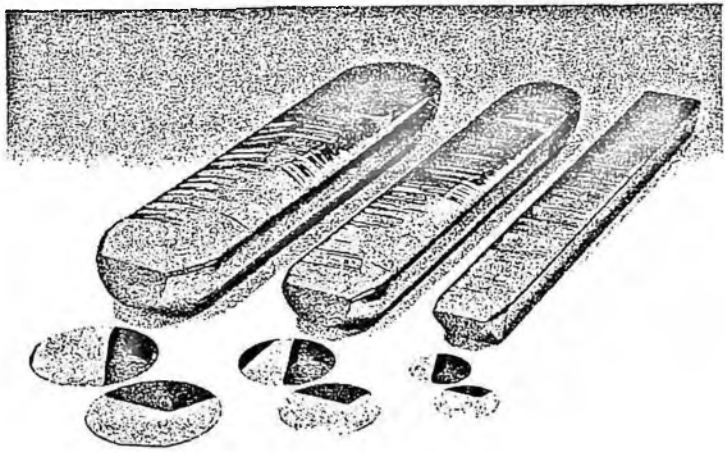

Fig. 8.3 GaAs single crystal ingots and wafers with dimensions of 100 mm, 75 mm and 50 mm VGF furnace (from Ref. 51 with permission).

The HGF method which can compete with the 3T-HB method has also been developed.[45-47] Fujii et al.[48, 49] discussed the thermodynamics in the Ga-As-Si-O system and the effect of the diffusion barrier temperature in the HGF method.

Mizutani et al.[50-52] have developed the HZM method to replace the HGF and HB methods and have grown 100 mm diameter SI-GaAs using Cr-doping (Fig. 8.2, 8.3).

(3) Reduction of dislocation densities

Horizontal boat growth methods have the advantage that low dislocation density crystals can be grown because the temperature gradient during crystal growth can be reduced.

Parsey et al.[53, 54] grew GaAs crystals by the HB method under controlled As vapor pressure and succeeded in reducing dislocation densities down to less than 500 cm^{-2}. Inoue et al.[55] have theoretically analyzed the thermal stress in HB crystals and discussed the procedure to decrease the dislocation densities. In fact, it is reported that crystals with low dislocation densities within range of dislocation-free (DF) ($<4x10^2\ cm^{-2}$) could be obtained.

Horizontal boat methods are highly developed and large diameter, long single crystals, 75-100 mm in diameter and 600 mm in length are industrially grown.[29, 44, 50-52]

Reduction of dislocation densities by In impurity hardening has been applied to HB crystal growth.[59-61] They showed that In-doping was effective in reducing dislocation densities not only for conductive GaAs crystals but also Cr-O doped semi-insulating GaAs.

(4) Semi-Insulating (SI) crystals

On the other hand, there is considerable contamination by silicon due to quartz ampoules and boats. This is the reason why undoped semi-insulating GaAs can not be obtained by the HB and HGF methods.

To overcome the above-mentioned disadvantage of HGF/HB/HZM methods, SI GaAs has been grown by doping Cr or Cr and O.[36, 37, 51, 60, 61] Since Cr acts as deep acceptor, it has the effect of compensating for Si in GaAs. Doping only with Cr, it is difficult to grow high quality crystals due to supercooling and precipitate formation. The Cr and O co-doping method has been therefore developed, and the SI mechanism has been considered by the four level model, where O provides deep donors.[60]

Undoped SI GaAs was also attempted by the HB method[62-66] using a pBN boat, liners and B_2O_3 encapsulant. It is claimed that uniform SI GaAs can be obtained by preventing Si contamination using pBN container materials and encapsulant. Growth of SI crystals of 50 mm diameter and 400 mm length has been reported.[66]

(5) <100> oriented growth

In most horizontal boat methods, GaAs crystals are grown to <111> orientation using a <111> oriented seed crystal. Murata et al.[67] have grown <100> oriented single crystals using a <100> oriented seed crystal.

8.3.2 Liquid Encapsulated Czochralski (LEC) Method

In 1979, it was found that undoped SI GaAs could be grown by in-situ synthesis in the LEC furnace and successive crystal growth.[68] Following this invention, the LEC method became the most appropriate one for growing SI GaAs. Various reviews have been published regarding the LEC method.[4, 27, 31, 69-72] There are many reports on the crystal growth of GaAs by the LEC method as summarized in Table 8.4. Typical LEC

Table 8.4 Crystal Growth of GaAs by the LEC method

Method	Result	Author	Year	Ref.
LEC	In-situ synthesis and crystal growth of SI GaAs	Aucoin et al.	1979	68
LEC	First In-doping for dislocation reduction	Jacob	1983	104
LEC	Dislocation-free Si-doped	Fornari et al.	1983	165
LEC	Growth of 75 mm ϕ SI crystals	Chen et al.	1983	73
LEC	Dislocation reduction by B-doping	Tada et al.	1984	102
LEC	Growth of 70mmϕ crystals under low temperature gradient	Elliot et al.	1984	74
LEC	Dislocation free SI crystals by In-doping	Barrett et al.	1984	108
LEC	Effect of In content on dislocation densities	Kimura et al.	1984	109
LEC	Typical LEC growth	Inada et al.	1984	75
LEC	Improved LEC with a window of suceptor	Shimada et al.	1984	92, 93
VM-FEC	Dislocation free crystal growth, In-doping with magnetic field application	Kohda et al.	1985	95, 96
MLEC	Strong magnetic field and homogeneity	Kimura et al.	1986	130
MLEC	Relationship between growth conditions and EL2 concentrations	Terashima et al.	1986	131
LEC	Elimination of grown-in dislocations in In-doping	Yamada et al.	1986	115
LEC	Dislocation-free Si and In doped crystal growth	Fujii et al.	1986	117
LEC	Cellular growth and In inclusions	Ono et al.	1986	118
LEC	Si-doped dislocation-free crystal	Orito et al.	1986	167
LEC	Uniform In concentration by the double crucible method	Matsumura et al.	1986	121
LEC	EPD<1000 cm^{-2} by an improved hot zone system	Okada et al.	1986	94
LEC	In-doping and mechanism of dislocation reduction	McGuigan et al.	1986	112, 113
LEC	As injection LEC method	Inada et al.	1986	82
MLEC	High pulling rate and properties	Kimura et al.	1987	132
MLEC	Magnetic field effect on residual impurity concentrations	Terashima et al.	1987	133
VM-FEC	In-doped vertical magnetic field applied FEC	Orito et al.	1987	97
PCZ	As pressure controlled LEC for dislocation reduction	Tomizawa et al.	1987	138, 139
As-LEC	Dislocation free crystals under low temperature gradient using an X-ray imaging system	Ozawa et al.	1987	141, 142
LEC	75 mm in diameter with 270 mm in length	Nambu et al.	1988	154
LEC	Intelligent processing of crystal growth	Goldberg	1990	152
LEC	100 mm diameter crystal with 9 kg	Kashiwa et al.	1991	155
LEC	Origin of polygonization	Tower et al.	1991	156
LP-LEC	Long-size crystal growth paying attention to the interface shape	Marshall	1991	172
LP-LEC	Si doping crystals with in-situ synthesis	Elliot et al.	1992	76
LEC	Long size single crystal growth	Onishi et al.	1993	159
VCZ	100 mm diameter crystal growth	Kawase et al.	1993	145
LEC	Long-size crystal growth, 75 mm in diameter with 500 mm in length, 100 mm diameter with 320 mm, 150 mm diameter with170 mm	Shibata et al.	1993	158
LEC	100 mm diameter crystal with more than 435 mm in length, maximum 900 mm	Ware et al.	1996	161
LEC	Growth of 150 mm diameter crystals	Flade et al.	1999	162
LEC	Growth of 200 mm diameter crystals	Wachi et al.	2003	164

LEC: Liquid Encapsulated Czochralski, MLEC: Magnetic LED, VM-FEC: Vertical Magnet Fully Encapsulated Czochralski, PCZ: Pressure-conrtolled LEC, As-LEC: Arsenic ambient controlled LEC, PCZ: Pressure controlled Czocralski, VCZ: Vapor controlled Czochralski

growth of GaAs and the characterization can be seen in Refs. 73-75.

The development of LEC-GaAs is based on the following items.

- Effect of melt composition
- Reduction of dislocation density by various methods
- Effect of magnetic field
- Vapor pressure control
- Diameter control
- Large diameter and long size crystal growth
- Growth of conductive GaAs
- Impurity control
- Low pressure LEC (LP-LEC) method

In the following subsections, the reported results and the present conclusions in each items are discussed.

(1) Melt composition

Melt composition control is one of the most important factors during crystal growth of GaAs. This is because when the melt composition is varied to the As-rich or Ga-rich side, the melt composition during crystal growth is greatly changed as shown in Fig. 8.4.[76] Since the point defect structure in grown GaAs is influenced by the melt composition,[77] the electrical properties are largely affected by the melt composition as explained in Sec. 8.6.2(2).[78, 79] The effect of melt composition on the electrical properties and defect concentrations of LEC-GaAs has been studied by several authors.[80-87]

Precise melt composition control is therefore of prime importance for the crystal growth of GaAs by the LEC method. Following the process in Fig. 8.5, the arsenic loss during each stage can be estimated. It is known that the arsenic loss is very great at the in-situ stage and cooling stage while that during crystal growth is negligible. Based on these estimations, the charge ratio As/Ga is controlled in order to make the melt composition during crystal growth as stoichiometric as possible. In order to control the As loss during in-situ synthesis, great care is taken with temperature control. By this method, the melt composition from which the crystal is grown is precisely controlled. An example of precise melt composition control is also found in the study by Nishio and Terashima.[84]

In order to control the melt composition precisely, the As injection method as shown in Fig. 8.6. has been developed.[82] In this method, As vapor generated by heating an As reservoir is injected into the GaAs melt in order to hold the As concentration constant during crystal growth.

(2) Reduction of dislocation densities

Since dislocations are postulated to affect the threshold voltage variation as explained in Section 8.8.3, various efforts have been devoted to reduce dislocation densities.

As explained in Sec. 3.5 and Sec. 4.3.3, the reduction of dislocation densities has been achieved mainly by improvements in the temperature distribution in the LEC furnace and by impurity hardening.

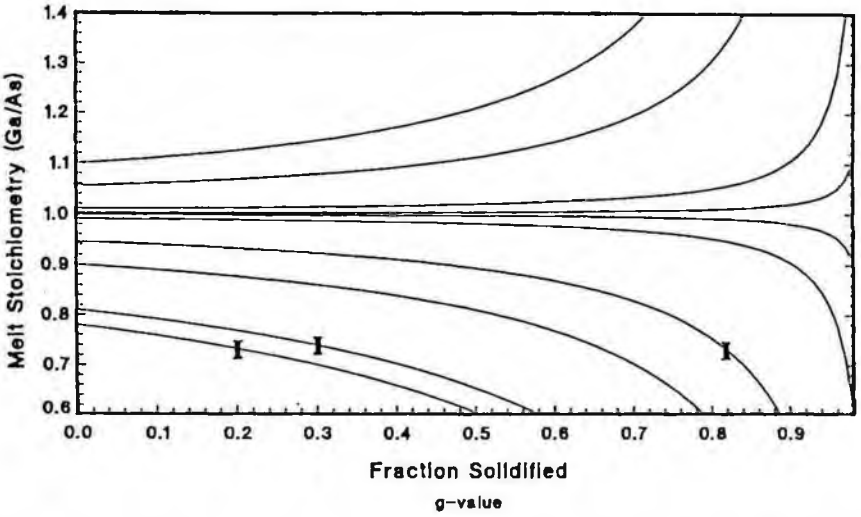

Fig. 8.4 Calculated segregation of Ga and As for various starting melt compositions. Data points (I) indicate measured g values for interface breakdown resulting from constitutional supercooling for crystals grown from the associated starting melt compositions (reprinted from Ref. 76 with permission, copyright 1992 Elsevier).

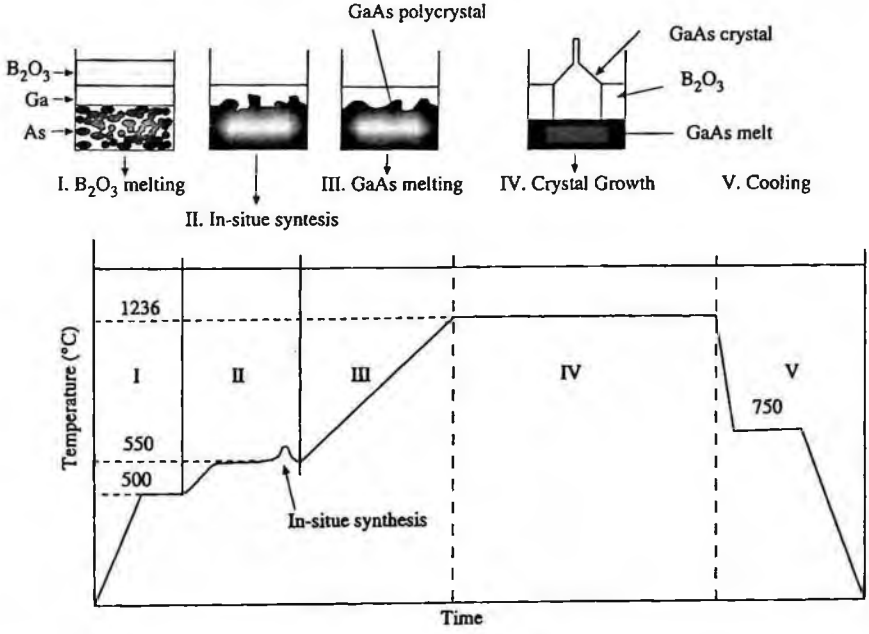

Fig. 8.5 In-situ synthesis and growth processes during LEC crystal growth.

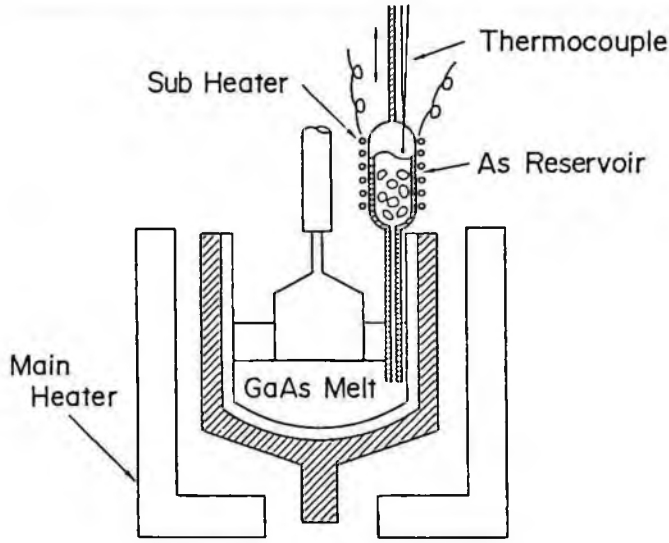

Fig. 8.6 Schematic cross-section of an As injection LEC furnace (reprinted from Ref. 82 with permission, copyright 1986 TMS).

- Necking procedure

The Dash method (Sec. 4.3.3), that is the necking procedure which was successful for Si crystal growth has also been applied in the case of LEC GaAs crystal growth.[73, 88-90] It was however found that although dislocation-free crystals could be obtained by necking, it was limited to small diameter crystals. For larger diameter crystals, since dislocations are generated from the grown crystal surface due to thermal stress and are propagated into the crystals and multiplied, the necking procedure is not effective.[91]

- Improvement of temperature distribution

The reduction of the temperature gradient during crystal growth is basically realized by the following methods.

(i) post-growth heating by sub-heaters set on the main heaters
(ii) reduction of applied inert gas
(iii) application of a thermal baffle
(iv) increasing the thickness of B_2O_3
(v) application of a slightly As rich melt

Of these, (i-iii) accelerate the dissociation of As so that their application is somewhat limited. (iv) can prevent the dissociation of As but the crystal growth yield is impaired when the thickness exceeds a certain limit.

Chen and Holmes[73] reported that the lowest dislocation densities obtained by optimizing some of these parameters for 75 mm diameter crystals was 6000 cm^{-2}.

Shimada et al.[92, 93] made windows in the susceptor which supports the crucible in

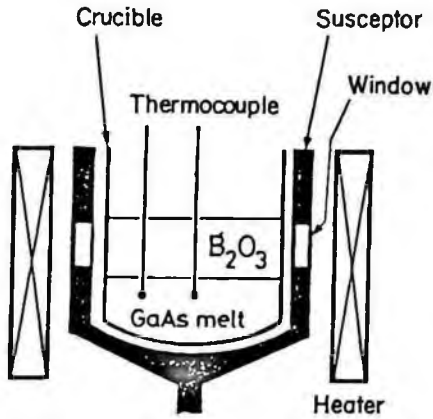

Fig. 8.7 Schematic cross-section of crystal growth using a susceptor with windows (from Ref. 92 with permission).

order effectively to heat the encapsulant B_2O_3 and reduce the axial temperature gradient (Fig. 8.7). This technique was combined with the application of a thermal baffle and the reduction of the inert gas atmosphere. With these improvements, they reported the realization of low dislocation densities of 1000 cm^{-2} for 50 mm diameter single crystals.

Elliot et al.[74] reported that they could obtain dislocation densities of 5000 cm^{-2} by decreasing the axial temperature gradient under 2.4 atm. nitrogen pressure. Okada et al.[94] improved the hot zone in order to make the axial temperature profile as linear as possible with a low axial temperature gradient. They reported also low dislocation densities down to 1000 cm^{-2} for 50 mm diameter crystals.

Nakanishi et al.,[95] Kohda et al.[96] and Orito et al.[97] developed the vertical magnetic-field-applied fully encapsulated Czochralski (VM-FEC) method (Fig. 8.9) in which they applied a magnetic field in order to reduce temperature fluctuations and grew crystals in a thick B_2O_3 encapsulant which covered the grown crystals entirely. The aim was to reduce the axial temperature gradient and to prevent the dissociation of As. This VM-FEC method was combined with In-doping which is effective in reducing dislocation densities as described below and dislocation-free 50 mm diameter single crystals were achieved.

- *Impurity hardening*

As explained in Sec. 4.3.4, some impurities have a hardening effect. For GaAs, impurities such as Si, S, Zn, B, N are known to have an impurity hardening effect.[74, 98-103] By doping these impurities, it becomes possible to grow low dislocation densities. Even dislocation-free crystals can be grown. Among n-type dopants, Si and S are known to reduce dislocation densities. Among p-type dopants, Zn is known to reduce dislocation densities.

Among various impurities for dislocation reduction, the effect of indium has been

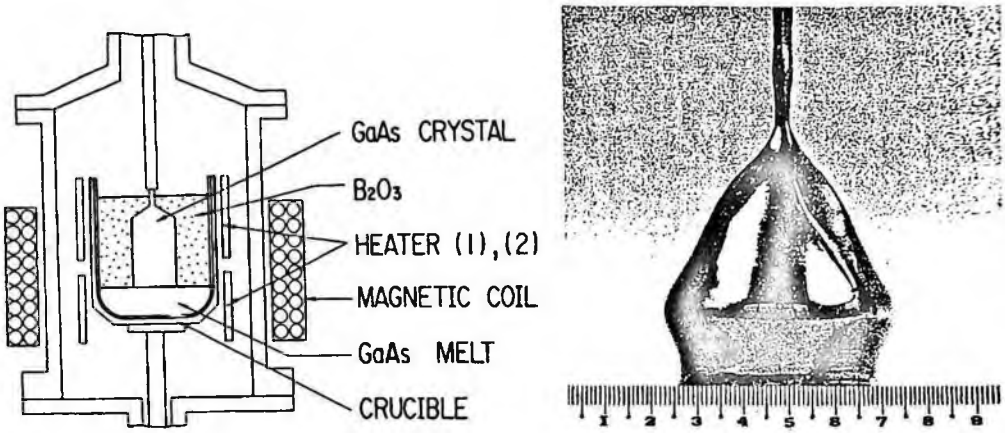

Fig. 8.8 (a) Growth apparatus for the VM-FEC and (b) the grown crystal (reprinted from Ref. 96 with permission, copyright 1985 Elsevier).

most extensively studied because indium does not affect the electrical properties since it acts as an isoelectronic impurity and does not impair the semi-insulating properties. Jacob et al.[104, 105] first tried to dope very high quantities of indium in order to reduce dislocation densities. Following his work, many studies have been performed.[74, 106-123]

Yamada et al.[115] analyzed the dislocation propagation from the seed to grown crystals and proposed the use of an In-doped seed whose In concentration is the same as that in grown crystals. Suzuki et al.[119] developed a technology for growing low dislocation density 75 mm diameter single crystals based on In-doping and showed the reduction of σV_{th} by using low EPD crystals.

The VM-FEC method (Fig. 8.8) has been developed, combining indium-doping in order to obtain dislocation-free crystals with lower In content.[96] Orito et al.[97] developed 100 mm diameter In-doped single crystals using the VM-FEC method and showed that the reduction of dislocation density improved the distribution of the sheet carrier concentration along the wafer.

In-doping can reduce the dislocation densities as shown in Fig. 8.9 and in Fig. 4.8. The mechanism of dislocation density reduction by In doping has been discussed by various authors as explained in Sec. 4.3.4.

Notwithstanding all these studies on indium doping, In-doping has not become the main industrial production method. The reason is that the doping level is too high to call it doping. Reducing dislocation densities needs more than 10^{20} cm^{-3}, and at this level it is really called alloying. At this high level of doping, supercooling takes place so that when long crystals are grown, polycrystallization takes place from the middle of the crystal. This polycrystallization can be avoided if the crystal growth rate is lowered but this lowers the productivity. This supercooling problem must be solved for this method to be industrially applied.

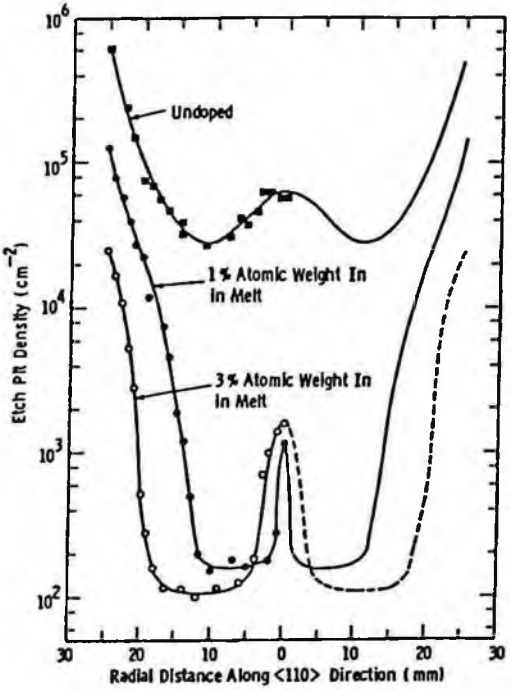

Fig. 8.9 EPD distributions of undoped and In-doped GaAs crystals (reprinted from Ref. 108 with permission, copyright 1984 Elsevier).

(3) Magnetic field application

The effectiveness of the application of a magnetic field is mainly due to the suppression of thermal convection in the melt, resulting from the high dynamic viscosity generated by the Fleming force as described in Sec. 3.5. Due to the suppression of thermal convection, the application of a magnetic filed has the effect of eliminating irregular growth striations and reducing the incorporation of impurities from the crucible to the melt. Because of these effects, the application of a magnetic field is effective in improving the quality of the crystal.

In the case of GaAs, the effect of the application of a magnetic field during LEC crystal growth was extensively studied mainly by Fukuda's group[124-134] and the NTT group[96, 135, 136] in the eighties. This application of a magnetic field to the LEC method is referred to as MLEC (Magnetic LEC). The application of a magnetic field was found to be effective in various ways.

(i) It has the effect of suppressing the temperature fluctuation (Fig. 8.10) and of eliminating striations.

(ii) Due to the suppression of convection, a high growth rate is achieved.

(iii) Because of the suppression of convection, the incorporation of impurities is affected.

Kimura et al.[130] examined the effect of magnetic fields up to 3000 Oe and found that the effective segregation coefficient of carbon approaches unity.

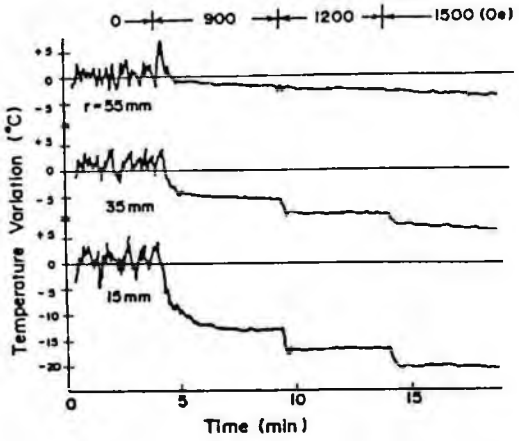

Fig. 8.10 Effect of magnetic field on melt temperature at 5 mm under the melt surface. Numerical r indicates the distance from the crucible center (from Ref. 135 with permission).

Terashima et al.[131] found that EL2 concentrations vary widely as a function of melt composition when a magnetic field is applied. Kimura et al.[132] showed that the homogeneity of the infrared absorption coefficient and of the resistivity of high pulling rate single crystals were greatly improved after ingot-annealing (Fig. 8.11). Terashima et al.[133] have discussed the impurity incorporation process thermodynamically (Fig. 8.12) and found that the oxidation of free Ga in the melt and the deoxidation rate of carbon and boron oxides are the rate limiting reactions. They also examined the effect of a magnetic field on these reactions and the incorporation of carbon and boron.

Notwithstanding these pioneering studies on the positive effects of the application of a magnetic field, this technique is not applied in the industrial production of GaAs. This is because most of the problems with GaAs were solved by other techniques. It was found that the concentration and distribution of EL2 can be well controlled by post-annealing technologies (Sec. 8.4). The carbon concentration can be precisely controlled by controlling the CO gas concentrations in the gas phase.

(4) Vapor pressure control

Since GaAs is a compound semiconductor, one of whose constituents has a high vapor pressure, several trials have been performed to grow crystals under arsenic vapor control.

Steimann and Zimmerli[88] were the first to apply arsenic vapor pressure control to the Czochralski method in growing GaAs in a furnace in which a crystal is pulled up by a magnetically driven movement. Leung and Allred[137] applied a new method where molten B_2O_3 is used as a push-pull, rotary seal and have grown low dislocation density crystals under arsenic vapor pressure. Nishizawa et al.[16] found an optimal arsenic vapor

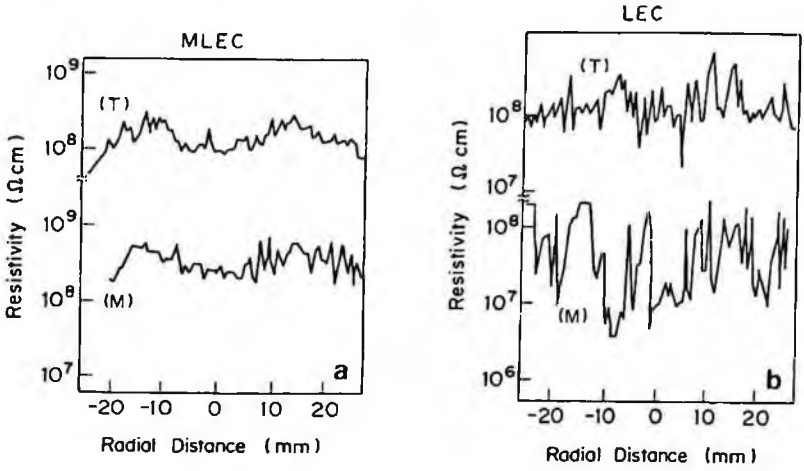

Fig. 8.11 Microscopic resistivity distribution across the wafer of (a) undoped MLEC GaAs and (b) LEC GaAs crystals. (T) top part of the crystal; (M) middle part of the crystal (reprinted from Ref. 130 with permission, copyright 1986 Elsevier).

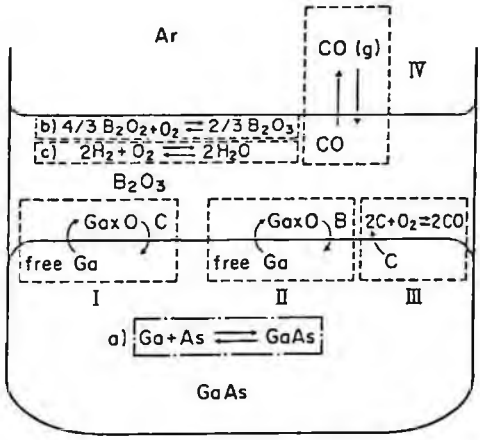

Fig. 8.12 Chemical reaction process related to impurity incorporation in the LEC and MLEC crystal growth technique (reprinted from Ref.133 with permission, copyright 1987 Elsevier).

pressure for stoichiometry as in Eq. 10.1.

Based on the above optimized As vapor pressure, Tomizawa et al.[138, 139] and Sasa[140] were the first to grow GaAs crystals under As vapor pressure in a furnace as seen in Fig. 8.13 and Fig. 2.16 (a) which is referred to as the arsenic Pressure Controlled Czochralski (PCZ) method. In this method, no encapsulant was used. They found that the dislocation density is affected by the As vapor pressure (Fig. 8.14). These studies are

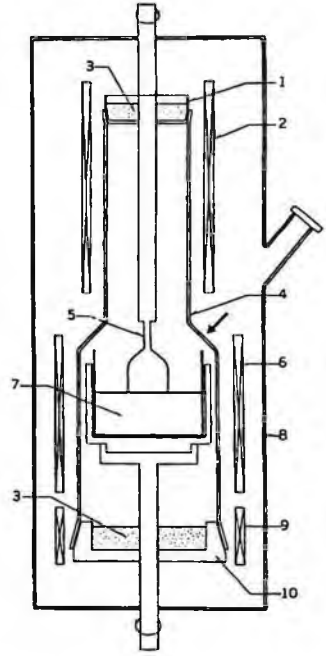

Fig. 8.13 Schematic diagram of the crystal puller for controlling vapor pressure. 1: upper lid, 2: heater A, 3: B_2O_3, 4: quartz chamber, 5: seed, 6: heater B, 7: GaAs melt, 8: metal chamber, 9: heater C, 10: lower lid (reprinted from Ref. 138 with permission of The Electrochemical Society).

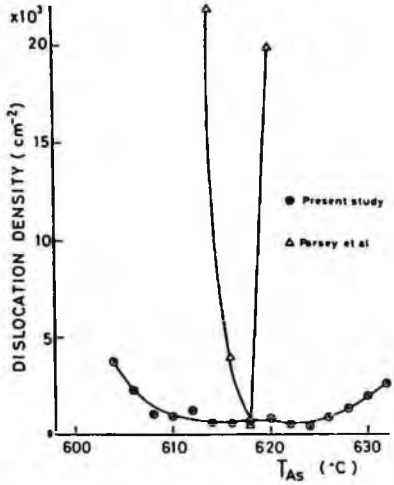

Fig. 8.14 Effect of As pressure on the EPD of PCZ grown GaAs (from Ref. 139 with permission). Parsey's data are from Ref. 54.

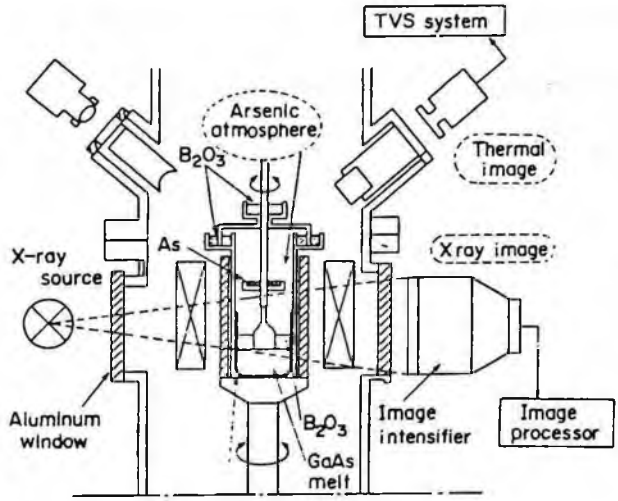

Fig. 8.15 Arsenic ambient controlled LEC (As-LEC) growth system (reprinted from Ref. 142 with permission, copyright 1987 Elsevier).

based on the idea that the crystal quality is affected by non-stoichiometry.

Ozawa et al.[141, 142] and Usuda et al.[143] have studied the As ambient controlled LEC (As-LEC) method (Fig. 8.15) in which an As reservoir is attached to the pulling rod to apply As vapor pressure during crystal growth. They showed that arsenic evaporation from the crystal surface is suppressed. It was also found that high resistive GaAs can be grown from a quartz crucible since the arsenic vapor application suppresses the silicon contamination from the quartz crucible.

Kawase et al.[144, 145] grew single crystals under arsenic vapor pressure with a B_2O_3 encapsulant, which is referred to as the Vapor-pressure Controlled Czochralski (VCZ) method. This method was first applied to the crystal growth of InP (Sec. 10.3.2 (3)). The principle of this method is based on decreasing the axial temperature gradient without the crystals decomposing. Because of the decrease in the axial temperature gradient, it became possible to reduce the dislocation density. They succeeded in growing 100 mm diameter single crystals with low dislocation densities.

These vapor pressure controlled LEC methods have been reviewed by Rudolph et al.[146-148] Computer simulation for the VCZ method has been performed by Frank et al.[149] and Smirnova et al.[150]

(5) Diameter control

Precise diameter control of growing GaAs crystals is important not only from the viewpoint of the availability of the material but also from the viewpoint of the growth of long crystals and the prevention of polycystallization as explained below. Various methods for diameter control have already been reviewed in Sec. 3.7 and these methods have been more or less applied to the growth of GaAs. Some examples for the growth

of GaAs are shown by Riedling,[151] Goldberg[152] and Washizuka et al.[153]

(6) Growth of large-diameter long single crystals

One of the most important techniques in GaAs crystal growth by the LEC method involves the growth of large-diameter long crystals. In fact, these techniques have been developed by various affiliations.[4, 73-74, 154, 155] It is well known that the growth of long

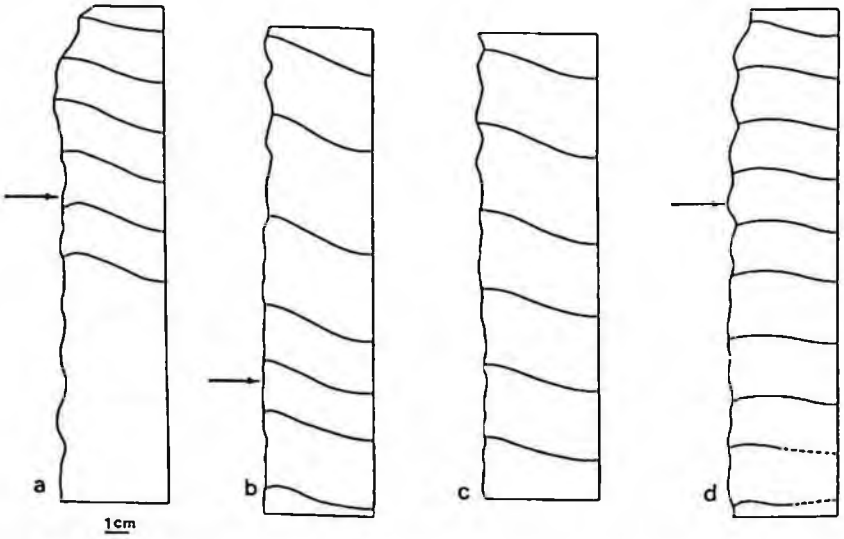

Fig. 8.16 Growth interface shapes of 8 kg, 75 mm diameter LEC GaAs crystals. Arrows indicate points of initial grain boundary formation. Crystal c is entirely single. (reprinted from Ref. 156 with permission, copyright 1991 Elsevier)

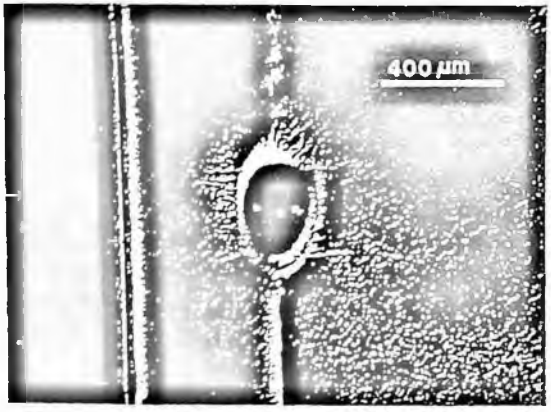

Fig. 8.17 Fissures occasionally originating from included gallium droplets (reprinted from Ref. 156 with permission, copyright 1991 Elsevier).

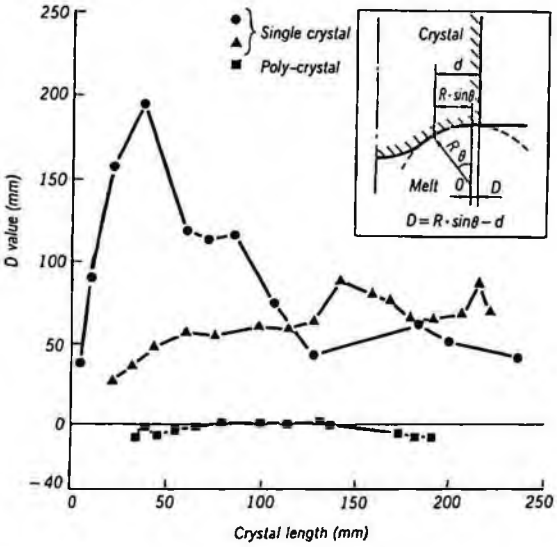

Fig. 8.18 Position of the center of curvature of the interface lines (D value) as a function of crystal length. The D value of a single crystal is generally positive and very large and that of a polycrystal is near zero or less (reprinted from Ref. 158 with permission, copyright 1993 Elsevier).

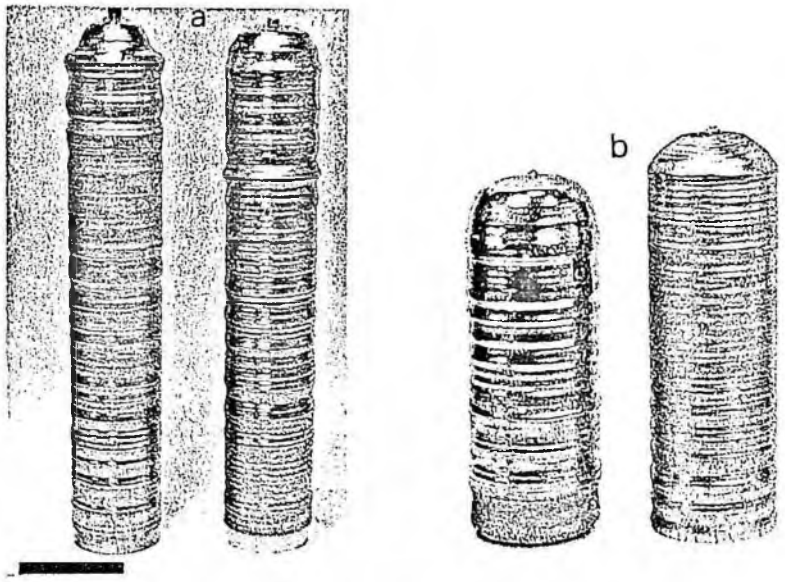

Fig. 8.19 (a) 500 mm-long 75 mm diameter GaAs crystals and (b) 350 mm-long 100 mm diameter GaAs crystals (reprinted from Ref. 158 with permission, copyright 1993 Elsevier).

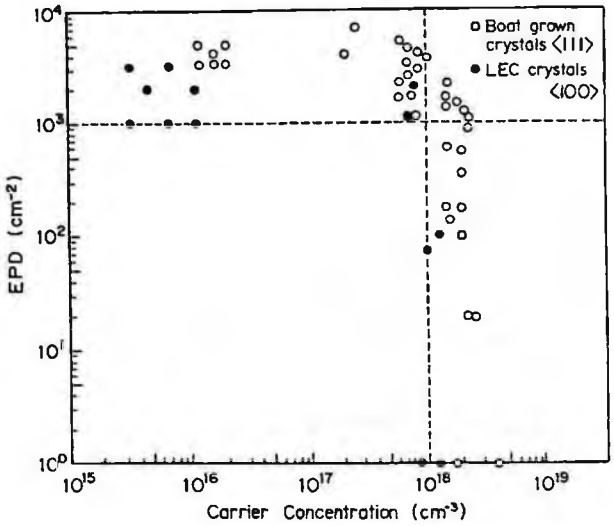

Fig. 8.20 Relationship between EPD and carrier concentration of Si-doped crystal (reprinted from Ref. 167 with permission, copyright 1986 TMS).

single crystals is very difficult since polycrystals are generated from lineages in part of the crystal. This phenomenon has been observed by many researchers.

The origin of this polycrystallization has been studied by Tower et al.[156] and Inada et al.[157-160] Tower et al. found that polygonization occurs depending on the interface shape (Fig. 8.16) due to the gallium droplet (Fig. 8.17) from which high density dislocations

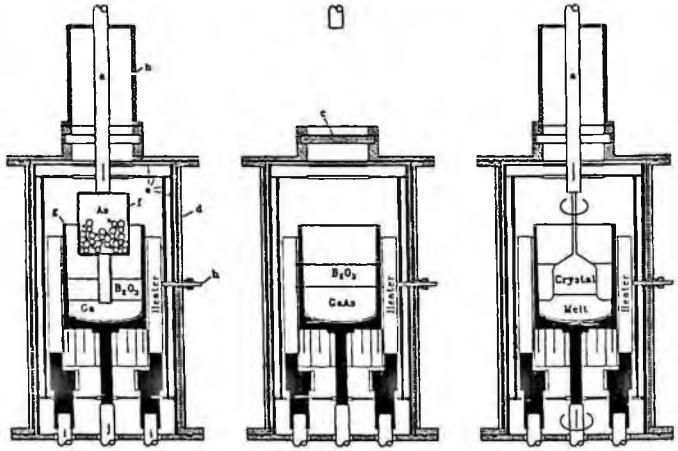

Fig. 8.21 Crystal growth by As injection synthesis and the subsequent crystal growth (reprinted from Ref. 76 with permission, copyright 1992 Elsevier).

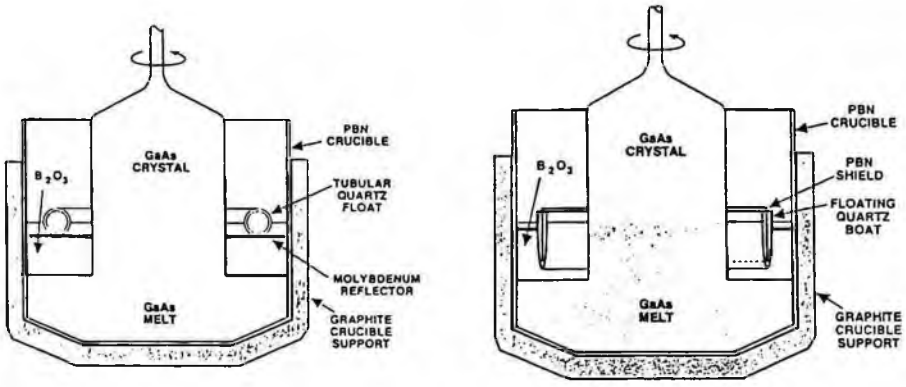

Fig. 8.22 (a) Floating Mo-quartz reflector simulating opaque B_2O_3 and (b) floating quartz-pBN shield to reduce "bleed" (reprinted from Ref. 172 with permission, copyright 1991 Elsevier).

are generated which propagate internally when diameter control can not be appropriately performed. Inada et al. claimed that polycrystal generation takes place because of the abnormal interface shape at the periphery of the grown crystals.[157-160] As shown in the center part of Fig. 8.18, the interface is concave to the melt, but is convex along the periphery of the crystal. This abnormal interface shape is believed to accumulate dislocations which appear as lineages and from these lineages, polycrystals spread. Inada et al. applied three zone furnaces in order to control the temperature distribution in such a way that the interface show no abnormalities. By this improvement, they succeeded in growing long crystals even up to 770 mm in length for 75 mm diameter (Fig. 8.19). Further large diameter crystal growth has continued to be achieved through 150 mm up to 200 mm.[161-164]

(7) Growth of conductive GaAs

As mentioned in the former section, conductive GaAs is mainly produced by the HB and HGF methods. There are however several studies of the growth of conductive GaAs by the LEC method with a view to producing it at low cost.

The effects of Si-, S-, Se- and Zn-doping on dislocation densities have been studied.[76, 165, 166] Orito et al.[167] have developed Si-doped dislocation-free GaAs crystals. They showed that dislocation-free crystals could be obtained with the Si concentration exceeding 10^{18} cm^{-3} as shown in Fig. 8.20, the same level as in the case of HB/HGF methods. Fujii et al. have studied the co-doping of Si and In.[168]

Hashio et al.[169] have applied the VCZ method to grow Si-doped conductive GaAs crystals. They examined the relationship between Si and B which are incorporated from encapsulant B_2O_3.

(8) Low Pressure LEC (LP-LEC) method

In the beginning of the development of SI GaAs, crystals were grown mainly by the high-pressure (HP-LEC) LEC method. This is because for in-situ synthesis, it is necessary to apply inert gas at high pressure in order to prevent the decomposition of the GaAs melt. However, the low-pressure LEC (LP-LEC) method was developed with a view to low cost production. This is based on using pre-synthesized GaAs material as the charge for growth.[170]

Mo et al. developed an in-situ synthesis LP-LEC method in which GaAs is synthesized by As injection into the Ga melt and GaAs crystals can be grown successively with melt composition control by As injection. They were able to grow undoped SI GaAs crystals reproducibly.[171] Elliot et al.[76] have grown Si-doped conductive GaAs by the LP-LEC method using the As injection process as shown in Fig. 8.21. Marshall[172] has studied the floating shield method (Fig. 8.22) in order to increase the crystal length. Wargo and Witt[173] have developed an imaging method for measuring the melt surface temperature distribution which is applicable to the LP-LEC method.

8.3.3 Vertical Boat Growth Methods

The vertical gradient freezing (VGF) method was first applied to the growth of GaAs by Chang et al.[174] in a pyrolytic boron nitride crucible without using seed crystals. The successful application of the VGF method was first reported by Gault et al. as reviewed in Refs. 175-177 for the growth of 50-75 mm diameter GaAs, using the same furnace as shown in Fig. 7.6 for GaP. Following this report, this became a new and promising method for GaAs crystal growth.

(1) Various modifications

The studies of VB/VGF methods are summarized in Table 8.5 [178-204]. There have been various modifications to these VGF and VB methods. In the first report of a VGF method, As vapor pressure was controlled by using a graphite container during crystal growth as shown in Fig. 7.7 (b). In this method, the container is not fully sealed so that arsenic loss is expected. Abemathy et al.[178] developed the VGF method and the VB method successively, where the GaAs melt in a pBN crucible is sealed in a quartz ampoule (Fig. 8.23, 8.24). In Fig. 8.25, GaAs crystals grown by Kremer et al.[179, 180] are shown. Hoshikawa et al.[181, 182] developed the LB-VB method (Fig. 8.26), in which arsenic pressure control is not applied and a B_2O_3 encapsulant is used to prevent the dissociation of arsenic. Bourret et al.[183, 184] have developed the VGF method, by using a B_2O_3 encapsulant in a pBN crucible and by controlling the As vapor pressure in a sealed quartz ampoule. Okabe et al.[185] developed a VGF method in which a small amount of B_2O_3 is used under arsenic pressure control (Fig. 8.27). Frank et al.[187] examined the effect of arsenic vapor pressure on EPD and Amon et al [188] have studied the influence of the crucible shape on twinning.

Based on these VB/VGF methods, the diameter of GaAs single crystals has been increased from 75 mm to 200 mm, and they are grown industrially.[189-194]

Table 8.5 Crystal Growth of GaAs by the VB and VGF Methods

Method	Result	Author	Year	Ref.
VGF	First application of VGF to GaAs	Chang et al.	1974	174
VGF	50 mm diameter single crystal growth undoped	Gault et al.	1986	175
VGF	75 mm diameter undoped SI <100> single crystal, EPD<2500 cm^{-2} SI and Si-doped crystals	Clemens et al.	1986 1988	176-177
VGF	50 mm diameter undoped and In alloyed crystals, addition of gallium oxide	Abernathy et al.	1987	178
VB	Undoped SI GaAs crystal growth up to 75 mm diameter	Kremer et al.	1989-1990	179-180
LE-VB	Liquid B_2O_3 encapsulated VB method, 75 mm diameter SI crystals	Hoshikawa et al.	1989 1991	181-182
DGF	62. 5mm <100> single crystal growth, EPD<1000 cm^{-2}	Bourret et al.	1990 1991	183-184
VGF	Undoped SI 80 mm diameter single crystals	Okabe et al.	1991	185
LE-VGF	Growth of 50 mm diameter low EPD crystals with 15 zone furnace. SI crystals by annealing	Buhrig et al.	1994 1997	198-199
LE-VB	Control of EL2 by annealing after growth	Nakanishi et al.	1995	186
MVGF	Effect of magnetic field on the suppression of Marangoni flow and striations	Park et al.	1995	202-203
VGF	Effect of As vapor pressure on EPD and electrical properties	Frank et al.	1996	187
LE-VGF	Growth of low EPD SI crystals with B_2O_3 encapsulant and the addition of Ga_2O_3	Frank et al.	1997	200-201
VGF	Effect of crucible shape on twinning	Amon et al.	1998	188
VGF	Industrial production of GaAs	Liu	1996	189
VB	Growth of 100 mm diameter SI crystals	Kawase et al.	1996	190
VGF	Growth of 100 mm diameter SI crystals under optimized conditions based on simulation	Birkmann et al.	2000	192
VB	Growth of 150 mm diameter crystals and characterization of their uniformity	Sawada et al.	2000	193
MVGF	Growth in a rotating magnetic field	Pätzold et al.	2002	204
VGF	Growth of 200 mm diameter crystals and resistivity as a function of carbon content	Stenzenberger	2003	194

VGF: Vertical Gradient Freezing, VB: Vertical Bridgman, LE-VGF: Liquid Encapsulated VGF, LE-VB: Liquid Encapsulated VB, MVGF: Magnetic VGF, DGF: Dynamic Gradient Freezing

(2) Dislocation reduction

It has been proved that VB/VGF methods are very effective in reducing dislocation densities. In fact, dislocation densities less than 3000 cm^{-2} for undoped SI GaAs and less than 1000 cm^{-2} for Si-doped GaAs are reported for 75 mm diameter crystals. Even 100 mm diameter single crystals with low dislocation densities are reported. The mechanism of dislocation reduction has been discussed.[195, 196]

(3) Semi-insulating VB/VGF GaAs

The VB/VGF methods are promising not only for conductive GaAs materials but also

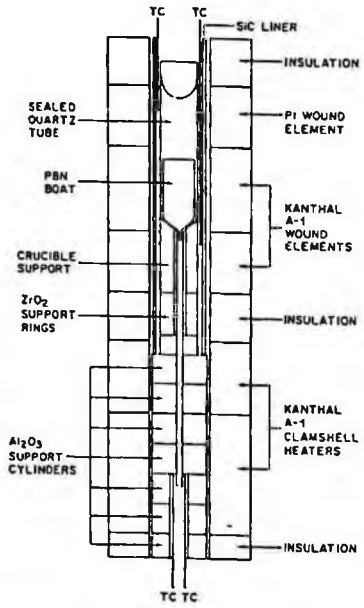

Fig. 8.23 Schematic view of VGF furnace (reprinted from Ref. 178 with permission, copyright 1987 Elsevier).

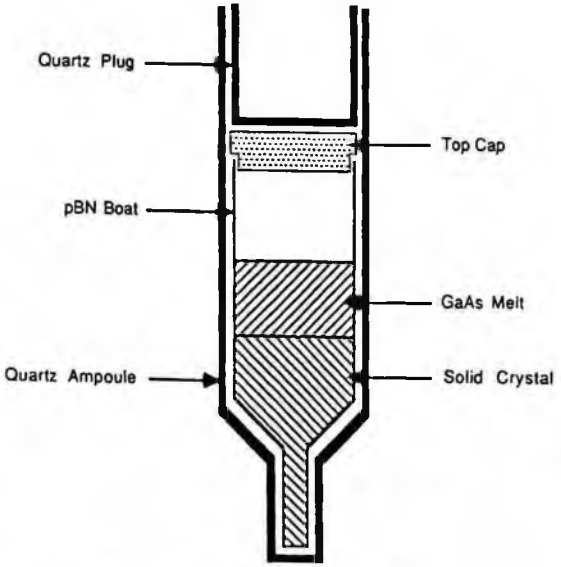

Fig. 8.24 Detailed drawing of the boat-quartz ampoule assembly (from Ref. 180 with permission).

for semi-insulating (SI) GaAs. In fact, the realization of semi-insulating GaAs and its characterization are reported by various authors.[185, 187, 190, 197-201] In many cases, grown crystals do not show semi-insulating properties until after they have been annealed.

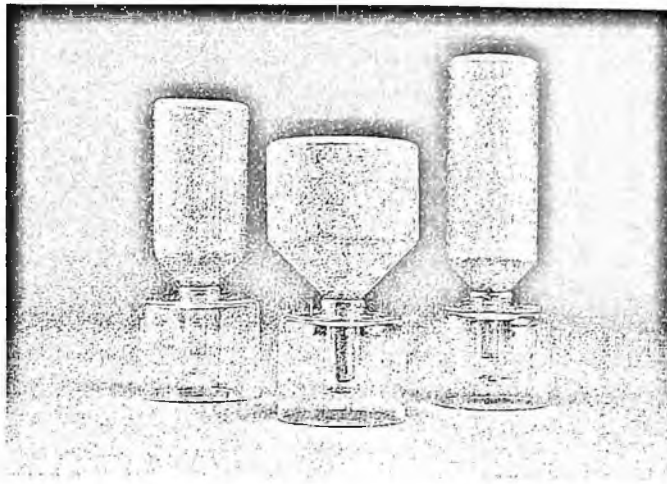

Fig. 8.25 Photographs of 50 mm and 75 mm diameter VB ingots (from Ref. 180 with permission).

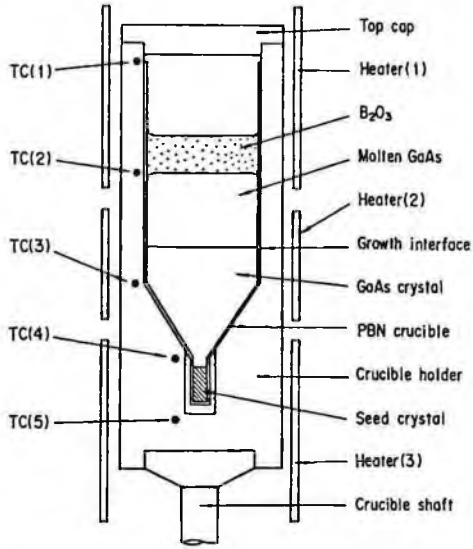

Fig. 8.26 Schematic representation of the LE-VB apparatus used to grow single crystals of GaAs (reprinted from Ref. 181 with permission, copyright 1989 Elsevier).

The critical condition for obtaining a SI crystal is to decrease the Si contamination in grown crystals. In order to realize this condition, the addition of Ga_2O_3 and the use of B_2O_3 are important.[200, 201] When this is brought about, the SI mechanism can be considered as the same as in the case of LEC crystals (Sec. 8.6.2).

(4) Magnetic field application

Magnetic fields have been applied to VGF growth in order to suppress the Marangoni

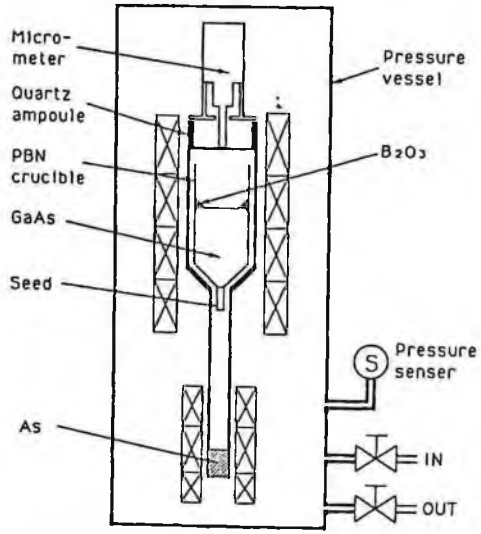

Fig. 8.27 Schematic drawing of VGF furnace (from Ref. 185 with permission).

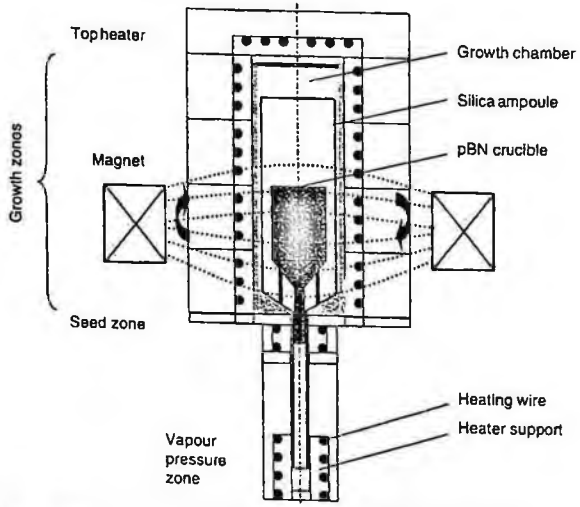

Fig. 8.28 Schematic view of vertical gradient freezing method with a rotating magnetic field (VGF-RMF) furnace (reprinted from Ref. 204 with permission, copyright 2002 Elsevier).

flow and to promote thermal stability to give stable growth with high growth yield and without twinning.[202, 203] Magnetic fields have also been effective in suppressing growth striations. Pätzold et al.[204] have applied a rotating magnetic field as shown in Fig. 8.28 in order to control the heat flux and have compared their results with the numerical

calculation of the melt flow.

(5) Simulation

Simulation studies have also been reported for the solid/liquid interface shapes in VGF,[205] LB-VB,[206] and magnetic applied VB.[207]

8.3.4 Other Methods

Various other methods of growing GaAs crystals have been studied other than those mentioned above, even if they have not yet been industrially applied.

Jacob[208] tried to grow GaAs single crystals in a conventional LEC furnace, without pulling the crystal but by solidifying the melt in the crucible after seeding. This is known as the LEK method, the modification of the Kyropoulos method, where the encapsulant B_2O_3 is used to prevent the decomposition of grown crystals. It was found that the dislocation density is decreased because a high thermal stress is not generated in the case of the LEK method as it is in the case of the LEC method.

Other melt growth methods including the Floating Zone (FZ),[209-211] Vertical Zone Melting (VZM),[212-216] Heat Exchange Method (HEM),[217-219] Liquid Encapsulated Stepanov (LES)[220] and Shaped Melt Lowering (SML)[221] methods have been studied for the growth of GaAs crystals. In Fig. 8.29, the growth arrangement and growth process observed by X-ray transmission for the LES method are shown. The effect of annealing on the grown crystals has been studied for the VZM method.[215]

In order to grow better quality bulk crystals, several solution growth methods such as synthesis by the solute diffusion (SSD),[222] temperature difference method by con-

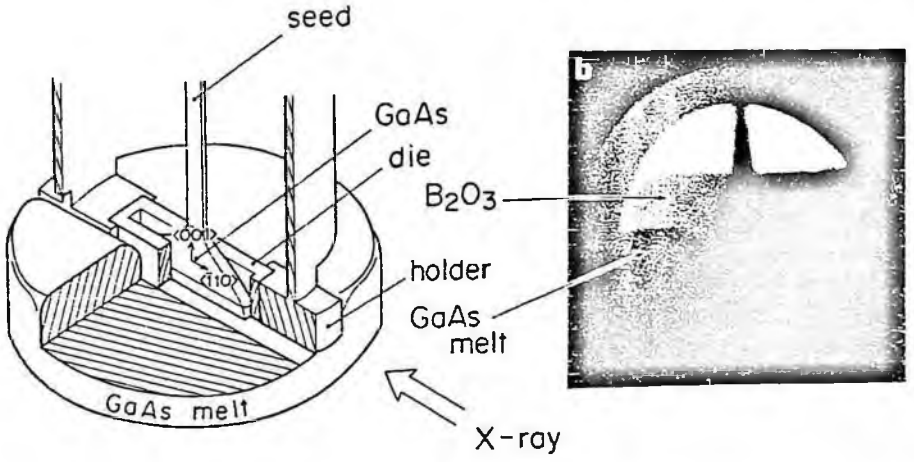

Fig. 8.29 (a) Schematic illustration of the growth system for GaAs plate crystal and (b) X-ray transmission image of a growing GaAs plate crystal (reprinted from Ref. 220 with permission, copyright 1988 Elsevier).

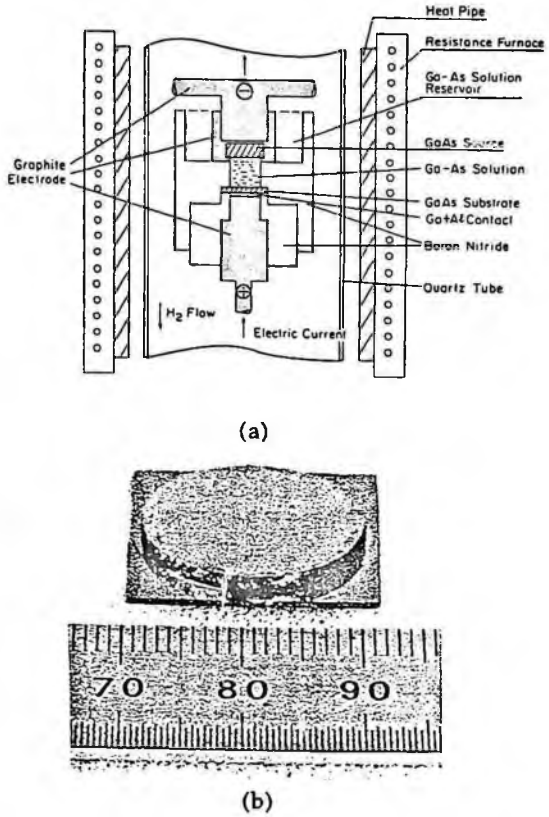

Fig. 8.30 (a) Illustration of the LPEE growth apparatus for the growth of bulk GaAs crystals and (b) photograph of GaAs crystal 1 cm thick with 19 mm diameter (reprinted from Ref. 228 with permission, copyright 1987 Elsevier).

trolled vapor pressure (TDM-CVP),[223-225] constant temperature steady-state (CTSS)[226] and Liquid Phase Electroepitaxy (LPEE)[227, 228] have been examined. By the LPEE method (Fig. 8.30), it was possible to grow thick GaAs crystals as shown in Fig. 8.30 (b) and it was found that dislocations could be eliminated.

Thick epitaxial layers have been grown by the chloride CVD methods and it was found that by wafer annealing, they can be converted to semi-insulating material.[229-230] It was also demonstrated that even dislocation-free epitaxial semi-insulating GaAs can be obtained by this method using Si-doped dislocation-free GaAs substrates.[231]

8.4 POST-GROWTH ANNEALING

8.4.1 Ingot Annealing

One of the main application of GaAs is for digital and analog ICs. For this application, it is necessary to homogenize the electrical properties of semi-insulating GaAs.

Inhomogeneity stems from the accumulation of EL2 along dislocation lines. In order to improve the quality of GaAs, it has been found that ingot annealing is an indispensable procedure to be incorporated in the preparation of bulk GaAs materials. Ingot annealing under various conditions has been performed and it is now known that annealing at about 850-950 °C for a long period is the best way to ensure good quality. In special cases, high temperature ingot annealing is also performed, depending on the device structure. The contribution of ingot annealing to the performance of devices is clearly proved by the examination of that performance.

It was first found that ingot annealing is effective in the improvement of the electrical properties of GaAs in 1993.[232] From that time, many investigations have been undertaken in order to optimize the annealing conditions, to clarify the mechanism of annealing and to examine the effect of annealing on various properties as seen in Table 8.6.[232-288] In this table, studies on wafer annealing (Sec. 8.1.2) are also summarized for convenience. These annealing investigations are also summarized in Ref. 289.

The most important new information gained from these experiments are as follows.

(i) The uniformity of electrical properties over the wafer is greatly improved by ingot annealing at moderate temperatures due to EL2 homogenization.[232-234, 236, 238, 240, 245, 255]

(ii) Appropriate annealing improves not only the electrical properties but also the uniformity of photoluminescence.[234, 238, 240, 249]

(iii) High temperature annealing dissolves arsenic precipitates and EL2, intrinsically existing in conventionally grown LEC-GaAs, and impairs the uniformity of electrical properties.[232, 241, 255, 268, 269, 277, 286]

(iv) Dissolved EL2 and arsenic precipitates regenerate reversibly after moderate temperature annealing.[241, 250, 276, 277, 285]

(v) The cooling rate after annealing greatly affects the electrical properties depending on the carbon concentration.[237, 258, 259, 278, 280]

Based on these results, multiple-step ingot annealing[241, 255, 274] has been applied and as the most sophisticated ingot annealing procedure, three-step ingot annealing[268, 269] has been invented, which shows good uniformity even from the viewpoint of IR scattering.

8.4.2 Wafer Annealing

Wafer annealing is the most recent annealing procedure for improving the uniformity of material quality. It is known that conventionally grown LEC-GaAs has many tiny arsenic precipitates as explained in Sec. 8.6.5, due to non-stoichiometry which is inevitable because the congruent point of the GaAs phase diagram is deviated toward the arsenic-rich side (Fig. 8.31). Since these arsenic precipitates were found to affect the device properties and the fabrication yield, a new material fabrication process was required which would reduce their number. For this purpose, wafer annealing has been studied as a technology replacing ingot annealing.

Wafer annealing was first applied by various authors[240, 290, 291] to as-cut wafers to improve the electrical properties as in the case of ingot annealing. This annealing was performed under similar conditions to ingot annealing at moderate temperatures (800-

Table 8.6 Post Growth Annealing of GaAs

Authors	Year	Content	Ref.
Matsumoto et al.	1982	Improvement of homogeneity by wafer annealing	290
Rumsby et al.	1983	First attempt of ingot annealing	232
Yokogawa et al.	1984	Improvement of PL, mobility, resistivity and pinch -off voltage by ingot annealing	233, 234
Martin et al.	1984	EL2 distribution before and after annealing	235
Holmes et al.	1984	Effect of annealing on EL2 distributions	236
Look et al.	1984	Reversibility between semiconducting and semi-insulating by annealing	237
Miyazawa et al.	1984	Homogeneity improvement by WA at 800 °C	291
Chin et al.	1985	Improvement of CL uniformity by annealing	238
Osaka et al.	1985	Ingot annealing of In-doped dislocation free crystals	239
Löhnert	1986	Improvement of IR absorption, scanning PL, CL and electrical properties by IA and WA	240
Lagowski et al.	1986	Observation of inverted thermal conversion (ITC)	241
Kitagawara et al.	1986	SI conversion after annealing of low carbon content GaAs	242
Ogawa	1986	Effect of melt composition and thermal history	243
Ford et al.	1986	Reversibility between SI and low resistivity by thermal cycling	244
Otoki et al.	1986	Change of IR scattering images caused by annealing	245
Osaka et al.	1986	Mechanism of annealing effect for In-doped GaAs	246
Miyazawa et al.	1986	EL2 increase along dislocation lines	247
Look et al.	1987	Reversibility between semiconducting and semi-insulating by annealing	248
Noto et al.	1986	PL intensity after annealing of In-doped GaAs	249
Kang et al.	1987	EL2 concentration increase as a function of annealing time	250
Kanber et al.	1987	Effect of ingot annealing on device performances	251
Kazuno et al.	1987	Behavior of As_{Ga} defects by annealing	252
Jin et al.	1987	Effect of annealing on dislocation configuration	253
Chichibu et al.	1987	Effect of arsenic vapor pressure during annealing	254
Clark et al .	1988	Uniformity as a function of annealing temperatures	255
Kitagawara et al.	1988	EL2 concentrations and arsenic precipitate densities	256-257
Reichlmaier et al.	1988	Resistivity drop of low carbon GaAs and its mechanism	258
Nakamura et al.	1988	Resistivity change by cooling rate after annealing	259
Asom et al.	1988	Ingot annealing of Bridgman-grown GaAs	260
Stirland et al.	1988	Effect of annealing on etching features and CL homogeneity	261
Sucht et al.	1988	Stability of ion-implantation annealing for post-growth annealed substrates	262
Ogawa	1988	Effect of arsenic fraction in the melt and thermal history on electrical properties	263
Miyazawa et al.	1988	Model of defects around dislocations and effect of annealing	264
Koschek et al.	1988	CL homogeneity and FET threshold behavior	265
Taharasako et al.	1988	Homogeneous wafer production by appropriate annealing procedure	266

Table 8.6 Post Growth Annealing of GaAs (continued)

Authors	Year	Content	Ref.
Stirland et al.	1989	Defect structures after annealing	267
Inada et al.	1989	Behavior of excess arsenic as a function of annealing	268
Kuma et al.	1989	Three-step ingot annealing	269
Chabli et al.	1989	Correlation among dislocations, point defects non-stoichiometry and thermal history	270
Lee et al.	1989	Relationship between excess As and EL2	271
Markov et al.	1989	Change of electrical properties caused by annealing	272
Fang et al.	1989	Effect of annealing on deep level behavior	273
Stirland	1990	Defect structure change by two step annealing	274
Molva et al.	1989	Mechanism of microscopic inhomogeneity	275
Otoki et al.	1990	IR scattering centers as a function of annealing temperatures	276
Clark et al.	1990	EL2 concentrations as a function of annealing temperature	277
Matsui et al.	1990	Effect of annealing temperatures and cooling rate	278
Menninger et al.	1990	Effect of annealing on CL uniformity	279
Mori et al.	1990	Multiple-step wafer annealing (MWA)	292
Kano et al.	1990	Effect of MWA on surface defects	293
Nakamura	1990	Effect of carbon and annealing on resistivity	280
Kitagawara et al.	1990	Effect of annealing process on EL2 concentrations	281
Yamada et al.	1990	Behavior of micro defects in dislocation-free crystals	282
Visser et al.	1990	Microstructure changes after annealing	283
Inoue et al.	1991	PL spectra after various annealing procedure	294
Oyake et al.	1991	Effect of various annealing procedures on MESFET Vth	295
Suemitsu et al.	1991-1992	EL2 kinetics during annealing	284-285
Oda et al.	1992	Mechanism of multiple-step wafer annealing and stoichiometry control by wafer annealing	296-297
Ohkubo et al .	1993	p-type thermal conversion after high temperature annealing	286
Priecel et al.	1993	CL images of lightly Cr-doped crystals after annealing	287
Oda et al.	1993	Effect of various annealing procedures on Vth of MESFETs	298
Imaizumi et al.	1993	Control of defects and electrical properties of chloride CVD epitaxial wafers by wafer annealing	229-230
Oda et al.	1994	Effect of MWA on Vth of SRAM ICs	299
Hoffman et al.	1996	Two-step ingot annealing	288
Noda et al.	1996	Dislocation-free SI GaAs by wafer annealing of chloride CVD thick epitaxial wafers	231

950 °C), and was found to have a similar effect as ingot annealing. Since there was no specific advantage compared with ingot annealing, this moderate temperature wafer annealing was then unnoticed for the reason that wafer-annealed material was less uniform than ingot-annealed material.

Wafer annealing was later noticed as a technology overcoming the disadvantages of ingot annealing and studied extensively.[292-299] Mori et al.[292] developed a multi-step wafer annealing (MWA) process where as-cut wafers are first annealed at high temperatures (>1100 °C) and then annealed at moderate temperatures (950° C). As-cut wafers

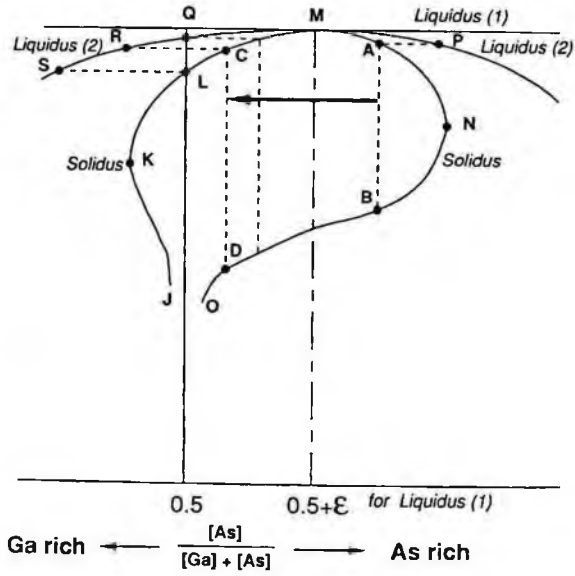

Fig. 8.31 Schematic phase diagram for the Ga-As system. Liquidus line (1) is illustrated on the same scale as solidus lines and liquidus line (2) is illustrated on a larger scale (reprinted from Ref. 296 with permission, copyright 1992 Elsevier).

are slightly etched and annealed in quartz ampoules with an appropriate arsenic overpressure at temperatures higher than 1100 °C. This is done to adjust the material composition to stoichiometry based on the arsenic exchange between the material and the vapor phase.[295, 296] GaAs after this process is not very uniformity so that it has to be reannealed at moderate temperatures as in the case of ingot annealing for homogenizing EL2 distributions. By this MWA process, it was found that nearly stoichiometric material with fewer arsenic precipitates and good uniformity of resistivity of 5 % can be obtained reproducibly.[295, 296] This MWA technique was proved to be effective in reducing the V_{th} variation.[296-299]

Wafer annealing was then applied even to high-purity CVD epitaxial wafers in order to convert conductive epitaxial wafers to semi-insulating ones.[229, 230] It was found that semi-insulating properties can be obtained even for lower EL2, carbon and impurity concentrations than those in bulk material. It was also found that the concentrations of various point defects such as EL3, EL5 and EL6 can be greatly reduced by wafer annealing.[231]

8.5 PURITY

8.5.1 Carbon

(1) Analysis

Carbon is a very important impurity for semi-insulating GaAs because its concentration is higher than that of residual donor impurities and it plays an important role in the

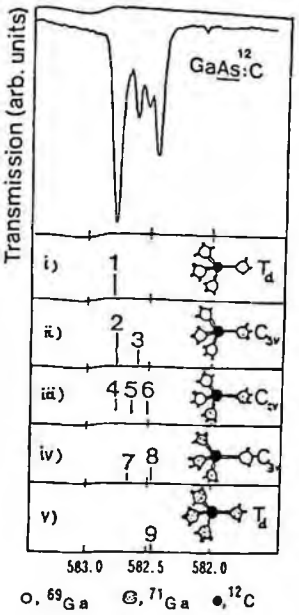

Fig. 8.32 Spectrum of localized mode and its explanation (T~80K). (reprinted from Ref. 301 with permission, copyright 1998 American Physical Society).

semi-insulating behavior.[300] It is therefore very important to analyze the concentration. Even though there is a correlation between the carbon concentration and resistivity, the resistivity itself depends not only on the carbon concentration but also on EL2 concentrations and boron concentrations. It is therefore even more important to analyze the carbon concentration precisely by an analytical method.

The concentration of carbon can be determined by infrared spectrometry, measuring the absorption by carbon in localized vibration mode (LVM). As shown in Fig. 8.32, there is a peak due to carbon at 582.4 cm^{-1} consisting of various localized vibrations.[301-304] The analysis of carbon by FT-IR has been extensively studied by several authors. The temperature dependence of the carbon peak has been studied by Sargent and Blakemore.[305] Other LVM lines due to carbon were found and studied.[306, 307]

Carbon concentration N_C to be measured by FT-IR can be represented as

$$N_C = f\,\alpha \quad \text{or} \quad f\,\alpha\,\Delta. \tag{8.2}$$

where, f is the conversion coefficient, α the absorption coefficient and Δ the halfwidth. Various conversion coefficients have been reported depending on the calibration methods as shown in Table 8.7.[308-315] Here, Kitagwara et al.[314] measured the conversion coefficient for carbon in In-doped GaAs while the others are for undoped GaAs.

As the absolute measurement method, charged particle activation analysis (CPAA)

Table 8. 7 Various Conversion Coefficients for the Analysis of Carbon by FT-IR

conversion coefficient ($x10^{15}cm^{-3}$)	absolute concentration measurement method	Temperature	Author	Year	Ref.
24	SSMS	Liq. N_2	Brozel	1978	308
31-41	SIMS, SSMS	Liq. N_2	Theis	1983	309
11	Hall Effect	Liq. N_2	Hunter	1984	310
9.5 ± 0.29	SIMS	Liq. N_2	Homma	1985	311
7 ± 1	CPAA	Liq. N_2	Kadota	1986	312
8 ± 2	carrier concentration	Liq. N_2	Brozel	1986	313
23 ± 10	SIMS	Liq. N_2	Kitagawa	1986	314
9.2 ± 2	CPAA, PAA	Liq. N_2	Arai et al.	1988	315
11.8 ± 2	CPAA, PAA	RT	Arai et al.	1988	315

has been applied to measure carbon concentrations in LEC grown GaAs by Wei et al.[316] and was also applied to their measurement in different LEC growth atmospheres.[317] Traces of carbon have been analyzed by means of ^{3}He-activation,[318] Deutron activation analysis has been performed by Shikano et al.[319] Kobayashi et al.[320] have applied SIMS analysis in order to measure the carbon concentration quantitatively. All these analysis methods were compared for the same GaAs samples.[315]

There is a large discrepancy in the conversion coefficients as shown in Table 8.7. Recently, it has been pointed out that it is necessary to take calibration coefficients for each FT-IR by using standard samples whose carbon concentration is determined by activation analysis.[315] Without this calibration, one can not compare the carbon concentrations determined by different FT-IR even using the same conversion coefficient.

Round-robin tests for carbon analysis have been performed by Tajima et al.[321] and Arai et al.[315] involving various affiliations, and was also performed among GaAs manufacturers[322-324] using the reference samples prepared by Arai et al.[315] Based on these round-robin tests, a standardized carbon analysis method by FT-IR has been proposed.[325]

(2) Segregation coefficient of carbon

The effective segregation coefficient (k_{eff}) of carbon has been determined as 1.44 ± 0.08 from the investigation of the ^{13}C concentration distribution along the growth axis in ^{13}C doped LEC GaAs crystals.[326] Desnica et al.[327, 328] have determined the equilibrium distribution coefficient, k_0, as 3.5, by measuring k_{eff} as a function of pulling rate in the LEC method, using measurement by LVM absorption. Complex behavior of the segregation of carbon has been studied theoretically.[329] Since carbon forms precipitates, not all carbon atoms are active electrically.[330, 331]

(3) Carbon control

The precise control of carbon concentration is one of the most important points for semi-insulating GaAs production. The factors which affect the carbon concentrations have been investigated by various authors.[150, 329, 332-339]

It was found that carbon concentration is influenced by the water content in the boric oxide, the water vapor content in the inert gas atmosphere, the melt composition

and the pretreatment of graphite hot-zones and the presence of a magnetic field during crystal growth. The incorporation of carbon is believed to be due to CO_2 gas which is dissolved into the GaAs melt via the boric encapsulant.

Because of this complex process, the precise control of carbon needs attention to the following during crystal growth.

(i) Precise control of the water content in the encapsulant boric oxide within $\pm$ 10 ppmw.

(ii) Appropriate pretreatment of graphite hot-zones, namely pre-annealing before crystal growth in order to desorb oxygen and water which will form CO gas by reacting with graphite.

(iii) Appropriate control of the graphite heater in order to prevent overheating which accelerates the generation of CO gas.

(iv) Precise control of the CO gas concentration in the inert gas according to the relationship between carbon and resistivity.

Hanning et al.[340] have discussed how to control the carbon concentration in the case of crystal growth by the VGF method. The substitution of carbon has been analyzed thermodynamically by Wenzl et al.[341]

8.5.2 Boron

Boron was found to affect the electrical properties even though it is an isoelectronic element. It was first pointed out that residual boron has an influence on the electrical properties, as well as the starting melt composition.[342]

The effect of boron on the electrical properties of semi-insulating GaAs has been examined precisely by Osaka et al.[343] They showed that the sheet carrier concentration after ion implantation and annealing is decreased as a function of the boron concentration. It is explained that boron reduces the Ga vacancy concentration which results in the reduction of the Si_{Ga} donor concentration. The effect of boron on the activation efficiency was also examined by Morrow.[344]

The relationship between the lattice parameter and boron as a residual impurity has been studied by Okada and Orito.[345] It was found that the lattice parameter is reduced as a function of boron concentration as shown in Fig. 8.33. The concentration of boron can be determined reproducibly by GD-MS. CPAA analysis was also studied for the determination of the absolute concentration. Thermodynamically, the relationship between boron and native point defects was analyzed theoretically.[341]

8.5.3 Oxygen

Oxygen is an unavoidable impurity in GaAs as long as B_2O_3 is used as the encapsulant and the concentration is assumed to be high. The effect of residual oxygen on the concentration of Si, B and O has been thermodynamically studied for the growth of GaAs by 3T-HB and LEC methods[35] as shown in Fig. 8.34.

Gatos et al. first pointed out the effect of oxygen on the carrier concentration and deep level formation.[346] Bourgoin et al.[347] have examined the interaction of oxygen with EL2 by DLTS comparing undoped and oxygen doped GaAs. Merkov et al.[348] has studied various deep levels in GaAs doped with oxygen. Ulrici et al.[349] have found an

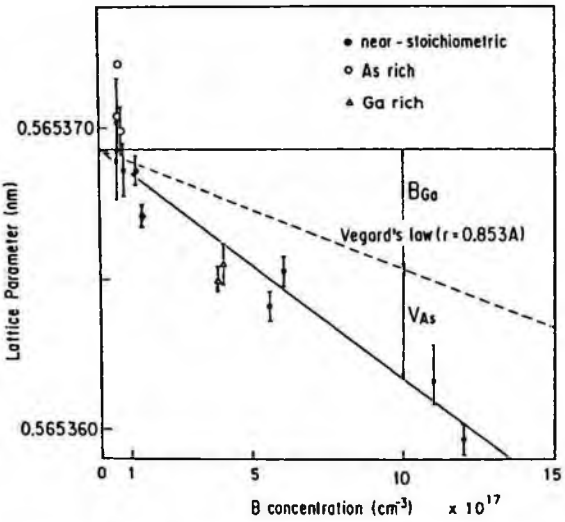

Fig. 8.33 Dependence of lattice parameter on boron concentration in undoped LEC GaAs crystal (reprinted from Ref. 345 with permission, copyright 1988 American Institue of Physics).

LVM line probably due to the Ga-O bond. CPAA analysis was performed to determine the absolute concentration of oxygen. Alt studied the oxygen related LVM peaks and found that the oxygen concentration is of the order of 10^{15} cm^{-3}.[350] Skowronski has used LVM spectroscopy to study the annealing behavior of oxygen-doped GaAs.[351]

8.5.4 Others Impurities

The analysis of trace impurities has been examined by SIMS[352, 353] and the distribution of impurities such as B, Si, Cr, Al across LEC-GaAs has been analyzed.

Round robin tests for various impurities have been performed by chemical analysis, SSMS and SIMS[354] using reference samples involving various affiliations.

The effect of various impurities on the properties of SI GaAs has been studied and the purity of various samples of GaAs and materials such as B_2O_3 and pBN from different manufacturers was compared by Markov et al.[355]

Local vibrational mode adsorption of silicon[356] and hydrogen[357] have been studied. The concentration of hydrogen in LEC GaAs has been determined[358] and the interaction of hydrogen with defects has been discussed.[359, 360] The behavior of Cu which can diffuse rapidly in GaAs has been studied to clarify its effect on the electrical properties.[361, 362] The segregation of Sn,[363] Si[364] and Cr[365] in LEC grown GaAs has been studied.

Residual impurities in LEC-GaAs are dependent on the holding time of the melt in the molten state before crystal growth, the water content in the encapsulant and the purity of the starting materials. The reason why the purity is dependent on the water content of the encapsulant, boric oxide is because there is a reduction-oxidation reaction between the GaAs melt and the encapsulant. The relationship has been studied in detail by Fukuda et al.[366] and Nishio and Terashima.[367] Fujii et al.[368] examined the ef-

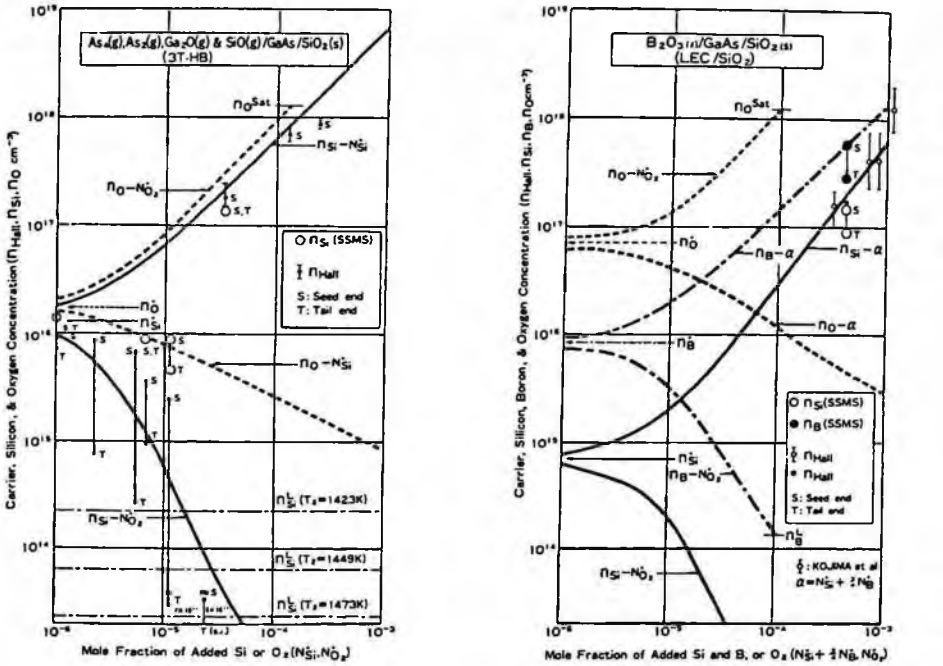

Fig. 8.34 Theoretical (lines) and experimental (dots) carriers. (a) Si and O concentrations for 3T-HB system as a function of mole fraction of added Si and O_2, (b) Si, B and O concentrations for LEC system as a function of mole fraction of added Si and B or O_2 (from Ref. 35 with permission).

fects of crucible materials such a sintered Si_3N_4, Si_3N_4 coated quartz, and AlN on LEC-GaAs purity. Immenroth et al. have studied the effect of arsenic purification on the purity of synthesized GaAs polycrystals.[369] Seifert et al.[370] have studied the effect of inert gas pressure on the purity of LEC grown crystals.

8.6 DEFECTS

8.6.1 Dislocations

Dislocations are known to be crucial defects in the application to lasers since they propagate dark lines during the operation of lasers.[371, 372] For conductive GaAs, it is important to grow crystals with low dislocation densities. For this purpose, HB and HGF methods have mainly been used for the growth of conductive GaAs, and recently VB and VGF methods have been replacing them.

For electronic device applications, it was postulated that dislocations greatly affect the threshold voltages[264, 373-379] so that many studies have been performed aimed at decreasing dislocation densities in the 70's, including In-doping etc.

The density of dislocations is measured mainly by etching procedures and several etchants have been reported. The old etchants only revealed dislocations on (111) faces.[380, 381] The AB etchant found by Abrahams and Buiocchi[382] is known to show dis-

locations and precipitates and has a memory effect.[383] A modified more sensitive ultrasonic AB etching method has also been reported.[384] A KOH etchant[385] is presently widely used for counting the dislocation density (etch pit density; EPD). A mixture of KOH and NaOH has also been found to be a dislocation etchant.[386] A sophisticated etchant, DLS, has been found to reveal precise dislocation structures.[387] The characteristics of various etchants have been reviewed by Stirland and Straughan.[388] The study of dislocation structures has been carried out using these etchants and comparing the results with those from observations using other methods.[389-400]

In order to establish the method of EPD measurement among various manufacturers, EPD round robin tests have been performed by various manufactures.[401] The EPD measurement standard has also been established by SEMI.[402]

A system based on the image-processing of the etch pit shape has been established for counting the EPD automatically, and is marketed by various equipment manufacturers. Another automatic EPD measurement method based on infrared transmission has been developed.[403]

Dislocation distribution in various forms of GaAs, such as Si-doped, In-doped, undoped SI LEC GaAs and VGF GaAs has been studied by etching, X-ray topography, and photoelasticity.[73, 404-415]

The microscopic observation of dislocations by TEM has been done in order to study the origin of dislocations.[416-421] Based on these studies, the origin of dislocations in GaAs has been discussed by several authors.[422-429]

The dynamics of dislocations have been studied by various authors.[430-438] In order to examine the dislocation generation process and to compare the dislocation densities deduced theoretically with those obtained in grown crystals, various computer simulations have been performed,[439-442] some of which were explained in Sec. 3.5

8.6.2 Residual Stress

The distribution of residual stress in LEC GaAs has been studied by Dobrilla and Blakemore using an optical method based on photoelasticity.[443, 444] The photoelastic method has also studied by Iwaki,[445] Zakhaarov et al.[446] and Gomi and Niitsu.[447]

Lattice distortion was measured by X-ray methods to evaluate residual stress and strain.[446, 448, 449] Kuriyama and Satoh applied RBS/PIXE methods to evaluate lattice strains.[450]

8.6.3 Lineages

Lineages are line defects due to the accumulation of dislocations[451] and their accumulation leads to the formation of subgrain boundaries.[452] They are observed, for example, in LEC GaAs. Even though HB and HGF GaAs have lower dislocation densities, lineages are puzzling defects for crystals since in other regions, hardly any dislocations can be observed. The origins of lineages have been discussed from the viewpoint of dislocation reactions.[451]

8.6.4 Striations

Ito et al.[453] have studied the growth striations of In-doped GaAs by SIMS. It was found

that the striation of indium is in phase with the concentration variations of B and Si, but in antiphase with that of carbon. Striations have also been studied by a photoetching method.[454-460]

8.6.5 Precipitates

The main precipitates in GaAs are arsenic precipitates which are formed due to non-stoichiometry of GaAs. These precipitates have been studied by many researchers using chemical etching based on AB etchant,[382] DSL photoetchant,[387] TEM,[425] IR tomography[461] and Raman spectroscopy.[462] Using these methods, the observation of precipitates in GaAs has been studied by many authors.[20, 263, 275, 276, 389, 417, 426-481]

Fig. 8.35(a) shows a photograph of arsenic precipitates revealed by AB etching. Precipitates are revealed along dislocation lines. The size of these arsenic precipitates is determined to be around 500-1000 Å by TEM observation (Fig. 5.6). It is known that the density of these precipitates is large in the case of LEC materials compared with HB materials.[389] The formation kinetics of arsenic precipitates was studied by various authors. It was found that they are eliminated by high temperature annealing. They however reappear when the crystal is reannealed at medium temperatures. The formation and annihilation of arsenic precipitates thus shows reversible kinetics.

It was also found that the existence of these arsenic precipitates impairs the performance of devices.[20, 482-485] The elimination of arsenic precipitates has been extensively studied by various researchers and it was found that they can be eliminated in such a way that the device properties become satisfactory by various annealing procedures as described in Section 8.5.

It was speculated that the reason why these arsenic precipitates exist in LEC-GaAs was due to the deviation of the congruent-point to the arsenic-rich side.[264, 275] This speculation was supported by an assumption that EL2 itself was related to arsenic pre-

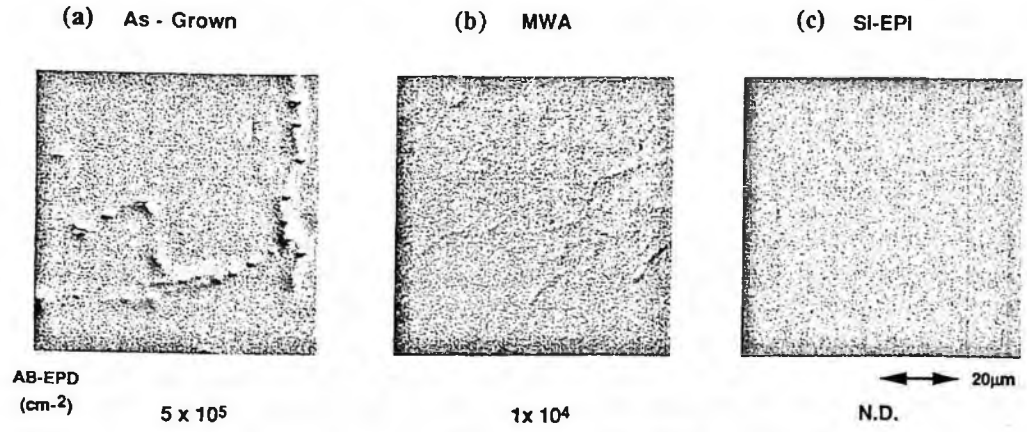

Fig. 8.35 Arsenic precipitates revealed by AB etching. (a) As-grown substrate, (b) multiple-wafer-annealed (MWA) substrate, (c) semi-insulating epitaxial substrate. (reprinted from Ref. 230 with permission, copyright 1994 American Institue of Physics)

cipitation.[264] In fact, EL2 and arsenic precipitates can be eliminated by high temperature annealing.[20, 241, 255, 268] The fact that the congruent-point is deviated to the arsenic-rich side was finally experimentally proved by annealing experiments and by coulometric titration analysis.[20] Because of this deviation, the appearance of arsenic precipitates is understood to be inevitable for as-grown and ingot-annealed LEC-GaAs.

Precipitate-like defects in V- and Cr-doped GaAs,[486] S-doped GaAs,[487, 488] Si-doped GaAs,[488, 489] and Te-doped GaAs[488] have also been studied.

8.6.6 Non-stoichiometry

Since GaAs is a material consisting of two elements, it is important to understand the non-stoichiometry. The problem of non-stoichiometry of compound semiconductors is discussed in Sec. 4.2.4. Non-stoichiometry greatly affects the electrical properties as explained in Sec. 8.7, so that it is important to control the stoichiometry. The phase diagram of GaAs from the viewpoint of non-stoichiometry has been examined theoretically[15] and experimentally.[16]

There have been many reports on the relationship between lattice parameter and non-stoichiometry and point defects. There however remain large discrepancird among these data.[77, 490-507] An accurate non-stoichiometry analysis method (Sec. 5.6.6) based on coulometric titration has been developed by several authors. This method gives a reliable estimation of non-stoichiometry and has helped in the determination of the congruent point.[20, 508-511]

The control of stoichiometry can be performed as follows.

(i) Crystal growth

In order to control the stoichiometry during crystal growth, Inada et al applied arsenic injection during LEC crystal growth[82] and Tomizawa et al. applied arsenic vapor pressure directly to the melt without encapsulant.[138, 139]

(ii) Wafer annealing

Oda et al.[20] have developed the wafer annealing process as a post growth annealing method (Sec. 8.4.2) and found that stoichiometry can be precisely controlled even after crystal growth.

(iii) Laser processing

Ruda et al.[512] developed a laser annealing process for stoichiometry control after crystal growth.

8.6.7 Native Defects and Deep Levels

Native point defects in undoped and doped GaAs have been theoretically considered in detail by Hurle,[513, 514] based on the point defect theory (Sec. 4.2). Bourgoin and Bardeleben reviewed native point defects in GaAs.[515] Jansen and Sankey[516] have calculated the formation energy of point defects in GaAs by an ab-initio pseudo-atomic method and showed the concentration of point defects as a function of stoichiometry. Wenzl et al.[341] and Tan[517, 518] performed a systematic theoretical calculation of various native defects. Point defects in GaAs were also studied by many researchers.[519-527]

Deep levels which were found in bulk GaAs by deep level transient spectroscopy

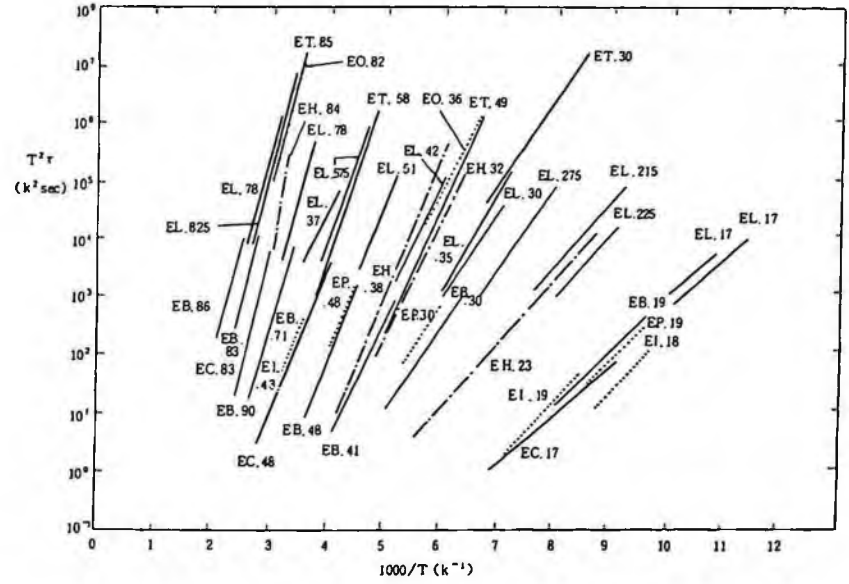

(a)

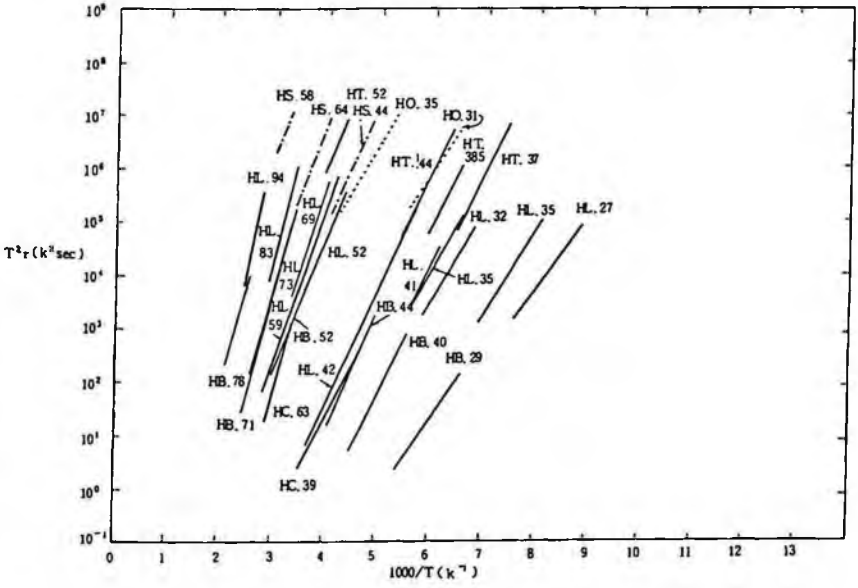

(b)

Fig. 8.36 Electron traps (a) and hole traps (b) measured by DLTS (from Ref. 557 with permission).

(DLTS),[53, 528-540] TSC[541-551] and other measurement methods[552-556] have been studied and are reviewed by various authors.[557-563] Some of them are shown in Fig. 8.36.[557] Desnica[562] reviewed the deep level characterization on SI GaAs by TSC and other methods. The origin of these defects has been extensively discussed. Look[563] has reviewed important defects in GaAs and discussed their effect on the compensation mechanism.

Among various defects, EL2 is the most important since it is indispensable for the semi-insulating properties of GaAs and it greatly affects the resistivity and activation efficiency and therefore the threshold voltage of MESFETs.

(1) EL2

EL2 is the best known deep level in GaAs and many studies have been performed in order to clarify the origin of EL2. The EL2 defect was first referred to as such by Martin et al.[558] EL2 behavior is reviewed by various researchers.[564-570] EL2 have been measured by various methods such as DLTS,[53, 528-540] absorption[571-587] and others[588-591] and it has been found that EL2 defects have the following features.[571, 592]

(i) The energy level is located at 0.75 eV below the conduction band.

(ii) The existence of a specific absorption in the near infrared region and its quenching behavior.

(iii) Thermal activation energy of 0.8 eV and capture cross section of 10^{-13} cm^{-2}. The capture cross section is temperature dependent.

Based on the absorption properties, the concentration of EL2 can be determined from absorption coefficients. Fig. 8.37 shows the correlation between the absorption coefficient and the EL2 concentration. The activation energy of EL2 is given by the following equation.

$$E'_{EL2} = 0.759 - 2.37 \times 10^{-4} \ (eVK^{-1}) \qquad (8.3)$$

The origin of EL2 has been investigated over a long period by various authors.[20, 347, 570, 593-650]

EL2 was first believed to be related to oxygen.[347, 593-596] Huber et al.[597] however found based on measurements by DLTS and SIMS that EL2 has no correlation with oxygen. It was also postulated that EL2 was related to dislocations but it was also later found that dislocations themselves were not the origin of EL2

EL2 was then believed to be due to intrinsic point defects which involve one or more As antisite defects as proposed below.

- Ga vacancy[598]
- As_{Ga} antisite defects[570, 599-601, 607, 608, 618, 620, 621, 625, 628, 640, 661, 646, 647, 650]
- As_{Ga} + As vacancy (V_{As}) complex[602]
- As_{Ga} + V_{Ga} complex[609]
- $V_{Ga}V_{As}As_{Ga}$[619]
- complex with several As_{Ga}[622, 629]
- As_{Ga}-V_{Ga}[623]
- As_{Ga}-As_i defect pair[624, 630-632, 634, 639, 649]

-$(As_i)_2$ at V_{Ga} [633]
-$As_{Ga}V_{As}V_{Ga}$ [603, 626, 635, 643]
-$As_{Ga}+2V_{Ga}$ [642]
-As_{Ga} and $V_{Ga}As_i$ [570]

In order to explain these various models, EL2 family concepts have been proposed by Taniguchi et al.[604, 610] and by others,[605, 606, 611, 612, 644] in which EL2 is a kind of agglomerate which takes the form of various defects depending on thermal and other conditions. Similar models such as the cluster model,[616, 637] the atomic model[636] and the cluster/precipitate model[20, 642] have been proposed. Suezawa and Sumino[642] studied the kinetics EL2 concentrations by adsorbance measurement as a function of annealing time.

Combining the foregoing large body of work from the viewpoint of point defects with the following features of EL2, the nature of EL2 can be explained as related to precipitation behavior.

(i) Semi-insulating behavior takes place when the melt composition As/Ga>0.46 which deviates greatly from stoichiometry. This fact gives rise to the understanding that EL2 are formed even when GaAs is Ga-rich. It is however pointed out that the congruent point is deviated to the As-rich side and stoichiometric GaAs can be obtained from a very Ga-rich melt. It is therefore possible that significant concentrations of EL2 can be obtained only when GaAs is As rich. These facts suggest that EL2 is a specific defect which is strongly related to precipitates or clusters.

(ii) Moderate temperature annealing homogenizes the distribution of EL2 defects which have a large inhomogeneity along dislocation cell boundaries.[264] This EL2 homogenization is the main reason for the improvement of the uniformity of resistivity.

(iii) EL2 as well as arsenic precipitates are completely eliminated when GaAs is annealed at temperatures higher than 1100 °C. This phenomenon was postulated as a thermodynamically reversible reaction from a consideration of the phase diagram[20, 264, 275, 276] and was experimentally proved by coulometric titration analysis.[20]

(iv) EL2 and arsenic precipitates are regenerated by reannealing at lower temperatures, typically lower than 1000 °C. This feature is very similar to the formation of precipitates and is explained by examining the phase diagram (Sec. 8.6.5) . The formation of these defects is also explained as a thermodynamic phenomenon. The relationship between EL2 and arsenic precipitates has also been discussed and their kinetics during annealing has been studied. It was found that the concentration of EL2 is increased as a function of annealing time at 1000 °C and then decreased.

All of this behavior suggests that EL2 can be understood as a specific native defect formed during the As precipitation process. When excess arsenic atoms have to precipitate according to the phase diagram, they gather as As_{Ga} or other native defects. When EL2 are explained as native defects which are formed during As precipitate formation, many defect models, EL2 family and cluster models can be understood in a unified concept.

EL2 distributions in crystals have been measured by various methods,[651-667] such as infrared absorption,[651] deep level transient spectroscopy (DLTS),[652] optical assisted resistance profile (OARP)[660] and reflectance mirowave prove (RMP).[666]

Table 8.8 Deep Levels in GaAs

Level	Activation energy	Capture cross section	DLTS peak temperature
EL2	0.80	6.6×10^{-14}	392
EL3	0.60	6.4×10^{-13}	275
EL5	0.37	2.0×10^{-14}	210
EL6	0.35	1.0×10^{-13}	179
EL9	0.215	2.3×10^{-15}	137
EL10	0.18	1.3×10^{-14}	109

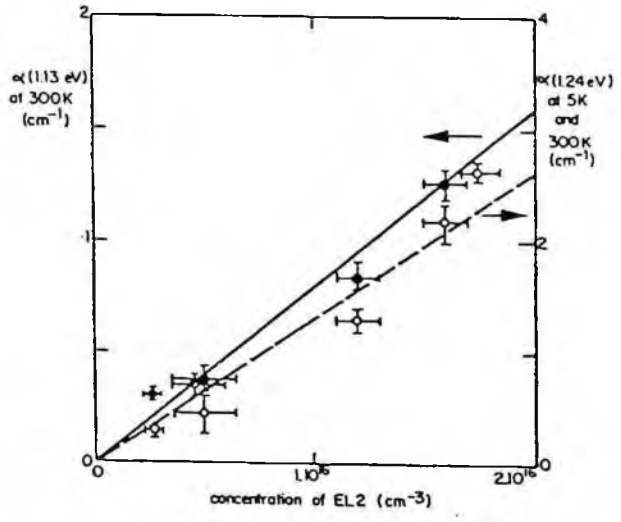

Fig. 8.37 Variation of the optical absorption coefficient in undoped n-type materials as a function of the concentration of EL2 determined by capacitance methods. Measurement at 5K (open circles) and room temperature (full circles). (reprinted from Ref. 571 with permission, copyright 1981 American Institue of Physics)

Hope et al.[659] compared the EL2 distribution in dislocation-free crystals with dislocated crystals and found a correlation of the distribution with the long range elastic strain. Holmes et al.[653, 654] showed the symmetric distribution of EL2 in LEC grown crystals and its correlation with the stress. They also discussed the correlation of the EL2 distribution with melt stoichiometry. Gray et al.[661] showed that the distribution of EL2 is uniform in VGF grown GaAs crystals being independent of the dislocation density. Fillard et al examined the microscopic distribution of EL2 in the vicinity of dislocations using IR tomography. McCann et al.[655] examined the EL2 distribution in Cr-doped LEC crystals.

EL2 distributions can be greatly improved by annealing procedures as explained in Sec. 8.4. Alt et al.[665] found a correlation between the distribution of EL2 and the resistivity, the activation efficiency of Si. The effect of EL2 on the threshold voltage of MESFETs has been discussed by several authors. Dobrilla et al.[668] showed the correla-

tion between the threshold voltage of ion-implanted MESFETs and the EL2 concentration. There was a linear correlation and Vth decreased by 63 meV/10^{15} EL2/cm^3. Anholt and Sigmon[669] discussed the out-diffusion of EL2 during post-annealing after implantation and the threshold voltage change.

(2) Other Deep Levels

There are many other deep levels such as EL3, EL5 and EL6 but most of them have not been studied as extensively as EL2. It was however found that some of them play important roles in the electrical properties of GaAs in the region of low carbon concentrations as explained in Sec. 8.7.2. Regarding these deep levels, stoichiometry dependent deep levels in p-GaAs,[670] non-radiative recombination centers[671] and vacancy-related deep levels[672] have been studied. Among these levels, EL6 has been found to have a very important effect on the electrical properties as much as EL2.[242, 243]

Fang et al.[673] identified EL6 as V_{Ga}-V_{As}. Levinson identified EL6 as an As_{Ga} antisite-related complex.[675] Hashizume and Nagabuchi[676] systematically studied the behavior of various defects during annealing, and showed that EL6 is reduced by annealing. The effect of ingot annealing on other defects was also studied by several authors[242, 243] and the influence of EL6 on the annealing behavior has been found as follows.

The electrical properties are converted reversibly between semi-insulating and semiconducting by annealing.[237] It is known that semi-insulating properties can not be held when semi-insulating GaAs with low carbon concentrations is cooled slowly after crystal growth or after annealing. Low temperature annealing at around 550-650 °C has the effect of increasing the concentration of midgap donors and the resistivity is converted to the semiconducting range (10^3-10^6 Ω·cm) when it exceeds the carbon concentration.[242, 258, 278] This phenomenon is now clearly explained from a Schockley diagram by the formation of EL6[242] as shown in Fig. 8.44.

8.7 ELECTRICAL PROPERTIES

8.7.1 Doping, Carrier Concentration and Mobility

Various impurities have energy levels as shown in Fig. 8.38. Among these impurities, Si and Zn are industrially used as the n-type dopant and the p-type dopant, respectively. The segregation coefficients of these dopants are shown in Table 8.9. Mobility as a function of carrier concentration and the effect of various scattering mechanisms (Fig. 8.39) have been systematically studied.[677-682] Electron drift velocity as a function of electric field has also been studied in detail.[683, 684] Mixed conductivity has also been studied as a function of carrier concentrations.[685, 686] Woods and Ainslie[687] have discussed the effect of oxygen on the silicon contamination and the mobility. Fornari made a precise study of the influence of melt composition on the electron mobility of Si-doped LEC GaAs.[688]

8.7.2 Semi-Insulating (SI) GaAs

(1) Mechanism of semi-insulation

The occurrence of SI GaAs has been known since 1958[209] and was studied by electrical

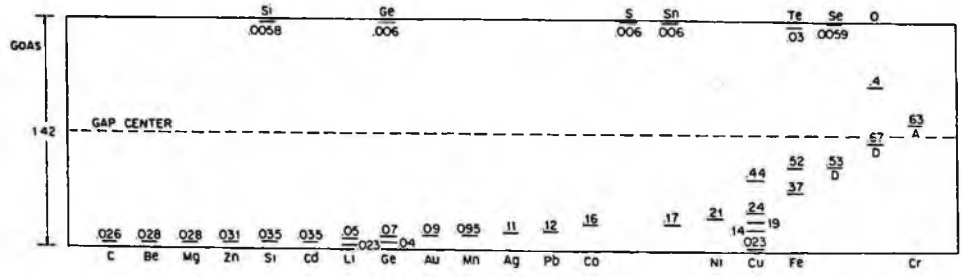

Fig. 8.38 Ionization energies for various impurities in GaAs (from Ref. 677 with permission).

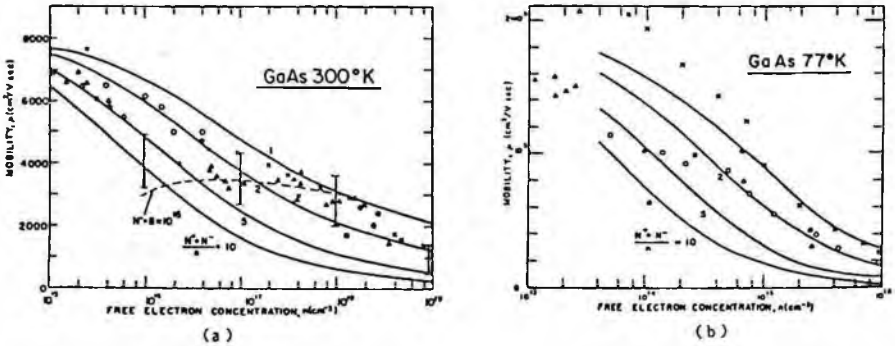

Fig. 8.39 Carrier concentration-mobility curves as a function of the compensation ratio (reprinted from Ref. 679 with permission, copyright 1971 American Physical Society).

measurement[689] and Z and O co-doping.[690] In 1964, it was found that GaAs can be made semi-insulating by doping Cr to create deep acceptors.[691] After that Cr-Oxygen co-doping was found to be more effective for semi-insulation. From that time, Cr-O doped semi-insulating GaAs has been grown by the HB method.

The mechanism of semi-insulation is known to be the compensation between shallow donor/acceptors and deep donor/acceptors.[692-697] In the case of Cr in Cr-O doping, semi-insulation is due to compensation between Cr and shallow donors.

Undoped semi-insulation occurs as the compensation between shallow acceptors and deep donors, which is due to the native defect, EL2 as seen in Fig. 1.14. The mechanism of undoped semi-insulation has then been studied.[563, 694, 696, 698-714] Based on this model, it becomes very important to control the concentrations of EL2 and carbon to obtain reproducibly and stably material whose resistivity is precisely controlled.

This three level model has however been found wanting because semi-insulating GaAs can not be stably obtained even though EL2 and carbon are controlled. From various results based on annealing experiments, it was finally found that another middle donor defect, EL6 has an important effect on the semi-insulating mechanism.

Based on these findings, high purity epitaxial layers which are conductive have been made semi-insulating.[229, 230]

- *The control of EL2*

The origin of EL2 is discussed in Section 8.5. The occurrence of EL2 during crystal growth has been studied by many researchers. Holmes et al. found that EL2 concentration is increased as a function of the As/Ga ratio of the melt from which crystals are grown as shown in Fig. 8.40. It was also found that various other crystal growth conditions affect the concentration of EL2.[79, 715]

It was however found later that these effects of crystal growth on EL2 concentrations are not so important since EL2 concentration can be changed reversibly by annealing. This was proved using epitaxial layers as shown in Fig. 8.41. Similar behavior to that shown in Fig. 8.40 can be obtained just by varying the annealing temperature. The only important point is in the manner of growing crystals with nearly stoichiometric conditions.

Since it is found that the threshold voltage depends greatly on the concentration of EL2, it is important to control EL2 concentrations from batch to batch.

- *Role of carbon and its control*

Carbon is known to be the most important impurity since it determines the electrical properties of semi-insulating GaAs. This is because the semi-insulation is due to the compensation of deep donor EL2 and shallow acceptor carbon. The influence of carbon

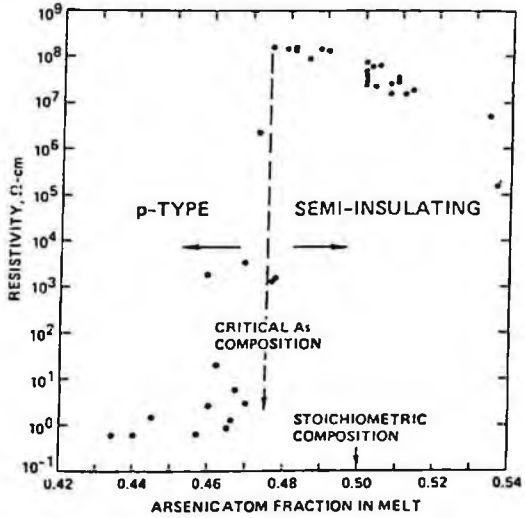

Fig. 8.40 Effect of melt composition on electrical properties of LEC GaAs (reprinted from Ref. 79 with permission, copyright 1982 American Institue of Physics).

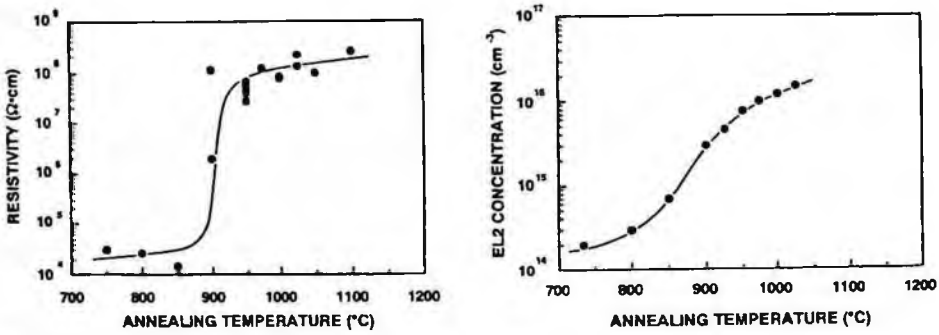

Fig. 8.41 Effect of arsenic vapor pressure on the resistivity (a) and EL2 concentration of wafer-annealed GaAs epitaxial layers (reprinted from Ref. 229 with permission, copyright 1993 American Institue of Physics).

on the electrical properties has been investigated by various authors.[242, 258, 259, 713, 716-728] It is known that the resistivity is increased as a function of carbon concentration not only for LEC-grown crystals[259, 721, 725, 726] but also for VGF-grown crystals.[194]

An example is shown in Fig. 8.42. The mobility is also affected by the carbon con-

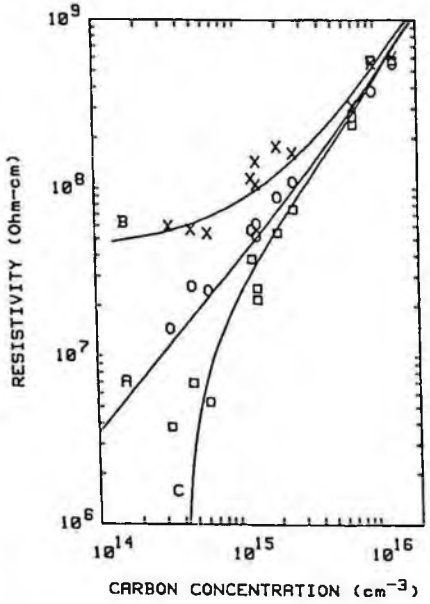

Fig. 8.42 Resistivity vs carbon concentration for as-grown (○) and annealed samples (×: rapid cooling, □: slow cooling). Solid lines are theoretical calculations (from Ref.259 with permission).

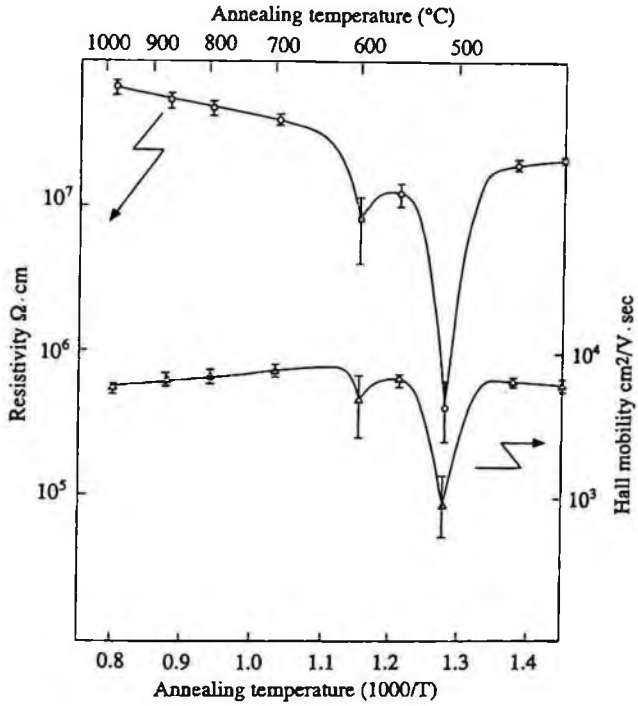

Fig. 8.43 Resistivity and mobility as a function of annealing temperature.

centration. It is found that the threshold voltage V_{th} of MESFETs depends linearly on the carbon concentration[716] as seen in Fig. 8.46. Carbon is also known to affect the thermal conversion behavior.[717, 718, 723] It is therefore important precisely to control the concentration of carbon and it has been performed as explained Sec. 8.5.1.

When the carbon concentration is lower than $1\text{-}3\text{x}10^{15}$ cm^{-3}, the resistivity is greatly decreased depending on the annealing conditions as seen in Fig. 8.42. It is also important to know that the mobility is increased as the carbon concentration is decreased but when the carbon concentration is lower than 10^{15} cm^{-3}, the mobility is drastically decreased. This decrease coincides with a drastic decrease in resistivity. The big reduction in mobility is not yet well understood but it may be related to the breakdown of semi-insulating properties which will vary the position of the Fermi level, resulting in the variation of the position of the bottom of the conduction band, thus interrupting the normal transport of electrons in the conduction band.

- Role of other defects - four level model

Semi-insulating behavior is in principle determined by the balance between shallow donor impurities, shallow acceptor carbon and deep donor EL2 as mentioned above. This semi-insulating behavior however can not be determined only by these three levels, especially in the case of low carbon GaAs. When GaAs crystals with low carbon

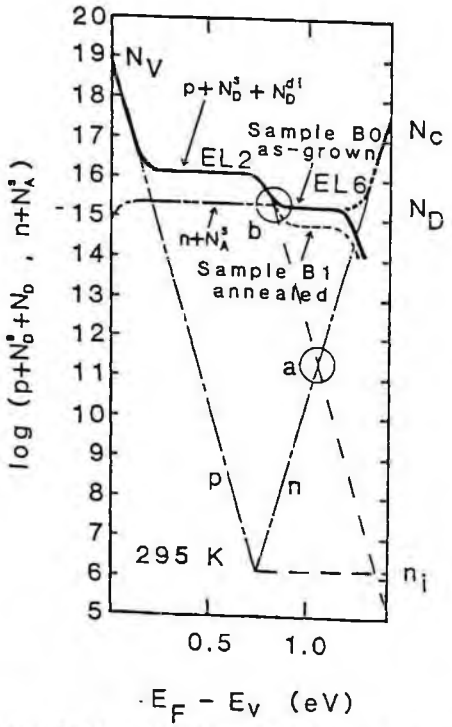

Fig. 8.44 Shockley diagram for four level model for the as-grown crystal B0 and the annealed crystal B1 (from Ref. 242 with permission).

concentrations less than 1-3x10^{15} cm^{-3} are grown by the LEC method, it happens very often that the grown crystals do not turn out semi-insulating, having resistivity of the order of 10^4-10^6 Ω·cm and n-type conductivity. This resistivity can not be explained by the above three level model. If the carbon concentration is lower than the EL2 concentration, the resistivity goes down to a few ohm·cm with p-type conductivity. These semi-conductive properties can be explained only by introducing another middle level donor type.

Fig. 8.43 shows the electrical properties of the above semiconducting GaAs measured as a function of annealing temperature. The resistivity and mobility are greatly changed depending on the annealing temperature. It is known that the resistivity becomes semiconducting when the crystal is subject to annealing at medium temperatures. This phenomenon can be explained using a Shockley diagram with a four level model including a middle donor level of EL6 as shown in Fig. 8.44.[242] This type of abnormal electrical property change can be avoided when the carbon concentration is higher than about 3x10^{15} cm^{-3}. This is because when the carbon concentration is higher than the maximum concentration of the middle-level donor, it becomes semi-insulating due to the compensation between EL2 and carbon only without the influence of the middle-level donor.

It is also found that in converting these semiconducting GaAs crystals with low

carbon concentrations, after annealing at 950 °C to improve the uniformity, it is necessary to cool the crystal at a sufficient cooling rate in order to prevent the formation of these middle donor levels.[259]

8.7.3 Measurement of Uniformity of Electrical Properties

The uniformity of electrical properties over the wafer is an important issue for the fabrication of electronic devices of reproducible performance. Various measurement methods have therefore been studied to evaluate it.[729-741] Resistivity uniformity of In-doped SI GaAs has been studied by Miyairi et al.[110]

8.7.4 Control of Electrical Properties

It has been proved by many authors that moderate temperature annealing greatly improves the uniformity of electrical properties such as resistivity and mobility as explained in Sec. 8.4.1. Microscopic uniformity has mainly been measured by the three guard ring method (Sec. 5.5.4) and it is known that the best uniformity achievable is less than 5%[20] which is near the detection limit. This uniformity is very important since it is directly correlated with the threshold voltage variation of FETs.[742]

Precise control of electrical properties can be achieved by stoichiometry control by wafer annealing. First step wafer annealing was found greatly to affect the electrical properties as a function of temperature and arsenic vapor pressure. When the temperature is increased and arsenic pressure is decreased, the semi-insulating properties are lost and it is converted to p-type conductive material.[20, 292] This p-type conversion behavior is very similar to the p-type conversion as a function of melt composition seen in crystal growth.[79] The p-type conversion is believed to correspond to non-stoichiometry resulting in the decrease of EL2 concentration. It was found that by optimizing annealing conditions, semi-insulating properties can be achieved with the composition closely approaching stoichiometry, such composition not being achievable by ingot-annealing.[20]

Uniformity of electrical properties can be improved by moderate temperature annealing at 950 °C as in the case of ingot annealing. This uniformity results from the homogenization of EL2 as in the case of ingot annealing. This multiple-step wafer annealing finally gives the same uniformity of electrical properties as the best ingot annealing.[20]

8.8 OPTICAL CHARACTERIZATION

8.8.1 Photoluminescence (PL)

Since photoluminescence is a very sensitive method for evaluating GaAs, many studies have been performed for the characterization of GaAs. The assignment of various peaks is summarized in Table 8.9, based on the report in Ref. 743.

Photoluminescence of EL2 has been studied by various authors[744-748] as reviewed by Tajima.[591] Out-diffusion of Cr and the 0.839 eV level have been studied by the PL method.[749] The behavior of other impurities such as Cu,[750, 751] O[752] and C[753] has been studied. Kirillow et al.[754] developed a room temperature photoluminescence method for

Table 8.9 Assignments of PL peaks in GaAs

Peak (eV)	Symbol	Assignment
Exciton Peaks		
1.5153	(F,X)n=1	free exciton, n=1 state of upper polariton branch
1.515	(F,X)	free exciton, lower polariton branch
1.5150-1.5145	(Do,X)	excited states of exciton bound to neutral
1.5133(6)	(D+,X)	exciton bound to ionized donor
1.5128	(Ao,X), J=1/2	exciton bound to neutral acceptor
1.5124	(Ao,X), J=3/2	
1.5122	(Ao,X), J=5/2	
Impurity related peaks		
1.4931(2)	FB	conduction band to C(As)
1.4915	FB	Be(Ga)
1.4911(4)	FB,	conduction band to Mg(Ga)
1.4894	FB	Zn(Ga)
1.4891(2)	DAP,	neutral donor to C(As)
1.4875	DAP,	neutral donor to Mg
1.4854	DAP	Zn(Ga)
1.4850(1)	FB,	conduction band to Si(As)
1.4848	FB	Cd(Ga)
1.4814(6)	DAP,	neutral donor to Si(As)
1.4781-1.479	FB,	conduction band to Ge(As)
1.4745(6)	DAP,	neutral donor to Ge(As)
1.406	FB	Mn-related
1.356	FB	Cu-related
1.349		
Broad band peaks		
0.65		
0.68		
0.80		

determining the indium content.

Macroscopic mapping examination of SI GaAs has also been extensively performed.[249, 755-767] It is known that depending on the improvement in the uniformity of the resistivity, PL intensity mapping is also improved. Compared with PL at low temperatures, room temperature scanning photoluminescence has been found to be a very effective and easy way to evaluate the uniformity. Microscopic mapping has also been studied in order to study the origin of non-uniformity in the vicinity of dislocations.[759, 768-771]

The effect of annealing on the PL spectra has been extensively studied.[234, 240, 249, 294, 760, 772-776] Inoue et al.[294] showed how the PL spectra are changed as a function of various annealing conditions as shown in Fig. 8.45. It was shown that MWA was the best way to yield the most uniform PL mapping.

By looking at the near band-edge emission, mainly that of the carbon related emission BA°_{c} (1.49 eV), it was found that the uniformity can be easily detected and this technique is applied often in GaAs manufacturing.[234, 240, 249, 294, 760, 774] It is known that the BA°_{c} intensity is increased and the uniformity is improved by moderate temperature

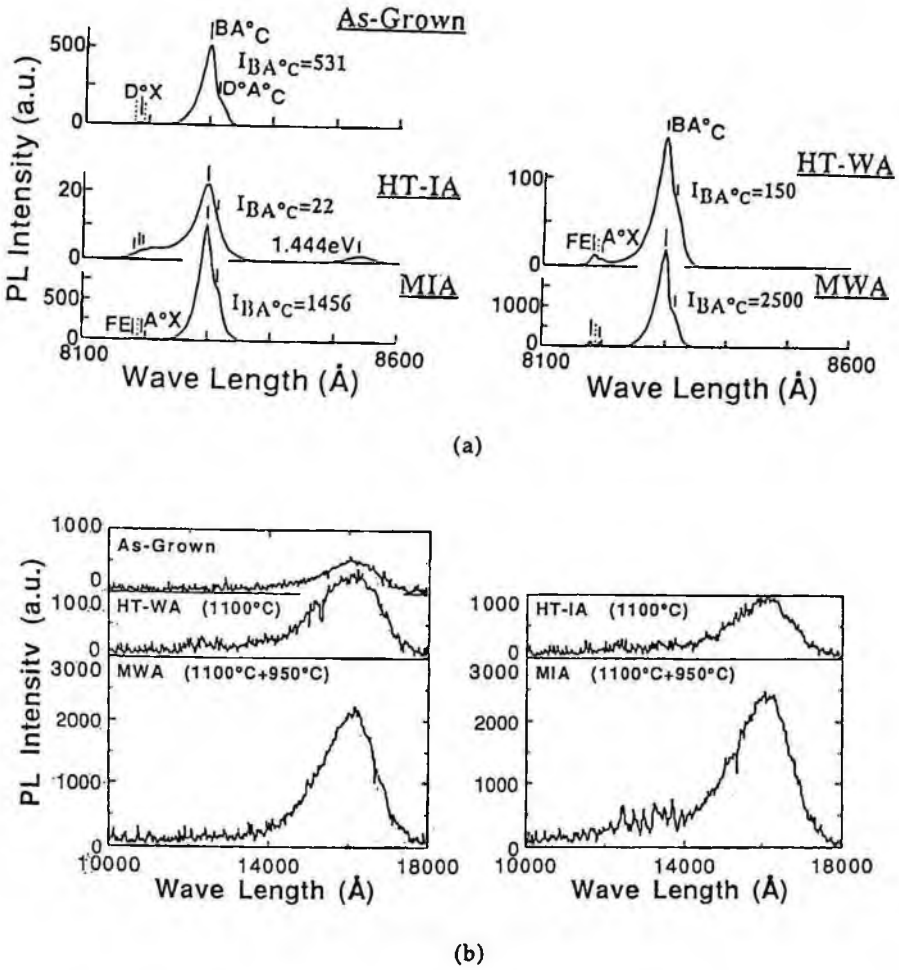

Fig. 8.45 PL spectra at the center of various wafers. HT-IA: high-temperature ingot annealing, MIA: multiple-step ingot annealing, HT-WA: high-temperature wafer annealing, MWA: multiple step wafer annealing. (a) PL intensity (I_{BA}) at the peak of BA (bound-accepter) recombination. (b) PL intensity due to deep level (from Ref. 294 with permission).

(800-950 °C) annealing. The increase of the $BA°_C$ intensity however does not literally mean that the carbon concentration is increased. The increase may be based on the decrease of non-radiative recombination centers,[249] possibly that of arsenic vacancy related point defects.[294] It is also known that the $BA°_C$ intensity becomes very small after high temperature (>1000 °C) annealing, about two orders of magnitude smaller than that after moderate temperature (800-950 °C) annealing.[294] The mechanism of photoluminescence homogenization by ingot annealing is not yet fully clarified even after many investigations so that a systematic and comprehensive study is required.

The annealing conditions affect the uniformity of photoluminescence as in the case of ingot annealing. By wafer annealing, similar uniformity of photoluminescence can be achieved as with ingot annealing.[294] The other feature is that CL uniformity can be greatly improved in the case of MWA compared with ingot annealing.[20, 292] In the case of ingot annealing, complete homogenization of the microscopic non-uniformity of cathodoluminescence can not be achieved, while in the case of wafer annealing, it can be completely homogenized. The reason has not yet been clarified, but it seems to be due to some defects other than EL2, being the origin of non-uniformity of cathodoluminescence .

8.8.2 Cathodoluminescence (CL)

Cathodoluminescence (CL) and electron beam induced current (EBIC) are very sensitive methods for evaluating the uniformity of SI GaAs at the far microscopic level. In fact, these methods have been applied by various authors.[20, 777-787] The origin of CL contrast has been discussed by Koschek et al.[777] and Frigeri and Wheyer.[399] In many cases it is known that non-uniformity is always present, especially along dislocation cell boundaries. The effect of defects such as dislocations,[435, 788-794] striations[795] and lineages[796] have also been studied.

Cathodoluminescence is also a convenient method for examining the effect of annealing. This method has a higher resolution than photoluminescence and is convenient for examining the microscopic uniformity. In fact, Miyazawa et al.[374, 797] showed that CL non-uniformity correlates with the threshold voltage variation of FETs. CL uniformity measurement is therefore a good, easy technique for evaluating the effect of annealing and precise studies have been performed by various authors.[238, 798, 799] It is known that uniformity can be improved by appropriate annealing[238, 240, 255, 279] but it has also been found that microscopic non-uniformity is not fully eliminated by ingot annealing.[292] This implies that CL information may include more information on defects other than EL2.[265] Only in the case of SI GaAs subjected to multiple wafer annealing (MWA) did cathodoluminescence show completely uniform images.[20]

8.8.3 Others

Brozel et al.[651, 800] and Skolnick et al.[801] have developed a simple IR transmission method for observing inhomogeneities such as striations, and dopant segregations of GaAs. Katsumata et al.[802-804] developed an IR transmission topography system using a video image processor, and have examined IR scattering and transmission images as a function of melt composition. Dobrilla and Blakemore[805] have developed an IR transmittance imaging method for observing the stress field in GaAs wafers. Carlson and Witt[806] used an IR microscope to determine the carrier concentration in Te-doped GaAs and to observe striations. Fillard[807] showed that by IR transmission imaging, the distribution of $EL2^{0}$ which is anti-correlated with that of $EL2^{+}$ can be observed. Tüzemen et al.[671] have developed a near-band-edge absorption measurement system to study non-recombination center distributions.

Ogawa[808] first showed the applicability of LST to GaAs characterization. Katsumata

et al.[809] have studied the scattering mechanism and observed As precipitates and Ga inclusions. The correlation between LST images and AB and DSL etched images, as regards micro-precipitates has been clarified.[461, 810, 811] Fillard et al.[812] compared LST and IR transmission images in In-doped GaAs to study the distribution of EL2 in the vicinity of a dislocation.

8.9 DEVICE PROPERTIES

8.9.1 Thermal Stability

Since the decomposition pressure due to arsenic is rather high, when GaAs is annealed at moderate temperatures, EL2 based on excess arsenic is out-diffused and the semi-insulating properties near the surface region are broken down. This is called thermal conversion and it should be suppressed for activation annealing after ion-implantation for MESFET fabrications. The detailed mechanism of thermal conversion has been studied by various authors.[80, 723, 813-817] This thermal conversion was attributed to out-diffusion of EL2, the concentration of which becomes lower than that of the shallow acceptor so that the surface region becomes p type conductive after annealing. Ohkubo et al.[723] examined the effect of carbon on the thermal conversion and concluded that thermal conversion is caused not only by the reduction in EL2 but also by the formation of native acceptors. It is concluded that the carbon concentration must be somewhat higher than that of EL2. If the difference is small, a slight out-diffusion of EL2 easily results in thermal conversion.

8.9.2 Activation efficiency

The activation efficiency after Si doping and annealing is important in the production of MESFETs. Kiyama et al.[818] made an exact study of the relationship between the activation efficiency and the crystal quality as a function of the axial position of wafers. The role of dislocations,[819] boron,[344, 820] EL2[344] and striations[821] on the activation efficiency has been studied.

8.9.3 Threshold Voltage (V_{th}) and its Variation

Since control of the absolute value of V_{th} is indispensable for the reproducible production of GaAs MESFETs, the factors which affect the V_{th} have been extensively studied experimentally and theoretically.[264, 375, 668, 669, 716, 822-848] The effect of dislocations, EL2, carbon and boron has been studied. It was first pointed out that dislocations affect the V_{th} of FETs.[375] Later studies clarified that the inhomogeneity of EL2 in the vicinity of dislocations is the main reason for that effect.

From these examinations, it was found that the precise control of EL2 and carbon is critical for the high yield production of discrete MESFETs. It should be noted that the precise control of EL2 correlates strongly with the precise control of non-stoichiometry because under the same post-annealing conditions, the EL2 concentration is dependent on the non-stoichiometry.

Beyond the control of the absolute V_{th}, the variation of V_{th} is the most important key factor for integrated circuit fabrication since the device chip yield depends strongly on

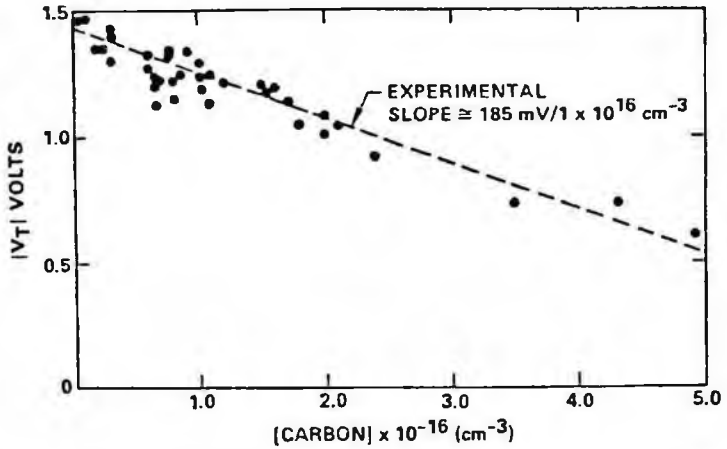

Fig. 8.46 Dependence of the absolute value of FET threshold voltage V_T on carbon concentration (reprinted from Ref. 716 with permission, copyright 1984 American Institue of Physics).

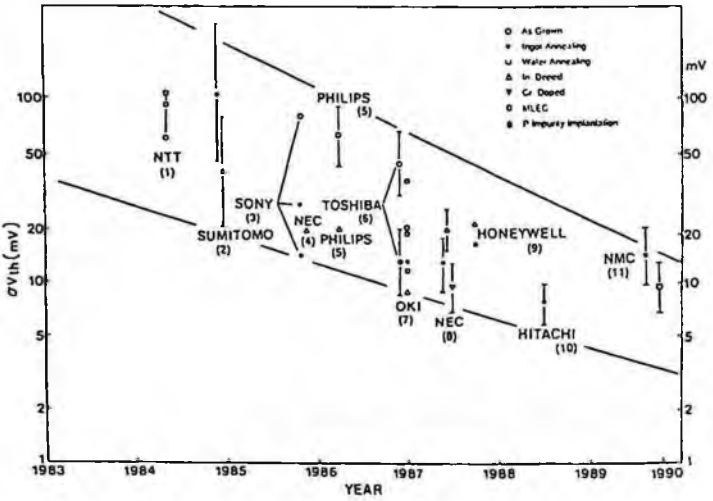

[1] Y. Ishi, S. Miyazawa and S. Ishida, *IEEE Electron Devices* ED-31 (1984) 800.
[2] S. Murai, K. Tada, S. Akai and T. Suzuki, *Oyo Buturi (Monthly Publ. Jpn. Soc. Appl. Phys.) (in japanese)* 53(1984) 1083.
[3] J. Kasahara, M. Arai and N. Watanabe, *Jpn. J. Appl. Phys.* 25 (1986) L85.
[4] Y. Tanaka, T. Matsumura, F. Shimura, M. Kanamori and A. Higashisaka, in *Extended Abstracts of the17th Conf. Solid Devices and Materials* (Tokyo, 1985) p. 433.
[5] J. Maluenda, G. M. Matin, H. Schink and G. Packeiser, *Appl. Phys. Lett.* 48 (1986) 715.
[6] I. Terashima and T. Nakanishi, *Nikkei Electronics (in japanese)* 11 (1986) 99.
[7] T. Egawa, Y. Sano, H. Nakamura, T. Ishida and K. Kaminishi, *Jpn. J. Appl. Phys.* 25 (1986) L973.
[8] S. Asai, N. Goto and T. Nozaki, *IEICE Tech. Rep.* CPM87 (1987) 55
[9] K. L. Tan, H. Cung and C. H. Chen, *IEEE Electron Devices Lett.* EDL-8 (1987) 440.
[10] Y. Fujisaki and Y. Takano, in *Proc. 5th Conf. Semi-insulating III-V Mateirals* (Malmö, Sweden, 1988) p. 247.
[11] M. Oyake, H. Yamamoto, G. Kano, T. Inoue and O. Oda, *Inst. Phys. Conf. Ser.* 112 (1991) 311.

Fig. 8.47 Reduction of threshold voltage variation (sV_{th}) with year (from Ref. 298 with permission).

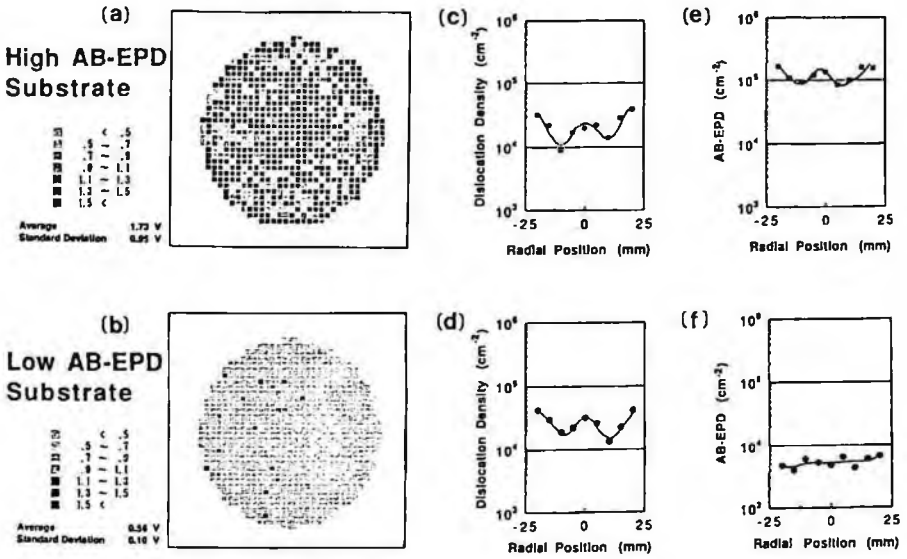

Fig. 8.48 g_m compression mapping (a,b), radial distribution of substrate dislocation density measured by KOH etching and (e,f) radial distribution of arsenic precipitate density measured by AB etching (reprinted from Ref. 484 with permission of The Electrochemical Society)

the σV_{th}.[849] Because of this importance, many studies have been performed aimed at the reduction of σV_{th} as summarized in Fig. 8.47.[298] It was finally found that the best achievable variation of less than 10 meV was obtained by appropriate ingot annealing. High temperature ingot annealing was also found to increase the microwave device fabrication yield.[483] This is due to the reduction of arsenic precipitates which greatly reduce the device fabrication yield when they land under the gate electrode (Fig. 8. 8).

The effect of wafer-annealed GaAs on device performance has been examined in various circumstances. Oyake et al.[295] proved that the threshold voltage variation can be improved by using MWA wafers, being comparable to ingot annealing. It was also found that the device fabrication yield can be improved for integrated circuit application.[299] This is the most expected effect of wafer annealed material since in the case of large scale ICs, a large number of defects such as arsenic precipitates will significantly impair the device fabrication yield as happens with silicon oxide in silicon ICs. This advantage of wafer-annealed GaAs achieves importance in the case of large scale devices rather than discrete devices.

As another feature of wafer-annealed material, it was found that it improves the characteristics and the morphology of epitaxial layers, especially in the case of MBE grown AlGaAs epitaxial layers.[293, 298] When wafer-annealed material is used for epitaxial growth, tiny oval defects due to arsenic precipitates along dislocations, which

differ from conventional oval defects due to gallium oxides, can be significantly reduced which naturally improves the device fabrication yield.

8.9.4 Device Yield

Among the factors of bulk properties which affect the device yield, Vth and its variation were recognized as those which are essentially important. It was however later found that the arsenic precipitates which inevitably appear in conventional bulk crystal growth and ingot-annealing, reduce the device yield to a large extent.[484, 485] This was decisively found by device fabrication studies.[485, 295] The arsenic precipitates can be eliminated by high-temperature ingot-annealing,[470, 483] three-step ingot annealing[288] and the MWA method.[20, 292] For large scale ICs up to 4k SRAM, it was found that the MWA process greatly improves the device chip yield.[299]

REFERENCES

1. C.J. Nuese, in *Crystal Growth: A Tutorial Approach*, eds. W. Bradsley, D.T.J. Hurle and J.B. Mullin (North-Holland, Amsterdam, 1979) p. 353.
2. *Ultra High Speed Compound Semicondcutor Devices*, eds. T. Sugano and M. Ohmori (Baifukan, Tokyo, 1986)
3. R. Szweda, in *Compoumnd Semiconductor Industry Directory* (Elsevier Sci., Amsterdam, 1997) p. 14.
4. R.N. Thomas, H. M. Hobgood, G. W. Eldridge, D. L. Barrett, T. T. Braggins, L. B. Ta and S. K. Wang, in *Semiconductors and Semimetals Vol. 20*, eds. R.K. Willardson and A.C. Beer (Academic Press, New York, 1984) p. 1.
5. H.C. Gatos and J. Lagowski, *Proc.Compound Semiconductor Growth, Processing and Devices for the 1990's: Japan.U.S. Perspectives* (Gaincesville, Florida, 1987) p. 8.
6. K. Fukita, in *Bulk Crystal Growth Technology* (Gordon and Breach, New York, 1989) p. 10.
7. M. Yokogawa, in *Bulk Crystal Growth Technology* (Gordon and Breach, New York, 1989) p. 46.
8. R.N. Thomas, H. M. Hobgood, P.S. Ravishankar and T. T. Braggins, *J. Crystal Growth* 99 (1990) 643.
9. G. Müller, G. Hirt and D. Hoffman, in *Proc. 7th Conf. Semi-Insulating III-V Materials* (Ixtapa, Mexico, 1992) p. 73.
10. *Landolt-Börnstein, Vol. 17 Semiconductors*, ed. O. Madelung (Springer-Verlag, Berlin, 1982) p. 218.
11. W. Köster and B. Thomas, *Z. Metalkunde* 46 (1955) 291.
12. J. van den Boomgaad and K. Schol, *Philips Res. Rept.* 12 (1957) 127.
13. M.B. Panish, *J. Crystal Growth* 27 (1974) 6.
14. H. Wenzl, A. Dahlen, A. Fattah, K. Mika and D. Henkel, in *Proc. 7th Conf. Semi-insulating III-V Materials* (Tronto, Canada, 1990) p. 306.
15. H. Wenzl, A. Dahlen, A. Fattah, S. Peterson, K. Mika and D. Henkel, *J. Crystal Growth* 109 (1991) 191.
16. J. Nishizawa, H. Otsuka, S. Yamakoshi, and K. Ishida, *Jpn. J. Appl. Phys.* 13 (1974) 46.
17. R.M. Logan and D.T.J. Hurle, *Phys. Chem. Solids* 32 (1971) 1739.
18. D.T.J. Hurle, *J. Phys. Chem. Solids* 40 (1979) 613.
19. H. Wenzl, K. Mika and D. Henkel, *J. Crystal Growth* 100 (1990) 377.
20. O. Oda, H. Yamamoto, M. Seiwa, G. Kano, M. Mori, H. Shimakura and M. Oyake, *Semicond. Sci. Technol.* 7 (1992) A215.
21. Y. Nakada and T.R. Imura, *phys. stat. sol. (a)* 102 (1987) 625.
22. D. Gerthsen and C.B. Cartier, *phys. stat. sol. (a)* 136 (1993) 29.
23. R. Shetty, R. Balasubramanian and W.R. Wilcox, *J. Crystal Growth* 100 (1990) 58.
24. R. Rupp and G. Müller, *J. Crystal Growth* 113 (1991) 131.

25. K. Kakimoto and T. Hibiya, *Appl Phys. Lett.* **52** (1988) 1576.
26. K. Kakimoto, H. Watanabe and T. Hibiya, *J. Electrochem Soc.* **133** (1986) 2649.
27. L. Zanotti, *Materials and Physics* **9** (1983) 19.
28. R.L. Lane, *Semicon Int.* **October** (1984) 68.
29. S. Akai, in *Compound Semiconductor Growth, Processing and Devices*, ed. P.H. Holloway and T.J. Anderson (Crc Pr I Lic, 1989) p. 3.
30. J. M. Parsey, Jr., *Semi-insualting III-V Materials* (Adam Hilger, 1988) p. 405.
31. M. Jurisch, F. Borner, Th. Bunger, St. Eichler, T. Flade, U. Kretzer, A. Kohler, J. Stenzenberger and B. Weinert, *J. Crystal Growth* **275** (2005) 283.
32. T. Suzuki, S. Akai and K. Kohe, in *Semiconductor Research Vol. 12 (in japanese)*, ed. J. Nishizawa (Kogyo Chousakai, Tokyo, 1976) p. 87.
33. J. Nakagawa and K. Mizuniwa, *Mater. Sci. (in japanese)* **February** (1985) 14.
34. K. Fujii, M. Hirata, S. Takeda and H. Fujita, *Semiconductor Research Vol. 37 (in japanese)*, ed. J. Nishizawa (Kogyo Chousakai, Tokyo, 1992) p. 3.
35. S. Akai, K. Fujita, M. Sasaki and K. Tada, *Inst. Phys. Conf. Ser.* **63** (1981) 13.
36. G.M. Martin, G. Jacob, J.P. Hallais, F. Grainger, J.A. Roberts, B. Clegg, P. Blood and G. Poiblaud, *J. Phys. C: Solid State Phys.* **15** (1982) 1841.
37. K. Shikano, K. Kobayashi, S. Miyazawa, *Appl. Phys. Lett.* **46** (1985) 391.
38. L. Stourac, *Crystal Prop. Prep.* **12** (1987) 101.
39. J. Leitner and F. Moravec, *J. Crystal Growth* **83** (1987) 376.
40. T.P. Chen, Y.D. Guo and T.S. Huang, *J. Crystal Growth* **94** (1989) 683.
41. T. Shimoda and S. Akai, *Jpn. J. Appl. Phys.* **8** (1969) 1352.
42. T. Suzuki and T. Akai, *Bussei (in Japanese)* **3** (1971) 144.
43. T. Suzuki, S. Akai, K. Kohe, Y. Nishida, K. Fujita and N. Kito, *Sumitomo Electric Tech. Rev.* **18** (1978) 105.
44. S. Akai, K. Fujita, S. Nishine, N. Kito, Y. Sato, S. Yoshitake and M. Sekinobu, in *Proc. Symp. III-V Opto-electron. Epi. Dev. Related Processes* (Electrochem. Soc., New Jersey, 1983) p. 41.
45. P. Mo, J. Yang, S. Li, D. Jiang and H. Zhao, *J. Crystal Growth* **65** (1983) 243.
46. F. Orito, Y. Tsujikawa and M. Tajima, *J. Appl. Phys.* **55** (1984) 1119.
47. A. Hruban, A. Mirowska and A. Materna, *Acta Phys. Polonica* **A71** (1987) 421.
48. K. Fujii, F. Orito, H. Fujita and T. Sato, *J. Crystal Growth* **121** (1992) 255.
49. K. Fujii, F. Orito and H. Fujita, *Mater. Sci. Forum* **117-118** (1993) 393.
50. S. Mizuniwa, M. Kashiwa, T. Kurihara, K. Nkamura, S. Okubo and K. Ikegami, *J. Crystal Growth* **99** (1990) 676.
51. S. Mizuniwa, M. Nakamori, K. Nakamura and S. Okubo, *Hitachi Cable Rev.* **10** (1991) 37.
52. S. Mizuniwa, H. Akiyama, M. Nakamori and K. Nakamura, *Hitachi Cables (in japanese)* **11** (1992) 33.
53. J. M. Parsey, Jr., Y. Nanishi, J. Lagowski and H. C. Gatos, *J. Electrochem. Soc.* **128** (1981) 936.
54. J. M. Parsey, Y. Nanishi, J. Lagowski and H. C. Gatos, *J. Electrochem. Soc.* **129** (1982) 388.
55. T. Inoue, T. Matsumoto, M. Yokogawa and K. Fujita, *J. Jpn. Assoc. Crystal Growth* **18** (1991) 494.
56. K.H. Lie, J.T. Hsu, Y.D. Guo and T.P. Chen, *J. Crystal Growth* **109** (1991) 205.
57. T. Inoue, S. Nishine, M. Shibata, T. Matsumoto, S. Yoshitake, Y. Sato, T. Shimoda and K. Fujita, *Inst. Phys. Conf. Ser.* **79** (1985) 7.
58. K. Fujita, *Oyo Buturi (Monthly Publ. Jpn. Soc. Appl. Phys.) (in japanese)* **56** (1987) 1473.
59. K. Fujita, T. Shimoda, S. Yoshitake, T. Inoue, T. Matsutomo, S. Nishine, Y. Sato and M. Shibata, *Sumitomo Electric Tech. Rev.* **26** (1987) 185.
60. K. Fujita, Y. Nishida, N. Kito, K. Kohe, S. Akai, T. Suzuki and A. Matsumura, *Sumitomo Electric Tech. Rev.* **19** (1980) 97.
61. J. Bonnafe, M. Castagne, B. Clerjaud, B. Deveaud, P.N. Favennec, J.P. Fillard, M. Gauneau, A Goltzene, B. Guennais, G. Guillot, A.M. Hennel, A.M. Huber, J. Jouglar, P. Leyral, J.C. Manifacier, G. Martinez, G. Picoli, A. Roizes, C. Schwab, N. Visentin and P.L. Vullermoz, *Mater.*

Res. Bull. **16** (1981) 1193.
62. E. M. Swiggrad, S. H. Lee and F. W. con Batchelder, *Inst. Phys. Conf. Ser.* **33b** (1977) 23.
63. K. M. Burke, S. R. Leavitt, A. A. Khan, E. Riemer, T. Stoebe, S. A. Alterovitz and E. J. Haugland, in *GaAs IC Symposium* (1986) p. 37.
64. A. A. Khan, M. Boss, S. A. Alterovitz, E. J. Haugland, W. P. Allred and K. M. Burke, *Semi-Insulating III-V Materials*, eds. H. Kukimotoa nd S. Miyazawa, (Ohmsha, Tokyo and North-Holland, Amsterdam, 1986) p. 71.
65. M. L. Gray, L. Sargent, K. M. Burke, K. A. Grim and J. S. Balkemore, *J. Appl. Phys.* **63** (1988) 4413.
66. T. Ishihara, K. Murata, M. Sato, N. KIto and M. Hirano, *J. Crystal Growth***137** (1994) 375.
67. K. Murata, T. Ishihara, M. Sato, N. Kito and M. Hirano, *J. Crystal Growth* **141** (1994) 29.
68. T. R. Aucoin, R. L. Ross, M. J. Wada and R. O. Savage, *Solid State Technol.* **January** (1979) 59.
69. C.G. Kirkpatrick, R.T. Chen, D.E. Holmes, P.M. Asbeck, K.R. Elliot, R.D. Fairman ad J.O. Oliver, in *Semiconductors and Semimetals Vol. 20*, ed. (Academic Press, New York, 1984) p. 159.
70. C.G. Kirkpatrick, R.T. Chen, D.E. Holmes and K.R. Elliot, in *Gallium Arsenide, Materials, Devices and Circuits* ed, M.J. Howes and D.V. Morgan (Wiley, New York, 1985) p. 86.
71. G. Jacob, in *Semi-Insulating III-V Materials*, eds. D.C. Look and J.S. Blakemore (Shiva, Nantwich, 1984) p. 2.
72. R.N. Thomas, H. M. Hobgood, P.S. Ravishankar and T. T. Braggins, Prog. Crystal Growth Character. **26** (1993) 219.
73. R. T. Chen and D. E. Holmes, *J. Crystal Growth* **61** (1983) 111.
74. A. G. Elliot, C. Wei, R. Farraro, G. Woolhouse, M. Scott and R. Hiskes, *J. Crystal Growth* **70** (1984) 169.
75. T. Inada, T. Simada J. Nakagawa and S. Okubo, *Hitachi Cable Rev.* **3** (1984) 23.
76. A.G. Elliot, A. Flat, and D.A. Vanderwater, *J. Crystal Growth* **121** (1992) 349.
77. V. T. Bublik, V. V. Karataev, R. S. Kulagin M. G. Mil'vidskii, V. B. Osvenskii, O. G. Stolyarov, and L. P. Kholodnyi, *Sov. Phys. Crystallogr.* **18** (1973) 218.
78. D. E. Holmes, R. T. Chen, K. R. Elliot, C. G. Kirkpatrick and P. W. Yu, *IEEE Trans. Electron. Devices* **ED-29** (1982) 1045.
79. D. E. Holmes, R. T. Chen, K. R. Elliot, C. G. Kirkpatrick, *Appl. Phys. Lett.* **40** (1982) 46.
80. L. B. Ta, H. M. Hobgood, A. Rohatgi and R. N. Thomas, *J. Appl. Phys.* **53** (1982) 5771.
81. T. Obokata, T. Katsumata and T. Fukuda, *Jpn. J. Appl. Phys.* **24** (1985) L785.
82. T. Inada, T. Sato, K. Ishida, T. Fukuda and S. Takahashi, *J. Electron. Mater.* **15** (1986) 169.
83. T. Katusmata, H. Okada, T. Kimura and T. Fukuda, *J. Appl. Phys.* **60** (1986) 3105.
84. J. Nishio and K. Terahsima, *J. Crystal Growth* **85** (1987) 469.
85. R. Fornari, E. Gombia and R. Mosca, *J. Electron. Mater.* **18** (1989) 151.
86. R. Fornari, *Cryst. Res. Technol.* **24** (1989) 767.
87. M.L. Young, G.T. Brown and D. Lee, *J. Appl. Phys.* **67** (1990) 4140.
88. A. Steinmann and U. Zimmerli, *J. Phys. Chem. Solids* **Suppl.** (1967) 81.
89. B. C. Grabmaier and J. G. Grabmaier, *J. Crystal Growth* **13/14** (1972) 635.
90. G. Jacob, J. P. Farges, C. Schemali, M. Duseaux, J. Hallais, W. J. Bartels and R. J. Roksnoer, *J. Crystal Growth* **57** (1982) 245.
91. S. Thono, S. Shinoyama, A. Yamamoto and C. Uemura, *J. Appl. Phys.* **54** (1983) 666.
92. T. Shimada, K. Terashima, H. Nakajima and T. Fukuda, *Jpn. J. Appl. Phys.* **23** (1984) L23.
93. T. Shimada, T. Obokata and T. Fukuda, *Jpn. J. Appl. Phys.* **23** (1984) L441.
94. H. Okada, T. Kastsumata, T. Obokata, T. Fukuda and W. Susaki, *J. Crystal Growth* **75** (1986), 319.
95. H. Nakanishi, K. Yamada, H. Kohda and K. Hoshikawa, in *Extended Abstr. 16th Int. Conf. Solid State Dev. Mater.* (Tokyo, 1984) p. 63.
96. H. Kohda, K. Yamada, H. Nakanishi, T. Kobayashi, J. Osaka and H. Hoshikawa, *J. Crystal Growth* **71** (1985) 813.
97. F. Orito and T. Ibuka, *Mitsubishi Chemical R&D Review* **1** (1987) 52.

98. Y. Seki, *Oyo Buturi (Monthly Publ. Jpn. Soc. Appl. Phys.) (in japanese)* **46** (1977) 637.
99. Y. Seki, H. Watanabe, J. Matsui, *J. Appl. Phys.* **49** (1978) 822.
100. T. Kamejima, J. Matsui, Y. Seki and H. Watanabe, *J. Appl. Phys.* **50** (1979) 3312.
101. G. Jacob, *J. Crystal Growth* **59** (1982) 669.
102. K. Tada, A. Kawasaki, T. Kotani, R. Nakai, T. Takebe, S. Akai and T. Yamaguchi,in *Proc. 3rd Conf. Semi-Insulating III-V Materials*, eds. S. Makram-Ebeid adn B. Tuck (Evian, 1982) p. 36.
103. I.V. Stepantsova, V.B. Osvensky, A.V. Markov, S.S. Shifrin, U.A. Grigoreiv and V.T. Bubik, *Crystal Prop. Prep.* **19&20** (1989) 41.
104. G. Jacob, in *Semi-Insulating III-V Materials*, eds. D.C. Look and J.S. Blakemore (Shiva, Nantwich, 1984) p. 2.
105. G. Jacob, M. Duseax, J. P. Farges, M. M. B. van den Boom and R. J. Roksnoer, *J. Crystal Growth* **61** (1983) 417.
106. M. Duseaux and S. Martin, in *Semi-Insulating III-V Materials*, eds. D.C. Look and J.S. Blakemore (Shiva, Nantwich, 1984) p. 118.
107. H. M. Hobgood, R. N. Thomas, D. L. Barrett, g. W. Eldrige, M. M. Sopira and M. C. Driver, in *Semi-Insulating III-V Materials*, eds. D.C. Look and J.S. Blakemore (Shiva, Nantwich, 1984) p. 149.
108. D. L. Barrett, S. McGuigan, H. M. Hobgood, G. W. Eldridge and R. N. Thomas, *J. Crystal Growth* **70** (1984) 179.
109. H. Kimura, C. B. Afable, H. M. Olsen, A. T. Hunter and H. V. Winston, *J. Crystal Growth* **70** (1984) 185.
110. H. Miyairi, T. Inada, T. Obokata, M. Nakajima, T. Katsumata and T. Fukuda, *Jpn. J. Appl. Phys.* **24** (1985) L729.
111. B. Pichaud, N. Nurle-Durbec and F. Minari, *J. Crystal Growth* **71** (1985) 648.
112. S. McGuigan, R. N. Thomas, D. L. Barrett, H. M. Hobgood and B. W. Swanson, *Appl. Phys. Lett.* **48** (1986) 1377.
113. S. McGuigan, R. N. Thomas, D. L. Barrett, G. W. Eldridga, R. L. Messham and B. W. Swanson, *J. Crystal Growth* **76** (1986) 217.
114. T. Shimada, K. Ohata and K. Kurata, *Hitachi Cable Rev.* **5** (1985) 25.
115. K. Yamada, H. Kohda, H. Nakanishi and K. Hishikawa, *J. Crystal Growth* **78** (1986) 36.
116. T. Matsumura, F. Sato, A. Shimura, T. KItano and J. Matsui, *J. Crystal Growth* **78** (1986) 533.
117. T. Fujii, M. Nakajima and T. Fukuda, *Mater. Lett.* **4** (1986) 189.
118. H. Ono, H. Watanabe, T. Kamejima and J. Matsui, *J. Crystal Growth* **74** (1986) 446.
119. T. Suzuki, S. Akai, K. Tada and S. Murai, *Sumitomo Electric Tech. Rev.* **26** (1987) 174.
120. H. Okada, T. Katsumata, M. Eguchi and T. Fukuda, JJ. *Crystal Growth* **82** (1987) 643.
121. K. Matsumoto, M. Yamashita, R. Nakai, S. Yazu, K. Tada and S. Akai, in *Proc. 5th Conf. Semi-insulating III-V Mateirals* (Malmö, Sweden, 1988) p. 447.
122. S. McGuigan, B.W. Swanson and R.N. Thomas, *J. Crystal Growth* **94** (1989) 75.
123. J. He and S. Kou, *J. Crystal Growth* **216** (2000) 21.
124. T. Fukuda, K. Terashima, T. Katsumata, F. Orito and T. Kikuta, in *Extended Abstr. 15th Int. Conf. Solid State Dev. Mater.* (Tokyo, 1983) p.153.
125. K. Terashima, T. Katsumata. F. Orito, T. Kikuta and T. Fukuda, *Jpn. J. Appl. Phys.* **22** (1983) L325.
126. K. Terashima and T. Fukuda, *J. Crystal Growth* **63** (1983) 423.
127. K Terashima, T. Katsumata, F. Orito and T. Fukuda, *Jpn. J. Appl. Phys.* **23** (1984) L302.
128. K. Terashima, F. Orito, T. Katsumata and T. Fukuda, *Jpn. J. Appl. Phys.* **23** (1984) L485.
129. T. Fukuda and K. Terashima, *Oyo Buturi (Monthly Publ. Jpn. Soc. Appl. Phys.) (in japanese)* **53** (1984) 42.
130. T. Kimura, T. Katsumata, M. Nakajima and T. Fukuda, *J. Crystal Growth* **79** (1986) 264.
131. K. Terashima, A. Yahata and T. Fukuda, *J. Appl. Phys.* **59** (1986) 982.
132. T. Kimura, T. Obokata and T. Fukuda, *J. Crystal Growth* **84** (1987) 394.

133. K. Terashima, J. Nishio, S. Washizuka and M. Watanabe, *J. Crystal Growth* **84** (1987) 247.
134. S. Ozawa, T. Inada, T. Kimura, H. Miyairi and T. Fukuda, in *Semi-Insulating III-V Materials*, eds. H. Kukimoto and S. Miyazawa (Ohmsha, Tokyo, 1986) p. 53.
135. J. Osaka, H. Kohda, T. Kobayashi and K. Hoshikawa, *Jpn. J. Appl. Phys.* **23** (1984) L 195.
136. J. Osaka and K. Hoshikawa, in *Semi-Insulating III-V Materials*, eds. D.C. Look and J.S. Blakemore (Shiva, Nantwich, 1984) p. 126.
137. P. C. Leung and W. P. Allred, *J. Crystal Growth* **19** (1973) 356.
138. K. Tomizawa, K. Sassa, Y. Shimanuki and J. Nishizawa, *J. Electrochem. Soc.* **131** (1984) 2394.
139. K. Tomizawa, K. Sassa, Y. Shimanuki and J. Nishizawa, *Inst. Phys. Conf. Ser.* **91** (1988) 435.
140. K. Sasa, *Semicon. Lab. Rept. (in japanese)* **28** (1993) 131.
141. S. Ozawa, H. Miyairi, M. Nakajima and T. Fukuda, *Inst. Phys. Conf. Ser.* **79** (1986) 25.
142. S. Ozawa, H. Miyairi, J. Kobayashi and T. Fukuda, *J. Crystal Growth* **85** (1987) 553.
143. K. Usuda and T. Fujii, *J. Crystal Growth* **151** (1995) 13.
144. T. Kawase, T. Araki, Y. Miura, T. Iwasaki, N. Yamabayashi, M. Tatsumi, S. Murai, K. Tada and S. Akai, *Sumitomo Electric Tech. Rev.* **29** (1990) 228.
145. T. Kawase, T. Wakamiya, S. Fujiwara, M. Tatsumi, T. Shirakawa , K. Tada and M. Yamada, *Sumitomo Electric Tech. Rev.* **35** (1993) 78
146. M. Neubert, M. Seifert, P. Rudolph, K. Trompa and M. Pietsch, in *Proc. 9th Conf. Semicond. Insul. Mater. (SIMC '9)* (Toulouse, 1996) p. 17.
147. P. Rudolph, M. Neubert, S. Arulkumaran and M. Seifert, *Cryst. Res. Technol.* **32** (1997) 35.
148. M. Neubert and P. Rudolph, *Prog. Crystal Growth Character. Mater.* **43** (2001) 119.
149. Ch. Frank, K. Jacob, M. Neubert, P. Rudolph, J. Fainberg and G. Müller, *J. Crystal Growth* **213** (2000) 10.
150. O.V. Smirnova, V.V. Kalaev, Yu.N. Makarov, Ch. Frank-Rotsch, M. Neubert and P. Rudolph, *J. Crystal Growth* **266** (2004) 67.
151. K. Riedling, *J. Crystal Growth* **89** (1988) 435.
152. H.S. Goldberg, in *Intelligent Processing of Materials*, eds. by H.N.G. Wadley and W. E. Eckhart, Jr. (Min. Met. & Mat. Soc., 1990) p. 83.
153. S.Washizuka, J. Ushizawa, Y. Kokubun, M. Watanabe, T. Fukuda, *Oyo Buturi (Monthly Publ. Jpn. Soc. Appl. Phys.) (in japanese)* **52** (1983) 515.
154. K. Nambu, R. Nakai, M. Yokogawa, K. Matsumoto, K. Koe and K. Tada, *Inst. Phys. Conf. Ser.* **91** (1988) 141.
155. M. Kashiwa, Y. Otoki, M. Seki, S. Taharasako and S. Okubo, *Hitachi Cable Rev.* **9** (1990), 55.
156. J.P. Tower, R. Tobin, P.J. Pearah and R.M. Ware, *J. Crystal Growth* **114** (1991) 665.
157. T. Inada, M. Shibata and S. Kuma, *J. Jpn. Assoc. Crystal Growth* **18** (1991) 462.
158. M. Shibata, T. Suzuki, S. Kuma and T. Inada, *J. Crystal Growth* **128** (1993) 439.
159. M. Onishi, M. Shibata, S. Mizuniwa and M. Wachi, *Hitachi Cable Rev.* **12** (1993) 39.
160. T. Inada, M. Wachi, T. Suzuki, M. Shibata and M. Kashiwa, *Hitachi Cable Rev.* **13** (1994) 53.
161. R.M. Ware, W. Higgins, K.O'Hearn and M. Tiernam, in *Technical Digest - GaAs IC Symp.* (1996) p. 54.
162. T. Flade, M. Juricsch, A. Kleinwechter, A. Kohler, U. Kretzer, J. Prause, Th. Reinhold and B. Weinert, *J. Crystal Growth* **198/199** (1999) 336.
163. A. Seidl, S. Eichler, T. Flade, M. Jurisch, A. Köhler, U. Kretzer and B. Weinert, *J. Crystal Growth* **225** (2001) 561
164. M. Wachi, S. Komata, T. Inada and S. Yabuki, *J. Jpn. Assoc. Crystal Growth* **30** (2003) 88.
165. R. Fornari, C. Paorici, L. Zanotti and G. Zuccalli, *J. Crystal Growth* **63** (1983) 415.
166. R. T. Chen, D. E. Holmes and C. G. Kirkpartrick, in *NASA Lewis Res. Center Space Photovolatic Res. Technol.* (1982) p. 109.
167. F. Orito, H. Okada, M. Nakajima, T. Fukuda and T. Kajimura, *J. Electron. Mater.* **15** (1986) 87.
168. T. Fujii, M. Nakajima and T. Fukuda, *Mater. Lett.* **4** (1986) 189.
169. K. Hashio, S. Sawada, M. Tatsumi, K. Fujita and S. Akai, *J. Crystal Growth* **173** (1997) 33.

170. P. Burggraaf, *Semicon. Intern.* **October** (1984) 60.
171. P.G. Mo, X.Q. Fan, Y.D. Zhou and J. Wu, *Cryst. Res. Technol.* 24 (1989) 1089.
172. H.D. Marshall, *J. Crystal Growth* **109** (1991) 218.
173. M. J. Wargo and A. F. Witt, *J. Crystal Growth* **116** (1992) 213.
174. C. E. Chang, V.S.F. Yip and W.R. Wilcox, *J. Crystal Growth* **22** (974) 247.
175. W. A. Gault, E.M. Monberg and J.E Clemans, *J. Crystal Growth* 74 (1986) 491.
176. J. E Clemans, W.A. Gault and E.M. Monberg, *AT&T Tech. J.* **65** (1986) 86.
177. J. E. Clemens and J. H. Conway, in *Proc. 5th Conf. Semi-insulating III-V Mateirals* (Malmö, Sweden, 1988) p. 423
178. C. R. Abernathy, A. P. Kinsella, A. S. Jordan, R. Caruso, S. J. Pearton, H. Temkin and H. Wade, *J. Crystal Growth* **85** (1987) 106.
179. R. E. Kremer, D. Francomano, G. H. Bekhart and K. M. Burke and T. Miller, in *Proc. Mater. Res. Soc. Symp. Vol. 144* (Mater. Res. Soc., Pittsburgh, 1989) p. 15.
180. R. E. Kremer, D. Francomano, G. H. Bekhart and K. M. Burke, *J. Mater. Res.* **5** (1990) 1468.
181. K. Hoshikawa, H. Nakanishi, H. Kohda and M. Sasaura, *J. Crystal Growth* **94** (1989) 643.
182. K. Hoshikawa, in *Semiconductor Research Vol. 35 (in japanese)*, ed. J. Nishizawa (Kogyo Chosakai, Tokyo, 1991) p. 3.
183. E. D. Bourret, J. B. Guitron, M. L. Galiano and E. E. Haller, *J. Crystal Growth* **102** (1990) 877.
184. E. D. Bourret and E. C. Merk, *J. Crystal Growth* **110** (1991) 395.
185. Y. Okabe, S. Shimoyama and A. Tanaka, *J. Jap. Assoc. Crystal Growth* **18** (1991) 502.
186. H. Nakanishi and H. Kohda, *J. Crystal Growth* **155** (1995) 171.
187. C. Frank, K. Hein, C. Hannig and G. Gartner, *Cryst. Res. Technol.* **31** (1996) 753.
188. J. Amon, F. Dumke and G. Muller, *J. Crystal Growth* **187** (1998) 1.
189. Z. Liu, *Microelectron. J.* **27** (1996) 4.
190. T. Kawase, Y. Hagi, M. Tatsumi, K. Fujita and R. Nakai, in *Proc. 9th Int. Conf. Semiconducting and Insulating Materials* (IEEE, Pisctaway, NJ, 1996) p. 275.
191. K. Sonnenberg and E. Kussel, *III-Vs Review* **10** (1997) 30.
192. B. Birkmann, M. Rasp, J. Stenzenberger and G. Muller, *J. Crystal Growth* **211** (2000) 157.
193. S. Sawada, T. kawase, Y. Hagi, H. Miyajima, T. Sakurada, M. Yamashita, H. Yoshida, M. Kiyama and R. Nakai, *Sumitomo Electric Tech. Rev.* 49 (2000) 111.
194. J. Stenzenberger, T. Bürber, F. Börner, S. Eichler, T. Flade, R. Hammer, M. Jurisch, U. Kretzer, S. Teichert and B. Weinert, *J. Crystal Growth* **250** (2003) 57.
195. Y. Okada, S. Sakuragi and S. Hashimoto, *Jpn. J. Appl. Phys.* **29** (1990) L1954.
196. J. Amon, J. Härtwig, W. Ludwig and G. Müller, *J. Crystal Growth* **198/199** (1999) 367.
197. L. Breivik, M.R. Brozel, D.J. Stirland and S. Tuzemen, *Semicon. Sci. Technol.* 7 (1992) A269.
198. E. Buhrig, C. Frank, G. Gartner, K. Hein, V Klemm, G. Kuhnel and U. Voland, *Mater. Sci. Engineer.* **B28** (1994) 87.
199. E. Buhrig, C. Frank, G. Gartner, K. Hein, V Klemm, G. Kuhnel and U. Voland, *Mater. Sci. Engineer.* **B44** (1997) 248.
200. C. Frank and K. Hein, *Erzmetall* **48** (1995) 422.
201. C. Frank and K. Hein, *Cryst. Res. Technol.* **30** (1995) 897.
202. Y.J. Park, S.-K. Min, S.-H. Hahn and J.-K. Yoon, *J. Crystal Growth* **154** (1995) 10.
203. Y.J. Park, E.K. Kim, M.H. Son and S.-K. Min, *J. Crystal Growth* **156** (1995) 487.
204. O. Pätzold, I. Grants, U. Wunderwald, K. Jenkner, A. Cröll and G. Gerbeth, *J. Crystal Growth* **245** (2002) 237.
205. H. Weimann, J. Amon, Th. Jung and M. Müller, *J. Crystal Growth* **180** (1997) 560.
206. T. Suzuki, Y. Okano, K. Hoshikawa and T. Fukuda, *J. Crystal Growth* **128** (1993) 435.
207. T.P. Lyubimova, A. Croell, P. Dold, O.A. Khlybov and I.S. Fayzrakhmanova, *J. Crystal Growth* **266** (2004) 404.
208. G. Jacob, *J. Crystal Growth* **58** (1982) 455.
209. J.M. Whelan and G.H. Wheatley, *J. Phys. Chem. Solids* **6** (1958) 169.

210. F. M. Herrmann, J. Baumgartl, T. Feulner and G. Müller, in *Proc. VIIIth Euro. Symp. Mater. Fluid Sci. Microgravity* (Brussels, Belgium, 1992) 57.
211. F.M. Herrmann and G. Müller, *J. Crystal Growth* **156** (1995) 350.
212. E. M. Swiggard, *J. Crystal Growth* **94** (1989) 556.
213. P. E. R. Nordquist, R. L. Henry, J. S. Balkemore, R. J. Gorman and S. B. Saban, *Inst. Phys. Conf. Ser.* **120** (1991) 61.
214. R.L. Henry, P. E. R. Nordquist, R. J. Gorman and S. B. Quadri, *J. Crystal Growth* **109** (1991) 228.
215. P. E. R. Nordquist, R. L. Henry, J. S. Balkemore, S. B. Saban and R. J. Gorman, *Inst. Phys. Conf. Ser.* **141** (1993) 343.
216. R.S. Tang, L. Sargent, J.S. Blakemore and E.M. Swiggard, *J. Crystal Growth* **103** (1990) 323.
217. C. P. Khattak, J. Lagowski, J. H. Wohlgemuth, S. Mil'shtein, V. E. White and F. Scchmid, *Inst. Phys. Conf. Ser.* 79 (1986) 31.
218. C.P. Khattak, S. di Gregorio and F. Schmid, *Inst. Phys. Conf. Ser.* **91** (1987) 133.
219. J.H. Wohlgemuth, C.P. Khattak, J. Lagowski and M. Skowronski, in *Semi-Insulating III-V Materials*, eds. H. Kukimoto and S. Miyazawa (Ohmsha, Tokyo, 1986) p. 191.
220. T. Fujii, M. Eguchi and T. Fukuda, *J. Crystal Growth* **87** (1988) 573.
221. S. Miyazawa, *J. Crystal Growth* **60** (1982) 331.
222. T. Kobayashi and J. Osaka, *J. Crystal Growth* **67** (1984) 319.
223. J. Nishizawa, S. Shinozaki and K. Ishida, *J. Appl. Phys.* **44** (1973) 1638.
224. J. Nishizawa, H. Otsuka, S. Yamakoshi, and K. Ishida, *Jpn. J. Appl. Phys.* **13** (1974) 46.
225. J.Nishizawa, Y.Okuno and H.Tadano, *J. Crystal Growth* **31** (1975) 215.
226. D.E. Holmes and G.S. Kamath, *J. Crystal Growth* **57** (1982) 607.
227. C. F. Bouccher, Jr., O. Ueda, T. Bryskiewicz and H. C. Gatos, *J. Appl. Phys.* **61** (1987) 359.
228. T. Bryskiewicz, C. F. Boucher, Jr., J. Lagowski and H. C. Gatos, *J. Crystal Growth* **82** (1987) 279.
229. T. Imaizumi, H. Okazaki and O. Oda, *Appl. Phys. Lett.* **63** (1993) 1390.
230. T. Imaizumi, H. Okazaki and O. Oda, *J. Appl. Phys.* **76** (1994) 7957.
231. A. Noda, K. Kohiro and O. Oda, *J. Electron. Mater.* **25** (1996) 1841.
232. D. Rumsby, R. M. Ware, B. Smith, M. Tyjberg, R. M. Brozel and E. J. Foulkes, in *1983 Tech. Dig. GaAs IC Symp.* (IEEE, New York, 1983) p. 34
233. M. Yokogawa, S. Nishine, K. Matsumoto, H. Morishita, K. Fujita and S. Akai, *Inst. Phys. Conf. Ser.* **74** (1984) 29.
234. M. Yokogawa, S. Nishine, M. Sasaki, K. Matsumoto, K. Fujita and S. Akai, *Jpn. J. Appl. Phys.* **23** (1984) L339.
235. S. Martin, M. Dusseaux and M. Erman, *Inst. Phys. Conf. Ser.* 74 (1984) 53.
236. D. E. Holmes, H. Kuwamoto, C. G. Kirkpatrick and R. T. Chen, in *Semi-Insulating III-V Materials*, eds. D.C. Look and J.S. Blakemore (Shiva, Nantwich, 1984) p. 204.
237. D. C. Look, P. W. Yu, W. M. Theis, W. Ford, G. Mathur, J. R. Sizelove, D. H. Lee and S. S. Li, *Appl. Phys. Lett.* **49** (1986) 1083.
238. A. K. Chin, I. Camlibel, R. Caruso, M. S. S. Young and A. R. Von Neida, *J. Appl. Phys.* **57** (1985) 2203.
239. J. Osaka, F. Huga, K. K. Watanabe, *Appl. Phys. Lett.* **47** (1985) 1307.
240. K. Löhnert, W. Wettling and G. Koschek, in *Semi-Insulating III-V Materials*, eds. H. Kukimoto and S. Miyazawa (Ohmsha, Tokyo, 1986) p. 267.
241. J. Lagowski, H. C. Gatos, C. H. Kang, M. Skowronski, K. Y. Ko and D. G. Lin, *Appl. Phys. Lett.* **49** (1986) 892.
242. Y. Kitagawara, N. Noto, T. Takahashi and T. Takenaka, in *Semi-Insulating III-V Materials*, eds. H. Kukimoto and S. Miyazawa (Ohmsha, Tokyo, 1986) p. 273.
243. O. Ogawa, in *Semi-Insulating III-V Materials*, eds. H. Kukimoto and S. Miyazawa (Ohmsha, Tokyo, 1986) p. 237
244. W. Ford, G. Mathur, D. Look and P. Yu, in *Semi-Insulating III-V Materials*, eds. H. Kukimoto and S. Miyazawa (Ohmsha, Tokyo, 1986) p. 227.

245. Y. Otoki, M. Nakamori, R. Nakazono and S. Kuma, in *Semi-Insulating III-V Materials*, eds. H. Kukimoto and S. Miyazawa (Ohmsha, Tokyo, 1986) p. 285.
246. J. Osaka, H. Okamoto, F. Huga, K. Watanabe and K. Yamada, in *Semi-Insulating III-V Materials*, eds. H. Kukimoto and S. Miyazawa (Ohmsha, Tokyo, 1986) p. 279.
247. S. Miyazawa, in *Defects in Semiconductors*, ed. by H. J. von Bardeleben (Trans. Tech., Switzerland, 1986) p.1
248. D. C. Look, W. M. Theis, P. W. Yu, J. R. Sizelove and G. Mathur, *J. Electron Mater.* **16** (1987) 63.
249. N. Noto, Y. Kitagawara, T. Takahashi and T. Takenaka, *Jpn. J. Appl. Phys.* **25** (1986) L394.
250. C. H. Kang, J. Lagowski and H. C. Gatos, *J. Appl. Phys.* **62** (1987) 3482.
251. H. Kanber and D. C. Wang, *IEEE Trans. Electron Devices* **ED-34** (1987) 1626.
252. T. Kazuno, Y. Takatsuka, K. Satoh, K. Chino and Y. Chiba, *Inst. Phys. Conf. Ser.* **91** (1987) 61.
253. N.Y. Jin and X.S. Huang, *Mater. Lett.* **5** (1987) 196.
254. S. Chichibu, N. Okubo and S. Matsumoto, *J. Appl. Phys.* **64** (1988) 3987.
255. S. Clark, D. J. Stirland, M. R. Brozel, M. Smith and C. A. Warwick, in *Semi-insulating III-V Materials* (Malmö, 1988) p. 31.
256. Y. Kitagawara, T. Takahashi, S. Kuwabara and T. Takenaka, in *Proc. 5th Conf. Semi-insulating III-V Mateirals* (Malmö, Sweden, 1988) p. 49.
257. Y. Kitagawara, N. Noto,T. Takahashi and T. Takenaka, *Appl. Phys. Lett.* **52** (1988) 221.
258. S. Reichlmaier, K. Löhnert and M. Baumgartner, *Jpn. J. Appl. Phys.* **27** (1988) 2329.
259. Y. Nakamura, Y. Ohtsuki and T. Kikuta, *Jpn. J. Appl. Phys.* **27** (1988) L1148.
260. M. T. Asom, J. M. Parsey Jr., L. C. Kimerling, R. Sauer adn F. A. Thiel, *Appl Phys. Lett.* **52** (1988) 1472.
261. D.J. Stirland, C.A. Warwick and G.T. Brown, in *Proc. 5th Conf. Semi-insulating III-V Mateirals* (Malmö, Sweden, 1988) p. 93.
262. P. Sucht, M. Duseaux, J. Le Bris, P. Deconinck and G. M. Martin, in *Proc. 5th Conf. Semi-insulat ing III-V Mateirals* (Malmö, Sweden, 1988) p. 99.
263. O. Ogawa, in *Proc. 5th Conf. Semi-insulating III-V Mateirals* (Malmö, Sweden, 1988) p. 477.
264. S. Miyazawa, K. Watanabe, J. Osaka and K. Ikuta, *Rev. Phys. Appl.* **23** (1988) 727.
265. G. Koschek, H. Lakner and E. Kubalek, *phys. stat. sol (a)* **108** (1988) 683.
266. S. Taharasako, Y. Otoki, T. Inada and K. Ikegami, *Hitachi Cable Rev.* **August** (1988) 55.
267. D.J. Stirland, P. Kidd, G.R. Booker, S. Clark, D.T.J. Hurle, M.R. Brozel and I. Grant, in *Microscopy of Semicondcutor Materials* (IOP, Bristol, 1989) p. 373.
268. T. Inada, Y. Otoki, K. Ohata, S. Taharasako and S. Kuma, *J. Crystal Growth* **96** (1989) 327.
269. S. Kuma, Y. Otoki and T. Inada, *Oyo Buturi (Monthly Publ. Jpn. Soc. Appl. Phys.) (in japanese)* **91** (1989) 327.
270. A. Chabli, E. Molva, J.P. Le Ludec, P. Bunod, C. Perret and F. Bertin, in *Defect Control in Semiconductors*, ed. K. Sumino (North-Holland, Amsterdam, 1990) p. 679.
271. B. Lee, E. D. Bourret, R. Gronsky and I. Park, *J. Appl. Phys.* **65** (1989) 1030.
272. A.V. Markov, I.V. Stepantsova, V.B. Osvenskii and S.P. Grishina, *Sov. Phys. Semicond.* **23** (1989) 1109.
273. Z.Q. Fang, L. Shan, J.H. Zhao, X.J. bao, T.E. Schlesinger, A.G. Milnes, G.R. Yang and W.M. Lau, *J. Elecrtron. Mater.* **18** (1989) 123.
274. D. J. Stirland, in *Defect Control in Semiconductors*, ed. K. Sumino (North-Holland, Amsterdam, (1990) p. 783.
275. E. Molva, Ph. Bunod, A. Chabli, A. Lombardot, S. Dubois and F. Bertin, *J. Crystal Growth* **103** (1990) 91.
276. Y. Otoki, M. Watanabe, T. Inada and S. Kuma, *J. Crystal Growth* **103** (1990) 85.
277. S. Clark, M. R. Brozel, D. J. Stirland, D. T. J. Hurle and I. Grant, in *Defect Control in Semiconductors*, ed. K. Sumino (North-Holland, Amsterdam, 1990) p. 807.
278. M. Matsui and T. Iino, *Sumitomo Metal Mining, Rep. Electron. Mater. Lab. (in japanese)* **8** (1990)

17.
279. H. Menninger, M. Beer, R. Cleichmann, H. Raidt, B. Ulrici and G. Voigt, *phys. stat. sol. (a)* **121** (1990) 95.
280. Y. Nakamura, *Heat Treatment (in japanese)* **30** (1990) 201.
281. Y. Kitagawara and T. Takenaka, in *Semi-insulating III-V Materials* (Toronto, Adam Hilger, 1990) p. 53.
282. K. Yamada, J. Osaka and K. Hoshikawa, *J. Appl. Phys.* **69** (1991) 6990.
283. E.P. Visser, J.L. Weyher and L.J. Gilling, *J. Appl. Phys.* **69** (1991) 4234.
284. M. Suemitsu, K. Terada, M. Nishijima and N. Miyamoto, *J. Appl. Phys.* **70** (1991) 2594.
285. M. Suemitsu, K. Terada, M. Nishijima and N. Miyamoto, *Jpn. J. Appl. Phys.* **31** (1992) L1654.
286. N. Ohkubo, M. Shishikura and S. Matsumoto, *J. Appl. Phys.* **73** (1993) 615.
287. I. Priecel, L. Duricek, V. Daniska and D. Korytar, *J. Crystal Growth* **126** (1993) 103.
288. B. Hoffmann, M. Jurisch, G. Kissinger, A. Kohler, G. Kuhnel, T. Reinhold, W. Siegel and B. Weinert, in *Proc. 9th Conf. Semiconducting and Insulating Materials* (Toulouse, France 1996) p. 63.
289. O. Oda, in *Properties of Gallium Arsenide*, eds. M.R. Brozel and G.E. Stillman (EMIS, No.16, INSPEC, 1996) p. 585.
290. Y. Matsumoto and H. Watanabe, *Jpn. J. Appl. Phys.* **21** (1982) L515.
291. S. Miyazawa, T. Honda, Y. Ishii and S.Ishida, *Appl. Phys. Lett.* **44** (1984) 410.
292. M. Mori, G. Kano, T. Inoue, H. Shimakura, H. Yamamoto and O. Oda, in *Semi-insulating III-V Materials* (Toronto, Adam Hilger, 1990) p. 155.
293. G. Kano G, M. Takakusaki, M. Oyake, H. Yamamoto and O. Oda, in *Semi-insulating III-V Materials* (Toronto, Adam Hilger, 1990) p. 59.
294. T. Inoue T, M. Mori, G. Kano, H. Yamamoto and O. Oda, *Inst. Phys. Conf. Ser.* **112** (1990) 219.
295. M. Oyake, H. Yamamoto, G. Kano, T. Inoue and O. Oda, *Inst. Phys. Conf. Ser.* **112** (1991) 311.
296. O. Oda, H. Yamamoto, M. Seiwa, G. Kano, M. Mori, H. Shimakura and M. Oyake, *Semicond. Sci. Technol.* **7** (1992) A215.
297. H. Yamamoto, *III-Vs Review* **5** (1992) 30.
298. O. Oda, H. Yamamoto, K. Kainosho, T. Imaizumi and H. Okazaki, *Inst. Phys. Conf. Ser.* **135** (1993) 285.
299. O. Oda, H. Yamamoto, K. Kainosho, T. Imaizumi and H. Okazaki, in *Semi-insulating III-V Materials*, ed. M. Godlewski (World Sci., Singapore, 1994) p. 27.
300. A.S. Jordan and J.M. Parsey, *MRS Bulletin* **13** (1988) 36.
301. D.N. Talwar, M. Vandevyer, K.K. Bajaj and W.M. Theis, *Phys. Rev. B* **33** (1986) 8525.
302. R.S. Leigh and R.C. Newman, *J. Phys. C: Solid State Phys.* **15** (1982) L1045.
303. P. Kleinert, *phys. stat. sol. (b)* **119** (1983) K37.
304. Y. Kadota, in *31th Semiconductor Speciality Short Course* (Yamagata, 1988) p. 1.
305. L. Sargent and J. S. Blakemore, *Appl. Phys. Lett.* **54** (1989) 1013.
306. H. Ch. Alt and B. Dischler, *Appl. Phys. Lett.* **66** (1995) 61.
307. H. Ch. Alt, *Mater. Sci. Forum* **196-201** (1995) 1577.
308. M. R. Brozel, J. B. Clegg and R. C. Newman, *J. Phys. D; Appl. Phys.* **11** (1978) 1331.
309. W.M. Theis, K.K. Bajaj, C.W. Litton and W.G. Spitzer, *Physica B* **117** (1983) 116.
310. A.T. Hunter, H. Kimura, J.P. Bukus, H.V. Winston and O.J. Marsh, Appl. Phys. Lett. **44** (1984) 74.
311. Y. Homma, Y. Ishii, T. Kobayashi and J. Osaka, *J. Appl. Phys.* **57** (1985) 2932.
312. Y. Kadota, K. Sakai, T. Nozaki, Y. Itoh and Y. Ohkubo, in *Semi-Insulating III-V Materials*, eds. H. Kukimoto and S. Miyazawa (Ohmsha, Tokyo, 1986) p. 201.
313. M.R. Brozel, F.J. Foulkes, R.W. Series and D.T.J. Hurle, *Appl. Phys. Lett.* **49** (1986) 337.
314. Y. Kitagawara, T. Itoh, N. Noto and T. Takenaka, *Appl. Phys. Lett.* **48** (1986) 788.
315. T. Arai, T. Nozaki, M. Tajima and J. Osaka, *J. Electronic Industry (in japanese)* **30** (1988) 38.
316. L. C. Wei, G. Blondiaux, A. Giovagnoli, M. Valladon and J. L. Debrun, *Nucl. Instrum. Methods*

Phys. Res. **B24/25** (1987) 999.
317. Y. Itoh, Y. Katoda, T. Nozaki, H. Fukusshima and K. Takeda, *Jpn. J. Appl. Phys.* **28** (1989) 210.
318. P. Misaelides, J. Krauskopf, G. Wolf and K. Bethge, *Nuc. Instr. Methods Phys. Res.* **B18** (1987) 281.
319. K. Shiakno, H. Yonezawa and T. Shigematsu, *J. Radioanal. Nuc. Chem.* **111** (1987) 51.
320. J. Kobayashi, M. Nakajima and K. Ishida, *J. Vac. Sci. Technol.* **A6** (1988) 86.
321. M. Tajima, K. Hoshikawa and T. Ogawa, *Oyo Buturi (Monthly Publ. Jpn. Soc. Appl. Phys.) (in japanese)* **54** (1985) 84.
322. R. Nakamura, Y. Itoh, M. Kashiwa, O. Oda, Y. Katsuno, K. Yamada, T. Sato, A Matsushima and M. Matsui, *III-Vs Review* **8** (1995) 34.
323. S. Yoshida, Y. Itoh, M. Kashiwa, Y. Katsuno, H. Mkishima, K. Haijima, T. Otaki, T. Sato, R. Nakai and M. Matsui, *III-Vs Review* **8** (1995) 42.
324. K. Ishii, A. Matsushita, M. Matsui, R. Nakamura, H. Matsushita, T. Inada, H. Yamamoto, Y. Katsuno and K. Yamada. *III-Vs Review* **11** (1998) 42.
325. SEMI Standard M30-0997 (annual publication from Semiconductor Equipment and Materials In ternational).
326. T. Kobayashi and J. Osaka, *J. Crystal Growth* **71**(1985) 240.
327. U.V. Desnica and M. Pawlowicz, *Inst. Phys. Conf. Ser.* **83** (1986) 33.
328. U.V. Desnica, M.C. Cretella, L.M. Pawlowicz and J. Lagowski, *J. Appl. Phys.* **62** (1987) 3639.
329. S. Eichler, A. Seidl, F. Borner, U. Kretzer and B. Weinnert, *J. Crystal Growth* **247** (2001) 69.
330. A.J. Moll, E.E. Haller, J.W. Agner III and W. Walukiewicz, *Appl. Phys. Lett.* **65** (1994) 1145.
331. A.J. Moll, J.W. Ager, III, Kin Man Yu, W. Walukiewicz and E.E. Haller, *Inst. Phys. Conf. Ser.* **141** (1994) 269.
332. T. Kikuta, H. Emori and T. Fukuda and K. Ishida, *J. Crystal Growth***76** (1986) 517.
333. T. Inada, T. Fujii, T. Kikuta and T. Fukuda, *Appl. Phys. Lett.* **50** (1987) 143.
334. J. Nishio and Y. Nakata, *J. Crystal Growth* **99** (1990) 680.
335. A.M. Nosovsky, Yu.N. Bolsheva, M.A. Ilyin, A.V. Markov, N.G. Mikhailova and V.B. Osvensky, *Acta Physica Hungarica* **70** (1991) 211.
336. H.D. Marshall and D.W. DeCuir, *J. Crystal Growth* **110** (1991) 960.
337. J. Nishio, *J. Crystal Growth* **108** (1991) 150.
338. J. Nishio and H. Fujita, *J. Crystal Growth* **134** (1993) 97.
339. W.M. Higgins, R.M. Ware, M.S. Tiernan, K.J. O'Hearn and D.J. Carlson, *J. Crystal Growth* **174** (1997) 208.
340. C. Hannig, E. Buhrig and G. Gartner, *Cryst. Res. Technol.* **34** (1999) 189.
341. H. Wenzl, K. Mika and D. Henkel, *Cryst. Res. Technol.* **25** (1990) 699.
342. L. B. Ta, H. M. Hobgood and R. N. Thomas, *Appl. Phys. Lett.* **41** (1982) 1091.
343. J. Osaka, F. Hyuga, T. Kobayashi, Y. Yamada and F. Orito, *Appl. Phys. Lett.* **50** (1987) 191.
344. R. A. Morrow, *J. Appl. Phys.* **62** (1987) 3671.
345. Y. Okada and F. Orito, *Appl. Phys. Lett.* **52** (1988) 582.
346. H.C. Gatos, M. Skowronski, L. Pawlowicz and J. Lagowski, *Inst. Phys. Conf. Ser.* **74** (1984) 41.
347. J.C. Bourgoin, D. Stievenard, D. Deresmes and J. M. Arroyo, *J. Appl. Phys.* **69** (1991) 284.
348. A.V. Markov, V.B. Osvensky, A.Y. Polyakov, M.V. Tishkin and E.M. Omeljanovsky, *Solid State Commun.* **73** (1990) 495.
349. B. Ulrici, R. Stedman and W. Ulrici, *phys. stat. sol. (b)* **143** (1987) K135.
350. H.Ch. Alt, *Appl. Phys. Lett.* **54** (1989) 1445.
351. M. Skowronski, *Phys. Rev. B* **46** (1992) 9476.
352. Y. Ishii, Y. Homma, K. Ikeda and H. Takaoka, *NTT Research Practization Report (in japanese)* **33** (1984) 707.
353. Y. Homma and Y. Ishii, *J. Appl. Phys.* **56** (1984) 1892.
354. S. Kurosawa, Y. Homma, Y. Nakamura, K. Nomura, Y. Yoshioka, M. Shibata, T. Yokoyama, K. Hoshikawa and T. Ogawa, *Oyo Buturi (Monthly Publ. Jpn. Soc. Appl. Phys.) (in japanese)* **54**

(1985) 1074.
355. A.V. Markov, Yu. N. Bol'sheva and V. B. Osvenskii, *Vysokochistye Veshchestva* **1** (1993) 86.
356. J. Woodhead, R.C. Newman, A.K. Tipping, J.B. Clegg, J.A. Roberts and I Gale, *J. Phys. D: Appl. Phys.* **18** (1985), 1575.
357. B. Ulrici, R. Stedman and W. Ulrici, *phys. stat. sol. (b)* **143** (1987) K135.
358. B. Clerjaud, D. Cote, C. Naud, M. Gauneau and R. Chaplain, *Appl. Phys. Lett.* **59** (1991) 2980.
359. E.M. Omeljavocsky, A.V. Pakhomov and A.V. Polyakov, in *Defect Control in Semiconductors*, ed. K. Sumino (Elsevier Sci., Amsterdam, 1990) p. 855.
360. A.Y. Polyakov, A.V. Pakhomov, M.V. Tishkin and E.M. Omeljanovsky, in *Proc. 6th Conf. Semi-insulating III-V Materials* (Toronto, Adam Hilger, 1990) p. 247.
361. D.A. MacQuistan and F. Weinberg, *J. Crystal Growth* **110** (1991) 745.
362. W.J. Moore and R.L. Henry, *Phys. Rev. B* **46** (1992) 7229.
363. M.R. Brozel, E.J. Foulkes, I.R. Grand and D.T.J. Hurle, *J. Crystal Growth* **80** (1987) 323.
364. A. Flat, *J. Crystal Growth* 109 (1991) 224.
365. M. R. Brozel, I. R. Grant, D. T. J. Hurle, *J. Crystal Growth* **80** (1987) 315.
366. T. Fukuda, K. Terashima and H. Nakajima, *Inst. Phys. Conf. Ser.* **65** (1982) 23.
367. J. Nishio and K. Terashima, *J. Crystal Growth* **96** (1989) 605.
368. T. Fujii, M. Eguchi, T. Inada and T. Fukuda, *J. Crystal Growth* **84** (1987) 237.
369. H. Immenroth, U. Lambert and E. Tomzig, *J. Crystal Growth* **142** (1994) 37.
370. M. Seifert, M. Neubert, W. Ulrici, B. Wiedemann, J. Conecker, J. Kluge, E. Wolf, D. Klinger and P. Rudolph, *J. Crystal Growth* **158** (1996) 409.
371. P. Petroff and R. L. Hartman, *Appl. Phys. Lett.* **23** (1973) 469.
372. P.M. Petroff, R.A. Logan and A. Savage, *Phys. Rev. Lett.* **44** (1980) 287.
373. R. T. Blunt, S. Clark and D. J. Stirland, *IEEE Trans. Microwave Theory and Techniques* **MTT-30** (1982) 943.
374. S. Miyazawa, Y. Ishii, S. Ishida and Y. Nanishi, *Appl. Phys. Lett.* **43** (1983) 305.
375. S. Miyazawa and Y. Ishii, *IEEE Trans. Electron. Devices* **ED-31** (1984) 1057.
376. H. V. Winston, A. T. Hunter, H. M. Olsen, R. P. Bryan and R. E. Lee, in *Proc. 4th Conf. Semi-Insulating III-V Materials*, eds. D.C. Look and J.S. Blakemore (Shiva, Nantwich, 1984) p. 402.
377. H. V. Winston, A. T. Hunter, H. M. Olsen, R. P. Bryan and R. E. Lee, *Appl. Phys. Lett.* **45** (1984) 447.
378. F. Hyuga, *Jpn. J. Appl. Phys.* 24 (1985) L160.
379. A. T. Hunter, H. Kimura, H. M. Olsen and H. V. Winston, *J. Electron. Mater.* **15** (1986) 215.
380. H.A. Schell, *Z. Metalkunde* **48** (1957) 158.
381. J.L. Richards and A.J. Crocker, *J. Appl. Phys.* 31(1960), 611.
382. M. S. Abrahams and C. J. Buiocchi, *J. Appl. Phys.* **36** (1965) 2855.
383. D.J. Stirland and R. Ogden, *phys. stat. sol. (a)* **17** (1973) K1.
384. N. Chen, H. He, Y. Wang, K. Pan and L. Lin, *J. Crystal Growth* **167** (1996) 766.
385. J. G. Grabmaier and C. B. Watson, *phys. stat. sol.* **32** (1969) K13.
386. H. Lessoff and R. Gorman, *J. Electron. Mater.* **13** (1984) 733.
387. J.L. Wehyer and J. van den Ven, *J. Crystal Growth* **78** (1986) 191.
388. D. J. Stirland and B. W. Straughan, *Thin Solid Films* **31** (1976) 139.
389. Y. Okada, *Jpn. J. Appl. Phys.* **22** (1983) 413.
390. D. A. O. Hope and B. Cockayne, *J. Crystal Growth* **67** (1984) 153.
391. J.L. Weyher and L.J. Giling, in *Defect Recognition and Image Processing*, ed. by J. P. Fillard (Elsevier Sci, Amsterdam, 1985) p. 63.
392. G.T. Brown and C.A. Warwick, *J. Electrochem. Soc.* **133** (1986) 2576.
393. L.J. Giling, J.L. Weyher, A. Montree, R. Fornari and L. Zanotti, *J. Crystal Growth* **79** (1986) 271.
394. G.T. Brown, *Ann. Rev. Mater. Sci.* **17** (1987) 123.
396. R. Gleichmann, H. Menniger and H. Raidth, *Crystal Prop. Prep.* **12** (1987) 17.

397. P. Dobrilla and D.C. Miller, *J. Electrochem. Soc.* **134** (1987) 3197.
398. J.L Weyher, in *Proc. 5th Conf. Semi-insulating III-V Mateirals* (Malmö, Sweden, 1988) p. 499.
399. C. Frigeri and J.L. Weyher, *J. Appl. Phys. 65 (1989) 4646.*
400. M.R. Brozel, L. Brevik, D.J. Stirland, G.M. Williams and A.G. Cullis, *Appl. Phys. Sci.* **50** (1991) 475.
401. K. Iwaki, M. Imai and A. Nakamura, *J. Crystal Growth* **103** (1990) 257.
402. SEMI Standard, M36-0699 (annual publication from Semiconductor Equipment and Materials International).
403. J.S. Sewell, S.C. Dudley, M.G. Mier, D.C. Look and D.C. Walters, *J. Electron. Mater.* **18** (1989) 191.
404. S. Clark and D. J. Stirland, *Inst. Phys. Conf. Ser.* **60** (1981) 339.
405. T. Kitano, T. Ishikawa, H. Ono and J. Matsui, *Jpn. J. Appl. Phys.* **25** (1986) L530, L761.
406. S. Thono, S. Shinoyama and A. Katsui, *Appl. Phys. Lett.* **49** (1986) 1204.
407. T. Ishikawa, T. Kitano and J. Matsui, *J. Appl. Cryst.* **20** (1987) 344.
408. H. Ono, T. Kitano and J. Matsui, *Appl. Phys. Lett.* **51** (1987) 238.
409. R. Fornari, C. Paorici, V. Pessina and L. Zecchina, *High Temperatures-High Pressures* **20** (1988) 379.
410. E. Zielinska-Rohozinska, *J. Crystal Growth* **87** (1988) 154.
411. M.R. Brozel and S. Tuzemen, *Inst. Phys. Conf. Ser.* **135** (1994) 187.
412. M. Tajima, R. Toba, N. Ishida and M. Warashina, in *Proc. 1st Int. Conf. Mater. Microelectron.* (Barcelona, 1994) p. 1.
413. M. Yamada, M. Fukuzawa and K. Ito, *Inst. Phys. Conf. Ser.* **155** (1996) 901.
414. P. Rudolph, Ch. Frank-Rtsch, U. Juda, M. Naumann and M. Neubert, *J. Crystal Growth* **265** (2004) 331.
415. B. Birkmann, J. Stenzenberger, M. Jurisch, J. Hartwig, V. Alex and G. Muller, *J. Crystal Growth* **276** (2005) 335.
416. S.K. Maksimov, M. Ziegler, I.I. Khodos, I.I. Snighiryova and M. Sh. Shikhsaidov, *phys. stat. sol. (a)* **84** (1984) 79.
417. E. A. Lodge, G. R. Booker, C. A. Warwick and G. T. Brown, *Inst. Phys. Conf. Ser.* **76** (1985) 217.
418. S.P. Ardren, C.A.B. Ball, J.H. Neethling and H.C. Snyman, *J. Appl. Phys.* **60** (1986) 965.
419. Y. Nakada and T. Imura, *phys. stat. sol. (a)* **103** (1987) 85.
420. Y. Nakada and T. Imura, *phys. stat. sol. (a)* **102** (1987) 625.
421. M. Jimenez-Melendo, A. Djemel, J.P. Riviere, J. Castaing, C. Thomas and M. Duseaux, *Rev. Phys. Appl.* **23** (1988) 251.
422. P.M. Petroff and L.C. Kimerling, *Appl. Phys. Lett.* **29** (1976) 461.
423. P.W. Hutchinson and P.S. Dobson, *Phil. Mag. A* **41** (1980) 601.
424. T. Figielski, *Appl. Phys. A* **29** (1982) 199.
425. J.P. Cornier, M. Duseaux and J.P. Chevalier, *Inst. Phys. Conf. Ser.* **74** (1984) 95.
426. J.P. Cornier, M. Duseaux and J.P. Chevalier, *Appl. Phys. Lett.* **45** (1984) 1105.
427. T. Figielski, *Appl. Phys. A* **36** (1985) 217.
428. B.C. De Cooman and C.B. Carter, *Appl. Phys. Lett.* **50** (1987) 40.
429. P. Sitch, R. Jones, S. Oberg and M.I. Heggie, *Phys. Rev. B* **50** (1994) 17718.
430. S.K. Choi and M. Mihara, *J. Phys. Soc. Jpn.* **32** (1972) 1154.
431. V. Swaminathan and S.M. Copley, *J. Am. Cer. Soc.* **58** (1975) 482.
432. S.K. Choi, M. Mihara and T. Ninomiya, *Jpn. J. Appl. Phys.* **16** (1977) 737.
433. I. Yonenaga, K. Sumino and K. Yamada, *Appl. Phys. Lett.* **48** (1986) 326.
434. I. Yonenaga and K. Sumino, *J. Appl. Phys.* **62** (1987) 1212.
435. K. Sumino, *Oyo Buturi (Monthly Publ. Jpn. Soc. Appl. Phys.) (in japanese)* **56** (1987) 860.
436. I. Yonenaga and K. Sumino, *J. Appl. Phys.* **71** (1992) 4249.
437. I. Yonenaga and K. Sumino, *phys. stat. sol. (a)* **131** (1992) 663.
438. V. P. Kisel, S. A. Erofeeva and M. Sh. Shikhsaaidov, *Phil. Mag. A* **67** (1993) 343.

439. A.S. Jordan, A.R. Von Neida and R. Caruso, *J. Crystal Growth* **76** (1986) 243.
440. P. Liu and C. T. Tsai, *Computational Methods in Materials Processing* **MD-39** (1992) 17.
441. C. T. Tsai, A. N. Gulluoglu and C. S. Hartley, *J. Appl. Phys.* **73** (1993) 1650.
442. N. Miyazaki, Y. Kuroda and M. Sakaguchi, *J. Crystal Growth* **218** (2000) 221.
443. P. Dobrilla and J. S. Blakemore, *Appl. Phys. Lett.* **48** (1986) 1303.
444. P. Dobrilla and J. S. Blakemore, *J. Appl. Phys.* **60** (1986) 169
445. T. Iwaki, *J. Jpn. Assoc. Crystal Growth* **17** (1990) 39.
446. S. N. Zakhaarov, S. A. Laptev, V. M. Kaganer, V. T. Bublik and V. L. Indenbom, *phys. stat. sol. (a)* **131** (1992) 143.
447. K. Gomi and Y. Niitsu, *Adv. Elecron. Pack.* **EPP-Vol.19-1** (1997),1129.
448. Y. Okada, Y. Tokumaru and Y. Kadota, *Appl. Phys. Lett.* **48** (1986) 975.
449. J. Matsui, *Appl. Surf. Sci.* **50** (1991) 1.
450. K. Kuriyama and M. Satoh, *Oyo Buturi (Monthly Publ. Jpn. Soc. Appl. Phys.) (in japanese)* **57**(1988) 1374.
451. H. Ono, *J. Crystal Growth* **89** (1988) 209.
452. H. Lessoff and R. Gorman, *J. Electron. Mater.* **18** (1989) 407.
453. T. Ito, S. Ushio, Y. Kitagawara, H. Harada and T. Abe, in *Proc. 29th Semicon. Integ. Circuit Technol. Symp.* (1985) p. 155.
454. M. Nakajima, T. Katsumata, K. Terashima and K. Ishida, *Jpn. J. Appl. Phys.* 24 (1985), L65.
455. J.M. Parsey and F.A. Thiel, *J. Crystal Growth* **85** (1987) 327.
456. C. Frigeri, J.L. Weyher and L. Zanotti, *Mater. Res. Soc. Symp. Proc.* **138** (1989) 527.
457. C. Frigeri, J.L. Weyher and L. Zanotti, *J. Electrochem. Soc.* **136** (1989) 262.
458. K. A. Pandelisev, R. P. Bult and D. Freschi, in *Proc. 6th Conf. Semi-insulating III-V Materials* (Toronto, Adam Hilger, 1990) p. 167.
459. J. L. Weyher, P. J. van der Wel, G. Frigerio and C. Mucchino, in *Proc. 6th Conf. Semi-insulating III-V Materials* (Toronto, Adam Hilger, 1990) p. 161.
460. D.J. Carlson and A.F. Witt, *J. Crystal Growth* **108** (1991) 508.
461. P. Sucht, M. Duseaux, . Gillardin, J. Le Bris and G. M. Martin, *J. Appl. Phys.* **62** (1987) 3700.
462. T. Katoda and K. Yano, *Inst. Phys. Conf. Ser.* **91** (1987) 101.
463. D. J. Stirland, P. D. Augustus and B. W. Straughan, *J. Mater. Sci.* **13** (1978) 657.
464. A. G. Cullis, P. D. Augustus and D. J. Stirland, *J. Appl. Phys.* **51** (1980) 2556.
465. P. D. Augustus and D. J. Stirland, *J. Microscopy* **118** (1980) 111.
466. D. J. Stirland, P. D. Augustus, M. R. Brozel and E. J. Foulkes, in *Proc. 4th Conf. Semi-Insulating III-V Materials*, eds. D.C. Look and J.S. Blakemore (Shiva, Nantwich, 1984) p. 68.
467. T. Ogawa, in *Defect Recognition and Image Processing*, ed. by J. P. Fillard (Elsevier Sci, Amsterdam, 1985) p. 11.
468. M. Duseaux, S. Martin and J.P. Cevalier, in *Proc. 5th Conf. Semi-Insulating III-V Materials*, eds. H. Kukimoto and S. Miyazawa (Ohmsha, Tokyo, 1986) p. 221.
469. P. Sucht and M. Duseaux, *Inst. Phys. Conf. Ser.* **91** (1988) 375.
470. P. Sucht, M. Duseaux, C. Schiller and G. M. Martin, in *Proc. 5th Conf. Semi-insulating III-V Mateirals* (Malmö, Sweden, 1988) p. 483.
471. J.P. Fillard, P. Gall, J.L. Wehyer, M. Asgarinia and P.C. Montgomery, in *Proc. 5th Conf. Semi-insulating III-V Mateirals* (Malmö, Sweden, 1988) p. 537.
472. K. Yamada and J. Osaka, *J. Appl. Phys.* **63** (1988) 2609.
473. P. Gall, J. P. Fillard, M. Castagne, J. L. Weyher and J. Bonnafé, *J. Appl. Phys.* **64** (1988) 5161.
474. B-T. Lee, R. Gronsky and E. D. Bourret, *J. Appl. Phys.* **64** (1988) 114.
475. B-T. Lee, R. Gronsky and E. D. Bourret, *J. Crystal Growth***96** (1989) 333.
476. P. Sucht, M. Duseam, C. Shiller and G. M. Martin, in *Proc. 5th Conf. Semi-insulating III-V Mateirals* (Malmö, Sweden, 1988) p. 1.
477. B-T. Lee, E. D. Bourret, R. Gronsky, I. Park, *J. Appl. Phys.* **65** (1989) 1030.
478. D.J. Stirland, P. Kidd, G.R. Booker, S. Clark, D.T.J. Hurle, M.R. Brozel and I. Grant, *Inst. Phys.*

Conf. Ser. **100** (1989) 373.
479. J.L. Weyner, P. Gall, L.S. Dang, J.P. Fillard, J. Bonnafé, H. Rüfer, M. Baumgartner and K. Löhnert, *Semicon. Sci. Technlol.* **7** (1992) A36.
480. P. Schlossmacher, K. Urban and H. Rüfer, *J. Appl. Phys.* **71** (1992) 620.
481. K. Mizushima, Y. Ogiso, M. Furusawa, S. Sugwwara, Y. Imashimizu amd J. Watanabe, *J. Jpn. Assoc. Crystal Growth* **24** (1997) 254.
482. S. Martin, M. Dusseaux and M. Erman, *Inst. Phys. Conf. Ser.* **74** (1984) 53.
483. S. Martin, P. Sucht and G. M. Martin, in *Proc. 6th Conf. Semi-insulating III-V Materials* (Toronto, Adam Hilger, 1990) p. 1.
484. H. Yamamoto, O. Oda, M. Seiwa, M. Taniguchi, H. Nakata and M. Ejima, *J. Electrochem. Soc.* **136** (1989) 3098.
485. H. Yamamoto, H. Shimakura, G. Kano, M. Seiwa, H. Nakata and O. Oda, in *Defect Control in Semiconductors*, ed. by K. Sumino (North-Holland, Amsterdam, 1990) p. 1273.
486. B. Cockayne, W. R. MacEwan, I. R. Harris and N. A. Smith, *J. Crystal Growth* **88** (1988), 180.
487. G.M. Pennock, F.W. Schapink and J.L. Weyher, *J. Mater. Sci. Lett.* **7** (1988) 353.
488. P. Fornari, P. Franzosi, G. Salviati, C. Ferrari and C. Ghezzi, *J. Crystal Growth* **72** (1985) 717.
489. G. Frigero, C. Mucchino, J.L. Weyher, L. Zanotti and C. Paorici, *J. Crystal Growth* **99** (1990) 685.
490. M. E. Straumanis and C. D. Kim, Acta Crystallogr. **19** (1965) 256 .
491. H. R. Pottes and G. L. Pearson, *J. Appl. Phys.* **37** (1966) 2098 .
492. A. F. W. Willoughby, C. M. H. Driscoll, and B. A. Beiiamy, *J. Mater. Sci.* **6** (1971) 1389.
493. C.M.H. Driscoll and A.F.W. Willoughby, in *Defects in Semiconductors, Session 8* (1972) p. 46.
494. I. Fujimoto, *Jpn. J. Appl. Phys.* **23** (1984) L287.
495. Y. Takano, T. Ishiba, N. Matsunaga, and N. Hashimoto, *Jpn. J. Appl. Phys.* **24** (1985) L239.
496. Y. Okada, Y. Tokumaru, and Y. Kadota, *Appl. Phys. Lett.* **48** (1986) 975.
497. H. Kuwamoto and D. E. Holmes, *J. Appl. Phys.* **59** (1986) 656.
498. M. Nakajima, T. Sato, T. Inada, T. Fukuda, and K. Ishida, in *Proc. 5th Conf. Semi-Insulating III-V Materials*, eds. H. Kukimoto and S. Miyazawa (Ohmsha, Tokyo, 1986) p. 181.
499. K. Terashima, O. Ohmori, A. Okada, M. Watanabe, and T. Nakanishi, in *Proc. 5th Conf. Semi-Insulating III-V Materials*, eds. H. Kukimoto and S. Miyazawa (Ohmsha, Tokyo, 1986) p. 187.
500. T, Matsuzaki, Y. Tomotake, F. Yajima and T. Okano, *Jpn. J. Appl. Phys.* **25** (1986) 291.
501. A.N. Morozov and V.T. Bublik, *J. Crystal Growth* **75** (1986) 491.
502. A.N. Morozov and V.T. Bublik, *J. Crystal Growth* **75** (1986) 497.
503. Y. Tomotake, I. Matsuzaki and F. Yajima, *Mitsubishi Chem R&D Rev.* **1** (1987) 1.
504. Y. Okada and K. Fujii, *Mater. Sci. Forum* **117** (1993) 381.
505. N.F. Chen, Y. Wang, H. He, Z. Wang, L.Lin and O. Oda, *Appl. Phys. Lett.* **69** (1996) 1.
506. N. Chen, Y. Wang, H. He and L. Lin, *Phys. Rev. B* **54** (1996) 8516.
507. N.F. Chen, H. He, Y. Wang and L. Lin, *J. Crystal Growth* **173** (1997) 325.
508. K. Terashima, J. Nishio, A. Okada, S. Washizuka and M. Watanabe, *J. Crystal Growth* **79** (1986) 463.
509. K. Kuramoto, T. Sato and K. Ishida, *J. Electrochem. Soc.* **134** (1987) 1286.
510. K. Kurusu, Y. Suzuki and H. Takami, *J. Electrochem. Soc.* **136** (1989) 1450.
511. M. Cullen and J. M. P. Mearns, *Anal. Chimica Acta.* **277** (1993) 113.
512. H.E. Ruda, Q. Liu, M. Ozawa, S. Zukotynski, J.M. Parsey, Jr., T.J. O'neill, D.J. Lockwoods and B. Lent, *J. Phys. D: Appl. Phys.* **25** (1992) 1538.
513. D.T.J. Hurle, *J. Phys. Chem. Solids* **40** (1979) 613, 627, 639, 647.
514. D.T.J. Hurle, *J. Appl. Phys.* **85** (1999) 6957.
515. J.C. Bourgoin and H.J. von Bardeleben, *J. Appl. Phys.* **64** (1988) R65.
516. R.W. Jansen and O.F. Sankey, *Phys. Rev. B* **39** (1989) 3192.
517. T.Y. Tan, *Mater. Sci. Engineer.* **B10** (1991) 227.
518. T.Y. Tan, *J. Phys. Chem. Solids* **55** (1994) 917.
519. N.P. Il'in and V.F. Masterov, *Sov. Phys. Semicond.* **10** (1978) 496.

520. G.A. Baraff and M. Schluterm, *Phys. Rev. Lett.* **55** (1985) 1326.
521. G.A. Baraff and M. Schluterm, *Phys. Rev. B* **33** (1986) 7346.
522. D.J. Chadi and s.B. Zhang, *Phys. Rev. B* **41** (1990) 5444.
523. H. Xu and U. Lidefelt, *Phys. Rev. B* **41** (1990) 5979.
524. G. Cox, K.H. Graf, D. Szynka, U. Poppe and K. Urban, *Vacuum* **41** (1990) 591.
525. U. Gosele, T.Y. Tan, M. Uematsu and K. Wada, *Mater. Sci. Forum* **117** (1993) 53.
526. S. Dannefaer, B. Hogg and D. Kerr, *Phys. Rev. B* **30** (1984) 3355.
527. S. Dannefaer and D. Kerr, *J. Appl. Phys.* **60** (1986) 591..
528. S. Brehme and R. Pickenhain, *Solid State Commun.* **59** (1986) 469.
529. M. Henini, B. Truck and C.J. Paull, *Solid-State Electron.* **29** (1986) 483.
530. Y. Kitagawara, N. Noto, T. Takahashi and T. Takenaka, *Appl. Phys. Lett.* **48** (1986) 1664.
531. G. Marrakchi, D. Barbier, G. Guillot and A. Nouailhat, *J. Appl. Phys.* **62** (1987) 2742.
532. K. Sassa, K. tomizawa, Y. Shimanuki and J. Nishizawa, *Inst. Phys. Conf. Ser.* **91** (1988) 81.
533. L. Montellius, S. Nilsson and L. Samuelson, in *Proc. 5th Conf. Semi-insulating III-V Mateirals* (Malmö, Sweden, 1988) p. 361.
534. L. Montellius, S. Nilsson, L. Samuelson, E. Janzen and M. Ahlström, *J. Appl. Phys.* **64** (1988), 1564.
535. P. Dobrilla, *J. Appl. Phys.* **64** (1988) 6767.
536. R. Fornari, E. Gombia and R. Mosca, *J. Electron. Mater.* **18** (1989) 151.
537. O. Breitestein, *Rev. Phys. Appl.* **24** (1989) C6-101.
538. V. Pandian, Y.N. Mohapatra and V. Kumar, *Jpn. J. Appl. Phys.* **30** (1991) 2815.
539. K.-H. Ko and J.-H. Ahn, *J. Korean Cer. Soc.* **28** (1991) 141.
540. T. Neffati and J.C. Bourgoin, *phys. stat. sol. (b)* **203** (1997) 459.
541. J.P. Fillard, M. Castagne, J. Bonnafe and M. de Murcia, *J. Appl. Phys.* **54** (1983) 6767.
542. J.P. Fillard, J. Bonnafe and M. Castagne, *J. Appl. Phys.* **56** (1984) 3020.
543. M. Tomozane and Y. Nannichi, *Jpn. J. Appl. Phys.* **25** (1986) L273.
544. M. Tomozane, Y. Nannichi, I. Onodera, T. Fukase and F. Hasegawa, *Jpn. J. Appl. Phys.* **27** (1988) 260.
545. Y.N. Mohapatra and V. Kumar, *J. Appl. Phys.* **64** (1988) 956.
546. H. Witte, W. Siegel, G. Kuhnel, T. Flade and H.A. Schneider, *phys. stat. sol. (a)* **117** (1990) 527.
547. Z-Q. Fang and D.C. Look, *J. Appl. Phys.* **69** (1991) 8177.
548. Z-Q. Fang and D.C. Look, *J. Appl. Phys.* **73** (1993) 4971.
549. J. Vaitkus, V. Kazukauskas, R. Kiliulis and J. Storasta, *Inst. Phys. Conf. Ser.* **136** (1993) 755.
550. Z-Q. Fang, D.C. Look, H. Yamamoto and H. Shimakura, *Appl. Phys. Lett.* **69** (1996) 3417.
551. D. Kabiraj and S. Ghosh, *Appl. Phys. Lett.* **84** (2004) 1713.
552. A.V. Markov, E.M. Omel'yanovski, V.B. Osvenskii, A.Ya. Polyakov, I.A. Koval'chuk, V.I. Raikhshtein and M.V. Tishkin, *Sov. Phys. Semicond.* **22** (1988) 27.
553. P. Kaminski and H. Thomas, *Acta Phys. Polonica* A77 (1990) 87.
554. M.R. Burd and R. Baunstein, *J. Phys. Chem. Solids* **49** (1988) 731.
555. E.K. Kim, H.Y. Cho, S.-K. Min, S.H. Choh and S. Namba, *J. Appl. Phys.* **67** (1990) 1380.
556. J. Nishizawa, Y. Oyama and K. Dezaki, *J. Appl. Phys.* **69** (1991) 1446.
557. T. Okumura, in *New Compound Semiconductor Handbook*, ed. T. Ikoma (Science Forum, Tokyo, 1982) p. 249.
558. G. M. Martin, A. Mitonneau and A. Mircea, *Electron. Lett.* **13** (1977) 191.
559. A. Mircea and D. Bois, *Inst. Phys. Conf. Ser.* **46** (1979) 82.
560. G.M. Martin, in *Proc. 2nd Conf. Semi-Insulating III-V Materials*, ed. G.J. Rees (Nantwich, Shiva, 1980) p. 13.
561. G. M. Martin and S. Makram-Ebeid, *Acta Electronica* **25** (1983) 133.
562. D.I. Desnica, *J. Electron. Mater.* **21** (1992) 463.
563. D.C. Look, in *Semiconductors and Semimetals Vol. 38*, eds. R.K. Willardson and A.C. Beer (Academic Press, New York, 1991) p. 91.

564. M. Taniguchi and T. Ikoma, *Oyo Buturi (Monthly Publ. Jpn. Soc. Appl. Phys.) (in japanese)* **7** (1984) 619.
565. S. Makram-Ebeid, P. Langlade and G. M. Martin, in *Proc. 4th Conf. Semi-Insulating III-V Materials*, eds. D.C. Look and J.S. Blakemore (Shiva, Nantwich, 1984) p. 184.
566. H. C. Gatos and J. Lagowski, in *Microscopic Identification of Electronic Defects in Semiconductors*, eds. by N. M. Johnson, S. G. Bishop and G. D. Watkins (Mater. Res. Soc., Pittsburgh, PA, 1985) p. 153.
567. G. M. Martin and S. Makram-Ebeid, in *Deep Centers in Semiconducrors*, ed. S. T. Pantelides (Gordon and Breach, New York, 1986) p. 399.
568. T. Ikoma and Y. Mochizuki, *J. Jpn. Assoc. Crystal Growth* **28** (1986) 103.
569. H. J. von Baardeleben, D. Stievenard, D. Deresmes, A. Huber and J. C. Bourgoin, *Phys. Rev. B* **34** (1986) 7192.
570. P. Trautman and J.M. Baranowski, *Int. J. Modern Phys.* **11** (1995) 1263.
571. G. M. Martin, *Appl. Phys. Lett.* **39** (1981) 747.
572. M Kaminska, M. Skowronski, J. Lagowski, J.M. Parsey and H.C. Gatos, *Appl. Phys. Lett.* **43** (1983) 302.
573. M. Castagne, J.P. Fillard and J. Bonnafe, *Solid State Commun.* **54** (1985) 653.
574. M. Skowronski, J. Lagowski and H. C. Gatos, *J. Appl. Phys.* **59** (1986) 2451.
575. J.P. Walczak, M. Kaminska and J.M. Baranowski, *Acta Phys. Polonica* **A71** (1987) 337.
576. C. Song, W. Ge, D. Jiang and C. Hsu, *Appl. Phys. Lett.* **50** (1987) 1666.
577. H.J. von Bardeleben, N.T. Bagraev and J.C. Bourgoin, *Appl. Phys. Lett.* **51** (1987) 1451.
578. F. Fuchs and B. Dischler, *Appl. Phys. Lett.* **51** (1987) 679.
579. F. Fuchs and B. Dischler, *Appl. Phys. Lett.* **51** (1987) 2115.
580. J. Lagowski, M. Bugajski, M. Matsui and H.C. Gatos, *Appl. Phys. Lett.* **51** (1987) 511.
581. W. Kuszko, M. Jezewski, M. Kaminska and J.M. Baranowski, *Crystal Prop. Prep.* **12** (1987) 195.
582. D.W. Fischer, *Appl. Phys. Lett.* **50** (1987) 1751.
583. P. Silverberg, P. Omling and L. Samuelson, *Appl. Phys. Lett.* **52** (1988) 1689.
584. Z. Zhong, D. Jiang, W. Ge and C. Song, *Appl. Phys. Lett.* **52** (1988) 628.
585. M. Tajima, H. Saito, T. Iino and K. Ishida, *Jpn. J. Appl. Phys.* 27 (1988) L101.
586. P. Trautmann, J.P. Walczak, M. Kaminska and J.M. baranowski, *Acta Phys. Polonica* **A73** (1988) 419.
587. W. Kuszko, M. Jezewski, M. Kaminska and J.M. Baranowski, *Acta Phys. Polonica* **A73** (1988) 215.
588. M. Jordan, T. Hangleiter and J.-M. Spaeth, *Semicon. Sci. Technol.* 7 (1992) 725.
589. J. Jimenez, A. Alvarez and M. Chafai, *Phys. Rev B* **50** (1994) 14112.
590. C. Le Berre, C. Corbel, M.R. Brozel, S. Kuisma, K. Saarinen and P. Hautojarvi, *J. Phys: Condens. Mater.* **6** (1994) L759.
591. M. Tajima, *Oyo Buturi (Monthly Publ. Jpn. Soc. Appl. Phys.) (in japanese)* **57** (1988) 2.
592. G. M. Martin, G. Jacob, G. Poiblaud, A. Goltzene and C. Shcwab, *Inst. Phys. Conf. Ser.* **59** (1982) 281.
593. J. Blanc and L. R. Sweisberg, *Nature* **192** (1961) 155.
594. A. D. Jonath and R. H. Bube, *J. Appl. Phys.* **46** (1975) 1745.
595. H. J. Stocker, *J. Appl. Phys.* **48** (1977) 4583.
596. P. K. Vasudev and R.. H. Bube, *Solid State Commun.* **27** (1978) 1095.
597. A.M. Huber, N.T. Linh, M. Valladon, J.L. Debrun, G.M. Martin, A. Mitonneau and A. Mirea, *J. Appl. Phys.* **50** (1979) 4022.
598. F. Hasegawa and A. Majerfeld, *Electron. Lett.* **11** (1975) 286.
599. E. R. Weber, H. Fnnen, U. Kaufmann, J. Windscheif, J. Schneider, and T. Wosinski, *J. Appl. Phys.* **53** (1982) 6140.
600. J. Lagowski, H. C. Gatos, J. M. Parsey, K. Wada, M. Kaminska and W. Walukewicz, *Appl. Phys. Lett.* **40** (1982) 342.

601. J. Lagowski, J. M. parsey, M. Kaminska, K. Wada, and H. C. Gatos, in *Proc. 3rd Conf. Semi-Insulating III-V Materials*, eds. S. Makram-Ebeid adn B. Tuck, (Nantwich, Shiva, 1982) p. 154.
602. J. Lagowski, H. C. Gatos, J. M. Parsey, M. Kaminska and W. Walukewicz, *Inst. Phys. Conf. Ser.* **65** (1982) 41.
603. Y. Zou, *Inst. Phys. Conf. Ser.* **63** (1982) p. 185.
604. M. Taniguchi and T. Ikoma, *J. Appl. Phys.* **54** (1983) 6448.
605. Y. Imamura and J. Osaka, *Jpn. J. Appl. Phys.* **22** (1983) L333.
606. M. O. Watanabe, A. Tanaka, T. Udagawa, T. Nakanishi and Y. Zohta, *Jpn. J. Appl. Phys.* **22** (1983) 923.
607. T. Figielski, T. Wosinski and A. Morawski, *J. Phys.* 44 (1983) C4-353.
608. T. Figielski and T. Wosinski, *Czech J. Phys.* **B34** (1984) 403.
609. E. Weber, in *Proc. 4th Conf. Semi-Insulating III-V Materials*, eds. D.C. Look and J.S. Blakemore (Shiva, Nantwich, 1984) p. 296
610. T. Ikoma, M. Taniguchi and Y. Mochizuki, *Inst. Phys. Conf. Ser.* **74** (1984) 65.
611. J. Lagowski, D. G. Lin, T. Aoyama and H. C. Gatos, *Appl. Phys. Lett.* **44** (1984) 336.
612. J.P. Fillard, J. Bonnafe and M. Castagne, *Solid State Commun.* **52** (1984) 855.
613. B.K. Meyer, J.-M. Spaeth and M. Scheffler, *Phys. Rev. Lett.* **52** (1984) 851.
614. K. Elliott, R.T. Chen, S.G. Greenbaum and R.J. Wagner, *Appl. Phys. Lett.* **44** (1984) 907.
615. M. Deiri, K.P. Homewood and B.C. Cavenett, *J. Phys. C* **17** (1984) L627.
616. K. Wada and N. Inoue, *Appl. Phys. Lett.* **47** (1985) 945.
617. M. Kaminska, in *Proc. 17th Conf. Phys. Semicon.* (San Francisco, 1984) p. 741.
618. M. Kaminska, M. Skowronski, and W. Kuszko, *Phys. Rev. Lett.* **55** (1985) 2204.
619. G. A. Baraff and M. Schluter, *Phys. Rev. Lett.* **55** (1985) 2340.
620. A.N. Morozov, V.T. Bublik, O. Yu. Morozova, *Cryst. Res. Technol.* **21** (1986) 859.
621. P. Omling, E.R. Weber and L. Samuelson, *Phys. Rev. B* **33** (1986) 5880.
622. W. Frank, in *Proc. 12th Int. Symp.CaAs and Related Compounds*, ed. M. Fujimoto (Hilger, Bristol, 1986) p. 217.
623. T. A. Kennedy, in *Proc. 14th Int. Conf. Defects in Semiconductors*, ed. by H. J. von Bardeleben (Aedermannsdorf, Switzerland, 1986) p. 293.
624. H. J. von Bardeleben, D. Stievenard, D. Deresmes, A. Huber, and J. C. Bourgoin, *Phys. Rev. B* **34** (1986) 7192.
625. B. Dischler, F. Fuchs and U. Kaufmann, *Appl. Phys. Lett.* **48** (1986) 1282.
626. J. Wu, Y. Zou and P. Mo, *Mater. Lett.* **5** (1986) 29.
627. H. Hasegawa and H. Ono, *Jpn. J. Appl. Phys.* **25** (1986) L319.
628. T. Hariu, T. Sato, H. Komori and K. Matsushita, *J. Appl. Phys.* **61** (1987) 1068.
629. T. Figielski and T. Wosinski, *Phys. Rev. B* **36** (1987) 1269.
630. B. K. Meyer, D. M. Hofmann, J. R. Niklas, and J. M. Spaeth, *Phys. Rev. B* **36** (1987) 1332 .
631. G. A. Baraff and M. Schluter, *Phys. Rev. B* **35** (1987) 6154.
632. G. A. Baraff, M. Lanno and M. Schluter, *Phys. Rev. B* **38** (1987) 6003.
633. H.J. von Bardeleben, J.C. Bourgoin, D. Stievenard and M. Lannoo, *Inst. Phys. Conf. Ser.* **91** (1987) 399.
634. R.A. Morrow, *J. Mater. Rev.* **2** (1987) 681.
635. Y. Zou, *Mater. Lett.* **5** (1987) 203.
636. J. F. Wagner and J. A. Van Vechten, *Phys. Rev. B* **35** (1987) 2330.
637. M. Kaminska, *Phys. Script.* **T19** (1987) 551.
638. J.L. Lagowski, M. Matsui, M. Bugajski, C.H. Kang, M. Skowronski, H.C. Gatos, M. Holinkis, E.R. Weber and W. Walukiewicz, *Inst. Phys. Conf. Ser.* **91** (1987) 395.
639. J.-M. Spaeth, D.M. Hofman, M. Heinemann and B.K. Meyer, *Inst. Phys. Conf. Ser.* **91** (1988) 391.
640. D. J. Chadi and K. J. Chang, *Phys. Rev. Lett.* **60** (1988) 2187.
641. J. Dabrowski and M. Scheffler, *Phys. Rev. Lett.* **60** (1988) 2183.
642. M. Suezawa and K. Sumino, *Jpn. J. Appl. Phys.* **27** (1988) L18.

643. G. Wang, Y. Zou, S. Benakki, A. Goltzene and C. Schwab, *J. Appl. Phys.* **63** (1988) 2595.
644. D.W. Fisher, *Phys. Rev.* **37** (1988) 2968.
645. H. Hoinkis, E. R. Weber, W. Walukiewicz, J. Lagowski, M. Matsui, H. C. Gatos, B. K. Meyer and J. M. Spaeth, *Phys. Rev. B* **39** (1989) 5538.
646. M. O. Manasreh, d. W. Fisher and W. C. Mitchel, *phys. stat. sol. (b)* **154** (1989) 11.
647. J. Dabrowski and M. Scheffler, *Phys. Rev. B* **40** (1989) 10391.
648. C. Minot and C. Demangeat, *J. Chem. Phys.* **87** (1990) 931.
649. S. W. Biernacki, *Solid State Commun.* **91** (1994) 245.
650. A. Alvarez, J. Jimenez and M.A. Gonzalez, *Appl. Phys. Lett.* **68** (1996) 2959.
651. M. R. Brozel, I. Grant, R. M. Ware and D. J. Stirland, *Appl. Phys. Lett.* **42** (1983) 610.
652. F. Hasegawa, N. Iwata, N. Yamamoto and Y. Nannichi, *Jpn. J. Appl. Phys.* **22** (1983) L502.
653. D.E. Holmes, R.T. Chen, K.R. Elliot and C.G. Kirkpatrick, *Appl. Phys. Lett.* **43** (1983) 305.
654. D.E. Holmes, R.T. Chen and J. Yang, *Appl. Phys. Lett.* **42** (1983) 419.
655. J.P. McCann, M.R. Brozel and L. Eaves, J. *Phys. D: Appl. Phys.* **17** (1984) 1831.
656. B. Gouteraux, N. Visentin, B. Lent and M. Bonnet, *Inst. Phys. Conf. Ser.* **74** (1984) 89.
657. M.R. Brozel, E.J. Foulkes and D.J. Stirland, *Inst. Phys. Conf. Ser.* **74** (1984) 59.
658. M. S. Skolnick, M. R. Brozel, L. J. Reed, I. Grand. D. J. Stirland and R. M. Ware, *J. Electronic Mater.* **13** (1984) 107.
659. D.A.O. Hope, M.S. Skolnick, B. Cockayne, J. Woodhead and R.C. Newman, *J. Crytal Growth* **71** (1985) 795.
660. F.-C. Wang, *J. Appl. Phys.* **59** (1986) 3737.
661. M.L. Gray, L. Sargent, J.S. Blakemore, J.M. Parsey, Jr. and J.E. Clemens, *J. Appl. Phys.* **63** (1988) 5689.
662. J.P. Fillard, P. Gall, M. Asgarinia, M. Castagne and M. Baroudi, *Jpn. J. Appl. Phys.* **27** (1988) L899.
663. J.P. Fillard, P. Montgomery, A. Baroudi, J. Bonnafe and P. Gall, *Jpn. J. Appl. Phys.* **27** (1988) L258.
664. J.P. Fillard, P. Montgomery, P. Gall, M. Gsgarinia and J. Bonnafe, *Jpn. J. Appl. Phys.* **27** (1988) 384.
665. H.Ch. Alt and H. Schink, *Appl. Phys. Lett.* **52** (1988) 1661.
666. A. Usami, A. Kitagaw a and T. Wada, *Mater. Res. Soc. Symp. Proc.* **146** (1989) 419.
667. M.R. Brozel and S. Tüzemen, *Mater. Sci. Engineer.* **B28** (1994) 130.
668. P. Dobrilla, J. S. Blakemore, A. J. McVamant, K. R. Gleason and R. Y. Koyama, *Appl. Phys. Lett.* **47** (1985) 602.
669. R. Anholt and T. W. Sigmon, *J. Appl. Phys.* **62** (1987) 3995.
670. J. Nishizawa, Y. Oyama and K. Dezaki, *J. Appl. Phys.* **69** (1991) 1446.
671. S. Tüzemen, L. Breivik and M. R. Brozel, *Semicon. Sci. Technol.* **7** (1992) A36.
672. C. Corbel, M. Stucky, P. Hautojärvi, K. Saarinen and P. Moser, *Phys. Rev. B* **38** (1988) 8192.
673. Z.-Q. Fang, T.E. Schlesinger and A.G. Milnes, *J. Appl. Phys.* **61** (1987) 5047.
674. J. Samitier, A. Herms, A. Cornet and J.R. Morante, *Phys. Script.* **35** (1987) 521.
675. M. Levinson, *Inst. Phys. Conf. Ser.* **91** (1988) 73.
676. T. Hashizume and H. Nagabuchi, *Semicond. Sci. Technol.* **4** (1989) 427.
677. S. M. Sze, *Physics of Semiconductor Devices* (John Wiley & Sons, New York, 1981) p. 21.
678. F.J. Reid, in *Compound Semiconductors, Vol. 1, Preparation of III-V Compounds*, eds. R.K. Willardson and H.L. Goering (Reinhold, New York, 1962) p. 158.
679. D.L. Rode and S. Knight, *Phys. Rev. B* **3** (1971) 2534.
680. W. Walukiewicz, L. Lagowski, L. Jastrzebski, M. Lichtensteiger and H.C. Gatos, *J. Appl. Phys.* **50** (1979) 899.
681. W. Walukiewicz, J. Lagowski and H.C. Gatos, *J. Appl. Phys.* **53** (1982) 769.
682. W. Walukiewicz, L. Wang, L.M. Pawlowicz, J. Lagowski and H.C. Gatos, *J. Appl. Phys.* **59** (1986) 3144.

683. C.S. Chang and H.R. Fetterman, *Solid-State Electron.* **29** (1986) 1295.
684. J. Xu, B.A. Bernhardt, M. Shur, C.-H. Chen and A. Peczalski, *Appl. Phys. Lett.* **49** (1986) 342.
685. J.J. Winter, H.A. Leupold, A. Ballato and T. Monahan, *J. Appl. Phys.* **61** (1987) 444.
686. R. Fornari, *Solid State Commun.* **29** (1986) 589.
687. J.F. Woods and N.G. Ainslie, *J. Appl. Phys.* **34** (1963) 1469.
688. R. Fornari, *J. Crystal Growth* **94** (1989) 433.
689. C.H. Gooch, C. Hilsum and B.R. Holeman, *J. Appl. Phys. Suppl.* **32** (1961) 2069.
690. R.W. Haisty, E.W. Mehal and R. Stratton, *J. Phys. Chem. Solids* **23** (1962) 829.
691. G. R. Cronin and R. W. Haisty, *J. Electrochem. Soc.* **111** (1964) 874.
692. R. Zucca, *J. Appl. Phys.* **48** (1977) 1987.
693. P.F. Lindquist, *J. Appl. Phys.* **48** (1977) 1262.
694. D. C. Look, *J. Appl. Phys.* **48** (1977) 5141.
695. G.M. Martin, in *Semi-insulating III-V Materials*, ed. G.J. Rees (Shiva, 1980) p. 13.
696. G. M. Martin, J. P. Farges, G. Jacob, J. P. Hallais and G. Poiblaud, *J. Appl. Phys.* **51** (1980) 2840.
697. J.S. Blakemore, *J. Appl. Phys.* **53** (1982) 520.
698. D. E. Holmes, R. T. Chen, K. R. Elliot, C. G. Kirkpatrick and P. W. Yu, *IEEE Trans. Electron Devices* **ED-29** (1982) 1045.
699. D.C. Look, D.C. Walters and J.R. Meyer, *Solid State Commun.* **42** (1982) 745.
700. E.J. Johnson, J.A. Kafalas and R.W. Davies, *J. Appl. Phys.* **54** (1983) 204.
701. S. Martin and G. Jacob, *Acta Electronica* **25** (1983) 123.
702. M. Bonnet, V. Visentin, B. Lent and C. Raffet, *Rev. Tech. Thomson-CSF* **15** (1983) 39.
703. W. Walukiewicz, J. Lgowski and H.C. Gatos, *Appl. Phys. Lett.* **43** (1983) 112.
704. T. Hashizume, *Bull. Kushiro National College Technol. (in japanese)* **18** (1984) 75.
705. L'. Hrivnák, *Czech. J. Phys. B* **34** (1984) 436.
706. W. Walukiewicz, *Phys. Rev. B* **37**(1988) 4760.
707. R. Fornari and L. Dozsa, *phys. stat. sol. (a)* **105** (1988) 21.
708. R.S. Tang, L. Sargent and J.S. Blakemore, *J. Appl. Phys.* **66** (1989) 256.
709. S.K. Brierley and H.T. Hendriks, *J. Appl. Phys.* **67** (1990) 6306.
710. W. Siegel, G. Kuhnel, H.A. Schneider, H. Witte and T. Flade, *J. Appl. Phys.* **69** (1991) 2245.
711. M. Suemitsu, M. Nishijima and N. Miyamoto, *J. Appl. Phys.* **69** (1991) 7240.
712. M. Jordan, M. Linde, T. Hangleiter and J.-M. Spaeth, *Semicon. Sci. Technol.* **7** (1992) 731.
713. Y. Otoki, S. Okubo, S. Shinzawa and S. Kuma, *Hitachi Cable Rev.* **11** (1992) 37.
714. M. Baeumler, U. Kaufmann, P. Mooney and J. Wagner, in *Proc. 6th Conf. Semi-insulating III-V Materials* (Toronto, Adam Hilger, 1990) p. 29.
715. D. E. Holmes, R. T. Chen, K. R. Elliott and C. G. Kirkpatrick, *Appl. Phys. Lett.* **57** (1990) 2464.
716. R. T. Chen, D. E. Holmes and P. M. Asbeck, *Appl. Phys. Lett.* **45** (1984) 459.
717. T. Obokata, H. Okada, T. Katsumata and T. Fukuda, *Jpn. J. Appl. Phys.* **25** (1986) L179.
718. Y. Nakamura, Y. Otsuki, T. Kikuta and Y. Kashiwayanagi, *Furukawa Electrics Rev.* **79** (1986) 37.
719. S. Chichibu, S. Matsumoto and T. Obokata, *J. Appl. Phys.* **62** (1987) 4316.
720. R.K. Boncek and D.L. Rode, *J. Appl. Phys.* **64** (1988) 6315.
721. M. Baumgartner, K. Löhnert, G. Nagel, H. Rüfer and E. Tomzig, *Inst. Phys. Conf. Ser.* **91** (1988) 97.
722. J. Wagner and H. Seelewind, *J. Appl. Phys.* **64** (1988) 2761.
723. N. Ohkubo, S. Chichibu and S. Matsumoto, *Appl. Phys. Lett.* **53** (1988) 1054.
724. P. J. Pearah, R. Tobin, J. P. Tower and R. M. Ware, in *Proc. 5th Conf. Semi-insulating III-V Mateirals* (Malmö, Sweden, 1988) p. 195.
725. R.M. Ware, P.J. Doering, B. Freidenreich, R.T. Koegl and T. Collins, *Semicon. Sci. Technol.* **7** (1992) A224.
726. Y. Otoki, M. Sahara, S. Shinzawa and S. Kuma, *Mater. Sci. Forum* **117-118** (1993) 405.
727. T.M. Schmidt, P.P.M. Venezuela, M.J. Caldas and A. Fazzio, *Appl. Phys. Lett.* **66** (1995) 2715.
728. W.J. Moore and R.L. Henry, *Appl. Phys. Lett.* **70** (1997) 738.

729. Y. Matsumoto and H. Watanabe, *Jpn. J. Appl. Phys.* **21** (1982) L515.
730. T. Matsumura, H. Emori, K. Terashima and T. Fukuda, *Jpn. J. Appl. Phys.* **22** (1983) L154.
731. N. Visentin, M. Bonnet, B. Gouteraaux, B. Lent and A. Lordereau, *Rev. Tech. Thomson-CSF* **16** (1984) 261.
732. D.C. Look and E. Pimentel, *Appl. Phys. Lett.* **51** (1987) 1614.
733. E. Pimentel and D.C. Look, *J. Electron. Mater.* **17** (1988) 63.
734. A.V. Kartavykh, S.P. Grishina, M.G. Mil'vidskii, N.S. Rytova, I.V. Stepantsova and E.S. Yurova, *Sov. Phys. Semicond.* **22** (1988) 633.
735. W. Siegel, H. Witte and G. Kuhnel, *phys. stat. sol. (a)* **112** (1989) K35.
736. J. Wagner, W. Wettling, J. Windscheif and W. Rothemund, *J. Appl. Phys.* **65** (1989) 5225.
737. P.D. Mumford and D.C. Look, *Rev. Sci. Instrum.* **62** (1991) 1666.
738. A. Usami, A. Kitagawa and T. Wada, *Appl. Phys. Lett.* **54** (1989) 831.
739. A. Usami, in *Semiconductor Research Vol. 31 (in japanese)*, ed. J. Nishizawa (Kogyo Chosakai, Tokyo, 1989) p. 37.
740. P.D. Mumford and D.C. Look, *Rev. Sci. Instrum.* **62** (1991) 1666.
741. W. Siegel, G. Kuhnel and U. Kretzer, *Mater. Sci. Engineer.* **B28** (1994) 84.
742. S. Asai, N. Goto and T. Nozaki, *IEICE Tech. Rep.* **CPM87** (1987) 55.
743. *Properties of Gallium Arsenide, EMIS Datareviews Series No.2* (INSPEC, 1986).
744. T. Kikuta, K. Terashima and K. Ishida, *Jpn. J. Appl. Phys.* **22** (1983) L541.
745. P.W. Yu, *Phys. Rev. B* **29** (1984) 2283
746. M. Tajima, in *Proc. 5th Conf. Semi-insulating III-V Mateirals* (Malmö, Sweden, 1988) p. 119.
747. M. Tajima and T. Iino, *Jpn. J. Appl. Phys.* **28** (1989) L841.
748. Y. Mori, Y. Yoshimura, H. Kamoda, H. Ohkura and Y. Shiba, *Jpn. J. Appl. Phys.* **28** (1989) L.417.
749. J. T. Hsu, T. Nishino and Y. Hamakawa. *Jpn. J. Appl. Phys.* **26** (1987) 685.
750. T. Hiramoto and T. Ikoma, in *Proc. 5th Conf. Semi-insulating III-V Mateirals* (Malmö, Sweden, 1988) p. 337.
751. C.J. Miner, A.J. Springthorpe, C. Blaauw, T. Lester and F.R. Shepherd, in *Proc. 5th Conf. Semi-Insulating III-V Materials*, eds. H. Kukimoto and S. Miyazawa (Ohmsha, Tokyo, 1986) p. 261.
752. T. Kazuno, Y. Sawada and T. Yokoyama, *Jpn. J. Appl. Phys.* **25** (1986) L878.
753. C.K. Teh, J. Tuszynski and F.L. Weichman, *J. Mater. Res.* **5** (1990) 365.
754. D. Kirillov, M. Vichr and R. A. Powell, *Appl. Phys. Lett.* **50** (1987) 262.
755. M. Tajima and Y. Okada, *Physica* **116B** (1983) 404.
756. K. Kitahara, M. Ozeki and A. Shibatomi, *Jpn. J. Appl. Phys.* **23** (1984), 207.
757. M. Yokogawa, S. Nishine and Y. Aota, *Sumitomo Electrics (in japanese)* **125** (1984) 141.
758. H.J. Hovel and D. Guidotti, *IEEE Trans. Electron Devices* **ED-32** (1985) 2331.
759. H.J. Hovel, M. Albert, E. Farrell, D. Guidotti and J. Bekcer, in *Proc. 5th Conf. Semi-Insulating III-V Materials*, eds. H. Kukimoto and S. Miyazawa (Ohmsha, Tokyo, 1986) p. 97.
760. S. Shinzawa, A. Hattori, Y. Otoki and S. Okubo, *Hitachi Cables (in japanese)* **6** (1987) 41.
761. K. Leo, W.W. Ruhle and N.M. Haegel, *J. Appl. Phys.* **62** (1987) 3055.
762. J. Oswald and J. Pastrnak, *Crystal Prop. Prep.* **12** (1987) 207.
763. W.W. Ruhle, K. Leo and N.M. Haegel, *Inst. Phys. Conf. Ser.* **91** (1988) 105.
764. P. Deconinck, L. Allain, G. Gillardin, J. Maluenda, J.P. Farges, G.M. Martin, G. Nagel and K. Lohnert, in *Proc. 5th Conf. Semi-insulating III-V Mateirals* (Malmö, Sweden, 1988) p. 531.
765. M. Tajima, *Appl. Phys. Lett.* **53** (1988) 959.
766. M. Tajima, *Jpn. J. Appl. Phys.* **27** (1988) L1323.
767. P. Santhanaraghavan, K. Sankaranarayanan, J. Arokiaraj, S. Anbukumar, J. Kumar and P. Ramasamy, *phys. stat. sol. (a)* **142** (1994) 521.
768. T. Kikuta, T. Katsumata, T. Obokata and K. Ishida, *Inst. Phys. Conf. Ser.* **74** (1984) 47.
769. J.L. Wehyer, L.S. Dang and E.P. Visser, *Inst. Phys. Conf. Ser.* **91** (1987) 109.
770. S.K. Krawczyk, M. Garrigues, A. Khoukh, C. Lallemand and K. Schobe, in *Proc. 5th Conf. Semi-insulating III-V Mateirals* (Malmö, Sweden, 1988) p. 555.

771. M. Tajima, Y. Kawate, R. Toba, M. Warashina and A. Nakamura, *Inst. Phys. Conf. Ser.* **149** (1996) 257.
772. P.W. Yu, D.C. Look and W. Ford, *J. Appl. Phys.* **62** (1987) 2960.
773. N.M. Haegel, A. Winnacker, K. Leo, W.W. Ruhle and S. Gisdakis, *J. Appl. Phys.* **62** (1987) 2946.
774. V. Swaminathan, R. Caruso and S.J. Pearton, *J. Appl. Phys.* **63** (1988) 2164.
775. A. Usami. A. Kitagawa and T. Wada, *Appl. Phys. Lett.* **54** (1989) 831.
776. C. Chao, V.A. Bykovskii and M.I. Tarasik, *Semiconductors* **28** (1994) 19.
777. G. Koschek, H. Lakner and E. Kubalek, *phys. stat. sol. (a)* **106** (1988) 651.
778. Y. Tokumaru and Y. Okada, *Jpn. J. Appl. Phys.* **23** (1984) L64.
779. A.K. Chin, R. Caruso, M.S.S. Young and A.R. Von Neida, *Appl. Phys. Lett.* **45** (1984) 552.
780. C.A. Warwick and G.T. Brown, *Appl. Phys.* **46** (1985) 574.
781. A.V. Govorkov, E.M. Omel'yanovskii, A.Ya. polyakov, V.I. Raikhshtein and V.A. Fridman, *Sov. Tech. Phys. Lett.* **13** (1987) 157.
782. J.M. Parsey, Jr., and F.A. Thiel, *J. Crystal Growth* **85** (1987) 327.
783. D.A. Johnson , S. Myhaklenko, J.L. Edwards, G.N. Maracas, R.J. Roedel and H. Goronkin, *Appl. Phys. Lett.* **51** (1987) 1152.
784. B. B. Méndez, J. Piqueras, F. Domíngez-Adame and N. de Diego, *J. Appl. Phys.* **64** (1988) 4466.
785. B. Méndez and J. Piqueras, *Inst. Phys. Conf. Ser.* **100** (1989) 789.
786. D. Köhler, G. Koschek and E. Kubalek, *Scann. Microscope* **3** (1989) 765.
787. B. Méndez and J. Piqueras, *J. Appl. Phys.* **65** (1991) 2776.
788. P. Franzosi and G. Salviati, *J. Crystal Growth* **63** (1983) 419.
789. Y. Tokumaru and Y. Okada, *Jpn. J. Appl. Phys.* **24** (1985) L364.
790. J. Ding, J.S.C. Chang and M. Bujatti, *Appl. Phys. Lett.* **50** (1987) 1089.
791. T.W. James, J.B. James and V.B. Harper, *J. Appl. Phys.* **64** (1988) 3885.
792. G. Weber, S. Dietrich, M. Huhne and H. Alexander, *Inst. Phys. Conf. Ser.* **100** (1989) 749.
793. P.J. Gallagher and F. Weinberg, *J. Crystal Growth* **94** (1988) 299.
794. R.J. Roedel, K. Rowley, J.L. Edwards and S. Myhajlenko, *J. Electrochem. Soc.* **138** (1991) 3120.
795. H. Ono, T. Kamejima, H. Watanabe and J. Matsui, *Jpn. J. Appl. Phys.* **25** (1986) L130.
796. J.P. Noad, *J. Appl. Phys.* **64** (1988) 1599.
797. S. Miyazawa, Y. Ishii, S. Ishida and Y. Nanishi, *Appl. Phys. Lett.* **43** (1983) 853.
798. C.E. Third, F. Weinberg and L. Young, *Appl. Phys. Lett.* **54** (1989) 2671.
799. A. Djemel, J. Castaing, N. Visentin and M. Bonnet, *Semicon. Sci. Technol.* **5** (1990) 1221.
800. M.R. Brozel, *Inst. Phys. Conf. Ser.* **91** (1987) 117.
801. M.S. Skolnick, L.J. Reed and A.D. Pitt, *Appl. Phys. Lett.* **44** (1984) 447.
802. T. Katsumata and T. Fukuda, *Rev. Sci. Instrum.* **57** (1986) 202.
803. T. Katsumata, T. Obokata, M. Nakajima and T. Fukuda, in *Defect Recognition and Image Process ing*, ed. by J. P. Fillard (Elsevier Sci, Amsterdam, 1985) p. 149.
804. T. Katsumata, H. Okada, T. Kikuta, T. Fukuda and T. Ogawa, in *Proc. 5th Conf. Semi-Insulating III-V Materials*, eds. H. Kukimoto and S. Miyazawa (Ohmsha, Tokyo, 1986) p. 145.
805. P. Dobrilla and J.S. Blakemore, in *Proc. 5th Conf. Semi-Insulating III-V Materials*, eds. H. Kukimoto and S. Miyazawa (Ohmsha, Tokyo, 1986) p. 103.
806. D.J. Carlson and A.F. Witt, *J. Crystal Growth* **91** (1988) 239.
807. J. P. Fillard, *Rev. Phys. Appl.* **23** (1988) 765.
808. T. Ogawa, *Jpn. J. Appl. Phys.* **25** (1986) L916.
809. T. Katsumata, H. Okada, T. Kikuta and T. Fukuda, *Appl. Phys. A* **42** (1987) 103.
810. J.P. Fillard, P. Gall, J.L. Weyher, M. Asgarinia and P.C. Montgomery, in *Proc. 5th Conf. Semi-insulating III-V Mateirals* (Malmö, Sweden, 1988) p. 537.
811. S. Kuwabara, Y. Kitagawara, N. Noto, S. Nagasawa and T. Takenaka, *J. Crystal Growth* **96** (1989) 572.
812. J. P. Fillard, P. Gall, A. Baaroudi and J. Bonnafe, *Solid State Commun.* **67** (1988) 321.
813. A. Mircea, A. Mitonneau, L. Hollan and A. Briere, *J. Appl. Phys.* **11** (1976) 153.

814. S. Markram-Ebeid, D. Gautard, P. Devillard and G. M. Martin, *Appl. Phys. Lett.* **40** (1982) 161.
815. M. Matsui and T. Kazuno, *Appl. Phys. Lett.* **51** (1987) 658.
816. P. W. Yu and D. A. Park, *J. Appl. Phys.* **50** (1979) 1097.
817. Y. J. Chan and M. S. Lin, *J. Appl. Phys.* **60** (1986) 2184.
818. M. Kiyama, K. Nanbu, T. Takebe, M. Yokoyama and N. Shirakawa, *Sumitomo Electrics (in japanese)* **133** (1985) 121.
819. F. Hyuga, *J. Appl. Phys.* **64** (1988) 3880.
820. F. Orito, S.Kawabata and Y. Yamada, *J. Appl. Phys.* **63** (1988) 2691.
821. H. Schink and R.D. Schnell, *Appl. Phys. Lett.* **53** (1988) 764.
822. S. Miyazawa and Y. Nanishi, *Jpn. J. Appl. Phys.* **22** (1983) Suppl. 22-1, p. 419.
823. S. Miyazawa, Y. Ishii, S. Ishida and Y. Nanishi, *Appl. Phys. Lett.* **42** (1983) 853.
824. Y. Ishii, S. Miyazawa and S. Ishida, *IEEE Trans. Electron. Devices* **ED-31** (1984), 1051.
825. G.M. Martin, M. Duseaux and J. Maluenda, *Inst. Phys. Conf. Ser.* **74** (1984) 13.
826. H. Matsuura, J. Nakamura, Y. Sano, T. Egawa, T. Ishida and K. Kaninishi, in *GaAs IC Symp. Technical Digest.* (1985) p. 67.
827. C.H. Chen, M. Shur and A. Peczalski, *IEEE Trans. Electron. Devices* **ED-33** (1986) 792.
828. S. Miyazawa and K. Wada, *Appl. Phys. Lett.* **48** (1986) 905.
829. S. Yasuami, K. Fukuta, M. Watanabe and T. Nakanishi, *Jpn. J. Appl. Phys.* **25** (1986) 1905.
830. S. Miyazawa and F. Hyuga, *IEEE Trans. Electron. Devices* **ED-33** (1986) 227.
831. W. De Raedt, M. Van Hove, M. de Potter, M. Van Rossum and J.L. Weyher, *Inst. Phys. Conf. Ser.* **91** (1987) 685.
832. S. Miyazawa, *Oyo Buturi (Monthly Publ. Jpn. Soc. Appl. Phys.) (in japanese)* **56** (1987) 19.
833. J. Kasahara, *Oyo Buturi (Monthly Publ. Jpn. Soc. Appl. Phys.) (in japanese)* **56** (1987) 26.
834. Y. Sano, T. Egawa, H. Nakamura and K. Kaminishi, *Oyo Buturi (Monthly Publ. Jpn. Soc. Appl. Phys.) (in japanese)* **56** (1987) 33.
835. P. Sucht, M. Duseaux, J. Maluenda and G.M. Martin, *J. Appl. Phys.* **62** (1987) 1097.
836. T. Inada, T. Fujii and T. Fukuda, *J. Appl. Phys.* **61** (1987) 5483.
837. R. Anholt and T.W. Sigmon, *IEEE Electon. Devices Lett.* **EDL-8** (1987) 16.
838. H. Kanber and D.C. Wang, *IEEE Electon. Devices* **ED-34** (1987) 1626.
839. R. Anholt and T.W. Sigmon, *J. Electron. Mater.* **17** (1988) 5.
840. H. Ch Alt, H. Schink and G. Packeizer, in *Proc. 5th Conf. Semi-insulating III-V Mateirals* (Malmö, Sweden, 1988) p. 515.
841. Y. Saito, *J. Appl. Phys.* **65** (1989) 846.
842. S. Asai and K. Ohata, *EICST Conf.* **ED89-109** (1989) 7.
843. S. Asai, *IEICE Tech Rep.* **ED-90-129** (1990) 27.
844. K. Watanabe, F. Hyuga and N. Inoue, *J. Electrochem. Soc.* **138** (1991) 2815.
845. S. Miyazawa, *Prog. Crystal Growth Characer.* **23** (1991) 23.
846. K. Kaminaka, H. Miyashima, K. Nambu, R. Nakai, M. Yokogawa and S. Murai, *Sumitomo Electrics (in japanese)* **138** (1991) 156.
847. Y. Saito, *J. Appl. Phys.* **72** (1992) 5451.
848. K. Kaminaka, H. Morishita, M. Kiyama and M. Yokogawa, *Sumitomo Electric Tech. Rev.* **35** (1993) 75.
849. S.I. Long, B.M. Welch, R. Zucca and R.C. Eden, *J. Vac. Sci. Technol.* **19** (1981) 531.

9. GaSb

9.1 INTRODUCTION

Since the lattice constant of GaSb is fairly large, GaSb is a promising material for mixed III-V compounds whose band gaps correspond to wavelengths longer than 1.5 μm.[1] This is important since transmission loss due to Rayleigh scattering is significantly low at these wavelengths.[2]

Quaternary GaInAsSb and GaAlAsSb epitaxial layers on GaSb substrates[1, 3, 4] are promising for LEDs and lasers in the range of 2-2.3 μm[5-7] as are AlGaSb photodetectors[8, 9] at wavelengths longer than 1.5 μm. InAs/GaSb superlattices are promising for ultrahigh speed electronic devices.[10] InGaSb Gunn oscillators have also been studied.[11] A recent attractive application of GaSb is for infrared solar cells combined with GaAs based solar cells and for thermophotovoltaic cells in order to convert wasted thermal energies to electric energies.[12]

9.2 PHYSICAL PROPERTIES

The physical properties of GaSb have been investigated and they are reported in various references.[13, 14] Typical data are shown in Table 9.1.

GaSb has a direct band gap of 0.72 eV at room temperature and a cubic lattice constant of 6.095 Å which permits the lattice matching with GaInAsSb quaternary materials for devices sensitive at long wavelengths. The melting point of GaSb is as low as 712 °C which is lower than those of other compound semiconductors.

The phase diagram of GaSb has been investigated[15] and a typical example is shown in Fig. 9.1.[16] Stoichiometric and P-T diagrams have been studied from the theoretical calculation of point defects.[17] The vapor pressure of Ga and Sb are reported as seen in Fig. 9.2.[18]

Thermodynamical calculations have been made for the system Ga-Sb and Ga-In-Sb.[20] The effect of oxygen on the formation of Ga_2O_3 has been discussed.[18]

Table 9.1. Physical Properties of GaSb

Crystal Structure	zincblende
Lattice Constant	6.094 Å
Density	5.613 g/cm^3
Melting Point	712 °C
Linear Expansion Coefficient	6.7 x10^{-6} /deg
Thermal Conductivity	0.33 W/cm•K
Dielectric Constant	15.69
Refractive index	3.82
Bandgap at Room Temperature	0.70 eV
Intrinsic Carrier Concentration	10^{14} cm^{-3}
Electron Mobility	7,700 cm^2/V•sec
Hole Mobility	1,400 cm^2/V•sec

The temperature dependence of the lattice constant has been measured and has been discussed from the viewpoint of non-stoichiometry.[21]

9.3 CRYSTAL GROWTH

The growth of GaSb crystals has been reviewed by various authors.[22-25] Several crystal growth methods used for GaSb are summarized in Table 9.2. Since the melting point of GaSb is as low as 712 °C, the main crystal growth methods are CZ and LEC methods and they are presently applied in industrial production.

9.3.1 Solution Growth

(1) Solution growth

Solution growth from Ga solution or Sb solution has been performed to grow GaSb to examine the electrical properties but the crystals grown are small and are only used for characterization of GaSb crystals.[26-28]

Watanabe et al.[29] grew GaSb bulk crystals by a modified CZ method known as the solute feeding CZ (SFCZ) method. In this method, GaSb crystals were grown from a Ga solution fed from a GaSb source using a two-chamber crucible at a constant temperature of 670 °C.

Bischopink and Benz[30] grew GaSb layers with a thickness of more than 3 mm and a diameter of 15 mm on GaSb substrates from a Ga-rich solution by a vertical Liquid Phase Electro Epitaxy (LPEE) method. The growth temperature was in the range of 550-575 °C and the current density was varied from 5 to 10 A/cm^2.

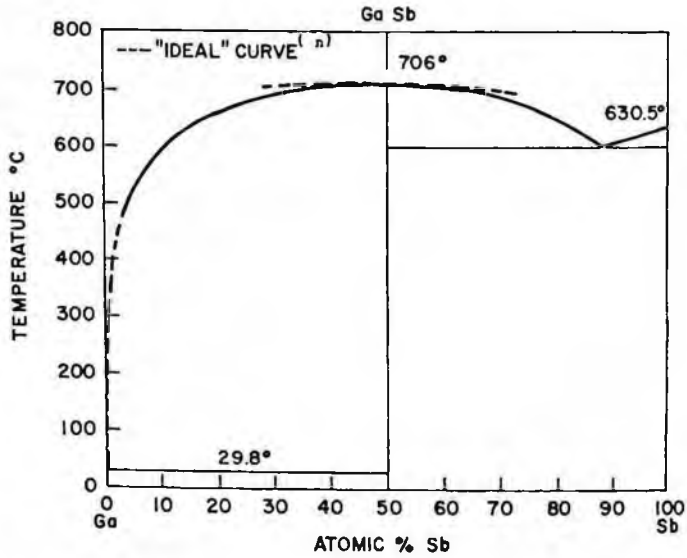

Fig. 9.1 Phase diagram of GaSb (from Ref. 16 with perimssion, copyrright 1958 McGraw-Hill).

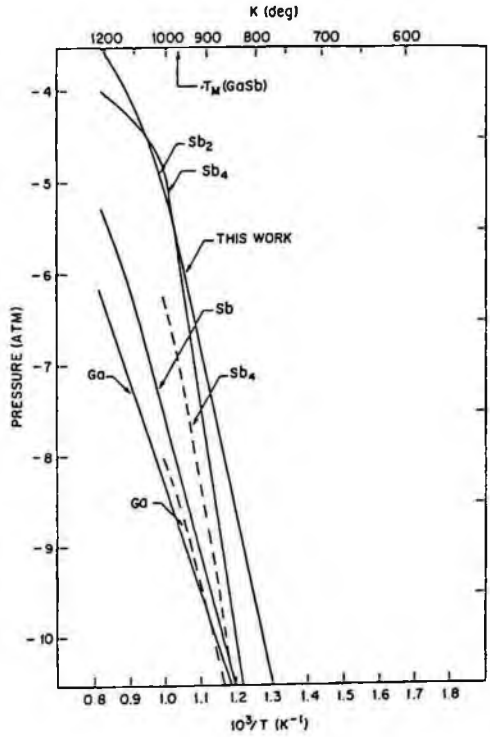

Fig. 9.2 Vapor pressures of Sb, Sb_2, Sb_4 and Ga above GaSb(s, l) for an equimolar mixture of Ga and Sb (reprinted from Ref. 18 with permission, copyright 1986 Elsevier). The dashed lines are calculations.[19]

(2) Travelling Heater Method (THM)

GaSb single crystals of diameter 10 mm and length 30 mm have been grown by the vertical THM method by Benz and Müller.[31] A horizontal THM method was also applied to the crystal growth of GaSb. The maximum growth rate of inclusion-free 10 mm diameter crystals was 2.5 ± 0.5 mm/day at 500 °C. EPD less than 103 cm-2 could be obtained. Müller and Neumann[32] have grown GaSb single crystals by the horizontal THM by forced convection on a centrifuge arrangement with a gravity 20 times higher than earth gravity and found that the growth rate is increased.

9.3.2 Melt Growth

(1) Bridgman growth

GaSb polycrystals were synthesized by a direct reaction between Ga and Sb and the crystallization was performed by a vertical Bridgman method.[33] It is however pointed out that because of the existence of oxide layers containing Ga_2O_3, twinning and polycrystals are easily formed.[34]

Dutta et al.,[35-37] using a furnace assembly as shown in Fig. 9.3, examined the factors

Table 9.2. Crystal Growth of GaSb

Method	Results	Authors	Year	Ref.
CZ	Double crucible method	Allred et al.	1961	41
CZ	Double crucible	Van der Meulen	1964	42
SG	Small crystal from a Ga solution	Miyauchi et al.	1965	27
SG, CZ	Growth from Sb-rich melt	Reid et al.	1966	28
CZ	Effect of growth direction polarity	Dasevskii	1969	43
THM	Diameter 10 mm, length 30 mm growth rate is low (2.5 ± 0.5 mm/day)	Benz et al .	1979	31
CZ	Effect of ultrasonic vibration	Kumagawa	1980	44
LEC	Encapsulant: NaCl-KCl	Miyazawa et al.	1980	62
LEC	Encapsulant: B_2O_3+Na_2AlF_6	Katusi et al.	1980	64
VB	Direct synthesis and crystal growth	Harsy et al.	1981	33
SML	Platelet single crystal growth	Miyazawa	1982	68
LEC	Encapsulant: NaCl-KCl, <111> single crystal	Kondo et al.	1982	65
LEC	Te-doped <100> single crystal growth	Ohmori et al.	1982	66
CZ	Growth under hydrogen, EPD 10^2-10^3 cm^{-2}	Cockayne et al.	1982	45
CZ	<115>,<112> , <111> directed crystal growth	Hirai et al.	1982	46
LEC	Effect of the polarity of <111> seed crystal on twinning	Katsui et al.	1982	64
CZ	Growth under hydrogen, 3.5 cm in diameter and 6 cm in length	Sunder et al .	1986	47
CZ, LEC	Crystal growth under hydrogen atmosphere	Moravec et al.	1987	48
CZ	Growth under hydrogen for <100>, <111> and <112> directions. Effect of seed orientation on twinning occurrence	Moravec et al.	1989	49, 50
LEC	Te-doped <111> GaSb with NaCl-KCl encapsulant	Matsumoto et al.	1989	24
VGF	<111> crystals with 10 mm diameter and 50 mm in length. EPD<100 cm^{-2}. Solidified fraction measurement	Garandet et al.	1989	40
CZ	<111> Te-doped single crystal growth	Stepanek et al.	1992 1994	34, 52-55
CZ	Effect of excess of Sb on the acceptor concentration	Moravec	1993	51
CZ	S-doping	Stepanek et al.	1993	56
CZ	Solute feeding growth from Ga solution	Watanabe et al.	1993	29
LPEE	Growth of thick AlGaSb and GaSb layers	Bishop et al.	1993	30
CZ	Upper-lower crucible technique	Mo et al	1993	61
VB	Crystal growth under planar solid-liquid interface shape	Dutta et al.	1994 1995	35-37
VB	Growth of $Ga_{1-x}Mn_xSb$ crystals	Basu et al.	1994	38
CZ	Careful recleaning of Ga, growth of 25 mm diameter <100> single crystal	Oliveira et al.	1995	60
CZ	Doping with Cu, In, Ge, N, S, Se, Te and Mn	Sestakova et al.	1995	57,58
CZ	Growth under ionized hydrogen atmosphere Decrease of carrier concentrations	Sestakova et al.	1996	59
HB	Growth of 25 mm diameter and 60n mm in length, EPD<10^2 cm^{-2}.	Sestakova et al.	1996	59
FZ	Growth under microgravity	Croll et al.	1998	69
EGF	Growth of ribbon and rod crystals	Nicoara et al.	2000	67
VB	Growth of Nd-doped GaSb crystals	Plaza et al.	2002	39
HTHM	Growth under 20 times earth gravity	Müller et al.	2005	32

CZ: Czochralski, LEC: Liquid Encapsulated CZ, VB: Vertical Bridgman, VGF: Vertical Gradient Freezing, SG: Solution Growth, THM: Travelling Heater Method, HTHM: Horizontal THM, SML: Shaped Melt Lowering, LPEE: Liquid Phase Electro-Epitaxy, EGF: Edge-defined, Film-fed Growth

affecting the melt-solid interface shape and found that high quality crystals can be grown with a flat melt-solid interface shape. They also examined the interface shape and the growth rate by quenching and etching methods and showed the results agreed well with the theoretical prediction .

Basu et al.[38] for the first time tried the growth of $Ga_{1-x}Mn_xSb$ which shows semimagnetic semiconducting (SMSC) behavior by the VB method using compositions of $0<x<0.15$. The effect of the Mn concentration was examined.

Since rare earth doped semiconductors show a temperature stable luminescence, Nd-doped GaSb bulk crystals have been grown by the vertical Bridgman method[39] and the effective segregation coefficient and the electrical properties have been examined.

(2) Vertical Gradient Freezing (VGF) method

Garandet et al.[40] applied a VGF method combined with a dilatometric method for growing GaSb while measuring the solidified fraction. Dislocation densities below 100 cm^{-2} could be obtained.

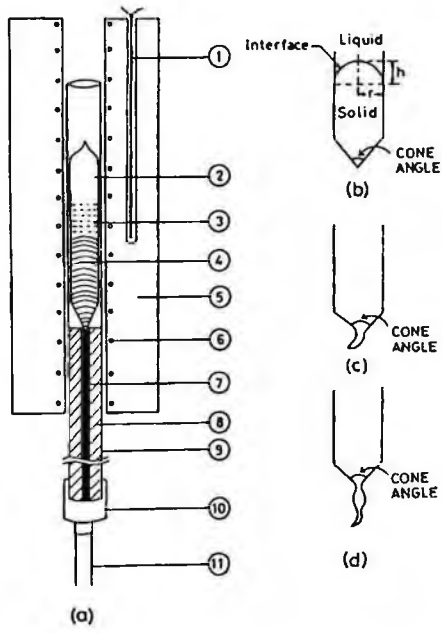

Fig. 9.3 (a) Schematic diagram of the furnace and crucible assembly: (1) NiCr/NiAl control thermocouple; (2) quartz ampoule; melt; (4) crystal; (5) furnace; (6) furnace element; (7) ampoule stem; (8) quartz wool; (9) quartz crucible holder; (10) stainless steel coupler; (11) stainless steel lower rod; (b), (c), (d) Various shapes of ampoule tip (reprinted from Ref. 35 with permission, copyright 1994 Elsevier).

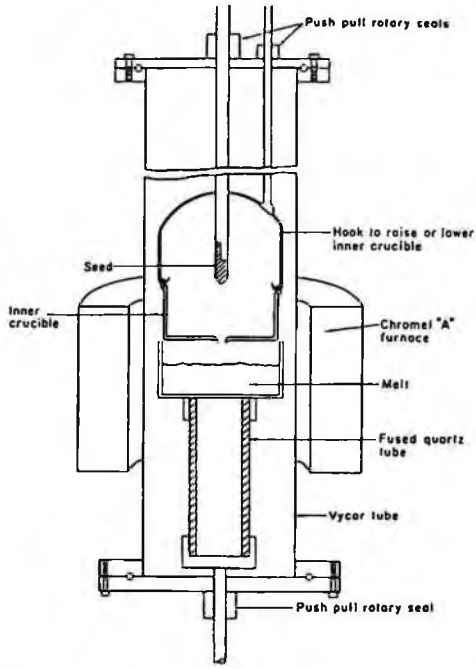

Fig. 9.4 GaSb crystal grower using double crucible method to eliminate oxide (reprinted from Ref. 41 with permission of The Electrochemical Society).

(3) Czochralski (CZ) method

For the growth of GaSb crystals, the main method is the CZ method and it has been studied by various researchers.[41-61]

In the CZ crystal growth of GaSb, the main problem is that after the GaSb melts, a film of Ga_2O_3 oxide is formed at the surface of the melt, as predicted by thermodynamical analysis.[20] This oxide film makes seeding difficult and twinning occurs easily because of the adherence of the film.

To prevent this problem, the double crucible method (Fig. 9.4) has been developed where the GaSb melt is made to flow through a hole in the bottom of the inner crucible and the oxide film is removed.[22, 41] It is however known that during crystal growth, oxide films are formed again[56] and the temperature gradient is so large that twins and dislocations are formed easily.

It is known that high-purity argon and nitrogen gas do not prevent the formation of oxide scum. To prevent the formation of oxide films, crystal growth has been performed by the CZ method under a hydrogen atmosphere.[47, 48, 51] Oxide films can be removed after several days' purging with high purity hydrogen.

Hirai and Obokata[46] grew <115>, <112> and <111> direction GaSb single crystals by the CZ method using a double carbon crucible under a hydrogen atmosphere, and showed that low dislocation density crystals can be grown by the <115> direction growth.

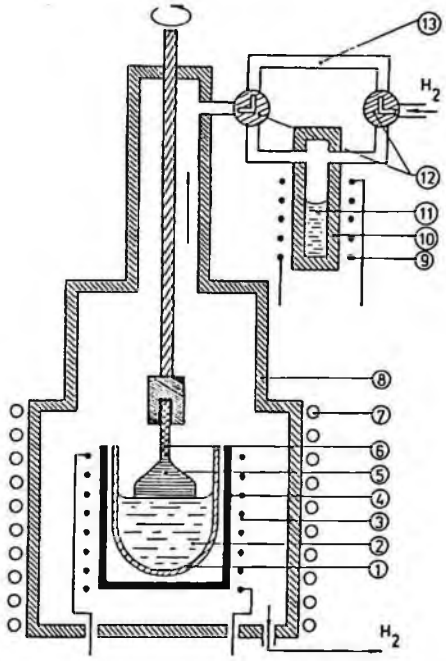

Fig. 9.5 Schematic diagram of the Czochralski apparatus for GaSb growth: (a) quartz crucible; (2) GaSb melt; (3) molybdenum wire coils; (4) graphite cylinder; (5) GaSb crystal; (6) seed; (7) water cooling coils; (8) quartz tube; (9) Kanthal wire coils; (10) quartz ampoule; (11) sulphur; (12) two-way cocks; (13) quartz bypass (reprinted from Ref. 57 with permission, copyright 1992 Elsevier).

Sunder et al.[47] have performed a two-step process for preventing the formation of oxide films, and have made systematic studies of CZ crystal growth, investigating the role of crystal stoichiometry, crystalline perfection, impurity distribution and interface shape on the electrical properties. They have grown GaSb single crystals of diameter 3.5 cm and length 6 cm reproducibly.

Moravec and Tomm[48] compared the CZ method with the LEC method and concluded that the CZ method is preferable from the viewpoint of twin-free crystal growth. Moravec et al. [49, 50] have grown GaSb single crystals in the direction of <100>, <111>, <112> and compared them for polycrystallization and twinning. Another phenomenon also examined was that Sb excess in the melt decreases the residual acceptor concentration.[51]

Sestakova et al.[34] examined various methods and found that the CZ method without encapsulant in a flow of hydrogen is the most suitable method (Fig. 9.5). They grew GaSb single crystals by this method doping with Te,[52-55] S,[56] In and N[57] and Cu, In, Ge, N, S, Se, Te, Mn.[58]

Crystal growth under an ionized hydrogen atmosphere without encapsulant was also examined and it was found that lower free carrier concentrations could be obtained,

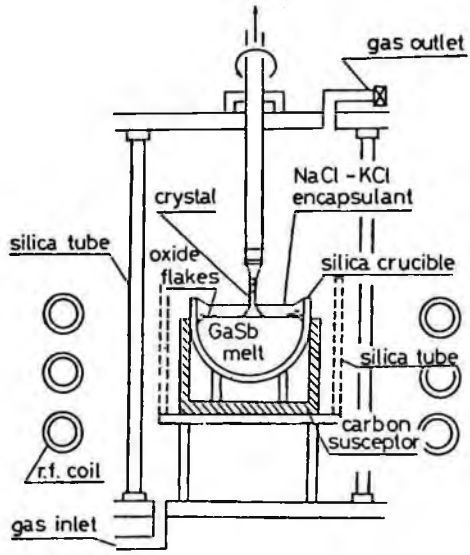

Fig. 9.6 LEC growth apparatus. The quartz tube was used to control temperature distribution (reprinted from Ref. 65 with permission, copyright 1982 Elsevier).

probably by the passivation of residual impurities or defects.[59]

Oliveira and de Garvalho[60] have grown 25 mm diameter GaSb single crystals, without using hydrogen, but by thermal treatment of gallium in a vacuum before crystal growth to yield a scum-free melt.

Mo et al.[61] applied a double crucible technique for growing GaSb crystals from a scum-free melt. In this method, the upper crucible is used to trap the scum on the melt surface. By this method, a growth cycle of only one-step can be performed instead of the conventional two-step growth cycle.

(4) Liquid Encapsulated Czochralski (LEC) method

The LEC method has the advantage that it is possible to remove oxide films and to obtain a lower temperature gradient than with the CZ method. It is however important to select an appropriate encapsulant. Boric oxide which is mainly used as the encapsulant for GaP, GaAs and InP is not appropriate for GaSb. This is because the viscosity of B_2O_3 at the melting temperature is high and bubbles can not easily be removed. The removal of oxide film is not effective neither.

In the selection of an appropriate encapsulant, the following criteria must be considered.[62]

(i) The melting point must be lower than that of GaSb (~712 °C)

(ii) That the viscosity is sufficiently low

(iii) That it does not react with GaSb and does not dissolve GaSb.

(iv) That the specific gravity is lower than that of GaSb
(v) Transparent when single crystals are grown
(vi) Evaporation is small
(vii) It wets well with GaSb
(viii) It is not toxic.

Katusi et al.[63, 64] used B_2O_3 with an additive of 3.3 mol % Na_2AlF_6 aimed at reducing the viscosity. They also examined the effect of the polarity of the <111> seed crystals and the melt composition on the occurrence of twinning. This method is however limited because when the removal of oxide film is not sufficient, the encapsulant becomes opaque.

Miyazawa et al.[62, 65] developed an encapsulant NaCl-KCl eutectic compound for crystal growth (Fig. 9.6). Since the NaCl-KCl eutectic encapsulant has good oxide film removing abilities, a eutectic temperature of about 645 °C, a specific gravity of about 2 g/cm^3 and it wets well with GaSb, it would appear to be an ideal encapsulant. It however has the disadvantage that it more or less evaporates under atmospheric pressure. By melting back the dislocation free seed crystal, a dislocation-free crystal could be obtained.[66]

Since GaSb has a tendency to generate twinning, it is important to control the melt composition with a view to stoichiometry control. Ohmori et al.[66] and Matusmoto et al.[24] in fact grew GaSb single crystals of diameter 50 mm while preventing twinning.

Moravec and Tomm[48] compared the above LEC method, with the encapsulant B_2O_3+3.3 mol % Na_2AlF_6 and NaCl-KCl, with the CZ method in pure hydrogen gas. 35-50 mm diameter Te-doped GaSb free of dislocations could be obtained by the LEC method with a B_2O_3 encapsulant. They however postulated the advantage of the CZ

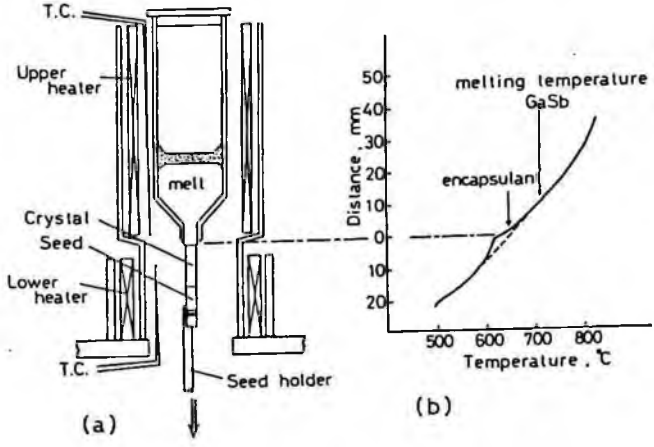

Fig. 9.7 Furnace setup. (a) SML growth apparatus and (b) temperature profile in the furnace (reprinted from Ref. 68 with permission, copyright 1982 Elsevier).

method from the viewpoint of crystal growth yield.

With the LEC method it is however pointed out that an oxide layer is formed between the encapsulant and the GaSb melt which sticks to the seed crystal and cause the local freezing.

(5) Others

GaSb crystals shaped as ribbons and rods were grown by pulling from the melt using a non-wetted floating shaper to control the crystal cross section shape and size.[67] Graphite was used as the shaper and the crucible material since it does not react chemically with molten gallium antimonide.

A novel Shaped Melt Lowering (SML) technique was first applied to GaSb by Miyazawa.[68] In this method, a shaped crystal is pulled down from the crucible using a seed crystal as seen in Fig. 9.7. Undoped and Te-doped platelet GaSb single crystals were grown with a pulling down rate of 18 mm/h.

9.3.3 Vapor Phase Growth

It is found that the Piper-Polish method is not effective in the crystal growth of GaSb because of its low vapor pressure.[70] When transport agents such as GaI_3 and SbI_3 are used in the vapor phase method, the growth rate is increased one order of magnitude but is still too low for industrial production.[22]

Shen et al.[71] applied the closed tube vapor phase growth method using iodine as the transport agent in order to grow $Ga_xAl_{1-x}Sb$ single crystals on GaSb substrates at 550-580 °C, and obtained smooth GaAlSb layers on (111)A and (100) GaSb substrates.

9.3.4 Doping

Distribution coefficients of various dopants are summarized in Table 9.3.[22, 72, 73] These data were mainly obtained from the electrical measurement of crystals grown by the CZ method. Other doping studies were mainly performed by Sestakova et al.[34, 52-59] using the CZ method in a hydrogen atmosphere.

The relationship between the distribution coefficient and growth parameters such as melt composition, growth rate and crystal orientation has been extensively discussed.[47]

Table 9.3 Distribution Coefficients

Impurity	Distribution Coefficient
Zn	0.16-0.3
Cd	<0.02-0.02
In	~1
Si	1
Ge	0.08-0.2
Sn	0.0002-<0.2
As	2-4
S	0.06
Se	0.18-0.4
Te	0.32-1

9.4 CHARACTERIZATION

9.4.1 Purity

When eutectic NaCl-KCl is used as the encapsulant, Na, K and Cl are incorporated in grown crystals in amounts of several ppm. Impurities such as Al from the source Ga material and Ca and S which are found in NaCl and KCl are also incorporated in grown crystals.

9.4.2 Defects

(1) Dislocations

Since GaSb has a higher critical yield stress than other III-V materials as explained Sec. 1.7.3, it is much easier to get low dislocation densities than with other III-V materials.

As dislocation etchants, H_2O_2:HCl:H_2O=1:1:2[74] and HNO_3:HF : CH_3COOH = 2:1:2[75] were first used but lately, Brown et al.[76] found that HCl:H_2O_2 = 2:1 is a useful etchant since it reveals two types of dislocations and also striations. Kondo et al.[65] showed that dislocations on the (111) Ga face can be revealed as triangular etch pits by etching with 2%Br-methanol after mirror etching by HF: HNO_3: CH_3COOH=1:9:20. The one-to-one correspondence between etch pits and dislocations is confirmed by X-ray topography.[65] Another dislocation etchant is a modified CP4 etch which is HNO_3:CH_3COOH: HF:H_2O = 5:3:3:11 by which dislocations on (111) Ga and (111)Sb can be revealed.[40] Cockanye et al.[45] revealed dislocations on the (100) surface using a concentrated HCl:H_2O_2 = 2:1 etchant. HCl:H_2O_2:H_2O=1:1:2 is also used as an EPD etchant.

When dislocation free crystals are used as seed, propagated dislocations take place from the seed crystal. This may be due to thermal shock on the occasion of seeding. Melt-back and necking procedures were effective in preventing these propagated dislocations and dislocations fewer than 10 cm^{-2} could be obtained.[65] When Te-doping is performed, dislocation free less than 1 cm^{-2} is realized.[66]

Undoped CZ grown GaSb has dislocation densities of 10^2-10^3 cm^{-3}. It is found that high Te doping ($\geqq 10^{19}$ cm^{-3}) is effective in reducing the dislocation densities to the level of less than 10^2 cm^{-2}.[45] Te thus has an impurity hardening effect.

In the case of <100> crystals, dislocations are mainly generated at the interface between the seed crystal and the melt, and propagated along (111) directions. It was found that no dislocations are generated during crystal growth.[45]

Heinz[77] showed that dislocations can be reduced by post growth annealing. They have annealed Zn doped (100) HGF-GaSb substrates at 680 °C for various durations and found that the initial dislocation density of about 2000 cm^{-2} was reduced 50 % to less than 2000 cm^{-2} (Fig. 9.8). The reduction of dislocations may be due to the annihilation and coalescence of dislocations by an enhanced dislocation movement under thermal stress during annealing.

Omri et al.[78] studied the plastic deformation of GaSb and examined the movement and structure of dislocations. Anthony et al.[79] showed that the dislocation density of GaSb substrates largely affects the lifetime of Ga(As,Sb) active layers grown on the substrate for 0.87 mm AlGaAs DH lasers. For Ga(As,Sb) active layers on high disloca-

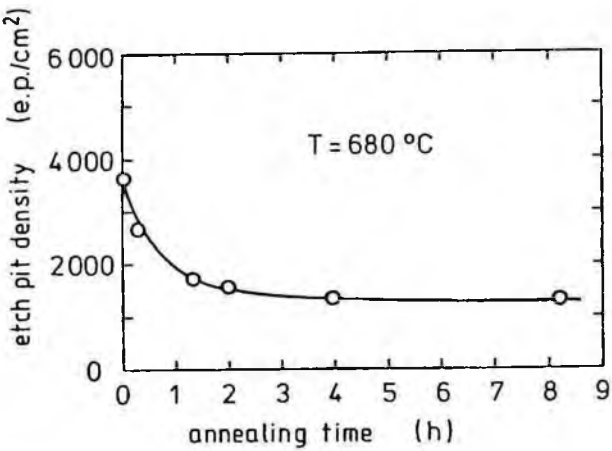

Fig. 9.8 Variation of etch pit density as a function of various annealing times at an annealing temperature of 680°C (reprinted from Ref. 77 with permission, copyright 1993 Taylor & Francis).

tion density substrates, dark line defects (DLD) formed very rapidly and the lifetime decreased three orders of magnitude for an increase of dislocation density of one order of magnitude.

(2) Striations and facets

Thono et al.[80] have observed striations in undoped GaSb single crystals grown by the LEC method. Striations could be observed by X-ray diffraction topography and etching technique. The origin of observed rotational and non-rotational striations was discussed.

Van der Meulen[81] first pointed out the effect of facets on the electrical conductivity. Kumagawa et al. has studied systematically the formation of microfacets in GaSb single crystals.[44, 82-88] He discussed the transition of microfacets to macrofacets and the role of impurities.

(3) Point defects

Van der Meulen first showed that the complex defect $V_{Ga}Ga_{Sb}$ is the origin of the residual acceptor in GaSb. Allegre et al.[89, 90] have shown how this complex defect is formed during an annealing experiment. Brescansin and Fazzio[91] have made a theoretical study of single vacancies in GaSb. Shaw[92] studied the diffusion of In in GaSb from the viewpoint of the diffusion mechanism involving divacancies. The behavior of structural defects in ternary compounds such as GaInSb and AlGaSb has also been studied.[90] Ling et al have studied the role of V_{Ga} as acceptors using positron annihilation and PL measurement.[93] Edelin and Mthiot[17] have calculated thermodynamically the concentrations of defects such as vacancies and anti-site defects and constructed the precise phase diagram.

(4) Deep levels

Polyakov et al. have studied the effect of hydrogen treatment on deep level passivation using the DLTS technique.[94] Hubik et al.[95] studied the deep levels in CZ-grown GaSb crystals doped with sulphur. They found sulphur related DX-like centers.

9.4.3 Electrical Properties

(1) Carrier concentration and mobility

Impurities in undoped GaSb are less than 0.1 ppma even though Si is in the range of 0.2-0.4 ppma, which is the contamination from the quartz crucible. Grown crystals have p-type conductivity and the residual acceptor is believed to be due to Sb_{Ga} antisite defects[89] or $V_{Ga}Ga_{Sb}$.[81] Undoped GaSb is p-type with carrier concentrations of (1.5-1.7)x10^{17} cm^{-3}, Hall mobilities of 550-800 $cm^2/V \cdot sec$ and resistivity of 10^{-2}-(5-9)x10^{-2} $\Omega \cdot cm$.[50, 57, 70]

Increasing the carrier concentration has been attempted by several methods. The first is doping donor impurities such as S, Se and Te etc. to compensate residual acceptors[52] but this method gives uneven carrier concentrations.[96] By growing from a non-stoichiometric melt, carrier concentrations of about 5x10^{16} cm^{-3} were realized.[97] Growth under an ionized hydrogen atmosphere makes it possible to obtain relatively high resistivity because of the passivation of acceptors by hydrogen.[54, 80, 98] Sestakova et al.[98] found that when GaSb crystals are grown under ionized hydrogen, the resistivity is increased one order of magnitude which is ascribed to hydrogen passivation of residual acceptors.

Te is doped as an n-type dopant. In <111> oriented grown crystals, there was non-uniformity due to facetting but <100> oriented grown crystals showed uniform carrier concentration distribution.[59]

Undoped GaSb shows carrier concentrations of the order of 1.7x10^{17} cm^{-3} with acceptors.[54] These acceptors are identified as $V_{Ga}Ga_{Sb}$ complexes which have a double ionized structure.[42]

To reduce acceptor concentrations, various attempts have been made.

(i) Doping with S, Se, Te, Cu, In, Ge, Mn, N for compensating these acceptors[56, 59]

(ii) Growth from a non-stoichiometric melt[97]

(iii) Growth using ionized hydrogen[55, 98]

The detailed study of the energy levels of various residual acceptors has been extensively carried out by Nakashima[99] and Meinardi et al.[100] and Baranov et al.[101] examined the effect of structure defects on the electrical properties.

9.4.4 Optical Properties

Photoluminescence spectra of undoped,[102] Te-doped,[102-106] Zn-doped,[102] Mn-doped[105] and In-doped[106] GaSb have been studied and the various peaks have been identified as seen in Table 9.4.[100, 102-106] A typical photoluminescence spectrum is shown in Fig. 9.9.

Chioncel et al.[107] have used cathodoluminescence for studying the plastic deformation behavior of GaSb. It was found that the quenching of the luminescence represents the increase of defect band A and of the 730 eV band related to the $V_{Ga}Ga_{Sb}Te_{Sb}$ centers.

Table 9.4. Assignments of Photoluminescence Lines of GaSb

Line	hυ (meV)	Assignment
FE	810	Free exciton (E_{ex} = 2 meV)
D	803	Shallow acceptor (Ea = 9 meV)
BE	795.5	Bound exciton
A	777.5	Bound-acceptor transition, E_a = 33 meV Native defect (single charged state)
BE-LO	766	BE phonon replica (hw = 29 meV)
B	757	Band-acceptor transition, E_a = 55 meV
A-LO	748.5	Phonon replica of line A (hυ = 29 meV)
B-LO	729.4	Phonon replica of line B
C	710	Band-acceptor transition, E_C = 100 meV

9.5 APPLICATIONS

Milnes and Polyakov[13] reviewed the physical properties of GaSb and its various applications. Lines[2] and Law et al.[108] also reviewed the application of GaSb substrates.

9.5.1 Photonic Devices

(1) LEDs and lasers

Quarternary GaInAsSb and GaAlAsSb devices based on GaSb are sensitive in the mid-infrared wavelength range of 2-2.3 μm (Ref. 3) so that they are promising as infrared LEDs and lasers.[5, 6] In fact, various lasers have been made.[5, 6, 109-111] Motosugi and Kawawa[5] have made AlGaAsSb/GaSb DH lasers on Te-doped n-GaSb substrates by the LPE method. Kano and Sugiyama have fabricated GaInAsSb/GaSb DH lasers oper-

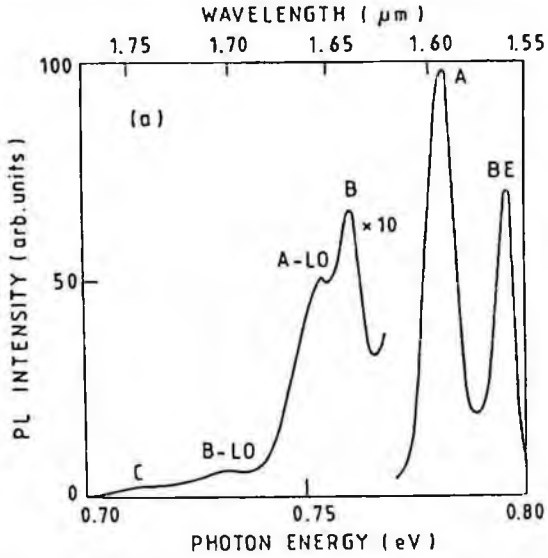

Fig. 9.9 PL spectra of undoped p-GaSb (reprinted from Ref. 106 with permission, copyright 1992 Elsevier).

ating at 2.0 μm CW operation (at 80K) by the LPE method.

(2) Photodetectors

Quarternary GaInAsSb and GaAlAsSb grown on GaSb substrates are also promising for long wavelength photodetectors. Law et al.[108] showed the possibility of applying GaAlAsSb material on GaSb substrates as light emitters and detectors in the 1.2-1.7 μm region.[111] Sukegawa et al.[11] have made a photodiode with the n-$Al_xGa_{1-x}Sb$/p-GaSb structure on a p-GaSb substrate. Capasso et al.[8] have fabricated GaSb mesa photodiodes with $Al_xGa_{1-x}Sb$ windows. Jun et al.[113] reported GaInAsSb/GaSb pin photodetectors sensitive to the wavelength of 2.4 μm. GaSb based avalanche photodiodes have also been investigated by several authors.[114, 115]

9.5.2 Electronic Devices

(1) High speed electronic devices

GaSb based HBTs, HETs and MODFETs have been reported. Even complementary HFETs have been reported. Esaki[116] has proposed a InAs/GaSb based super lattice structure for ultra high speed electronic devices.

(2) Gunn diodes

Segawa et al.[11] showed Gunn diode oscillations in $Ga_xIn_{1-x}Sb$ (x = 0.82, 0.91) LPE epitaxial layers on GaSb (100) substrates. A peak/valley ratio of about 2 was obtained.

(3) Tunneling diodes

Kang and Ko[117] fabricated planar tunneling diodes on (111) GaSb substrates. A peak to valley current ratio of eight was obtained routinely, with a maximum value of eighteen. The peak current gauge factor was in the range of 180 to 240, higher than the highest gauge factor obtained for Si or Ge devices. GaSb planar tunneling diodes are thus promising for strain gauges or pressure transducers.[118] Fay et al.[119] reported logic circuits which operate at 12 GHz based on a InAs/AlSb/GaSb resonant interband tunneling diode (RITD).

9.5.3 Solar Cells

Gruenbaum et al.[120] fabricated GaSb infrared solar cells to be mechanically stacked with GaAs solar cells. The efficiency of these GaSb solar cells was 6 % under a GaAs filter and was found to be very radiation resistive. Andreev et al.[121] have reported a solar cell with a high efficiency up to 11.3 %.

9.5.4 Thermophotovoltaic (TPV) Generators

Photovoltaic cells based on GaSb have a maximum energy conversion in the long wavelength region in the range of 2-4 μm so that these cells are applicable for power generation from flames and other sources which generate heat. In fact, GaSb thermophoto-voltaic cells have been realized[122] and it has been demonstrated that high

power could be generated from a candle flame, Bunsen burner flame, room heater and from exhausted heat. This application suggests a future possibility for new energy sources and helps the environmental problem. The cost performance of GaSb TPV systems was calculated against Si and it was found that they are effective at lower emitter temperatures than Si TPV systems.[123]

REFERENCES

1. R.A. Laudise, *J. Crystal Growth* **65** (1983) 3.
2. M.E. Lines, *J. Appl. Phys.* **55** (1984) 4058.
3. M. Astles, A. Hill, A.J. Williams, P.J. Wright and M.J. Young, *J. Electon. Mater.* **15** (1986) 41.
4. H.M. Manasevit and K.L. Hess, J. *Electrochem. Soc.* **126** (1979) 2031.
5. G. Motosugi and T. Kagawa, *Jpn. J. Appl. Phys.* **19** (1980) 2303.
6. M.B.E. Morosini, J.L. Herrera-Perez, M.S.S. Loural, A.A.G. Von Zuben, A.C.F. da Silveira and N.B. Patel, *IEEE J. Quantum Electron.* **QE-29** (1993) 2103.
7. T. Sukegawa, T. Hiraguchi, A. Tanaka and M. Hagino, *Appl. Phys. Lett.* **32** (1978) 316.
8. F. Capasso, M.B. Panish, S. Ssumski, and P.W. Foy, *Appl. Phys. Lett.* **36** (1980) 165.
9. O. Hildebrand, W. Kuebart, K.W. Benz and M.H. Pilkuhn, *IEEE J. Quantum Electron.* **QE-17** (1981) 284.
10. L. Esaki, *J. Crystal Growth* **52** (1981) 227.
11. K. Segawa, H. Miki, M. Otsubo and K. Shirahata, *Electron. Lett.* **12** (1976) 124.
12. L.M. Fraas, G.R. Girard, J.E. Avery, B.A. Arau, V.S. Sundaram, A.G. Thomson and J.M. Gee, *J. Appl. Phys.* **66** (1989) 3866.
13. A.G. Milnes and A.Y. Polyakov, *Solid-State Electron.* **36** (1993) 803.
14. *Landolt-Börnstein, Vol. 17 Semiconductors*, ed. O. Madelung (Springer-Verlag, Berlin, 1982) p. 258.
15. W. Köster and B. Thomas, *Z. Metallkunde* **46** (1955) 291.
16. M. Hansen, in *Constitution of Binary Alloys*, (MacGraw-Hill, New York, 1958) p. 755.
17. G. Edelin and D. Mthiot, *Phil. Mag.* **B42** (1980) 95.
18. K.B. McAfee, Jr., D.M. Gay, R.S. Hozack, R.A. Laudise, G. Schwartz and W.A. Sunder, *J. Crystal Growth* **76** (1986) 263.
19. Yu. T. Zakharov and M. S. Mirgalovskaya, *Izv. Akad. Nauk SSSR, Neorg. Mater.* **3** (1967) 1998.
20. T.L. Aselage and T.J. Anderson, *High Temp. Sci.* **20** (1985) 207.
21. V.T. Bublik, J. Wilke and A.T. Pereversev, *phys. stat. sol. (a)* **73** (1982) K271.
22. W.P. Allred, in *Compound Semiconductors, Vol. I, Preparation of III-V Compounds*, eds. R.K. Willardson and H.L. Goering (Reinhold, New York, 1962) p. 187.
23. K.W. Benz, *Metall* **37** (1983) 696.
24. K. Matsumoto, in *Bulk Crystal Growth Technology* (Gordon & Breach Sci., Amsterdam, 1989) p. 158.
25. S. Miyazawa, in *Crystal Growth Handbook*, ed. Jpn. Assoc. Crystal Growth (Kyoritsu, Tokyo, 1995) p. 445.
26. G. Woff, P.H. Jeck and J.D. Broder, *Phys. Rev.* **94** (1954) 753.
27. T. Miyauchi and H. Sonomura, *Jpn. J. Appl. Phys.* **4** (1965) 317.
28. F.J. Reid, R.D. Baxter and S.E. Miller, *J. Electrochem. Soc.* **113** (1966) 713
29. A. Watanabe, A. Tanaka and T. Sukegawa, *J. Crystal Growth* **128** (1993) 462.
30. G. Bischopink and K.W. Benz, *J. Crystal Growth* **128** (1993) 466.
31. K.W. Benz and G. Müller, *J. Crystal Growth* **45** (1979) 154, **46** (1979) 35.
32. G. Müller and G. Neumann, *J. Crystal Growth* **63** (1983) 58.
33. M. Harsy, T. Gorog, E. Lendvay and F. Koltai, *J. Crystal Growth* **53** (1981) 234.
34. V. Sestakova, B. Stepanek, and J. Sestak, *J. Crystal Growth* **165** (1996) 159.
35. P.S. Dutta, K.S. Sangunni, H.L. Bhat and V. Kumar, *J. Crystal Growth* **141** (1994) 44.

36. P. S. Dutta, K. S. Sangunni, H. L. Bhat and V. Kumar, *J. Crystal Growth* **141** (1994) 476.
37. P. S. Dutta, H. L. Bhat and V. Kumar, *J. Crystal Growth* **154** (1995) 213.
38. S. Basu and T. Adhikari, *J. Alloy Compounds* **205** (1994) 81.
39. J.L. Plaza, P. Hidalgo, B. Mendez, J. Piqueras and E. Dieguez, *J. Crystal Growth* **241** (2002) 283.
40. J.P. Garandet, T. Duffar and J.J. Favier, *J. Crystal Growth* **96** (1989) 888.
41. W.P. Allred and R.T. Bate, *J. Electrochcm. Soc.* **108** (1961) 258.
42. Y.J. Van der Meulen, *J. Phys. Chem. Solids* **28** (1967) 25.
43. M.A. Dasevskij, G.V. Kukuladze and M.S. Mirgalovskaja, *Sov. Inorg. Mater.* **5** (1969) 1141.
44. M. Kumagawa, H. Oka, N.V. Quang and Y. Hayakawa, *Jpn. J. Appl. Phys.* **19** (1980) 753.
45. B. Cockayne, V.W. Steward, G.T. Brown, W.R. MacEwan, M.L. Young and S. J. Courtney, *J. Crystal Growth*
46. I. Hirai and T. Obokata, *Jpn. J. Appl. Phys.* **21** (1982) 956.
47. W.A. Sunder, R.L. Barns. T. Y. Kometani, J. M. Parsey, Jr. and R. A. Laudise, *J. Crystal Growth* **78** (1986) 9.
48. F. Moravec and Y. Tomm, *Cryst. Res. Technol.* **22** (1987) K30.
49. F. Moravec, V. Sestakova, B. Stepanek and V. Charbat, *Cryst. Res. Technol.* **24** (1989) 275.
50. F. Moravec, V. Sestakova, V. Charbat and B. Stepanek, *Crystal Prop. Prep.* **19/20** (1989) 145.
51. F. Moravec, *J. Crystal Growth* **128** (1993) 457.
52. V. Sestakova and B. Stepanek, *Thermochim. Acta* **198** (1992) 213.
53. B. Stepanek and V. Sestakova, *Thermochim. Acta* **209** (1992) 285.
54. B. Stepanek, V. Sestakova and J. Sestak, *Mater. Sci. Engineer.* **B20** (1993) 249.
55. B. Stepanek, Z. Sourek, V. Sestakova, J. Sestak and J. Kub, *J. Crystal Growth* **135** (1994) 290.
56. B. Stepanek, V. Sestakova, P. Hubik, V. Smid and V. Charvat, *J. Crystal Growth* **126** (1993) 617.
57. B. Stepanek and V. Sestakova, *J. Crystal Growth* **123** (1992) 306.
58. V. Sestakova and B. Stepanek, *J. Crystal Growth* **146** (1995) 87.
59. V. Sestakova, B. Stepanek, J.J. Mares and J. Sestak, *Mater. Chem. Phys.* **45** (1996) 39.
60. C.E.M. de Oliveira, M.M.G. de Carvalho, *J. Crystal Growth* **151** (1995) 9.
61. P.G. Mo, H.Z. Tan, L.X. Du and X.Q. Fan, *J. Crystal Growth* **126** (1993) 613.
62. S. Miyazawa, S. Kondo and M. Naganuma, *J. Crystal Growth* **49** (1980) 670.
63. A. Katsui and C. Uemura, *Jpn. J. Appl. Phys.* **19** (1980) L318,
64. A. Katsui and C. Uemura, *Jpn. J. Appl. Phys.* **21** (1982) 1106.
65. S. Kondo and S. Miyazawa, *J. Crystal Growth* **56** (1982) 39.
66. Y. Ohmori, K. Sugii, S. Akai and K. Matsumoto, *J. Crystal Growth* **60** (1982), 79.
67. I. Nicoara, D. Nicoara, A.G. Ostrogorsky, C. Marin and T. Peignier, *J. Crystal Growth* **220** (2000) 1.
68. S. Miyazawa, *J. Crystal Growth* 60 (1982) 331.
69. A. Croll, Th. Kaiser, M. Schweizer, A.N. Danilewsky, S. Lauev, A. Tesetmeier and K.W. Benz, *J. Crystal Growth* **191** (1998) 365.
70. K.Th Wilke, in *Kristallzüchtung* (VEB Deutsher Verlag der Wissenschaften, Berlin, 1973) p. 71.
71. J. Shen, N. Kitamura, M. Kakehi and T. Wada, *Jpn. J. Appl. Phys.* 20 (1981) 1169.
72. K, B. Stepanek and V. Sestakov, *Cryst. Res. Technol.* 19 (1984) K41.
73. R.N. Hall and J.H. Racette, *J. Appl. Phys.* **32** (1961) 856.
74. J. W. Faust and A. Sagar, *J. Appl. Phys.* **31** (1960) 331.
75. H. C. Gatos and M. C. Lavine, *J. Electrochem. Soc.* **107** (1964) 427.
76. G.T. Brown, B. Cockayne, W.R. MacEwan and V.W. Steward, *J. Mater. Sci.* **1** (1982) 253.
77. C. Heinz, *Int. J. Electron.* **75** (1993) 285. http;//www.tandf.co.uk./journals
78. M. Omri, J-P. Michel and A. George, *Phil. Mag. A* **62** (1990) 203.
79. P.J. Anthorny, R.L. Hartsman, N.E. Schumaker and W.R. Wagner, *J. Appl. Phys.* **53** (1982) 756.
80. S. Tohno and A. Katsui, *J. Electrochem. Soc.* **128** (1981) 1614.
81. Y.J. van der Meulen, *Solid-State Electron.* 7 (1964) 767.
82. M. Kumagawa, *Jpn. J. Appl. Phys.* **16** (1977) 2297.

83. M. Kumagawa, Y. Asabe and S. Yamada, *J. Crystal Growth* **41** (1977) 245.
84. M. Kumagawa, *J. Crystal Growth* **44** (1978) 291.
85. M. Kumagawa and N.V. Quang, *Jpn. J. Appl. Phys.* **19** (1980) 2509.
86. N. V. Quang and M. Kumagawa, *Jpn. J. Appl. Phys.* **20** (1981) 817.
87. M. Kumagaya, *Jpn. J. Appl. Phys.* **21** (1982) 804.
88. M. Kumagawa and Y. Hayakawa, *J. Jpn. Assoc. Crystal Growth* **13** (1986), 131.
89. J. Allegre, M. Averous and G. Bougnot, *Crystal Lattice Defects* **1** (1970) 343.
90. J. Allegre and M. Averous, *Inst. Phys. Conf. Ser.* **46** (1979) 379.
91. L.M. Brescansin and A. Fazzio, *phys. stat. sol. (b)* **105** (1981) 339.
92. D. Shaw, *J. Phys. C: Solid State Phys.* **16** (1983) L839.
93. C.C. Ling, W.K. Mui, C.H. Lam, C.D. Beling, S. Fung, M.K. Lui, K.W. Cheah, K.F. Li, Y.W. Zhao and M. Gong, *Appl. Phys. Lett.* **80** (2002) 3934.
94. A.Y. Polyakov, S.J. Pearton, R.G. Wilson, P. Rai-Choudhury, R.J. Hillard, X.J. Bao, M. Stam, A.G. Milnes, T.E. Schlesinger and J. Lopata, *Appl. Phys. Lett.* 60 (1992) 1318.
95. P. Hubik, V. Smid, J. Kristofik, B. Stepanek and V. Sestakova, *Solid State Commun.* **86** (1993) 19.
96. V. Sestakova and B. Stepanek, *Thermochim. Acta* 209 (1992) 277.
97. D. Effer and P.I. Etter, *J. Phys. Chem. Solids* **25** (1964) 451.
98. V. Sestakova, B. Stepanek, J.J. Mares and J. Sestak, *J. Crystal Growth* **140** (1994) 426.
99. K. Nakashima, *Jpn. J. Appl. Phys.* **20** (1981) 1085.
100. F. Meinardi, A. Parisini and L. Tarricone, *Semicond. Sci. Technol.* **8** (1993) 1985.
101. A.N. Baranov, T.I. Voronina, T.S. Langunova, I.N. Timchenko, Z.I. Chugueva, V.V. Sherstnev and Yu.P. Yakovlev, *Sov. Phys. Semicond.* **23** (1989) 490.
102. P. S. Dutta, H. L. Bhat and V. Kumar, *J. Crystal Growth* **154** (1995) 213.
103. A.S. Filipchenko, T.B. Kurenkeev, L.P. Bolshakov and E.I. Chaikina, *phys. stat. sol. (a)* **48** (1978) 281.
104. E.I. Chaikina, S.Sh. Egemberdieva and A.S. Filipchenko, *phys. stat. sol. (a)* **84** (1984) 541.
105. E.I. Georitse, L.M. Gutsulyak, V.I. Ivanov-Omskii, V.A. Smirov and Sh. U. Yuldashev, *Sov. Phys. Semicond.* **25** (1991) 1180.
106. S. Basu, U.N. Roy, B.M. Arora and A.K. Srivastava, *Appl. Surf. Sci.* **59** (1992) 159.
107. M.F. Chioncel, C. Diaz-Guerra and J. Piqueras, *Semicon. Sci. Technol.* **19** (2004) 490.
108. H.D. Law, J.S. Harris, K.C. Wong and L.R. Tomasetta, *Inst. Phys. Conf. Ser.* **45** (1979) 420.
109. L.M. Dolginov, L.V. Druzhinina, P.G. Elisev, A.N. Lapshin, M.G. Milvidskij and B.N. Sverdlov, *Sov. J. Quantum Electron.* **8** (1978) 416.
110. H. Kano and K. Sugiyama, *Electron. Lett.* **16** (1980) 146.
111. Y. Horikoshi, in *Semiconductors and Semimetals Vol. 22*, eds. R.K. Willardson and A.C. Beer (Academic Press, New York, 1985) p. 93.
112. C. Heinz, *Electron. Lett.* **22** (1986) 276.
113. L. Jun, S. Hang, Y. Jin, J. Hong, G. Miao and H. Zhao, *Semicond. Sci. Technol.* **19** (2004) 690.
114. O. Hildebrand, W. Kuebart, K.W. Benz and M.H. Pilkuhn, *IEEE J. Quantum Electron.* **QE-17** (1981) 284.
115. O.V. Sulima, M.G. Mauk, Z.A. Shellenbarger, J.A. Cox, J.V. Li, P.E. Sims, S. Datta and S.B. Rafol, *IEE Proc. Optoelectron.* **151** (2004) 1.
116. L. Esaki, *J. Crystal Growth* **52** (1981) 227.
117. S.D. Kang and W.H. Ko, *Int. Electron Devices Meeting.* **No. 1976** (1976) 267.
118. A.S. Kyuregyan and V.M. Stuchebnikov, *Sov. Phys. Semicond.* **4** (1971) 1365.
119. P. Fay, G.H. Bernstein, D. Chow, J. Schulman, P. Mazymder, W. Williamson and B. Gilbert, in *9th Great Lakes Symp. VLSI*, March 04-06 (1999) p. 162.
120. P.E. Gruenbaum, V.T. Dinh and V.S. Sundaram, *Solar Ener. Mater. Solar Cells* **32** (1994) 61.
121. V.M. Andreev, V.P. Khvostikov, V.D. Rumyantsev, S.V. Sorokina, M.Z. Shvarts and V.I. Vasil'ev, Ioffe Institute, http;//www.ioffe.rssi.ru/index.en.html.
122. L. Fraas, H.H. Xiang, J. Samaras, T.R. Ballan, D. Williams, S. Hui and L. Ferguson, in *Conf. Rec.*

IEEE Photovoltaic Spec. Conf., 25th (1996) p. 125.
123. P.E. Gruenbaum, M.S. Kuryla and V.S. Sundaram, in *AIP Conf. Proc.* No. 321 (Am. Inst. Phys., 1995) p. 357.

10. InP

10.1 INTRODUCTION

Since the transmission losses in quartz optical fibers has been reduced by reducing the numbers of hydroxyl (OH) groups, the minimum loss can be obtained at around 1.3 μm and 1.55 μm.[1] These are therefore the wavelength region used for fiber communications. For quaternary InGaAsP III-V alloys in these wavelength regions, InP is an indispensable material since it has good lattice matching with these alloys as seen in Fig. 1.12. InP is therefore a key material for the production of InP photonic devices such as laser diodes (LDs), light emitting diodes (LEDs) and photodetectors for this type of communication.[2]

InP is also promising for high frequency devices such as high-electron-mobility transistors (HEMTs) and hetero-bipolar-transistors (HBTs). Because the carrier concentrations and the electron mobilities are large enough in InGaAs layers lattice-matching to InP, these InP-based devices can be used in the frequency range exceeding several tens of GHz.[3] These devices are expected to be useful in new applications in millimeter wave communications, anticollision systems and imaging sensors.[4] Optoelectronic integrated circuits (OEICs) with the integration of lasers, photodetectors and amplifiers are indispensable for second generation communication systems working at 40 Gb/sec.[5]

Since InP has a band gap of around 1.4 eV with a high energy conversion efficiency, it is also promising for solar cells especially for space satellites, because of its high resistivity against radiation.[6] In fact, InP based solar cells with p-n junctions have been fabricated for a space satellite.[7]

For the above applications, there are variously doped InP substrates commercially available as shown in Table 10.1. Sn-doped and S-doped n-type InP are for laser diodes and S-doped n-type InP is for photodiodes. Impurity hardening renders S-doped InP dislocation-free and makes it indispensable for photodiodes because dislocations increase the dark current in photodiodes.[8] For high power laser diodes, p-type Zn-doped InP is preferred and for solar cell applications, lightly Zn-doped InP is used. Fe-doped

Table 10.1 Various Types of InP and their Applications

Dopant	Concentrations	EPD	Applications
Sn	$0.5\text{-}6\times10^{18}$ cm^{-3}	$<5\times10^{4}$ cm^{-2}	laser diodes, LEDs
S	$>=4\times10^{18}$ cm^{-3}	no dislocation area	photodiodes
	>6.5 cm^{2} (<500 cm^{-2})		
Zn	$>=4\times10^{18}$ cm^{-3}	$<5\times10^{3}$ cm^{-2}	high power laser diodes
	$2\text{-}5\times10^{16}$ cm^{-3}	$<5\times10^{4}$ cm^{-2}	solar cells
Fe	$2\text{-}8\times10^{16}$ cm^{-3}	$<5\times10^{4}$ cm^{-2}	electronic devices
Undoped	($<10^{16}$ cm^{-3})	$<1\times10^{5}$ cm^{-2}	source material for LPE
	(Fe$<2.5\times10^{15}$ cm^{-3})	$<5\times10^{4}$ cm^{-2}	electronic devices

semi-insulating InP is indispensable for high frequency electronic devices such as HEMTs and HBTs. Semi-insulating InP may also find its application even for photonic devices with higher transmission rate than 40 GHz/sec because of the necessity to reduce parasitic noise.[9, 10]

The development of InP, crystal growth, characterization and devices are reviewed in Refs. 11-15.

10.2 PHYSICAL PROPERTIES

The main physical properties of InP are summarized in Table 10.2. More detailed data can be found in Refs. 12 and 16.

Fig. 10.1(a) shows the pressure-temperature (P-T) phase diagram and Fig. 10.1(b) shows the composition-temperature (X-T) phase diagram of InP.[17, 18] The detail of these phase diagrams has also been studied and discussed from the viewpoint of defect formation.[19, 20] The non-stoichiometric region of InP is not yet well known but a preliminary study by coulometric titration analysis[21] showed that the deviation of the composition is quite small in the case of InP, compared with the case of GaAs (Sec. 8.6.6). It is predicted that this could be the reason why InP does not show many precipitates with native defects such as EL2 in GaAs.[22]

InP is one of the compound semiconductors whose stacking fault energy is small as shown in Fig. 1.24. In the crystal growth of InP, twinning occurs much more easily than with GaAs and GaP, and this is a serious difficulty with InP crystal growth.

The resolved shear stress is a factor which predicts the ease of the dislocation generation as explained in Sec. 1.7.3. Among various compound semiconductor materials, InP has a lower resolved shear stress as seen in Table 1.11. This is one of the reasons why the growth of low dislocation density InP single crystals is difficult.

The hardness of InP is lower than that of Si, GaP and GaAs. This is the main reason why InP is more brittle than Si, GaP and GaAs and the thickness of InP wafers is specified to be greater than that of Si. The dimensions of InP wafers are standardized by SEMI International.[23]

Table 10.2 Physical Properties of InP

Crystal Structure	zincblende
Lattice Constant	5.869 Å
Density	4.8 g/cm^3
Melting Point	1062 °C
Linear Expansion Coefficient	4.5x10^{-6}/deg
Thermal Conductivity	0.70 W/cm·K
Dielectric Constant	12.5
Refractive index	3.45
Bandgap at Room Temperature	1.35 eV
Optical Transition Type	direct
Intrinsic Carrier Concentration at R.T.	2x10^7 cm^{-3}
Electron Mobility at R.T.	4500 cm^2/V·sec
Hole Mobility at R.T.	150 cm^2/V·sec
Intrinsic Resistivity	8x10^7 Ω·cm

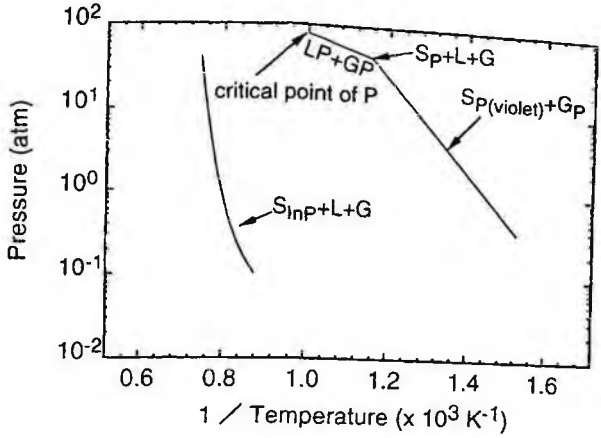

(a)

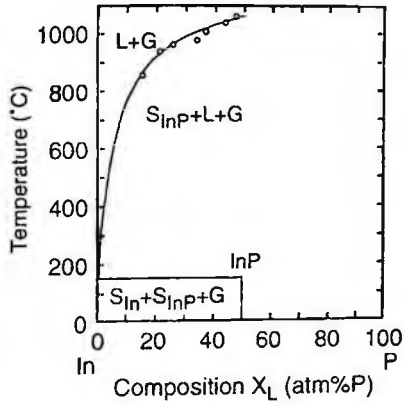

(b)

Fig. 10.1 Phase diagrams of InP (from Ref. 17 with permission). (a) P-T phase diagram, (b) X-T phase diagram.

The drift velocity of InP under a strong electric field is greater than those of GaAs and Si as seen in Fig. 1.22 so that InP is believed to be a good material for higher speed devices.[24] InP has quite high thermal conductivity so that InP is a good material for electronic devices from the viewpoint of power dissipation. The precise thermal conductivity as a function of temperature is discussed by Jordan.[25]

InP has another advantage in having lower localized state densities than those of GaAs, so that it is also promising for metal-insulator-semiconductor FETs (MISFETs) and metal-oxide-semiconductor (MOSFETs).[26]

10.3 CRYSTAL GROWTH

The polycrystal synthesis and crystal growth of InP have been reviewed by several authors as seen in Refs. 13, 22 and 27-33.

10.3.1 Polycrystal Synthesis

InP has a high decomposition pressure of about 27 atm. so that it is difficult to synthesize InP polycrystals directly from indium and phosphorus in the crystal growth furnace. Polycrystals must therefore be pre-synthesized prior to crystal growth. Various methods such as synthesis by solute diffusion (SSD), horizontal Bridgman (HB), horizontal gradient freezing (HGF) and phosphorus injection methods have been studied in order to synthesize polycrystals (Table 10.3).

(1) Solute Solution Diffusion (SSD) method

The SSD method (Sec. 5.3.3), first proposed for GaP crystal growth has been applied to InP polycrystal synthesis.[31, 34-46] A typical furnace configuration for this method is shown in Fig. 10.2.[31] In the SSD method, InP crystals are grown at lower temperatures (900-1000 °C) from an indium rich solution. From the bottom reservoir with a lower temperature, phosphorus is supplied as the vapor and is dissolved in the indium melt. InP crystals are grown from the bottom of the crucible and the lack of phosphorus in the melt is supplied from the vapor phase. Since crystals can be grown at lower temperatures, silicon contamination from the quartz ampule can be minimized. Other impurities with segregation coefficients less than unity can be accumulated in the solution so that high purity crystals can be grown. In fact, very low carrier concentrations of the level of 10^{14} cm^{-3} are reported.[31, 43] The growth rate of this method is however very low since the diffusion of phosphorus in the solution is very slow.

(2) Horizontal Bridgman (HB) and Horizontal Gradient Freezing (HGF) methods

HB and HGF methods have been extensively studied by various researchers[19, 31, 47-63] from the earliest stages of InP crystal development. In these methods, phosphorus vapor is made to react with the indium melt to be synthesized. When the temperature of the indium melt is higher than the melting point of InP, phosphorus vapor is absorbed in the indium melt till all of the indium melt is converted to InP melt. Since the temperature of the indium melt is higher than the melting point, the synthesis rate is quite high but the contamination by silicon from the quartz ampoule is significant.

The HB method with three heater zones as shown in Fig. 10.3 was developed in order to overcome this disadvantage of the former HB/HGF methods. Indium in a boat-type crucible and red phosphorus block are charged and vacuum-sealed in a quartz ampoule. The ampoule is then heated under the temperature distribution as seen in Fig. 10.3. Phosphorus vaporized from the one side of the ampoule is dissolved into the indium melt up to its solubility. In the RF heating region, where the temperature is the highest but still lower than the melting point of InP, the phosphorus content is increased because of its higher solubility. InP polycrystals are precipitated from the indium solution at the end of the boat and are grown with the translation of the ampoule. An inert gas such as nitrogen or argon at an overpressure of up to 40 atm. is applied to prevent the rupture of the quartz ampoule during synthesis. This method is presently adopted as the industrial synthesis method because of its reasonable synthesis rate and

Table 10.3 Polycrystal Synthesis of InP

Method	Result	Author	Year	Ref.
HGF	First synthesis report of InP	Richman	1962	47
HGF	Small scale synthesis	Bachmann et al.	1974	19, 48
HGF	Directional freezing at 950 °C	Antypas	1977	49
HGF	Synthesis by gradient freezing	Henry et al.	1978	50
SSD	First application of SSD method to InP	Marshall et al.	1978	34
SSD	$3x10^{14}$ cm^{-3} < C/C < $2x0^{16}$ cm^{-3}	Yamamoto et al.	1978	35
SSD	Large diameter polycrystal with low C/C	Sugii et al.	1979	36
HGF/HB	Synthesis by two-zone furnace	Iseler	1979	51
HB	C/C=$6.8x10^{14}$ cm^{-3}	Barthruff et al.	1979	52
DS	First application of P-injection method to InP	Wardill et al.	1980	64
SSD	C/C=$6.4x10^{14}$ cm^{-3} after In baking	Kubota et al.	1981	37
HGF	150 g synthesis with C/C=2-5x10 cm^{-3}	Bonner	1981	53
HGF	Rapid synthesis up to 2 kg within two hours	Allred et al.	1981	54
HB	Three zone HB method for 1.6 kg InP synthesis	Rumsby et al.	1981	55
HB	Reduction of Si contamination	Yamamoto et al.	1981	56
DS	1 kg polycrystal synthesis by P-injection	Farges	1982	65
HB	Purity improvement by pre-baking of indium	Adamski	1982	57
DS	Synthesis by phosphorus injection	Tongnien et al.	1982	66
DS	Polycrystal InP synthesis by the P-injection method	Hyder et al.	1983	67
HB	Effect of synthesis conditions on the purity of synthesized InP	Adamski	1983	58
HGF	C/C~$1x10^{15}$ cm^{-3} by presynthesis purification	Bonner et al.	1983	59
HGF	Effect of synthesis conditions on the purity of synthesized InP	Coquille et al.	1983	60
HGF	C/C<$5x10^{15}$ cm^{-3}, 1.6 kg, 10-20 mm/hr	Wardill et al.	1983	61
SSD	Growth-rate controlled SSD method	Kubota et al.	1984	38
SSD	P-type InP doped with Mg, Ca and Zn	Kubota et al.	1984	39
SSD	Preparation of Fe-doped semi-insulating InP	Chung et al.	1984	40
SSD	C/C~$1x10^{14}$ cm^{-3} after prebaking of sources	Ohoka et al.	1985	41
HB	C/C=1-$3x10^{15}$ cm^{-3} by using pBN boats	Kusumi et al.	1985	62
SSD	Dependence of growth rate on growth temperature and temperature gradient	Aikawa et al.	1985	42
SSD	Growth rate as a function of temperature	Kainosho et al.	1985	43
DS	3 kg synthesis by P-injection	Sasaki et al.	1985	68
SSD	Growth of undoped n-type and Zn-doped p-typed InP	Siegel et al.	1986	44
SSD	Identification of shallow donors as Si and S	Kubota et al.	1986	45
HGF	Use of sandblasted quartz boat, C/C<$5x10^{15}$ cm^{-3}	Yoshida et al.	1987	63
DS	Liquid phosphorus encapsulated method	Inada et al.	1987	69, 70
DS	10-11 kg large scale synthesis by P-injection	Dowling et al.	1988	71
SSD	Calculation of diffusion constant of phosphorus	Oda et al.	1990	29
DS	Simulation analysis of P-injection synthesis	Prasad et al.	1994	72
SSD	Synthesis by using glassy-carbon crucibles in In melt	Miskys et al.	1996	46
DS	Large-scaled P-injection synthesis furnace with successive crystal growth facility	Bliss et al.	2001	73
DS	P-injection synthesis in a magnetic LEC furnace with 3 kg charge	Higgins et al.	2000-2001	74-75

SSD: Solute Solution Diffusion, HB; Horizontal Bridgman, HGF: Horizontal Gradient Freezing, DS: Direct Synthesis

the prevention of silicon contamination.

The stoichiometry of synthesized InP polycrystals is critical for InP single crystal growth. When the InP polycrystal is indium-rich, the composition of the InP melt in the LEC growth becomes indium-rich and it becomes difficult to grow single crystals because of supercooling. The stoichiometry can be analyzed by coulometric titration analysis. It is known that stoichiometric InP polycrystals can be obtained by optimizing the conditions of synthesis.[22]

Yoshida et al.[63] developed a horizontal gradient freezing (HGF) method for polycrystal synthesis and crystal growth. InP polycrystals were synthesized from indium and red phosphorus in a quartz boat which was sandblasted and thermally finished to

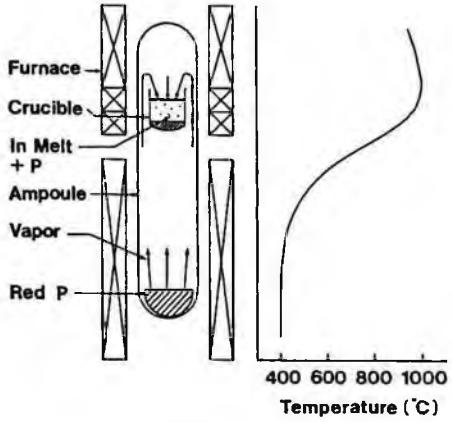

Fig. 10.2 Solute Solution Diffusion (SSD) method (reprinted from Ref. 31, with permission, copyright 1990 Elsevier).

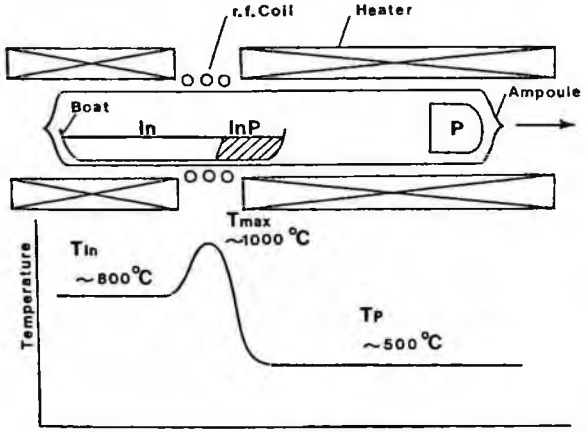

Fig. 10.3 Horizontal Bridgman method (reprinted from Ref. 31 , with permission, copyright 1990 Elsevier).

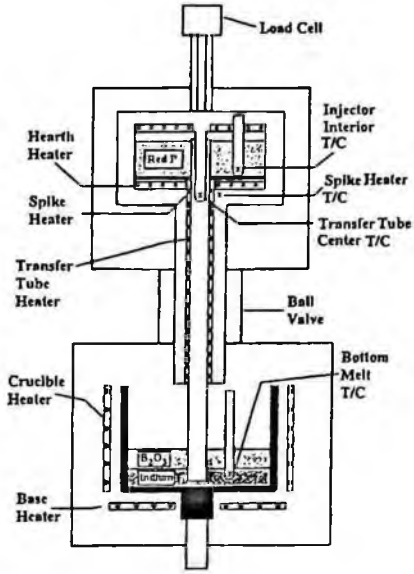

Fig. 10.4 Schematic drawing of phosphorus injection system (reprinted from Ref. 75 with permission, copyright 2001 Elsevier).

prevent the synthesized InP polycrystal sticking to the quartz surface and Si contamination from the quartz boat. Carrier concentrations less than $5x10^{15}$ cm^{-3} could be obtained even though the quartz boat was used.

(3) Direct Synthesis (DS) methods

Direct synthesis methods in which phosphorus is injected into the indium melt in high pressure vessels are promising methods with the potentiality to replace the HB method because of the higher growth rate and the lower production cost, and they have been extensively studied.[64-75] In the injection method, phosphorus reacts with indium very quickly so that the rapid polycrystal synthesis is possible. It also lends itself easily to increasing the scale of production, so that the method is very promising for future large-scale production. In fact, Bliss et al.[73-75] have developed a new system for this purpose (Fig. 10.4).

Inada et al.[69, 70] invented a direct synthesis method in which indium is reacted with white phosphorus which is circulated in the furnace as vapor/liquid transformation (Fig. 10.5). After the synthesis, crystal growth can be performed in the same furnace. In this method, indium and phosphorus are charged in a crucible, the top of which is covered by a thermal shield. Phosphorus vaporized from the crucible during heating deposits on the wall of the shield as white phosphorus which is in the liquid state in this temperature range. Liquid phosphorus then drops down into the indium melt and phosphorus which does not react with the liquid indium thus circulates in the furnace till all

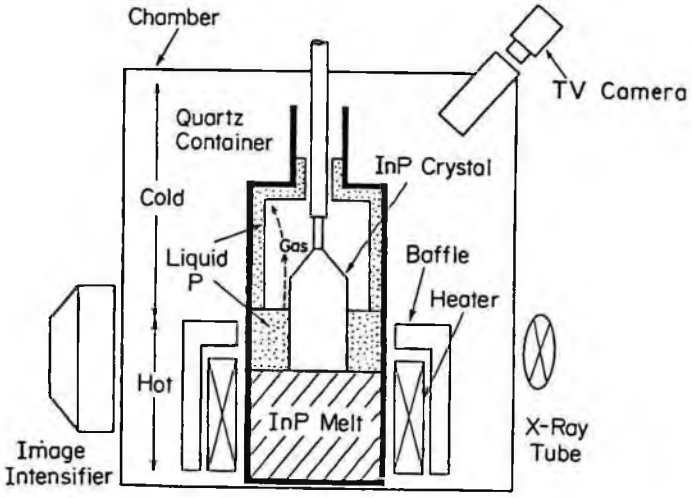

Fig. 10.5 Schematic diagram of the furnace for the liquid phosphorus encapsulated Czochralski (LPCZ) method (reprinted from Ref. 69 with permission, copyright 1987 American Institue of Physics).

indium reacts to form InP. The residual liquid phosphorus plays a role as an encapsulant to prevent the decomposition of the synthesized InP. After the synthesis is completed, the crystal growth is performed in the furnace directly without interruption for cooling.

10.3.2 Single Crystal Growth

The crystal growth of InP has been performed by several methods such as the LEC method, modified LEC method, vapor pressure-controlled LEC (VLEC) method, VGF method and the HB/HGF method. These studies are summarized in Table 10.4.

(1) Liquid Encapsulated Czochralski (LEC) method

Mullin et al.[76, 77] first applied the LEC method to the crystal growth of InP and then the conventional LEC method became the main growth method.[49, 55, 66, 78-94] The diameter of crystals has also been increased. The growth of 75 mm diameter single crystals has been achieved with and without magnetic field application.[83, 85] LEC growth has also been performed using directly-synthesized InP polycrystals.[65, 67-69, 71] Synthesis by phosphorus injection and successive direct crystal growth methods have also been studied.[66, 73-75] Prasad et al.[72] made a theoretical hydrodynamic consideration of synthesis by phosphorus injection and the direct crystal growth process. Based on these preliminary works, Bliss et al. developed an in-situ synthesis and crystal growth system, being able to grow crystals of diameter up to 150 mm.[73-75] The growth of 150 mm diameter single crystals has been reported.[91] Computer simulations of the effect of gas flow

Table 10.4 Crystal Growth of InP

Method	Result	Author	Year	Ref.
LEC	First crystal growth of InP by the LEC method	Mullin et al.	1968	76
LEC	Effect of growth parameters on the crystal perfection and electrical properties	Mullin et al.	1970	77
LEC	Growth of undoped, Zn-doped and Cd-doped crystals	Bachmann et al	1975	78
LEC	Twin-free <100> single crystal growth with a diameter increase angle less than 19.68°	Bonner	1980	79
LEC	Growth of dislocation-free crystals by the necking procedure	Shinoyama et al.	1980-1981	80-82
LEC	Single crystal growth with 80 mm diameter and 3 kg weight	Rumsby et al.	1981	55
LEC	Direct synthesis of polycrystals by P-injection and the successive crystal growth	Farges et al.	1982	65
DS-LEC	Phosphorus injection synthesis and in-situ crystal growth	Tong-nien et al.	1982	66
DS-LEC	Direct synthesis of polycrystals by phosphorus injection and the successive crystal growth	Hyder et al.	1983	67
LEC	Effect of crystal growth conditions on the purity of grown crystals	Coquille et al.	1983	60
DS-LEC	LEC growth from polycrystals synthesized by P-injection	Sasaki et al.	1985	68
LEC	75 mm diameter <100> Sn-, S-doped single crystals	Katagiri et al.	1986	83
VGF	First growth of InP by the VGF method	Gault et al	1986	116
VCZ	50 mm diameter InP under dT/d=30 °C/cm, EPD=$2x10^3$ cm^{-2}	Tada et al.	1987	103
LEC	50 mm diameter dislocation-free crystals by S-doping	Farges et al	1987	84
VGF	50 mm diameter <111>InP, EPD=several 10^2 cm^{-2}	Monberg et al.	1987	117, 118
LPCZ	Crystal growth by the CZ method with encapsulation by liquid phosphorus	Inada et al.	1987-1990	69-70
DS-LEC	10-11 kg large scale synthesis by P-injection	Dowling et al.	1988	71
HGF	(100) grain of about 40x30 mm	Yoshida et al.	1988	63
MLEC	75 mm diameter Fe-doped InP under magnetic field	Hofmann et al.	1988	85
VGF/DGF	50 mm diameter <111> Fe-doped InP with low EPD	Monberg et al.	1988	119
VGF/DGF	50 mm diameter <111> Zn-doped InP, doping level less than 10^{18} cm^{-3}	Monberg et al.	1989	120
VGF/DGF	Details of the VGF/DGF furnace configuration	Monberg et al.	1989	121
MLEK	Growth of 70 mm diameter crystals under magnetic field	Ahern et al. 1989	1989	141-142
VCZ	Low EPD 50 mm diameter crystals grown by phosphorus vapor pressure application	Tatsumi et al.	1989	8, 104
PC-LEC	Low EPD 75 mm diameter crystals grown by phosphorus vapor pressure application	Kohiro et al.	1991-1996	73, 110-112
VGF	<100> InP crystal growth with a double-wall crucible containing $CdCl_2$	Ejim et al.	1991	122
HGF	<100> 22x6 mm crystals with stoichiometry control	Schäfer et al.	1991	138
VGF	Elliptical <111> InP crystal growth with EPD < 50 cm^{-2}	Shahid et al.	1991	123
LE-VB	Growth in open ampoules using B_2O_3 encapsulant	Fornari et al.	1991	124
MLEK	Effect of magnetic field on EPD and Sn concentration distribution	Bliss et al.	1991-1993	143-144
VCZ	Low EPD 75 mm diameter crystals grown by phosphorus vapor pressure application	Hosokawa et al.	1992	105
TB-LEC	Thermal baffle application for EPD reduction	Hirano et al.	1992	97
VB	Liquid encapsulated VB method using the same diameter seed crystal	Matsumoto et al.	1993	125

Table 10.4 Crystal Growth of InP (continued)

Method	Result	Author	Year	Ref.
VGF	Growth in a multiple heater furnace, prevention of twinning	Müller et al	1993	126
TB-LEC	Application of a double thermal baffle with an outer thermal insulator for EPD reduction	Hirano et al.	1995 1999	98-102
VGF	Numerical simulation for VGF crystal growth with the same diameter seed crystal	Zemke et al.	1996	127
VGF	Numerical simulation of interface curvature for VB crystal growth with the same diameter seed	Rudolph et al.	1996	128
VGF	First report on <100> oriented single crystal growth	Liu	1996	129
LEC	Growth using glassy carbon crucibles	de Oliveira	1996 1998	86-88
LEC	Growth using a double crucible system	Fornari et al.	1996	89
MLEK	Fabrication of a large scaled direct synthesis and LEC crystal growth system	Bliss et al.	1998	73
VCZ	Single crystal growth of 100 mm diameter <100> InP	Hosokawa et al.	1998	107, 108
VGF	Single crystal growth of 75 mm diameter <100> InP	Young et al.	1998	130, 131
VGF	Single crystal growth of 100 mm diameter <100> InP, EPD=2000 cm^{-2}	Asahi et al.	1998 1999	132-135
LEC	Fragility of 75-100 mm diameter InP wafers	Ware	2000	90
HB	Effect of boat material and phosphorus vapor pressure	Shimizu et al.	2000	139, 140
PC-LEC	Dislocation free 75 mm diameter Fe-doped single crystals	Noda et al.	2001	113-115
MLEC	Phosphorus injection synthesis and LEC growth under magnetic field	Higgins et al.	2000-2001	74-75
LEC	Growth of 150 mm diameter single crystals	Sato et al.	2003	91
LEC, VCZ	Comparison of various crystal growth methods	Kawase et al .	2004	109
DS-LEC	P-injection synthesis and growth of 100 mm diameter single crystals	Zhou et al.	2004	92
LEC	Growth of 75-100 mm diameter single crystals	Sun et al.	2004	93
LEC	Growth from a phosphorus-rich melt	Sun et al.	2004	94

LEC: Liquid Encapsulated Czochralski, MLEC: Magnetic LEC, DS-LEC: Direct Synthesis and LEC, PC-LEC: Pressure-Controlled LEC, TB-LEC: Thermal Baffle LEC, VCZ: Vapor pressure controlled Czochralski, VGF: vertical gradient freezing, DGF: Dynamic Gradient Freezing, VB: Vertical Bridgman, HGF: Horizontal Gradient Freezing, HB: Horizontal Bridgman, LEK: Liquid Encapsulated Kyropolous, MLEK: Magnetic LEK, LPCZ: Liquid Phosphorus encapsulated Czochralski

on the melt flow and S/L interface, and the thermal stress and dislocation distribution during LEC crystal growth have also been performed.[95, 96]

(2) Improved LEC method

To reduce the dislocation density, modified LEC methods have been developed, such as Thermal Baffle LEC (TB-LEC) methods, in which thermal baffles are used to reduce the temperature gradient in the furnace (Fig. 10.6).[97-102] Since the upper part of the melt crucible is covered by thermal baffles, the axial temperature gradient can be reduced as well as the radial temperature gradient. When the axial temperature gradient is reduced, the temperature of the surface of the boric oxide encapsulant is increased so that it promotes the decomposition of phosphorus from the surface of the growing InP crystal. The decomposition of phosphorus however can be prevented because of the ther-

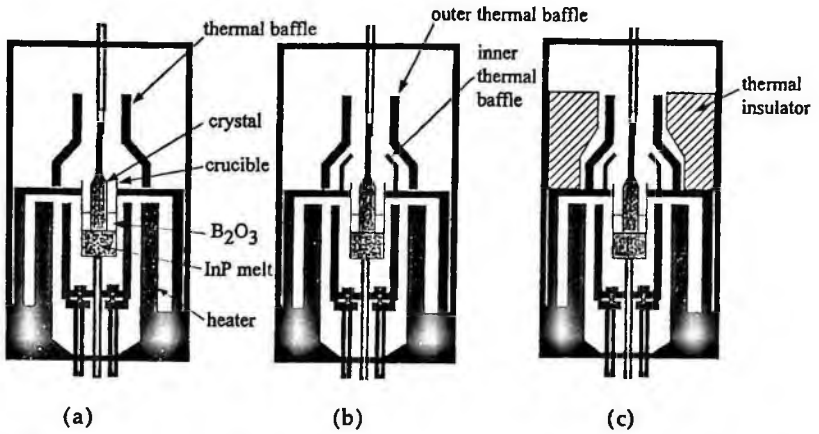

Fig. 10.6 Various thermal baffle structure for TB-LEC methods (from Ref. 133 with permission). (a) Single thermal baffle, (b) double thermal baffle, (c) double thermal baffle with outer thermal insulator.

mal baffle from which the effusion of phosphorus vapor is suppressed due to the small outlet cross section over the thermal baffle.

(3) Vapor-Pressure-Controlled LEC (VLEC) methods

VLEC methods, such as the Vapor-pressure-controlled Czochralski (VCZ) method[8, 103-109] and the Pressure-Controlled LEC (PC-LEC) method have been developed[110-115] to reduce dislocation densities. In these methods, the phosphorus vapor pressure is applied from the phosphorus reservoir during crystal growth as shown in Fig. 10.7(b), in order to prevent the dissociation of phosphorus from the surface of growing crystals. Because decomposition can be prevented by the applied vapor pressure, the axial temperature gradient can be decreased as seen in Fig. 10.7. This decrease leads to the reduction of dislocation densities as explained in Section 2.3. Fig. 10.8 shows a 75 mm diameter InP single crystal grown by the PC-LEC method. Hosokawa et al. have applied the VCZ method to the growth of 100 mm diameter single crystals.[107-109] Noda et al. developed the PC-LEC to grow Fe-doped semi-insulating (SI) crystals with hardly any dislocations.[113-115]

(4) Vertical Gradient Freezing (VGF) and Vertical Bridgman (VB) methods

The VGF/VB methods for InP have been developed by the ATT group and others.[116-123] It is reported that low dislocation density crystals can be grown as shown in Table 10.7. The growth was however limited to <111> oriented crystals because twinning readily occurs. To grow <100> oriented crystals, the use of an ellipsometric crucible and of $CaCl_2$ material around the outside of the crucible have been examined.[122, 123] The same diameter seed crystal as that of grown crystals is applied to prevent twinning[125] and the

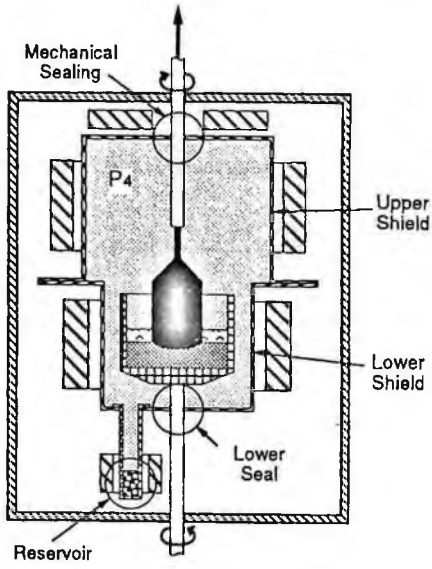

(a)

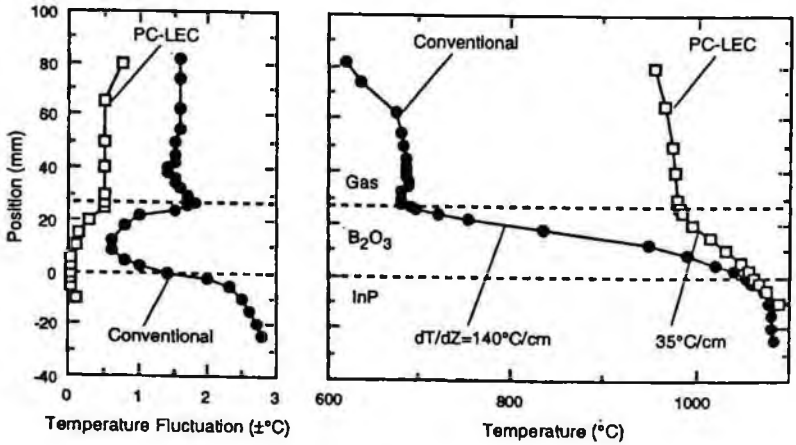

(b)

Fig. 10.7 Pressure-Controlled LEC (PC-LEC) method (reprinted from Ref. 112 with permission, copyright 1996 Elsevier). (a) Furnace configuration and (b)Temperature fluctuations and distributions for conventional LEC method and PC-LEC method.

process has been examined by numerical simulation.[127, 128] It is reported that <100> oriented single crystals have been obtained.[129] The perspective of VGF/VB methods has been reviewed by Müller.[126] The difficulty of growing <100> oriented InP single crystals has however been finally overcome by the growth of 75 mm diameter single crystals[131] and 100 mm diameter single crystals.[132-135] Fig. 10.10 shows a 100 mm diameter single crystal of length 80 mm grown by the VGF method using a six-heater zone furnace. This success is mainly thanks to precise temperature control using six heaters

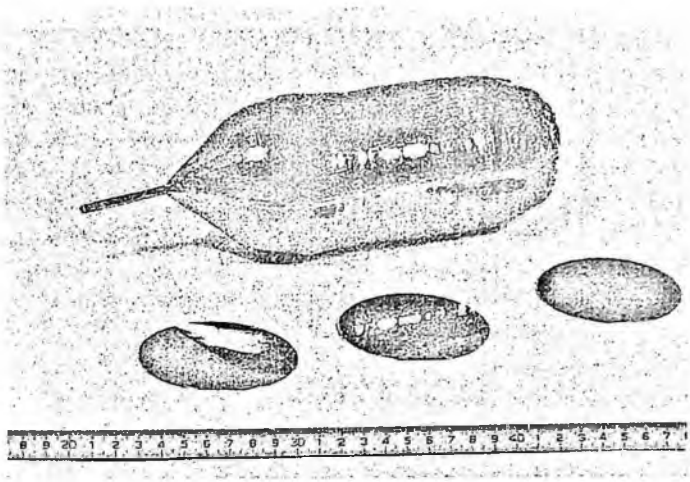

Fig. 10.8 75 mm diameter long (240 mm) InP single crystal grown by the PC-LEC method (reprinted from Fig. 17 at p. 36 in Ref.22 with permission).

(Fig. 10.9) and the reduction of temperature fluctuations which is effective in preventing twinning as mentioned in Sec. 4.4. Simulations for VB methods have been performed.[136, 137]

(5) Horizontal Bridgman (HB) and Horizontal Gradient Freezing (HGF) methods

The HGF method has been applied to the synthesis of InP polycrystals and the successive crystal growth by Yoshida et al.[63] A large grain of 40x35 mm could be obtained but the entire single crystal could not be obtained. Using 22 mm inner diameter ampoules, Schäfer et al.[138] obtained <100> oriented single crystals by the HGF method. Shimizu et al.[139, 140] have grown InP crystals by the HB method and studied the effect of boat material and the phosphorus vapor pressure on the dislocation density.

In the HB/HGF furnaces, wide temperature fluctuations and strong convection in the melt occur because the melt surface and the solid/liquid interface are always exposed to high pressure gas of several tens of atmospheres. This high pressure causes strong gas convection which influences the solid/liquid interface exposed to the melt surface and makes it difficult to grow single crystals.

(6) Other Methods

As mentioned in Section 10.3.1, Inada et al.[69, 70] invented a simultaneous polycrystal synthesis and crystal growth method. In this method, indium and phosphorus are directly synthesized in a Czochralski crystal grower and crystals are grown successively in the same furnace. Liquid phosphorus covering the InP melt plays the role of encapsulant instead of B_2O_3 during crystal growth. <111> oriented 20 mm diameter single

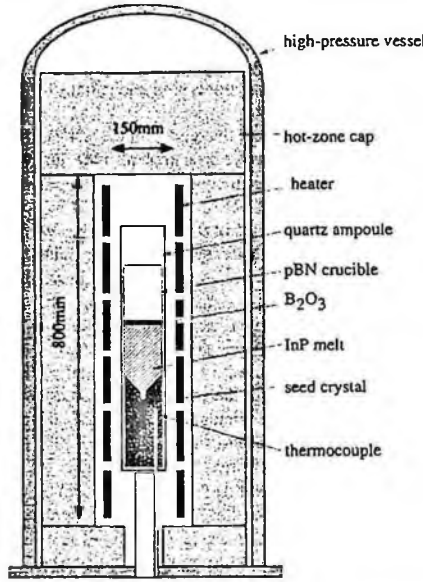

Fig. 10.9 Schematic diagram of a high-pressure VGF furnace with multiple heaters (from Ref. 134 with permission).

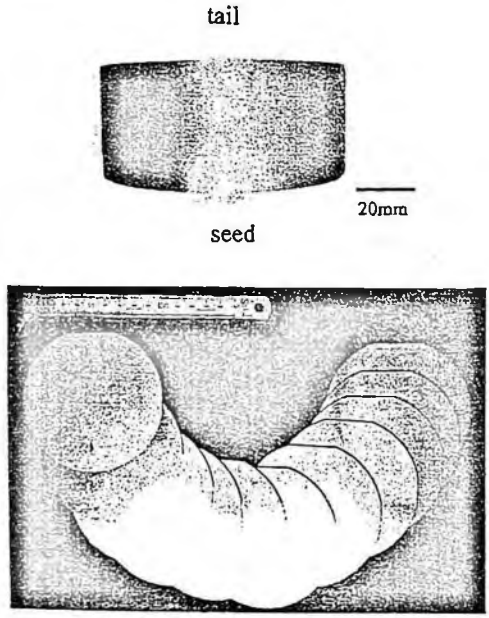

Fig. 10.10 100-mm diameter single crystal grown by a high-pressure VGF method and wafers (from Ref. 134 with permission).

crystals could be successfully grown.

The Liquid Encapsulated Kyropolous (LEK) method was also studied.[141-144] A magnetic field was applied in order to reduce the temperature fluctuation. In this method, crystal growth is performed in the crucible without pulling the seed crystal so that a lower axial temperature gradient can be realized as in the case of the VGF method. 50-75 mm diameter <100> oriented single crystals have been grown by Bliss et al.[143, 144] They reported the characteristic dislocation densities, growth interfaces and impurity segregations.

10.3.3 Prevention of Twinning

Since the stacking fault energy of InP is lower than for GaAs and GaP as shown in Table 1.11, twinning takes place very easily during crystal growth. Various crystal growth factors which affect the occurrence of twinning have been discussed in Section 4.4. Bachmann et al. pointed out that twinning is due to the entrapped gas bubbles between InP and B_2O_3.[78]

Tono and Katsui[145] used X-ray topography for observing twin formation in LEC-grown InP crystals and found that twin crystals are formed by a 180° angle rotation around the <111> axis. By micro Raman scanning spectroscopy, it has been shown that fluctuation of stoichiometry is the origin of twin formation.[146] Twinning occurrence in the initial stage of InP crystal growth has been examined by Wei[147] and the mechanism has been discussed. By synchrotron white beam X-ray topography, Chung et al.[148] also examined the occurrence of twinning. They basically showed that the prediction by Hurle[149] is correct in certain cases but also showed a new twin formation mechanism. Using magnetic field LEC (MLEC) grown crystals, the origin of twins has been studied systematically.[150, 151] Han and Lin[152] have discussed stress, non-stoichiometry and inhomogeneous impurity distribution as the origin of twinning. Antonov et al.[153] have discussed the possibility of twinning being due to the transition from a dislocation-free mechanism region to one where the dislocation growth mechanism depends on the crystal diameter.

The prevention of twinning has been attempted by Yoshida et al.[154] by enlarging the shoulder part of the crystal as flat as possible in the LEC crystal growth using a low pulling rate just after seeding. This high growth rate can prevent twinning. This may be because when the growth rate is made quite high, the fluctuation of the interface position due to the temperature fluctuation is reduced since the interface position itself moves quickly due to the high growth rate. The disadvantage of this method may be the occurrence of polygonization because of the insufficient dissipation of the latent heat of solidification during crystal growth.

In order to prevent twinning in the VGF method, a large diameter seed crystal, the same diameter as the grown crystal has been applied in the VGF method by Matsumoto et al.[125] and Zemke et al.[127] They showed that twin-free <001> oriented single crystals can be obtained. This method seems to be reasonable from the viewpoint of the three phase equilibrium (Sec. 4.4). Since the seed crystal has the same diameter as the grown crystal, the contact angle between the solid and the environment gas phase θ_{SG} and that

between the solid and the liquid θ_{SL} are constant during crystal growth while in the shoulder part of LEC and VGF methods, they are not constant. This arrangement therefore seems to make the factor control more easily.

When the vapor pressure-controlled LEC (VLEC) methods such as PC-LEC and VCZ methods are used, twinning occurs more readily because the axial temperature gradient is decreased so that the solid/liquid (S/L) interface fluctuation distance becomes large when the temperature fluctuation is the same as the LEC method. In these methods, in order to minimize the S/L interface distance, it is essential to reduce temperature fluctuations to prevent twinning. In fact, in the PC-LEC method, the temperature fluctuation is reduced from 1.3 °C to less than 0.2 °C at the S/L interface[111, 112] and 75 mm single crystals without twins could be reproducibly grown. Hosokawa et al.[107, 108] showed that the temperature fluctuation in the VCZ method can be reduced from 1 °C to 0.5 °C to grow 100 mm diameter single crystals.

In the case of VGF methods, the axial temperature gradient becomes even smaller and the S/L interface distance much larger. In fact, the growth of <100> oriented InP single crystals becomes difficult. In order to grow< 100> oriented 100 mm diameter InP single crystals, Asahi et al. examined the gas flow in the VGF furnace by a computer simulation and found that the gas flow is greatly affected by the furnace configuration.[132-135] They also showed that the temperature fluctuation in the VGF furnace can be reduced from 0.2 °C to 0.03 °C by improving the furnace configuration. After this improvement, it beocmes possible reproducibly to grow < 100> oriented 100 mm diameter InP single crystals.

10.3.4 Reduction of Dislocation Densities

The reduction of the commonest defects, dislocations, is one of the key issues in InP crystal growth. The effect of dislocation densities is twofold. Firstly, in InP based photodetectors, it is known that dislocations are the cause of high current leakage.[8] Secondly, high dislocation densities exceeding $5x10^4$ cm^{-2} are undesirable from the viewpoint of wafer warpage and brittleness. This is more critical for large diameter wafers since the breakage of InP wafers becomes significant during device processing.

Dislocation densities can be reduced by two methods, by impurity hardening and by reducing the temperature gradient as explained in Sec. 4.3.3 and Sec. 3.5 respectively. The first is achieved by doping appropriate impurities and the second is achieved by various crystal growth methods.

(1) Impurity hardening

In the case of InP, it is known that S, Zn, and Te are very effective in reducing dislocation densities.[84, 155, 156] Some studies of the effect of isoelectronic impurities such as Ge, Ga, Sb and As have also been carried out.[157-162] These isoelectronic impurities have been examined to see if dislocation densities can be reduced without any change in electrical properties, aiming at semi-insulating Fe-doped InP whose dislocation densities are similar to undoped InP.

Industrially, only S-doped and Zn-doped InP are commercialized as dislocation-free

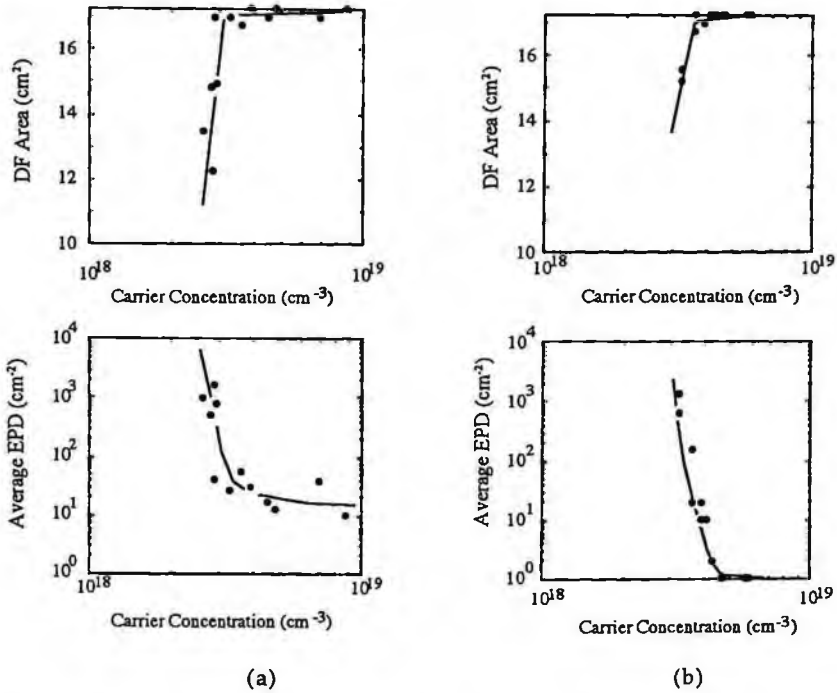

Fig 10.11 Average etch pit density (EPD) and dislocation-free (DF) area of (a) S-doped and (b) Zn-doped InP (from Ref. 13 with permission).

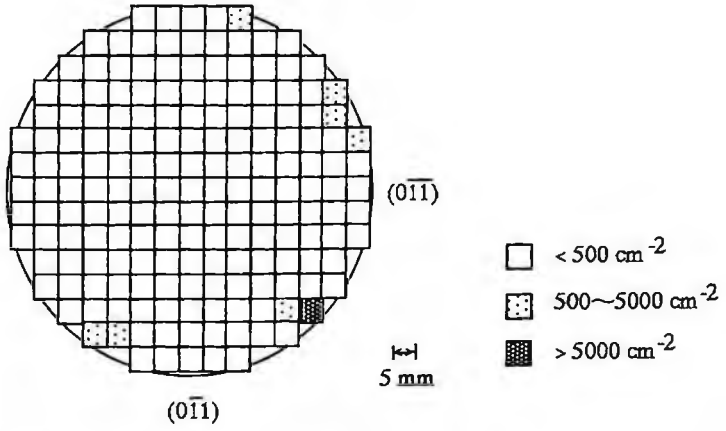

Fig. 10.12 Dislocation-free (DF) area for 75 mm diameter S-doped InP (from Ref. 13 with permission).

n-type material and p-type material, respectively. The effect of S-doping and Zn-doping on the reduction of dislocation densities is shown in Fig. 10.11 as a function of dopant concentrations. For 75 mm diameter InP, it is known that a very large dislocation-free area can be obtained as seen in Fig. 10.12.

Si-doping has not been successful because Si is gettered as SiO_2 in the encapsulant B_2O_3 and sufficient doping can not be achieved. The other disadvantage is due to the possibility of amphoteric behavior of Si. Cd is expected to be an effective p-type dopant compared with Zn since it has a lower diffusion coefficient.[162]

The effect of co-doping, e.g. with Zn+S, Ga+Sb, Ge+S, Ga+As, Ga+As+Sb, Fe+Ge, Cd+S, has also been examined extensively.[163-169] In this co-doping, various effects have been pursed. One is to use two dopants, one of which has a segregation coefficient less than unity and the other of which has a segregation coefficient larger than unity. The dislocation densities can be then reduced to the same extent along the crystal growth axis with one dopant compensating for the effect of the other. Improving carrier concentration consistency along the crystal growth axis has also been attempted by the co-doping method.

The reduction of dislocations by impurity hardening in InP has been theoretically analyzed by Jorden et al.[170] based on the quasi static state (QSS) heat transfer/thermal stress model as explained in Sec. 3.5.

(2) Reduction of temperature gradient

The dislocation distribution in LEC grown crystals has been studied based on the QSS model and the Haasen model.[171-173] Müller et al.[173] have studied systematically the effect of the temperature distribution in crystals on the dislocation density distribution.

As explained in Section 3.5, lowering the temperature gradient is effective in lowering the dislocation densities. In fact, Shinoyama et al.[81] showed the relationship between the axial temperature gradient ($\partial T/\partial z$) and the critical diameter D_c for obtaining dislocation free crystals as

$$(\partial T/\partial z)\, D_c = 124 \text{ deg} \cdot \text{cm}. \qquad (10.1)$$

The temperature gradient can be reduced in three ways. The first simple way is to use some thermal baffles on top of the heat insulating zone surrounding the crucible as in the TB-LEC methods. By this method, dislocation densities of the level of 200-5000 cm^{-2} for 50 mm diameter Sn- and Fe-doped InP can be achieved and dislocation-free crystals can be grown with lower S or Zn concentrations.

The second method is to apply the phosphorus vapor pressure directly during crystal growth as in the PC-LEC and VCZ methods. It is known that by reducing the axial temperature gradient, the dislocation densities can be decreased as shown in Fig. 10.13, even in the case of 75 mm diameter single crystals. Hoshikawa et al.have grown 100 mm diameter single crystals by the VCZ method under a magnetic field and could obtain dislocation densities of the order of $(0.4\text{-}1.7)\times10^4$ cm^{-2}.[107] Noda et al.[114, 115] have shown that even dislocation free Fe-doped single crystals 75 mm in diameter can be grown.

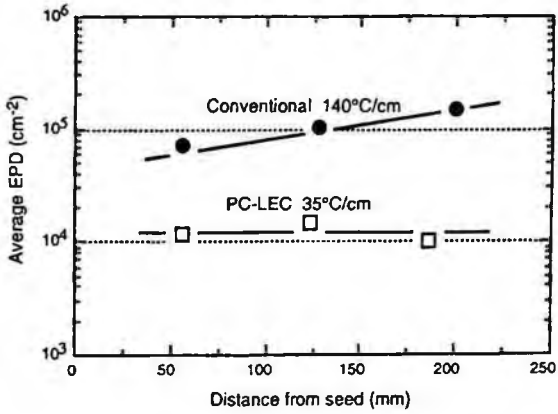

Fig. 10.13 Average dislocation densities for crystals grown by a conventional LEC method and by the PC-LEC method (reprinted from Ref. 112 with permission, copyright 1996 Elsevier).

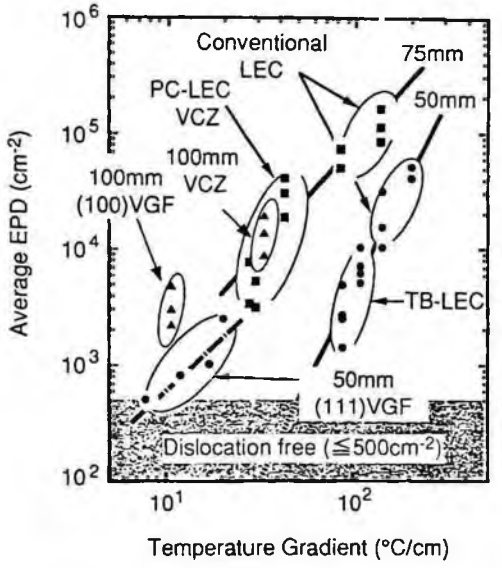

Fig. 10.14 Relationship between the average dislocation density (EPD) and the axial temperature gradient among various crystal growth methods (reprinted from Fig. 25 at p. 47 in Ref.22 with permission).

The third method is to use the VGF/VB methods where crystals can be grown directly in the crucible in which the axial temperature gradient can be decreased. Using the VGF/VB methods, a lower axial temperature gradient than that using the LEC/PC-

LEC methods can easily be obtained so that lower dislocation densities than those using the LEC/PC-LEC methods can obtained (Fig. 10.14). The VGF method has been applied to 75 mm and 100 mm diameter crystal growth[131, 132] and it was found that <100> oriented single crystals could be grown with low dislocation densities.

10.3.5 Crystal Growth with Various Dopants

Various types of doping are performed to produce n-type, p-type and semi-insulating InP. For each type of doping, it is important to know the segregation coefficient. These data[19, 51, 62, 160, 161, 169, 174-178] are summarized in Table 10.5.

For n-type InP, Sn and S doping are common in industrial production. Since Sn does not have any impurity hardening effect, Sn-doped InP grown by the conventional LEC method has a dislocation density in the range of $1\text{-}3\times10^4$ cm^{-2}.[31] N-type S-doped InP is used not only for laser diodes but also for photodetectors. For photodetectors, S-doped InP is valuable since these devices need dislocation-free materials to prevent leakage current caused by dislocations. Since sulphur has an impurity-hardening effect, dislocation-free materials can easily be obtained as shown in Fig. 10.11(a) as well as increasing the carrier concentration.

For p-type InP, Zn is mainly used for industrial production aiming at applications in high power laser diodes. Zinc also has an impurity hardening effect as does sulphur and is also effective in reducing dislocation densities. The relationship between the dislocation-free area and carrier concentration is shown in Fig. 10.11(b).

S however has rapid diffusivity and Zn stimulates the out-diffusion of Fe. In order to overcome these disadvantages, Cd has been examined as another dopant for conductive InP[178] but has not yet reached industrial production.

For semi-insulating InP, since undoped InP is n-type conductive due to residual donor impurities and native defects, it is necessary to dope deep acceptors such as transition metal impurities such as Fe, Co and Cr. Among them, Fe is an important dopant for

Table 10.5 Segregation Coefficients

Impurity	Segregation Coefficient	Author	Year	Ref.
Fe	1.6×10^{-3}	Lee et al.	1977	174
	2×10^{-4}	Iseler	1979	51
	2.5×10^{-4}	Cockayne et al.	1981	175
	$1\text{-}4\times10^{-4}$	Cockayne et al.	1981	175
	$2.9\text{-}4.7\times10^{-4}$	Kusumi et al.	1985	62
Sn	2x10-2	Mullin et al.	1972	176
S	0.5	Mullin et al.	1972	176
Zn	8x10-3	Mullin et al.	1972	176
	0.7	Bachmann et al.	1974	48
Cd	0.16	Fornari et al.	1991	169, 177
Mg	0.20	Kubota et al.	1984	178
Ca	0.025	Kubota et al.	1984	178
Ga	2.5-4.0	Katsui et al.	1986	160
Al	3.0	Tohno et al.	1986	161
Sb	0.12	Tohno et al.	1986	161
As	0.4	Thono et al.	1986	161

industrial production[51, 174, 175, 179-183] because of its high solubility limit compared with Co and Cr which have lower solubility limits.[184, 185] Semi-insulating properties can be obtained when the Fe-doping level is higher than $1x10^{16}$ cm^{-3}. It is known that Fe precipitates are segregated when the concentration exceeds $1x10^{17}$ cm^{-3}.[180]

It has been found that semi-insulating InP can be prepared by Ti-doping.[186, 187] Since Ti acts as a deep acceptor, it is necessary that the main residual impurity in InP is a shallow acceptor if semi-insulating properties are to be achieved. In order to realize Ti-doped semi-insulating InP, it is necessary to dope shallow acceptors such as Zn, Cd, Be with Ti because the conductivity of undoped InP is n-type due to impurities and defects. Cu doping is also reported to make InP semi-insulating.[188]

These dopants show macroscopic and microscopic inhomogeneities. The former is mainly due to the solid-liquid interface shape determined by the crystal growth method and growth conditions. The latter inhomogeneity is caused by temperature fluctuations and is revealed as striations. These inhomogeneities have been investigated by various methods.[189-202] Since these dopant inhomogeneities give rise to fluctuations in electrical properties and influence the properties of devices, it is best to minimize them.

10.4 CHARACTERIZATION

10.4.1 Purity

Various approaches towards improving the purity of InP have been tried, such as In baking,[203] usage of AlN crucibles,[204] pre-encapsulation of starting material[205] and improvement of polycrystal synthesis.[31] Quantitative trace analysis of InP has also been performed by secondary ion mass spectroscopy (SIMS)[206] and glow discharge mass spectroscopy (GD-MS).[207, 208] In the early days of InP crystal production, all manufacturers found agglomerated defects which were called " grappes ". They looked like bunches of grapes after etching for the measurement of etch pit densities as explained in Sec 10.4.2. These defects however could be eliminated by purifying the raw materials such as metal sources and polycrystal sources as explained. These defects may therefore be due to some impurities present at very low concentrations which can not be detected by state-of-the-art analysis technologies. The behavior of hydrogen in InP and its effect on the electrical properties has been studied by various authors.[209, 210]

10.4.2 Defects

(1) Dislocations and residual stress

Various etchants for revealing dislocations are summarized by Adachi[211] and some of them[212-226] are shown in Table 10.6. Dislocations in InP can be revealed by the Huber etchant[217] or the AB etchant used for GaAs.[213] BCA solutions[225, 226] are found to be effective in determining the inclination of the dislocation line. The correlation between lattice defects and etch pits has been studied using X-ray topography, TEM and cathodoluminescence.[227, 228]

Automatic measurement of etch pits has been examined by Peiner et al.[224] for various etchants and it was found that automatically counted EPD is in good agreement with the naked-eye measurement for most etchants.

Table 10.6 Etchants for Dislocation Measurement

Etchant	Author	Year	Ref.
20 HCl + 10 HNO_3 +0.25 Br_2	Clarke et al.	1973	215
various etchants	Tuck et al.	1973	216
2 H_3PO_4(85%)+1 HBr(47%) (Huber etchant)	Huber et al.	1975	217
H_3PO_4	Gottschalch et al	1979	218
1 HBr + 60 CH_3COOH	Akita et al.	1979	219
1 HBr + 2 H_3PO_4 (solution H)	Brown et al.	1980	220
1g CrO_3 + 8mg $AgNO_3$ in 2 m*l* H_2O + 1m*l* 47% HF (AB etchant)	Brown et al.	1980	220
1 HNO_3 + 3HBr	Chu et al.	1982	221
20 HBr + 2H_2O_2 + 20 HCl +20 H_2O	Huo et al.	1989	222
2.5 HBr + 1 C_2H_5OH	Nishikawa et al.	1989	223
1 HBr(47%) + 1 HCl(37%) + 10 CH_3COOH	Peiner et al.	1992	224
20 HBr(47%) + 0.5 H_2O_2(30%) + 20 HCl(37%) + 10 H_2O	Peiner et al.	1992	224
20 HBr(47%) + 2 HNO_3(65%) + 20 HCl(37%)	Peiner et al.	1992	224
3 HBr + 1 CH_3OH	Peiner et al.	1992	224
HBr + $K_2Cr_2O_7$ + H_2O (BCA solution)	Weyher et al.	1994	225, 226

Thono et al.[229] used X-ray diffraction topography to examine the propagation of dislocations from the seed crystal to the grown crystal and found that most dislocations from the seed crystal go throughout the crystal to its periphery but the dislocations nucleated at the crystal periphery propagate into the crystal and are multiplied.

Yonenaga et al.[230] measured the velocities of α, β and screw dislocations for variously doped InP and found that Zn doping retards the motion of all types of dislocations while S doping retards the motion of b and screw dislocations and enhances the motion of a dislocations. The mechanical strength of Ge-doped InP has been examined by Brown et al.[159] Azzaz et al.,[231] Müller et al.[232] and Völkl et al.[233, 234] and Luysberg[235] reported the plastic deformation behavior of InP. The hardness of various forms of InP has been examined by various authors.[236-238]

Yamada et al.[239-241] examined the residual stress in various forms of InP and found that it is very dependent on the crystal growth conditions. Since the brittleness of InP becomes a serious obstacle to the application of InP wafers in electronic devices, the elucidation of the origin of residual stress and the clarification of the relationship between dislocations and residual stress is becoming very important.

(2) Microtwins

Microtwins are defects which appear in bulk crystals as parallel twin planes close together. These microtwins exist in the bulk in isolation with lengths ranging from several microns to several millimeters. These microtwin defects seem to be a kind of large stacking fault defect and may be caused by temperature fluctuation.

(3) Precipitates

In the early days of InP crystal growth, there were many precipitates in InP. They were

known as grappe defects or clusters.[220, 242-249] The origin of these precipitates was not clear and they were believed to be impurity and/or dislocation related. Cockayne et al.[247] postulated that these grappe and cluster defects could be eliminated by controlling the moisture of B_2O_3 and by controlling the stoichiometry of the melt. It was found that when high purity polycrystals were used for single crystal growth, the density of precipitates was greatly decreased as explained in Sec. 10.4.1. It was also found that when pBN crucibles were used instead of quartz crucibles, the density of precipitates were reduced. Hirano et al.[250] found that if the melt before crystal growth was left for a prolonged period before crystal growth, the density was reduced. He also found that the density in the grown crystals decreases from the top part to the tail part. Kohiro et al.[251] showed by coulometric titration analysis that S-type pits seemed to be related to the stoichiometry of the InP melt.

Other precipitates formed in variously doped InP have been observed for Fe-doping,[174, 252-254] V-doping,[255] Ti-, Cr-, Ni-doping,[256] Zn-doping,[257-259] Sn-doping,[259] Cd, S-co-doping,[260] Co-doping[261] and C-precipitates.[262]

(4) Native defects

Native defects such as vacancies,[263-265] interstitials,[265] antisite defects[266, 267] and various complexes[268, 269] have been studied by various methods and have been theoretically analyzed.[270, 271]

Kainosho et al.[272] found that carrier concentrations after Si ion implantation are greatly increased and may exceed the net Si concentration under conditions where phosphorus dissociation may take place. This implies that phosphorus vacancies will play an important role in the electrical properties of InP. Inoue et al.[273] also found that the carrier concentration is greatly decreased by appropriate annealing, which implies native defects play an important role in InP.

(5) Deep levels

Deep levels in InP are investigated by various methods. In Fig. 10.15, deep level measurement by deep level transient spectroscopy (DLTS) is summarized.[274] In Table 10.7, various impurity deep levels so far reported are summarized.[51, 186, 275-282] Among these deep levels, the 0.4 eV peak is an important one since it appears during annealing and was considered to be the origin of semi-insulating behavior.

Zozime et al.[282] have measured deep levels related to dislocations. Backhouse et al.[283] analyzed the temperature dependence of low-frequency current oscillation and found a deep level with an activation energy of 0.47 eV. The effect of annealing on deep levels has been examined by Paris et al.[284] Fang et al. have measured deep levels in semi-insulating InP by TSC measurement.[285, 286]

10.4.3 Electrical Properties

(1) Carrier concentrations

The relationship between the carrier concentration and mobility was calculated by Walukiewicz et al.[287] as shown in Fig. 1.17. Undoped InP is known to show n-type

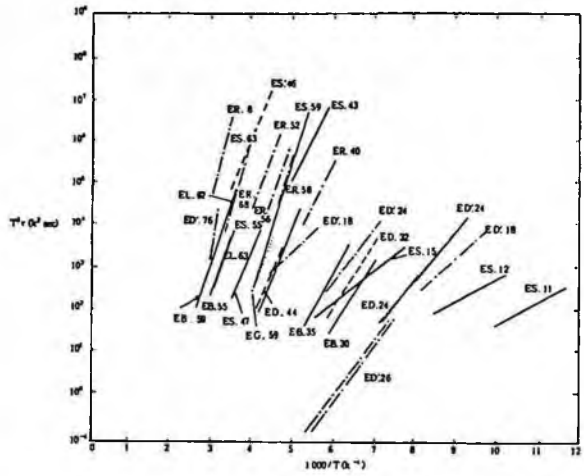

(a)

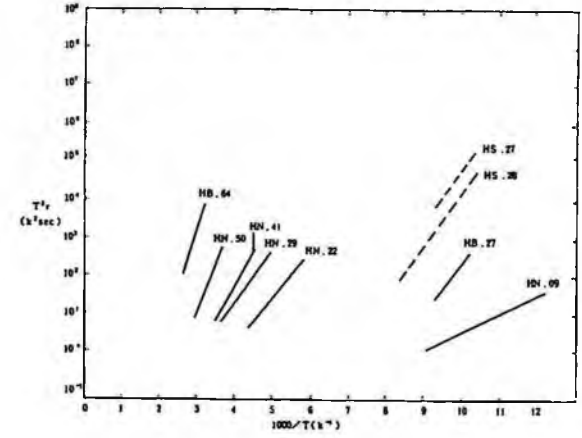

(b)

Fig. 10.15 Various deep levels in InP (from Ref. 274 with permission). (a) Electron traps and (b) hole traps.

Table 10.7 Deep Levels due to Impurities in InP

Impurity	Energy Level (eV)	Conductivity Type	Author	Year	Ref.
Au	Ec-0.55	deep donor	Parguel et al.	1987	278
Fe	Ec-0.65	deep acceptor	Iseler	1979	51
Cr	Ec-0.39	deep acceptor	Iseler	1979	51
	Ev+0.56	deep donor	Toudic et al.	1988	279
Ni	Ev+0.48	deep acceptor	Korona et al.	1990	281
Ti	Ec-0.62	deep donor	Iseler et al.	1986	186
Co	Ev+0.32	deep acceptor	Skolnick et al.	1983	275
	Ev+0.24	deep acceptor	Rojo et al.	1984	276
Mn	Ev+0.22	deep acceptor	Lambert et al.	1985	277
V	Ev+0.2	deep donor	Delerur et al.	1989	280

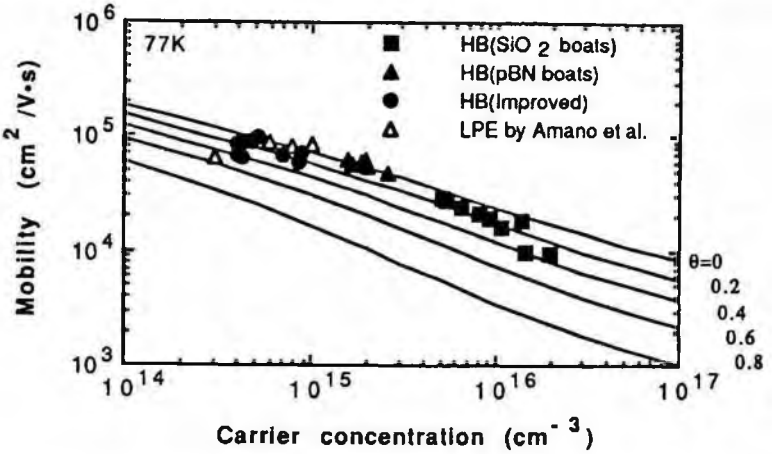

Fig. 10.16 Relationship between mobility and carrier concentration (from Ref. 29 with permission, copyright 1990 Routledge/Taylor & Francis Group). Theoretical data (solid lines) are from Ref. 287 with permission.

conductivity and it is believed to be due to silicon incorporation from quartz material when the carrier concentration is high.[288]

When the carrier concentration is less than 10^{15} cm^{-3}, the carrier concentration seems not to be determined by silicon impurity alone. When single crystals with carrier concentrations of 2-4x10^{15} cm^{-3} are annealed at 620 °C, the carrier concentration is drastically decreased down to 5x10^{14} cm^{-3}.[273] This fact seems to imply that the carrier concentration is determined by native defects such as phosphorus vacancies which will be reduced by appropriate annealing conditions.

The purity of polycrystals grown by the three-zone HB method is dependent on the conditions of synthesis. The purity of polycrystals has been improved as shown in Fig. 10.16 by changing the conditions of synthesis. The carrier concentration exceeds 10^{16} cm-3 when quartz boats are used. The carrier concentration could however be decreased to the level of 10^{15} cm^{-3} when pBN boats are used. Even carrier concentrations of the order of ~5x10^{14} cm^{-3} have been obtained under optimized conditions of synthesis. This carrier concentration level is similar to the purity level of SSD polycrystals and InP epitaxial layers prepared by liquid phase epitaxy.[288] Because of the good linearity between carrier concentrations and spark source mass spectroscopy (SSMS) analysis results, it is concluded that the impurity which dominates the carrier concentration is silicon in the case of carrier concentrations higher than 10^{15} cm^{-3}. The origin of the silicon contamination is considered to be the quartz ampoule material.[289] It is predicted that silicon is involved in the grown polycrystals as high vapor pressure SiO gas.

(2) Fe doped semi-insulating InP

Semi-insulating InP is industrially produced by Fe doping with high Fe concentrations exceeding 10^{16} cm^{-3} (>0.2 ppmw).[173, 290, 291] Zach has discussed in detail the mechanism of the semi-insulating behavior of Fe-doped InP[292, 293] and has concluded that since

some of the Fe atoms are ionized and compensate shallow donors, a larger amount of Fe is necessary. This is the reason why the concentration of Fe is about one order of magnitude higher than that of shallow donors. The electrical properties of Fe-doped InP have been studied in detail by Kim et al.[294] and Fornari et al.[295] The redistribution phenomenon seen with annealing has been studied and discussed.[296-298]

High Fe concentrations are however undesirable from the viewpoint of device performance and reliability. The disadvantages of Fe-doped InP are manifold as follows.

(i) Fe concentrations themselves change along the crystal growth axis[299] because of the low segregation coefficient of Fe of the order of 10^{-3}-10^{-4}, as explained in Sec. 3.4. The Fe concentration therefore changes in wafers from top to tail of one single crystal ingot.

(ii) When Si ions are implanted into Fe-doped InP, the activation efficiency of implanted Si is greatly decreased as the Fe concentration is increased.[272] The decrease of the activation efficiency is significant when the Fe concentration exceeds 0.2 ppmw.

(iii) Fe atoms diffuse out from the substrate into the epitaxial layer, depending on the epitaxial growth conditions, and impair the properties of the epitaxial layer.[300]

(iv) The out-diffusion of Fe is stimulated when Zn-doped layers are epitaxially grown on Fe-doped substrates.[301]

(v) Through high-resolution scanning photoluminescence, bright spots are often seen in Fe-doped substrates.[302]

(3) Low Fe-doped semi-insulating InP produced by annealing

A desirable objective therefore is to realize undoped or extremely low Fe-doped semi-insulating InP with Fe concentrations lower than 0.2 ppmw. High resistive nominally undoped InP of 3.6×10^5 Ωcm was first obtained by Klein et al. after annealing undoped conductive InP at 900-950 °C under 6 bars of phosphorus overpressure.[303] It was also shown by Hirano et al.[304, 305] that high resistive InP of about 10^5 Ωcm can be obtained when slightly Zn-doped InP is annealed at 650 °C for 3 hrs. Hofmann et al.[306] first obtained semi-insulating InP with resistivity higher than 10^7 Ωcm by annealing high purity undoped InP at 900 °C under 5 atm. phosphorus overpressure. Hirt et al.[307] and Kiefer et al.[308] have studied the effect of phosphorus overpressure on the resistivity from the viewpoint of the decrease of intrinsic donor V_P. Kainosho et al.[309] also showed that whole 50 mm diameter semi-insulating InP wafers can be obtained by annealing 50 mm diameter undoped InP wafers at 900 °C under 15 atm. phosphorus overpressure.

After this preliminary work, many studies have been carried out in order to produce high-quality InP. These studies however clarified the difficulty of preparing semi-insulating InP reproducibly. Hirt et al.[307] showed that the reproducibility depends on the purity of the starting InP materials. It was also found by Fornari et al.[310-312] that the reproducible preparation of semi-insulating InP is possible when InP is annealed in a vacuum. Under high phosphorus vapor pressure, it was found that slight contamination by Fe occurs during annealing.[313, 314] The poor reproducibility was also found to be due to contamination by Cr and Ni from phosphorus during annealing.[315, 316] Based on these extensive studies, it is now possible to prepare semi-insulating InP reproducibly by annealing InP wafers with extremely low Fe concentrations under lower vapor pres-

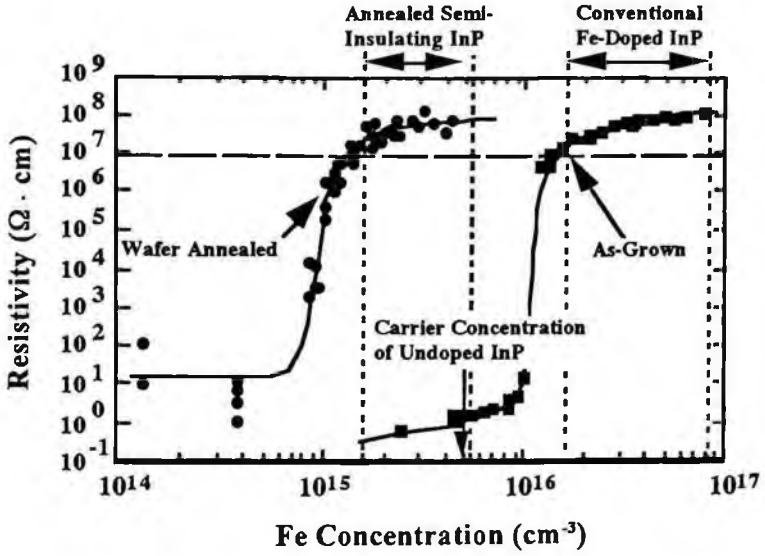

Fig. 10.17 Relationship between resistivity and Fe concentration for Fe-doped InP and annealed InP (from Ref. 13 with permission).

sure.[316-320] As shown in Fig. 10.17, semi-insulating InP with Fe concentrations less that 0.2 ppmw becomes possible and the preparation becomes reproducible when one applies one atm. phosphorus vapor pressure instead of 25 atm. phosphorus vapor pressure to prevent the contamination detrimental to the semi-insulating behavior.[318] Semi-insulating VGF InP was also obtained by Hirt et al. using the annealing procedure.[321]

The resistivity of the semi-insulating InP thus prepared however is not uniform to a satisfactory degree.[316] In order to overcome this disadvantage, the Multiple-step Wafer Annealing (MWA) process (Sec. 8.4.2) was applied to InP by Uchida et al.[318, 322, 323] The process consists of two steps, the first step annealing to convert conductive wafers to semi-insulating and the second step annealing to improve the uniformity of resistivity. By increasing the phosphorus overpressure up to 30 atm., it was found that the uniformity of both resistivity and mobility could be greatly improved. In Fig. 10.18, the uniformity of electrical properties of 75 mm diameter InP wafers subjected to the MWA process is shown.

In order to overcome the segregation of Fe during crystal growth, direct Fe doping by wafer annealing has been developed. It was first shown that Fe can be doped from a phosphide vapor atmosphere during annealing.[317] This first suggestion was applied to wafers larger than 50 mm in diameter by Uchida et al.[324] They showed that the Fe doping level is a function of the Fe/P molar fraction in the ampoule. It was found that Fe doping can be achieved efficiently when the phosphide vapor of composition of FeP_2 is formed during annealing

The mechanism of semi-insulating behavior has been extensively studied by various methods such as the Hall effect,[306] TSC,[325, 326] deep level transient spectroscopy

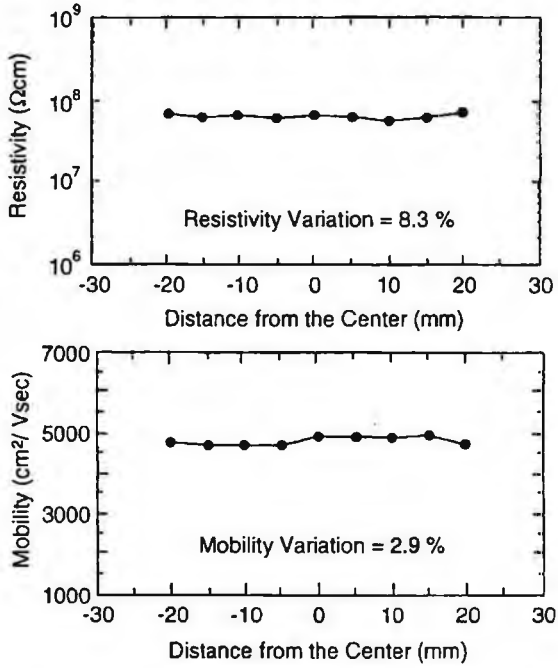

Fig. 10.18 Uniformity of resistivity and mobility of semi-insulating InP after wafer annealing (reprinted from Ref. 323 with permission, copyright 1998 TMS).

(DLTS),[327, 328] PICTS[329] and PL measurements.[308, 309, 330] The following four mechanisms are proposed based on these examinations.

(i) A slight amount of Fe is activated by annealing and the concentration of shallow donors which may be mainly native defects such as phosphorus vacancies, is decreased to a level less than the concentration of activated Fe.[313, 314, 331]

(ii) Shallow donors due to the complex defect (hydrogen-indium vacancy) can be eliminated by annealing to a point lower than the concentration of residual Fe.[332]

(iii) Indium related defects which act as shallow acceptors are created under low phosphorus vapor pressure annealing and they compensate residual shallow donors.[311, 312]

(iv) Phosphorus antisite defects which act as deep donors are created upon annealing and are compensated by shallow or deep acceptors.[333]

10.4.4 Optical Properties

In Table 10.8, the main photoluminescence (PL) peaks[334-336] are summarized.

The exciton peaks are data from Refs. 273, 337-340. As shown in Fig. 10.19, when the carrier concentration of polycrystal InP is decreased, the PL peaks resolve better. When the carrier concentration is less than 10^{15} cm^{-3}, even free exciton peaks can be observed. It was also found that in LE-VB crystals, strong band to band recombination can be observed due to low dislocation densities.[341]

Table 10.8 Photoluminescence Data for InP

Peak (eV)	Notation	Assignment
Exciton Peaks		
1.4188	$(F,X)_{n=1}$	Free exciton, n=1 state of upper polariton branch
1.4185	$(D_0,X)_{n=5}$	Exciton bound to neutral donor
1.4183	$(D_0,X)_{n=4}$	Exciton bound to neutral donor
1.4178	$(D_0,X)_{n=3}$	Exciton bound to neutral donor
1.4176	$(D_0,X)_{n=2}$	Exciton bound to neutral donor
1.4173	$(D_0,X)_{n=1}$	Exciton bound to neutral donor
1.4168	(A_0,h)	neutral donor to hole
1.4166	(D^+,X)	Exciton bound to ionized donor
1.4144	(A_0,X)	Exciton bound to neutral acceptor
1.4142	(A_0,X)	Exciton bound to neutral acceptor
Impurity related peaks		
1.40		Surface state unidentified
1.3988	BA	Ge
1.386	BA	Si_P
1.384-1.380	BA	C
1.3833	DAP	Si_P
1.381	DAP	Si_{In}
1.3785	DAP	Mg
1.3783	DAP	Al
1.3782	DAP	Be
1.378	DAP	Ca
1.3755-1.3790	DAP	C
1.3732	DAP	Zn
1.35		Defect-induced Cu
1.369		Cd
Deep level related peaks		
1.27-1.28		Point defect-oxygen complex
1.21		Acceptor, V(In) or Si
1.14		Acceptor, V(In) impurity
1.10		Ge, Fe
1.08		Acceptor, D-A complex
0.99		Donor, V(P) impurity
0.75		Unknown
0.35		Fe

Residual donor identification has been done using PL measurement for InP single crystals and S and Si are found to be the main donors in InP.[342]

Peaks due to acceptor impurities have also been identified.[343-349] There are several Donor-Acceptor (D-A) pair peaks depending on acceptor impurities.[39, 347, 350-352] It is known that three peaks can be observed due to Zn, Mg, and Ca for polycrystalline raw materials, but in grown single crystals, only Zn peaks are observed. The explanation proposed is that Mg and Ca are gettered in the encapsulant B_2O_3 during crystal growth.[348]

For Sn-doped, S-doped InP, several PL spectra are reported and the PL intensity distribution across the wafer has been examined.[353] The PL spectra for semi-insulating (SI) Fe-doped InP have been examined by various authors. In the case of semi-insulat-

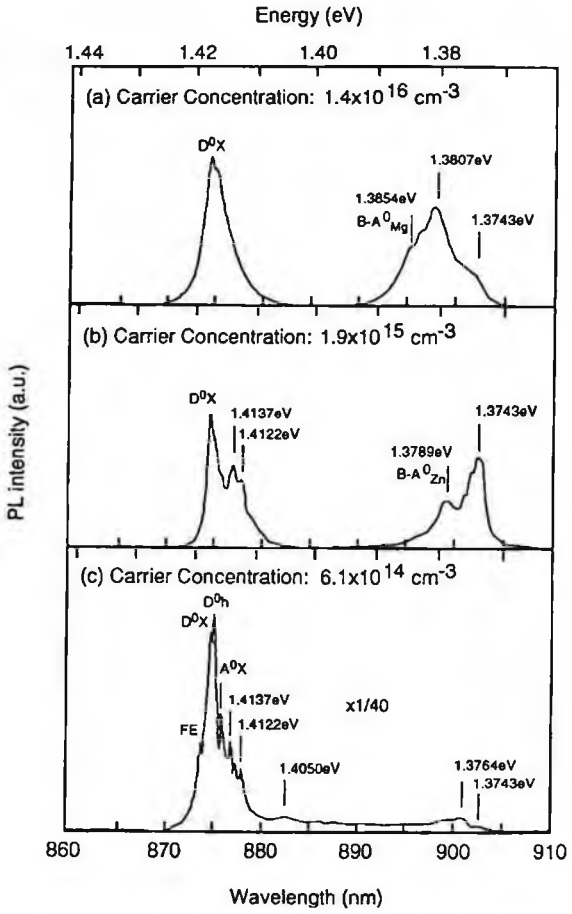

Fig. 10.19 PL spectra of various types of polycrystalline InP (reprinted from Ref. 31 with permission, copyright 1990 Elsevier).

ing Fe-doped InP, very broad peaks due to the recombination through Fe impurities are observed.[354]

The effect of annealing on PL spectra has been extensively studied.[273, 284, 330, 355] When undoped conductive InP single crystals are annealed, it is found that free exciton peaks which are not distinct for as-grown crystals become clear as a function of the annealing temperature. Undoped semi-insulating InP shows a very fine spectrum which competes with the best data ever reported for high purity MOCVD InP with carrier concentrations of the order of several 10^{14} cm^{-3}.[273]

Annealed InP shows very interesting features in its photoluminescence spectra. Makita et al.[356-358] reported that annealed materials show highly resolved photoluminescence spectra after high temperature annealing. It has been shown that the resolution improves with decreasing Fe concentrations. In their data, very strong peaks due to phosphorus vacancies can be clearly seen. Uchida et al.[330] found that during multiple-

step wafer annealing to prepare highly uniform semi-insulating InP with extremely low Fe-doped InP, after the second step of annealing, a peak due to phosphorus vacancies is greatly decreased.

Carrier lifetime and surface recombination velocities have been studied from the temperature dependence of time-resolved PL.[359] PL is also known to be sensitive to the surface state of InP.[360-365]

Scanning PL has been used to examine the inhomogeneity of variously doped InP.[366, 367] Room-temperature scanning PL was found to be effective in evaluating the surface quality and the inhomogeneity over wafers.[368, 369] A PL topography system has also been developed to examine the propagation of defects from substrate to epitaxial layers, as demonstrated in the case of InGaAsP/InP.[370] Polishing damage can also be observed by room temperature PL.[371] Cathodoluminescence is also a high resolution effective technique for observing the inhomogeneity with a high resolution.[372] Recently, a near-infrared (NIR) transmittance technique has been developed to observe the homogeneity of large diameter InP substrates.[373]

10.5 APPLICATIONS

10.5.1 Substrates for Epitaxy

Since InP is a material difficult to polish and is used as a substrate for epitaxial growth for high grade devices such as high speed optoelectronics, the polishing technique is important for its application. In fact, high quality polishing has been described in several reports.[31, 208, 374-379] The damaged layer after polishing has also been evaluated by X-ray diffraction,[31, 380, 381] Makyo topography,[382] photoluminescence (PL)[365] and etching.[383-386] Surface cleanliness of polished substrates and etched substrates has been evaluated by X-ray photoemission spectroscopy (XPS),[387, 388] ion scattering spectroscopy (ISS) and Auger electron spectroscopy (AES),[389] PL,[390] IR spectroscopy,[391] contact angle measurement[31, 392] and time of flight SIMS (TOM-SIMS).[393, 394] The surface quality after polishing can be protected by appropriate surface oxide formation.[395]

The relationship between the quality of the substrate and the epitaxial surface is therefore very important. In order to examine the quality of substrates for various epitaxial growth processes such as liquid phase epitaxy (LPE), metalorganic chemical vapor deposition (MOCVD), molecular beam epitaixy (MBE), epitaxial growth has been performed and the quality examined by various characterization methods such as PL[302] and etching.[385, 386]

Katsura et al.[396] found that after appropriate substrate polishing and cleaning, the quality of InAlAs/InGaAs epitaxial layers for high electron mobility transistor (HEMT) structures is better than that obtained by using substrate pretreatment at the side of epitaxial growers.

Nakamura et al.[397] found that the very slight off-angle is very important for high quality epitaxial growth by MOCVD. When the normal orientation is within 0.02 degrees of <100>, many hillocks are formed. They found that a very slight off-angle greater than >0.05 degrees abolishes the formation of hillocks, a greater off-angle than that reported by other researchers.

In thick epitaxial layers grown on Fe-doped substrates, slip-like defects were often observed even though they were not observed in the substrates themselves. These slipline-like defects are attributed to Fe precipitates in the substrate which cause a local thermal stress during epitaxial growth.[302]

10.5.2 Optoelectronic Devices

InP is becoming a more and more important materials for optoelectronic devices such as laser diodes[2, 398-400] and pin-PDs[401] and APDs[402-405] for wavelengths of 1.3 μm and 1.55 μm for optical fiber communications. Even infrared LEDs for this wavelength have been studied.[406, 407] The strong demand for internet systems with bit rate information exchange higher than 40 Gb/s needs semi-insulating substrates even for laser diodes and photodetectors.[408] OEICs based on InP lasers and detectors have also been developed.[5, 409-411] Terabit/sec communication systems are also in the future target.

The other possible applications of InP optoelectronic devices are interconnection using optical devices. In fact, many studies have been performed for these applications.

There are trials to fabricate visible LEDs using II-VI layers[412] and long wavelength detectors using GaSb layers[413] and GaInAs/GaAsSb layers[414] on InP substrates.

10.5.3 High Frequency Devices

InP has the highest drift mobility compared with silicon and GaAs as shown in Fig. 2.22 and InP was expected to be useful for high frequency devices and MESFETs[415-418] and MISFETs[26, 419, 420] have been extensively studied in the past. Since localized states in the metal-insulator interface are smaller for InP than for GaAs, MISFETs were extensively studied. The formation of a stable Schottky contact was difficult in the case

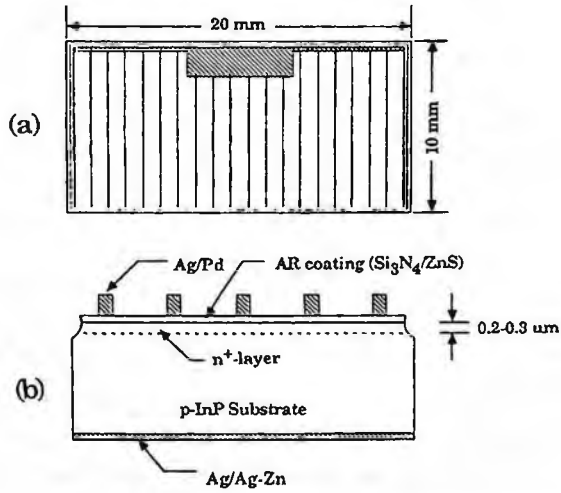

Fig. 10.20 Schematic diagram of (a) front surface and (b) cross section of a InP solar cell (reprinted from Ref. 7 with permission, copyright 1988 IEEE).

of InP, probably because the surface native oxide is unstable so that MESFETs seemed to be impossible. Sawatari et al.[421, 422] however showed that the formation of a very thin atomic layer of another metal oxide could make stable Schottky contacts and allow reproducible MESFET fabrication. These MISFETs and MESFETs have not however reached industrial production.

On the other hand, MOCVD and MBE epitaxial growth technologies have been quickly developed and high frequency high electron mobility transistors (HEMTs),[423, 424] hetero bipolar transistors (HBTs),[425, 426] microwave/millimeter wave monolithic ICs (MMICs)[427-430] and optoelectronic ICs (OEICs)[409-411] have been developed based on these epitaxial layers. The highest cutoff frequencies exceeds 500 GHz. These InP based electronic devices are expected to find applications in high-speed fiber communications and anticollision radars.[430]

10.5.4 Solar Cells

InP is a promising candidate for solar cells[6] since the bandgap of InP is 1.4 eV and it is expected to have a high energy conversion efficiency as explained in Sec. 6.4. InP is also known to be highly resistive to radiation damage[431] so that it is expected to be a good solar cell materials for space satellites.[6, 432] Because of these possibilities, there have been many studies of InP solar cells. Okazaki et al.[7] succeeded in fabricating InP solar cells with a simple diffusion p-n structure with a conversion efficiency of about 17% (Fig. 10.20). Spitzer et al.[433] have fabricated homo epitaxial solar cells by MOCVD epitaxial growth with a conversion efficiency of about 20.4 %. Solar cells with InGaAs/InP layers on InP substrates have also been studied.[434]

REFERENCES

1. M.E. Lines, *J. Appl. Phys.* **55** (1984) 4058.
2. K. Onabe, *Jpn. J. Appl. Phys.* **21** (1982) 791.
3. See papers in *Proc. 8th Int. Conf. on InP and Related Materials* (Schwäbisch Gmünd, 1996) and in *Proc. 9th Int. Conf. on InP and Related Materials* (Hyaniss, 1997)
4. D. L. Lile, in *Proc. 10th Int. Conf. on InP and Related Materials* (Tsukuba, 1998) p. 6.
5. O. Wada, in *Proc. 9th Int. Conf. on InP and Related Materials* (Hyaniss, 1997) p. 7.
6. T. J. Coutts and M. Y. Yamaguchi, in *Current Topics in Photovoltaics Vol. 3*, eds. T. J. Coutts and J. D. Meakin (1988) p. 79.
7. H. Okazaki, T. Takamoto, H. Takamura, T. Kamei, M. Ura, A. Yamamoto and M. Yamaguchi, in *Proc. 12th Int. Conf. on Photovoltaic Science and Engineering* (Las Vegas, IEEE, 1988) p. 886.
8. M. Tatsumi, T. Kawase, T. Araki, N. Yamabayashi, T. Iwasaki, Y. Miura, S. Murai, K. Tada and S.Akai, in *Proc. First Int. Conf. on InP and Related Materials* (Oklahoma, 1989) p. 18.
9. K. Kato and Y. Akatsu, in *Proc. 7th Int. Conf. on InP and Related Materials* (Sapporo, 1995) p. 349.
10. I. H. Tan, J. E. Bowers and E. L. Hu, in *Proc. 7th Int. Conf. on InP and Related Materials* (Sapporo, 1995) p. 365.
11. *Indium Phosphide: Crystal Growth and characterization*, Semicon. Semimet. Vol. 31, eds. R.K. Willardson and A.C. Beer (Academic Press, New York, 1990).
12. *Properties of Indium Phosphide*, ENIS Datareviews Series, No.6, (INSPEC, 1991).
13. O. Oda, K. Kohiro, K. Kainosho, M. Uchida and R. Hirano, in *Recent Development of Bulk Crystal Growth*, ed. M. Isshiki (Research Signpost, India, 1998) p. 97.
14. *InP-Based Materials and Devices -Physics and Technology*, eds. O. Wada and H. Hasegawa (John Wiley & Sons, 1999).

15. *InP and Related Compounds: Materials, Applications and Devices*, ed. M.O. Manasreh (Gordon & Breach Sci., Amsterdam, 2000)
16. *Landolt-Börnstein, Vol. 17 Semiconductors*, ed. O. Madelung (Springer-Verlag, Berlin, 1982) p. 281.
17. J. Boomgaard and K. Schol, *Philips Res. Rept.* **12** (1957) 127.
18. R.N. Hall, *J. Electrcochem. Soc.* **110** (1963) 385.
19. K.J. Bachmann and E. Buehler, *J. Electrochem. Soc.* **121** (1974) p. 835.
20. R. Fornari, A. Brinciotti, A. Sentiri, T. Görög, M. Curti and G. Zuccalli, *J. Appl. Phys.* 75 (1994) 2406.
21. K. Kainosho, O. Oda, G. Hirt and G. Müller, *Mater. Res. Soc. Symp. Proc.* **325** (1994) 101.
22. O. Oda, T. Fukui, R. Hirano, M. Uchida, K. Kohiro, H. Kurita, K. Kainosho, S. Asahi and K. Suzuki, *InP and Related Compounds: Materials, Applications and Devices*, ed. M.O. Manasreh (Gordon & Breach Sci., Amsterdam, 2000) p. 9.
23. SEMI International Standards, M-23 (annual publication from Semiconductor Equipment and Materials International).
24. L.D. Nielsen, *Phys. Lett.* **A38** (1972) 221.
25. A.S. Jordan, *J. Crystal Growth* **71** (1985) 559.
26. H. Hasegawa and T. Sawada, *Oyo Buturi (Monthly Publ. Jpn. Soc. Appl. Phys.) (in japanese)* **50** (1981) 1289.
27. G. W. Iseler, *J. Electron. Mater.* **13** (1984) 989.
28. M. Morioka, K. Tada and S. Akai, *Ann. Rev. Mater. Sci.* **17** (1987) 75.
29. O. Oda, K. Kainosho, K. Kohiro, H. Shimakura, T. Fukui, R. Hirano and S. Katsura, in *Proc. 6th Conf. Semi-insulating III-V Materials*, eds. by A. Milnes and C. J. Miner (Toronto, Adam Hilger, 1990) p. 189
30. J.P. Farges, in *Indium Phosphide: Crystal Growth and Characterization*, Semicon. Semimet. Vol.
31. eds. R.K. Willardson and A.C. Beer (Academic Press, New York, 1990) p. 1.
31. O. Oda, K. Katagiri, K. Shinohara, S. Katsura, Y. Takahashi, K. Kainosho, K. Kohiro and R. Hirano, in *Indium Phosphide: Crystal Growth and Characterization*, Semicon. Semimet. Vol. 31, eds. R.K. Willardson and A.C. Beer (Academic Press, New York, 1990) p. 93.
32. K. Tada, M. Tatsumi, M. Morioka, T. Araki and T. Kawase, in *Indium Phosphide: Crystal Growth and Characterization*, Semicon. Semimet. Vol. 31, eds. R.K. Willardson and A.C. Beer (Academic Press, New York, 1990) p. 175.
33. D. Bliss, in *InP-Based Materials and Devices -Physics and Technology*, eds. O. Wada and H. Hasegawa (John Wiley and Sons, 1999) p. 109.
34. A. J. Marshall and K. Gillessen, *J. Crystal Growth* **44** (1978) 651.
35. A. Yamamoto and C. Uemura, *Jpn. J. Appl. Phys.* **17** (1978) 1869.
36. K. Sugii, E. Kubota and H. Iwasaki, *J. Crystal Growth* **46** (1979) 289.
37. E. Kubota and K. Sugii, *J. Appl. Phys.* **52** (1981) 2983.
38. E. Kubota and J. Sugii, *J. Crystal Growth* **68** (1984) 639.
39. E. Kubota, Y. Ohmori and K. Sugii, *J. Appl. Phys.* **55** (1984) 3779.
40. C.H. Chung, S.K. Noh and M.W. Kim, *Jpn. J. Appl. Phys.* **23** (1984) 784.
41. M. Ohoka, H. Tsuchiya and H. Araki, in *Extended Abstr.* (46th Autumn Meeting, Jpn. Soc. Appl. Phys., 1985) p. 630.
42. H. Aikawa, K. Iwasaki and K. Nakanishi, *Electrochemistry (Denki Kagaku) (in japanese)* **53** (1985) 253.
43. K. Kainosho, M. Ohoka, D. Kusumi and O. Oda, in *Extended Abstr.* (33rd Spring Meeting, *Jpn. Soc. Appl. Phys.* 1985) p. 743.
44. W. Siegel, G. Kühnel, H. Koi and W. Gerlach, *phys. stat. sol. (a)* **95** (1986) 309.
45. E. Kubota, A. Katsui and S. Yamada, *Electron. Lett.* **22** (1986) 21.
46. C.R. Miskys, C.E.M. de Oliveira and M.M.G. de Carvalho, in *Proc. 8th Int. Conf. on InP and Related Materials* (Schwäbisch Gmünd, 1996) p. 291.

47. D. Richman, in *Preparation of Indium Phosphide, Compound Semiconductors, Vol.1*, eds R.K. Willardson and H.L. Goering (Reinhold, New York, 1962) p. 214.
48. K.J. Bachmann and E. Buehler, *J. Electron. Mater.* **3** (1974) 279.
49. G.A. Antypas, *Int. Phys. Conf. Ser.* **33b** (1977) 55.
50. R.L. Henry and E.M. Swiggard, *J. Electron. Mater.* **7** (1978) 647.
51. W. Iseler, *Inst. Phys. Conf. Ser.* **45** (1979) 144.
52. D. Barthruff and K.W. Benz, *J. Electron. Mater.* **8** (1979) 485.
53. W.A. Bonner, *J. Crystal Growth* **54** (1981) 21.
54. W.P. Allred, J.W. Burns and W.L. Hunter, *J. Crystal Growth* **54** (1981) 4144.
55. D. Rumsby, R.M. Ware and M. Whitaker, *J. Crystal Growth* **54** (1981) 32.
56. A. Yamamoto, S. Shinoyama and C. Uemura, *J. Electrochem. Soc.* **128** (1981) 585.
57. J.A. Adamski, *J. Crystal Growth* **60** (1982) 141.
58. J.A. Adamski, *J. Crystal Growth* **64** (1983) 1.
59. W.A. Bonner and H. Temkin, *J. Crystal Growth* **64** (1983) 10.
60. R. Coquille, Y. Toudic, M. Gauneau, G. Grandpierre and J.C. Paris, *J. Crystal Growth* **64** (1983) 23.
61. J.E. Wardill, D.J. Doling, R.A. Brunton, D.A.E. Crouch, J.R. Stockbridge and A.J. Thompson, *J. Crystal Growth* **64** (1983) 15.
62. D. Kusumi, K. Kainosho, K. Katagiri, O. Oda and H. Araki, in *Extended Abstr.* (46th Autumn Meeting, Jpn. Soc. Appl. Phys., 1985) p. 743.
63. S. Yoshida, N. Nishibe and T. Kikuta, *Inst. Phys. Conf. Ser.* **91a** (1988) 137.
64. J.E. Wardill, D.J. Dowling, S.F. Lovett, A.E. Crouch and A.I. Thomson, *Proc. NATO-sponsored InP Workshop* **RADC-TM-80-07** (1980) p. 65.
65. J.P. Farges, *J. Crystal Growth* **59** (1982) 665.
66. S. Tong-nien, L. Szu-lin and K. Shu-tseng, in *Proc. 3rd Conf. Semi-Insulating III-V Materials*, eds. S. Makram-Ebeid adn B. Tuck (Shiva, Nantwich, 1982) p. 61.
67. S.B. Hyder and C.J. Jr. Holloway, *J. Electron. Mater.* **12** (1983) 575.
68. Y. Sasaki, S. Kuma and J. Nakagawa, *Hitachi Cables (in japanese)* **5** (1985) 33.
69. T. Inada, T. Fujii, M. Eguchi and T. Fukuda, *Appl. Phys. Lett.* **50** (1987) 86.
70. T. Inada and T. Fukuda, in *Indium Phosphide: Crystal Growth and Characterization*, Semicon. Semimet. Vol. 31, eds. R.K. Willardson and A.C. Beer (Academic Press, New York, 1990) p. 71.
71. D.J. Dowling, R.A. Brunton, D.A.E. Crouch, A. Thompson and J.E. Wardill, *J. Crystal Growth* **87** (1988) 137.
72. V. Prasad, D.F. Bliss and J.A. Admski, *J. Crystal Growth* **142** (1994) 21.
73. D. Bliss, G. Bryant, I. Jafri, V. Prasad, K. Gupta, R. Farmer and M. Chandra, in *Proc. 10th Int. Conf. on InP and Related Materials* (Tsukuba, 1998) p. 38.
74. W.M. Higgins, G.W. Iseler, D.F. Bliss, G. Bryant, V. Tassev, I. Jafri, R.M. Ware and D.J. Carlson, in *Proc. 12th Int. Conf. on InP and Related Materials* (Williamsburg, 2000) p. 522.
75. W.M. Higgins, G.W. Iseler, D.F. Bliss, G. Bryant, V. Tassev, I. Jafri, R.M. Ware and D.J. Carlson, *J. Crystal Growth* **225** (2001) 225.
76. J.B. Mullin, R.J. Herifage, C.H. Holliday and B.W. Strgughan, *J. Crystal Growth* **3/4** (1968) 281.
77. J.B. Mullin, A. Royle and B.W. Straughan, in *Proc. Int. Symp. Gallium Arsenide* (Archen, 1970) p. 41.
78. K.J. Bachmann, E. Buehler, J.L. Shay and A.R. Strand, *J. Electron. Mater.* **4** (1975) 389.
79. W.A. Bonner, Mater. Res. Bull. **15** (1980) 63, *J. Electrochem. Soc.* **127** (1980) 1798.
80. S. Shinoyama, C. Uemura, A. Yamamoto and S. Tohno, *Jpn. J. Appl. Phys.* **19** (1980) L331.
81. S. Shinoyama, S. Tohno and C. Uemura, *Inst. Phys. Conf. Ser.* **63** (1981) 25.
82. S. Shinoyama and C. Uemura, *J. Mater. Sci. Soc. Jpn. (in japanese)* **21** (1985) 273.
83.K. Katagiri, S. Yamazaki, A. Takagi, O. Oda, H. Araki and I. Tsuboya, *Inst. Phys. Conf.Ser.* **79** (1986) 67.
84. J. P. Farges, C. Schiller and W.J. Bartes, *J. Crystal Growth* **83** (1987) 159.

85. D. Hofmann, in *Proc. 5th Conf. Semi-insulating III-V Mateirals* (Malmö, Sweden, 1988) p. 429.
86. C.E.M. de Oliveira, C.R. Miskys and M.M.G. de Carvalho, in *Proc. 8th Int. Conf. on InP and Related Materials* (Schwäbisch Gmünd, 1996) p. 290.
87. C.E.M. de Oliveira, M.M.G. de Carvalho and C.R. Miskys, *J. Crystal Growth* **173** (1997) 214.
88. C.E.M. de Oliveira, M.M.G. de Carvalho, C.A.C. Mendonca, C.R. Miskys, G.M. Guadalpi, M. Battagliarin and M.I.M.S. Bueno, *J. Crystal Growth* **186** (1998) 487.
89. R. Fornari, E. Gilloli, G. Mignoni and M. Masi, *Cryst. Res. Technol.* **32** (1997) 1085.
90. R. Ware, in *Proc. 12th Int. Conf. on InP and Related Materials* (Williamsburg, 2000) p. 546.
91. T. Sato, K. Aoyama, K. Sao, S. Numao, I. Homma, S. Sugano, T. Hoshina and K. Iwasaki, *J. Jpn. Assoc. Crystal Growth (in japanese)* **30** (2003) 89.
92. X. Zhou, Y. Zhao, No. Sun, G. Yang, Y. Xu and T. Sun, *J. Crystal Growth* **264** (2004) 17.
93. N. Sun, L. Mao, X. Zhou, X. Wu, W. Guo, M. Hu, L. Li, M. Xiao, B. Liao, G. Yang, J. Fu, Z. Yao, Y. Zhao, K. Yang and T. Sun, in *Proc. 16th Int. Conf. on InP and Related Materials* (Kagoshima, 2004) p. 326.
94. N. Sun, L. Mao, X. Zhou, X. Wu, W. Guo, M. Hu, L. Li, M. Xiao, B. Liao, G. Yang, J. Fu, Z. Yao, Y. Zhao, K. Yang and T. Sun, in *Proc. 16th Int. Conf. on InP and Related Materials* (Kagoshima, 2004) p. 595.
95. N. Miyazaki, H. Uchida, T. Munakata and T. Fukuda, *JSME Int. J.* **A37** (1994) 124.
96. H. Zhang, V. Prasad and D.F. Bliss, *J. Crystal Growth* **169** (1996) 250.
97. R. Hirano, T. Kanazawa and M. Nakamura, in *Proc. 4th Int. Conf. on InP and Related Materials* (Newport, 1992) p. 546.
98. R. Hirano and M. Uchida, in *Proc. 7th Int. Conf. on InP and Related Materials* (Sapporo, 1995) p. 97.
99. R. Hirano and M. Uchida, *J. Electron. Mater.* **25** (1996) 347.
100. R. Hirano, in *Proc. 10th Int. Conf. on InP and Related Materials* (Tsukuba, 1998) p. 80.
101. R. Hirano, *Jpn. J. Appl. Phys.* **38** (1999) 969.
102. R. Hirano, *Thesis*, Gakushuin University (1999).
103. K. Tada, M. Tatsumi, M. Nakagawa, T. Kawase and S. Akai, *Inst. Phys. Conf. Ser.* **91** (1987) 439.
104. T. Kawase, T. Araki, M. Tatsumi, S. Murai, K. Tada and S. Akai, *Sumitomo Electrics (in japanese)* **135** (1989) 156.
105. Y. Hosokawa, S. Kowarabayashi, Y. Yabuhara, M. Morioka, M. Yokogawa, K. Fujita, S. Akai, Proc. in *Proc. 4th Int. Conf. on InP and Related Materials* (Newport, 1992) p. 258.
106. M. Tatsumi, T. Kawase and K. Tada, in *Non-Stroichiometry in Semiconductors*, eds. K.J. Bachmann, H.L. Hwang and C. Schwab (Elsevier Sci., Amsterdam, 1992) p. 107.
107. Y. Hosokawa, Y. Yabuhara, R. Nakai and K. Fujita, in *Proc. 10th Int. Conf. on InP and Related Materials* (Tsukuba, 1998) p. 34.
108. Y. Hosokawa, Y. Yabuhara, R. Nakai and K. Fujita, *Sumitomo Electrics Tech. Rev.* **48** (1999) 53.
109. T. Kawase, N. Hosaka, K. Hashio and Y. Hosokawa, in *Proc. 16th Int. Conf. on InP and Related Materials* (Kagoshima, 2004) p. 589.
110. K. Kohiro, K. Kainosho and O. Oda, in *Proc. 3rd Int. Conf. on InP and Related Materials* (Cardiff, 1991) p. 8.
111. K. Kohiro, K. Kainosho and O. Oda, *J. Electron. Mater.* **20** (1991) 1013.
112. K. Kohiro, M. Ohta and O. Oda, *J. Crystal Growth* **158** (1996) 197.
113. R. Hirano and A. Noda, in *Proc. 13th Int. Conf. on InP and Related Materials* (Nara, 2001) p. 529.
114. A. Noda, K. Suzuki, A. Arakawa, H. Kurita and R. Hirano, in *Proc. 14th Int. Conf. on InP and Related Materials* (Stockholm, 2002) p. 397.
115. A. Noda, M. Nakamura, A. Arakawa and R. Hirano, in *Proc. 16th Int. Conf. on InP and Related Materials* (Kagoshima, 2004) p. 552.
116. W.A. Gault, E.M. Monberg and J.E Clemans, *J. Crystal Growth* **74** (1986) 491.
117. E.M. Monberg, W.A. Gault, F. Simchock and F. Dominguez, *J. Crystal Growth* **83** (1987) 174.
118. E.M. Monberg, W.A. Gault, F. Dominguez, F. Simchock, S.N.G. Chu and C.M. Stiles, *J.*

Electrochem. Soc. **135** (1988) 500.
119. E.M. Monberg, H. Brown, S.N.G. Chu and J.M. Parsey, in *Proc. 5th Conf. Semi-insulating III-V Mateirals* (Malmö, Sweden, 1988) p. 459.
120. E.M. Monberg, H. Brown. C.E. Bonner, *J. Crystal Growth* **94** (1989) 109.
121. E.M. Monberg, P.M. Bridenbaugh, H. Brown and R.L. Barns, *J. Electron. Mater.* **18** (1989) 549.
122. T.I. Ejim, in *Proc. 3rd Int. Conf. on InP and Related Materials* (Cardiff, 1991) p. 196.
123. M.A. Shahid and F. Simchock, in *Proc. 3rd Int. Conf. on InP and Related Materials* (Cardiff, 1991) p. 319.
124. R. Fornari, M. Curti, R. Magnanini, G. Mignoni and G. Zuccalli, *Crystal Prop. Prep.* **36-38** (1991) 306.
125. F. Matsumoto, Y. Okano, I. Yonenaga, K. Hoshikawa and T. Fukuda, *J. Crystal Growth* **132** (1993) 348.
126. G. Müller. D. Hofmann and N. Schäfer, in *Proc. 5th Int. Conf. on InP and Related Materials* (Paris, 1993) p. 313.
127. D. Zemke, H.J. Leister and G. Müller, in *Proc. 8th Int. Conf. on InP and Related Materials* (Schwäbisch Gmünd, 1996) p. 47.
128. P. Rudolph, F. Matsumoto and T. Fukuda, *J. Crystal Growth* **158** (1996) 43.
129. X. Liu, *Microelectronics J.* **27** (1996) 4.
130. M. Young, X. Liu, D. Zhang, M. Zhu and X.Y. Hu, in *Proc. 10th Int. Conf. on InP and Related Materials* (Tsukuba, 1998) p. 30.
131. X. Hu, M. Young, H. Helava and D. Zhang, Post Deadline Papers in *Proc. 10th Int. Conf. on InP and Related Materials* (Tsukuba, 1998) p. 15.
132. T. Asahi, K. Kainosho, T. Kamiya, T. Nozai, Y. Matsuda and O. Oda, Post Deadline Papers in *Proc. 10th Int. Conf. on InP and Related Materials* (Tsukuba, 1998) p. 1.
133. T. Asahi, R. Hirano, K. Kohiro, K. Kainosho, M. Uchida and O. Oda, *J. Jpn. Crystal Growth Assoc. (in japanese)* **25** (1998) 220.
134. T. Asahi, K. Kainosho, T. Kamiya, T. Nozai, Y. Matsuda and O. Oda, *Jpn. J. Appl. Phys.* **38** (1999) 977.
135. T. Asahi, K. Kainosho, K. Kohiro, A. Noda, K. Sato and O. Oda, in *Book on Crystal Growth Technology*, ed. H.J. Scheel (John Wiley & Sons, New York, 2004) p. 323.
136. A.N. Gulluoglu and C.T. Tsai, *Acta Mater.* **47** (1999) 2313.
137. P. Schwesig, M. Hainke, J. Friedrich and G. Müller, *J. Crystal Growth* **266** (2004) 224.
138. N. Schäfer, J. Stierlen and G. Müller, *Mater. Sci. Engineer.* **B9** (1991) 19.
139. A. Shimizu, J. Nishizawa, Y. Oyama and K. Sato, *J. Crystal Growth* **209** (2000) 21.
140. A. Shimizu, J. Nishizawa, Y. Oyama and K. Sato, *J. Crystal Growth* **237/239** (2000) 1697.
141. B.S. Ahern, S. Bachowski, R.M. Hilton and J.A. Adamski, *Mater. Lett.* **8** (1989) 486.
142. S. Bachowski, D.F. Bliss, B. Ahern, R.M. Hilton, J. Adamski and D.J. Carlson, in *Proc. 2nd Int. Conf. InP and Related Materials* (Denver, 1990) p. 30.
143. D.F. Bliss, R.M. Hilton, S. Bachowski and J.A. Adamski, *J. Electon. Mater.* **20** (1991) 967.
144. D.F. Bliss, R.M. Hilton and J.A. Adamski, *J. Crystal Growth* **128** (1993) 451.
145. S. Thono and A. Katsui, *J. Crystal Growth* **74** (1986) 362.
146. P. Martin, J. Jimenez, E. Martin, A. Torres, M. A. Gonzalez and J. Ramos, *J. Mater. Sci.: Mater. Electronics* **5** (1994) 315.
147. J. Wei, *Cryst. Res. Technol.* **30** (1995) K73.
148. H. Chung, M. Dudley, D.J. Larson, Jr., V. Prasad, D.T.J. Hurle and D.F. Bliss, in *Proc. 10th Int. Conf. on InP and Related Materials* (Tsukuba, 1998) p. 84.
149. D. T. J. Hurle, *J. Crystal Growth* **147** (1995) 239.
150. H. Chung, M. Dudley, D.J. Larson, Jr., D.T.J. Hurle, D.F. Bliss and V. Prasad, *J. Crystal Growth* **187** (1998) 9.
151. M. Dudley, B. Raghothamachar, Y. Guo, X.R. Huang, H. Chung, D.T.J. Hurle and D.F. Bliss, *J. Crystal Growth* **192** (1998) 1.

152. Y. Han and L. Lin, *Solid State Commun.* **110** (1999) 403.
153. V.A. Antonov, V.G. Elsakov, T.I. Olkhovikova and V.V. Selin, *J. Crystal Growth* **235** (2002) 35.
154. S. Yoshida, S. Ozawa, T. Kijima, J. Suzuki and T. Kikuta, *J. Crystal Growth* **113** (1991) 221.
155. Y. Seki, J. Matsui and H. Watanabe, *J. Appl. Phys.* **47** (1976) 3374.
156. P. J. Roksnoer and M. M. B. Van Rijbroek-van den Boom, *J. Crystal Growth* **66** (1984) 317.
157. G. T. Brown, B. Cockayne and W. R. MacEwan, *J. Crystal Growth* **51** (1981) 369.
158. G. Jacob, M. Duseaux, J.P. Farges, M.M.B. van den Boom and P.J. Roksnoer, *J. Crystal Growth* **61** (1983) 417.
159. G. T. Brown, B. Cockayne and W. R. MacEwan and D.J. Ashen, *J. Mater. Sci. Lett.* **2** (1983) 667.
160. A. Katsui, S. Thono, Y. Homma and T. Tanaka, *J. Crystal Growth* **74** (1986) 221.
161. S. Thono and A. Katsui, *J. Crystal Growth* **78** (1986) 249.
162. C. B. Wheeler, R. J. Roedel, R. W. Nelson, S. N. Schauer and P. Williams, *J. Appl. Phys.* **68** (1990) 969.
163. A. A. Ballman, A. M. Glass, R. E. Nahory and H. Brown, *J. Crystal Growth* **62** (1983) 198.
164. S. Thono, E. Kubota, S. Shinoyama, A. Katsui and C. Uemura, *Jpn. J. Appl. Phys.* **23** (1984) L72.
165. B. Cockayne, T. Bailey and W.R. MacEwan, *J. Crystal Growth* **76** (1986) 507.
166. A. Katsui and S. Thono, *J. Crystal Growth* **79** (1986) 287.
167. A. Shimizu, S. Nishine, M. Morioka, K. Fujita and S. Akai, in *Proc. 5th Conf. Semi-Insulating III-V Materials*, eds. H. Kukimoto and S. Miyazawa (Ohmsha, Tokyo, 1986) p. 41.
168. R. Coquille, Y. Toudic, L. Haji, M. Gauneau, G. Moisan and D. Lecrosnier, *J. Crystal Growth* **83** (1987) 167.
169. R. Fornari, J. Kumar, M. Curti and G. Zuccalli, *J. Crystal Growth* **96** (1989) 795.
170. A.S. Jordan, G.T. Brown, B. Cockayne, D. Brasen and W.A. Bonner, *J. Appl. Phys.* **58** (1985) 4383.
171. A. S. Jordan, R. Von A. R. Neida and J. W. Nielsen, *J. Appl. Phys.* **52** (1981) 3331.
172. S. Fogliani, M. Masi, S. Carra, G. Guadalupi, B. Molinas and L. Meregalli, *Mater. Sci. Forum* **203** (1996) 187.
173. G. Müller, J. Völk and E. Tomzig, *J. Crystal Growth* **64** (1983) 40.
174. R. N. Lee, M. K. Norr, R. L. Henry, and E. M. Swiggard, *Mater. Res. Bull.* **12** (1977) 651.
175. B. Cockayne, W. R. MacEwan, G. T. Rown and W. H. E. Wilgoss, *J. Mater. Sci.* **16** (1981) 554.
176. J.B. Mullin, A. Royle, B.W. Straunghan, P.J. Tufton and E.W. Williams, *J. Crystal Growth***13/14** (1972) 640.
177. R. Fornari, T. Taddia and D. Ranno, *Mater. Lett.* **10** (1991) 404.
178. E. Kubota and A. Katsui, *Jpn. J. Appl. Phys.* **24** (1985) L344.
179. D. Rumsby, R. M. Ware and M. Whittaker, in *Proc. 2nd Conf. Semi-Insulating III-V Materials*, ed. G.J. Rees (Nottingham, 1980) p. 59.
180. E. Kubota, Y. Ohmori and K. Sugii, *Inst. Phys. Conf. Ser.* **63** (1981) 31.
181. M. Morioka, K. Kikuchi, K. Kohe and S. Akai, *Inst. Phys. Conf. Ser.* **63** (1981) 37.
182. R. Fornari and J. Kumar, *Appl. Phys. Lett.* **56** (1990) 638.
183. R. Fornari, E. Gilioli, M. Morglioni, M. Thirumavalavan and A. Zappettini, *J. Crystal Growth* **166** (1996) 572.
184. I. R. Harris, N. A. Smith, B. Cockayne and W. R. MacEwan, *J. Crystal Growth* **64** (1983) 115.
185. B. W. Straughan, D. T. J. Hurle, K. Lloyd and J. B. Mullin, *J. Crystal Growth* **21** (1974) 117.
186. G. W. Iseler and B. S. Ahern, *Appl. Phys. Lett.* **48** (1986) 1656.
187. C. D. Brandt, A. M. Hennel, T. Bryskiewicz, K.Y. Ko, L. M. Pawlowicz and H.C. Gatos, *J. Appl. Phys.* **65** (1989) 3459.
188. R. P. Leon, M. Kaminska, K. M. Yu and E. R. Weber, *Phys. Rev. B* **46** (1992) 46.
189. D. Wruck and A. Knauer, *phys. stat. sol. (a)* **107** (1988) 321.
190. A. Knauer, R. Sprenger and U. Zeimer, *Crystal Prop. Prep.* **12** (1987) 37.
191. E. Tomzig, M. Baumgartner, K. Löhnert, D. Schmitz, H. Jurgensen, M. Heyen, M. Renaud, G. Gillardin and J.L. Bris, in *Proc. 5th Conf. Semi-Insulating III-V Materials* (Malmö, Sweden,

1988) p. 577.
192. V. Montgomery, J.G. Swanson and P.J.Claxton, *J. Crystal Growth* **94** (1989) 721.
193. K. Kainosho, H. Shimakura, H. Yamamoto, T. Inoue and O. Oda, in *Proc. First Int. Conf. on InP and Related Materials* (Oklahoma, 1989) p. 312.
194. K.D.C. Trapp, M.T. Asom, G.E. Carver, E.M. Monberg, F.A. Thiel and R.L. Barns, *Mater. Res. Soc. Symp. Proc.* **145** (1989) 499.
195. G.E. Carver, R.D. Moore, K.D.C. Trapp, P.M. Kahora and F.A. Stevie, in *Proc. 2nd Int. Conf. InP and Related Materials* (Denver, 1990) p. 428.
196. H. L'Haridon, R. Callec, R. Coquillé, P.N. Favennec, J.P. Fillard, P. Gall, M. Gauneau and Y. Le Guillou, *J. Crystal Growth* **113** (1991) 39.
197. H. L'Haridon, P.N. Favennec, R. Coquille, M. Salvi, M. Gauneau, Y. Le Guillou and R. Callec, *J. Crystal Growth* **113** (1991) 39.
198. W. Meler, H.Ch. Alt, Th. Vetter, J. Volkl and A. Winnacker, *Semicon. Sci. Technol.* **6** (1991) 297.
199. J. Jimenez, M.A. Avella, M.A. Gonzalez, P. Martin, L.F. Sanz and M. Chafai, *Mater Res. Soc. Symp. Proc.* **299** (1994) 71.
200. A. Seidl, F. Mosel and G. Muller, *Mater. Sci. Engineer.* **B28** (1994) 107.
201. J. Jimenez, M. Avella, A. Alvarez, M. Gonzalez and R. Fornari, *Inst. Phys. Conf. Ser.* **149** (1996) 269.
202. A. Alvarez, M. Avella, J. Jimenez, M.A. Gonzalez and R. Fornari, *Semicond. Sci. Technol.* **11** (1996) 941.
203. M. Janson, *J. Electrochem.* **130** (1983) 960
204. E. Kubota and A. Katsui, *Jpn. J. Appl. Phys.* **24** (1985) L69.
205. E. Kubota and A. Katsui, *Jpn. J. Appl. Phys.* **25** (1986) L249.
206. T. Tanaka, Y. Homma and S. Kurosawa, in *Extended Abstr. 15th Int. Conf. Solid State Dev. Mater.* (Tokyo, 1986) p. 631.
207. G. Jacob, R. Coquille and Y. Toudic, in *Proc. 6th Conf. Semi-insulating III-V Materials*, eds. by A. Milnes and C. J. Miner (Toronto, Adam Hilger, 1990) p. 149.
208. O. Oda, K. Kainosho, K. Kohiro, R. Hirano, H. Shimakura, T. Inoue, H. Yamamoto and T. Fukui, *J. Electron. Mater.* **20** (1991) 1007.
209. D. F. Bliss, G. G. Bryanl, D. Gabble, G. Iseler, E. E. Haller and F. X. Zach, in *Proc. 7th Int. Conf. on InP and Related Materials* (Sapporo, 1995) p. 678.
210. N. Sun, X. Wu, X. Wu, Y. Zhao, L. Cao, Q. Zhao, W. Guo, J. Zhang, K. Bi and T. Sun, *J. Crystal Growth* **225** (2001) 244.
211. S. Adachi, in *Properties of.Indium Phosphide*, ENIS Datareviews Series, No.6 (INSPEC, 1991) p. 337.
212. H.C. Gatos and M.C. Lavine, *J. Electrochem. Soc.* **107** (1960) 427.
213. M.S. Abraham and C.J. Buiocchi, *J. Appl. Phys.* **36** (1965) 2855.
214. J.B. Mullin, A. Royle and W. Straughan, in *Proc. Int. Symp. Gallium Arsenide* (Archen, 1970) p. 41.
215. R.C. Clarke, D.S. Robertson and A.W. Vere, *J. Mater. Sci.* **8** (1973) 1349.
216. B. Tuck and A.J. Baker, *J. Mater. Sci.* **8** (1973) 1559.
217. A. Huber and N. T. Linh, *J. Crystal Growth* **29** (1975) 80 .
218. V. Gottschalch, W. Heinig, E. Butter, H. Rosin, and G. Freydank, *Kristall und Technik* **14** (1979) 563.
219. K. Akita, T. Kusunoki, S. Komiya, and T. Kotani, *J. Crystal Growth* **46** (1979) 783.
220. G.T. Brown, B. Cockaye and W.R. MacEwan, *J. Mater. Sci.* **15** (1980) 2539.
221. S. N. G. Chu, C. M. Jodlauk, and A. A. Ballman, *J. Electrochem. Soc.* **129** (1982) 352 .
222. D. T. C. Huo, J. D. Wynn, M. F. Yan, and D. P. Wilt, *J. Electrochem. Soc.* **136** (1989) 1804.
223. H. Nishikawa, T. Soga, T. Jimbo, N. Mikuriya, and M. Umeno, *Jpn. J. Appl. Phys.* **28** (1989) 941.
224. E. Peiner and A. Schlachetzki, *J. Electron. Mater.* **21** (1992) 887.
225. J.L. Weyher, R. Fornari, T. Görög, J.L. Kelly and B. Erné, *J. Crystal Growth* **141** (1994) 57.

226. I.J. Weyher, R. Fornari, T. Görög, *Mater. Sci. Engineer.* **B28** (1994) 488.
227. A. Kauer, U. Zeimer and R. Sprenger, *Cryst. Res. Technol.* **24** (1989) 1245.
228. M.M. Al-Jassim, C.A. Warwick and G.R. Booker, *Inst. Phys. Conf. Ser.* 60 (1981) 357.
229. S. Thono, S. Shinohara, A. Yamamoto and C. Uemura, *J. Appl. Phys.* **54** (1983) 666.
230. I. Yonenaga and K. Sumino, *J. Appl. Phys.* **74** (1993) 917.
231. M. Azzaz, J-P. Michel and A. George, *Phil. Mag. A* 69 (1994) 903
232. G. Müller, R. Rupp, J. Völkl, H. Wolf and W. Blum, *J. Crystal Growth* **71** (1985) 771.
233. J. Völkl, G. Müller and W. Blum, *J. Crystal Growth* **83** (1987) 383.
234. J. Völkl and G. Müller, in *Proc. 5th Conf. Semi-insulating III-V Mateirals* (Malmö, Sweden, 1988) p. 489.
235. M. Luysberg and D. Gerthsen, *Phil. Mag. A* **76** (1997) 45.
236. D. Brasen, *J. Mater. Sci.* **11** (1976) 791.
237. D. Y. Watts and A. F. W. Willoughby, *J. Appl. Phys.* **56** (1984) 1869.
238. C. Ascheron, C. Haase, G. Kühn and H. Neumann, *Cryst. Res. Technol.* **24** (1989) K33.
239. M. Yamada, K. Ito and M. Fukuzawa, in *Proc. 9th Int. Conf. on InP and Related Materials* (Hyaniss, 1997) p. 209.
240. M. Yamada, M. Fukuzawa, M. Akita, M. Hermes, M. Uchida and O. Oda, in *Proc. IEEE Semicon. Insul. Mater. Conf.* (IEEE, Cat., 1998) p. 45.
241. M. Fukuzawa, M. Hermes, M. Uchida, O. Oda and M.Yamada, *Jpn. J. Appl. Phys.* **38** (1999) 1156.
242. B. Cockayne, G.T. Brown and W.R. MacEwan, *J. Crystal Growth* **51** (1981) 461.
243. C.R. Elliott and J.C. Regnault, *J. Electrochem. Soc.* **128** 1981) 113.
244. C.R. Elliot and J.C. Regnault, *Inst. Phys. Conf. Ser.* 60 (1981) 365.
245. M.M. Al-Jassim, C.A. Warwick and G.R. Booker, *Inst. Phys. Conf. Ser.* 60 (1981) 357.
246. P.D. Augustus and D.J. Stirland, *J. Electrochem. Soc.* **129** (1982) 614.
247. B. Cockayne, G.T. Brown and W.R. MacEwan, *J. Crystal Growth* **64** (1983) 48.
248. D.J. Stirland, D.G. Hart, S. Clark, J.C. Regnault and C.R. Elliott, *J. Crystal Growth* **61** (1983) 645.
249. G.T. Brown, B. Cockayne, C.R. Elliot, J.C. Regnault, D.J. Stirland and P.D. Augustus, *J. Crystal Growth* 67 (1984) 495.
250. R. Hirano, T. Kanazawa and S. Katsura, *J. Crystal Growth***134** (1993) 81.
251. K. Kohiro, R. Hirano and O. Oda, *J. Electron. Mater.* **25** (1996) 343.
252. S. Miyazawa and H. Koizumi, *J. Electrochem. Soc.* **129** (1982) 2335.
253. N.A. Smith, I.R. Harris, B. Cockayne and W.R. MacEwan, *J. Crystal Growth* **68** (1984) 517.
254. R. Fornari, C. Friteri, J.L. Wehyer, S.K. Krawczk, F. Kraft and G. Mignoni, in *Proc. 7th Conf. Semi-Insulating III-V Materials* (Ixtapa, Mexico, 1992) p. 39.
255. B. Cockayne, W.R. MacEwan, S.J. Courtney, I.R. Harris and N.A. Smith, *J. Crystal Growth* **69** (1984) 610.
256. B. Cockayne, W.R. MacEwan, I.R. Harris and N.A. Smith, *J. Crystal Growth* **76** (1986) 251.
257. C. Frigeri, C. Ferrari, R. Fornari, J.L. Weyher, F. Longo and G.M. Guadalupi, *Mater. Sci. Engineer.* **B28** (1994) 120.
258. C. Frigeri, R. Fornari, J.L. Weyher, G.M. Guadalupi and F. Longo, *Inst. Phys. Conf. Ser.* **146** (1995) 423.
259. P. Franzosi, G. Salvati, M. Cocito, F. Taiariol and C. Ghezzi, *J. Crystal Growth* **69** (1984) 388.
260. R. Fornari, P. Franzosi, J. Kumar and G. Salviati, *Semicon. Sci. Technol.* **7** (1992) A141.
261. I. R. Harris, N. A. Smith, B. Cockayne and W. R. MacEwan, *J. Crystal Growth* 64 (1983) 115.
262. A.J. Moll, E.E. Haller, J.W. Ager III and W. Walukiewicz, *Appl. Phys. Lett.* **65** (1994) 1145.
263. M. Alatalo, H. Kauppinen, K. Saarinen, M.J. Puska, J. Mäkinen, P. Hautojärvi and R.M. Nieminen, *Phys. Rev. B* **51** (1995) 4176.
264. C. Corbel, C. LeBerre, K. Saarinen and P. Hautojarvi, *Mater. Sci. Engineer.* **B44** (1997) 173.
265. A. Martinatis, A. Sakalas and G. Steponkus, *Crystal Prop. Prep.* **19&20** (1989) 49.
266. H.J. Sun, H.P. Gislason, C.F. Rong and G.D. Watkins, *Phys. Rev. B* **48** (1993) 17092.
267. T.A. Kennedy, N.D. Wilsey, P.B. Kelin and R.L. Henry, *Mater. Sci. Forum* **10-12** (1986) 271.

268. G. Dlubek, O. Brummer, F. Plazaola, P. Hautojarvi and K. Naukkarinen, *Appl. Phys. Lett.* **46** (1985) 1136.
269. C.P. Eweil, S. Oberg, R. Jones, B. Pajot and P.R. Briddon, *Semicon. Sci. Technol.* **11** (1996) 502.
270. R.W. Jansen, *Phys. Rev. B* **41**(1990) 7666.
271. A.P. Seitsonen, R. Virkkunen, M.J. Puska and P.M. Nieminen, *Phys. Rev. B* **49** (1994) 5253.
272. K. Kainosho, H. Shimakura, T. Kanazawa, T.Inoue and O. Oda, *Inst. Phys. Conf. Ser.* **106** (1990) 25.
273. T. Inoue, H. Shimakura and K. Kainosho, *J. Electrochem. Soc.* **137** (1990) 1283.
274. T. Okumura, in *New Compound Semiconductor Handbook (in japanese)*, ed. T. Ikoma (Science Forum, Tokyo, 1982) p. 249.
275. M.S. Skolnick, *J. Phys. C: Solid State Phys.* **16** (1983) 7003.
276. P. Rojo, P. Leyral, A. Nouailhat, G. Guillot, B. Lambert, B. Deveaud and R. Coquille, *J. Appl. Phys.* **55** (1984) 395.
277. B. Lambert, B. Clerjaud, C. Naud, B. Deveaud, G. Picoli and Y. Toudic, in *Proc. 13th Int. Conf. on Defects in Semiconductors* (Colorado, 1985) p. 1141.
278. V. Parguel, P.N. Favennec, M. Gauneau, Y. Rihet, R. Chaplain, H. L'Haridon and C. Vaudry, *J. Appl. Phys.* **62** (1987) 824.
279. Y. Toudic, B. Lambert, R. Coquillé, G. Grandpierre and M. Gauneau, *Semicon. Sci. Technol.* **3** (1988) 464.
280. C. Delerur, M. Lannoo, G. Bremond, G. Guillot and A. Nouailhat, *Europhys. Lett.* **9** (1989) 373.
281. K. Korona, K. Karpinska, A. Babinski and A. M. Hennel, *Acta Phys. Polonica* **A77** (1990) 71.
282. A. Zozime and W. Schöter, *Appl. Phys. Lett.* **57** (1990) 1326.
283. C. Backhouse, V.A. Samuilov and L. Young, *Appl. Phys. Lett.* **60** (1992) 2906.
284. J.C. Paris, M. Gauneau, H. L'Haridon and G. Pelous, *J. Crystal Growth* **64** (1983) 137.
285. Z.Q. Fang and D.C. Look, *Appl. Phys. Lett.* **61** (1992) 589.
286. Z.Q. Fang, D.C. Look, M. Uchida, K. Kainosho and O. Oda, *J. Electron. Mater.* **27** (1998) L68.
287. W. Walukiewicz, J. Lagowski, L. Jastrzebski, P. Rava, M. Lichtensteiger, C.H. Gatos and H.C. Gatos, *J. Appl. Phys.* **51** (1980) 2659.
288. T. Amano, S. Kondo and H. Nagai, in *Extended Abstr.* (34th Spring Meeting, Jpn. Soc. Appl. Phys. and Related Socs., 1987) p. 126.
289. G. Müller, J. Pfannenmuller, E. Tomzig and J. Volkl, *J. Crystal Growth* **64** (1983) 37.
290. O. Mizuno and H. Watanabe, *Electron. Lett.* **11** (1975) 118.
291. C. R. Zeiss, G. A. Antypas and C. Hopkins, *J. Crystal Growth* **64** (1983) 217.
292. F. X. Zach, *J. Appl. Phys.* **75** (1994) 7894,
293. F. X. Zach, *J. Crystal Growth* **64** (1983) 217.
294. H.K. Kim, J.S. Hwang, S.K. Noh and C.H.Chung, Jpn. *J. Appl. Phys.* **25** (1986) L888.
295. R. Fornari, *J. Electron. Mater.* **20** (1991) 1043.
296. G. Bahir, J.L. Merz, J.R. Abelson and T.W. Sigmon, *J. Appl. Phys.* **65** (1989) 1009.
297. H. Kamada, S. Shinoyama and A. Katsui, *J. Appl. Phys.* **55** (1984) 2881.
298. M. Gauneau, R. Chaplain, A. Rupert, E.V.K. Rao and N. Duhamel, *J. Appl. Phys.* **57** (1985) 1029.
299. A. Seidl, F. Mosel, J. Friedrich, U. Kretzer and G. Müller, *Mater. Sci. Engineer.* **B21** (1993) 321.
300. D. E. Holmes, R. G. Wilson and P. W. Yu, *J. Appl. Phys.* **52** (1981) 3396.
301. E. W. A. Young and G. M. Fontijn, *Appl. Phys. Lett.* **56** (1990) 146.
302. C. J. Miner, D. G. Knight, J. M. Zorzi, R. W. Strater, N. Puetz and M. Ikisawa, *Inst. Phys. Conf. Ser.* **135** (1994) 181.
303. P. B. Klein, R. L. Henry, T. A. Kennedy and N. D. Wilsey, *Mater. Sci. Forum* **10-12** (1986) 1259.
304. R. Hirano and T. Kanazawa, *J. Crystal Growth* **106** (1990) 531.
305. R. Hirano, T. Kanazawa and T. Inoue, *J. Appl. Phys.* **71** (1992) 659.
306. D. Hofmann, G. Müller and N. Streckfuss, *Appl. Phys.* **A48** (1989) 315.
307. G. Hirt, D. Hofmann, F. Mosel, N. Schäfer and G. Müller, *J. Electron. Mater.* **20** (1991) 1065.
308. P. Kipfer, J. Lindolf, D. Hofmanna and G. Müller, *J. Appl. Phys.* **69** (1991) 3860.

309. K. Kainosho, H. Shirnakura, H. Yamamoto and O. Oda, *Appl. Phys. Lett.* **59** (1991) 932.
310. R. Fornari, A. Brinciotti, E. Gombia, R. Mosca and A. Sentiri, *Mater. Sci. Engineer.* **B28** (1994) 95.
311. R. Fornari, B. Dedavid, A. Sentiri and N. Curti, in *Semi-insulating III-V Materials*, ed. M. Godlewski (World Sci., Singapore, 1994) p. 35.
312. R. Fornari, A. Brinciotti, E. Gombia, R. Mosca, A. Huber and C. Grattepain, in *Semi-insulating I II-V Materials*, ed. M. Godlewski (World Sci., Singapore, 1994) p. 283.
313. K. Kainosho, H. Okazaki and O. Oda, in *Post-Deadline Papers of Proc. 5th Int. Conf. on InP and Related Materials* (Paris, 1993) p. 33.
314. K. Kainosho, O. Oda, G. Hirt and G. Müller, *Mater. Res. Soc. Symp. Proc.* **325** (1994) 101.
315. K. Kainosho, M. Ohta and O. Oda, in *Proc. 7th Int. Conf. on InP and Related Materials* (Sapporo, 1995) p. 37.
316. K. Kainosho, M. Ohta, M. Uchida, M. Nakamura and O. Oda, *J. Electron. Mater.* **25** (1996) 353.
317. D. Wolf, G. Hirt and G. Müller, J. Electron. Mater. **24** (1995) 93, D. Wolf, G. Hirt, F. Mosel, G. Müller and J. Völkl, *Mater. Sci. Engineer.* **B28** (1994) 115.
318. M. Uchida, K. Kainosho, M. Ohta and O. Oda, in *Proc. 8th Int. Conf. on InP and Related Materi als* (Schwäbisch Gmünd, 1996) p. 43.
319. R. Fornari, A. Zappettini, E. Gombia, R. Mosca and M. Curti, in *Proc. 8th Int. Conf. on InP and Related Materials* (Schwäbisch Gmünd, 1996) p. 292
320. R. Fornari, A. Zappettini, E. Gombia, R. Mosca, K. Cherkaoui and G. Marrakchi, *J. Appl. Phys.* **81** (1997) 7604.
321. G. Hirt, B. Hoffmann, U. Kretzer, A. Woitech, D. Zemke and G. Müller, in *Proc. 7th Int. Conf. on InP and Related Materials* (Sapporo, 1995) p. 33.
322. O. Oda, M. Uchida, K. Kainosho, M. Ohta, M. Warashina and M. Tajima, in *Proc. 9th Int. Conf. on InP and Related Materials* (Hyaniss, 1997) p. 404.
323. M. Uchida, K. Kainosho, M. Ohta and O. Oda, *J. Electron. Mater.* **27** (1998) 8.
324. M. Uchida, T. Asahi, K. Kainosho, Y. Matsuda and O. Oda, *Jpn. J. Appl. Phys.* **38** (1999) 985.
325. G. Hirt, T. Mono and G. Müller, *Mater. Sci. Engineer.* **B28** (1994) 101.
326. Z.Q. Fang, D.C. Look, M. Uchida, K. Kainosho and O. Oda, *J. Electron. Mater.* **27** (1998) L68.
327. G. Hirt, S. Bornhorst, J. Friedrich, N. Schäfer and G. Müller, in *Proc. 5th Int. Conf. on InP and Related Materials* (Paris, 1993) p. 313.
328. G. Hirt, D. Wolf and G. Müller, *J. Appl. Phys.* 74 (1993) 5538.
329. K. Cherkaoui, S. Kallel, M. Marrakchi and A. Karoui, in *Proc. IEEE Semicon. Semi-insulating. Mater. Conf* (Piscataway, USA, 1996) p.59.
330. M. Uchida, O. Oda, M. Warashina and M. Tajima, *J. Electrochem. Soc.* **145** (1998) 1048.
331. M. Uchida and O. Oda, *J. Jpn. Assoc. Crystal Growth (in japanese)* **28** (2001) 37.
332. D. F. Bliss, G. G. Bryanl, D. Gabble, G. Iseler, E. E. Haller and F. X. Zach, in *Proc. 7th Int. Conf. on InP and Related Materials* (Sapporo, 1995) p. 678.
333. Y.W. Zhao, X.L. Xu, M. Gong, S. Fung, C.D. Beling, X.D. Chen, N.F. Sun, T.N. Sun, S.L. Liu, G.Y. Yang, X.B. Guo, Y.Z. Sun, L. Wang, Q.Y. Zheng, Z.H. Zhou and J. Chen, *Appl. Phys. Lett.* **72** (1998) 2126.
334. T.S. Kim and B.G. Streetman, in *Properties of Indium Phosphide*, ENIS Datareviews Series, No.6 (INSPEC, 1991) p. 165.
335. T. Inoue, in *Properties of Indium Phosphide*, ENIS Datareviews Series, No.6 (INSPEC, 1991) p. 182.
336. T. Inoue, in *Properties of Indium Phosphide*, ENIS Datareviews Series, No.6 (INSPEC, 1991) p. 191.
337. M. Razeghi, Ph. Maurel, M. Defour, F. Omnes, G. Neu and A. Kozacki, *Appl. Phys. Lett.* **52** (1988) 117.
338. L.D. Zhu, K.T. Chen, D.K. Wagner and J.M. Ballantyne, *J. Appl. Phys.* **57** (1985) 5486.
339. T. Inoue, K. Kainosho, R. Hirano, H. Shimakura, T. Kanazawa and O. Oda, *J. Appl. Phys.* **67**

(1990) 7165.
340. P.J. Dean, M.S. Skolnick, *J. Appl. Phys.* **54** (1983) 346.
341. J. Kang, F. Matsumoto and T. Fukuda, *J. Appl. Phys.* **81** (1997) 905.
342. P.J. Dean, M.S. Skolnick, B. Cockayne and W.R. MacEwan, *J. Crystal Growth* **67** (1984) 486.
343. J.U. Fischbach, G. Benz, N. Stath and M.H. Pilkuhn, *Solid-State Commun.* **11** (1972) 725.
344. K. Hess, N. Stath and K.W. Benz, *J. Electrochem. Soc.* **121** (1974) 1208.
345. D. Barthruff, K.W. Benz, G.A. Antypas, *J. Electron. Mater.* **8** (1979) 485.
346. M. Yamaguchi, A. Yamamoto, S. Shinoyama and H. Sugiura, *J. Appl. Phys.* **53** (1982) 633
347. B.J. Skromme, G.E. Stillman, J.D. Oberstar and S.S. Chan, *J. Electron. Mater.* **13** (1984) 463.
348. E. Kubota, A. Katusi and K. Sugii, *J. Appl. Phys.* **59** (1986) 3841.
349. T.S. Kim, S.D. Lester and B.G. Streeman, *J. Appl. Phys.* **61** (1987) 1363.
350. J.B. Mullin, A. Royle, B.W. Straughan, P.J. Tufton and E.W. Williams, *Inst. Phys. Conf. Ser.* **17** (1973) 118.
351. E.W. Willams, W. Elder, M.G. Astles, M. Webb, J.B. Mullin, B. Straughan and P.J. Tufton, *J. Electrochem. Soc.* **120** (1973) 1741.
352. P.J. Dean, D.J. Robbins and S.G. Bishop, *J. Phys. C* **12** (1979) 1741.
353. T. Inoue and J. Takahashi, *Jpn. J. Appl. Phys.* **26** (1987) L249.
354. S.G. Bishop, P.B. Klein, R.L. Henry and B.D. McCombe, in *Proc. 2nd Conf. Semi-Insulating III-V Materials*, ed. G.J. Rees (Nantwich, Shiva, 1980) p. 161.
355. T.S. Kim, S.D. Lester and B.G. Streeman, *J. Appl. Phys.* **61** (1987) 4598.
356. Y. Makita, A. Yamada, H. Yoshinaga, T. Iida, S. Niki, S. Uekusa, T. Matsumori, K. Kainosho and O. Oda, in *Proc. 4th Int. Conf. on InP and Related Materials* (Newport, 1992) p. 626.
357. H. Yoshinaga, Y. Makita, A. Yamada, T. Iida, S. Niki, T. Matsumori, K. Kainosho and O. Oda, in *Proc. 5th Int. Conf. on InP and Related Materials* (Paris, 1993) p. 317.
358. H. Yoshinaga, Y. Makita, A. Yamada, T. Iida, H. Shibata, A. Obara, T. Matsumori, S. Uekusa, K. Kainosho and O. Oda, in *Proc. 5th Int. Conf. on InP and Related Materials* (Paris, 1993) p. 630.
359. B.M. Keyes, D.J. Dunlavy, R.K. Ahrenkiel, G. Shaw, G.P. Summers, N. Tzafaras and C. Lentz, *J. Appl. Phys.* **75** (1994) 4249.
360. S.D. Lester, T.S. Kim and B.G. Streetman, *J. Appl. Phys.* **60** (1986) 4209.
361. S.K. Krawczyk and G. Hollinger, *Appl. Phys. Lett.* **45** (1984) 870.
362. R.R. Chang, R.Iyer and D.L. Lile, *J. Appl. Phys.* **61** (1987) 1995.
363. A. Knauer, S. Gramlich and R. Staske, *Sov. J. Quantum Electron.* **18** (1988) 1424.
364. H.J. Frenck, W. Kulisch and R. Kassing, in *Proc. First Int. Conf. on InP and Related Materials* (Oklahoma, 1989) p. 250.
365. Z. Laczik, G.R. Booker and A. Mowbray, *J. Crystal Growth* **158** (1996) 37.
366. M. Erman, g. Gillardin, J. le Bris, M. Renaud and E. Tomzig, *J. Crystal Growth* **96** (1989) 469.
367. Th. Vetter and A. Winnacker, *J. Mater. Res.* **6** (1991) 1055.
368. S.K. Krawczyk, M. Garrigues, K. Schohe and C. Lallemand, *Le Vide, les Couches Minces* **241** (1988) 171.
369. S.K. Krawczyk, J.Y. Lonére, K. Schohe and J. Tardy, *Le Vide, les Couches Minces* **251** (1990) 94.
370. B. Sartorius, D. Franke and M. Schlak, *J. Crystal Growth* **83** (1987) 238.
371. H.J. Hovel and D. Guidotti, *IEEE Trans. Electron Devices* **ED-32** (1985) 2331.
372. D.B. Holt, R. Fornari, P. Franzosi, J. Kumar and G. Salviati, *Inst. Phys. Conf. Ser.* **100** (1989) 421.
373. R. Shiomi, T. Kawase and M. Yamada, in *Proc. 16th Int. Conf. on InP and Related Materials* (Kagoshima, 2004) p. 599.
374. B.H. Chin and K.L. Barlow, *J. Electrochem. Soc.* **135** (1988) 3120.
375. Y. Morisawa, I. Kikuma, N. Takayama and M. Takeuchi, *Surface Technlolgy (in japanese)* **44** (1993) 86.
376. Y. Morisawa, I. Kikuma, N. Takayama and M. Takeuchi, *Appl. Surface Sci.* **92** (1996) 147.
377. Y. Morisawa, I. Kikuma, N. Takayama and M. Takeuchi, *J. Electron. Mater.* **26** (1997) 34.
378. J. Wei and L.X. Lang, *Cryst. Res. Technol.* **32** (1997) 243.

379. T. Fukui, H. Kurita and N. Makino, in *Proc. 9th Int. Conf. on InP and Related Materials* (Hyaniss, 1997) p. 272.
380. Y. Takahashi, T. Fukui and O. Oda, *J. Electrochem. Soc.* **134** (1987) 1027.
381. J. Caulet and R. Coquille, *Le Vide, les Couches Minces* **241** (1988) 175.
382. Z. Laczik, G.R. Booker and A. Mowbray, *J. Crystal Growth* **153** (1995) 1.
383. K.P. Quinlan, *J. Electrochem. Soc.* **137** (1990) 1991.
384. A.M. Huber and C. Gratepain, *Mater. Sci. Forum* **38-41** (1989) 1345.
385. A.M. Huber, C. Gratepain and P. Collot, in *Defect Control in Semiconductors*, ed. by K. Sumino (North-Holland, Amsterdam, 1990) p. 1523.
386. A.M. Huber and N. Briot, *Mater. Sci. Engineer.* **B28** (1994) 61.
387. J. Massiers, F. Turco and J.P. Contour, *Jpn. J. Appl. Phys.* **25** (1986) L664.
388. E. Kurth, A. Reif, V. Gottschalch, J. Finster and E. Butter, *Cryst. Res. Technol.* **23** (1988) 117.
389. S.J. Hoekje and G.B. Hoflund, *Appl. Surface Sci.* **47** (1991) 43.
390. S.K. Krawczk, M. Garrigues and H. Bouredocen, *J. Appl. Phys.* **60** (1986) 392.
391. A.S. Barriere, B. Desbat, B. Mombelli and V. Tournay, *Appl. Surface Sci.* **64** (1993) 225.
392. S. das Neves and M. De Paoll, *Semicon. Sci. Technol.* **9** (1994) 1719.
393. N. Thomas, G. Jacob and H. Hardtegen, in *Proc. 10th Int. Conf. on InP and Related Materials* (Tsukuba, 1998) p. 96.
394. G. Jacob, Ph. Regeny, N. Tomas and H. Hardtegen, in *Proc. 9th Int. Conf. on InP and Related Materials* (Hyaniss, 1997) p. 420.
395. D. Gallet, M. Gendry, G. Hollinger, A. Overs, G. Jacob, B. Boudart, M. Gauneau, H. L'Haridon and D. Lecrosnier, in *Proc. 3rd Int. Conf. on InP and Related Materials* (Cardiff, 1991) p. 85.
396. S. Katsura, Y. Sugiyama, O. Oda and M. Tacano, *Appl. Phys. Lett.* **62** (1993) 1910.
397. M. Nakamura, S. Katsura, N. Makino, E. Ikeda, K. Suga and R. Hirano, *J. Crystal Growth* **129** (1993) 456.
398. J.J. Hsieh, J.A. Rossi and J.P. Donnelly, *Appl. Phys. Lett.* **28** (1976) 707.
399. *Heterostructure Lasers, Part B*, eds. T. Casey, Jr. and M. Panish (Academic Press, New York, 1978).
400. K. Mito, *Optoelectronics Material Manual* (in japanese) (Optronics, Tokyo, 1986) p. 281.
401. H. Terauchi, A. Yamaguchi, N. Yamabayashi, H. Nishizawa, Y. Kuhara, M. Kuroda and N. Iguchi, *umitomo Electrics (in japanese)* **127** (1985) 106.
402. Y. Matsushima, Y. Noda, Y. Kushiro, K. Sakai, S. Akiba and K. Utaka, in *Tech. Digest 4th Int. Conf. Integ. Opt. Fiber Comm.* (Tokyo, 1983) p. 226.
403. K. Yasuda, Y. Kishi, T. Shirai, T. Mikawa, S. Yamazaki and T. Kaneda, *Electron. Lett.* **20** (1984) 158.
404. T. Mikawa, S. Yamazaki and T. Kaneda, *Electron. Lett.* **20** (1984) 158.
405. Y. Matsushima, Y. Noda and Y. Kushiro, *IEEE Quantum Electron.* **QE-21** (1985) 1257.
406. T. Kamiya and N. Kamata, *Oyo Buturi (Monthly Publ. Jpn. Soc. Appl. Phys.) (in japanese)* **52** (1983) 485.
407. M. Hirotani, T.E. Sale, J. Woodhead, J.S. Roberts, P.N. Robson, T. Saak and T. Kato, *J. Crystal Growth* **170** (1997) 390.
408. l.-H. Tan, J. Bowers, E.L. Hu, B.I. Miller and R.J. Capik, in *Proc. 7th Int. Conf. on InP and Related Materials* (Sapporo, 1995) p. 365.
409. O. Wada, T. Sakurai and T. Nakagami, *IEEE J. Quantum Electron.* **QE-22** (1986) 805.
410. T.L. Koch and U. Koren, *IEE Proc. J.* **138** (1991) 139.
411. T. Otsuji, *Oyo Buturi (Monthly Publ. Jpn. Soc. Appl. Phys.) (in japanese)* **71** (2002) 1352.
412. T. Saithoh, I. Nomura, Y. Takashima, Y. Nakai, T. Yamazaki, A. Kikuchi and K. Kishino, in *Proc. 16th Int. Conf. on InP and Related Materials* (Kagoshima, 2004) p. 64.
413. S. Tiwari, M.C. hargis, Y. Wang, M.C. Teich and W.I. Wang, *IEEE Photonics Technol. Lett.* **4** (1992) 256.
414. R. Sidhu, N. Duan, J.C. Campbell and A.L. Holmes, *IEEE Photonics Technol. Lett.* **17** (2005)

2715.
415. K. Asano, K. Kasahara and T. Itoh, *IEEE Electron Device Lett.* **EDL-8** (1987) 289.
416. H.M. Dauplaise, K. Vaccaro, A. Davis, W.D. Waters and J.P. Lorenzo, in *Proc. 10th Int. Conf. on InP and Related Materials* (Tsukuba, 1998) p. 455.
417. H. Hasegawa, in *Proc. 10th Int. Conf. on InP and Related Materials* (Tsukuba, 1998) p. 455.
418. H. Takahashi and H. Hasegawa, in *Proc. 10th Int. Conf. on InP and Related Materials* (Tsukuba, 1998) p. 463.
419. T. Itoh, K. Kasahara, T. Ozawa and K. Ohata, in *Proc. Int. Electron Dev. Meeting (IEDM)* (Los Angels, 1986) p. 771.
420. T. Itoh and K. Ohata, *Semiconductor Technologies, JARET, Vol. 19*, ed. J. Nishizawa (Ohmsha and North-Holland, Amsterdam, 1986) p. 147.
421. H. Sawatari, M. Oyake, K. Kainosho, H. Okazaki and O. Oda, in *Proc. 5th Int. Conf. on InP and Related Materials* (Paris, 1993) p. 297.
422. H. Sawatari and O.Oda, *J. Appl. Phys.* **72** (1992) 5004.
423. P.M. Smith, *IEEE Trans. Microwave Theory and Technol.* **44** (1996) 2328.
424. M. Schlechtweg, A. Leuther, A. Tessmann, C. Schwörer, H. Massler, W. Reinert, M. Lang, U. Nowotny, O. Kappler, M. Walther and R. Lösch, in *Proc. 16th Int. Conf. on InP and Related Materials* (Kagoshima, 2004) p. 609.
425. M. Sokolich, *Compound Semicon.* **October** (2001) 51.
426. M. Feng, W. Hafez and J-W. Lai, in *Proc. 16th Int. Conf. on InP and Related Materials* (Kagoshima, 2004) p. 653.
427. N.X. Nguyen, J. Fierro, K.T. Feng and C. Nguyen, in *Proc. 16th Int. Conf. on InP and Related Materials* (Kagoshima, 2004) p. 653.
428. J. Berenz, *Microwave J.* **August** (1993) 113.
429. K. Murata, K. Sano, T. Enoki, H. Sugahara and M. Tokumitsu, in *Proc. 16th Int. Conf. on InP and Related Materials* (Kagoshima, 2004) p. 10.
430. N.P. Morec, in *IEEE MTT-S Digest* (IEEE, New York, 1996) p. 39.
431. M. Yamaguchi and Y. Yamamoto, *J. Appl. Phys.* **55** (1984) 1429.
432. I. Weinberg and D.J. Brinker, in *Proc. 21st Intersoc. Energy Convers. Eng. Conf.* (1986) p. 1431.
433. M.B. Spitzer, c.J. Keavney, S.M. Vernon and V.E. Haven, *Appl. Phys. Lett.* **51** (1987) 364.
434. T. Takamoto, in *InP and Related Compounds: Materials, Applications and Devices*, ed. M.O. Manasreh (Gordon & Breach Sci., Amsterdam, 2000) p. 787.

11. InAs

11.1 INTRODUCTION

InAs is a narrow bandgap semiconductor and is useful in very high speed electronic devices. It is also used as a substrate for infrared detectors and Hall devices and used as source material for multinary compound epitaxial growth.[1]

11.2 PHYSICAL PROPERTIES

The physical properties of InAs[2,3] are summarized in Table 11.1. The melting point of InAs is 943 °C, rather low compared with other III-V materials. The bandgap is as low as 0.356 eV and electron mobility is as high as 33,000 $cm^2/V\cdot sec$ so that it can be expected to be a good material for long wavelength photodetectors and high speed electronic devices. The phase diagram of InAs is as shown in Fig. 11.1.[4,5] The decomposition pressure of InAs is as low as 0.33 atm. at the melting point.[6] The thermoelectrical properties of InAs have been evaluated and found to be 210-310 μV/K.[7]

11.3 CRYSTAL GROWTH

11.3.1 Melt Growth

InAs is industrially grown by the Liquid Encapsulated Czochralski (LEC) method using B_2O_3 as encapsulant. At the melting point, the viscosity of B_2O_3 is sufficiently low so that it does not affect the crystal quality. Indium and arsenic are charged and can be synthesized directly and crystals are grown as in the case of GaAs. It is also possible to charge polycrystal material and to grow single crystals.

Since the stacking fault energy of InAs is lower than that of GaAs and GaP (Sec. 1.7.2), it is easily twinned. In order to prevent twinning, it is necessary to pay attention to various factors as explained in Sec. 3.4.

Table 11.1 Physical Properties of InAs

Crystal Structure	zincblende
Lattice Constant	6.058 Å
Density	5.667 g/cm^3
Melting Point	943 °C
Linear Expansion Coefficient	5.19 $x10^{-6}$/deg
Thermal Conductivity	0.26 W/cm·K
Dielectric Constant	14.55
Refractive index	3.52
Bandgap at Room Temperature	0.356 eV
Intrinsic Carrier Concentration	$1.25x10^{15}/cm^3$
Electron Mobility	33,000 $cm^2/V\cdot sec$
Hole Mobility	460 $cm^2/V\cdot sec$
Conductivity	0.2 Ω·cm

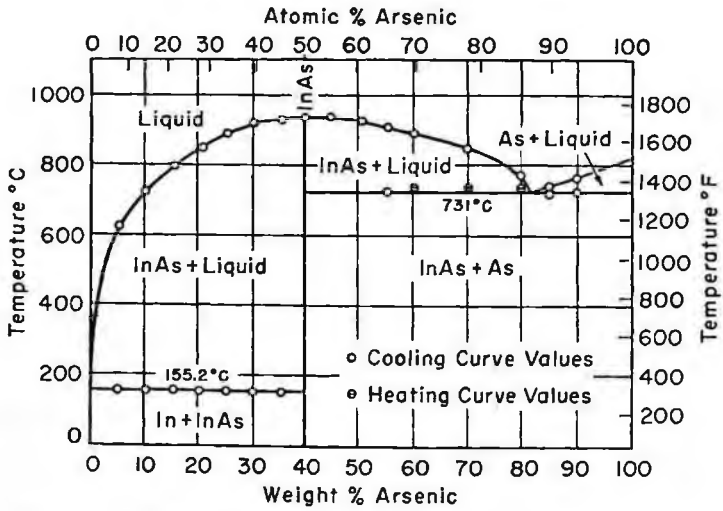

Fig. 11.1 Phase diagram of InAs (from Ref. 4 with permission).

(i) Elimination of scum on the melt surface
(ii) Crystal shape control
(iii) Control of the solid-liquid interface shape
(iv) Reduction of temperature fluctuation
(v) Stoichiometry control

Growth of 50 mm diameter InAs has been reported by Matsumoto[8] and Iwanami et al.[9] A typical InAs single crystal is shown in Fig. 11.2.

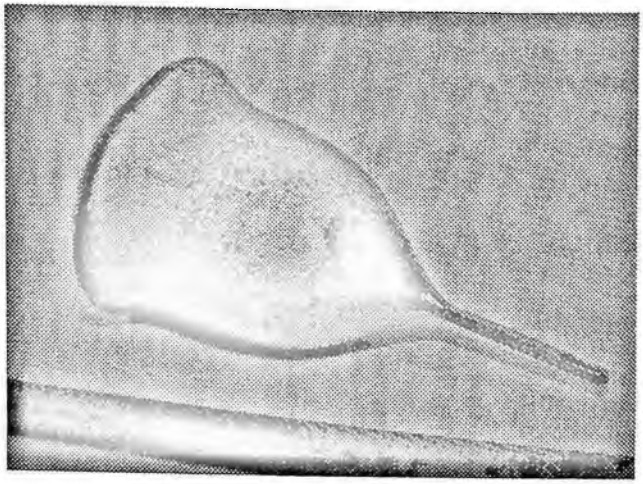

Fig. 11.2 Typical InAs single crystal grown by the LEC method.[9]

Table 11.2 Segregation Coefficients k_0

Mg	Zn	Cd	Si	Ge	Sn	S	Se	Te
0.70	0.77	0.13	0.40	0.07	0.09	1.0	0.93	0.44

11.3.2 Solution Growth

Wolff et al.[10] have grown InAs crystals from indium solvent containing 10-20 at.% arsenic. In order to grow crystals, a very slow freezing rate less than 1 mm/hr was required.

11.3.3 Vapor Phase Growth

Antell and Effer[11] have grown InAs crystals using $InCl_3$ and InI_3 as the transport reagent in the temperature range of 830-840°C, with the starting materials held at 875-890 °C. Holonyak[12] has grown InAs crystals using $ZnCl_2$ as the transport reagent and obtained p-type crystals from n-type starting materials.

11.4 CHARACTERIZATION

11.4.1 Purity

Segregation coefficients of various impurities have been measured by electrical prop-

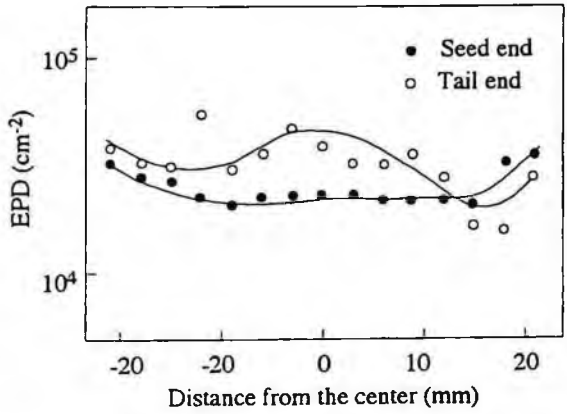

Fig. 11.3 Typical dislocation distribution along <-1-10) direction in <100> oriented 50 mm diameter InAs single crystal grown by the LEC method.[9]

Table 11.3 Purity of Typical InAs Single Crystal (reprinted from Table 6.6 at p. 176 in Ref. 8 with permission). (ppmw)

B	Mg	Si	S	Zn	Cd	Sn	Mn	Cu
0.004	0.009	0.03	0.03	ND	ND	ND	ND	ND

ND: not detected

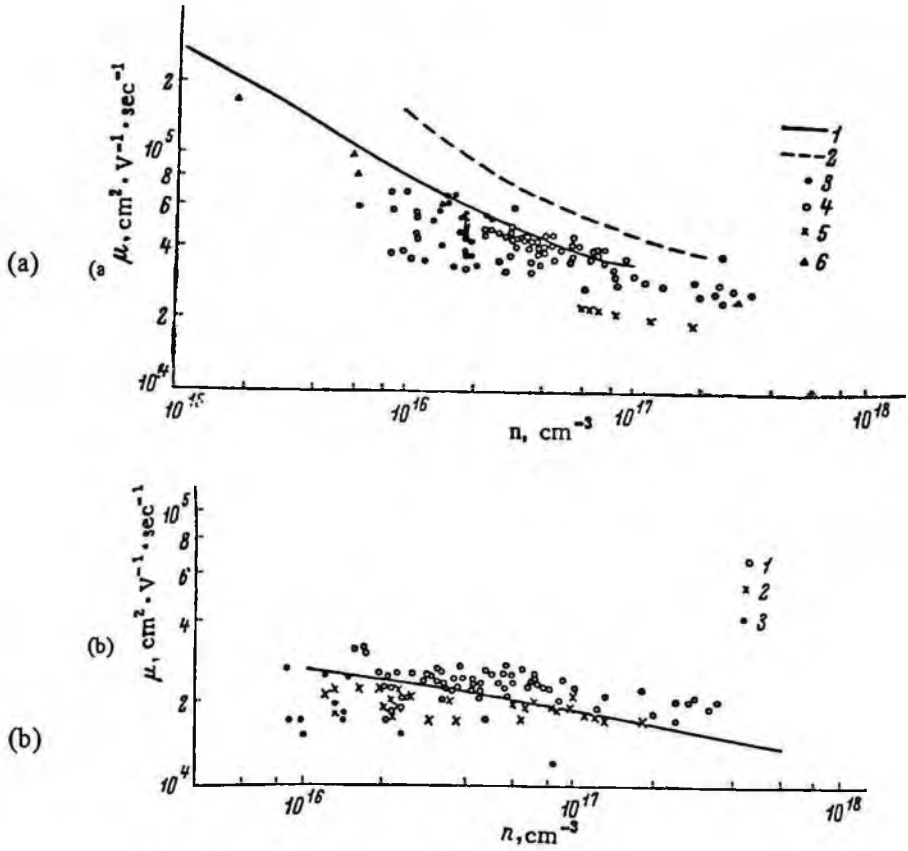

Fig. 11.4 Relationship between Hall mobility and carrier concentration of n-type InAs at 77 K (a) and 300 K (b) (from Ref. 16 with permission). The lines are calculated curves. The detail of this figure is explained in the reference.

erty characterization and were determined[13] as shown in Table 11.2. The systematic purification process of InAs has been reported by Enright.[14] The lowest carrier concentration after appropriate purification was 1.3×10^{16} cm^{-3}.[15] A typical purity of InAs grown by the LEC method is shown in Table 11.3.[8] The main impurity in InAs is sulphur since its vapor pressure and segregation coefficient are close to those of arsenic so that it is difficult to eliminate it in the purification process before crystal growth. The purity of InAs is however of a high order and the carrier concentration is not predominantly determined by any specific impurities.[8]

Table 11.4 Ionization Energies of Shallw Acceptors

Sn	Ge	Si	Cd	Zn
0.01	0.014	0.02	0.015	0.01

11.4.2 Defects

The dislocation density can be measured by etching with conc. HCl etching for 1 min. on (100) surfaces and with an etchant ($HF:HNO_3:H_2O$ = 1:1:2) on (111) surfaces.[8] Fig. 13.3 shows the dislocation density distribution for a <100> oriented 50 mm diameter InAs single crystal. The average dislocation density was about $2x10^4$ cm^{-2}.

11.4.3 Electrical Properties

The relationship between mobility and carrier concentration is shown in Fig. 11.4.[16] The carrier concentration is not determined by residual impurities but by point defects whose concentration varies according to annealing conditions.[17-19] Hilsum et al.[20, 21] showed that copper introduced from quartz materials is the impurity which is moved between the matrix and dislocation traps by annealing. The drift velocity as a function of the electric field was calculated by Brennan and Hess.[22] Ionization energies of shallow donors such as Se, S, Te, Ge, Si, Sn and Cu were as low as 0.001 eV and those of shallow acceptors[23, 24] are as shown in Table 11.4. Commercially, Zn is used as the dopant for p-type crystals and S for n-type crystals, with the highest carrier concentration reaching $3x10^{18}$ cm^{-3}.

11.5 APPLICATIONS

InAs is used as a substrate for infrared detectors in the wavelength range of 1.0-3.8 μm.[25-27] InAs photodetectors based on photodiode structures are industrially commercialized for applications in laser warning receivers, process control monitors, temperature sensors, pulsed laser monitors, infrared spectroscopy and power meters.[28, 29] It is also used as a substrate for mid-IR lasers and LEDs based on InAsSbP layers.[30] InAs is also a sensitive material for Hall devices. Various types of Hall sensors have been commercialized.[31, 32] InAs is used as a high purity source material for the multinary compound epitaxial growth of InGaAsP.

REFERENCES

1. J. B. Schroeder, in *Compound Semiconductors, Vol. I, Preparation of III-V Compounds*, eds. R.K. Willardson and H.L. Goering (Reinhold, New York, 1962) p. 222.
2. *Landolt-Börnstein, Vol. 17 Semiconductors*, ed. O. Madelung (Springer-Verlag, Berlin, 1982) p. 297.
3. S. Adachi, *Physical Propeties of III-V Semiconductor Compounds: InP, InAs, GaAs, GaP, InGaAs and InGaAsP* (John Wiley & Sons, New York, 1992)
4. T.S. Liu and E.A. Peretti, *Trans. AIME* **45** (1953) 677.
5. M. Hansen, *Constitution of Binary Alloys* (McGraw-Hill, 1958) p. 166.
6. J. van den Boomgaard and K. Schol, *Philips Res. Rept.* **12** (1957) 127.
7. M.I. Aliyev, Sh. Sh. Rashidova, I.M. Aliyev, M.A. Huseynova and M.A. Jafarova, *Cryst. Res. Technol.* **39** (2004) 598.
8. K. Matsumoto, in *Bulk Crystal Growth Technology* (Gordon and Breach, New York, 1989) p. 158.
9. K. Iwanami, Y. Yamamoto and O. Oda, presented at 46th Spring Meeting, Jpn. Soc. Appl. Phys. and Related Socs., 1985)
10. G.A. Wolff, P.H. Keck and J.D. Broder, *Phys. Rev.* **94** (1954) 753.
11. G.R. Antell and E.Effer, *J. Electrochem. Soc.* **106** (1959) 509.
12. described as a private communication in J. B. Schroeder, in *Compound Semiconductors Vol. I,*

Preparation of III-V Compounds, eds. R.K. Willardson and H.L. Goering (Reinhold, New York, 1962) p. 222.
13. E. Schillmann, *in Compound Semiconductors, Vol. I, Preparation of III-V Compounds*, eds. R.K. Willardson and H.L. Goering (Reinhold, New York, 1962) p. 390.
14. D.P. Enright, *US Govt. Res. Repts 31,366 (a)* (1959) PB 137457.
15. D. Effer, *J. Electrochem. Soc.* **108** (1961) 357.
16. V.V. Karataev, M.G. Mil'vidskii, N.S. Rytova and V.I. Fistul', *Sov. Phys. Semicond.* **11** (1977) 1009.
17. J.R. Dixon and D.P. Enright, *J. Appl. Phys.* **30** (1959) 753.
18. J.R. Dixon, *J. Appl. Phys.* **30** (1959) 1412.
19. J.R. Dixon and D.P. Enright, *J. Appl. Phys.* **30** (1959) 1463.
20. J.T. Edmond and C. Hilsum, *J. Appl. Phys.* **31** (1960) 1300.
21. C. Hilsum, *Proc. Phys. Soc. (London)* **73** (1959) 685.
22. K. Brennan and K. Hess, *Solid-State Electron.* **27** (1984) 347.
23. M.I. Guseva, N.V. Zotova, A.V. Koval' and D.N. Nasledov, *Sov. Phys. Semocon.* **8** (1974) 34.
24. M.I. Guseva, N.V. Zotova, A.V. Koval' and D.N. Nasledov, *Sov. Phys. Semocon.* **8** (1975) 1323.
25. Judson Technologies, www.judsontecnologies.com.
26. Polytec, www.polytec-pi.fr.
27. NEOPT, www.neopt.cp.jp
28. Hamamatsu Photonics, www.hpk.co.jp
29. Y. Horikoshi, in *Semiconductors and Semimetals, Vol. 22*, eds. (Academic Press, New York, 1985) p.93.
30. R. Szweda, *III-Vs Review* **25** (2002) 38.
31. F.W. Bell, www.fwbell.com
32. Toyo Technica, www.toyo.co.jp/bell.

12. InSb

12.1 INTRODUCTION

InSb has a small bandgap of 0.18 eV and is sensitive to longer wavelengths of the region of 3-5 μm so that it is a promising material for infrared detectors.[1-5] It is also an important substrate material for infrared detectors in the 9-12 μm long wavelength region.[1] Since the effective mass of electrons of InSb is very low and therefore the electron mobility very high, InSb is an important material for Hall devices[5-8] and magnetoresistance devices.[9] The crystal growth of InSb is reviewed by Liang[10] and Matsumoto.[11]

12.2 PHYSICAL PROPERTIES

InSb has a small bandgap and low effective mass so that it has a large electron mobility up to 78,000 cm^2/V·sec. This is the reason why InSb is a very interesting material for IR detectors, Hall devices and magnetoresistance devices. The main physical properties of InSb can be found in Ref. 12 and some data are summarized in Table 12.1. The phase diagrams of InSb have been reported in Refs. 13 and 14, and a typical X-T phase diagram is shown in Fig. 12.1. In and Sb self-diffusion coefficients have been measured in the temperature range of 400-500 °C by the radioactive tracer diffusion method.[15] The self-diffusion coefficient of In is

$$D\ (cm^2/sec) = 6.0 \times 10^{-7} \exp[-(1.45 \pm 0.09)\ eV/kT] \qquad (12.1)$$

and that of Sb is

$$D\ (cm^2/sec) = 5.35 \times 10^{-4} \exp[-(1.91 \pm 0.08)\ eV/kT]. \qquad (12.2)$$

12.3 CRYSTAL GROWTH

12.3.1 Synthesis and Purification

Table 12.1 Physical Properties of InSb

Lattice Constant	6.48937 Å
Density	5.775 g/cm^3
Melting Point	525 °C
Linear Expansion Coefficient	5.37 x10^{-6}/K
Thermal Conductivity	0.18 W/cm·K
Dielectric Constant	17.72
Refractive index	4.0
Bandgap at Room Temperature	0.180 eV
Intrinsic Carrier Concentration	2.04x10^{16} /cm^3
Electron Mobility	78,000 cm^2/V·sec
Hole Mobility	850 cm^2/V·sec
Intrinsic Resistivity	4.5x10^{-3} Ω·cm

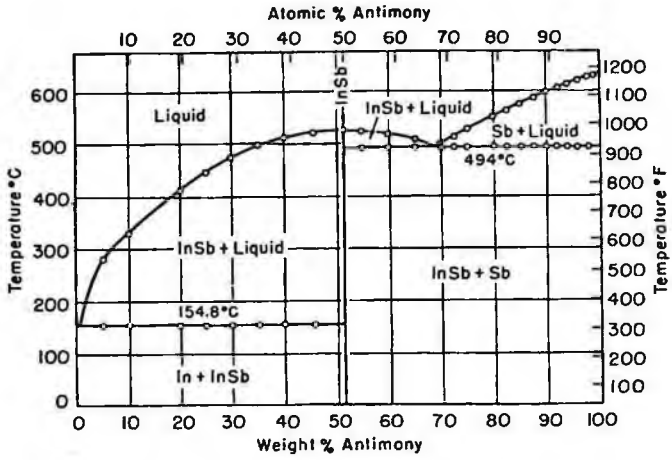

Fig. 12.1 Phase diagram of InSb (from Ref.14 with perimssion, copyright 1958 McGraw-Hill).

The synthesis of InSb can be easily performed by reacting pure In and Sb metals directly together. However, special attention must be paid to avoid oxidation. This is because the oxides of In and Sb form easily and are difficult to reduce. After synthesis, the purity of InSb can be improved by zone-melting. Since Zn, Te and Cd are impurities difficult to remove by zone-melting,[16] attention must be paid to the purity of the starting material metals with respect to these impurities. It is also reported that vacuum treatment is very effective in removing volatile impurities such as Cd.[17]

12.3.2 Crystal growth

Large diameter InSb crystals are mainly grown by the Czochralski (CZ) method but various other methods have been applied as shown in Table 12.2.

(1) Solution growth

Simple solution growth has been performed but is reported to be ineffective in growing single crystals.[18] Benz and Müller[19] applied a horizontal THM and could obtain a single crystal of 10 mm diameter and 23 mm length. The maximum growth rate for inclusion-free crystals was 2.5 ± 0.5 mm/day.

(2) Horizontal Bridgman (HB) and Horizontal Zone Melting (HZM) methods

The HB method, combined with zone refining for purification has been applied to InSb single crystal growth.[20] Since InSb has a strong tendency to grow along the <111> axis, single crystals can be grown by self-seeding, with a high growth rate of 2 mm/min without twinning.[10] It is reported that high purity material with mobility exceeding 10^6 $cm^2/V \cdot sec$ and a carrier concentration of 1.2×10^{13} cm^{-3} could be obtained by the HZM

Table 12.2 Crystal Growth of InSb

Method	Result	Authors	Year	Ref.
HZM	Growth of hihg purity crystals	Vinogradova et al.	1959	21
CZ	Growth of InSb in the <111> polar direction	Gatos et al.	1960	28
CZ	Se-doped InSb with the double crucible method	Allred et al.	1961	29
HZM	Seed orientation and twinning	Müler et al.	1961	22
DC	Diffusion-controlled steady-state segeragtion in space	Witt et al.	1975	39
THM	10 mm diameter crystals of length 30 mm	Benz et al.	1979	19
CZ	Effect of rotation conditions on the strain formation	Miller	1979	30
CZ	Effect of ultrasonic wave application	Kumagawa et al.	1980	31
HZM	Growth of high purity InSb by in-situ synthesis	Ohno et al.	1982	23
CZ	Uniform carrier concentration using inclined seed crystals for <111> oriented single crystal growth	Terashima	1982	32
CZ	Diameter control by a colling plot	Burstein et al.	1984	33
CZ	Crystal growth of 40 mm diameter with 350 mm length	Matsumoto	1989	11
DS	Growth in space satellite	Zemskov et al.	1991	41
MCZ	Magnetic field application on the recombination characteristics	Vekshina et al.	1992	34
DS	Growth in a cnetrifuge appartus in reduced gravity	Derebail et al.	1992	42, 43
SHM	Te-doped InSb with diffusion-controlled segregation of Te	Ostrogorsky et al.	1993	38
DS	Application of ACRT	Zhou et al.	1993	26
VB	Radioactive visualization of the growth interface	Campbell et al.	1995	24
CZ	Effect of ultrasonic vibration	Kozhemyakin	1995	35
CZ	Segragation control using floating crucibles	Lin et al.	1995	36
VGF	Growth in aergel crusibles for visualization	Tscheuschner et al.	1999	27
VB	Growth of inclusion-free InSb crystals	Mohan et al.	2000	25
DS	Detached solidification of Ga-doped InSb growth	Wang et al.	2004	44

HB: Horizontal Bridgaman, HZM: Horizontal Zone Melting, VB: Vertical Bridgman, VGF: Vertical Gradinet Freezing, CZ: Czochralski, MCZ: Magnetic field CZ, THM: Traveling Heater Method, DS: Direct Synthesis, SHM: Submerged Heated Method

method.[21] Dislocation densities are normally high up to 10^5-10^6 cm^{-2}, but it is also reported that low dislocation density InSb crystals can be obtained.[10]

Crystal growth by horizontal zone melting in a vacuum has been performed by Ohno et al.[23] and n-type crystals with carrier concentration 10^{13}-10^{14} cm^{-3} and having maximum mobility of $8x10^5$ $cm^2/V \cdot s$ have been obtained.

(3) Vertical Bridgman (VB) and Vertical Gradient Freezing (VGF) methods

Campbell et al.[24] used X-ray radioscopy to examine the shape of the solid-liquid interface during crystal growth by the VB method of Te-doped InSb. Because of the density difference between the melt and the solid, the shape of the solid-liquid interface could be observed in real time as the difference in contrast.

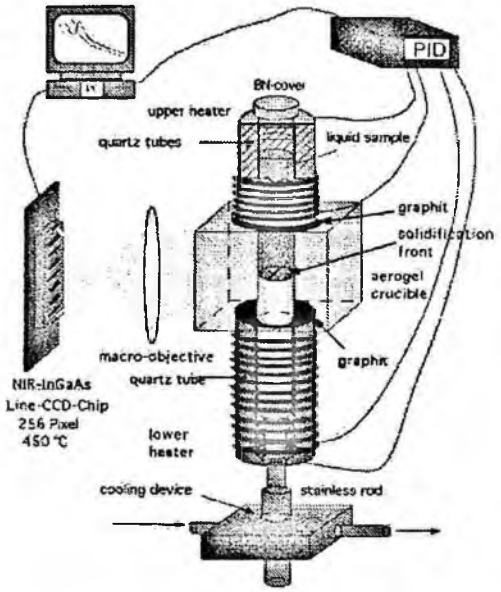

Fig. 12.2 VGF method with an aerozol crucible for the in-situ observation of the interface shape during crystal growth (from Ref. 27 with permission).

Mohan et al.[25] examined factors which affect the formation of inclusions, such as synthesis temperature, synthesis time, thermal gradient, ampoule lowering rate and ampoule geometry, and worked out the optimal conditions to minimize inclusions.

The effect of the accelerated crucible rotation technique (ACRT) on the shape of the solid-liquid interface has been studied for crystal growth by the VB method.[26] The variation of the growth rate was examined from the viewpoint of the heat transfer process across the interface.

Tscheuschner et al.[27] developed a VGF furnace, equipped with an IR-CCD camera, using an aerogel crucible (Fig. 12.2) in order to observe the crystallization front, and demonstrated its effectiveness in crystal growth.

(4) Czochralski (CZ) method

Since the melting point of InSb is low (525 °C) and the dissociation pressure is very low ($<10^{-5}$ atm.), no encapsulant is necessary for the Czochralski method. Various CZ growth results are summarized in Table 12.2.

In <111> oriented crystal growth, the polarity of the seed crystal is very important as pointed out by Gatos et al.[28] When a seed crystal with a <111>B face with Sb atoms is used, single crystals can be grown, while when a seed crystal with a <111>A face with In atoms is used, twinning and polycrystallization occur easily.

Single crystals with orientations <111> and <110> doped with Se have been grown

using a CZ furnace [29] as shown in Fig. 9. 4, the same as for GaSb crystal growth. InSb has a strong tendency to grow along the <111> direction and twinning and lineage easily occur for <110> and <100> oriented crystal growth.

It is reported by several researchers[11, 29] that when crystals are grown in the <111> direction, a strong radial segregation of impurities occurs. This is thought to be due to the strong <111> facet growth because the segregation coefficient is greater in a facet region than that in a off-facet region. It has also been shown that the inhomogeneity due to <111> directed growth can be eliminated when <311> oriented crystals are grown.[11]

Matsumoto[11] pointed out that InSb crystals can be grown directly from the InSb melt without any encapsulant but the scum on the melt makes crystals in which twins readily form. They showed that prebaking under hydrogen can eliminate the scum and have grown a crystal of diameter 40 mm and length 350 mm. The dislocation density was less than 2.5×10^2 cm^{-2} in all regions.

Miller,[30] using X-ray anomalous transmission topography, studied the effect of the rotation of crystal and crucible on the strain configuration in Te-dope crystals grown by the CZ method and discussed the mechanism of strain formation. Kumagawa et al.[31] applied ultrasonic wave during crystal growth and found that the effect was to eliminate the facet region and homogeneous crystals were grown.

InSb single crystals have been grown by the CZ method in high purity nitrogen gas

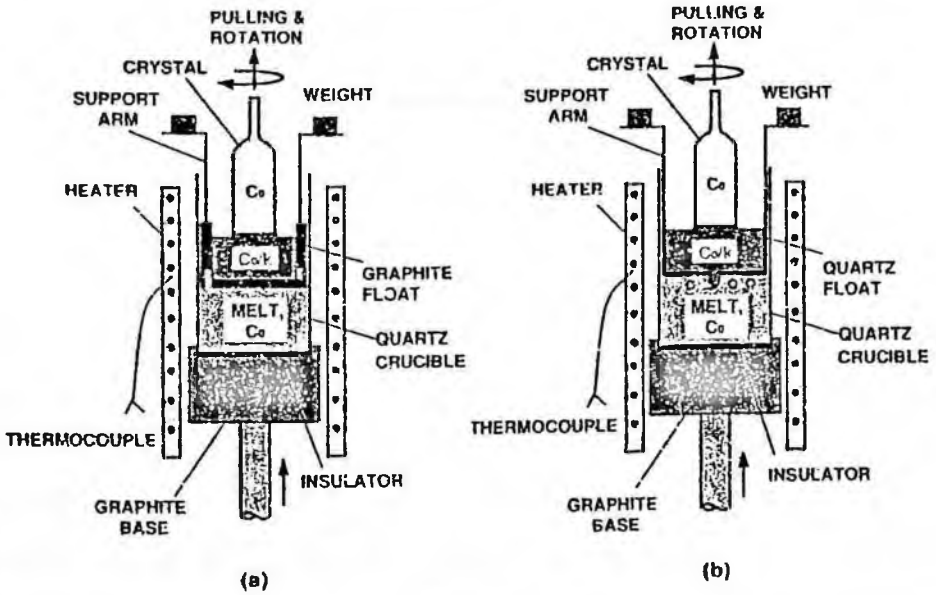

Fig. 12.3 Segregation control in Czochralski pulling with a floating crucible having a very long melt passageway to suppress dopant back diffusion: (a) a graphite floating crucible; (b) a quartz floating crucible (reprinted from Ref. 36 with permission, copyright 1962 Elsevier).

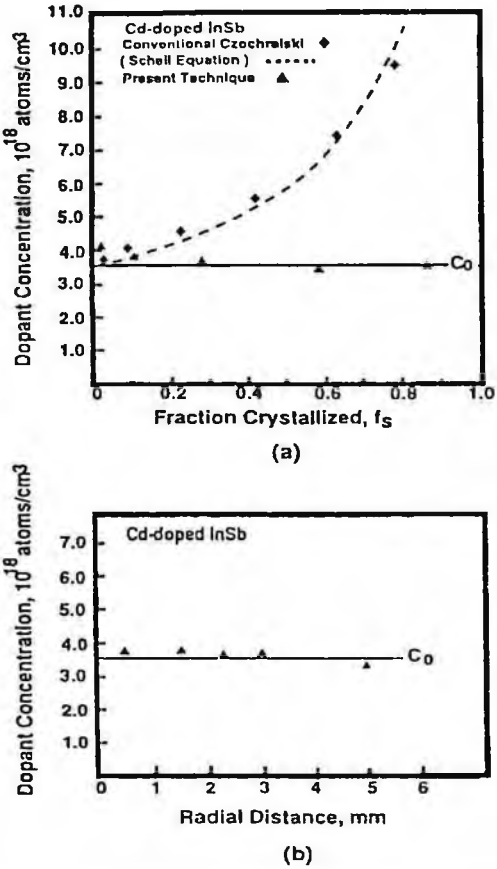

Fig. 12.4 Dopant concentration profiles in an InSb crystal grown with the graphite crucible. (a) axial; (b) radial (reprinted from Ref. 36 with permission, copyright 1995 Elsevier). The dashed line represents axial segregation by conventional Czochralski pulling.

containing 10 % hydrogen.[32] It was found that high quality crystals could be grown using a seed inclined 5-10 degrees from the [111] to the [110] direction.

Burnstein et al.[33] showed a simple diameter control method based on programming the cooling from a calculation of mass balance and applied this method to the growth of 50 mm diameter InSb crystals.

Vekshina et al.[34] studied the effect of the application of a magnetic field on the electrical properties. The application of a transverse magnetic field of 1.5×10^3 A/m was found to be effective in reducing the concentration of structural defects, thus increasing the lifetime and mobility of carriers.

Cd-doped InSb single crystals were grown from a floating crucible in order to obtain uniform Cd concentrations in crystals[36] as shown in Fig. 12.3. The floating crucible method allows feeding and pulling to occur simultaneously automatically. It was found that Cd can be doped uniformly along the axial and the radial directions for a crystal of

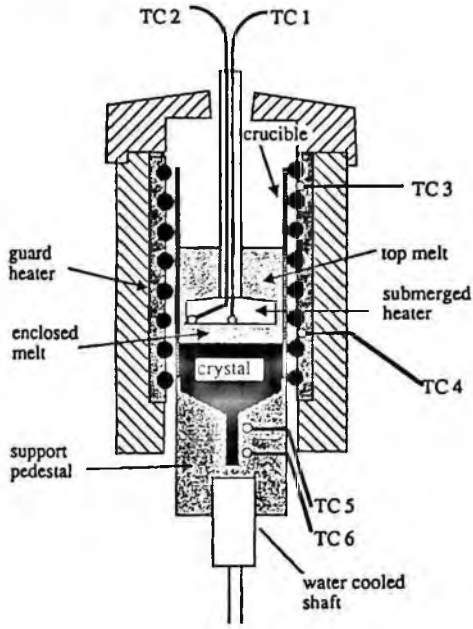

Fig. 12.5 Schematic drawing of the experimental apparatus for crystal growth by the Submerged Heater Method (SHM) (reprinted from Ref. 38 with permission, copyright 1993 Elsevier).

length 19 cm and diameter 1 cm as shown in Fig. 12.4.

Simulation of Czochralski (CZ) growth has been performed by Bouhennache et al.[37] and the temperature distribution, thermal strain in growing crystals, heat distribution in the crucible and meniscus shape have been analyzed.

(5) Other Methods

The Submerged Heater Method (SHM) was applied to the growth of Te-doped InSb crystals as shown in Fig. 12.5.[38] It was found that diffusion-controlled steady state segregation could be achieved for Te-doped crystal growth.

The crystal growth of InSb by directional freezing in microgravity has been performed and the effect of microgravity was studied[39] and the result was analyzed for the effect on thermal convection.[40] Te-doped InSb was grown in a space satellite.[41] Undoped, Te-doped and Se-doped InSb crystals were grown in spacecraft and in a large centrifuge[42, 43] and the numbers of grain boundaries, twins and striations were examined as a function of acceleration, compared with crystal growth on the ground. Detached solidification of Ga-doped InSb on earth has been examined by using ampoules coated with hexagonal boron nitride.[44]

Table 12.3 Segregation Coefficients

Impurity	Segregation Coefficient
Te	0.54-4.2
Se	0.17-1.9
Cu	6.6×10^{-4}
Ag	4.9×10^{-5}
Au	1.9×10^{-6}
Zn	2.3-3.52
Cd	0.26
Ga	2.4
Sn	5.7×10^{-2}
Tl	5.2×10^{-4}
P	0.16
As	5.4
Fe	4.0×10^{-2}
Ni	6.0×10^{-5}
S	0.1

12.3.3 Doping

Segregation of various impurities in InSb has been studied[27, 45-47] and their segregation coefficients have been determined as in Table 12.3.

12.4 CHARACTERIZATION

12.4.1 Defects

(1) Dislocations

The orientation of an InSb single crystal can be determined by an etching procedure.[48] Dislocations in InSb can be revealed by EPD etchants as 5 HNO_3 + 2 HF + 6 H_2O + 20-50% lactic acid and 1(48% HF) + 2 (30% H_2O_2) + 2 H_2O.[32] Modified CP-4 etchant (2 HNO_3 + 1 HF + 1 glacial CH_3COOH) can reveal α-dislocations and the etchant, 1 (30% H_2O_2) + 1 (48% HF) + 8 H_2O + 0.4% n-butylthiobutane can reveal β-dislocations.[49]

The typical dislocation density for CZ-grown InSb is less than $2.5\times10^2\,cm^{-2}$,[11] which is a very low level compared with other compound semiconductors. This is due to the high critical resolved shear stress (CRSS) of InSb. The effect of inclusions on the dislocation density has been studied,[49] comparing space-grown crystals with CZ-grown crystals.

Since it is easy to obtain dislocation-free InSb single crystals, many studies have been performed to measure dislocation velocities by observing plastic deformation by applying stress on these crystals.

In III-V materials, 60° dislocations such as α and β dislocations exist as first found by Haasen.[50] As shown in Fig. 4.7, α and β and screw dislocations are related and their relationship has been studied by etching techniques.[51] The velocity of these dislocations has been measured by the etching method,[52-55] stress-strain curve measurement,[56-59] TEM observation[60] and the bending test.[61-67]

The velocity of various dislocations has been measured as a function of temperature and it was found that the velocity of α dislocations is 10^2 to 10^3 times faster than β- and screw dislocations. The activation energies of dislocation motion for α- and β-dislocations were 0.6 eV and 1.1 eV respectively.

The effect of annealing on the screw dislocation velocity was also studied and discussed from the viewpoint of the interaction of point defects with dislocations.[64-67] Optical properties such as absorption spectra of plastically deformed InSb were studied and the effect of dislocations was discussed.[68] The ductile-to-brittle transition temperature was measured by the micro Vickers hardness method and was found to be 0-100 °C.[69]

Müller and Jacombson[70] have grown a crystal with grain boundaries consisting of a and β dislocations using A[111] and A[-1-1-1] oriented seed crystals. They have studied the current flow through these grain boundaries and found that dislocations behave as acceptors and donors.

(2) Microtwins

Vanderschaeve and Calliard[71] have submitted InSb single crystal samples to tensile strain in the temperature range of 443-593 K and observed microtwin formation by TEM. Through an analysis of dislocation formation, the mechanism of twinning was discussed.

(3) Facets and striations

It is known that in the CZ growth of InSb, strong facets are formed due to the facet formation mechanism.[11, 72, 73]

Witt and Gatos[74] were the first to apply interference contrast microscopy to investigating the formation of striations and found the existence of six types of striations, three rotational striations and three non-rotational as explained in Sec. 4.7. Morizane et al.[75-77] have studied impurity striations in the CZ growth of InSb in an experimental arrangement where the thermal and rotational axes did not coincide and theoretically analyzed the resulting striations. Utech and Flemings[78] have shown that the application of a vertical magnetic field is effective in eliminating the formation of striation bands during the HGF growth of Te-doped InSb crystals.

Miller[28] has studied the striation in CZ grown crystals using X-ray anomalous transmission topography and discussed growth striation and the residual strain existing mainly in the core region.

Hayakawa et al.[79, 80] have explained striation phenomena using a two-dimensional model and developed a CZ growth method using alternate rotation in order to minimize dopant striations.

(4) Deep levels

Kosarev et al. [81] have analyzed the Hall measurement data and deduced the concentrations of deep carriers. Deep levels were studied by DLTS.[82-84] Volkov et al.[83] have measured deep levels for n-type InSb and Ge-doped p-type InSb at temperatures of 4.2-

Table 12.4. Deep Levels in InSb (from Ref. 83 with permission)

		Energy Level (eV)	Capture cross sections (cm^2) Electrons (σ_n)	Holes (σ_p)	Trap concentration (cm^{-3})
Electron traps					
n-type	E1	E_c-0.120	$5x10^{-16}$		$5x10^{12}$
	E2	E_c-0.101	$2x10^{-14}$		$1x10^{13}$
p-type	E	E_c-0.015			$1x10^{13}$
Hole traps					
n-type	H1	E_v+0.050	$3x10^{-14}$	$5x10^{12}$	
	H2	E_v+0.010	$2x10^{-17}$	$2x10^{12}$	
p-type	H3	E_v+0.100	$6x10^{-17}$		$2x10^{13}$
	H4	E_v+0.108	$2x10^{-14}$		$2x10^{13}$
	H5	E_v+0.120	$9x10^{-14}$		$1.5x10^{13}$
	H6	E_v+0.047	$4x10^{-14}$		$4x10^{12}$
	H7	E_v+0.020			$4x10^{12}$

300 K. Electron traps at E_c-0.120 eV and E_c-0.101 eV have been observed. Littler[85] has applied a magneto-optical method to determine various deep levels and summarized his and previous data.

12.4.2 Electrical Properties

Since InSb has a very small bandgap, it has a relatively high intrinsic carrier concentration ($1\text{-}2x10^{16}$ cm^{-3}). Electron and hole mobilities have been measured as a function of carrier concentration as shown in Fig. 12. 6.[10] The radial segregation of impurities during crystal growth makes for a large difference in mobility from the center to the edge by a factor of 10. Energy levels of various shallow impurities so far reported[12] are as shown in Table 12.5.

Otsuka[86] calculated electron scattering by impurities using a simplified square well-

Table 12.5 Energy Levels of Shallow Impurities

Type	Impurity	Energy level (eV)
n	Te	0.05
n	Se	0.15
n	S	0.25
p	Cd	0.00986
p	Zn	0.0091
p	Ge	0.00925
p	Cr	0.07
p	Mn	0.0095
p	Fe	0.0013
p	Co	0.008
p	Cu^o	0.028
p	Cu^-	0.056
p	Ag^o	0.0298
p	Ag^-	0.056
p	X	0.120

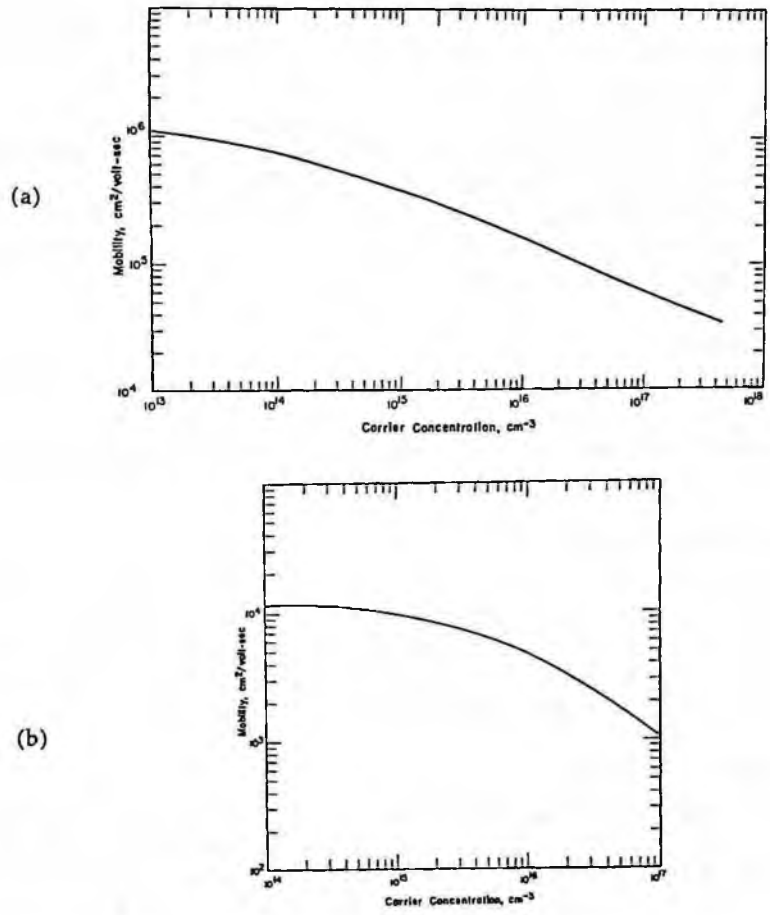

Fig. 12.6 Electron (a) and hole (b) mobilities at 77 K as a function of carrier concentration.[10]

or-hump potential model and showed that the scattering cross-section by a screened acceptor is much smaller than that by a screened donor. The donor to acceptor ratio of the cross section σ_n/σ_a amounted to 550.

The electrical resistivity of Mn-doped and Ge-doped p-type InSb has been measured with high acceptor concentrations of $4.5\text{x}10^{16}$-$2\text{x}10^{17}\,\text{cm}^{-3}$ and the metal-insulator transition was reported.[87] Magnetoresistance and transverse magnetophonon resonance[88] have been measured for crystals grown by the horizontal zone melting (HZM) method.

12.5 APPLICATIONS

12.5.1 Optical Devices

(1) Focal-plane array (FPA) detectors

InSb based focal-plane array (FPA) detectors are sensitive to near the infrared wave-

length region (1-5.5 μm) and various array devices have been developed.[89-100] One dimensional InSb FPAs[89] employing line scanning to obtain two dimensional images have been used in thermal imaging, earth resources remote sensing, a visible infrared mapping spectrometer for Mars observation and night-vision instruments. One dimensional FPAs have limited sensitivity. Two dimensional InSb staring FPAs have been developed from 8x8 pixels,[90] 128x128 pixels[97-99] to 1024x768 pixels[100] cameras in the 3-5um range for thermal sensing, IR astronomy[94-96] and night vision systems.[98] Treado et al.[101] and Lewis et al.[102] showed the application of (FPA) detectors to an absorption spectroscopic microscope sensitive in the range of 1-5.5 μm.

(2) Photodetectors

InSb,[103] InAsSb[104] and InTlSb[6] are good materials for long wave length photodetectors. Su et al.[105] examined the 1/f noise for InSb photodiodes as a function of temperature, gate bias, diode voltage, junction area and photon flux and discussed the origin of 1/f noise.

12.5.2 Electronic Devices

P channel MOS transistors were fabricated using n-type InSb substrates and a threshold voltage of −3V with an effective hole mobility of 330 $cm^2/V \cdot s$ was reported.[106] Calster et al.[107] have developed thin film transistors using InSb films on glass substrates. Margalit et al.[108, 109] showed a field induced tunneling diode based on InSb. There is a promising future possibility of InSb replacing Si in MOS devices.[110]

12.5.3 Sensors and Others

InSb thin films on GaAs substrates are used as Hall sensors in mass production.[111, 112] Woelk et al.[113] showed the large scale production of position sensors for automobile engines, based on InSb thin films on GaAs wafers. Ghoshi et al.[114] showed that a (111) InSb crystal can be used as an X-ray monochromator and showed that it has a strong reflecting power and high resolving power. Its low thermal expansion coefficient (4.9×10^{-6}/C) and chemical stability facilitates the high precision measurement of radiation from ^{14}Si to ^{92}U (Ma). Nesmelova et al.[115] showed that InSb is promising as a small, quick-response medical thermometer. The operating principle is based on the temperature dependence of the electrical resistance in the intrinsic conductivity region.

REFERENCES

1. K.F. Hulm and J.B. Mullin, *J. Solid State Electron.* **5** (1962) 211.
2. S.R. Jost, V.F. Meikleham, T.H. Myers, *Mater. Res. Soc. Symp. Proc.* **90** (1987) 429.
3. R.D. Thom, T.L. Koch, J.D. Langan and W.J. Parrish, *IEEE Trans. Electron Devices* **ED-27** (1980) 160.
4. C-Y. Wei, K.L. Wang, E.A. Taft, J.M. Swab, M.D. Gibbon and W.E. Davern, *IEEE Trans. Electron Devices* **ED-27** (1980) 170.
5. R.A. Stradling, *Semicon. Sci. Technol.* **6** (1991) C52.
6. M. van Schilfgaarde, A. Sher, A-B. Chen, *Appl. Phys. Lett.* **62** (1993) 1857.
7. J.D. Kim, D. Wu, J. Wojkowski, J. Piotrowski, J. Xu and M. Razegi, *Appl. Phys. Lett.* **68** (1996) 99.
8. Y.Z. Gao and T. Yamaguchi, *Cryst. Res. Technol.* **34** (1999) 285.

9. G.S. Nadkarni, A. Simoni and J.G. Simmons, *Solid State Electron.* **18** (1975) 393.
10. S.C. Liang, *Compound Semiconductors, Vol.1. Preparation of III-V Compounds*, eds. R.K. Willardson and H.L. Goering (Reinhold, New York, 1962) p. 227.
11. K. Matsumoto, in *Bulk Crystal Growth Technology* (Gordon and Breach, New York, 1989) p. 169.
12. *Landolt-Börnstein, Vol. 17 Semiconductors*, ed. O. Madelung (Springer-Verlag, Berlin, 1982) p. 310.
13. T.S. Liu and E.A. Peretti, *Trans. AIME* **44** (1952) 539.
14. M. Hansen, in *Constitution of Binary Alloys* (MacGraw-Hill, 1958) p. 859.
15. A. Rastogi and K.V. Reddy, *J. Appl. Phys.* **75** (1994) 4984.
16. T.C. Harman, *J. Electrochem. Soc.* **103** (1956) 128.
17. K.F. Hulm, *J. Electronics and Control* **6** (1959) 397.
18. G. Wolff, P.H. Keck and J.D. Broder, *Phys. Rev.* **94** (1954) 753.
19. K. W. Benz and G. Müller, *J. Crystal Growth* **46** (1979) 35.
20. R.C. Bourke, S.E. Miller and W.P. Allred, *J. Electrochem. Soc.* **106** (1959) 61C.
21. K.I. Vinogradova, V.V. Galavanov, D.N. Nasledov and L.I. Solov'yeva, *Sov. Phys.-Solid State* **1** (1959) 364.
22. R.K. Müler and R.L. Jacobson, *J. Appl. Phys.* **32** (1961) 550.
23. I. Ohno, N. Iwasaki and T. Yoneyama, *Jpn. J. Appl. Phys.* **18** (1979) 285.
24. T.A. Campbell and J.N. Coster, *J. Crystal Growth* **147** (1995) 408.
25. P. Mohan, N. Senguttuvan, S. Moorthy Babu and P. Ramasamy, *J. Crystal Growth* **211** (2000) 207.
26. J. Zhou, M. Larrousse, W.R. Wilcox and L.L. Regal, *J. Crystal Growth* **128** (1993) 173.
27. D. Tscheuschner and L. Ratke, *Cryst. Res. Technol.* **34** (1999) 167.
28. H.C. Gatos, P.L. Moody and M.C. Lavine, *J. Appl. Phys.* **31** (1960) 212. 1265?
29. W.P. Allred and R.T. Bate, *J. Electrochem. Soc.* **108** (1961) 258.
30. D.C. Miller, *J. Crystal Growth* **46** (1979) 31.
31. M. Kumagawa, H. Oka, N.V. Quang and Y. Hayakawa, *Jpn. J. Appl. Phys.* **19** (1980) 753.
32. K. Terashima, *J. Crystal Growth* **60** (1982) 363.
33. Z. Burnstein and M. Azulay, *Mater. Res. Bull.* **19** (1984) 49.
34. V.S. Vekshina, D.G. Letenko, O.V. Nagibin, A. Ya Polyakov, A.B. Fedorstov and Yu V. Churki n, *Sov. Tech. Phys. Lett.* **18** (1992) 33.
35. G.N. Kozhemyakin, *J. Crystal Growth* **149** (1995) 266.
36. M.H. Lin and S. Kou, *J. Crystal Growth* **152** (1995) 256.
37. T. Bouhennache, L. Fairbairn, I. Frigaard, J. Ho, A. Hodge, H. Huang, M. Kamali, M.H.K. Kharrazi, N. Lee, R. LeVeque, M. Liang, S. Liang, T. Marquez-Lago, A. Majdanac, W.F. Micklethwaite, M. Muck, T. Myers, A. Rasekh, J. Rossmanith, A. Sanaie-Fard, J. Stockie, R. Westbrook, J.F. Williams, J. Zarestky and C.S. Bohun, in *Proc. 5th PIMS Industrial Problem Solving Workshop*, ed. J. Macki (Pacific Inst. Math. Sci., 2001) p. 17.
38. A.G. Ostrogorsky, H.J. Sell, S. Scharl and G. Muller, *J. Crystal Growth* **128** (1993) 201.
39. A.F. Witt, H.C. Gatos, M. Lichtensteiger, M.C. Lavine and C.J. Herman, *J. Electrochem. Soc.* **122** (1975) 276.
40. S.V. Jr. Bourgois, and L.W. Spradley, *Less Heat Mass Transfer* **3** (1976) 193.
41. V.S. Zemskov, M.R. Raukhman, E.A. Kozitsina and I.M. Arsent'ev, *Phys. Chem. Mater. Treat.* **25** (1991) 493.
42. R. Derebail, W.R. Wilcox and L.L. Regal, *J. Crystal Growth* **119** (1992) 98.
43. R. Derebail, B. Hoekstra, W.R. Wilcox and L.L. Regel, in *Proc. 30th Aerospace Sci. Meet. Exhibit.* (Am. Inst. Aeronaut. Astronaut., Washington, 1992) p. 1.
44. J. Wang, L.L. Regal and W.R. Wilcox, *J. Crystal Growth* **260** (2004),590.
45. J.B. Mullin, *J. Electronics and Control* **4** (1958) 358.
46. A.J. Strauss, *J. Appl. Phys.* **30** (1958) 559.
47. J.B. Mullin, in *Compound Semiconductors, Vol.1. Preparation of III-V Compounds*, eds. R.K. Willardson and H.L. Goering, (Reinhold, New York, 1962) p. 365.

48. R.E. Maringer, J. *Appl. Phys.* **29** (1958) 1261.
49. H.U. Walter, *J. Electrochem. Soc.* **124** (1977) 250.
50. P. Haasen, *Acta Met.* **5** (1957) 598.
51. J.D. Venables and P.M. Broudy, *J. Appl. Phys.* **29** (1958) 1025.
52. Y. A. Osip'yan and S. A. Erofeeva, *Sov. Phys.-Solid State* **11** (1969) 770.
53. H. Steinhardt and S. Schäfer, *Acta Met.* **19** (1971) 65.
54. M. Mihara and T. Ninomiya, *J. Phys. Soc. Jpn.* **25** (1968) 1198.
55. M. Mihara and T. Ninomiya, *phys. stat. sol. (a)* **32** (1975) 43.
56. P. Haasen, *Z. Phys.* **167** (1962) 461.
57. S.A. Erofeeva and Yu. A. Osip'yan, *Sov. Phys.-Solid State* **15** (1973) 538.
58. D. Ferre andJ.L. Farvacque, *phys. stat. sol. (a)* **49** (1978) 737.
59. J.L. Farvacque and D. Ferre, *J. Phys. Colloq.* **40** (1979) C6.157.
60. M. Fnaiech and F. Louchet, *Physica* **116B** (1983) 641.
61. V.I. Barbashov, V.I. Zaitsev, V.M. Mostovoi and V.I. Alekseenko, *Sov. Tech. Phys. Lett.* **12** (1986) 214.
62. V.I. Barbashov, V.I. Zaitsev, V.M. Mostovoi and V.I. Alekseenko, *phys. stat. sol. (a)* **111** (1987) K135.
63. V.I. Barbashov and T.V. Rodzina, *phys. stat. sol. (a)* **121** (1990) K27.
64. V.I. Alekseenko, V.I. Barbashov, L.A. Zilberman, V.M. Mostovoi and M. Ya. Skorokhod, *phys. stat. sol. (a)* **111** (1989) K145.
65. V.I. Alekseenko and V.M. Mostovoi, *Sov. Tech. Phys. Lett.* **15** (1989) 968.
66. V.I. Alekseenko, *Sov. Tech. Phys. Lett.* **17** (1991) 668.
67. V.I. Alekseenko, *Tech. Phys.* **38** (1993) 967.
68. D. Vignaud and J. L. Farvacque, *phys. stat. sol. (a)* **125** (1984) 785.
69. R.K. Banerjee and P. Feltham, *J. Mater. Sci.* **11** (1976) 1171.
70. R. K. Müller and R. L. Jacobson, *J. Appl. Phys.* **33** (1962) 2341.
71. G. Vanderschaeve and D. Caillard, *Twinning Adv. Mater. Symp. Twinning Adv. Mater.* (1994) p. 297.
72. K.F. Hulme and J.B. Mullin, *Phil. Mag.* **4** (1959) 1286.
73. A. Trainer and B.E. Bartlett, *Solid State Electron.* **2** (1961) 106.
74. A.F. Witt and H.C. Gatos, *J. Electrochem. Soc.* **113** (1966) 808.
75. K. Morizane, A. Witt and H.C. Gatos, *J. Electrochem.* Soc. **113** (1966) 51.
76. K. Morizane, A. Witt and H.C. Gatos, *J. Electrochem.* Soc. **114** (1967) 738.
77. K. Morizane, A. Witt and H.C. Gatos, *J. Electrochem.* Soc. **115** (1968) 747.
78. H.P. Utech and M.C. Flemings, *J. Appl. Phys.* **37** (1966) 2021.
79. Y. Hayakawa, K. Ishikawa and M. Kumagawa, *Jpn. J. Appl. Phys.* **25** (1986) 528.
80. Y. Hayakawa, M. Nagura and M. Kumagawa, *Semicond. Sci. Technol.* **3** (1988) 372.
81. V.V. Kosarev, V.V. Popov, V.S. Vekshina and N.I. Pepik, *phys. stat. sol. (a)* **107** (1988) K43.
82. L.V. Druzhinina, E.V. Molodtsova, E.A. Kozhukhova, A.Ya Polyakov, A.N. Popkov, M.V. Tishkin and A.L. Shlenskii, *Sov. Phys. Semicond.* **23** (1989) 1292.
83. V.V. Volkov, A.G. Padalko, S.V. Belotelov, V.B. Lazarev and V.V. Bozhko, *Sov. Phys. Semicond.* **23** (1989) 871.
84. O.S. Shemelina, Yu F. Novotoskii-Vlasov, *Sov. Phys. Semicond.* **26** (1992) 569.
85. C. Littler, *Proc. SPIE* **2021** (1993) 184.
86. E. Otsuka, *Jpn. J. Appl. Phys.* **22** (1983) 292.
87. S.A. Obukhov, *Sov. Phys. Semicond.* **22** (1988) 19.
88. I. Ohno, I. Fujisawa, K. Imamura and K. Haruna, *Jpn. J. Appl. Phys.* **21** (1982) 1174.
89. R.D. Thom, T.L. Koch and W.J. Parrish, *Pap. Am. Inst. Aeronaut. Astronaut.* **78-1728** (1978) 1.
90. J.P. Chatard, A. Lussereau, A. Salaville, M. Sirieix, D. Esteve, J.J. Simonne, J. Farre and J. Rahobisoa, *Rev. Phys. Appl.* **13** (1978) 637.
91. C-Y. Wei, K.L. Wang, E.A. Taft, J.M. Swab, M.D. Gibbons, W.E. Davern and D.M. Brown, *IEEE*

Trans. Electron. Devices **ED-27** (1980) 170.
92. R.D. Thom, T.L. Koch, J.D. Langan and W.J. Parrish, *IEEE Trans. Electron Devices* **ED-27** (1980) 160.
93. G.C. Bailey, K. Matthews and C.A. Niblack, *Proc. SPIE* **430** (1983) 52.
94. W.J. Forrest and J.L. Pipher, *NASA Tech. Mem.* **88213** (1986) 11.
95. A.H. Lockwood and W.J. Parrish, *Opt. Engineer.* **26** (1987) 228.
96. A.M. Fowler, R.G. Probst, J.P. Britt, R.R. Joyce and F.C. Gillett, *Opt. Engineer.* **26** (1987) 232.
97. S.R. Jost, V.P. Meikleham and T.H. Myers, *Mater. Res. Soc. Symp. Proc.* **90** (1987) 429.
98. W.J. Parrish, J. Blackwell, R. Paulson and H. Arnold, *Proc. SPIE* **1512** (1991) 68.
99. H.Fujisada, M. Nakayama and A. Tanaka, *Proc. SPIE* **1341** (1992) 80.
100. T.J. Phillips, *III-Vs Review* **15** (2002) 32.
101. P.J. Treado, I.W. Levin and E.N. Lewis, *Appl. Spectrosc.* **48** (1994) 607.
102. E.N. Lewis and I.W. Levin, *Appl. Spectrosc.* **49** (1995) 672.
103. Catalog of Hamamatsu Photonics Co., http://www.hpk.co.jp.
104. J.D. Kim, D. Wu, J. Wojkowski, J. Piotrowski, J. Xu and M. Razeghi, *Appl. Phys. Lett.* **68** (1996) 99.
105. Y.K. Su, U.H. Liaw, T-P. Sun and G-S Chen, *J. Appl. Phys.* **81** (1997) 739.
106. J. Shappir, S. Margalit and I. Kidron, *IEEE Trans Electron Devices* **22** (1975) 960.
107. V. Calster, *Solid State Electron.* **22** (1979) 77.
108. S. Margalit, J. Shappir and I. Kidron, *J. Appl. Phys.* **46** (1975) 3999.
109. S. Margalit and J. Shappir, *Solid State Electron.* **19** (1976) 789.
110. M. Cooke, *III-Vs Review* **18** (2005) 34.
111. A. Okamoto, A. Ashihara, T. Akaogi and I. Shibasaki, *J. Crystal Growth* **227/228** (2001) 619.
112. I. Shibasaki, *III-Vs Review* **16** (2003) 26.
113. E. Woelk, H. Jürgensen, R. Rolph and T. Zielinski, *J. Electron. Mater.* **24** (1996) 1715.
114. Y. Gohshi, O. Hirao, M. Murata, T. Tanoue and M. Tsuruoka, *X-ray Spectrom.* **4** (1975) 74.
115. I.M. Nesmelova, O.A. Petrova, E.M. Zonshain, V.V. Paslavskii, I.M. Lavrent'eva and V.N. Ryzhkov, *Sov. J. Opt. Technol.* **60** (1993) 654.

PART 3

II-VI MATERIALS

13. CdS
14. CdSe
15. CdTe
16. ZnS
17. ZnSe
18. ZnTe

13. CdS

13.1 INTRODUCTION

After the photovoltaic effect was first observed by Reynolds et al.,[1] much interest was focused on CdS. CdS is a material which is of importance in phosphors and photoconductors. Since the bandgap of CdS is 2.38 eV and of direct transition type, it is a candidate for green light photoelectric conversion devices. CdS is also promising for lasers so that the growth of large single crystals have been attempted.

13.2 PHYSICAL PROPERTIES

Typical physical properties are shown in Table 13.1.[2-6] Precise melting point and vapor pressures were determined by Addamiano et al.[7,8]

The phase diagram of CdS was reported by Woodbury[9] as shown in Fig. 13.1. The lattice parameter of CdS_xSe_{1-x} has been measured by Al-Bassam et al.[10]

Vaporization of CdS has been studied precisely by Somorjai et al.,[11-14] considering doping, surface, temperature and light exposure. The dependence of the vaporization rate on the orientation of the basal planes was also studied.[15] These fundamental studies became the basis for the vapor phase growth of CdS.

13.3 CRYSTAL GROWTH

Since CdS has quite a high melting point and decomposition pressure, it is mainly grown by vapor phase growth methods but other methods have also been examined as shown in Table 13.2.

13.3.1 Melt Growth

The first experiment to melt CdS in a high pressure furnace was carried out very long

Table 13.1 Physical Properties of CdS

Crystal Structure	wurtzite
Lattice Constant	a=4.1368 Å
	c=6.7163 Å
Density	4.82 g/cm^3
Melting Point	1475 °C
Linear Expansion Coefficient	5.0-6.5x10^{-6} / deg ($\perp$ c)
	2.5-4.0x10^{-6} / deg (// c)
Thermal Conductivity	0.3 W/cm·K
Dielectric Constant	10.33 (//), 9.35 ($\perp$)
Refractive index	2.674
Bandgap at Room Temperature	2.38 eV
Optical Transition Type	direct
Intrinsic Carrier Concentration	16.7x10^{15} / cm^3 (1173 K)
Electron Mobility at R.T.	350 cm^2/V·sec
Hole Mobility at R.T.	15 cm^2/V·sec

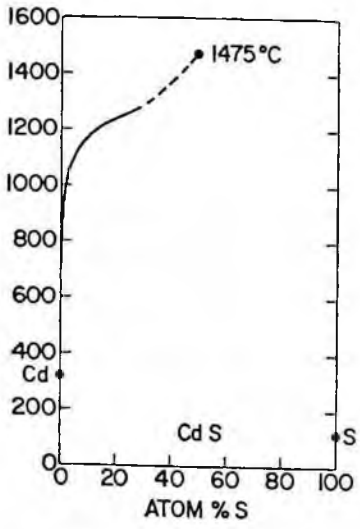

Fig. 13.1 Phase diagram of CdS (reprinted from Ref. 9 with permission, copyright 1963 American Chemical Society).

time ago.[16] Medcalf et al.[17] grew CdS single crystals by the VGF method using a high pressure furnace as shown in Fig. 13.2. The temperature is raised to 1500 °C under an Ar atmosphere of 1500 psi, and the furnace is cooled down to grow crystals. Crystal growth was performed under various pressures and it was found that when the pressure went down to 250 psi, only polycrystalline ingots were obtained. The segregation coefficients of various impurities during growth were measured as shown in Fig. 13.3.

Fischer[18-20] has grown CdS single crystals using a high pressure furnace by a soft ampoule method as shown in Fig. 13.4. In this method, a quartz ampoule is covered by a graphite susceptor so that the softened ampoule can be used even at high temperatures up to 1500 °C.

Kobayashi et al.[21] have grown CdS single crystals weighing 50 g, at a temperature of about 1400 °C by lowering the crucible at a rate of 3-20 mm/hr.

13.3.2 Solution Growth

Rubenstein[24] has measured the solubility of CdS in Sn and has grown CdS single crystals with the process shown in Fig. 13.5, at temperatures of 800-900 °C with a temperature difference between the surface of the solution and the bottom of the ampoule. Crystal growth was performed without any seed crystal and grown crystals were platelets of 4x4x2 mm^3 or rods of 2x2x6 mm^3. Crystal growth was also performed from lead, cadmium, and the eutectics of Cd-Bi-Pb-Sn and Bi-Pb-Sn.

Aoki et al.[25-27] have grown CdS single crystals from a Te solvent. The solubility of CdS in Te was measured and CdS was grown from solution at temperatures of 700-1000 °C with a cooling rate of 15 °C/hr. CdS single crystal platelets several mm in size were obtained.

Table 13.2 Crystal Growth of CdS

Method	Results	Author	Year	Ref.
HP-VGF	First melt growth of CdS	Tiede et al.	1920	16
DS	Direct synthesis by the reaction of Cd vapor with H_2S	Frerichs	1947	28
PVT	Sublimation growth under inert gas	Stanley	1956	30
PVT	Sublimation growth under H_2 H_2S	Grillot.	1956	31
HP-VGF	Growth under various Ar pressures (250-1500 psi)	Medcalf et al.	1958	17
PVT	Morphology of sublimation grown crystals	Reynolds et al.	1958	32
PVT	Growth of 20 mm^3 crystals	Green et al.	1958	33
PVT	Growth under H_2S or argon atmosphere	Boyd et al.	1959	34
PVT	Vaporization of CdS powders	Nishimura et al.	1959	35, 36
HP-VB	Soft ampoule method for preventing ampoule failure	Fisher	1959 -1961	18-20
VG	Direct synthesis from elements. Growth of CdZnS	Vitrikhovskii et al.	1960	29
CVT	Growth using iodine as the transport reagent	Nitsche	1960 -1962	57-60
PVT	Sublimation in a vertical furnace	Fujizaki et al.	1960	37
PVT	Self-sealing sublimation method	Piper et al.	1961	38
HP-VB	Growth of 50 g crystals under 76 atm.	Kobayashi	1966	21
PVT	Modified Piper-Polish method	Clark et al.	1966	39
CVT	Thermodynamical principle of CVT method	Shäfer et al.	1966	61
HP-VB	High pressure furnace arrangement	Kozielski	1967	22
PVT	Direct synthesis of CdS from the elements and PVT growth in a closed system	Hemmat et al.	1967	40
SG	Solubility in Sn, Cd, Bi. Growth of small crystals	Rubenstein	1968	24
PVT	Growth in a vertical furnace with sulphur vapor pressure control	Clark et al.	1968	41
PVT	Growth with sulfur vapor pressure control	Fochs et al.	1968	42
PVT	Growth of ZnCdS measuring 15x3x4 mm^3	Indradev et al.	1968	43
PVT	Theory of growth rate and comparison with experimental result	Ballentyne et al.	1970	44
CVT	Growth of $Cd_{1-x}Zn_xS$ using iodine as the reagent	Cherin et al.	1970	62
open PVT	Sublimation under various atmospheres	Corsini-Mena et al.	1971	45
PVT	Contactless growth in vertical and horizontal arrangements	Markov et al.	1971	46
PVT	Vertical PVT growth of crystals measuring several cm^3	Blanconnier et al.	1972	47
HP-VB	Composition analysis after melt growth	Kikuma et al.	1973	23
PVT	Theory of growth rate and comparison with experimental result	Tempest et al.	1974	48
PVT	40 mm diameter crystal growth by a seeding method	Dierssen et al.	1978	49
SG	Growth of plate-like crystals from Te solution	Aoki et al.	1979 -1982	25-27
PVT	Effect of Cd and S vapor pressures on the growth rate	Mochizuki et al.	1979	50

Table 13.2 Crystal Growth of CdS (continued)

Method	Results	Author	Year	Ref.
PVT	Contamination by CO_2 from silica capsule	Russel et al.	1979	51
PVT	Modification of Piper-Polish method	Morimoto et al.	1982	52
PVT	Theory of growth rate and comparison with experimental result	Su et al.	1987	53
PVT	Growth in a three-zone furnace	Su et al.	1990	54
CVD	Subatomical CVD for large area window material	Goela et al.	1988	63
PVT	Growth of $CdS_{0.99}Te_{0.01}$ crystal	Korostelin	1996	55
PVT	Growth of Cr-doped $CdS_{0.8}Se_{0.2}$ crystals	Roy et al.	2004	56
HS	Growth CdS nanocrystals	Nie et al.	2004	64

13.3.3 Vapor Phase Growth

(1) Direct Synthesis (DS) method

In the early days of the crystal growth of CdS, a dynamic crystal growth method was applied in which hydrogen sulfide and a carrier gas were passed over heated cadmium metal.[28] By the reaction between hydrogen sulfide and cadmium metal, cadmium sulfide was prepared and deposited as single crystals in a cooler position of the reaction tube. This method however gives only small crystals such as ribbons and platelets. Vitrikhovskii et al.[29] haveJ r grown CdS and $Cd_{1-x}Zn_xS$ crystals by the direct reaction of elemental vapors.

(2) Physical Vapor Transport (PVT) method

Stanley[30] has used a dynamic method in which a carrier gas is passed over heated cadmium sulfide powder. This method gives plate like crystals. Based on a method of

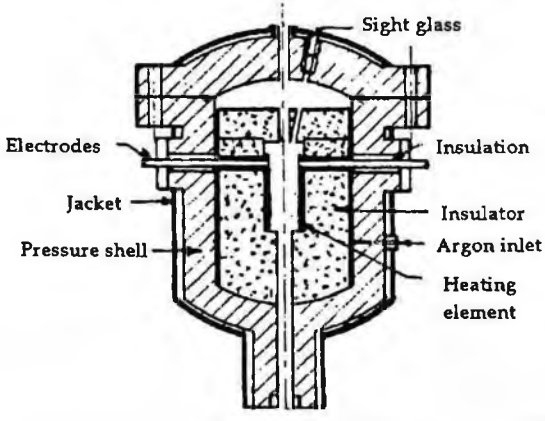

Fig. 13.2 Design of furnace used for the growth of CdS crystals from the melt (reprinted from Ref. 17 with permission of The Electrochemical Society).

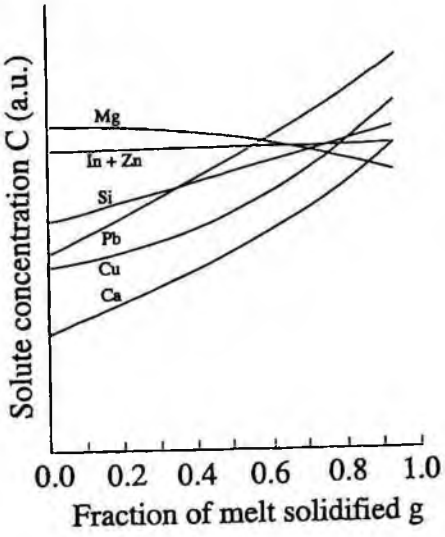

Fig. 13.3 Experimental concentration profiles for segregation of impurities in normal freezing of CdS melt (reprinted from Ref. 17 with permission of The Electrochemical Society).

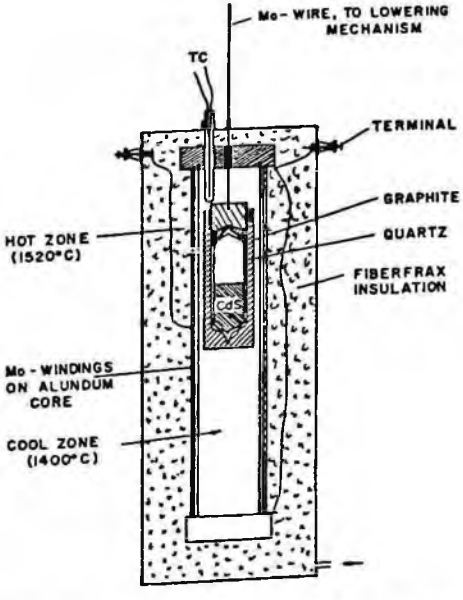

Fig. 13.4 High pressure Bridgman furnace for the growth of CdS crystals by "soft ampoule" method (reprinted from Ref. 20 with permission of The Electrochemical Society).

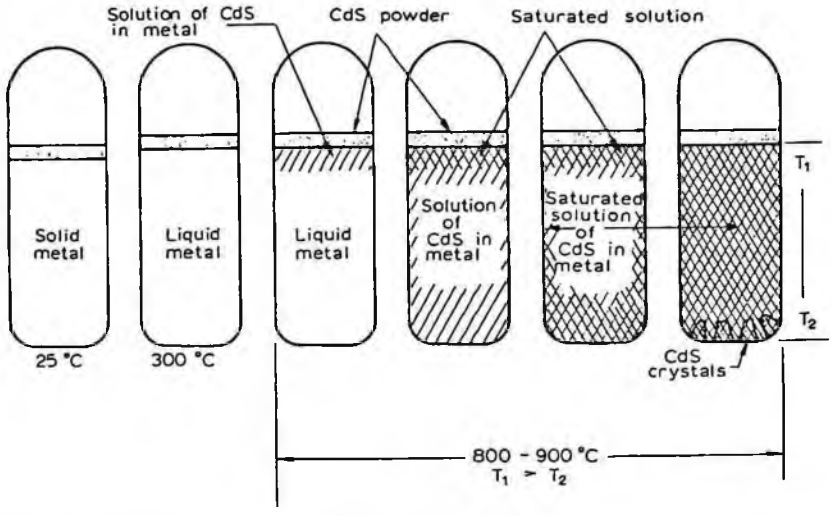

Fig. 13.5 Solvent transport growth of CdS crystals (reprinted from Ref. 24 with permission, copyright 1968 Elsevier).

Grillot,[31] Reynolds and Greene[32] have tried to grow CdS crystals by placing a CdS charge at one end of a quartz tube, the other end of which served as a substrate in a flat plane. The charge was heated at 1250 °C and the substrate was held at about 1150 °C. Large grains in excess of 50 g which were proved to be single crystals by X-ray measurement could be obtained.

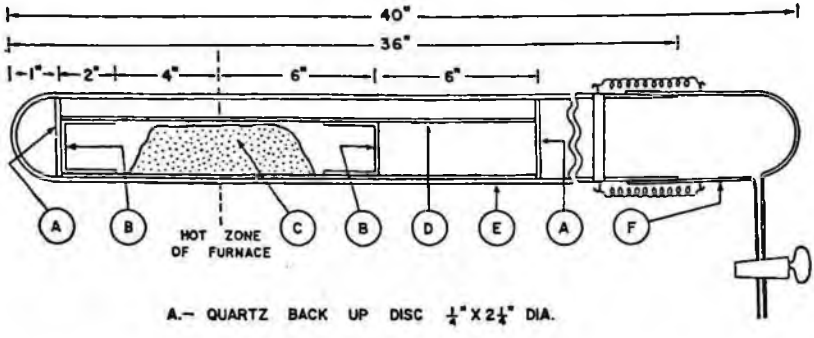

Fig. 13.6 Cross section of vapor phase transport growth furnace. A: quartz back up disc, B: quartz cup, C: CdS powder, D: quartz liner, E: mullite tube with one end ground to pit, F: ground glass vacuum cap (reprinted from Ref. 33 with permission, copyright 1958 American Institue of Physics)

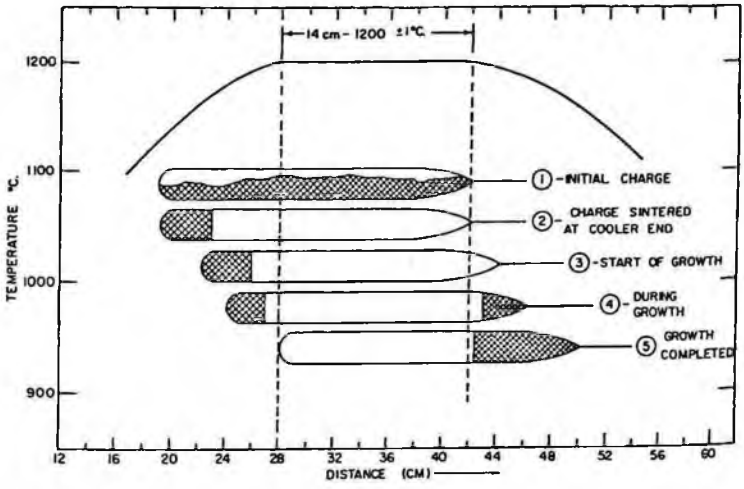

Fig. 13.7 Position of the ampoule relative to the temperature profile at various stages of PVT crystal growth (reprinted from Ref. 40 with permission of The Electrochemical Society).

Greene et al.[33] obtained CdS single crystals as large as 20 cm^3 by the sublimation method shown in Fig. 13.6. The center zone was heated at about 1250-1300 °C and the growth zone was heated at about 1135-1175 °C under various reduced gas pressure of H_2S, H_2 or N_2. CdS powder was sealed under H_2S or argon pressure of 1 atm. or less and heated by using a three-zone furnace at a maximum temperature of 1250 °C.[34] It was found that various types of crystals, depending on the temperature gradient, could be obtained.

Piper and Polish[38] first applied their PVT method (Fig. 2.15) to the crystal growth of CdS and obtained single crystals of a few cm^3 in size. In this method, self-sealing is performed after evacuation.

Hemmat and Weinstein[40] have synthesized CdS material directly in a closed system as shown in Fig. 13.7 and have grown crystals 9 cm in length and 25 mm in diameter successively in the same closed tube.

Clark and Wood[41] modified the former PVT method by putting a reservoir of Cd or S in order to control the vapor pressure during crystal growth. Fochs et al.[42] applied a vertical PVT method in which vapor pressure is controlled by using a reservoir as shown in Fig. 13.8. The feature of their method is that a small orifice is placed between the CdS charge and the crystal growth region to ensure that the crystal growth region is hotter than the charge region.

Ballentyne et al.[44] and Tempest et al.[48] examined the growth kinetics theoretically and compared the theory with the experimental result of the growth of CdS. Markov and Dabilov[46] applied a contactless PVT method to CdS crystal growth in vertical and horizontal arrangements.

Dierssen et al.[49] used a semi-closed system as seen in Fig. 13.9 and have success-

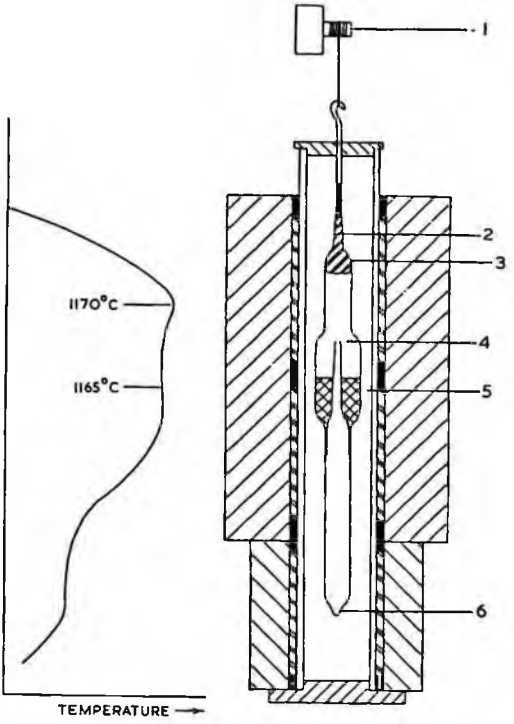

Fig. 13.8 Temperature profile and schematic diagram of silica capsule in furnace. (1) pulling motor, (2) capillary, (3) CdS crystal, (4) orifice , (5) CdS charge, (6) reservoir (reprinted from Ref. 42 with permission, copyright 1968 Elsevier).

fully grown <0001> directed 40 mm diameter single crystals using a seeding method (Fig. 13.10). For the seed crystal, a CdS single crystal wafer was prepared from crystals grown by the seed-cup method.

Mochizuki and Igaki[50] studied CdS single crystal growth by sublimation using Prior's method and showed that the growth rate was a function of partial vapor pressure of sulphur and cadmium as shown in Fig. 13.11.

Morimoto et al.[52] applied a modified Piper-Polish method, in which the furnace itself was moved through a sealed ampoule and studied the impurities in grown crystals by SIMS analysis.

Su[53] studied the vapor transport growth of CdS experimentally and compared the results with theoretical considerations in order to clarify the effect of various factors on the growth rate. They also studied growth in a three-zone furnace.[54]

$CdS_{0.8}Se_{0.2}$ crystals doped with Cr (Fig. 13.12) were grown by the self-seeded PVT method in a vertical configuration at a temperature of 950 °C. This crystal has been grown for near and mid-IR tunable laser applications.[56]

(3) Chemical Vapor Transport (CVT) method

Chemical vapor transport using iodine as the transport reagent was first applied to CdS

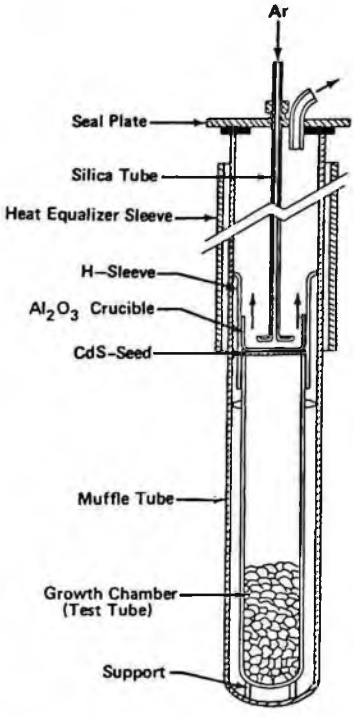

Fig. 13.9 Cross section through PVT growth assembly (reprinted from Ref. 49 with permission, copyright 1978 Elsevier).

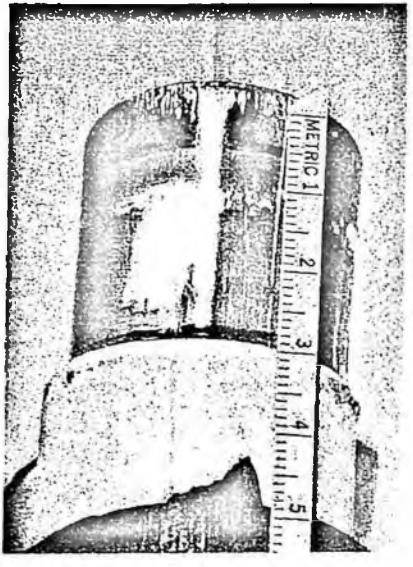

Fig. 13.10 Scale view of CdS boule grown in the (0001) direction (reprinted from Ref. 49 with permission, copyright 1978 Elsevier).

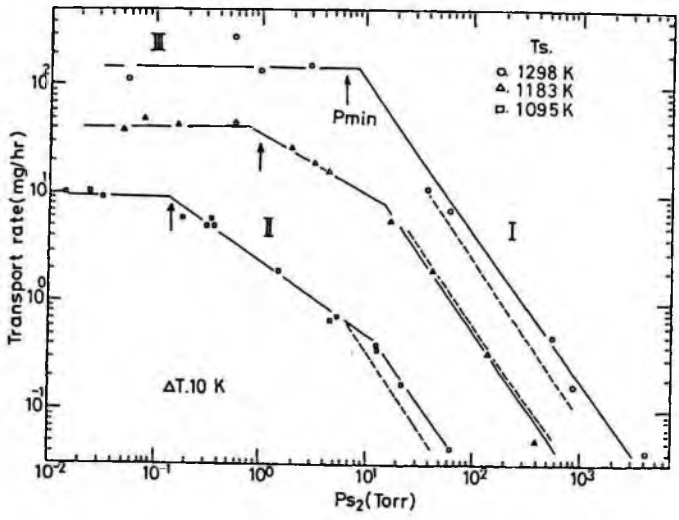

(a)

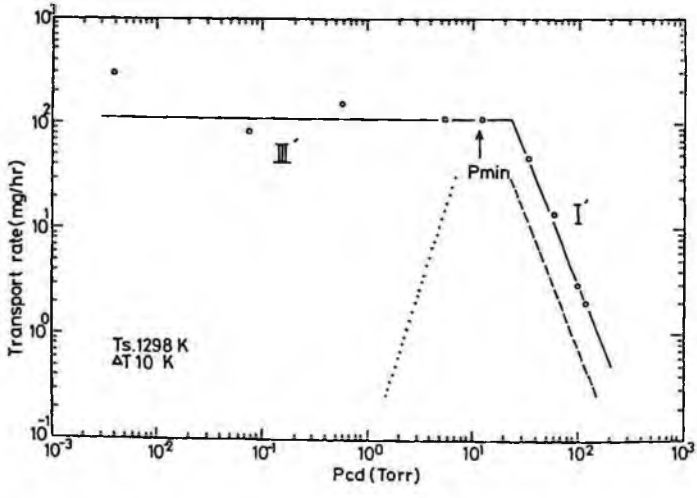

(b)

Fig. 13.11 Transport rate as a function of (a) S_2 partial pressure and (b) Cd partial pressure with fixed ΔT (10 K)(from Ref. 50 with permission).

by Nitsche.[57-60] Schäfer and Odenbach[61] also studied the growth of CdS by the same method. Cherin et al.[62] prepared $Cd_{1-x}Zn_xS$ materials by the iodine transport CVD method.

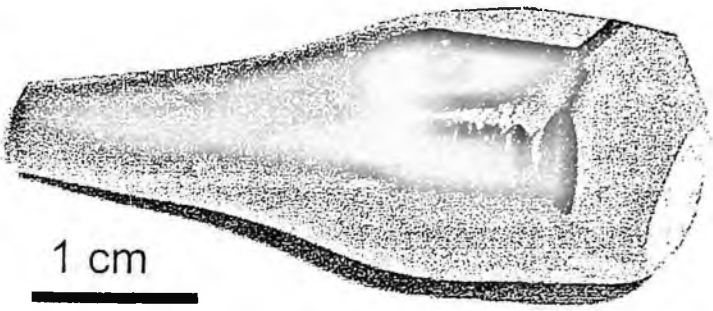

Fig. 13.12 Cr-doped $CdS_{0.8}Se_{0.2}$ crystal grown by self-seeded PVT method (reprinted from Ref. 56 with permission, copyright 2004 Elsevier).

13.3.4 Other Methods

Large polycrystals of CdS can be prepared by the CVD method.[63] This method is however limited to growing polycrystalline materials for infrared-optical applications. Nie et al.[64] have synthesized CdS nanocrystallites by the hydrothermal synthesis method.

13.4 CHARACTERIZATION

13.4.1 Defects

(1) Dislocations

Dislocation densities can be measured by counting the etch pits revealed by HPC etchant[40] (35% phosphoric acid saturated with CrO_3 with 65 % HCl). Typical dislocation densities for PVT CdS single crystals are $1\text{-}2\text{x}10^4$ cm^{-2}.[54]

(2) Deep levels

Grill et al.[65] have found various electron traps with activation energies of Ec-0.21 eV, Ec-0.2 7eV, Ec-0.33 eV, Ec-0.42 eV, Ec-0.47 eV, Ec-0.625 eV, Ec-0.735 eV in low resistive CdS crystals, and Verity et al.[66] reported two electron traps at Ec-0.50 eV and Ec-0.31 eV by DLTS.

13.4.2 Electrical Properties

Because of the self compensation mechanism (Sec. 4.2.5), CdS is of n-type conductivity and it is difficult to obtain p-type conductive material. The temperature dependence of electron mobility has been measured as shown in Fig. 13.13[67] and the dependence on the carrier concentration is as shown in Fig. 13.14.[68] The effect on the resistivity of

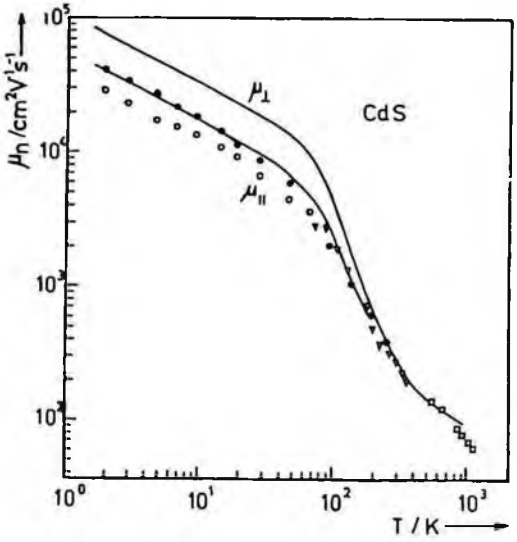

Fig. 13.13 Theoretical electron drift mobility (solid curve) of pure CdS compared with experimental Hall mobility data (reprinted from Ref. 67with permission, copyright 1975 Elsevier).

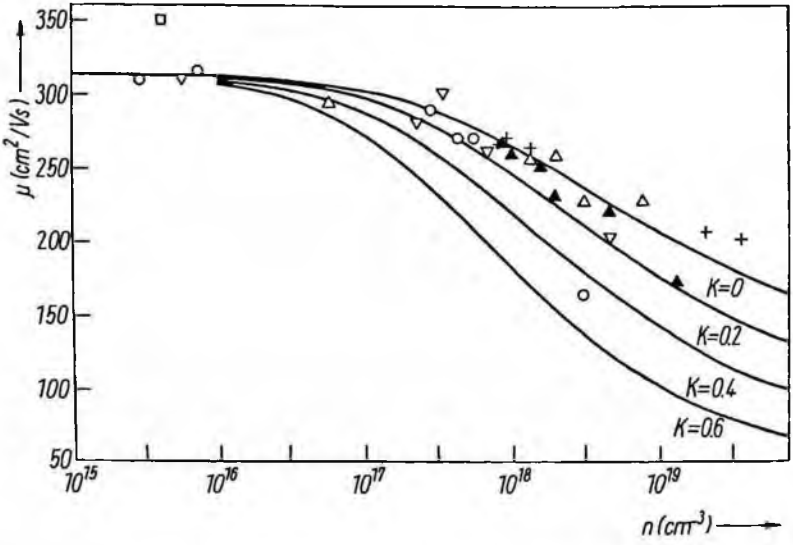

Fig. 13.14 Room temperature electron mobility of CdS as a function of electron concentration (from Ref. 68 with permission).

annealing under S overvapor has been studied by Susa et al.[69] The energy levels of donors and acceptors of CdS are determined[6] as shown in Table 13.3.

Table 13.3 Energy Levels of Donors and Acceptors in CdS

Impurity	Donor or Acceptor	Energy level from conduction band (eV)	Energy level from valence band (eV)
Ag	A		0.260
As	A		0.750
Br	D	0.0325	
Cl	D	0.0327	
Cu	A		1.100
F	D	0.0351	
Ga	D	0.0331	
I	D	0.0321	
In	D	0.0338	
Li	D	0.028	
	A		0.165
Na	A		0.169
P	A		0.120

13.4.3 Optical Properties

Edge emission characteristics have been discussed by Lambe et al.[70] Shionoya et al.[71] observed luminescence attributed to excitonic molecules as shown in Fig. 13.15. Susa et al.[69] have studied the effect of annealing in Cd or S vapor on the photoluminescence

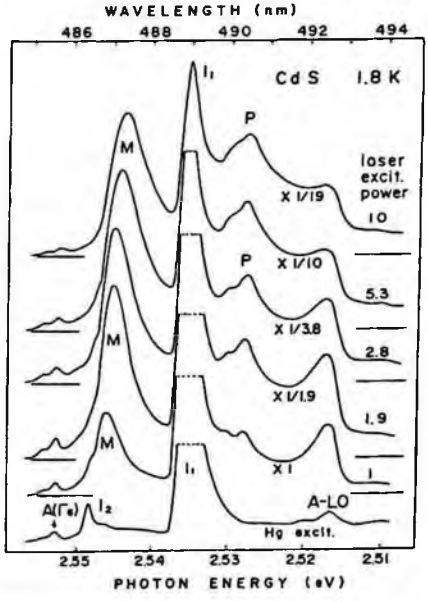

Fig. 13.15 Luminescence spectra of a CdS crystal at 1.8K under 337.1 nm laser light excitation as a function of laser excitation power (reprinted from Ref. 71 with permission, copyright 1973 Elsevier).

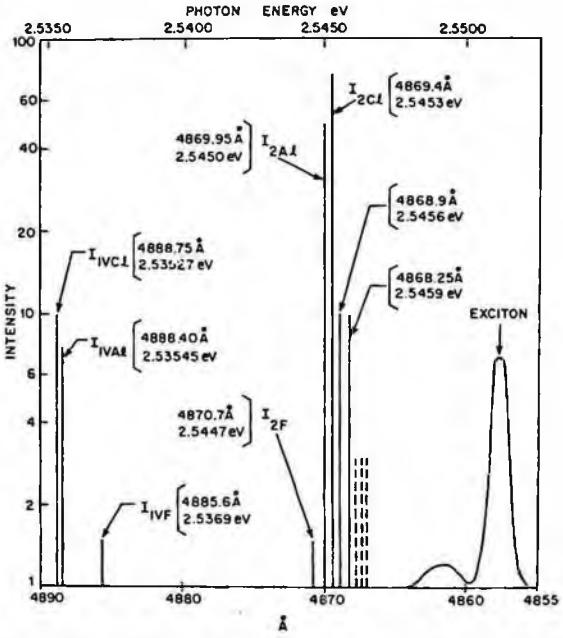

Fig. 13.16 Representation of some bound exciton emission lines seen from a CdS crystal.[73]

of melt-grown and PVT-grown crystals. Bouchenaka et al.[72] compared the luminescence spectra of bulk CdS crystals with epitaxially grown CdS. Typical edge emission lines are as shown in Fig. 13.16.

13.5 APPLICATIONS

As shown in Fig. 6.15, photoconductive devices using CdS polycrystalline films are produced industrially for camera sensors. CdS crystals were considered good material for green light lasers and much work went into putting this into practice but in vain and the activity has presently ceased.[74, 75] Since it is difficult to fabricate pn junction devices, MIS light emitting diodes have been studied using CdS single crystals.[76] A structure such as Au-SiO_x-CdS has been fabricated, paying attention to surface contamination and green light emitting devices have been demonstrated. Their efficiency was however limited.

REFERENCES

1. D.C. Reynolds, G. Leies, L.L. Antes and R.E. Marburger, *Phys. Rev.* **96** (1954) 533.
2. B. Ray, *II-VI Compounds* (Pergamonn, Oxford, 1969) p. 1.
3. *Physics and Cehmistry of II-VI Compounnds*, eds. M. Aven and J.S. Prener (Northe-Holland, Amsterdam, 1967).
4. *Landolt-Börnstein, Vol. 17 Semiconductors*, ed. O. Madelung (Springer-Verlag, Berlin, 1982) p. 166
5. H. Hartmann, R. Mach and B. Selle, in *Currents Topics in Materials Science, Vol. 9*, ed. E. Kaldis (North-Holland, Amsterdam, 1982) p. 1.

6. *Databook of II-VI Compound Semiconductor Crystals* (JEIPA, Tokyo, 1983)
7. A. Addamiano and P.A. Dell, *J. Phys. Chem.* **61** (1957) 1020.
8. A. Addamiano, *J. Phys. Chem.* **61** (1967) 1253.
9. H.H. Woodbury, *J. Phys. Chem.* **24** (1963) 881.
10. A.A.I. Al-Bassam, A.A. Al-Juffali and A.M. Al-Dhafiri, *J. Crystal Growth* **135** (1994) 476.
11. G.A. Somorjai and D.W. Jepsen, *J. Chem. Phys.* **41** (1964) 1389.
12. G.A. Somorjai and D.W. Jepsen, *J. Chem. Phys.* **41** (1964) 1394.
13. G.A. Somorjai and J.E. Lester, *J. Chem. Phys.* **43** (1965) 1450.
14. G.A. Somorjai and H.B. Lyon, *J. Chem. Phys.* **43** (1965) 1456.
15. R.B. Leonard and A.W. Searcy, *J. Appl. Phys.* **42** (1971) 4047.
16. E. Tiede and A. Schleede, *Ber. Deutschen. Chem. Gesellschaft Berlin* **53B** (1920) 1717.
17. W.E. Medcalf and R.H. Fahrig, *J. Electrochem. Soc.* **105** (1958) 719.
18. A.G. Fischer, *J. Electrochem. Soc.* **106** (1959) 838.
19. A.G. Fisher, *Bull. Am. Phys. Soc.* **6** (1961) 17.
20. A.G. Fishcer, *J. Electrochem. Soc.* **117** (1970) 41C.
21. S. Kobayashi, T. Seki, M. Wada and A. Nishizawa, in *Extend. Abstr.* (13th Spring Meeting, Jpn. Soc. Appl. Phys. Related Soc., 1966) p. 165.
22. M.J. Kozielski, *J. Crystal Growth* **1** (1967) 293.
23. H. Kimura and H. Komiya, *J. Crystal Growth* **20** (1973) 283.
24. M. Rubensein, *J. Crystal Growth* **3/4** (1968) 309.
25. M. Washiyama, K. Sato and M. Aoki, *Jpn. J. Appl. Phys.* **18** (1979) 869.
26. M. Aoki, M. Washiyama, H. Nakamura and K. Sakamoto, *Jpn. J. Appl. Phys.* **21** (1982) Suppl.21-1, p. 11.
27. M. Aoki, M. Washiyama and H. Nakamura, *Annual Rep. Fac. Eng. Univ. Tokyo* **41** (1982) 99.
28. R. Frerichs, *Phys. Rev.* **72** (1947) 594.
29. N.I. Vitrikhovskii and I.B. Mizetskaya, *Fizika Tverdogo Tela* **2** (1960) 2579.
30. J.M. Stanley, *J. Chem. Phys.* **24** (1956) 1279.
31. M.E. Grillot, *Compt. Rend.* **242** (1956) 779.
32. D.C. Reynolds and L.C. Greene, *J. Appl. Phys.* **29** (1958) 559.
33. L.C. Greene, D.C. Reynolds, S.J. Czyzak and W.A. Baker, *J. Chem. Phys.* **29** (1958) 1375.
34. D.R. Boyd and Y.T. Sihvonen, *J. Appl. Phys.* **30** (1959) 176.
35. J. Nishimura and J. Tanabe, *J. Phys. Soc. Jap.* **14** (1959) 850.
36. J. Nishimura, *J. Appl. Phys.* **28** (1959) 651.
37. H. Fujizaki and J. Tanabe, *J. Phys. Soc. Jap.* **15** (1960) 204.
38. W.W. Piper and S.J. Polish, *J. Appl. Phys.* **32** (1961) 1278.
39. L. Clark and J. Woods, Br. *J. Appl. Phys.* **17** (1966) 319.
40. N. Hemmat and M. Weinstein, *J. Electrochem. Soc.* **114** (1967) 851.
41. L. Clark and J. Woods, *J. Crystal Growth* **3/4** (1968) 126.
42. P.D. Fochs, W. George and P.D. Augustus, *J. Crystal Growth* **3/4** (1968) 122.
43. Indradev, L.J. Van Ruyven and F. Williams, *J. Appl. Phys.* **39** (1968) 3344.
44. D.W.G. Ballentyne, S. Wetwatana and E.A.D. White, *J. Crystal Growth* **7** (1970) 79.
45. A. Corsini-Mena, M. Elli, C. Paorici and L. Pelosini, *J. Crystal Growth* **8** (1971) 297.
46. E.V. Markov and Dabilov, *Izv. Acad. Nauk SSSR Neogan. Mater.* **7** (1971) 575.
47. P. Blanconnier and P. Henoc, *J. Crystal Growth* **17** (1972) 218.
48. P.A. Tempest and D.W.G. Ballentyne, *J. Crystal Growth* **21** (1974) 219.
49. G.H. Dierssen and T. Gabor, *J. Crystal Growth* **43** (1978) 572.
50. K. Mochizuki and K. Igaki, *Jpn. J. Appl. Phys.* **18** (1979) 1447.
51. G.J. Russel and J. Woods, *J. Crystal Growth* **46** (1979) 323.
52. J. Morimoto, T. Ito, T. Yoshida and T. Miyakawa, *J. Crystal Growth* **57** (1982) 362.
53. C.-H. Su, *J. Crystal Growth* **80** (1987) 333.
54. C.-H. Su, S.L. Lehoczky and F.R. Szofran, *J. Crystal Growth* **101** (1990) 221.

55. Yu.V. Korostelin, V.I. Kozlovsky, A.S. Nasbov and P.V. Shapkin, *J. Crystal Growth* **159** (1996) 181.
56. U.N. Roy, O.S. Babalola, Y. Cui, M. Groza, T. Mounts, A. Zavalin, S. Morgan and A. Burger, *J. Crystal Growth* **265** (2004) 453.
57. R. Nitsche, *Phys. Chem. Solids* **17** (1960) 163.
58. R. Nitsche, H.U. Bolsterli and M. Lichensteiger, *J. Phys. Chem. Solids* **21** (1961) 199.
59. R. Nitsche and D. Richman, *Z. Elektrochem.* **66** (1962) 709 (Part II).
60. R. Nitsche, in *Crystal Growth*, ed. H.S. Peiser (Pergamon Press, Oxford, 1967) p. 215.
61. V. H. Schäfer and H. Odenbach, *Z. Anorg, Allg. Chem.* **346** (1966) 127.
62]. P.Cherin, E.L. Lind and E.A. Davis, *J. Electrochem. Soc.* **117** (1970) 233.
63. J.S. Goela and R.L. Taylor, *J. Mater. Sci.* **23** (1988) 4331.
64. Q. Nie, Q. Yuan, W. Chen and Z. Xu, *J. Crystal Growth* **265** (2004) 420.
65. C. Grill, G. Bastide, G. Sagnes and M. Rouzeyre, *J. Appl. Phys.* **59** (1979) 1375.
66. D. Verity, F.J. Bryant, C.G. Scott and D. Shaw, *J. Crystal Growth* **59** (1982) 234.
67. D.L. Rode, in *Semiconductors and Semimetals, Vol. 10*, eds. R.K. Willardson and A.C. Beer (Academic Press, New York, 1975) p. 84.
68. B. Pödör, *phys. stat. sol. (a)* **20** (1973) K143.
69. N. Susa, H. Watanabe and M. Wada, *Jpn. J. Appl. Phys.* **15** (1976) 2365.
70. J.J. Lambe, C.C. Klick and D.L. Dexter, *Phys. Rev.* **103** (1956) 1715.
71. S. Shionoya, H. Saito, E. Hanamura and O. Akimoto, *Solid State Commun.* **12** (1973) 223.
72. C. Bouchenaki, B. Ulrich and J.P. Zielinger, *J. Lumin.* **48/49** (1991) 649.
73. D.G. Thomas, R. Dingle and J.D. Cuthbert, in *II-VI Semiconducting Compounds*, ed. D.G. Thomas (Benjamin, New York, 1967) p. 865.
74. L.D. DeLoach, R.H. Page, G.D. Wilke, S.A. Payne, W.F. Krupke, *OSA Proc. Adv. Solid State* Lasers **24** (1995) p. 127.
75. R.H. Page, *IEEE J. Quantum Electron.* **33** (1997) 609.
76. D.L. Wheeler and D. Haneman, *Solid State Electron.* **16** (1973) 875.

14. CdSe

14.1 INTRODUCTION

CdSe whose band gap is 1.70 eV is an interesting material for solar cells, photodetectors, optoelectronics, light amplifiers, electrophotography, light emitting diodes, lasers and photoelectrochemical cells. There are however very few studies of the bulk growth of CdSe even though its melting point is rather low (1239 °C).

14.2 PHYSICAL PROPERTIES

The physical properties of CdSe are shown in Table 14.1.[1-5] The phase diagram is as shown in Fig. 14.1.[6] Al-Bassam et al.[7] have measured the lattice parameter of CdS_xSe_{1-x} as a function of the composition.

14.3 CRYSTAL GROWTH

Various methods of crystal growth are summarized in Table 14.2.[8-25]

14.3.1 Melt Growth

Heinz and Banks[8] have grown a CdSe single crystal weighing 17 g using a high pressure VGF method, as shown in Fig. 14.1. Libicky[9] applied a zone refining method for the growth of CdSe.

14.3.2 Solution Growth

The Temperature Gradient Solution Growth (TGSG) method with excess Se has been applied to the growth of CdSe crystals[13, 14] and crystals 14 mm in diameter and 30-40

Table 14.1 Physical Properties of CdSe

Crystal Structure	wurtzite
Lattice Constant	a = 4.2985 Å
	c = 7.0150 Å
Density	5.684 g/cm^3
Melting Point	1239 °C
Linear Expansion Coefficient	4.4x10^{-6}/deg
Thermal Conductivity	0.09 W/cm·K
Dielectric Constant	10.65 (//), 9.70 (⊥)
Refractive index	2.6448
Bandgap at Room Temperature	1.74 eV
Optical Transition Type	direct
Intrinsic Carrier Concentration at R.T.	6x10^{13} cm^{-3} (800 K)
Electron Mobility at R.T.	650 cm^2/Vsec
Hole Mobility at R.T.	50 cm^2/Vsec
Intrinsic Resistivity	1x10^3 Ω·cm (800 K)

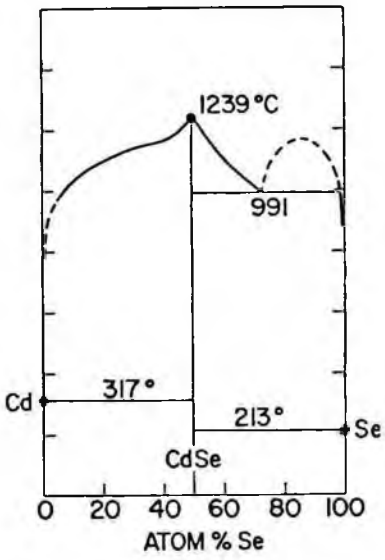

Fig. 14.1 Phase Diagram of CdSe (reprinted from Ref. 6 with permission of The Electrochemical Society).

Table 14.2 Crystal Growth of CdSe

Method	Results	Author	Year	Ref.
DR	Reaction of Cd vapor with H_2Se	Frerichs	1947	17
VGF	Growth of 17 g crystals under 150 lb/in²	Heinz et al.	1956	8
CVT	Growth using iodine as the transport reagent	Nitsche	1960 1961	18, 19
HPVT	Effect of vapor pressure on the growth rate	Hoschl et al.	1965	20
ZM	Synthesis of CdSe and growth by zone melting	Libicky et al.	1967	9
SG	Solubility in Sn, Cd, Bi. Growth of small crystals	Rubenstein	1968	12
TGSG	Growth from Se excess solution	Steininger	1968	13
Open PVT	Sublimation under various atmospheres	Corsini-Mena et al.	1971	21
HP-VB	Composition analysis after melt growth	Kimura et al.	1973	10
PVT	Crystals measuring 17 mmϕ x 40mm by the Piper-Polish method	Hatano et al.	1975	22
PVT	Growth of 30 g crystals of radiation detector grade	Burger et al.	1983	24
TGSG	Crystals measuring 14 mmϕ x 30-40 mm	Burger et al.	1984	14
SG	Growth of Cr-doped CdSe from Se solution	Ndap et al.	1984	15
PVT	Growth of $CdSe_{1-x}S_x$ mixed crystals	Al-Bassam et al.	1994	7
SSSR	Self-sealing growth under 5-7atm N_2 overpressure	Fitzpatrick et al.	1986	11
PVT	Growth of Cr-doped crystals (8x8x10mm³)	Schepler et a.l	1997	25
SG	Growth of Cr and Co-doped CdSe from Se solution	Adetunji et a.l	2002	16

VGF: Vertical Gradient Freezing, HP-VB: High Pressure Vertical Bridgman, ZM: Zone Melting, SG: Solution Growth, TGSG: Temperature Gradient Solution Growth, DR: Direct Reaction, PVT: Physical Vapor Transport, HPVT: Horizontal PVT, CVT: Chemical Vapor Transport, SSSR: Self-sealing Self-Releasing

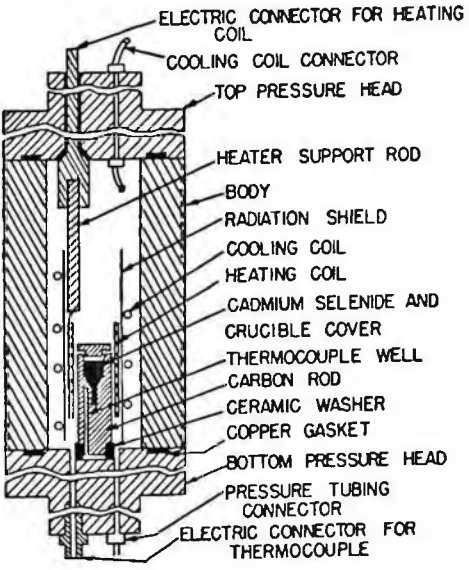

Fig. 14.2 High pressure Bridgman furnace for the growth of CdSe crystals (reprinted from Ref. 8 with permission, copyright 1956 American Institue of Physics).

mm in length have been routinely obtained.

Cr- and Co-doped CdSe crystals with doping levels of 4000 ppm were grown by the gradient freezing solution growth method from high temperature selenium solutions in order to prepare tunable mid-IR laser materials.[15, 16] The segregation coefficients of Cr and Co have been determined.

14.3.3 Vapor Phase Growth

Frerichs[17] has grown CdSe crystals by reacting Cd vapor with H_2Se gas. Nitsche[18, 19] have grown CdSe crystals by the CVT method using iodine as transport reagent. Grown crystals were however small only measuring a few mm^3.

Hatano et al.[22] have grown CdSe crystals with 17 mm in diameter and 40 mm in length by the Piper-Polish method (Fig. 2.13). They examined the effect of the ampoule travelling speed and annealing on the resistivity of the crystals grown.

Al-Bassam et al.[7] have grown CdS_xSe_{1-x} mixed crystals at a temperature of 1165 °C by the Clark and Woods vapor phase method[23] and by the Piper-Polish method (Fig. 2.13). Burger et al. have grown CdSe crystals weighing about 30 g by the unseeded PVT method.

14.4 CHARACTERIZATION

Because of the self compensation mechanism (Sec. 4.2.5), CdSe is of n-type conductivity and it is difficult to obtain p-type conductive material. The carrier concentration is mainly determined by Se vacancies. Tubota[26] has studied the electrical properties of

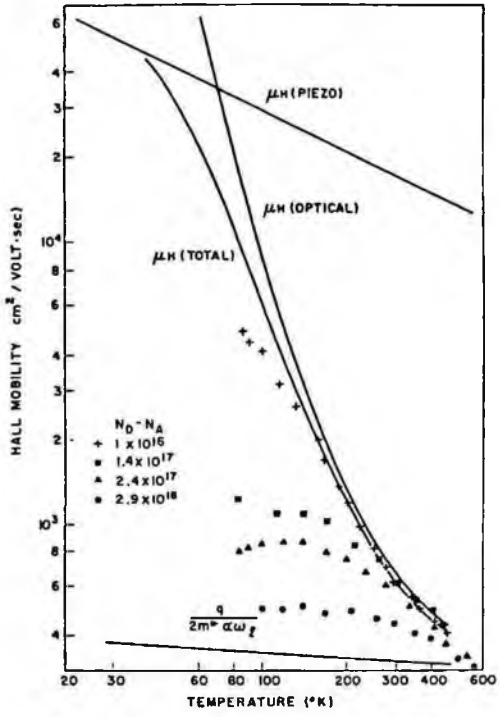

Fig. 14.3 Temperature dependence of the Hall mobility in several forms of n-type CdSe (reprinted from Ref. 27 with permission, copyright 1967 Elsevier).

CdSe crystals doped with various impurities such as Cu, Ag, Cd, In, Pb, Sn. The energy levels of Li and P acceptors are determined as 0.109 and 0.083 eV from the valence band, respectively.[5] The temperature dependence of Hall mobility is as shown in Fig. 14.3. Shionoya et al.[28] observed luminescence attributed to excitonic molecules.

14.5 APPLICATIONS

CdSe doped with Cr^{2+} is very promising for solid-state tunable lasers in the mid-IR region.[25, 29, 30] These lasers are expected to be useful for applications in remote sensing, environmental monitoring and surgical applications. CdSe is also promising for radiation detectors (Table 6.3). Burger et al.[24] have fabricated radiation detectors using PVT grown CdSe crystals of high resistivity obtained by heat treatment.

REFERENCES

1. B. Ray, *II-VI Compounds* (Pergamonn, Oxford, 1969) p. 1.
2. *Physics and Cehmistry of II-VI Compounnds*, eds. M. Aven and J.S. Prener (Northe-Holland, Amsterdam, 1967).
3. *Landolt-Börnstein, Vol. 17 Semiconductors*, ed. O. Madelung (Springer-Verlag, Berlin, 1982) p. 202.
4. H. Hartmann, R. Mach and B. Selle, in *Currents Topics in Materials Science, Vol. 9*, ed. E. Kaldis (North-Holland, Amsterdam, 1982) p. 1.

5. *Databook of II-VI Compound Semiconductor Crystals* (JEIPA, Tokyo, 1983)
6. A. Reisman and M. Berkenblit, *J. Electrochem. Soc.* **109** (1962) 1111.
7. A.A.I. Al-Bassam, A.A. Al-Juffali and A.M. Al-Dhafiri, *J. Crystal Growth* **135** (1994) 476.
8. D.M. Heinz and E. Banks, *J. Chem. Phys.* **24** (1956) 391.
9. A. Libicky, in *II-VI Semicond. Comp. Inter. Conf.*, ed. D.G. Thomas (Benjamin, New York, 1967) p. 389.
10. H. Kimura and H. Komiya, *J. Crystal Growth* **20** (1973) 283.
11. B. J. Fitzpatrick, T. F. McGee III and P. M. Harnack, *J. Crystal Growth* **78** (1986) 242.
12. M. Rubensein, *J. Crystal Growth* **3/4** (1968) 309.
13. J. Steininger, *Mater. Res. Bull.* **3** (1968) 595.
14. A. Burger and M. Roth, *J. Crystal Growth* 67(1984) 507.
15. J.-O. Ndap, O.O. Adetunji, K. Chattopadhyay, C.I. Rablau, S.U. Egarievwe, X. Ma, S. Morgan and A. Burger, *J. Crystal Growth* **211** (2000) 290.
16. O.O. Adetunji, N. Roy, Y. Cui, G. Wright, J.-O. Ndap and A. Burger, *J. Electron. Mater.* 7 (2002) 795.
17. R. Frerichs, *Phys. Rev.* **72** (1947) 594.
18. R. Nitsche, *Phys. Chem. Solids* **17** (1960) 163.
19. R. Nitsche, H.U. Bolsterli and M. Lichensteiger, *J. Phys. Chem. Solids* **21** (1961) 199.
20. P. Hoschl and C. Konak, *phys. stat. sol.* 9 (1965) 167.
21. A. Corsini-Mena, M. Elli, C. Paorici and L. Pelosini, *J. Crystal Growth* **8** (1971) 297.
22. H. Hatano, Y. Kokubun, H. Watanabe and M. Wada, *Jpn. J. Appl. Phys.* **14** (1975) 1059.
23. L. Clark and J. Woods, *J. Crystal Growth* **3/4** (1968) 126.
24. A. Burger, I. Shilo and M. Schieber, *IEEE Trans. Nucl. Sci.-NS* **30** (1983) 368.
25. K.L. Schepler, S. Kuck, L. Shiozawa, *J. Lumin.* **72-74** (1997) 116.
26. H. Tubota, *Jpn. J. Appl. Phys.* **2** (1963) 259.
27. S.S. Devlin, in *Physics and Cehmistry of II-VI Compounnds*, eds. by M. Aven and J.S. Prener, (Northe-Holland, Amsterdam, 1967) p. 551.
28. S. Shinoyama, H. Saito, E. Hanamura and O. Akimoto, *Solid State Commun.* **12** (1973) 223.
29. J. McKay, K.L. Schepler and G. Catella, in *Proc. CLEO Annual Meeting '99* (Baltimor, May, 1999) p. 547.
30. J. MaKay and K.L. Schepler, *Opt. Lett.* **24** (1999) 1575.

15. CdTe

15.1 INTRODUCTION

CdTe and $Cd_{1-x}Zn_xTe$ are materials which are mainly used as substrates for the epitaxial growth of $Hg_{1-x}Cd_xTe$ (MCT) in applications for far infrared detectors.[1-5] CdTe is also a promising material for use in radiation detectors[1, 6-8] since it has high stopping power and it can be made to have high resistivity at room temperature. CdTe is also promising for solar cells[6, 9-10] because the bandgap is appropriate to obtain a high conversion efficiency. Other applications of CdTe are in electro-optical modulators,[11] infrared windows[12] and photorefractive materials.[13]

Even though CdTe and related materials thus have a range of practical applications, the growth of these materials was difficult and it was a long time before large crystals with good qualities could be grown. This difficulty of growing high-quality large single crystals prevented the development of many devices based on CdTe and related materials. Crystal growth technologies for CdTe and related materials have rapidly developed in the last few decades. Large single crystals exceeding 100 mm diameter can now be grown. These circumstances allow CdTe and related materials to be applied industrially in the above mentioned applications.

15.2 PHYSICAL PROPERTIES

The physical properties of CdTe[1, 2, 14-19] are summarized in Table 15.1. Since the melting point (1092 °C) is relatively low and the dissociation pressure is close to one atmosphere, CdTe crystals can be grown in atmospheric pressure furnaces by using quartz ampoules.

Since CdTe has a wide band gap (1.49 eV), relatively high mobility ($\mu_n \sim 10^3$, $\mu_p \sim 10^2$ $cm^2/V \cdot s$), a wide transmission range (1-30 μm), a very low optical absorption coefficient (0.005 ± 0.002 cm^{-1} at 10.6 μm) and a large photoelectric coefficient (18×10^{-12} m/V), a piezoelectric coupling coefficient K of about 0.026 and emission in the infrared region (1.34, 1.41, 1.49 eV), CdTe is a promising material for the applications referred to above.

The phase diagram of CdTe is shown in Fig. 15.1. The phase diagrams of CdTe and related materials have been investigated by various authors[20-33] in the past. It is known that the congruent point is shifted to the Te-rich side and therefore precipitation occurs very often in the growth of CdTe crystals. Steininger et al.[22] and Vydyanath et al.[29] examined the vapor phase equilibria for the $Cd_{1-x}Zn_xTe$ alloy system. Yu et al.[30] examined the phase diagram for the Hg-Cd-Zn-Te system. The phase diagram of Cd-Mn-Te has also been studied.[33] The vapor pressure of CdTe has also been investigated.[34]

Because of the physical properties as shown in Table 15.2 which is extracted from Chapter 1, CdTe is a material of which it is difficult to grow high-quality single crystals for the following reasons.

Table 15.1 Physical Properties of CdTe

Lattice Constant	6.482 Å
Density	5.86 g/cm³
Melting Point	1092 °C
Linear Expansion Coefficient	4.9×10^{-6} /deg
Thermal Conductivity	0.075 W/cm•K
Dielectric Constant	10.3
Refractive index	2.91
Bandgap at Room Temperature	1.52 eV
Optical Transition Type	direct
Electron Mobility	1,200 cm²/V•sec
Hole Mobility	100 cm²/V•sec

(i) The thermal conductivity at the melting point is low so that the dissipation of heat during the solidification of the melt is difficult. Because of this difficulty, a convex solid/liquid interface can not easily be achieved in the melt.

(ii) Since the critical resolved shear stress is low as discussed in Sec. 1.7.3 and in Refs. 35 and 36, dislocations are easily generated by thermal stress. Dislocation densities in CdTe higher than 10^6 cm^{-2} are commonly observed for this reason.

(iii) Twins are easily formed because the stacking fault energy is very low as discussed in Sec. 1.7.2 and in Ref. 37.

The lattice constants of solid solutions, CdTe-HgTe, CdTe-ZnTe and HgTe-ZnTe have been measured by Woolley et al.[38] The relationship between the lattice constant of $Cd_{1-x}Zn_xTe$ (CZT) and $Hg_{1-y}Cd_yTe$ (MCT) is shown in Fig. 15.2.[39] For 10 μm far infrared detectors, MCT material with x = 0.8 has an appropriate bandgap for this wavelength.[40, 41] It is seen from Fig. 15.2 that CZT of composition with x = 0.96 has a lattice constant close to this MCT composition. For this reason, $Cd_{0.96}Zn_{0.04}Te$ is mainly produced at present as a substrate for MCT epitaxial growth, much more often than pure CdTe.

The diffusion constant of chalcogens,[42] phosphorus[43] and chlorine[44] have been measured. The hardness of CdTe has been measured by Hwang et al.[45] The thermal conductivity has been measured by Jougler et al.[46] and it was found to be very low.

15.3 CRYSTAL GROWTH

Various crystal growth methods have been investigated for CdTe and related crystals. In the early days, the sublimation method, THM, solution VB method, and the solvent evaporation method were most often investigated. This was because the rupture of

Table 15. 2 Properties of Various Semiconductor Materials

Material	Melting Point (°C)	Thermal Conductivity (W/cm•K)	Critical Resolved Shear Stress (MPa)	Stacking Fault Energy (erg/cm²)
Si	1420	0.21	1.85	70
Ge	960	0.17	0.7	63
GaAs	1238	0.07	0.4	48
InP	1070	0.1	0.36	20
CdTe	1092	0.01	0.11	10

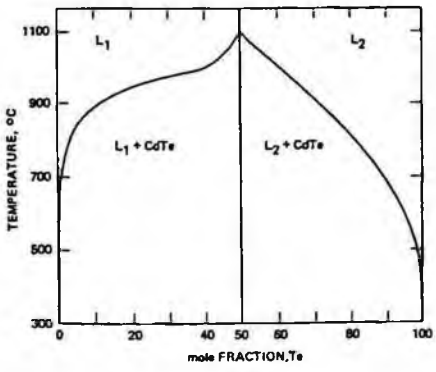

(a)

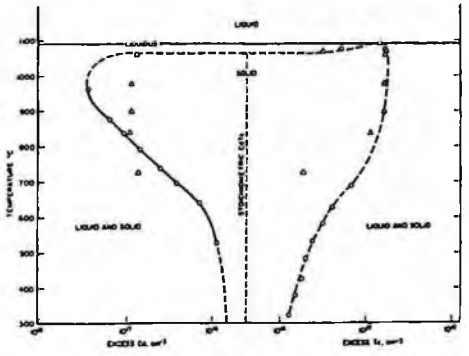

(b)

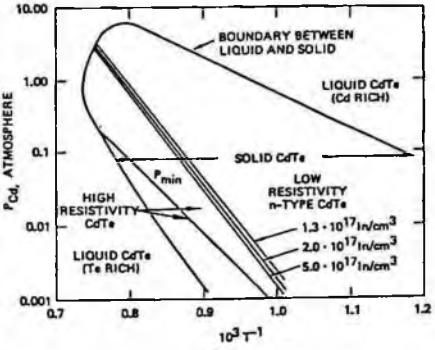

(c)

Fig. 15.1 Phase diagrams of CdTe. (a)X-T diagram and (b) P-T diagram(reprinted from Ref. 24 with per-mission, copyright 1980 AIChE) and (c) non-stoichiometric range (reprinted from Ref. 1 with permission, copyright 1980 Elsevier)

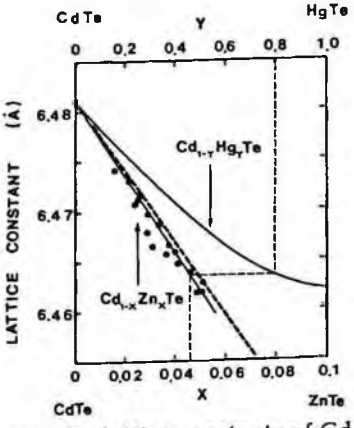

Fig. 15.2 Relationship between the lattice constants of $Cd_{1-x}Zn_xTe$ (CZT) and $Hg_{1-y}Cd_yTe$ (MCT). It is seen that the appropriate composition of CZT is x=0.04 for the common composition of MCT (y=0.8) for 10 μm far infrared detectors (reprinted from Ref. 39 with permission, copyright 1986 Elsevier).

quartz ampoules was a concern and the purity of the source materials Cd and Te was not sufficiently high. More recently, vertical Bridgman, vertical gradient freezing and horizontal Bridgman methods are more often investigated because of the development of the purification process of the raw materials and of improvements in the method of synthesis. The physical vapor transport method is however still extensively studied because of its advantage in growing low dislocation density materials. For materials applicable to radiation detectors, THM is a prominent crystal growth method but the VB method has been further examined for growing high resistive materials. These crystal growth methods have been reviewed by various authors.[1, 47-55]

15.3.1 Melt Growth

(1) Vertical Bridgman (VB) and Vertical Gradient Freezing (VGF) methods

CdTe is easily grown by the VB and VGF methods. These methods have been extensively studied over a long period because they offer the possibility of growing large crystals. In Table 15.3, most of the results of VB and VGF methods are summarized.[56-170] By using these methods, crystals of diameter exceeding 100 mm can be grown.

- Vertical Bridgman (VB) method

Kyle et al.[57] have grown CdTe single crystals using a modified VB method in a furnace as shown in Fig. 15.3, in which the Cd or Te reservoir temperature was controlled in order to vary the stoichiometry.

Oda et al.[64, 65] were the first to grow large CdTe single crystals up to 40-75 mm diameter applicable as industrial substrates as shown in Fig. 15.4. High quality crystals with EPD less than 10^4 cm^{-2}, X-ray rocking curve width less than 20 arcsec and without mosaic structure have been grown using purified Cd and Te sources.

Mochizuki et al.[70] have grown CdTe crystals while controlling the temperature of

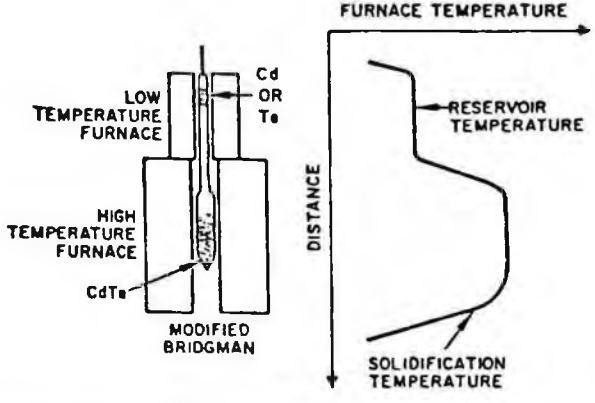

Fig. 15.3 Schematic illustration of apparatus used in the modified Bridgman method for growth of single crystals together with the temperature profile (reprinted from Ref. 57 with permission of The Electrochemical Society).

Table 15.3 Vertical Bridgman (VB) and Vertical Gradient Freezing (VGF) Methods for CdTe and CdZnTe

Method	Results	Authors	Year	Ref.
VB	Growth of CdTe and the measurement of physical properties	Yamada	1960	56
VB	Modified VB, defect chemistry and electrical properties	Kyle	1971	57
HP-VB	Composition analysis after melt growth	Kikuma et al.	1973	58
VB	Comparison with zone refining	Triboulet et al.	1973	59
VB	Growth of $CdTe_{1-x}Se_x$ ($0.05 \leqq x \leqq 0.15$)	Klausutis	1975	60
VB	CdTe single crystals of 15 cm^2	Wood et al.	1982	61
VB	25 mm diameter CdTe growth under different Cd(Te) overpressure	Muranevich et al.	1983	62
VB	Interface shape study using In radiotracer	Route et al.	1984	63
VB	40-50 mm diameter CdTe with low EPD	Oda et al.	1985	64
VB	75 mm diameter CdTe with low EPD	Oda et al.	1986	65
VB	Modified VB, CdZnTe single crystals of 10-12 cm^2	Bell et al.	1985	66
VB	Growth of CdTe and mixed crystals	Lay et al.	1986	67
VB	50 mm diameter CdTe with seeding	Masa et al.	1986	68
VGF	First growth of CdZnTe by the modified VGF method	Trivedi et al.	1987	135
VGF	p-type CdTe and the relationship between the resistivity and PL intensity	Seto et al.	1987	136
VB	Growth of CdZnTe using a CdZnTe seed	Kennedy et al.	1988	69
VB	CdTe growth with Cd or Te reservoir	Mochizuki et al.	1988	70
VB	Computer controlled multiple-zone VB furnace, growth of 50 mm diameter crystals	Sen et al.	1988	71
VB	Modified VB under Cd pressure control	Wen-Bin et al.	1988	72
VB/VGF	Slow cooling rate, effect of Zn doping for EPD reduction	Tanaka et al.	1988	137
HP-VB	High pressure vertical Bridgman method	Raiskin et al.	1988	102
VGF	75 mm diameter crucible, 75 mm square single crystal	Tanaka	1988	138
VB	Optical studies of the impurity distribution	Becker et al.	1989	73
VB	Effect of residual gas pressure on the resistivity	Yokota et al.	1989	74
VGF	CdTe co-doped with Zn and Se	Tanaka et al.	1989	139
VB	Moving the furnace to prevent mechanical disturbance	Bruder et al.	1990	75
VB	CdTe crystal growth by a multi-zone Bridgman furnace, mechanism of sticking of the grown ingot to the ampoule wall	Yasuda et al.	1990	76
VB	Coupled vibrational stirring method applied to VB growth of CdTe	Lu et al.	1990	77
VB	Effect of low temperature gradient on the crystal quality	Muhlberg et al.	1991	78
VGF	<111> seeding VGF, 50 mm in diameter, 40 mm in length	Azoulay et al.	1990	140
VB	CdTe-MnTe phase diagram, growth of (Cd, Mn) Te crystals	Triboulet et al.	1990	33
VGF	CdZnTe growth with a Zn/Cd reservoir for homogenizing the Zn distribution	Azoulay et al.	1991	141
VB	Growth by VB and characterization by TEM	Sabinina et al.	1991	84
VB	Fundamental investigation of various factors	Rudolph et al.	1992	79
VGF	Cl-doped CdTe, electrical properties in crystals	Suzuki et al.	1992	145
VB	Effect of the aspect ratio of the ingot on the interface shape	Pfeiffer et al.	1992	80
VB	Comparison of defect formation with THM grown crystals	Milenov et al.	1992	85
VB	50 mm diameter 120 mm length, $CdCl_2$ or CdI_2 doping	Milenov et al.	1992	86
VB	V-doped semi-insulating (SI) crystals	Launay et al.	1992	120
HP-VB	Growth of CdZnTe with full composition range	Doty et al.	1992	103

Table 15.3 Vertical Bridgman (VB) and Vertical Gradient Freezing (VGF) Methods for CdTe and CdZnTe (continued)

Method	Results	Authors	Year	Ref.
VGF	Zn segregation under Cd/Zn pressure control	Azoulay et al.	1992	142
VGF	Correlation between crystal quality distribution and interface shape	Azoulay et al.	1992	143
VGF	Growth of cubic $Cd_{0.6}Zn_{0.4}Te$ under a low axial temperature gradient (3 °C/cm)	Azoulay et al.	1993	144
HP-VB	CdZnTe growth of resistivity higher than $10^{11}\,\Omega \cdot cm$ without impurity doping	Butler et al.	1993	104
VB	Correlation between superheating and supercooling	Muhlberg et al.	1993	81
VB	64 mm diameter CdTe in a multi-zone furnace	Casagrande et al.	1993	87
VB	Discussion of the basic problems of VB methods	Rudolph et al.	1993	82
VB	Effect of the Cd vapor pressure and the CdTe melt surface temperature on the stoichiometry	Rudolph et al.	1994	83
VB	Thermally-annealed VB crystals grown with Cl, In doping	Alexiev et al.	1994	122
VB	3 kg ingots of 64 mm diameter	Casagrande et al.	1994	88, 89
VB	Growth of CdTe doped with V, Zn and Cl	Steer et al.	1994	90
VB	Large-scale VB method, 6 kg ingots of 100 mm diameter	Neugebauer et al.	1994	91
VB	Homogenization of Zn in CdZnTe using (Cd, Zn) alloy source in touch with the melt	Lee et al.	1995	92
VB	Application of ACRT for Zn homogenization	Capper et al.	1995	93
VB	CdTe, CdZnTe doped with V, Co, Ni	Aoudia et al.	1995	121
VGF	100 mm diameter CdZnTe and characterization	Asahi et al.	1995-1996	146-147
HP-VB	Growth of p-type semi-insulating CdZnTe with $0.2 < x < 0.4$	Kolesnikov et al.	1997	105
VB	Segregation reduction by melt supply from a second crucible	Tao et al.	1997	94
VB	In-situ synthesis, Cd vapor control and pBN crucible low Cu impurity crystals	Glass et al.	1998	95
VGF	Large-scale VGF with 2 kg charge, growth from the melt surface	Ivanov	1998	148
VGF	26 mm in diameter, 50-60 mm in length, effect of growth parameters on the crystal/melt interface shape	Okano et al.	2002	149
VB	Growth of high-resistive CdZnTe from Cd rich material	Li et al.	2001	96
VB	Growth of In-doped CdZnTe	Li et al.	2004	97
VB	Effect of the Zn composition on the crystal quality	Li et al.	2004	98
LE-VB	Undoped semi-insulating CdTe from stoichiometry-controlled material by the LE-VB method	Zha et al.	2002	99, 100
VB	Effect of In doping on the properties of CdZnTe	Yang et al.	2005	101

VB: Vertical Bridgman, VGF: Vertical Gradient Freezing, HP-VB: High-Pressure VB, LE-VB: Liquid Encapsulated VB

the Cd or Te reservoir in order to examine the effect of stoichiometry on the resistivity. Sen et al.[71] have developed a multi-zone furnace in order to control the temperature profile precisely as shown in Fig. 15.5. Bruder et al.[75] have grown CdZnTe single crystals weighing 1.5 kg and of diameter 47 mm and length 280 mm in a graphitized quartz ampoule. In order to avoid mechanical disturbance, the furnace is moved while the ampoule is fixed. Yasuda et al.[76] have controlled the temperature gradient from 26 to 0 °C/cm They examined the mechanism of the grown crystal sticking to the quartz am-

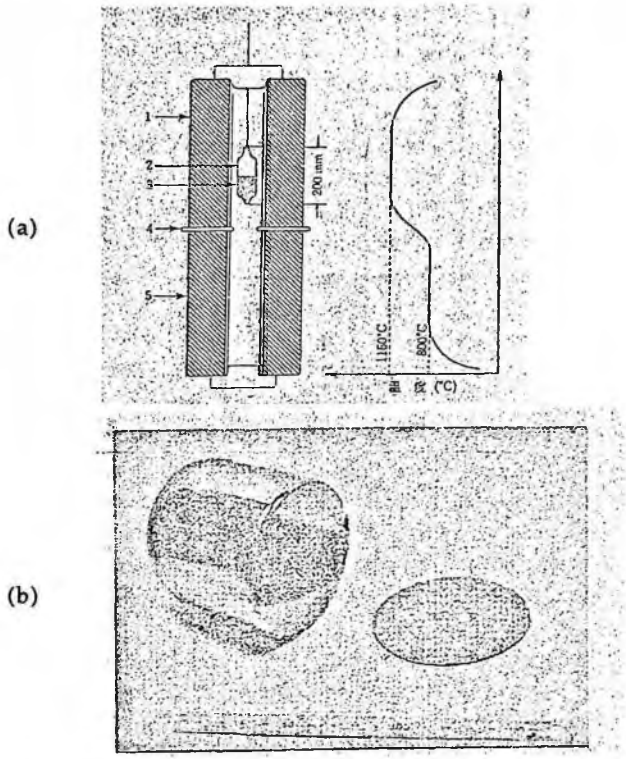

Fig. 15.4 (a) Vertical Bridgman furnace. 1: upper furnace, 2: quartz ampoule, 3: CdTe, 4: reflection plate, 5: lower furnace. (b) 75 mm diameter CdTe ingot and single crystal wafer (from Ref. 65 with permission).

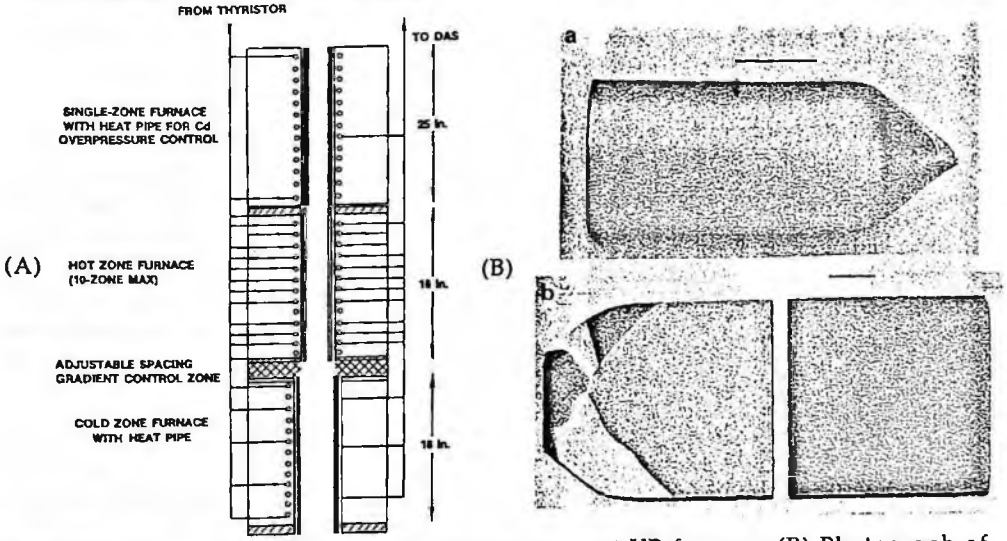

Fig. 15.5 (A) Schematic diagram of multiple-segment VB furnace. (B) Photograph of $Cd_{0.96}Zn_{0.04}Te$ boule (a) and longitudinal cut section showing favorable grain selection (b). Markers represent 25 mm (reprinted from Ref. 71 with permission, copyright 1988 Elsevier).

poule wall and found that the use of a pBN crucible is effective in avoiding this problem. Lu et al.[77] have applied coupled vibrational stirring (CVS) to the vertical Bridgman method as shown in Fig. 15.6 and examined its effect on the distribution of doped phosphorus.

Rudolph et al.[78-83] systematically studied various growth factors, using the a modified vertical Bridgman assembly as shown in Fig. 15.7. They clarified the effects of superheating on supercooling, the Cd vapor pressure and the CdTe melt surface temperature on the stoichiometry, the segregation behavior of the excess component, and the distribution of impurities, precipitates, and vacancies. These effects were analyzed with attention to thermodynamical considerations and stoichiometry.

Casagrande et al.[87-89] have grown $Cd_{0.96}Zn_{0.04}Te$ single crystals by the VB method with a computer controlled furnace. 3 kg ingots of diameter 64 mm have been grown. Neugebauer et al.[91] have developed a large-scale VB furnace in order to grow 6 kg ingots with diameters as large as 100 mm and routinely produced 4x6 cm^2 (Cd, Zn)Te substrates.

Capper et al.[93] have applied the accelerated crucible rotation technique (ACRT) to the VB method in order to homogenize the Zn concentration distribution. Glass et al.[95] have grown CdZnTe single crystals by a modified Bridgman method, using in situ synthesis, Cd vapor-pressure control and pBN crucibles. It was found that low Cu impurity crystals can be grown.

Li et al.[96-98] have grown 20ϕ x 50 mm $Cd_{0.8}Zn0.2Te$ single crystals from Cd rich material by a modified Bridgman method. In order to make sure that the cadmium vapor pressure remains uninterrupted, excess Cd is added to the stoichiometric starting material. They also examined the effect of the Zn composition on the crystal quality.

Zha et al.[99, 100] have grown semi-insulating (SI) CdTe crystals by the B_2O_3 encapsulated VB method under nitrogen pressure of 5 atm., using an open quartz ampoule. It was found that the yield of SI crystal growth was about 50 %.

Simulation studies on heat transfer, thermal convection, crystal-melt interface shape, and thermal stress in crystals have also been made for the VB method.[36, 123-134]

- *High Pressure Vertical Bridgeman (HP-VB) method*

The HP-VB method has been developed in order to obtain undoped semi-insulating (SI) CdTe.[102-119] Raiskin[102] has developed a method in which crystal growth is performed in a high pressure vessel using unsealed ampoules. Doty et al.[103] have grown CdZnTe over the full range of alloy composition. This was done without the use of sealed ampoules. Undoped semi-insulating CdZnTe single crystals whose resistivity exceeded 109 $\Omega \cdot$ cm for radiation detectors could be obtained.[104, 105] The present status of HP-VB CdZnTe crystals is summarized by James.[106] These SI CdTe and CdZnTe crystals have been evaluated by various methods.[109-119]

- *Vertical Gradient Freezing (VGF) method*

Tanaka et al.[136-139] have grown CdTe single crystals by the VGF method. They also have grown CdTe crystals co-doped with Zn and Se in order to obtain crystals lattice match-

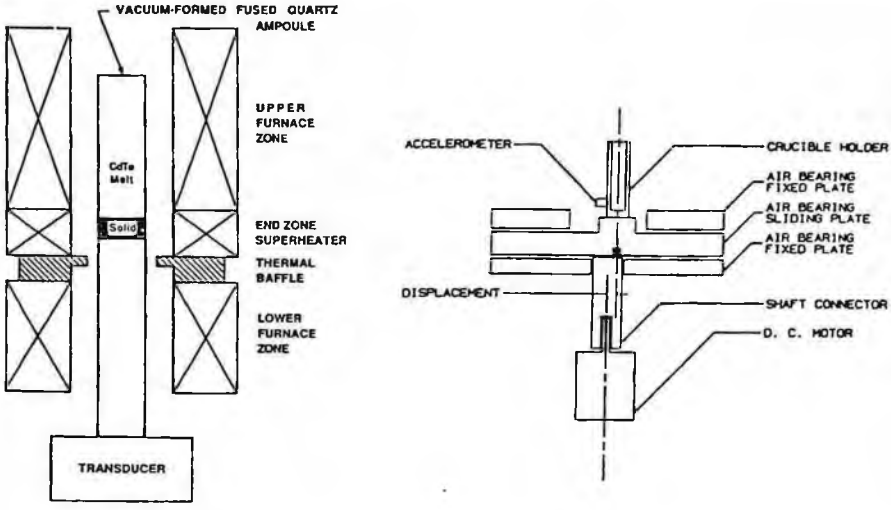

Fig. 15.6 (a) Schematic diagram of a vertical Bridgman (VB) growth furnace and (b) coupled vibrational stirring (CVS) apparatus (reprinted from Ref. 77 with permission, copyright 1990 Elsevier).

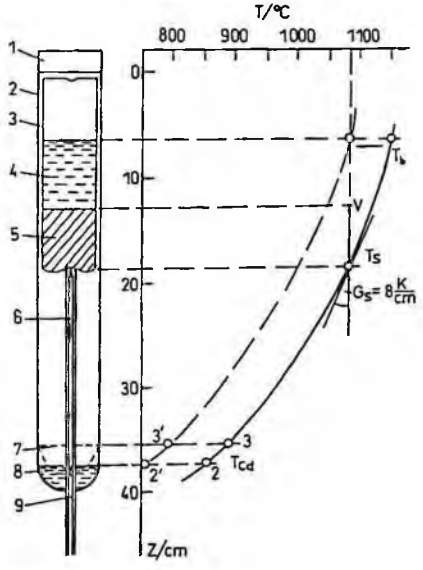

Fig. 15.7 Vertical Bridgman growth arrangement for CdTe. (a) plug, (2) outer silica container, (3) inner silica growth ampoule, (4) CdTe melt, (5) solidified fraction of CdTe, (6) capillary with thermocouple, (7, 8) position of Cd source, (9) thermocouple. Gs, temperature gradient at the interface; Th, the temperature at the CdTe melt surface (reprinted from Ref. 83 with permission, copyright 1994 Elsevier).

ing with HgCdTe. Azoulay et al.[140-144] developed systematically the VGF method not only for CdTe but also CdMnTe. Suzuki et al.[145] have developed semi-insulating CdTe by the VGF method.

Asahi et al.[146, 147] finally succeeded in growing 100 mm diameter, 50 mm long $Cd_{0.97}Zn_{0.03}Te$ single crystals as shown in Fig. 15.8 by the optimized VGF method. They were able to grow <111> oriented single crystals with no twins or polycrystals throughout the ingot except for the 5 mm thick tail part.

Ivanov[148] has developed a large-scale VGF method as shown in Fig. 15.9. In this method, unseeded crystals were grown from the surface of the melt, firstly from the center to the periphery on the melt surface and then from the surface to the bottom. Okano et al.[149] have developed a VGF method and compared the simulation result with the experimental one.

- Doping for semi-insulating CdTe

Yokota et al.[74] have grown In-doped CdTe crystals from a Te excess melt. Alexiev et al.[120] have grown Cl- and In-doped crystals and evaluated their radiation detector performance. Launay et al.[121] and Audia et al.[122] studied V-doping and Alexiev et al.[120] studied Cl-, In-doping for obtaining semi-insulating CdTe and have evaluated the properties of the crystals grown.

(2) Horizontal Bridgman (HB) and Horizontal Gradient Freezing (HGF) methods

In the HB and HGF methods (Table 15.4), it is very difficult to control the solid/liquid interface because the melt is put in a horizontal boat and the melt surface is exposed to the gas phase so that the solid/liquid interface is also exposed to the gas phase. Since the heat radiation from the melt surface is large, the solid/liquid interface is not perpendicular to the direction of growth but is inclined to the surface. Polygonization therefore happens easily. For these reasons, these methods are not industrially applied. The following researches have been reported.

Matveev et al.[150-152] attempted crystal growth using a HGF furnace under Cd overpressure control as shown in Fig. 15.10. It was shown that the type of conduction and carrier concentration could be varied by changing the Cd overpressure. Matveev also examined the convection flow in the growth crucible in the arrangement as shown in Fig. 15.10.

Khan et al.[153] have grown CdTe crystals using the HB method. The 5 cm diameter semi-round quartz boat was sealed in an evacuated quartz ampoule and the furnace was moved according to a pre-programmed sequence. The growth was seeded in the <110> direction but no attempt was made to provide Cd overpressure. Crystals with low EPD of the order of 10^4 cm^2, high resistivity of the order of 10^7 Ω·cm and X-ray rocking curve FWHM of 9 arcsec could be obtained.

Lay et al.[154] have grown CdTe crystals (Fig. 15.11) having EPD as low as 2×10^4 cm^{-2} and with X-ray rocking curve FWHM as low as 10 arcsec, by using a ten-zone HB furnace. Crystal growth was performed without seeding by gradient freezing.

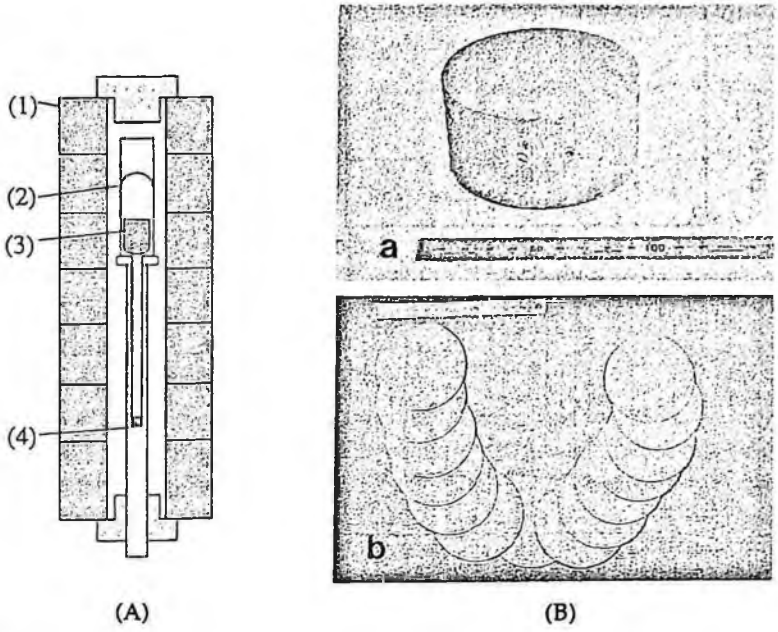

Fig. 15.8 (A) Schematic diagram of the VGF furnace; (1) multiple-zone heater, (2) quartz ampoule, (3) CdTe, (4) Cd reservoir. (B) Photograph of a VGF grown $Cd_{0.97}Zn_{0.03}Te$ single crystal. (a) 100 mm diameter CdTe ingot after cylindrical grinding, (b) <111> wafers sliced from top to tail (reprinted from Ref. 146 with permission, copyright 1995 Elsevier).

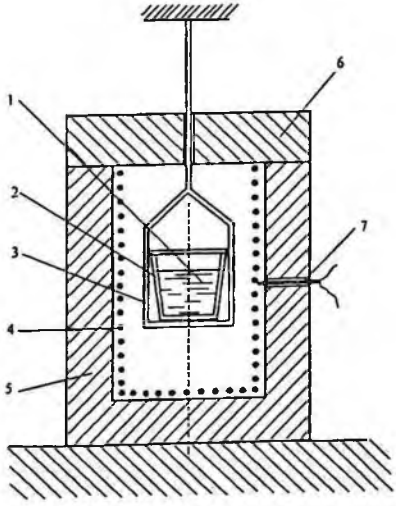

Fig. 15.9 Large-scale VGF furnace: (a) CdTe melt, (2) crucible with a lid, (3) protective ampoule, (4) heater, (5) heat insulation, (6) furnace cover (heat inclusion) and (7) thermocouple (reprinted from Ref. 148 with permission, copyright 1998 Elsevier).

Table 15.4 Horizontal Bridgman (HB) and Horizontal Gradient Freezing (HGF) Methods for CdTe and CdZnTe

Method	Result	Authors	Year	Ref.
HGF	Directional cooling under a constant Cd vapor pressure	Matveev et al.	1969	150
HB	EPD~10^4 cm^{-2}, FWHM 9 arcsec	Khan et al.	1986	153
HB	EPD~$2x10^4$ cm^{-2}, FWHM 10 arcsec, single crystal 75 %	Lay et al.	1988	154
HB	28 cm^2 (111) substrates obtained by optimizing the growth conditions	Cheuvart et al.	1990	155
HB	Effect of purity on the resistivity	Yokota et al.	1990	156
HB	Examination of temperature profile	Rudolph et al.	1994	50
HGF	Effect of convective flow on the carrier distribution	Matveev et al.	1994	151
HGF	Effect of temperature gradient and Cd vapor pressure on the carrier distribution	Matveev et al.	1995	152

Cheuvart et al.[155] used a multi-zone HB furnace, a transverse gradient freezing technique, and a seed crystal and controlled the Cd vapor pressure. Optimizing the growth conditions, they obtained (111) semi-insulating substrates up to 28 cm^2, of resistivity 10^6 Ω·cm and with an X-ray rocking curve FWHM of about 70 arcsec.

Yokota et al.[156] prepared high resistive CdTe in quartz ampoules evacuated to vacuum using a HB method. They showed that increasing the vacuum level of the ampoules increased the resistivity up to 10^7 Ω·cm. This was attributed to the residual oxygen which reacts with Te.

(3) Liquid Encapsulated Czochralski (LEC) method

The LEC method has been applied to the growth of CdTe crystals (Table 15.5) in the past but it was unsuccessful.[47, 60, 157] This is due to the tendency of CdTe to form twins.

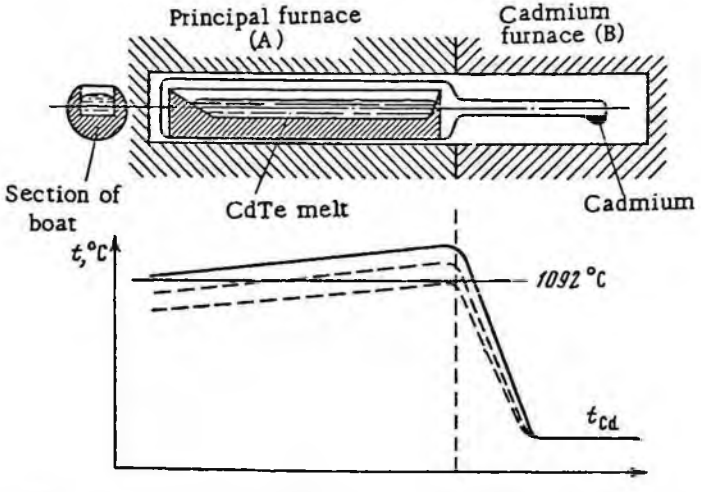

Fig. 15.10 Diagrams of apparatus for directional cooling of CdTe melt (from Ref. 150 with permission).

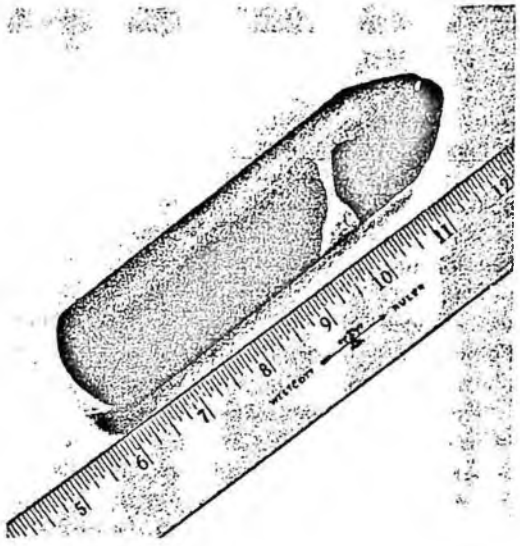

Fig. 15.11 CdTe ingot grown by a horizontal Bridgman (HB) method (reprinted from Ref. 154 with permission, copyright 1988 Elsevier).

Hobgood et al.[158] used the LEC method (Fig. 15.12) to grow CdTe and $Cd_{1-x}Mn_xTe$ (CMT) under an axial temperature gradient of about 450 °C/cm under an Ar atmosphere at 20 atm. The CdTe crystals that were grown became polycrystals (Fig. 15.13) and CMT crystals had large amounts of twins (Fig. 15.14). No single crystals could be obtained. Blackmore et al.[159] showed a significant incorporation of boron to CdTe crystals from the encapsulant. Kotani et al.[160, 161] have grown a CMT single crystal of diameter 45 mm and length 50-60 mm with an axial temperature gradient of 30-46 °C/cm by optimizing the growth conditions.

Only a few attempts at LEC crystal growth have been reported as explained above and it has been concluded that the method is not appropriate for growing CdTe and related materials because of the following reasons.

(i) The thermal conductivity of CdTe is lower than that of B_2O_3 so that there is little thermal conduction through a seed crystal.

(ii) The III group element, boron, is incorporated from B_2O_3 and it acts as a donor so changing the electrical properties.

(iii) The axial temperature gradient of the LEC method is normally high (150-450 °C/cm) so that the dislocation densities are greatly increased because the critical resolved shear stress of CdTe is very small.

In fact, the analysis of heat transfer in the LEC growth of CdTe made it clear that heat flow at the CdTe interface is about 50 times lower than that in the growth of GaAs. Most of the heat transfer occurs in the encapsulant B_2O_3 layer and the heat flow through the grown crystal is too low for the growth of single crystals.[35]

For these reasons, the growth of CdTe and related materials by the LEC method has

Table 15.5 Liquid Encapsulated Czochralski (LEC) Method and Other Methods

Method	Result	Authors	Year	Ref.
LEC	Growth of CdTe of 1x3 cm	Meiling et al.	1968	157
HZM	Effect of temperature gradient on the single crystal yield	Matveev et al.	1969	150
VZR	Sealed-ingot zone refining with vertical oscillations	Woodbury et al.	1971	165
VZM	Effect of zone melting on the purity of grown crystals	Triboulet et al.	1973	59
LEC	Growth of $CdTe_{1-x}Se_x$ ($0.05 \leq x \leq 0.15$)	Klausutis	1975	60
VZR	Purity improvement by zone passing technique	Triboulet	1977	166
LEC	Growth of CdTe with B_2O_3 encapsulant	Mullin et al.	1979	47
ZL	Growth of MnCdTe, CdSeTe and ZnCdTe	Lay et al.	1986	67
SSSR	Self-sealing growth under 5-7 atm. N_2 overpressure	Fitzpatrick et al.	1986	170
LEC	Boron segregation in LEC CdTe crystals	Blackmore et al.	1987	159
LEC	Growth of CdTe and CdMnTe by B_2O_3 encapsulated LEC	Hobgood et al.	1987	158
LEC	Growth of CdMnTe of 30-40 mm diameter	Kotani et al.	1987	160, 161
HEM	Growth of 7.5 cm diameter CdTe ingots	Khataak et al.	1989	168
LEC	Growth of CdTe and CdMnTe by B_2O_3 encapsulated LEC	Thomas et al.	1990	35
Casting	High resistive CdTe by casting and unidirectional solidification	Rudolph et al.	1995	169
VZM	Growth of CdZnTe and the distribution of Zn	Bueno et al.	2000	167

HZM: Horizontal Zone Melting, VZM: Vertical Zone Melting, VZR: Vertical Zone Refining, ZL: Zone Leveling, SSSR: Self-Sealing Self-Releasing, HEM: Heat Exchange Method

almost been abandoned. For LEC growth to be successful, heat transfer must be improved.

(4) Other Melt Growth Methods

-Zone-melting

Matveev[151] first applied the Horizontal Zone Melting (HZM) method to grow CdTe

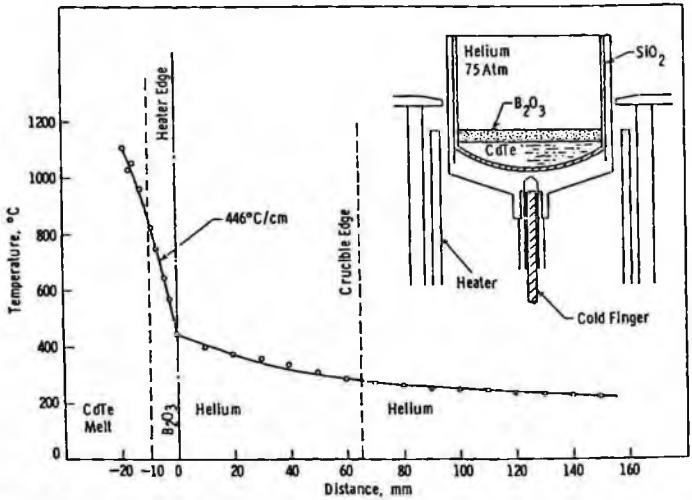

Fig. 15.12 Axial temperature distribution conductive to growth of large LEC CdTe boules (reprinted from Ref. 158 with permission, copyright 1987 Elsevier).

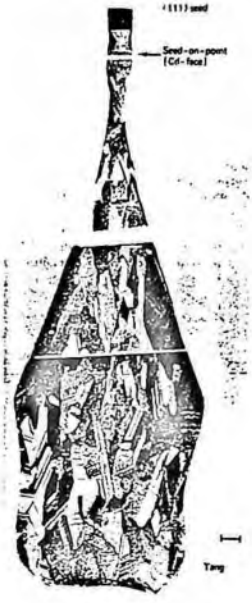

Fig. 15.13 Axial cross section of LEC CdTe boule. Marker represents 5 mm (reprinted from Ref. 158 with permission, copyright 1987 Elsevier).

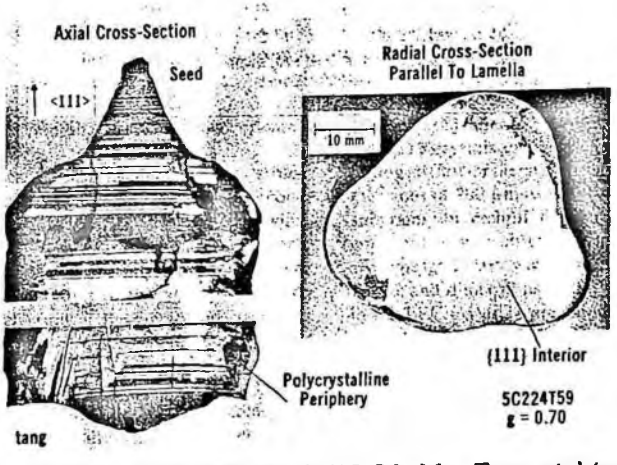

Fig. 15.14 Axial and radial cross sections of LEC $Cd_{0.9}Mn_{0.1}Te$ crystal (reprinted from Ref. 158 with permission, copyright 1987 Elsevier).

crystals using a furnace as shown in Fig. 15.15. Woodbury et al.[165] have applied the sealed-ingot zone melting method (Sec. 2.2.2 (3)) using a furnace arrangement as shown in Fig. 15.16, imposing large vertical oscillations during the last zone pass and grew CdTe single crystals of volume 10 cm^3. The segregation of Fe, Co, Sn, W and Bi has been investigated using their radiotracers. Triboulet et al.[59,166] also applied the same

method in order to examine the influence of the growth conditions on the electrical properties. It was however difficult to obtain high resistive CdTe reproducibly by this method. Bueno et al. applied the zone-melting method to the growth of $Cd_{1-x}Zn_xTe$ single crystals with high Zn concentrations ($0.45 < x < 0.85$) and it was found that Te precipitate formation depends largely on the Zn concentration.

- Heat Exchange Method (HEM)

Khattak and Schmid[168] used the HEM (Sec. 2.2.6) and obtained CdTe ingots weighing 1300 g and measuring 7.5 cm in diameter . It was found that large grains could be obtained whose EPD was in the range 10^3 to $5x10^5$ cm^{-2} and whose resistivity was 10^5 $\Omega \cdot cm$.

- Casting

Rudolph et al.[169] have grown radiation detector grade CdTe by a casting and unidirectional solidification method as shown in Fig. 15.17. Crystals with average resistivity of $5x10^9$ $\Omega \cdot cm$ could be obtained. The advantage of this method is that CdTe crystals of shape and size necessary for radiation detectors can be grown by casting.

- Self-Sealing and Self-Releasing (SSSR) method

A low pressure melt growth method, the SSSR has been developed for the growth of ZnSe (Sec. 17.3.1(4)).[170] This method is based on growth in a graphite crucible sealed

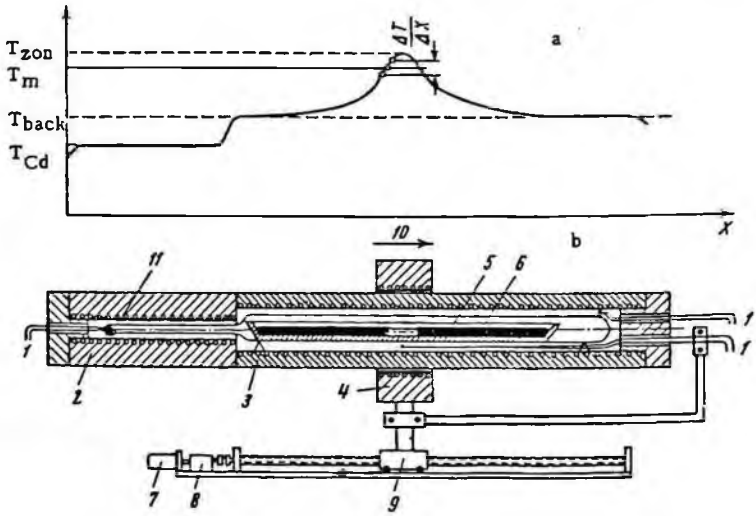

Fig. 15.15 Diagram of apparatus for zone melting CdTe crystal growth. (a) Temperature profile, (b) apparatus arrangement; 1: thermocouple, 2: furnace for control of CdTe vapor pressure in tube, 3: background furnace, 4: zone furnace, 5: quartz tube, 6: graphite boat containing CdTe, 7: motor, 8: reduction gear, 9: trolley for moving zone furnace, 10: direction of motion of zone, 11: excess Cd (from Ref. 150 with permission).

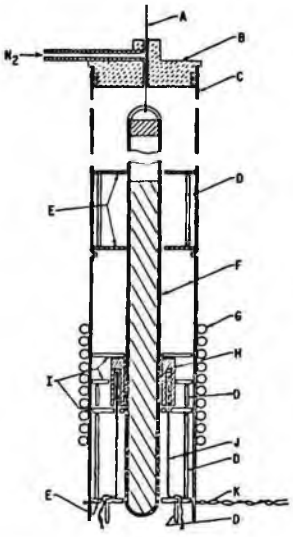

Fig. 15.16 Sealed-ingot zoning apparatus of CdTe. A: nylon string to puller wheel, B: metal cup with O-ring seal, C: quartz envelope, D: quartz tubing for vertical spacing and support, E: ceramic disks, F: quartz sealed CdTe ingot, G: rf induction coil, H: graphite susceptor, I: quartz disk, J: thermocouple (reprinted from Ref. 165 with permission, copyright 1971 Elsevier).

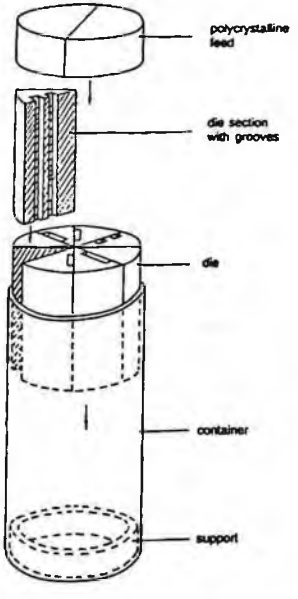

Fig. 15.17 Schematic drawing of the crystal growth arrangement by casting with ampoule diameter of 40 mm (reprinted from Ref. 169 with permission, copyright 1995 Elsevier)

by the condensed vapor of the constituents of the II-VI compound as described by Fitzpatrick et al.[170] and shown in Fig. 17.12. This method has been applied to the growth of CdTe and the possibility of in-situ synthesis has been suggested.

15.3.2 Solution Growth

(1) Traveling Heater Method (THM)

Since the THM is effective in purification, it is mainly applied to the growth of high resistive materials which are used for radiation detectors. Many studies have been reported using the THM method, mainly by the group of Wald in USA, Triboulet and Siffert in France and Taguchi in Japan. The studies of THM methods are summarized in Table 15.6.[171-196]

Te is mainly used as the solvent for the THM and donor impurities such as In or Cl are doped in order to obtain high resistive materials. When dopants such as Cl or In whose distribution coefficients are less than 0.1 are used, high resistive crystals with good uniformity from top to tail can be obtained. This is because the concentration of dopants in the Te solvent zone which moves from tail to top does not change during growth. THM is thus believed to be an appropriate method for preparing high resistive materials of good uniformity.

Bell et al.[171] have first applied the THM which was invented for growing GaP to CdTe (Fig. 15.18(a)). Wald and Bell[176] have grown CdTe by THM using accelerated rotation (Fig. 15.18(b)) in order to control the forced convection. Wald[178] has grown CdTe using In as solvent and shown that high resistive compensated material can be obtained. Tranchart and Bach[179] have developed a gas bearing system for the growth of CdTe by THM and have grown undoped and halogen doped CdTe crystals. Taguchi et al.[180] have grown high resistive CdTe crystals, examined their electrical and optical properties, and have applied this crystal to gamma-ray detectors. Dinger and Fowler[181] have examined the occurrence of Te inclusions in THM and shown how to grow crystals free from inclusions.

Triboulet and Marfaing[185] have grown CdTe by the multipass THM as shown in Fig. 15.19(a). Triboulet et al. [186] have grown a complete series of $Cd_{1-x}Zn_xTe$ ($0 \leqq x \leqq 1$) crystals by a single THM pass, and studied the properties in the whole composition range. Triboulet et al.[187] have grown CdTe using Cd as the solvent and compared the physical properties with CdTe grown from a Te solution.

Schoenholz et al.[188] have applied a mirror heating method as seen in Fig. 15.20 for growing CdTe by the THM. Mochizuki et al.[189] have compared solution-grown CdTe and THM-grown CdTe from the viewpoint of point defects and of the nuclear response. Bigrali et al.[190] have grown high resistive CdTe doped with Cl and examined the mechanism of the electrical properties.

Trioulet et al.[191] have invented a method which is called as the "Cold Travelling Heater Method (CTHM)" as shown in Fig. 15.19(b) in which synthesis and purification can be simplified. As shown in the figure, Cd and Te raw materials can be charged directly in the ampoule and the solution zone has an effect in purification. Sabina et al.[84] have grown CdTe crystals by the Bridgman method and THM and compared the

Table 15.6 Solution Growth Methods for CdTe Crystal Growth

Method	Result	Authors	Year	Ref.
SG	Solubility in Sn, Cd, Bi. Growth of small crystals	Rubenstein	1968	201
THM	Net carrier concentrations less than 10^{11} cm^{-3}	Bell et al.	1970	171
SG	Growth from Te solution, segregation coefficient measurement	Zanio	1974	202
THM	High purification before THM growth	Triboulet et al.	1974	174
THM	Te and $CdCl_2$ solution	Taguchi et al.	1974	175
SG	Growth from Te solution doped with halogens	Hoschl et al.	1975	203
THM	Calculation of natural and forced convection	Wald et al.	1975	176
THM	Room temperature resistivity ~$10^6 \Omega \cdot$cm	Taguchi et al.	1976	177
THM	Growth from In solvent	Wald	1976	178
THM	Gas bearing system for THM	Tranchart	1976	179
THM	Growth from Te-solution	Taguchi et al.	1977	166
THM	Te-solution THM under Cd vapor control	Taguchi et al.	1977	180
SG, THM	10 mm diameter crystal growth	Dinger et al.	1977	181
SG	Growth from Te solution, 45 mm x 150 mm	Schaub et al.	1977	204
SE	Evaporation of Cd by controlling Cd vapor pressure	Lunn et al.	1977	205
THM	Semi-insulating crystal with Tl doping	Wald et al.	1977	182
THM	Semi-insulating crystals grown by optimizing the growth conditions	Taguchi et al.	1978	183
THM	Growth parameters and micro-precipitate concentrations	Jougler et al.	1980	184
MTHM	Purification by multipass process	Triboulet et al.	1981	185
SE	Crystals doped with In, Ga, Cl, Cr	Mullin et al.	1982	207
THM	Growth of Cd1-xZnxTe alloys with $0 < x < 1$	Triboulet et al.	1983	186
SE	Growth of CdTe from Cd-rich solvent	Vere et al.	1985	208
THM	Growth from a Cd solvent	Triboulet et al.	1985	187
IR-THM	IR mirror radiation heating, seeding THM, 20 mm diameter and 60 mm length	Schoenholz et al.	1985	188
SG, THM	Growth from In-doped Te solution	Mochizuki et al.	1985	189
THM	Cl-doped high resistive CdTe	Biglari et al.	1987	190
CTHM	THM starting from constituent elements	Triboulet et al.	1990	191
THM, SG	Growth of CdMnTe for optical isolators	Onodera et al.	1991	192
THM	TEM investigation for grown crystals	Sabinina et al.	1991	84
THM	Doping with V, Zn and Cl	Steer et al.	1994	90
THM	Industrial growth of 75 mm diameter crystals Application to radiation detectors	Ohno et al.	1991-2000	193-196
SG	Growth of CdZnTe from Te solution	Suzuki et al.	1993	205
SE	Large scale growth up to 300 mm diameter	Pelliciari et al.	2005	209

SG: Solution Growth, SE: Solvent Evaporation, THM: Travelling Heater Method, CTHM: Cold THM, MTHM: Multipass THM

crystal quality by TEM observation.

The THM was however for a long time limited to small crystals of diameter 10 mm. Ohmori et al.[193, 194] however succeeded in growing large grain crystals of 32 mm diameter and 80 mm long as shown in Fig. 15.21. Ohno et al.[195, 196] succeeded in growing high resistive large diameter CdTe crystals on an industrial scale. Their grown crystals are shown in Fig. 15.22. They grew crystals up to 75 mm in diameter.

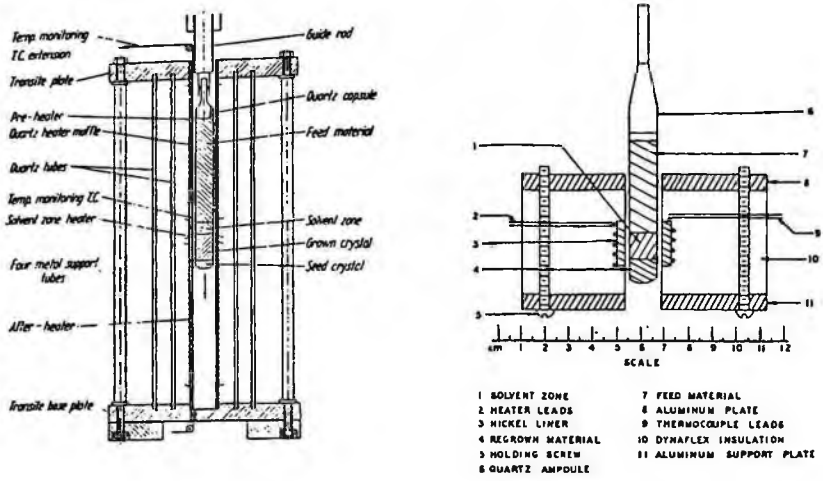

Fig. 15.18 Schematic THM growth furnaces. (a) from Ref. 171 with permission and (b) from Ref. 176 with permission, copyright 1975 Elsevier.

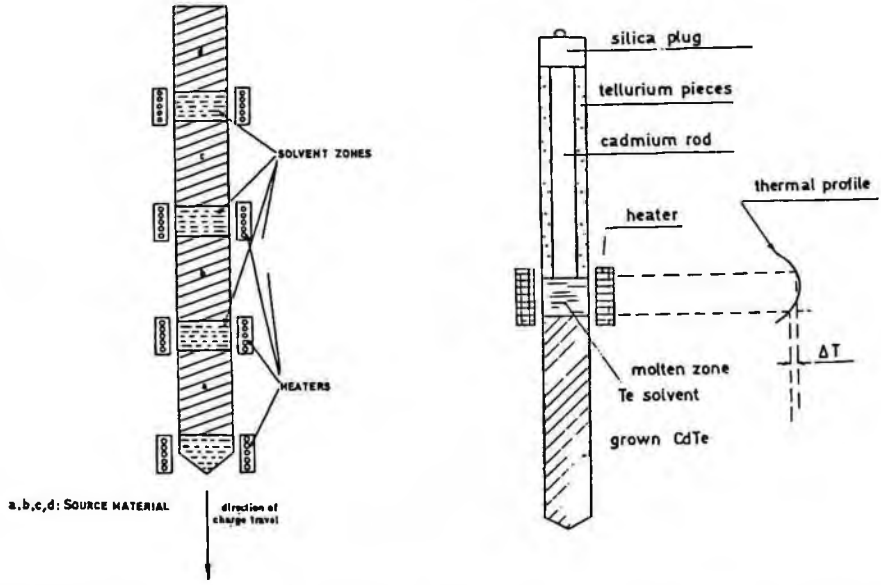

Fig. 15.19 (a) Multi-zone THM (reprinted from Ref. 185 with permission, copyright 1981 Elsevier) and (b) cold THM (CTHM)(reprinted from Ref. 191 with permission, copyright 1990 Elsevier).

Simulation studies on the temperature distribution,[197] melt convection[198] and heat and mass transfer during crystal growth[199] have been performed.

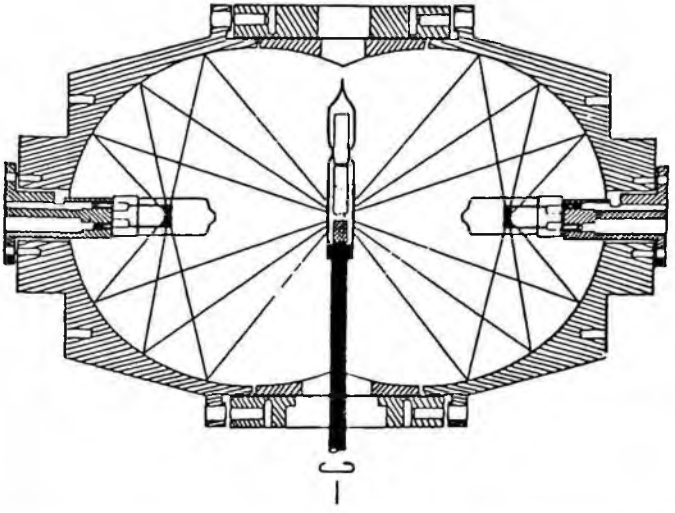

Fig. 15.20 Sketch of a THM mirror furnace with camera in front (reprinted from Ref. 188 with permission, copyright 1985 Elsevier).

(2) Other Solution Growth Methods

Zanio[202] applied a simple solution growth method for CdTe in the growth temperature range of 600-900 °C as shown in Fig. 15.23 and measured the segregation coefficient of various impurities. The solution VB method[203, 204] has also been examined for growing CdTe crystals. This method is a simple modification of the conventional VB method differing only by charging a Te rich solution in the ampoule instead of the close-stoichiometric melt. The crystal growth rate is of course lower but it is expected that the purity is improved because of the purification effect of the solvent Te. Hoschl et al.[203] have grown undoped CdTe and CdTe doped with halogens from a Te solution in a VB furnace by pulling up the ampoule with Cd and Te with Te in excess. The electrical properties of the crystals grown were examined precisely.

In-doped CdTe has been grown from a Te solution in order to obtain high resistive material for γ-ray detectors Mochizuki.[189]

Suzuki et al.[205] have grown $Cd_{1-x}Zn_xTe$ ($x < 0.2$) from a Te solution and determined the effective segregation coefficient of Zn as 1.62. It was also found that the EPD is of the order of 2.3×10^4 cm^{-2} and the purity is high with the residual impurity Cu of the order of 2×10^{14} cm^{-3}.

Lunn et al.[206-208] and successors applied the Solvent Evaporation (SE) method to grow CdTe crystals. As explained in Sec. 2.3.4, this method is based on the evaporation of the Cd solvent. The Cd concentration in the solution is decreased by evaporation so that CdTe crystals start to grow in the solution since the CdTe concentration exceeds the solubility limit. Pelliciari et al.[209] have recently developed a horizontal SE method by which 300 mm diameter crystals can be grown aiming at growing radiation grade high resistive crystals.

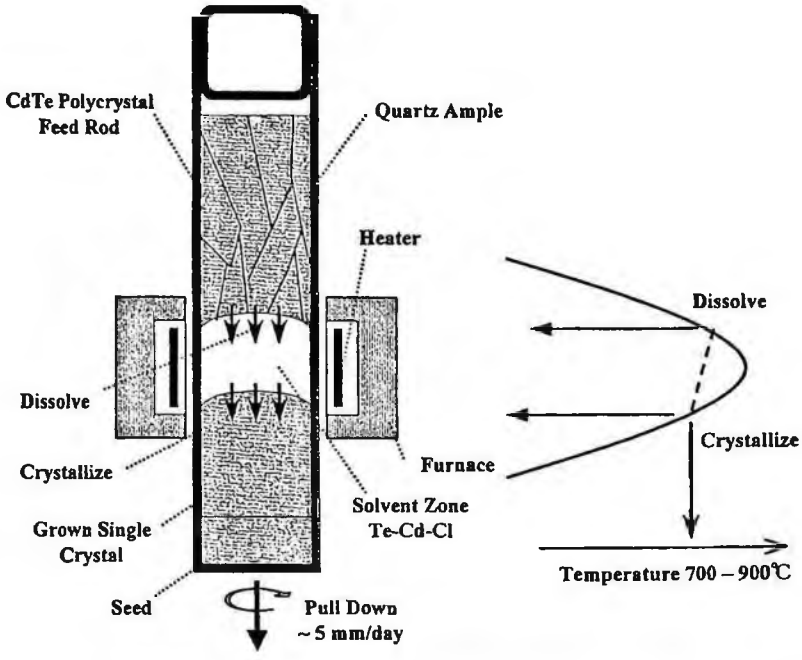

Fig. 15.21 Principle of CdTe radiation detector (from Ref. 196 with permission).

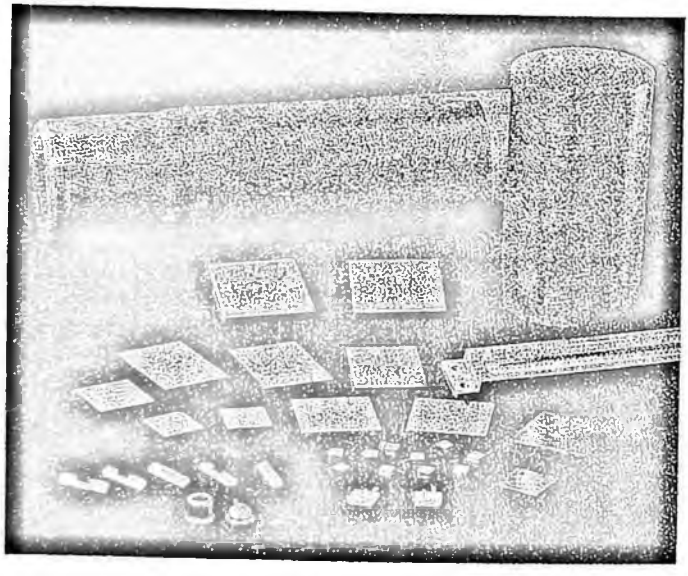

Fig. 15.22 Large diameter THM-grown CdTe crystal and wafers (from Ref. 196 with permission)

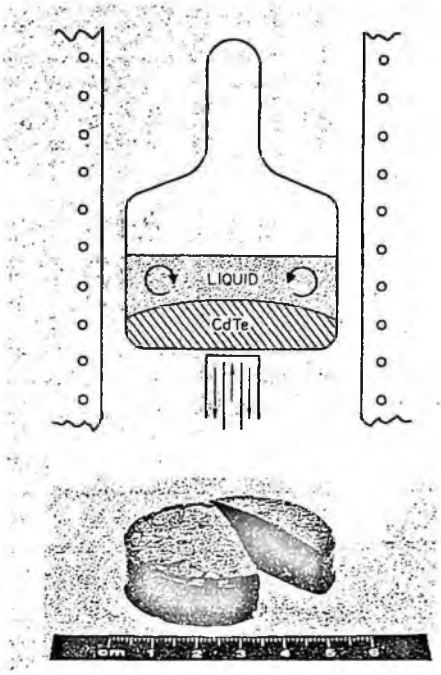

Fig. 15.23 (Top) schematic drawing of solution growth system and (bottom) 25 mm^3 CdTe boule which is 80% single crystal (reprinted from Ref. 202 with permission, copyright 1974 TMS).

15.3.3 Vapor Phase Growth

Vapor phase growth especially physical vapor phase growth has been extensively investigated in the past as summarized in Table 15.7. Among vapor phase growth methods, direct synthesis, chemical vapor transport, and sublimation recrystallization (physical vapor transport) have been investigated.

(1) Direct Synthesis (DS) method

Freiches[210] and Lynch[211] (Fig. 15.24) have synthesized CdTe by the direct reaction of Cd and Te vapors. Vanukov et al.[212] have made lamellar and acicular CdTe crystals by direct synthesis from Cd and Te vapors. They have examined the dislocation structures in crystals grown. Tuller et al.[213] have studied the growth of polycrystalline CdTe bulk materials by the reaction of Cd and Te vapors using a horizontal furnace, for preparing laser window materials. Polycrystalline blanks up to 15 cm^2 x 2 mm thick were grown at rates of 0.02-1.5 mm/hr.

(2) Physical Vapor Transport (PVT) method

CdTe source material is transferred by sublimation and recrystallized in a lower temperature part.

This method has the following advantages.

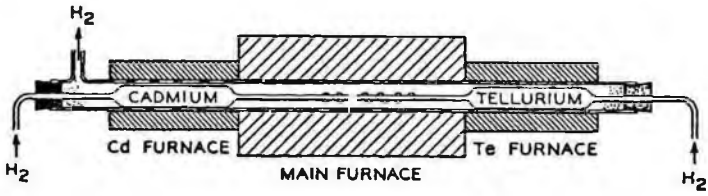

Fig. 15.24 Schematic diagram of apparatus for direct synthesis of CdTe (reprinted from Ref. 211 with permission, copyright 1962 American Institue of Physic).

(i) Crystal growth can be performed at relatively low temperatures.

(ii) The dissociation pressure of Cd is low and ampoule rupture does not occur. The apparatus can be made relatively simple.

(iii) The source material is sublimated so that there is a purification effect for impurities with low vapor pressures.

(iv) When the configuration for crystal growth is made in a way that there is no stress from the container, the dislocation density can be greatly reduced.

This method has however the disadvantage that the growth rate is extremely low. The method has however been extensively studied because high quality crystals can be obtained.

- Open tube PVT

In the early days of physical vapor transport growth of CdTe, crystals were grown in open tube furnaces. A typical example is shown in Fig. 15.25. This method has been studied using various carrier gases such as Ar, N_2, H_2S, H_2 and H_2S+H_2.[215-217]

- Closed tube PVT

Hoschl et al.[218-220] first applied the physical vapor transport method in closed tubes and examined the relationship between the total pressure and the partial pressure, and the dependence of growth rate on the pressure thermodynamically and experimentally.

Akutagawa and Zanio[221] applied the modified Piper-Polish method (Fig. 15.26) to the growth of CdTe and have grown large single crystals (< 3 cm^3). Lauer et al.[222] have applied the self-sealing Piper-Polish method (Fig. 15.27) to the growth of (Zn, Cd)S and (Zn, Cd)Te.

Igaki and Mochizuki[214, 223-227] have grown CdTe single crystals in a closed tube while controlling vapor pressure of one of the constituents as shown in Fig. 15.28(a), and have examined systematically the effect of the partial pressure on the growth rate and the growth mechanism. It was found that at lower partial vapor pressure, the surface reaction is rate-determining while at higher partial vapor pressure, diffusion in the vapor phase is rate-determining (Fig. 15.28(b)).

Buck et al.[228] first applied a vapor-pulling method in which the closed tube is moved

Table 15.7 Vapor Phase Growth of CdTe and CdZnTe

Method	Result	Authors	Year	Ref.
DS	Direct synthesis by the reaction of Cd vapor with H_2S	Frerichs	1947	210
DS, PVT open PVT	Growth of CdTe from elemental Cd and Te	Lynch	1962	211
open PVT	Growth of CdTe in an open tube furnace	Teramoto et al.	1963	215, 216
HPVT	Relationship between vapor pressures	Hoschl et al.	1963	218, 219
HPVT	Effect of vapor pressure on the growth rate	Hoschl et al.	1965	220
CVT	Growth in the Cd:Te:Cl system	Alferov et al.	1965	272
open PVT	Sublimation under various atmospheres, 8x6x3 mm^3 crystals	Corsini -Mena et al.	1971	217
HPVT	Modified Piper-Polish method, growth of $\leqq$ 250 mm^3 crystals	Akutagawa et al.	1971	221
HPVT	Modified Piper-Polish method for the growth of (Zn, Cd)Te	Lauer et al.	1971	222
CVT	Growth using NH_4Cl as the agent	Paorici et al.	1973	273
DS	Growth of CdTe from elemental Cd and Te	Vanyukov et al.	1975	212
HPVT	Growth under Te vapor pressure control	Igaki et al.	1974	223, 224
CVT	Growth in the system of Cd:Te:H:I	Paorici et al.	1974 1975	274, 275
DS	Growth of CdTe from elemental Cd and Te	Tuller et al.	1977	213
CVT	Growth in the system of CdTe:I_2	Paorici et al.	1977	276
STHM	Sublimation growth in THM	Triboulet et al.	1977	166
HPVT	Growth of 3.5 cm^3 single crystals	Buck et al.	1980	228
VPVT	Contactless seeded growth in a large ampoule (50 mm ϕ x250 mm)	Glebkin et al.	1980	229
STHM	Purity improvement by sublimation	Triboulet et al.	1981	185
HPVT	Sublimation under controlled partial pressures	Mochizuki et al.	1981	225-227
VPVT	Seeding vertical PVT, no contact with ampoule	Golacki et al.	1982	230
VPVT	Maximum growth rate ~ 2 g/day, dependence of growth rate on the excess Te	Yellin et al.	1982	231
VPVT	Seeding from the lower part, stress calculation	Zhao et al.	1983	232
HPVT	Growth of $(CdTe)_{1-x}(ZnSe)_x$ mixed crystal	Chandrasekharam	1983	233
VPVT	~18 cm^3 CdTe single crystals on a seed plate, epitaxial growth on (111)	Kuwamoto et al.	1984	234
VPVT	Dependence of mass transport on the material stoichiometry	Yellin et al.	1984	235
VPVT	Focused mirror furnace, crystals of 15 mm diameter and 50 mm length	Bruder et al.	1985	236
VPVT	$Cd_{0.96}Zn_{0.05}Te$ single crystals, 1-2 cm^3	Ben-Dor et al.	1985	237
HPVT, DS	Examination of activation energies for vapor transport	Mochizuki et al.	1985	214
Durham method	Pulling an evacuated capsule at a rate of ~15 mm/day	Durose et al.	1985	238
PVT	Unseeded PVT growth with different stoichiometric composition	Yellin et al.	1985	239
PVT	Pb doping	Lauck et al.	1986	24
PVT	Oriented growth using sapphire substrates	Klinkova et al.	1988	243
PVT	Modified Piper-Polish method under argon atmosphere in an open silica tube	Durose et al.	1988	241

Table 15.7 Vapor Phase Growth of CdTe and CdZnTe (continued)

Method	Result	Authors	Year	Ref.
HPVT	Capillary tube for seed selection	Geibel et al.	1988	242
HPVT	Growth temperature 900 °C, temperature gradient 0.1-0.2 °C/cm	Golacki et al.	1989	244
HPVT	Systematic study of mass transport rate	Wiedemeier et al.	1990	245
VPVT	In-situ nucleation, no wall contact, 8 cm^3, EPD ~$2x10^3 cm^{-2}$	Grasza et al.	1992	246
HPVT	No contact between crystal and ampoule wall, determination of optimal temperature conditions	Grasza	1993	247
PVT	Theoretical computation of mass flux, consideration of factors affecting the growth rate	Palosz et al.	1993	248
HPVT	Seeded growth, growth rate 35 mm/day (highest rate), temperature gradient 40 °C/cm	Wiedemeier et al.	1993	249, 250
CVT	Growth of CdTe:X (X=Cl, Br, I)	Schwarz et al.	1994	277
HPVT	30-50 mm ϕ, 250-300 g CdTe	Boone et al.	1994	251
STHM	Growth using a mirror furnace	Laarsch et al.	1994	270
HPVT	Growth of CdZnTe and effect of growth parameters on the Zn distribution	Palosz et al.	1995	248
STHM	Growth of V-doped, Ti-doped crystals	Schwarz et al.	1995	271
PVT	Contactless growth with self-seeding under low hydrogen atmosphere	Grasza	1995	252
VPVT	In-situ growth rate measurement by laser diffraction	Bailiang et al.	1995	253
HPVT	Effect of growth conditions on the composion of CdZnTe crystals	Palosz et al.	1995	258
VPVT	Seeding growth of CdZnTe	Palosz et al.	1996	259
HPVT	Improved ampoule structure	Yang et al.	1997	261
VPVT	Contact-free growth by seeding	Laarsch et al.	1997	256
HPVT	CdZnTe 50mm single crystal growth	Mycielski et al.	1998	262
VPVT	Free-growth of CdZnTe on oriented seeds	Melnikov et al.	1999	264
CVT	Growth of CdTe:NH_4X (X = Cl, Br, I)	Ilchuk et al.	1999	278 -280
MPVT	Multitube growth system for mass transport control	Mullins et al.	2000 2002	267-268
PVT	High purity crystal growth using stoichiometric charge	Zha	2002	103
VPVT	Contact-free sublimation growth	Palosz et al.	2003	269

DS: Direct Synthesis, PVT: Physical Vapor Transport, HPVT: Horizontal PVT, VPVT: Vertical PVT, CVT: Chemical Vapor Transport, STHM: Sublimation Travelling Heater Method

during crystal growth to effect appropriate seeding. Klinkova et al.,[243] Glebkin et al.[229] and Golacki et al.[230] and have applied a contactless growth method based on the Markov method (Sec.2.4.2). An example is shown in Fig. 15.29. Kuwamoto[234] has used a vertical three-zone furnace as shown in Fig. 15.30(a), and has grown large CdTe single crystals as shown in Fig. 15.30(b) of size up to 18 cm^3 by using seed crystals.

Yellin et al.[231, 235, 237, 239] have grown CdTe single crystals controlling partial vapor pressure but without seeding. They have systematically studied the effect of the non-stoichiometry on the growth rate. Bruder et al.[236] have used a mirror furnace (Fig.

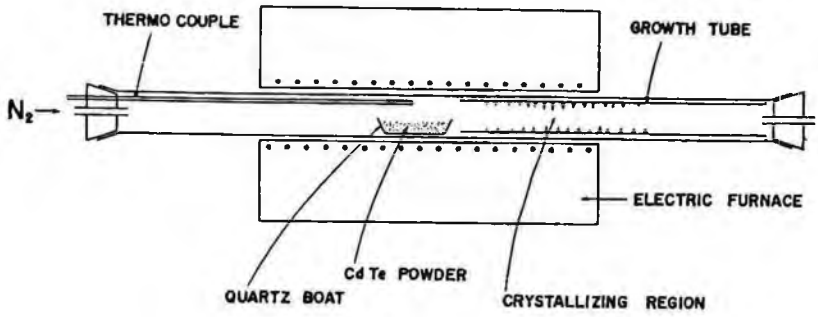

Fig. 15.25 Schematic diagram of apparatus for physical vapor transport of CdTe in an open tube furnace (reprinted from Ref. 215 with permission, copyright 1963 Taylor & Francis).

15.31) for growing crystals by seeding.

Grasza et al.[246, 247] have applied an in-situ nucleation method to crystal growth by vertical PVT as shown in Fig. 15.32(a). In this method, the source material is vaporized as shown in Fig. 15.32(b) for seeding.

Wiedmeier and Wu have grown CdTe[249] and $Cd_{1-x}Zn_xTe$[250] single crystals by a seeded growth technique with a very fast growth rate (15 mm/day) and obtained a dislocation density of about 10^4 cm^{-2}. Boone et al.[251] have applied the horizontal PVT method as shown in Fig. 15.33, where crystals are grown in both sides of the furnace. They obtained 45-50 mm diameter 250-300 g CdTe single crystals with an EPD of $7x10^4$ cm^{-2}. Laarsch et al.[254-256] have grown CdTe single crystals using a contactless seeded PVT method (modified Markov method).

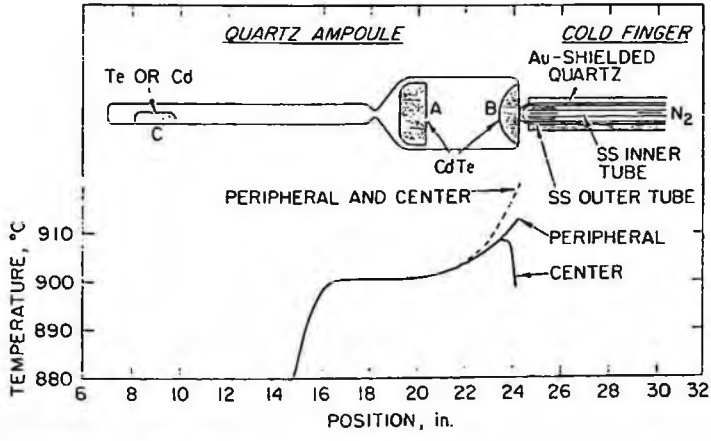

Fig. 15.26 PVT furnace for CdTe crystal growth under Cd or Te vapor pressure control. A: vaporizing CdTe, B: condensing CdTe, C: reservoir of Cd or Te (reprinted from Ref. 221 with permission, copyright 1971 Elsevier).

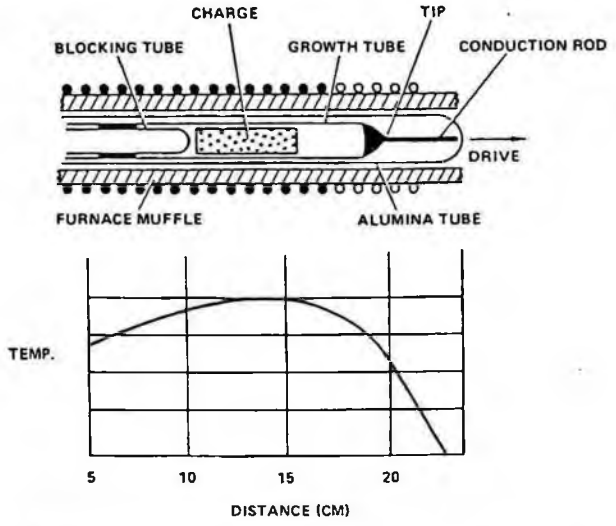

Fig. 15.27 Furnace and temperature profile for the growth of (Zn, Cd)S and (Zn, Cd)Te graded composition crystals. The charge is a homogeneous physical mixture of the starting materials (reprinted from Ref. 222 with permission, copyright 1971 Elsevier).

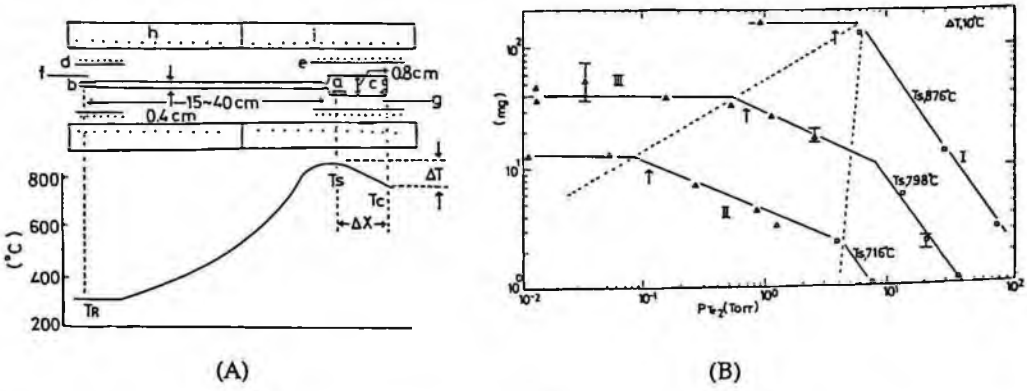

Fig. 15.28 (A) Schematic construction of the electric furnace and an example of temperature profile for vapor phase transportation. (a) source chamber; (b) reservoir chamber; (c) growth chamber; (d), (e) auxiliary heater; (f), (g) almel-chromel thermocouple; (h), (i) main heater. (B) Transport quantity after 1hr as a function of Te_2 partial pressure for several source temperatures with fixed ΔT (10 °C) and ΔX (4.0cm) (reprinted from Ref. 223 with permission, copyright 1974 Elsevier).

Palosz and Wiedemeier[257] discussed the effect of growth conditions without the partial vapor pressure control on growth rate and compared them with theoretical predictions. It was found that the Cd or Te vapor pressure is a significant factor which determines the mass flux. Palosz et al.[257-259, 269] have studied the growth of $Cd_{1-x}Zn_xTe$ single crystals by the contactless PVT method both theoretically and experimentally. They

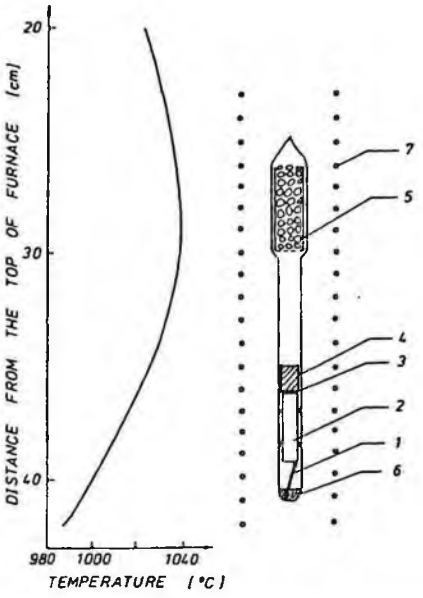

Fig. 15.29 Schematic diagram of the experimental set up and temperature profile: (a) quartz rod, (2) sapphire stick, (3) monocrystalline seed, (4) growing crystal, (5a) joint, (5b) joint with leak slits, (6) rest of the material after products, (7) vertical furnace (reprinted from Ref. 230 with permission, copyright 1982 Elsevier).

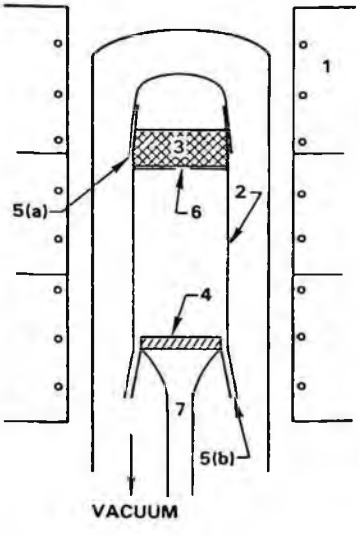

(a)

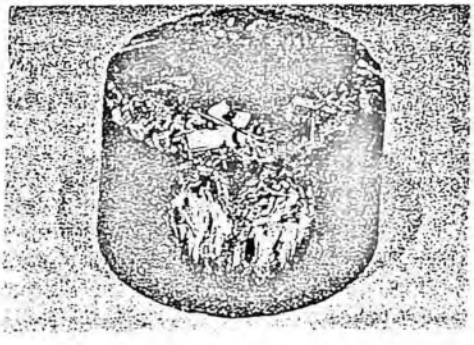

(b)

Fig. 15.30 (a) Schematic of apparatus: (1) three-zone furnace, (2) growth ampoule, (3) source, (4) seed plate, (5a) joint, (5b) joint with leak slits, (6) hole, (7) heat pipe. (b) CdTe single crystal grown on a triangular seed surrounded by polycrystals (reprinted from Ref. 234 with permission, copyright 1984 Elsevier).

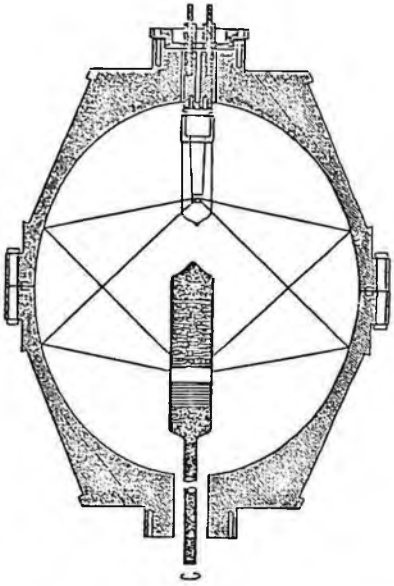

Fig. 15.31 Monoellipsoid mirror furnace with growth ampoule (reprinted from Ref. 236 with permission, copyright 1985 Elsevier).

also studied, using the apparatus as shown in Fig. 15.34, the effect of contactless growth and post-growth cool-down on the defect structure of CdTe crystals.

Yang et al.[261] improved the PVT method in order to achieve better purity, by heating the ampoule charge before sealing. Sanghera et al.[268] have studied the growth by a multi-tube physical vapor transport (MTPVT) method as shown in Fig. 15.35.

(3) Sublimation Travelling Heater Method (STHM)

The STHM was first proposed by Triboulet et al.[166] The principle of this method is as shown in Fig. 2.14. An empty space is kept between source material and grown crystal. It was found that STHM can overcome several drawbacks.[185]

Laarsch et al.[270] have grown undoped and halogen-doped CdTe crystals in a monoellipsoid mirror furnace using the sublimation travelling heater method (STHM), in closed ampoules. Not only chlorine but also bromine and iodine have been doped in order to obtain highly resistive materials for radiation detectors. It was found that resistive materials could be made ranging from 1.2×10^6 to $8 \times 10^8\ \Omega \cdot$cm. Schwarz et al.[271] have grown V-, Ti-doped CdTe crystals by the STHM and evaluated their defect structures by photo-induced current transient spectroscopy (PICTS).

(4) Chemical Vapor Transport (CVT) method

The deposition of CdTe by chemical vapor transport in an open tube technique was first reported in the Cd: Te: H: Cl system for the epitaxial growth of CdTe. Alferov et al.[272] then reported growth in the Cd: Te: Cl system using a closed tube technique.

Paorici et al.273-276 systematically studied the growth of CdTe by the CVT

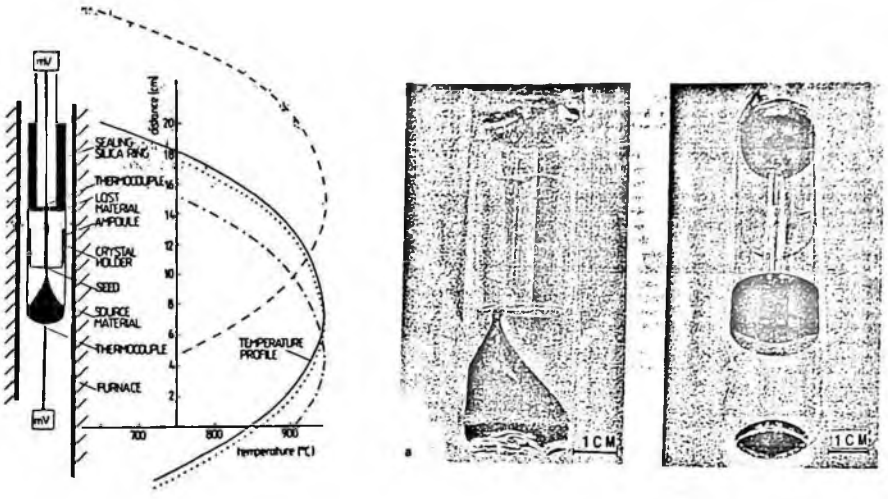

Fig. 15.32 (A) Experimental system with temperature profiles corresponding to source compaction (———), cone formation (——), seed separation (· · · · · ·) and growth (— · —). (B) (a) ampoule pulled from the furnace at the moment when the seed is separating from the source material. (b) ampoule in the last stage of crystal growth (reprinted from Ref. 246 with permission, copyright 1992 Elsevier).

method. They used NH_4Cl as the transport reagent.[273] NH_4Cl is a more easily used reagent than corrosive halogens which are difficult to handle. Solid NH_4Cl dissociates at 340 °C. When a small amount of NH_4Cl is sealed with CdTe and heated, NH_4Cl disso-

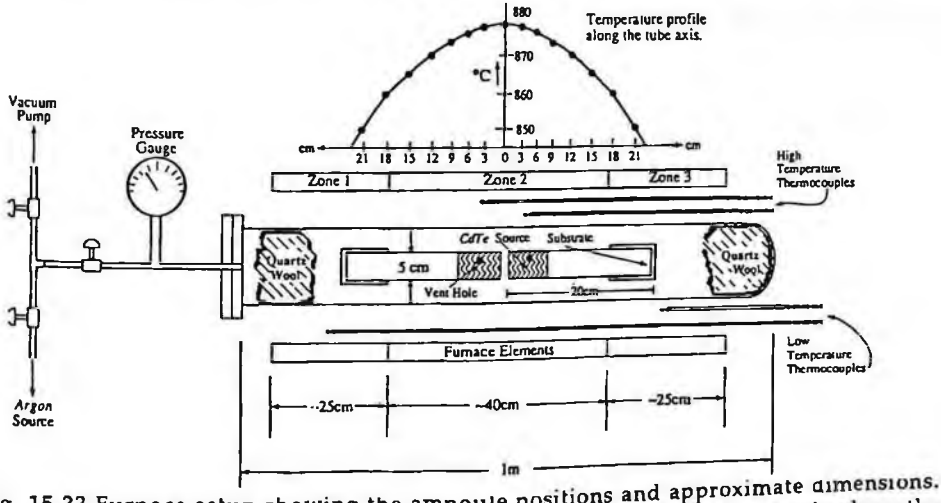

Fig. 15.33 Furnace setup showing the ampoule positions and approximate dimensions. The temperature profile at the top was obtained by moving a thermocouple along the tube axis without the ampoule and the end flange (reprinted from Ref. 251 with permission, copyright 1994 Elsevier).

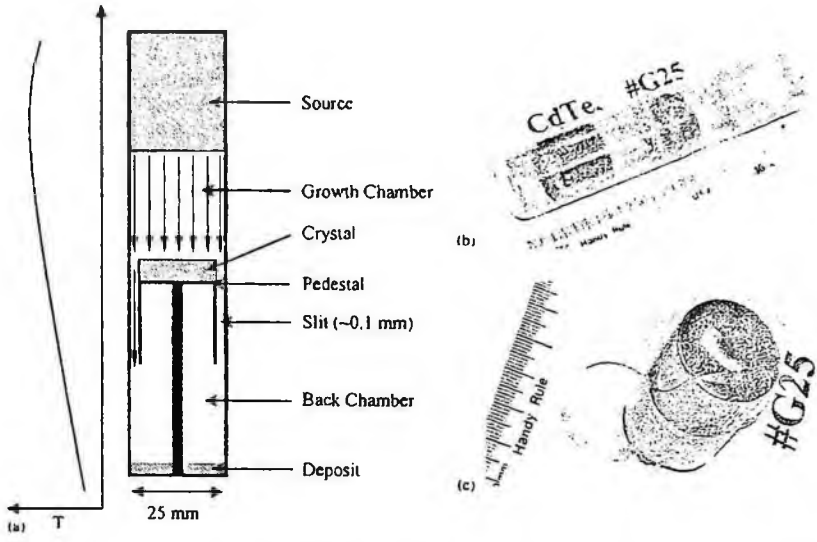

Fig. 15.34 (a) Semi-closed PVT furnace, (b) the ampoule after growth and (c) the crystal (reprinted from Ref. 269 with permission, copyright 2003 Elsevier).

ciates completely and the following reaction will occur.

$$CdTe(s) + 2HCl(g) = CdCl_2(g) + H_2(g) + 1/2Te_2(g) \qquad (15.1).$$

Crystal growth of CdTe using I_2 as the transport reagent has also been performed.[274-276] Schwarz et al.[277] have calculated thermodynamically the vapor phase species for CdTe: X (X = Cl, Br, I) systems.

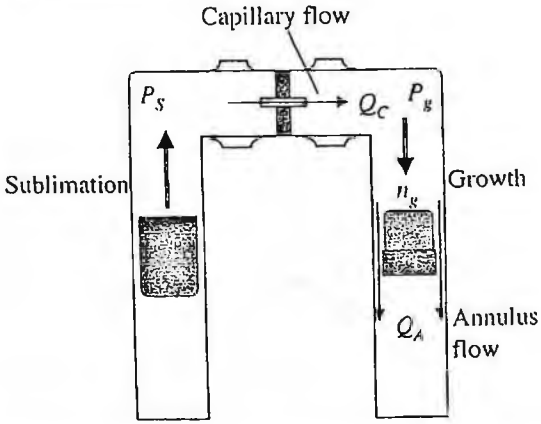

Fig. 15.35 Schematic diagram of the Multi-Tube PVT system (reprinted from Ref. 268 with permission, copyright 2002 Elsevier).

Ilchuk et al.[278-280] have calculated the thermodynamics of the CVT of CdTe using NH_4X (X=Cl, Br, I) as the transport reagent and have grown CdTe single crystals and evaluated their purities by the activation analysis method.

15.3.4 Segregation Coefficients

(1) Impurities

The segregation coefficients of various impurities have been determined during melt crystal growth experiments.[1, 73, 165, 202, 281-287] Woodbury et al.[165] and Isshiki et al.[283] have used radioactive tracers to determine the segregation coefficients. Chibani et al.[284] have determined the segregation coefficient of carbon using the charged particle activation analysis (CPAA) method. Rudolph et al.[286] have examined them using SSMS, SIMS and AAS analysis methods. These various data are summarized in Table. 19.9. Schiever et al.[287] have determined the segregation coefficients of various impurities in undoped, Ga-doped and Al-doped $Cd_{1-x}Zn_xTe$ grown by the HP-VB method using glow discharge mass spectroscopy (GD-MS) analysis.

(2) Mixed crystal

In the case of $Cd_{1-x}Zn_xTe$, it is important to grow single crystals whose Zn composition is homogeneous. The segregation of Zn has been studied by various authors[142, 139, 167, 205] and the segregation coefficient of Zn is measured as $k_{Zn} = 1.35\text{-}1.62$

15.3.5 Impurity Hardening

In the case of CdTe, it was found that Zn has an impurity hardening effect so that the dislocation density is lower for $Cd_{1-x}Zn_xTe$ than for CdTe. This effect is however seen when the Zn content is somewhat higher than with other impurity hardening effects. The mechanism of this impurity hardening has been discussed by various authors.[67, 288-290] Guergouri et al.[290] have calculated the critical resolved shear stress (CRSS) and compared it with the experimental values obtained from plastic deformation and microhardness measurements. It was found that as Zn concentrations increase, CRSS increases so that the EPD decreases by about one order of magnitude. This was explained by the difference of Cd-Te and Zn-Te bonding lengths.

15.4 CHARACTERIZATION

15.4.1 Purity

In the past, the purity of Cd and Te was not of sufficient grade so that the crystal growth was faced with the difficulty of the sticking of grown crystals to the wall of the quartz ampoules, which causes the ampoule to crack during crystal growth. This difficulty was however solved by using purified starting materials.

In the beginning, purity was tested mainly by solid source mass spectroscopy (SSMS) but recently glow discharge mass spectroscopy (GD-MS) which has good accuracy and sensitivity has been used. Table 15.9 shows a typical analysis result for VGF 100 mm diameter CdZnTe. It can be seen that most impurities are below the

Table 15.8 Segregation Coefficients k_0 of Various Impurities in CdTe

Impurity		CdTe	$Cd_{1-x}Zn_xTe$
Ia	Li	0.3-0.6	
	Na	0.01-~0.05, 0.001	0.088
	K	~0.01-~0.2	
IIa	Mg	0.5-,1.5, 1	0.29
	Ca		0.028
Ib	Cu	0.2	0.038
	Ag	0.009, 0.07, 0.2	
	Au	0.1	
IIb	Zn	4-6	
	Hg	0.3	
IIIb	B	<1	0.404
	Al	~0.1, 3.6	0.016
	Ga		0.43
	In	0.06, 0.11, 0.49-0.085, 0.43	
	Tl	<0.01	
IVb	C	0.09-~0.5	
		0.001-0.007	
	Si	1.05-1.1	0.021
	Sn	0.025, 0.06	
	Pb	<0.005, 0.05	
Vb	N	~0.005-~0.4	
	As	0.13	
	Sb	0.01-0.2, 0.013	
	Bi	0.001, 0.02	
VIb	O	~0.02	
	S	4-~10	3.2
	Se	2-7	1.61
VIb	Cl	0.005	
	I	<0.5, 0.22	
Transition Metals			
	Cr	<1, 0.01	0.007
	Mn	0.7	0.008
	Fe	0.47-0.58	0.006
	Co	0.03, 0.27, 0.3, 1.05-1.1	
	Pt	<0.02	

detection limits, and even the detected impurities are less than 0.1 ppmw.

Pautrat et al.[291] have studied microscopically using Auger Electron Spectroscopy (AES) and cathodoluminescence (CL) methods, how impurities are segregated to Te precipitates/inclusions and their behavior during annealing. Bowman et al.[292] have examined the relationship between Fe impurities and electron paramagnetic resonance (EPR) signals and photoluminescence (PL) peaks. Chibani et al. studied the behavior of carbon since carbon is the contaminant which comes from the coating of quartz ampoules by carbon hydrides. Rudolph et al.[286] analyzed impurities in source materials (Cd, Te), CdTe substrates and epitaxial layers by SSMS, SIMS and AAS and examined the behavior of impurities. Bagai et al.[293] have studied the incorporation of hydroxyl and carbonyl groups as polymerized chelate complexes to CdTe by analyzing infrared absorption spectra. Akutagawa et al.[294] have studied the solubility of Au in CdTe.

15.4.2 Defects

(1) Twinning

Because of the low stacking fault energy, twinning occurs easily in the case of the

Table 15.9 Typical Purity of VGF Grown CdTe (reprinted from Ref. 147 with permission, copyright 1996 Elsevier).

Element	Concentration (ppm)	Element	Concentration (ppm)
Li	<0.005	Zr	<0.005
Be	<0.005	Ru	<0.05
B	<0.005	Ag	<0.05
Na	0.1	Sn	<0.01
Mg	<0.05	Sb	<0.05
Al	0.05	Cs	<0.005
Si	<0.01	Gd	<0.005
P	<0.005	Tb	<0.001
S	<0.01	Dy	<0.005
Ca	<0.05	Tm	<0.001
Ti	<0.005	Tb	<0.005
V	<0.001	Lu	<0.005
Cr	<0.05	Hf	<0.005
Co	<0.005	W	<0.005
Ni	<0.05	Re	<0.005
Cu	<0.05	Os	<0.005
Ga	<0.05	Tr	<0.005
Ge	<0.05	Hg	<0.05
Rb	<0.005	Tl	<0.005
Sr	<0.001	Tb	<0.005
Y	<0.001	Bi	<0.005
Sc	<0.005		

crystal growth of CdTe. This makes it difficult to grow single crystals with a high growth yield. Vere et al.[37] have studied the origin of twinning in CdTe and found that it was due to growth irregularity at the liquid-solid interface rather than mechanical deformation after solidification. To reduce the occurrence of twinning, it is very important to control temperature fluctuations (Sec. 4.4).

(2) Dislocations

Dislocations in CdTe are investigated using various etchants as shown in Table 15.10.[295-303] In the early days of the investigation of CdTe crystal growth, the EAG1 etchant[295-297] was believed to be the etchant of choice for dislocations. It was however found that this etchant was not successful in revelling every single dislocation. These days, the Nakagawa etchant[298] based on a solution of HF is mainly used as the dislocation etchant. Gilabert et al.[304] have compared these etchants and discussed their suitability as dislocation etchants.

The polarity determination of the Cd face and the Te face for (111) faces was also in confusion in the past. The polarity was however concluded from studies by X-ray abnormal scattering,[305] ion-channeling,[306] X-ray Photoemission Spectroscopy (XPS),[307] electron diffraction,[307, 308] chemical etching,[309] and Auger Electron Spectroscopy (AES).[310] Some etchants[65] for polarity determination are also shown in Table 15.10.

Table 15.10 Etching Solutions for Dislocation and Polarity Evaluation

Etchant	Composition	Etch Pit Shape (111)A	(111)B	Ref.
EAg-1	HNO_3:H_2O:$K_2Cr_2O_7$:$AgNO_3$ 10 ml:20 ml:4 g:1 mg	deep triangular pit shallow triangular pit		295
Nakagawa	HF:H_2O_2:H_2O 30 ml:20 ml:20 ml	rounded pit	no change	298
Bagai	HF:H_2O_2:H_2O 4:0.5:2			300
Wermke	HF:HNO_3:1%$AgNO_3$ 1:2:			301
Hanert	HF:50%CrO_3:HNO_3 1:1:1:20			302
Watson	35 g $FeCl_3.(H_2O)_6$+10 mg H_2O			303
H_2SO_4 system	H_2SO_4:H_2O_2:H_2O	darkish surface	no change	65
Lactic acid system	Lactic acid:HNO_3:HF 50 ml:8 ml:2 ml 25 ml:4 ml:1 ml	no change	darkish surface	65

As explained in Sec. 15.2, since the critical resolved shear stress in CdTe is very low compared with other compound semiconductor materials, dislocations are easily generated in CdTe crystals. This is the reason why the dislocation density of CdTe crystals reaches levels above 10^6 cm^{-2} and dislocation cell structures are formed in grown crystals as seen in Fig. 15.36(a). In order to reduce dislocation densities, it is necessary to reduce the axial temperature gradient during crystal growth, and to find appropriate container structures and materials in order to prevent stress from the container. Various attempts have been made to this end. In the case of PVT growth, crystals have been grown by the contactless method, without attaching the grown crystal to the container wall.

Considering dislocation densities, it is known that the LEC method which has high axial temperature gradients is not appropriate. In the case of VB and VGF methods, when the temperature gradient is lowered below 5 °C/cm and attention is paid to the container, it is found to be possible to grow crystals with the dislocation densities lower than $5x10^4$ cm^{-2}. To reduce the dislocation density below 10^4 cm^{-2}, it has been shown that the PVT method is the most appropriate one. It is reported that 50 mm diameter single crystals with no twins or grain boundaries can be obtained with dislocation density below $3x10^3$ cm^{-2}.

For evaluating CdTe crystals, double crystal X-ray diffraction (DCXD) method is the main method used. It is known that there is a correlation between the rocking curve width of DCXD and dislocation densities.[311, 312] Since CdTe has a tendency to grow with cell structures as shown in Fig. 15.36 (a), the FWHM is normally wide as shown in Fig. 15.37(a). When crystal growth conditions are carefully optimized, crystals with FWHM of less than 20 arcsec can be obtained as shown in Fig. 15.37(b), with good uniformity even for 100 mm diameter crystals. In such materials, no cell structures can be observed as seen in Fig. 15.36(b) and the uniformity of dislocation densities and the

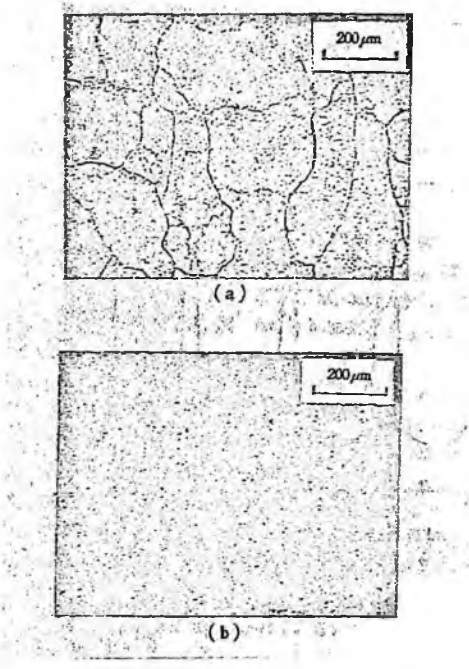

Fig. 15.36 Dislocation etch pits. (a) high dislocation density with cell structures, (b) low dislocation density with no cell structures (from Ref. 65 with permission).

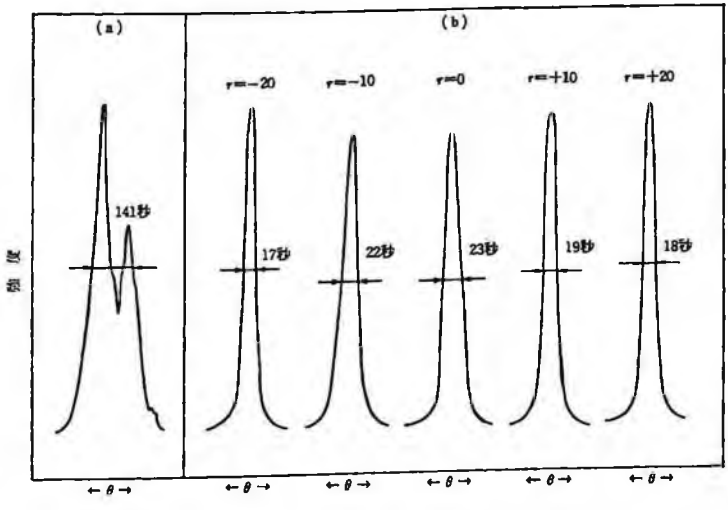

Fig. 15.37 Double crystal X-ray diffraction FWHM for (a) crystal with cell structures and (b) crystal without cell structures (from Ref. 65 with permission).

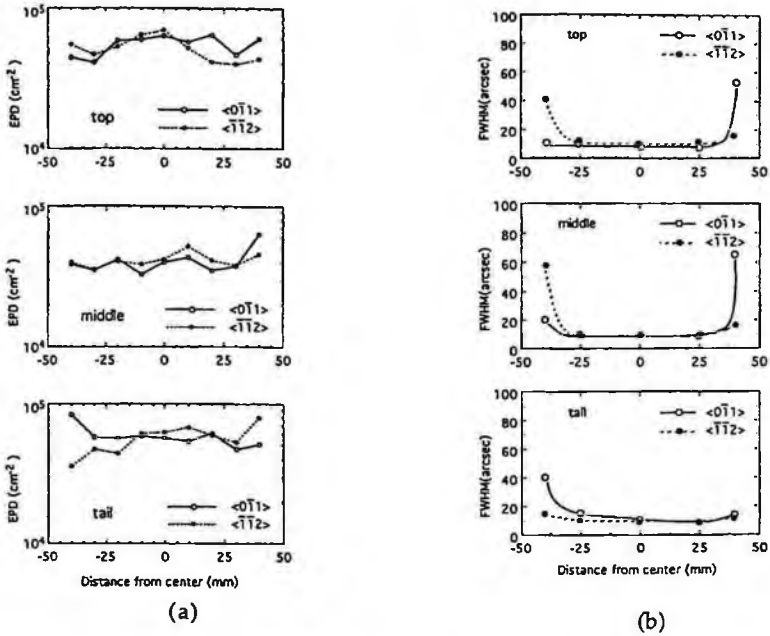

Fig. 15.38 Distributions of EPD (a) and double crystal X-ray diffraction FWHM (b) for 100 mm diameter $Cd_{1-x}Zn_xTe$ single crystals (reprinted from Ref. 147 with permission, copyright 1996 Elsevier).

FWHM in the whole crystal is satisfactory as shown in Fig. 15.38. To obtain crystals with no cell structures is very important since layers epitaxially grown on these substrates will also show cell structures.

CL methods[313-318] are also effective especially for examining the microscopic distributions of dislocations. Maeda and Takeuchi found one-to-one correspondence of dark spots on CL with dislocations.[313] The EBIC method has also been used to evaluate dislocation distributions.[318] Dislocations in CdTe and $Cd_{1-x}Zn_xTe$ have also been studied by various methods such as X-ray topography,[287, 319-321] X-ray double crystal topography,[322, 323] and TEM.[324-327]

Guergouri et al.[328] have studied the effect of dislocations introduced by indentation on electrical and optical properties. Wu and Slade[329] have examined the structure of CdMnTe by X-ray diffraction. Dislocation movement in CdTe during plastic deformation has been studied by various authors.[243, 330-334]

(3) Lineages

When there are lineages in grown crystals, they affect the epitaxial morphology of $Hg_{1-x}Cd_xTe$ layers grown on CdTe substrates so that it is desirable to have fewer lineages. Lineages are mainly formed at the intersection of grain boundaries as seen in Fig. 15.38(a) so that growing single crystals with no grain boundaries is one way to have fewer lineages. Lineages are also formed at the periphery of the crystals near the inner

wall of the crucible since they are formed because of the thermal stress due to the contraction from the container. It is therefore necessary to design the container in such a way as to reduce the stress from it as far as possible.

(4) Precipitates and inclusions

Precipitates and inclusions in CdTe and $Cd_{1-x}Zn_xTe$ have been characterized by various methods such as infrared microscopy,[335-337] infrared spectroscopy,[338-340] Raman Scattering,[341, 342] calorimetry[336] and reflected X-ray diffraction.[343]

In the past, precipitates and inclusions were considered to be the same defects, but recently they were better defined.[337] Precipitates are due to segregation during the cooling process caused by the deviation from the phase diagram while inclusions are due to the incorporation of excess Te from a non-stoichiometric melt during crystal growth.

Inclusions are generated due to the non-stoichiometry of the melt from which crystals are grown in the VB method.[344] Inclusions are also often observed in the case of THM growth because the melt differs widely from the stoichiometric composition.[345] The stoichiometry of the CdTe melt can be controlled by controlling the partial vapor pressure. It is therefore desirable to grow crystals by controlling the Cd vapor pressure in such a way that the melt composition approaches stoichiometry.

Asahi et al.[147] examined systematically the size of inclusions as a function of the Cd reservoir temperature. It was found that when the Cd vapor pressure is about 1.7 atm., the peak inclusion size reaches a minimum as shown in Fig. 15.40. Under this vapor pressure, it was also found that the electrical conductivity type was in the region of p/n conversion. When the Cd vapor pressure is higher than 1.7 atm., inclusions due to excess Cd appeared. Inclusions are thus related to non-stoichiometry of the melt composition.

Since the congruent point of the phase diagram tends towards a Te-rich composition, the composition of the grown crystals shows a Te excess even at about 10^{17} cm^{-3}. When the grown crystals are cooled down, the excess Te above the solidus line precipitates in the CdTe matrix.[346]

The elimination of Te precipitates has been achieved by annealing and it was found that by annealing at appropriate temperatures,[347-349] Te precipitates can be eliminated completely as seen in Fig. 15.41. This process is very similar to that of wafer annealing of GaAs (Sec. 8.7.2).

(5) Point defects and stoichiometry

The main point defects in CdTe are known to be Schottky type defects, that is Cd vacancy V_{Cd} and Cd interstitial Cd_i. The thermodynamics of native defects in CdTe have been studied systematically by de Nobel[20] and Kröger.[350, 351] When foreign impurities such as In and Au are incorporated, the concentrations of native defects change according to the thermodynamical mass action law. Chern and Kröger[352] have calculated native defect concentrations and their diffusion coefficients.

The self-compensation mechanism of CdTe has been discussed by many researchers. Pautrat et al. have explained this mechanism from the viewpoint of the segregation

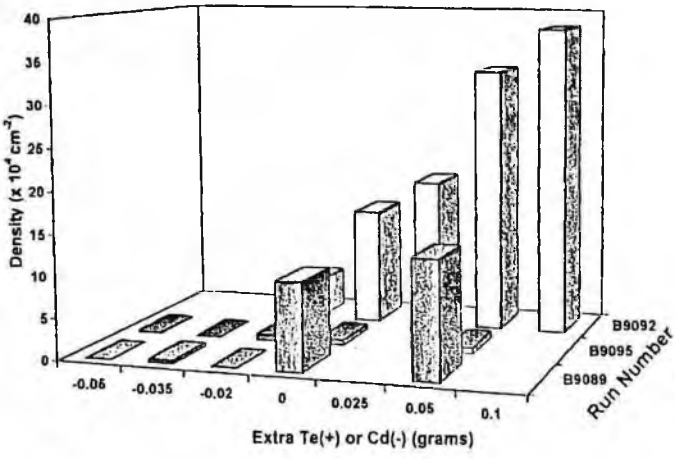

Fig. 15.39 Inclusion density as a function of Te (positive) or Cd (negative) addition for three runs each containing five boulettes (reprinted from Ref. 95 with permission, copyright 1998 Elsevier).

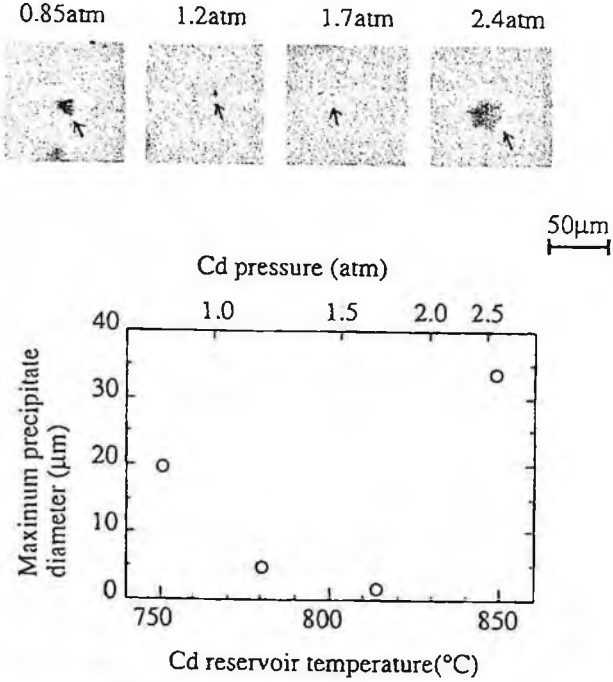

Fig. 15.40 Relationship between Cd pressure and the maximum diameter of inclusion (reprinted from Ref. 147 with permission, copyright 1996 Elsevier).

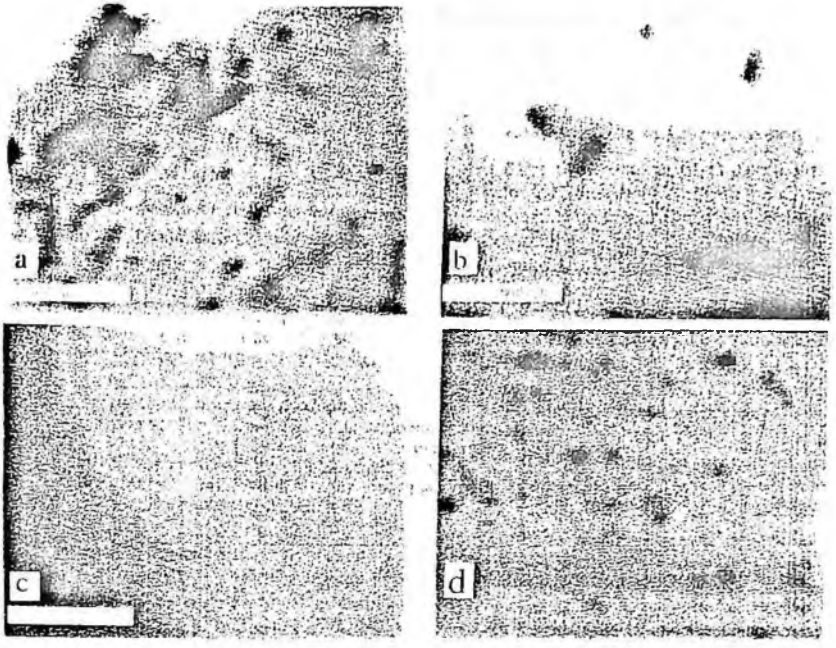

Fig. 15.41 CL images of a cross section of CdTe wafers at 80K. (a) as grown; (b) center part after annealing in Ga melt at 600°C for 2h; (c) wafer surface in contact with the Ga melt after annealing at 600°C, 24h; (d) the opposite surface after 24h Ga melt annealing. (reprinted from Ref. 349 with permission, copyright 1995 Elsevier)

of impurities to Te precipitates/inclusions.[291, 353] Ouyang et al.[354] have established the stoichiometry analysis method for CdTe by EDTA titration. Defect equilibrium has been calculated for semi-insulating CdTe doped with Cl.[355]

Zimmermann et al. have established the method to determine the concentration of V_{Cd}[356] and studied the state and distributions of point defects of doped and undoped VB grown CdTe.[357] Rudolph et al.[358] have studied the correlation between carrier concentrations and those of important substitutional acceptors and thus determined the non-stoichiometry curve of CdTe.

The defect structure of In-doped CdTe has been studied.[359] Meyer et al.[360] have identified V_{Cd} and V_{Te} by EPR and discussed the relationship between crystal quality and these intrinsic defects. Yujie et al.[361] have calculated thermodynamically the concentrations of various defects and have shown how the Fermi level varies as a function of Cd partial pressure and temperature.

(6) Deep levels

Deep levels in CdTe have been evaluated by various methods such as thermal stimulated current (TSC),[362-366] thermal stimulated capcitance (TSCAP),[366] photo-capacitance (PHCAP),[363, 367] deep level transient spectroscopy (DLTS),[363,368-373] capacitance

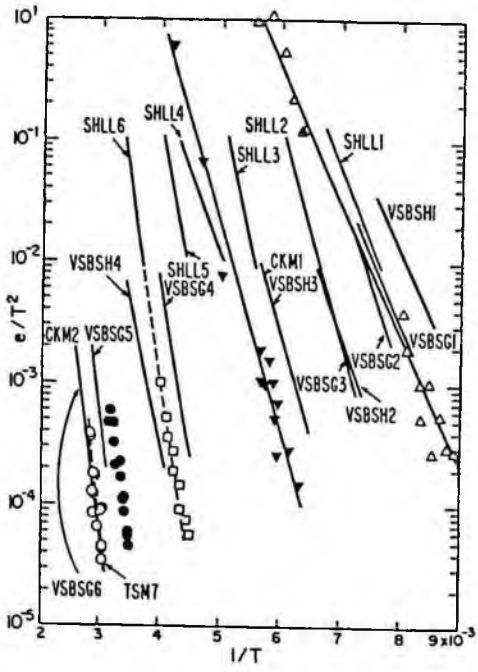

Fig. 15.42 Emission trap data for electron traps in n-CdTe (reprinted from Ref. 369 with permission, copyright 1984 American Institue of Physics). Labeled solid lines are literature data found in Ref. 369.

voltage transient (CCVT) measurement,[374] optical DLTS (ODLTS),[371] spectral analysis DLTS (SADLTS)[354] and photo induced current transient spectroscopy (PICTS).[373] Those evaluated in the past are summarized by Zanio.[1] Subsequently, deep levels have been evaluated by more precise methods such as DLTS and PDLTS. Some results reported on electron traps are summarized in Fig. 15.42.

15.4.3 Electrical Properties

(1) Electrical Properties

Among the various II-VI materials, CdTe is the one whose electrical conductivity can be controlled between n type and p type. It is known that as the Cd vapor pressure is increased, the conductivity type changes from p type to n type. This conductivity change is explained by Cd vacancies. The conductivity type of CdTe can be controlled by the partial vapor pressure of the constituent element. De Noble[20] and Carlsson and Ahlquist [376] showed that the carrier concentration and the conductivity type can be controlled as a function of Cd vapor pressure (Fig. 15.43). p-type and n-type CdTe crystals can thus be easily obtained. The conductivity mechanism has been discussed by several authors.[377-387]

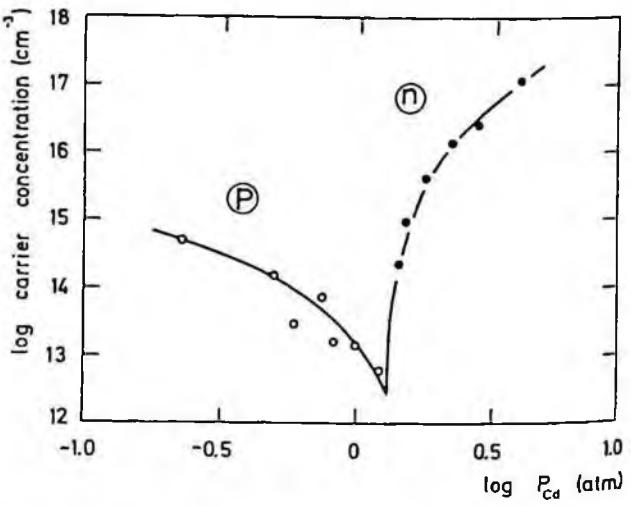

Fig. 15.43 Concentration of free electrons and holes measured at room temperature on CdTe single crystals after reheating under various partial pressures of Cd at 1200 K (reprinted from Ref. 376 with permission, copyright 1972 American Institue of Physics).

The typical temperature dependence of Hall mobility and carrier concentration of n-type CdTe is as shown in Fig. 15.44.[379] Yokota et al.[74] have studied the influence of oxygen incorporated from the residual gas in the ampoules on the electrical properties.

(2) Doping

Donor impurities for CdTe are III group elements such as Al and In and IX group elements, halogens. Acceptor impurities are V group elements such as P, As, Sb and I group elements, alkali metals. The energy levels of donors and acceptors of CdTe have been determined[17] as shown in Table 15.11.

The behavior of shallow acceptor states such as P, Li and Na has been studied by Crowder and Hammer.[389] Arkad'ev et al. studied the behavior of Li[390] and P[391] and Saraie[392] studied that of P. Alnajjar et al.[393] have studied the post-growth doping of P by wafer annealing. Pautrat et al.[353] examined the behavior of various impurities microscopically. Kikon et al.[394] have studied theoretically the energy levels of 3d elements. Chen et al.[395] have calculated the energy levels of various impurities.

(3) Self compensation and semi-insulating

Since the bandgap E_g of CdTe is 1.53 eV at room temperature, in principle it is possible to realize semi-insulating crystals of resistivity $10^{10}\,\Omega$·cm. For this degree of semi-insulation, it would be necessary for the residual carrier concentration to be less than $10^6\,cm^{-3}$. In reality, it is impossible to obtain such a high purity materials.

In practice, semi-insulating materials can be obtained by doping In or Cl in crystals

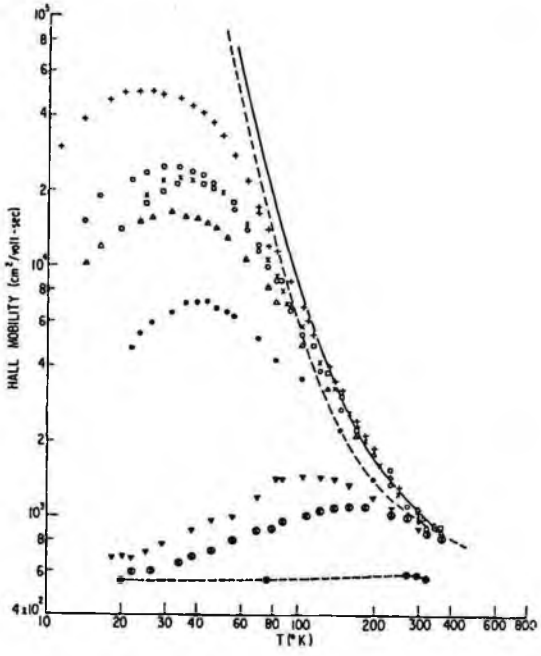

Fig. 15.44 Temperature dependence of Hall mobility of several examples of n-type CdTe grown by multiple zone refining (reprinted from Ref. 379 with permission, copyright 1963 American Physical Society).

grown under Te-rich conditions. This relies on the self-compensation mechanism as discussed by various researchers.[396-404] In order to compensate shallow donor impurities such as In or Cl, divalent Cd vacancies are formed as deep donor levels in crystals. These semi-insulating crystals are mainly grown by the THM. Recently, it has been reported that high resistive undoped materials with resistivity higher than $10^9\ \Omega \cdot cm$ can be grown by the high-pressure vertical Bridgman (HP-VB) method. Stuck et al.[397] proposed a theoretical model for the concentration of defects in pure and halogen compensated CdTe grown by the THM.

Table 15.11 Energy Levels of Donors and Acceptors in CdTe

Impurity	Donor or Acceptor	Energy levelfrom conduction band (eV)	Energy level from valence band (eV)
Ag	A		0.108
Cl	D	0.0141	
Cu	A		0.147
In	D	0.0145	
Li	D	0.0139	
	A		0.0578
Na	A		0.0588
P	A		0.060

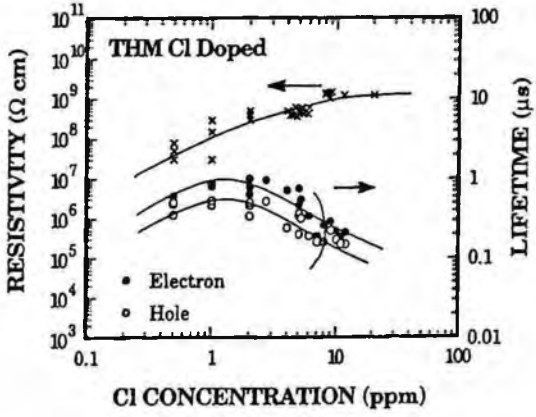

Fig. 15.45 Resistivity and carrier lifetime as a function of Cl concentration (reprinted from Ref. 193 with permission, copyright 1993 Elsevier).

Table 15.12 Analysis of Impurities through THM-grown Ingot (reprinted from Ref. 193 with permission, copyright 1993 Elsevier).

Sampling position	Weight in ppm						
	Cl	Cu	Ag	Fe	Ni	Al	Si
9[a]	410	0.02	-	-	-	-	-
8[b]	1.3	-	-	-	-	-	-
7[b]	1.4	-	-	-	-	-	-
6[b]	1.4	-	-	-	-	-	-
5[b]	1.5	-	-	-	-	-	-
4[b]	1.5	-	-	-	-	-	-
3[b]	1.5	-	-	-	-	-	-
2[b]	1.5	-	-	-	-	-	-
1[b]	1.6	-	-	-	-	-	-
Detection limit	0.1	0.02	0.01	0.02	0.02	0.02	0.02

a Amount remained solvent.
b Grown crystal ingot

For radiation detectors, it is necessary to achieve not only high resistivity but also long carrier lifetime. The addition of In or Cl reduces carrier lifetime. The carrier lifetime is measured by using the time of flight method developed for amorphous materials. Ohmori et al.[193] examined the electrical properties of THM grown crystals as a function of Cl concentrations (Fig. 15.45, Table 15.12). They found that the resistivity increases and the carrier lifetime is reduced as the Cl concentration increases. It was concluded that from the viewpoint of resistivity, carrier lifetime and mobility, the appropriate Cl concentration is about 1 ppmw.

15.4.4 Optical Properties

Photoluminescence (PL) from CdTe has been extensively studied from the viewpoint of purity examination and defect structure. Various photoluminescence lines have been observed[405-416] and are assigned as shown in Table 15.13.

(1) Purity

Near band edge emission of PL is often used for evaluating the purity of CdTe. Chamonal et al.[419] studied Cu and Ag. Molva et al.[420, 421] studied the effect of Au, N, P, and As on PL and electrical properties. James et al.[423] studied the effect of Cu on the PL spectra.

Krol et al.[422] have measured the infrared absorption of CdTe doped with Al, Ga, In and Li and found absorption bands ascribed to localized vibrational modes of strongly coupled acceptor-donor pairs. Pautrat et al.[353] have examined precisely the effect of donor and acceptor impurities on the PL spectra.

Cooper et al.[426] have measured near band edge photoluminescence (NBEP) for various CdTe crystals and shown the effect of crystal quality on the PL spectra.

Seto et al.[427] have studied the PL of p-type CdTe crystals grown by the VGF method and examined its correlation with purity and electrical properties. Becker et al.[73] have studied the impurity distribution of acceptors in CdTe crystals grown by the VB method.

Zimmermann et al.[428] examined the correlation between impurity concentrations and bound exciton to free exciton intensity ratios and determined the concentrations of Cu, Ag, P and Li. Schmidt et al.[415] have calculated the power dependence of the near band edge emission and found that it is in good agreement with the measured data on CdTe.

Seto et al.[136, 429, 430] studied the two electron transition (TFT) peaks of the D^0,X lines and identified the dominant residual donors in undoped CdTe crystals grown by the Bridgman method to be Al and Cl.

(2) High resistive materials

Saminadayar et al.[433] studied the EPR and PL of Cl-doped CdTe submitted to heat treatment. It was found that it enhanced the solubility of Cl. Seto et al.[434] examined the PL of high-resistive Cl-doped CdTe and discussed the origin of the Cl-related PL line at 1.5903 eV.

(3) Defects

Furgolle[439] studied the effect of donor-Cd vacancy complexes on the PL spectra. Norris examined systematically the cathodoluminescence of Te-rich CdTe:In with various In concentrations and discussed the origin of the 1.4 eV luminescence. Figueroa et al.[444] found that Cd vacancies are responsible for the 1.55 eV narrow band and the 1.591 eV bound exciton peaks. Becker et al.[73] studied various p-type Bridgman crystals by infrared extinction spectra and discussed the effect of Te precipitates and Cd vacancies.

The annealing behavior of CdTe has been examined by Seto et al.[446] and it was found

Table 15.13 Photoluminescence assignment of CdTe

Energy (eV)	Wavelength (Å)	Assignment
1.606		Fundamental energy gap
1.603		$(X)_{n=2}$
1.599		FE
1.5955(1.595)	7772	$(X)_{n=1}$
1.595(1.593)		(D^0, X)
1.5932(1.595)	7783	(D^0, X)
1.5907(1.590)		(A^0, X)
1.5901		Recombination of an exciton localized at the chlorine center A (V_{Cd}-Cl_{Te})
1.590		Exciton bound at an acceptor complex (V_{Cd}-$2Cl_{Te}$)
1.5896		Recombination of excitons bound to a neutral acceptor Cu (A^0, X) Cd Vacancy V^{2-}_{Cd} V_{Cd}/donor (D^+) complex ($V^{2-}Cd D^+$) Substitution of a Cd site by Cu
1.587		(D^+, X) or D
1.584		Unknown
1.577		FE-LO
1.569(1.570)		(A^0, X)-LO
1.564		Cl donor complex
	7870	X-LO
1.549	8010	(e, A^0), transition between a free electron and an acceptor complex (V_{Cd}-D)
1.5588	7955	(F, A)
1.5539(1.541)	7980-8050	(D, A) or DAP
1.548(1.545)		(A^0,X)-2LO
1.54	narrow band	Unknown
1.528		(e, A^0)-LO
1.519		(D, A)-LO
1.477		Y
1.456		Y-LO1
1.434		Y-LO2

that the neutral acceptor-bound exciton peak (A_0X) was drastically reduced by annealing under Cd overpressure and was increased reversibly by annealing under Te overpressure. They ascribed the A_0X peak to the recombination of excitons trapped at Cd-vacancy/donor-impurity complexes. Kvit et al.[448] also examined the effect of annealing and aging on the PL structure, especially Z centers and the self-activation bands.

(4) CdTe crystal quality

Giles-Taylor et al.[449] has compared the crystal qualities of CdTe single crystals grown by various methods. Taguchi et al.[180] have examined the relationship between the electrical properties and the PL spectra and found that a peak at 1.42 eV can be made small

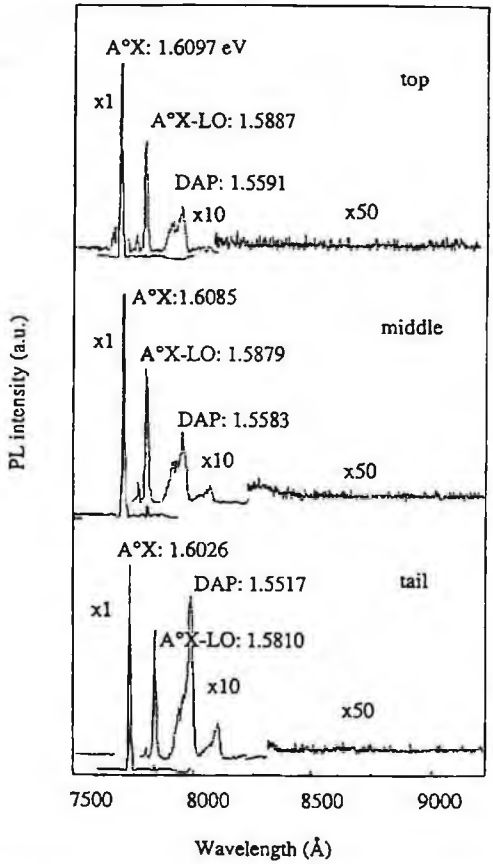

Fig. 15.46 PL spectra distribution of 100 mm diameter $Cd_{1-x}Zn_xTe$ single crystal (reprinted from Ref. 147 with permission, copyright 1996 Elsevier).

by appropriate THM growth conditions.

(5) $Cd_{1-x}Zn_xTe$

Taguchi et al.[450] studied the (A^0, X) emission of $Cd_{1-x}Zn_xTe$ crystals grown by THM. Cohen et al.[451] have studied the PL and Raman scattering from Cd1-xZnxTe. Gonzalez-Hernandez et al.[452] studied the PL spectra of $Cd_{1-x}Zn_xTe$ crystals grown by the modified VB method. Lopez-Cruz et al.[453] made PL and photoconductivity studies of $Cd_{1-x}Zn_xTe$ crystals grown by the VB method. Oettinger et al.[454] have examined the PL structure of $Cd_{1-x}Zn_xTe$ crystals grown by THM over the complete range of x = 0 to x = 1 and measured the excitonic line broadening as a function of the alloy composition.

Asahi et al.[146, 147] evaluated by PL the crystal quality of 100 mm diameter $Cd_{1-x}Zn_xTe$ single crystals grown by the VGF method as shown in Fig. 15.46. It was found that the whole ingot shows good uniformity of PL spectra.

15.5 APPLICATIONS

CdTe and $Cd_{1-x}Zn_xTe$ have various applications as explained below. These applications have been reviewed in Refs 1, 6 and 455.

15.5.1 Far-Infrared Detectors

The main application of CdTe and $Cd_{1-x}Zn_xTe$ is as substrates for the epitaxial growth of $Hg_{1-x}Cd_xTe$ which is sensitive to far infrared of wavelength 10 μm. Far-infrared detectors in this wavelength region are very useful since objects at room temperature can be detected by detecting their thermal radiation. It is also useful since this wavelength region corresponds to the atmospheric window in air where objects can be detected even in the presence of atmospheric obstacles such as clouds or fog.

As shown in Fig. 15.2, the lattice constant of $Hg_{1-x}Cd_xTe$ does not vary so greatly as a function of composition. CdTe has a good lattice constant to match that of $Hg_{1-x}Cd_xTe$ so that CdTe is used as a substrate for the epitaxial growth of $Hg_{1-x}Cd_xTe$. $Cd_{1-x}Zn_xTe$ has better lattice matching with $Hg_{1-x}Cd_xTe$ so more $Cd_{1-x}Zn_xTe$ is industrially produced than CdTe.

For far-infrared applications, two dimensional array devices are required for rapid image processing and therefore a large area substrate is required. It is therefore necessary to prepare large area crystals. In the beginning of the development of $Hg_{1-x}Cd_xTe$ detectors, bulk $Hg_{1-x}Cd_xTe$ materials were used.[456] There were however limitations to bulk $Hg_{1-x}Cd_xTe$ in obtaining large area substrates because of the difficulties in preparing large single crystals. The practiece has therefore changed to the use of large area CdZnTe substrates in order to realize large area two dimensional arrays. Epitaxial growth has been extensively studied by LPE,[4, 457, 458] VPE,[459] MOCVD[3, 456] and MBE.[3, 5] In Fig. 19.47, a typical $Hg_{1-x}Cd_xTe$/CdTe detector is shown.[457]

15.5.2 Radiation Detectors

As reviewed by several authors,[6-8, 460] CdTe is known among the various compound semiconductor materials as one of the most appropriate materials for high efficiency radiation detectors. Since CeTe has a large average atomic number, Z = 50, the stopping power for radiation is relatively high as explained in Sec. 6.5.1, so that less thickness is sufficient for detecting radiation than with other materials. Another advantage stems from the bandgap of CdTe (1.49 eV) which allows CdTe detectors to operate at room temperature. From this point of view, CdTe was studied as a radiation detector material in the past.[177, 461-466]

The main CdTe detectors are based on photoconductive devices as shown in Fig. 15.48 so that highly resistive material is required. The intrinsic resistivity of CdTe is of the level of 10^{10} Ωcm and this can be achieved using high purity CdTe mainly produced by the THM method doped with Cl to arrive at semi-insulating materials by the compensation mechanism.[193-196] It is important to have homogeneous Cl concentrations to obtain homogeneous detection performances for detector arrays as shown in Fig. 15.49. Recently, CdTe and CdZnTe grown by the HP-VB method were also found to be

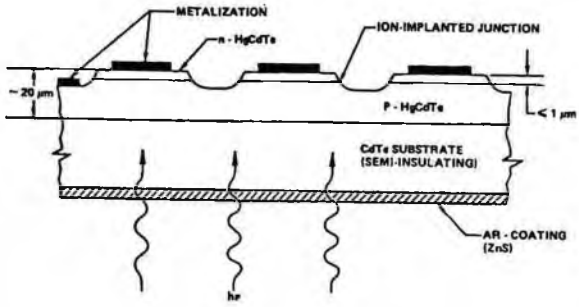

(a)

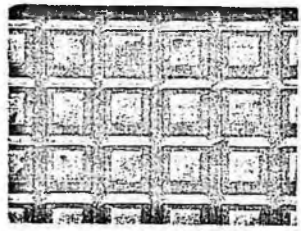

(b)

Fig. 15.47 (a) Cross section of mesa -type $Hg_{1-x}Cd_xTe$ detector and (b) the photograph of the portion of the mesa mosaic structure (reprinted from Ref.457 with permission, copyright 1980 IEEE).

good materials for radiation detectors.[107-119, 467-471]

CdTe radiation detectors were first developed as discrete devices for X-ray and gamma-ray detection.[472-474] These detectors however are one-dimensional. Two-dimensional more sophisticated devices for X-ray tomography and gamma-ray detectors for medical applications have been developed.[475-478] These detectors compete against ionization boxes or oxide scintillators, but are expected to perform as high-speed and high-resolution solid-state detectors.

15.5.3 Solar Cells

Since CdTe has a bandgap of 1.52 eV and has a high conversion efficiency as shown in Fig. 6.29 and has a high optical absorption coefficient, it is a promising material for solar cells. Since the absorption coefficient is so large that a thickness of less than 2 μm is sufficient to absorb all usable energy from the solar spectrum. Therefore, CdTe thin films have been studied extensively as solar cells.[9, 10, 479, 480]

It should however be noted that bulk CdTe single crystals are not obtained on a large industrial scale so that most CdTe solar cells are based on thin films or polycrystalline CdTe.

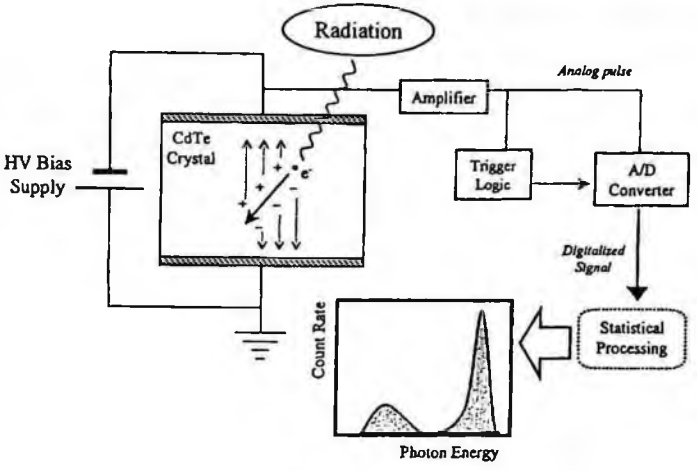

Fig. 15.48 Principle of CdTe photoconductive radiation detectors (from Ref. 196 with permission).

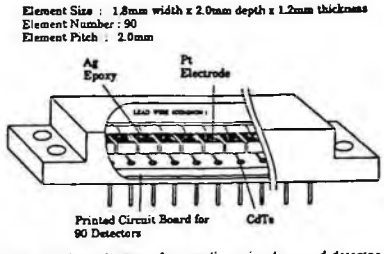

Fig. 12. Schematic view of a one-dimensional arrayed detector. Each element is mounted on a printed circuit board.

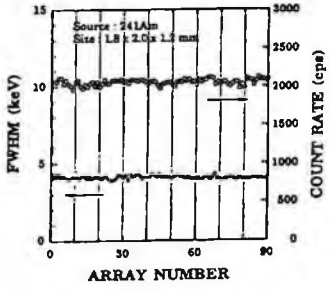

Fig. 15.49 (a) Schematic view of a one-dimensional arrayed detector. (b) FWHM and count rate for 90-element cell detectors. (reprinted from Ref. 193 with permission, copyright 1993 Elsevier)

15.5.4 Electro-Optic Modulators

The high electro-optical figure of merit, $n_o^3 r_{41}$, absence of natural birefringence and low optical absorption in the infrared region make it possible to use high resistive CdTe in electro-optical modulators. Kiefer and Yariv[481] measured the electro-optical properties of CdTe at 10.6 μm and compared them with those of semi-insulating GaAs. CdTe doped with In was studied in intracavity electro-optical modulators for Q-switched CO_2 lasers at 10.2 μm.[482] The material properties of CdTe:In used at 1.5 μm have been investigated by Milani et al.[483] who discussed its possible use in electro-optical modulators.

15.5.5 Infrared Windows

For window materials for high power CO_2 lasers, extremely low optical losses at this wavelength are required. The absorption coefficient of CdTe has been calculated and it has been found to be promising for infrared window material.[484] Gentile et al.[12] have examined the effect of point defects in CdTe and improved the absorption coefficient by a thermal annealing procedure. Deuche[485] has reviewed this application and discussed the problems and trade-offs of CdTe in very high power laser window applications.

15.5.6 Photorefractive Materials

It was first found by Bylsma et al.[486] that V doped semi-insulating CdTe demonstrates high sensitivity for optical processing applications. Partovi et al.[487] have reported on the photorefractive energy transfer at 1.5 μm for V-doped CdTe and shown that it is promising as a photorefractive material for real-time holography and optical phase conjugation . Launary et al.[120] have grown semi-insulating V-doped CdTe single crystals and characterized their photorefractive properties precisely. Marfaing[13] has reviewed the photorefractive properties of V-doped CdTe and CdZnTe crystals.

REFERENCES

1. K. Zanio, *Semiconductors and Semimetals, Vol. 13* (Academic Press, New York, 1978).
2. *Properties of Narrow Gap Cdmium Based Compounds*, ed. P. Capper, (INSPEC, London, 1994).
3. W.E. Tennant, C.A. Cockrum, J.B. Gilpin, M.A. Kinch, M.B. Reine and R.P. Ruth, *J. Vac. Sci. Technol.* **B10** (1992) 1359.
4. Y. Nemirovsky, S. Magalit, E. Finkman, Y. Shacham-Diamond and I. Kidron, *J. Electron. Mater.* **11** (1982) 133.
5. J. P. Faurie, A. Million and J. Piaguet, *J. Crystal Growth* **59** (1982) 10.
6. F.V. Wald, *Rev. Phys. Appl.* **12** (1977) 277.
7. Y. Eisen, *Nucl. Instr. Meth.* **A322** (1992) 596.
8. Y. Eisen, A. Shor and I. Mardor, *Nucl. Instr. Meth.* **A428** (1999) 158.
9. R.H. Bube, A.L. Fahrenbruch, R. Sinclair, T.C. Anthony, C. Fortmann, W. Huber, C.-T. Lee, T. Torpe and T. Yamashita, *IEEE Trans. Electron Devices* **ED-31**(1984) 528.
10. D. Bonnet and P. Meyers, *J. Mater. Res.* **13** (1998) 2740.
11. J. Kiefer and A. Yariv, *Appl. Phys. Lett.* **15** (1969) 26
12. A.L. Gentile, J.E. Kiefer, N.R. Kyle and H.V. Winston, *Mater. Res. Bull.* **8** (1973) 523.

13. Y. Marfaing, *J. Crystal Growth* **197** (1999) 707.
14. B. Ray, *II-VI Compounds* (Pergamon, Oxford, 1969) p. 1.
15. *Physics and Chemistry of II-VI Compounnds*, eds. M. Aven and J.S. Prener (North-Holland, Amsterdam, 1967).
16. H. Hartmann, R. Mach and B. Selle, in *Currents Topics in Materials Science, Vol. 9*, ed. E. Kaldis (North-Holland, Amsterdam, 1982) p. 1.
17. *Databook of II-VI Compound Semiconductor Crystals*, (JEIPA, Tokyo, 1983).
18. *Landolt-Börnstein, Vol. 17 Semiconductors*, ed. O. Madelung (Springer-Verlag, Berlin, 1982) p. 225.
19. R. Horch and Nieke, *Ann. Physik* **16** (1965) 289.
20. D. de Nobel, *Philips Res. Rept.* **14** (1959) 361.
21. M.R. Lorenz, *J. Phys. Chem. Solids* **23** (1962) 939.
22. J. Steininger, A. J. Strauss and R. F. Brebrick, *J. Electrochem. Soc.* **117** (1970) 1305.
23. S. Szapiro, *J. Electron. Mater.* 5 (1976) 223.
24. A. L. Gentile, *AIChE Symposium Series* **229** (1980) 143.
25. T. Tung, C.-H. Su, P.-K. Liao and R.F. Brebrick, *J. Vac. Sci. Technol.* **21**(1982) 117.
26. N. Yellin and S. Szapiro, *J. Crystal Growth* **73** (1985) 77.
27. K. Peters, A. Wenzel and P. Rudolph, *Cryst. Res. Technol.* **25** (1990) 1107.
28. J. H. Greenberg, V. N. Guskov and V. B. Lazarev, *Mater. Res. Bull.* **27** (1992) 997.
29. H. R. Vydyanath, J. A. Ellsworth, R. F. Fischer, J. J. Kennedy, C. J. Johnson and G. T. Neugebauer, *J. Electron. Mater.* **22** (1993) 1067.
30. T. C. Yu and R. F. Brebrick, *J. Phase Equilibria* **14** (1993) 271.
31. J.H. Greenberg, *J. Crystal Growth* **161** (1996) 1.
32. Yu. M. Ivanov, *J. Crystal Growth* **161** (1996) 12.
33. R. Triboulet, A. Heurtel and J. Rioux, *J. Crystal Growth* **101** (1990) 131.
34. J. H. Greenberg, V. N. Guskov, V. B. Lazarev and O.V. Sherbershneva, *J. Solid State Chem.* **102** (1993) 382.
35. R.N. Thomas, H.M. Hobgood, P.S. Ravishankar and T.T. Braggins, *J. Crystal Growth* **99** (1990) 643.
36. C. Parfeniuk , F. Weinberg I. V. Samarasekera , C. Schvezov and L. Li, *J. Crystal Growth* **119** (1992) 261.
37. A.W. Vere, S. Cole and D.J. Williams, *J. Electron. Mater.* **12** (1983) 551.
38. J.C. Woolley and B. Ray, *J. Phys. Chem. Solids* **13** (1960) 151.
39. K. Hirata and O. Oda, *Mater. Lett.* **5** (1986) 42.
40. H. Booyens and J.H. Basson, *phys. stat. sol. (a)* **85** (1984) 449.
41. A. Sher, A. Raizman and D. Eger, *J. Crystal Growth* **87** (1988) 507.
42. H.N. Woodbery and R.B. Hall, *Phys. Rev.* **157** (1967) 157.
43. R.B. Hall and H.H. Woodbury, *J. Appl. Phys.* **39** (1968) 5361.
44. E.D. Jones, J. Malzbender, J.B. Mullin and N. Shaw, *J. Phys. Condens. Mater.* **6** (1994) 7499.
45. Y. Hwang, H. Kim, S. Cho, Y. Um and H. Park, *J. Crystal Growth* **249** (2003) 391.
46. J. Jougler, C. Hetroit, P.L. Vuillermoz and R. Triboulet, *J. Appl. Phys.* **51** (1980) 3171.
47. J.B. Mullin and B.W. Straughan, *Rev. Phys. Appl.* **12** (1977) 105.
48. C.J. Johnson, *Proc. SPIE* **1106** (1989) 56.
49. P. Capper and A.W. Brinkman, in *Properties of Narrow Gap Cdmium Based Compounds*, ed. P. Capper, (INSPEC, London, 1994) p. 369.
50. P. Rudolph, *Prog. Crystal Growth Character.* **29** (1994) 275.
51. S. Sen and J.E. Stannard, *Mater. Res. Soc. Symp. Proc.* **229** (1994) 143.
52. M. Hage-Ali and P. Siffert, *Mater. Res. Soc. Symp. Proc.* **299** (1994) 231.
53. T. Asahi, A. Koyama, Y. Taniguchi and O. Oda, *J. Jpn. Assoc. Crystal Growth (in japanese)* **22** (1995) 3.
54. P. Rudolph, in *Recent Development of Bulk Crystal Growth*, ed, M. Isshiki (Research Signpost,

India, 1998) p. 127.
55. K. Sato, Y. Seki, Y. Matsuda and O. Oda, *J. Crystal Growth*197 (1999) 413.
56. S. Yamada, *J. Phys. Soc. Jpn.* **11** (1960) 1940.
57. N. R. Kyle, *J. Electrochem. Soc.* **118** (1971) 1790.
58. H. Kimura and H. Komiya, *J. Crystal Growth* **20** (1973) 283.
59. R. Triboulet and Y. Marfaing, *J. Electrochem. Soc.* **120** (1973) 1260.
60. N. Klausutis, A. Adamski, C.V. Collins, M. Hunt, H. Lipson and J.R. Weiner, *J. Electron. Mater.* **4** (1975) 625.
61. L. Wood, E.R. Gartner, W.E. Tennant and L.O. Bubulac, *Proc. SPIE* **350** (1982) 30.
62. A. Muranevich, M. Roitberg abd E. Finkman, *J. Crystal Growth* **64** (1983) 285.
63. R. K. Route, M. Wolf, R. S. Feigelson, *J. Crystal Growth* **70** (1984) 379.
64. O. Oda, K. Hirata, K. Matusmoto and I. Tsuboya, *J. Crystal Growth* **71** (1985) 273.
65. O, Oda, K. Hirata, K. Imura and F. Tsujino, *Oyo Buturi (Monthly Publ. Jpn. Soc. Appl. Phys.) (in japanese)* **55** (1986) 1084.
66. S.L. Bell and S. Sen, *J. Vac. Sci. Technol.* **A3** (1985) 112.
67. K.Y. Lay, N.C. Giles-Taylor, J.F. Schetzina and K.J. Bachmann, *J. Electrochem. Soc.* **133** (1986) 1049.
68. Y. Masa, A. Tanaka, S. Seto, Y. Saito, S. Yamauchi and T. Kawasaki, *Sumitomo Metal Mining Res. Rept. (in japanese)* **4** (1986) 14.
69. J.J. Kennedy , P.M. Amirtharaj , P.R. Boyd , S.B. Qadri , R.C. Dobbyn and G.G. Long, *J. Crystal Growth* **86** (1988) 93.
70. K. Mochizuki, K. Matsumoto and K. Miyazaki, *Mater. Lett.* **6** (1988) 119.
71. S. Sen , W. H. Konkel , S. J. Tighe , L. G. Bland , S. R. Sharma and R. E. Taylor, *J. Crystal Growth* **86** (1988) 111.
72. S. Wen-Bin, Y. Mei-Yun and W. Wen-Hai, *J. Crystal Growth* **86** (1988) 127.
73. U. Becker, H. Zimmermann, P. Rudolph and R. Boyn, *phys. stat. sol. (a)* **112** (1989) 569.
74. K. Yokota, T. Yoshikawa, S. Inano and S. Katayama, *Jpn. J. Appl. Phys.* **28** (1989) 1556.
75. M. Bruder, H. J. Schward , R. Schmitt , H. Maier and M. O. Moller, *J. Crystal Growth* **101** (1990) 266.
76. K. Yasuda, Y. Iwakami and M. Saji, *J. Crystal Growth* **99** (1990) 727.
77. Y. C. Lu, J. J. Shiau, R. S. Feigelson and R. K. Route, *J. Crystal Growth* **102** (1990) 807.
78. M. Muhlberg, P. Rudolph and A. Wenzel, *Crystal Prop. Prep.* **35** (1991) 129.
79. P. Rudolph and M. Muhlberg, *EMRS 1992 Spring Meet. Symp. F* F-VII (1992) p. 23.
80. M. Pfeiffer and M. Mühlberg, *J. Crystal Growth* **118** (1992) 269.
81. M. Muhlberg, P. Rudolph and M. Laasch, *J. Crystal Growth* **128** (1993) 571.
82. P. Rudolph and M. Muhlberg, *Mater. Sci. Engineer.* **B16** (1993), 8.
83. P. Rudolph, U. Rinas and K. Jacobs, *J. Crystal Growth* **138** (1994) 249.
84. I.V. Sabinina, A.K. Gutakovski, T.I. Milenov, N.N. Lyakh, Y.G. Sidorov and M.M. Gospodinov, *Cryst. Res. Technol.* **26** (1991) 967.
85. T.I. Milenov and M.M. Gospodinov, *Nucl. Instr. Meth.* Phys. Res. **A322** (1992) 363.
86. T.I. Milenov and M.M. Gospodinov, *Nucl. Instr. Meth.* Phys. Res. **A322** (1992) 368.
87. L. G. Casagrande , D. D. Marzio , M. B. Lee , D. J. Larson Jr. , M. Dudley and T. Fanning, *J. Crystal Growth* **128** (1993) 576.
88. L.G. Casagrande, D.J. larson, Jr., D. D. Marzion, J. Wu, M. Dudley, D.R. Black and H. Burdette, *Proc. SPIE* **2228** (1994) 21.
89. L.G. Casagrande, D.J. Larson, Jr., D. Di Marzio, J. Wu and M. Dudley, *J. Crystal Growth* **137** (1994) 195.
90. C. Steer, L. Chibani, J.M. Koebel, M. Hage-Ali and P. Siffert, *Mater. Res. Soc. Symp. Proc.* **229** (1994) 209.
91. G.T. Neugebauer, R. Shetty, C.K. Ard, R.A. Lancaster and P. Norton, *Proc. SPIE* **2228** (1994) 2.
92. T.S. Lee, S.B. Lee, J.M. Kim, J.S. Kim, S.H. Suh, J.H. Song, I.H. Park, S.U. Kim and M.J. Park, *J.*

Electron. Mater. **24** (1995) 1057.
93. P. Capper, J.E. Harris, E.S. O'Keefe and C.L. Jones, *Adv. Mat. Opt. Electron.* **5** (1995) 101.
94. Y. Tao and S. Kou, *J. Crystal Growth* **181** (1997) 301.
95. H.L. Glass, A.J. Socha, C.L. Parfeniuk and D.W. Bakken, *J. Crystal Growth* **184/185** (1998) 1035.
96. Q. Li, S. Zhu, B. Zhao, Y. Jing, D. Gao and L. Cai, *J. Crystal Growth* **233** (2001) 791.
97. G. Li, W. Jie, Z. Gu, G. Yang, T. Wang and J. Zhang, *J. Crystal Growth* **265** (2004) 159.
98. G. Li, W. Jie , Z. Gu and H. Hua, *J. Crystal Growth* **263** (2004) 332.
99. M. Zha, T. Gorog, A. Zappettini, F. Bissoli, L. Zanotti and C. Paorici, *J. Crystal Growth* **234** (2002) 184.
100. M. Zha, A. Zappettini, F. Bissoli, L. Zanotti, V. Corregidor and E. Dieguez, *J. Crystal Growth* **260** (2004) 291.
101. G. Yang, W. Jie, Q. Li, T. Wang, G. Li and H. Hua, *J. Crystal Growth* **283** (2005) 431.
102. E. Raiskin and J.F. Butler, *IEEE Trans. Nucl. Sci.* **35** (1988) 81.
103. F.P. Doty, J.F. Butler, J.F. Schetzina and K.A. Bowers, *J. Vac. Sci. Technol.* **B10** (1992) 1418.
104. J.F. Butler, F.P. Doty, B. Apotovsky, J. Lajzerowicz and L. Verger, *Mater. Sci. Engineer.* **B16** (1993) 291.
105. N.N. Kolesnikov, A.A. Kolchin, D.L. Alov, Yu.N. Ivanov, A.A. Chernov, M. Schiever, H. Hermon, R.B. James, M.S. Goorsky, H. Yoon, J. Toney, B. Brunett and T.E. Schlesinger, *J. Crystal Growth* **174** (1997) 256.
106. R.B. James, *J. Jpn. Assoc. Crystal Growth* **27** (2000) 67.
107. C.Johnson, E.E. Eissler, S.F. Cameron, Y. Kong, S. Fan, S. Jovanovic and K.G. Lynn, *Mater. Res. Soc. Symp. Proc.* **302** (1993) 463.
108. C.J. Johnson, E.E. Eissler, S.E. Cameron, Y.Kong, S. Fan, S. Jovanovic and K.G. Lynn, *Mater. Res. Soc. Symp. Proc.* **299** (1994) 215.
109. M. Schieber, H. Hermon, R.B. James, J. Lund, A. Antolak, D. Morse, N.N. Kolesnikov, Yu.N. Ivanov, M.S. Goorsky, H. Yoon, J. Toney and T.E. Schlesinger, *Proc. SPIE* **3115** (1997) 305.
110. M. Schieber, H. Hermon, R.B. James, J. Lund, A. Antolak, D. Morse, N.N. Kolesnikov, Yu.N. Ivanov, M.S. Goorsky, J.M. Van Scyoc, H. Yoon, J. Toney, T.E. Schlesinger, F.P. Doty and J.P.D. Cozzatti, *IEEE Trans. Nucl. Sci.* **44** (1997) 2566.
111. J.R. Heffelfinger, D.L. Medlin, H. Yoon, H. Hermon and R.B. James, *Proc. SPIE* **3115** (1997) 40.
112. P. Fougeres, M. Hage-Ali, J.M. Koebel, P. Siffert, S. Hassan, A. Lusson, R. Triboulet, G. Marrakchi, A. Zerrai, K. Cherkaoui, R. Adhiri, G. Bremond, O. Kaitasov, M.O. Ruault and J. Crestou, *J. Crystal Growth* **184/185** (1998) 1313.
113. E.Y. Lee, B.A. Brunett, R.W. Olsen, J.M. Van Scyoc III, H. Hermon and R.B. James, *Proc. SPIE* **3446** (1998) 40.
114. H. Hermon, M. Schieber, R.B. James, N. Yang, A.J. Antolak, D.H. Morse, N.N.P. Kolesnikov, Yu.N. Ivanov, V. Komar, M.S. Goorsky, H. Yoon, J. Toney and T.E. Schlesinger, *Mater. Res. Soc. Symp. Proc.* **487** (1998) 223.
115. H. Hermon, M. Schieber, RB. James, E. Lee, E. Cross, M. Goorsky, T. Lam, T.E. Schlesinger and M. Greaves, *Proc. SPIE* **3768** (1999) 138.
116. H. Hermon, M. Schieber, R.B. James, A.J. Antolak, D.H. Morse, B. Brunett, C. Hackett, E. Tarver, V. Komar, M.S. Goorsky, H. Yoon, N.N. Kolesnikov, J. Toney and T.E. Schlesinger, *Nucl. Instr. Meth. Phys. Res.* **A428** (1999) 30.
117. E.Y. Lee, R.B. James, R.W. Olsen and H. Hermon, *J. Electron. Mater.* **28** (1999) 766.
118. H. Hermon, M. Schieber, M. Goorsky, T. Lam, E. Meerson, H. Yao, J. Erickson and R.B. James, *Proc. SPIE* **4141** (2000) 186.
119. H. Hermon, M. Schieber, E.Y. Lee, J.L. McChesney, M. Goorsky, T. Lam, E. Meerson, H. Yao, J. Erickson and R.B. James, *Nucl. Instr. Meth. Phys. Res.* **A458** (2001) 503.
120. D. Alexiev, K.S.A. Butcher and A.A. Williams, *J. Crystal Growth* **142** (1994) 303.
121. J. C. Launay, V. Mazoyer, M. Tapiero, J. P. Zielinger, Z. Guellil, Ph. Delaye and G. Roosen, *Appl.*

Phys. **A55** (1992) 33.
122. A. Aoudia, e. Rzepka, A. Lusson, A. Tromson-Carli, D. Schneider, Y. Marfaing and R. Triboulet, *Opt. Mater.* 4 (1995) 241.
123. C.E. Huang, D. Elwell and R.S. Feigelson, *J. Crystal Growth* **64** (1983) 441.
124. T. Jasinski, A. F. Witt and W. M. Rohenow, *J. Crystal Growth* **67** (1984) 173.
125. F. M. Carlson, A. L. Fripp and R. K. Crouch, *J. Crystal Growth* **67** (1984) 747.
126. T. Jasinski and A. F. Witt, *J. Crystal Growth* **71** (1985) 295.
127. D.H. Kim and R.A. Brown, *J. Crystal Growth* **96** (1989) 609.
128. S. Motakef, *J. Crystal Growth* **104** (1990) 833.
129. S. Kuppurao, S. Brandon and J.J. Derby, *J. Crystal Growth* **158** (1996) 459.
130. A. Yeckel amd J.J. Derby, *J. Crystal Growth* **209** (2000) 734.
131. L. Xiaohua, J. Wanqi and Z. Yaohe, *J. Crystal Growth* **219** (2000) 22.
132. C. Martinez-Tomas and V. Munoz, *J. Crystal Growth* **222** (2001) 435.
133. K. Lin, S. Boschert, P. Dold, K.W. Benz, O. Kriessl, A. Schmidt, K.G. Siebert and G. Dziuk, *J. Crystal Growth* **237/239** (2002) 1736.
134. A. Yeckel, G. Compere, A. Pandy and J.J. Derby, *J. Crystal Growth* **263** (2004) 629.
135. S.B. Trivedi and H. Wiedemeier, *J. Electrochem. Soc.* **134** (1987) 3199.
136. S. Seto, M. Hino, R. Taniguchi, S. Yamauchi and A. Tanaka, *Sumitomo Metal Mining (in japanese)* **5** (1987) 12.
137. A. Tanaka , Y. Masa , S. Seto and T. Kawasaki, *Mater. Res. Symp. Proc.* **90** (1986) 111.
138. A. Tanaka, Y. Masa, S. Seto and T. Kawasaki, in *Electron. Mater. Meet. Papers.* (Inst. Electr. Enginner. Jpn.) **EFM-88-18** (1988) p. 63.
139. A. Tanaka, Y. Masa, S. Seto and T. Kawasaki, *J. Crystal Growth* **94** (1989) 166.
140. M. Azoulay, A. Raizman, G. Gafni and M. Roth, *J. Crystal Growth* **101** (1990) 256.
141. M. Azoulay , H. Feldstein, G. Gafni, S. Rotter and M. Roth, *Crystal Prop. Prep.* **36-38** (1991) 103.
142. M. Azoulay , S. Rotter , G. Gafni, R. Tenne and M. Roth, *J. Crystal Growth* **117** (1992) 276.
143. M. Azoulay , S. Rotter , G. Gafni and M. Roth, *J. Crystal Growth* **117** (1992) 515.
144. M. Azoulay, A. Raizman, R. Weingarten, H. Shacham and H. Feldstein, *J. Crystal Growth* **128** (1993) 588.
145. K. Suzuki and A. Tanaka, *Jpn. J. Appl. Phys.* **31** (1992) 2479.
146. T. Asahi, O. Oda, Y. Taniguchi and A. Koyama, *J. Crystal Growth* **149** (1995) 23.
147. T. Asahi, O. Oda, Y. Taniguchi and A. Koyama, *J. Crystal Growth* **161** (1996) 20.
148. Yu. M. Ivanov, *J. Crystal Growth* **194** (1998) 309.
149. Y. Okano, H. Kondo, W. Kishimoto, L. Li and S. Dost, *J. Crystal Growth* **237-239** (2002) 1716.
150. O.A. Matveev, S. V. Prokof'ev and Y. V. Rud', Akad. *Nauk SSSR, Neorgan. Mater.* **5** (1969) 1175.
151. O.A. Matveev and A.I. Terent'ev, *Tech. Phys. Lett.* **20** (1994) 781.
152. O.A. Matveev and A.I. Terent'ev, *Semiconductors* **29** (1995) 191.
153. A.A. Khan, W. P. Allred, B. Dean, S. Hooper, J.E. Hawkey and C.J. Johnson, *J. Electron. Mater.* **15** (1986) 181.
154. K. Y. Lay D. Nichols, S. McDevitt, B. E. Dean and C. J. Johnson, *J. Crystal Growth* **86** (1988) 118.
155. P. Cheuvart , U. El-Hanani , D. Schneider and R. Triboulet, *J. Crystal Growth* **101** (1990) 270.
156. K. Yokota , T. Yoshikawa , S. Inano , T. Morioka , H. Nakai and S. Katayama, *Technol. Rep. Kansai Univ.* **32** (1990) 103.
157. G.S. Meiling and R. Leombruno, *J. Crystal Growth* **3/4** (1968) 300.
158. H. M. Hobgood , B. W. Swanson and R. N. Thomas, *J. Crystal Growth* **85** (1987) 510.
159. G.W. Blackmore, S.J. Courtney, A. Royle, N. Shaw and A.W. Vere, *J. Crystal Growth* **85** (1987) 335.
160. T. Kotani, F. Nakanishi, H. Yasuo, M. Shibata and K. Tada, *Sumitomo Electrics (in japanese)* **130** (1987) 95.
161. T. Kotani, F. Nakanishi, M. Tatsumi and K. Tada, , in *Electron. Mater. Meet. Papers.* (Inst. Electr.

Enginner. Jpn.) **87(9-15)** (1987) p. 31.
162. M.R. Lorenz and R.E. Halsted, *J. Electrochem. Soc.* **110** (1963) 343.
163. A. Libicky, in *II-VI Semicond. Comp. Int. Conf.*, ed. D.G. Thomas (Benjamin, New York, 1967) p. 389.
164. A. Cornet, P. Siffert and A. Coche, *J. Crystal Growth* 7 (1970) 329.
165. H. H. Woodbury and R. S. Lewandowski, *J. Crystal Growth* **10** (1971) 6.
166. R. Triboulet, *Rev. Phys. Appl.* **12** (1977) 123.
167. J.J. Perez Bueno, M.E. Rodriguez, O. Zelaya-Angel, R. Baquero, J. gonzalez-Hernandez, L. Banos and B.J. Fitzparrick, *J. Crystal Growth* **209** (2000) 701.
168. C.P. Khattak and F. Schmid, *Proc. SPIE* **1106** (1989) 47.
169. P. Rudolph, S. Kawasaki, S. Yamashita, Y. Usuki, Y. Konagaya, S. Matada, S. Yamamoto and T. Fukuda, *J. Crystal Growth* **149** (1995) 201.
170. B. J. Fitzpatrick, T. F. McGee III and P. M. Harnack, *J. Crystal Growth* **78** (1986) 242.
171. R. O. Bell, N. Hemmat and F. Wald, *phys. stat. sol. (a)* **1** (1970) 375.
172. R. O. Bell, N. Hemmat and F. Wald, *IEEE Trans. Nucl. Sci.* **NS-17** (1970) 241.
173. R. Triboulet, Y. Marfaing, A. Cornet and P. Siffert, *Nat. Phys. Sci.* **245** (1973) 12.
174. R. Triboulet, Y, Marfaing, A. Cornet and P. Siffert, *J. Appl. Phys.* **45** (1974) 2759.
175. T. Taguchi, J. Shirafuji and Y. Inuishi, *Jpn. J. Appl. Phys.* **13** (1974) 1169.
176. F. V. Wald and R. O. Bell, *J. Crystal Growth* **30** (1975) 29.
177. T. Taguchi, J. Shirafuji, T. Kobayashi and Y. Inuishi, *Jpn. J. Appl. Phys.* **15** (1976) 267.
178. F. V. Wald, *phys. stat. sol. (a)* **38** (1976) 253.
179. J. C. Tranchart and P. Bach, *J. Crystal Growth* **32** (1976) 8.
180. T. Taguchi, J. Shirafuji and Y. Inuishi, *Rev. Phys. Appl.* **12** (1977) 117.
181. R. J. Dinger and I. L. Fowler, *Rev. Phys. Appl.* **12** (1977) 135.
182. F.V. Wald and R.O. Bell, *Rev. Phys. Appl.* **12** (1977) 203.
183. T. Taguchi, J. Shirafuji, T. Kobayashi and Y. Inuishi, *Jpn. J. Appl. Phys.* **17** (1978) 1331.
184. J. Jouglar, C. Hetroit, P. L. Vuillermoz and R. Triboulet, *J. Appl. Phys.* **51** (1980) 3171.
185. R. Triboulet and Y. Marfaing, *J. Crystal Growth* **51** (1981) 89.
186. R. Triboulet, G. Neu and B. Fotouhi, *J. Crystal Growth* **65** (1983) 262.
187. R. Triboulet, R. Legros, A. Heurtel, B. Sieber, G. Didier and D. Imhoff, *J. Crystal Growth* **72** (1985) 90.
188. R. Schoenholz, R. Dian and R. Nitsche, *J. Crystal Growth* **72** (1985) 72.
189. K. Mochizuki, T. Yoshida, K. Igaki, T. Shoji and Y. Hiratate, *J. Crystal Growth* **73** (1985) 123.
190. B. Biglari, M. Samimi, J. M. Koebel, M. Hage-Ali and P. Siffert, *phys. stat. sol. (a)* **100** (1987) 589.
191. R. Triboulet, K. P. Van and G. Didier, *J. Crystal Growth* **101** (1990) 216.
192. K. Onodera, T. Oikawa and K. Watanabe, *Tokin Tech. Rev.* **18** (1991) 29.
193. M. Ohmori, Y. Iwase and R. Ohno, *Mater Sci. Enginer.* **B16** (1993) 283.
194. R. Ohno, M. Funaki and T. Ozaki, *Radiation* **22** (1996) 9.
195. M. Funaki, T. Ozaki, K. Satoh and R. Ohno, *Nucl. Instr. Meth.* **A436** (1999) 120.
196. R. Ohno, *J. Jpn. Assoc. Crystal Growth* **27** (2000) 65.
197. R. O. Bell, *J. Electrochem. Soc.* **121** (1974) 1366.
198. J. Boucherie, J. C. Launay and E. Arquis, *Ann. Chim. Fr.* **16** (1991) 57.
199. Y. V. Apanovich and E. D. Ljumkis, *J. Crystal Growth* **110** (1991) 839.
200. F.F. Morehead and G. Mandel, *Phys. Rev.* **137** (1965) A924.
201. M. Rubensein, *J. Crystal Growth* **3/4** (1968) 309.
202. K. Zanio, *J. Electron. Mater.* **3** (1974) 327.
203. P. Hoschl, P. Polivka, V. Prosser and A. Sakalas, *Czech. J. Phys.* **B25** (1975) 585.
204. B. Schaub, J. Gallet, A. Brunet-Jailly and B. Pelliciari, *Rev. Phys. Appl.* **12** (1977) 147.
205. K. Suzuki, A. Nishihata, T. Haga and A. Odajima, *Mem. Hokkaido Inst. Technol.* **21** (1993) 23.
206. B. Lunn and V. Bettridge, *Rev. Phys. Appl.* **12** (1977) 151.

207. J. B. Mullin, C. A. Jones, B. W. Straughan and A. Royle, *J. Crystal Growth* **59** (1982) 35.
208. A. W. Vere, V. Steward, C. A. Jones, D. J. Williams and N. Shaw, *J. Crystal Growth* **72** (1985) 97.
209. B. Pelliciari, F. Dierre, D. Brellier and B. Schaub, *J. Crystal Growth* **275** (2005) 99.
210. R. Frerichs, *Phys. Rev.* **72** (1947) 594.
211. R. T. Lynch, *J. Appl. Phys.* **33** (1962) 1009.
212. A. V. Vanyukov, R. P. Boronenkova, I. I. Krotov and G. V. Indenbom, *Sov. Phys. Cryst.* **19** (1975) 635.
213. H.L. Tuller, K. Uematsu and H.K. Bowen, *J. Crystal Growth* **42** (1977) 150.
214. K. Mochizuki, *J. Crystal Growth* **73** (1985) 510.
215. I. Teramoto, *Phil. Mag.* **8** (1963) 357, http://www.tandf.co.uk./journals.
216. I. Teramoto and M. Inoue, *Phil. Mag.* **8** (1963) 1593.
217. A. Corsini-Mena, M. Elli, C. Paorici and L. Pelosini, *J. Crystal Growth* **8** (1971) 297.
218. P. Hoschl and C. Konak, *Czech. J. Phys.* **B13** (1963) 850.
219. P. Hoschl and C. Konak, *Czech. J. Phys.* **B13** (1963) 785.
220. P. Hoschl and C. Konak, *phys. stat. sol.* **9** (1965) 167.
221. W. Akutagawa and K. Zanio, *J. Crystal Growth* **11** (1971) 191.
222. R. B. Lauer and F. Williams, *J. Crystal Growth* **8** (1971) 333.
223. K. Igaki and K. Mochizuki, *J. Crystal Growth* **24/25** (1974) 162.
224. K. Igaki, N. Ohashi and K. Mochizuki, *Jpn. J. Appl. Phys.* **15** (1976) 1429.
225. K. Mochizuki, *J. Crystal Growth* **53** (1981) 355.
226. K. Mochizuki, *J. Crystal Growth* **51** (1981) 453.
227. K. Mochizuki and K. Masumoto, *J. Jpn. Assoc. Crystal Growth* **12** (1985) 293.
228. P. Buck and R. Nitsche, *J. Crystal Growth* **48** (1980) 29.
229. A.A. Glebkin, A.A. Davydov and N.I. Garba, *Inorg. Mater.* **16** (1980) 19.
230. Z. Golacki, M. Gorcka, J. Makowski and A. Szczerbakow, *J. Crystal Growth* **56** (1982) 213.
231. N. Yellin, D. Eger and A. Shachna, *J. Crystal Growth* **60** (1982) 343.
232. S.N. Zhao, C.Y. Yang, C. Huang and A.S. Yue, *J. Crystal Growth* **65** (1983),370.
233. P. Chandrasekharam, D. Raja Reddy and B.K. Reddy, *J. Crystal Growth* **63** (1983) 304.
234. H. Kuwamato, *J. Crystal Growth* **69** (1984) 204.
235. N. Yellin and S. Szapiro, *J. Crystal Growth* **69** (1984) 555.
236. M. Bruder and R. Nitsche, *J. Crystal Growth* **72** (1985) 705.
237. L. Ben-Dor and N. Yellin, *J. Crystal Growth* **71** (1985) 519.
238. K. Durose, G. J. Russel and J. Woods, *J. Crystal Growth* **72** (1985) 386.
239. N. Yellin, A. Zamel and T. Tenne, *J. Electron. Mater.* **14** (1985) 85.
240. R. Lauck, G. Muller-Vogt and W. Wendl, *J. Crystal Growth* **74** (1986) 520.
241. K. Durose and G. J. Russel, *J. Crystal Growth* **86** (1988) 471.
242. C. Geibel , H. Maier and R. Schmitt, *J. Crystal Growth* **86** (1988) 386.
243. L.A. Klinkova and S.A. Erofeeva, *Izves. Akad. Nauk SSSR* **24** (1988) 397.
244. Z. Golacki, J. Majewski and J. Makowski, *J. Crystal Growth* **94** (1989) 559.
245. H. Wiedemeier and Y.C. Bai, *J. Electron. Mater.* **19** (1990) 1373.
246. K. Grasza, U. Zuzga-Grasza, A. Jedrzejczak, R.R. Galazka, J. Majewski, A. Szadkowski and E. Grodzicka, *J. Crystal Growth* **123** (1992) 519.
247. K. Grasza, *J. Crystal Growth* **128** (1993) 609.
248. W. Palosz and H. Wiedemeier, *J. Crystal Growth* **129** (1993) 653.
249. H. Wiedemeier and G. Wu, *J. Electron. Mater.* **22** (1993) 1121.
250. H. Wiedemeier and G. Wu, *J. Electron. Mater.* **22** (1993) 1369.
251. J.L. Boone, G.Cantwell, W.C. Harsch, J.E. Thomas and B.A. Foreman, *J. Crystal Growth* **139** (1994) 27.
252. K. Grasza, *J. Crystal Growth* **146** (1995) 65.
253. Y. Bailiang, M. Isshiki, Z. Chuanping, H. Ximin and Y. Xiling, *J. Crystal Growth* **147** (1995) 399.
254. M. Laasch, R. Schwarz, W. Joerger, C. Eiche, M. Fiederle, K.W. Benz and K. Grasza, *J. Crystal*

Growth **146** (1995) 125.
255. M. Laasch, G. Kloess, T. Kunz, R. Schwarz, K. Grasza, C. Eiche and K.W. Benz, *J. Crystal Growth* **161** (1996) 34.
256. M. Laasch, T. Kunz, C. Eiche, M. Fiederle, W. Joerger, G. Kloess and K.W. Benz, *J. Crystal Growth* **174** (1997) 696.
257. W. Palosz, F.R. Szofran and S.L. Lehoczky, *J. Crystal Growth* **148** (1995) 49.
258. W. Palosz, F.R. Szofran and S.L. Lehoczky, *J. Crystal Growth* **148** (1995) 56.
259. W. Palosz, K. Grasza, D. Gillies and G. Jerman, *J. Crystal Growth* **169** (1996) 20.
260. B. Yang, Y. Ishikawa, T. Miki, Y. Doumae, T. Tomizono and M. Isshiki, *J. Crystal Growth* **159** (1996) 171.
261. B. Yang. Y. Ishikawa, Y. Doumae, T. Miki, T. Ohyama and M. Isshiki, *J. Crystal Growth* **172** (1997) 370.
262. A. Mycielski, E.Lusakowsaka, A. Szadkowski and L. Kowalczyk, *J. Crystal Growth* **184/185** (1998) 1044.
263. K. Chattopadhyay, S. Feth, H. Chen, A. Burger and C.-H. Su, *J. Crystal Growth* **191** (1998) 377.
264. A.A. Melnikov, A.S. Sigov, K.A. Vorotilov, A.A. Davydov, L.I. Topalova and N.V. Zhavoronkov, *J. Crystal Growth* **197** (1999) 616.
265. K. Graza, W. Palosz and S.B. Trivedi, *J. Crystal Growth* **207** (1999) 179.
266. N.M. Aitken, M.D.P. Potter, D.J. Buckley, J.T. Mullins, J. Carles, D.P. Halliday, K. Durose, B.K. Tanner and A.W. Brinkman, *J. Crystal Growth* **199** (1999) 984.
267. J.T. Mullins, J. Carles, N.M. Aitken and A.W. Brinkman, *J. Crystal Growth* **208** (2000) 211.
268. H.K. Sanghera, B.J. Cantwell, N.M. Aitken and A.W. Brinkman, *J. Crystal Growth* **237** (2002) 1711.
269. W. Palosz, K. Grasza, K. Durose, D.P. Halliday, N.M. Boyall, M. Dudley, B. Raghothamachar and L. Cai, *J. Crystal Growth* **254** (2003) 316.
270. M. Laasch, R. Schwarz, P. Rudolph and K.W. Benz, *J. Crystal Growth* **141** (1994) 81.
271. R. Schwarz, W. Joerger, C. Eiche, M. Fiederle and K.W. Benz, *J. Crystal Growth* **146** (1995) 92.
272. Z.I. Alferov, V.I. Korolkov, I.P. Mikhailova-Mikheeva, V.N. Romanenko and V.M. Tuchkevitch, *Sov. Phys. Solid State* **6** (1965) 1865.
273. C. Paorici, G. Attolini, C. Pelosi and G. Zuccalli, *J. Crystal Growth* **18** (1973) 289.
274. C. Paorici, G. Attolini, C. Pelosi and G. Zuccalli, *J. Crystal Growth* **21** (1974) 227.
275. C. Paorici, G. Attolini, C. Pelosi and G. Zuccalli, *J. Crystal Growth* **28** (1975) 358.
276. C. Paorici and C. Pelosi, *Rev. Phys. Appl.* **12** (1977) 155.
277. R. Schwarz, M. laasch and K.W. Benz, *Mater. Res. Soc. Symp. Proc.* **340** (1994) 593.
278. V.O. Ukrainets, G.A. Ilchuk, N.A. Ukrainets, Yu.V. Rud'. V.I. Ivanov-Omskii, *Tech. Phys. Lett.* **25** (1999) 642.
279. G.A. Ilchuk, N.A. Ukrainets, V.I. Ivanov-Omskii, Yu.V. Rud' and V.Yu. Rud', *Semiconductors* **33** (1999) 518.
280. G. Ilchuk, V. Ukrainetz, A. Danylov, V. Masluk, J. Parlag and O. Yaskov, *J. Crystal Growth* **242** (2002) 41.
281. M. Yokozawa, S. Otsuka and S. Takayanagi, *Jpn. J. Appl. Phys.* **4** (1965) 1018.
282. M.R. Lorenz and S.E. Blum, *J. Electrochem. Soc.* **113** (1966) 559.
283. M. Isshiki, M. Sato and K. Masumoto, *J. Crystal Growth* 78 (1986) 58.
284. H. Chibani, J.P. Stoquert, M. hage-Ali, J.M. Koebel, M. Abdesselam and P. Siffert, *Appl. Surface Sci.* **50** (1991) 177.
285. L. Kuchar, J.M. Ivanov and J.M. Drapala, *Scientific Papers of the School of Mines (VSB) Ostrava*, Vol. 32, 1st Met. Ser. (Ostrva, 1986)
286. P. Rudolph, M. Muhlberg, M. Neubert, T. Boeck, P. Mock, L. Parthier and K. Jacobs, *J. Crystal Growth* **118** (1992) 204.
287. M. Schiever, R.B. James, H. Hermon, A. Vilensky, I. Baydjanov, M. Goorsky, T. Lam, E. Meerson, H.W. Yao, J. Erickson, E. Cross, A. Burger, J.O. Ndap, G. Wright and M. Fiederle, *J.*

Crystal Growth **231** (2001) 235.
288. S.B. Qadri, E.F. Skelton, A.W. Webb and J. Kennedy, *Appl. Phys. Lett.* **46** (1985) 257.
289. A. Sher, A.B. Chen, W.E. Spicer and C.K. Shin, *J. Vac. Sci. Technol.* **A3** (1985) 105.
290. K. Guergouri, R. Triboulet, A. Tromson-Carli and Y. Marfaing, *J. Crystal Growth* **86** (1988) 61.
291. J.L. Pautrat, N. Magnea and J.P. Faurie. *J. Appl. Phys.* **53** (1982) 8668.
292. R.C. Bowman, Jr. and D.E. Cooper, *Appl. Phys. Lett.* **53** (1988) 1521.
293. R.K. Bagai, R.D.S. Yadava, B.S. Sundersheshu, G.L. Seth, M. Anandan and W.N. Borle, *J. Crystal Growth* **139** (1994) 259.
294. W. Akutagawa, D. Turnbull, W. K. Chu and J.W. Mayer, *J. Phys. Chem. Solid* **36** (1975) 521.
295. M. Inoue, I. Teramoto and S. Takayanagi, *J. Appl. Phys.* **33** (1962) 2578.
296. M. Inoue, I. Teramoto and S. Takayanagi, *J. Appl. Phys.* **34** (1963) 404.
297. M. Inoue, I. Terarnoto and S. Takayanagi, *Natl. Tech. Rep.* **9** (1963) 111.
298. K. Nakagawa, K. Maeda and S. Takeuchi, *Appl. Phys. Lett.* **34** (1979) 574.
299. P. Gaugash and A.G. Milnes, *J. Electrochem. Soc.* **128** (1981) 924.
300. R.K. Bagai, g. Mohan, G.L. Seth and W.N. Borle, *J. Crystal Growth* **5** (1987) 386.
301. B. Wermke and N. Muhlberg, *Cryst. Res. Technol.* **24** (1989) 365.
302. I. Hahnert and M. Schenk, *J. Crystal Growth* **101** (1990) 251.
303. C.C.R. Watson, K. Durose, A.J. Banister, E. O'Keefe and S.K. Bains, *Mater. Sci. Engineer.* **B16** (1993) 113.
304. U. Gilabert, A.B. Trigubo and N.E. Walsoe de Reca, *Mater. Sci. Engineer.* **B27** (1994) L11.
305. P.F. Fewster and P.A.C. Whiffin, *J. Appl. Phys.* **54** (1983) 4668.
306. A. Tanaka, Y. Masa, S. Seto and T. Kawasaki, in *Extended Abstr. 17th Int. Conf. Solid State Dev. Mater.* (Tokyo, 1985) p. 160.
307. C. Hsu, S. Sivananthan, X. Chu and J.P. Faurie, *Appl. Phys. Lett.* **48** (1986) 908.
308. Y. C. Lu, C. M. Stahle, J. Morimoto, R. H. Bube and R. S. Feigelson, *J. Appl. Phys.* **61** (1987) 924.
309. H. Iwanaga, T. Yoshiie, S. Takeuchi and K. Mochizuki, *J. Crystal Growth* **61** (1983) 691.
310. E. A. Hewat, L. DiCioccio, A. Million, M. Dupuy and J. P. Gaailliard, *J. Appl. Phys.* **63** (1988) 4929.
311. S. B. Qadri,and J. H. Dinan, *Appl. Phys. Lett.* **47** (1985) 1066.
312. S. B. Qadri, M. Fatemi and J. H. Dinan, *Appl. Phys. Lett.* **48** (1986) 239.
313. Y. Maeda and S. Takeuchi, *Solid Physics* **13** (1978) 461.
314. J.P. Chamonal, L.E. Molva, M. Dupuy, R. Accomo and J.L. Pautrat, *Physica* **116B** (1983) 519.
315. P.E. Sulewski, R.D. Dynes, S. mahajan amd D.J. Bishop, *J. Appl. Phys.* **54** (1983) 5711.
316. L.O. Bublac, W.E. Tennant, D.D. Edwall, E.R. Gertner and J.C. Robinson, *J. Vac. Sci. Technol.* **A3** (1985) 163.
317. C. Diaz-Guerra, U. Pal, P. Fernandez and J. Piqueras, *phys. stat. sol. (a)* **147** (1995) 75.
318. M. Wada, J. Suzuki and H. Hosomatsu, *Jpn. J. Appl. Phys.* **25** (1986) L780.
319. P. Buck and M. Nagel, *Z. Kristall.* **157** (1981) 291.
320. J. Auleytner, Z. Liliental, E. Mizera and T. Warminski, *phys. stat. sol. (a)* **55** (1979) 603.
321. D.J. Larson Jr., R.P. Silberstein, D. DiMarzio, F.C. Carlson, D. Gillies, G. Long, M. Dudley and J. Wu, *Semicond Sci. Technol.* **8** (1993) 911.
322. M. Muhlberg, P. Rudolph, C. Genzel, B. Wermke and U. Becker, *J. Crystal Growth* **101** (1990) 275.
323. I. Hahnert, M. Muhlberg, H. Berger and Ch. Genzel, *J. Crystal Growth* **142** (1994) 310.
324. K. Suzuki, M. Ichihara, K. Nakagawa, K. Maeda and S. Takeuchi, *Phil. Mag.* **A43** (1981) 499.
325. A. Orlova, J.P. Riviere and J. Castaing, *Rev. Phys. Appl.* **20** (1985) 449.
326. R. S. Rai, S. Mahajan, S. McDevitt and C. J. Johnson, *J. Vac. Sci. Technol.* **B9** (1991) 1892.
327. D.R. Acosta and F. Rabago, *Mater. Res. Soc. Symp. Proc.* **324** (1994) 433.
328. K. Guergouri, N. Brihi and R. Triboulet, *J. Crystal Growth* **209** (2000) 709.
329. A.Y. Wu and R.J. Sladek, *J. Appl. Phys.* **53** (1982) 8589.
330. K. Matsuura, N. Itoh and T. Suita, *J. Phys. Soc. Jpn.* **22** (1967) 1118.

331. E.L. Hall and J.B.V. Sande, *J. Am. Cer. Soc.* **61** (1978) 417.
332. E.L. Hall and J.B.V. Sande, *Phil. Mag. A* **37** (1978) 137.
333. K. Nakagawa, K. Maeda and S. Takeuchi, *J. Phys. Soc. Jpn.* **49** (1980) 1909.
334. P. Haasen, Müller and G. Zoth, *J. Phys.* **44** (1983) C4-365.
335. H.G. Brion, c. Mewes, I. Hahn and U. Schaufele, *J. Crystal Growth* **134** (1993) 281.
336. H.N. Jayatirtha, D.O. Henderson, A. Burger and M.P. Volz, *Appl. Phys. Lett.* **62** (1993) 573.
337. P. Rudolph, A. Engel. I. Schentke and A. Grochocki, *J. Crystal Growth* **147** (1995) 297.
338. T.J. Magee, J.Peng and J. Bean, *phys. stat. sol. (a)* **27** (1975) 557.
339. W.J. Kim, M.J. Park, S.U. Kim, T.S. Lee, J.M. Kim, W.J. Song and S.H. Suh, *J. Crystal Growth* **104** (1990) 677.
340. R.D.S. Yadava, B.S. Sundersheshu, M. Anandan, R.K. Bagai and W.N. Borle, *J. Electron. Mater.* **23** (1994) 1349.
341. S.H. Shin, J. Bajaj, L.A. Moudy and D.T. Cheung, *Appl. Phys. Lett.* **43** (1983) 68.
342. M.E. Rodriguez, O. Zelaya-Angel, J.J. Perez Bueno, S. Jimenez-Sandoval and L. Tirado, *J. Crystal Growth* **213** (2000) 259.
343. P. Franzosi, G. Salviali and M. Scoffardi, *J. Electrochem. Soc.* **142** (1995) 3185.
344. P. Rudolph, M. Neubert and M. Mühlberg, *J. Crystal Growth* **128** (1993) 582.
345. R.U. Barz and P. Gille, *J. Crystal Growth* **149** (1995) 196.
346. R.D.S. Yadava, R.K. Bagai and W.N. Borle, *J. Electron. Mater.* **21** (1992) 1001.
347. T.S. Lee, Y.T. Jeoung, H.K. Kim, J.M. Kim, I.H. Park, J.M. Chang, S.U. Kim and M.J. Park, in *Proc. 2nd Int. Symp. Long Wave Infrared Arrays Phys. Appl.* (1994, Miami) p. 242.
348. N.V. Sochinskii, M.D. Serrano, E. Dieguez, F. Agullo-Rueda, U. Pal, J. Piqueras and P. Fernandez, *J. Appl. Phys.* 77 (1995) 2806.
349. N.V. Sochinskii, E. Dieguez, U. Pal, J. Piqueras, P. Fernandez and F. Agullo-Rueda, *Semicond. Sci. Technol.* **10** (1995) 870.
350. F.A. Kröger, *Rev. Phys. Appl.* **12** (1977) 205.
351. F.A. Kröger, in *The Chemistry of Imperfect Crystals Vol. 2, 2nd ed.* (North Holland, Amsterdam, 1974) p. 728.
352. S.S. Chern and F.A. Kröger, *J. Solid State Chem.* **14** (1975) 44.
353. J.L. Pautrat, J.M. Francou, N. Magnea, E. Molva and K. Saminadayar, *J. Crystal Growth* **72** (1985) 194.
354. H. Ouyang, M.L. Peng, Y.M. Lin, M.H. Yang and H.L. Hwang, *J. Crystal Growth* **72** (1985) 232.
355. P. Hoschl, P. Moravec, J. Franc, E. Beltas and R. Grill, *Nucl. Instr. Meth. Phys. Res.* **A322** (1992) 371.
356. H. Zimmermann, R. Boyn, P. Rudolph, J. Bollmann and a. Klimakow, *Mater. Sci. Engineer.* **B16** (1993) 139.
357. H. Zimmermann, R. Boyn, P. Rudolph, C. Albers, K.W. Benz, d. sinerius, C. Eiche, B.K. Meyer and D.M. Hoffmann, *J. Crystal Growth* **128** (1993) 593.
358. P. Rudolph, H. Schroter, U. Rinas, H. Zimmermann and R. Boyn, *Adv. Mater. Opt. Electron.* **3** (1994) 2
359. V. Ostheimer, T. Filz, J. Hamann, St. Lauer, D. Weber, H. Wolf and Th. Wichert, *Mater. Sci. Forum* **258** (1997) 1341.
360. B.K. Meyer, D.M. Hofmann, W. Stadler, P. Emanuelsson, P. Omling, E. Weigel, G. Muller-Vogt, F. Wienecke and M. Schenk, *Mater. Res. Soc. Symp. Proc.* **299** (1994) 185.
361. L. Yujie, M. guoli and J. Wanqi, *J. Crystal Growth* **256** (2003) 266.
362. R. Stuck, J. C. Muller and P. Siffert, *Phys. Appl.* **12** (1977) 185.
363. T. Takebe, J. Saraie and H. Matsunami, *J. Appl. Phys.* **53** (1982) 457.
364. S.G. Elkomoss, M. Samimi, M. Hage-Ali and P. Siffert, *J. Appl. Phys.* **57** (1985) 5313.
365. S.G. Elkomoss, M. Samimi, S. Uramuno, M. Hage-Ali and P. Siffert, *J. Appl. Phys.* **61** (1987) 2230.
366. R. Lergos, Y. Marfaing and R. Triboulet, *J. Phys. Chem. Solids* **39** (1978) 179.

367. T. Takebe, M. Ono, J. Saraie and T. Tanaka, *Solid State Commun.* **37** (1981) 391.
368. D. Verity, F.J. Bryant, C.G. Scott and D. Shaw, *J. Crystal Growth* **59** (1982) 234.
369. L.C. Isett and P.K. Raychadhuri, *J. Appl. Phys.* **55** (1984) 3605.
370. M. Tomitori, M. Kuriki S. Ishii, S. Fuyuki and S. Hayakawa, *Jpn. J. Appl. Phys.* **24** (1985) L329.
371. T. Ido, A. Heurtel, Y. Marfaring and R. Triboulet, in *Extended Abstr. 18th Int. Conf. Solid State Dev. Mater.* (Tokyo, 1986) p. 31.
372. M. Tomitori, M. Kuriki and S. Hayakawa, *Jpn. J. Appl. Phys.* **26** (1987) 588.
373. A. Castaldini, A. Cavallini, B. Fraboni, J. Piqueras and L. Polenta, *Inst. Phys. Conf. Ser.* **149** (1996) 115.
374. J.-J. Shiau, A.L. Fahrenbruch and R.H. Bube, *J. Appl. Phys.* **61** (1987) 1340.
375. J. Morimoto, M. Fudamoto, S. Tashiro, M. Arai, T. Miyakawa and R. Bube, *Jpn. J. Appl. Phys.* **27** (1988) 2256.
376. L.Carlsson and C.N. Ahlquist, *J. Appl. Phys.* **43** (1972) 2529.
377. M.R. Lorenz and B. Segall, *Phys. Lett.* **7** (1963) 18.
378. M.R. Lorenz and H.H. Woodbury, *Phys. Rev. Lett.* **10** (1963) 215.
379. B. Segall, M.R. Lorenz and R.E. Halsted, *Phys. Rev.* **129** (1963) 2471.
380. M.R. Lorenz, B. Segall and H.H. Woodbury, *Phys. Rev.* **134** (1964) A751.
381. R.C. Whelan and D. Shaw, *phys. stat. sol.* **29** (1968) 145.
382. K.R. Zanio, *App. Phys. Lett.* **15** (1969) 260.
383. N.V. Agrinskaya, E.N. Arkad'eva, O.A. Matveev and Yu.V. Rud', *Sov. Phys. Semicon.* **2** (1969) 776.
384. V.A. Chapin, *Sov. Phys. Semicon.* **3** (1969) 481.
385. F.T. Smith, *Met. Trans.* **1** (1970) 617.
386. B.M. Vul, V.S. Vavilov, V.S. Ivanov, V.B. Stopachinskii and V.A. Chapnin, *Sov. Phys. Semicon.* **6** (1973) 1255.
387. K. Mochizuki, *Jpn. J. Appl. Phys.* **20** (1981) 671.
388. E.N. Arkad'eva, O.A. Matveev and Yu. V. Rud', *Sov. Phys. Solid State* **6** (1964) 798.
389. B.L. Crowder and W.H. Hammer, *Phys. Rev.* **150** (1966) 150.
390. E.N. Arkad'eva, O.A. Matveev and Yu. V. Rud', *Sov. Phys. Solid State* **8** (1967) 2260.
391. E.N. Arkad'eva, O.A. Matveev and V.A. Sladkova, *Sov. Phys. Semicon.* **2** (1969) 1264.
392. J. Saraie, *Oyo Buturi (Monthly Publ. Jpn. Soc. Appl. Phys.) (in japanese)* **49** (1980) 941.
393. A.A. Alnajjar, C.C.R. Watson, A.W. Brinkman and K. Durose, *J. Crystal Growth* **117** (1992) 385.
394. K.A. Kikoin, I.G. Kurek and S.V. Mel'nichuk, *Sov. Phys. Semicon.* **24** (1990) 371.
395. A.-B. Chen and A. Sher, *Phys. Rev. B* **31** (1985) 6490.
396. N.V. Agrinskaya, M.V. Alekseenko, E.N. Arkad'eva, O.A. Matveev and S.V. Prokof'ev, *Sov. Phys. Semicon.* **9** (1975) 208.
397. R. Stuck, A. Cornet, C. Scharager and P. Siffert, *J. Phys. Chem. Solids* **37** (1976) 989.
398. M. Baj, L. Dmowski, M. Konczykowski and S. Porwoski, *phys. stat. sol. (a)* **33** (1976) 421.
399. A. Zoul and E. Klier, *Czech. J. Phys.* **B27** (1977) 789.
400. M. Hage-Ali, C. Scharager, J.M. Koebel and P. Siffert, *Nucl. Instr. Meth.* **176** (1980) 499.
401. Y. Marfaing, *Prog. Crystal Growth Character.* **4** (1981) 317.
402. O.M. Matveev and A.I. Terent'ev, *Semiconductors* **27** (1993) 1043.
403. M. Hage-Ali and P. Siffert, *Nucl. Instr. Meth. Phys. Res.* **A322** (1992) 313.
404. O.M. Matveev and A.I. Terent'ev, *Semiconductors* **32** (1998) 144.
405. J. P. Noblanc, J. Loudette and G. Duraffourg, *J. Lumin.* **1/2** (1970) 528.
406. S. Suga, W. Dreybrodt, F. Willman, P. Hiesinger and K. Cho, *Solid State Commun.* **15** (1974) 871.
407. K. Cho, W. Drebrodt, P. Hiesinger, S. Suga and F. Willman, in *Proc. 12th Int. Conf. Phys. Semicon.* (1974) p. 945.
408. Taguchi, J. Shirafuji, and Y. Inuishi, *phys. stat. sol. (b)* **68** (1975) 727.
409. P. Hiesinger, S. Suga, F. Willman and W. Drebrodt, *phys. stat. sol. (b)* **67** (1975) 641.
410. Z. C. Feng, A. Mascarenhas and J. f. Schetzina, *J. Lumin.* **35** (1986) 329.

411. N. C. Giles, R. N. Bicknell and J. F. Schetzina, *J. Vac. Sci. Technol.* **A5** (1987) 3064.
412. Z. C. Feng, M. J. Bevan, W. J. Choyke and S. V. Krishnaswamy, *J. Appl. Phys.* **64** (1988) 2595.
413. Z. C. Feng, M. G. Burke and W. J. Choyke, *Appl. Phys. Lett.* **53** (1988) 128.
414. H. Zimmermann, R. Boyn, C. Michel and P. Rudolph, *J. Crystal Growth* **101** (1990) 691.
415. T. Schmidt, G. Daniel and K. Lischka, *J. Crystal Growth* **117** (1992) 748.
416. D.P. Halliday, M.D.G. Potter, J.T. Mullins and A.W. Brinkman, *J. Crystal Growth* **220** (2000) 30.
417. M. S. Brodin, Y. P. Gnatenko, M. V. Kurik and V. M. Matlak, *Sov. Phys. Semicon.* **3** (1970) 835.
418. E. Molva, J. P. Chamonal, and J. L. Pautrat, *phys. stat. sol. (b)* **109** (1982) 635.
419. P. Chamonal, E. Molva, and J. L. Pautrat, *Solid State Commun.* **43** (1982) 801.
420. E. Molva, K. Saminadayar, J. L. Pautrat, and E. Ligeon, *Solid State Commun.* **48** (1983) 955.
421. E. Molva, J. M. Francou, J. L. Pautrat, K. Saminadayal and L. S. Dang, *J. Appl. Phys.* **56** (1984) 2241.
422. A. Krol, R. Zielinska and W. Nazarewicz, *J. Crystal Growth* **72** (1985) 242.
423. M. James, J. L. Merz, and C. E. Jones, *Appl. Phys. Lett.* **46** (1985) 424.
424. E. Molva and Le Si Dang, *Phys. Rev. B* **32** (1985) 1156.
425. K. M. James, J. D. Flood, J. L. Merz, and C. E. Jones, *J. Appl. Phys.* **59** (1986) 3596 .
426. E. Cooper, J. Bajaj, and P. R. Newman, *J. Crystal Growth* **86** (1988) 544.
427. S. Seto, A. Tanaka, and M. Kawashima, *J. Appl. Phys.* **64** (1988) 3658 .
428. H. Zimmermann, R. Boyn, C. Michel and P. Rudolph, *phys. stat. sol. (a)* **118** (1990) 225.
429. S. Seto and A. Tanaka, *Mater. Sci. Forum* **117/118** (1993) 471.
430. S. Seto, *Ishikawa Nat. College Technol. Bull.* **25** (1993) 39.
431. D.P. Halliday, M.D.G. Potter, J.T. Mullins and A.W. Brinkman, *J. Crystal Growth* **220** (2000) 30.
432. C. E. Barnes and K. Zanio, *J. Appl. Phys.* **46** (1975) 3959.
433. K. Saminadayar, J. M. Francou and J. L. Pautrat, *J. Crystal Growth* **72** (1985) 236.
434. S. Seto, A. Tanaka, Y. Masa and M. Kawashima, *J. Crystal Growth* **117** (1992) 271.
435. T. Shoji, K. Ohba, T. Suehiro and Y. Hiratate, *IEEE Trans. Nucl. Sci.* **40** (1993) 405.
436. T. Shoji, H. Onabe, K. Ohba, T. Suehiro and Y. Hiratate, *IEEE Trans. Nucl. Sci.* **40** (1993) 50.
437. R.E. Halsted and M. Aven, *Phys. Rev.* **14** (1963) 64.
438. F. J. Bryant, D. H. Totterdell and W. E. Hagston, *J. Phys.* **C4** (1971) 641.
439. B. Furgolle, M. Hoclet and M. Vandevyver, *Solid State Commun.* **14** (1974) 1237.
440. C. B. Norris and C. E. Barnes, *Rev. Phys. Appl.* **12** (1977) 219.
441. C. B. Norris, *J. Lumin.* **16** (1978) 297.
442. C. B. Norris, *J. Elecron. Mater.* **9** (1980) 499.
443. C. B. Norris and K. R. Zanio, *J. Appl. Phys.* **53** (1982) 6347.
444. J. M. Figueroa, F. Sanchez-Sinencio, J. M. Mendoza-Alvarez, O. Zelaya, C. Vazquez-Lopez and J. S. Helman, *J. Appl. Phys.* **60** (1986) 452.
445. W. J. Choyke, M. G. Burke, Z. C. Feng, M. H. Hanes and A. Masscarenhas, in *Defects in Semicon ductors Vols. 10-11*, ed. H. J. von Bardeleben (Schetzina, 1986) p. 769.
446. S. Seto, A. Tanaka, Y. Masa, S. Dairaku and M. Kawashima, *J. Appl. Phys.* **53** (1988) 1524.
447. L.O. Bublac, J. Bajaj, W.E. Tennant, P.R. Newman and D.S. Lo, *J. Crystal Growth* **86** (1988) 536.
448. A.V. Kvit, Yu, V. Klevkow, S.R. Oktyabrsky and B.G. Zhurkin, *Semicon. Sci. Technol.* **9** (1994) 1805.
449. N.G. Giles-Taylor, R.N. Bicknell, D.K. Blanks, T.H. Myers and J.F. Schetzina, *J. Vac. Sci. Technol.* **A3** (1975) 76.
450. T. Taguchi, *phys. stat. sol. (a)* 77 (1983) K115.
451. E. Cohen, R. A. Street and A. Muranevich, *Phys. Rev.* **B28** (1983) 7115.
452. J. Gonzalez-Hernandez, E. Lopez-Curz, D. D. Allred, W. P. Allred, *J. Vac. Sci. Technol.* **A8** (1990) 3255.
453. E. Lopez-Curz, J. Gonzalez-Hernandez, D. D. Allred and W. P. Allred, *J. Vac. Sci. Technol.* **A8** (1990) 1934.
454. K. Oettinger, D. M. Hofmann, Al. L. Etros and B. K. Meyer, *J. Appl. Phys. 71 (1992) 4523.*

455. J.F. Butler, A.W. Brinkman, in *Narrow Gap Cdmium Based Compounds*, ed. P. Capper (INSPEC, London, 1994) p. 587.
456. P. Capper, J. Gosney, J.E. Harris, E. O'Kefefe and C.D. Maxey, *GEC J. Res.* **13** (1996) 164.
457. C.C. Wang, M. Chu, S.H. Shin, W.E. Tennant, J.T. Cheung, M. Lanir, A.H.B. Vanderwyck, G.M. Williams, L.O. Bubulac and R.J. Eisel, *IEEE Trans. Electron. Devices* **ED-27** (1980) 154.
458. P. Capper, J. Gosney, J.E. Harris, E. O'Kefefe and C.D. Maxey, *GEC J. Res.* **13** (1996) 175.
459. P. Vohl and Ch.M. Wolfe, *J. Electron. Mater.* 7 (1978) 659.
460. M. Cuzin, *Nucl. Instr. Meth.* **A253** (1987) 407.
461. E.N. Arkad'eva, O.A. Matveev, Yu. V. Rud' and S.M. Ryvkin, *Sov. Phys. Tech. Phys.* **11** (1966) 846.
462. E.N. Arkad'eva, L.V. Maslova, O.A. Matveev, Yu. V. Rud' and S.M. Ryvkin, *Sov. Phys. Semicon.* **1** (1967) 669.
463. R.O. Bell and F.V. Wald, *IEEE Trans. Nuclear Sci.* **NS-21** (1974) 331
464. K. Zanio, F. Krajenbrink and H. Montano, *IEEE Trans. Nucl. Sci.* **NS-21** (1974) 315.
465. P. Siffert, A. Cronte, R. Stucj, R. Triboulet and Y. Marfaing, *IEEE Trans. Nucl. Sci.* **NS-22** (1975) 211.
466. T. Taguchi, T. Shoji, Y. Hiratate and Y. Inuishi, *Inst. Phys. Conf. Ser.* **46** (1979) 399.
467. J.F. Buttler, C.L. Lingren and F.P. Doty, *IEEE Trans. Nucl. Sci.* **39** (1992) 605.
468. A. Niemela and H. Sipila, *IEEE Trans. Nucl. Sci.* **41** (1994) 1054.
469. L. Verger, N. Baffert, M. Rosaz and J. Rustique, *Nucl. Instr. Meth. Phys. Res.* **A380** (1996) 121.
470. M. Fiederle, T. Feltgen, J. Meinhardt, M. Rogalla and K.W. Benz, *J. Crystal Growth* **197** (1999) 635.
471. A.A. Melnikov, *J. Crystal Growth* **197** (1999) 663.
472. T. Shoji, K. Ohba and Y. Hiratate, *phys. stat. sol. (a)* **57** (1980) 765.
473. L. Verger, M. Cuzin, G. Gaude, F. Glasser, F. Mathy, J. Rustique and B. Schaub, *Nucl. Instr. Meth. Phys. Res.* **A323** (1992) 357.
474. C. Matsumoto, T. Takahashi, K. Takizawa, R. Ohno, T. Ozaki and K. Mori, *IEEE Trans. Nucl. Sci.* **45** (1998) 428
475. M. Fiederle, T. Feltgen, J. Meinhardt, M. Rogalla and K.W. Benz, *J. Crystal Growth*h **197** (1999) 635.
476. M.R. Squilliante, and G. Entine, *Nucl. Instr. Meth. Phys. Res.* **A322** (1992) 569.
477. K. Hori and T. Fujimoto, *Nucl. Instr. Meth. Phys. Res.* **A380** (1996) 397.
478. Y. Eisen and A. Shor, *J. Crystal Growth* **184/185** (1998) 1302.
479. M. Rodot, *Rev. Phys. Appl.* **12** (1977) 411.
480. V.P. Singh, H. Brafman, J. Makwana and J.C. McClure, *Solar Cells* **31** (1991) 23.
481. J. Kiefer and A. Yariv, *Appl. Phys. Lett.* **15** (1969) 26.
482. G.L. Herrit, H.E. Reedy, in *Optical materials, Process. Sci. Symp.* (San Diego, USA, 1989, Mater. Res. Soc.) p. 169.
483. A. Milani, E. Bocchi, A. Zappettini, S.M. Pietralunga and M. Martinelli, *J. Crystal Growth* **214/215** (2000) 913.
484. B. Bendow and R.D. Gianini, *Opt. Commun.* **9** (1973) 306.
485. T.F. Deuche, *J. Electron. Mater.* **4** (1975) 663.
486. R.B. Bylsma, P.M. Brindenbaugh, D.H. Olson and A.M. Glass, *Appl. Phys. Lett.* **51** (1987) 889.
487. A. Partovi, J. Millerd, E.M. Garmire, M. Ziari, W.H. Steler, S.B. Trivedi and M.B. Klein, *Appl. Phys. Lett.* **57** (1990) 846.

16. ZnS

16.1 INTRODUCTION

ZnS has a wide bandgap (3.65 eV) with direct transition and is a promising material for blue light LEDs and LDs. Therefore many studies have been performed for a long period of time but these light emitting devices have still not been realized. The main reason is that high quality ZnS single crystals can not be grown because the melting point is as high as 1830 °C and the dissociation pressure is high (3.7×10^4 Pa). ZnS also has a transformation transition from a high temperature wurtzite phase to a low temperature zincblende phase at about 1060 °C. The p-n control of ZnS is also difficult as with other II-VI materials due to self compensation phenomena. Blue light emitting diodes were first attempted by Aven[1] and since then many studies have been performed as reviewed in Refs. 2-4.

16.2 PHYSICAL PROPERTIES

The physical properties of ZnS can be found in Refs. 5-9 and are summarized in Table 16.1. Precise melting point and vapor pressures were determined by Addamiano et al.[10] Crystal growth must therefore take place at lower temperatures than this temperature. So far, about 150 polytypes have been reported.[11] Some typical examples are shown in Fig. 16.1. The phase diagram of ZnS has been determined by Sharma et al.[12] as shown in Fig. 16.2.

16.3 CRYSTAL GROWTH

Since ZnS has a high melting point of 1830 °C and the decomposition pressure is as high as 3.7×10^4 Pa, melt growth and solution growth are rather difficult. Because of the phase transition at about 1060 °C, crystals grown at high temperatures will contain

Table 16.1 Physical Properties of ZnS

	α-ZnS	β-ZnS
Crystal Structure	wurtzite	zincblende
Lattice Constant	a = 3.820 Å c = 6.260 Å	a = 5.4093 Å
Density	4.087 g/cm³	4.102 g/cm³
Melting Point	1830 °C	
Linear Expansion Coefficient	6.48×10^{-6} / deg	$\times 10^{-6}$ / deg
Thermal Conductivity	0.27 W/cm·K	W/cm·K
Dielectric Constant	8.3	9.6
Refractive index	2.705	
Bandgap at Room Temperature	3.66 eV	3.54 eV
Optical Transition Type	direct	direct
Electron Mobility at R.T.	140 cm²/V·sec	cm²/V·sec
Hole Mobility at R.T.	10-15 cm²/V·sec	cm²/V·sec

defects such as stacking faults so that vapor phase crystal growth at lower temperatures is the main method used. Crystal growth of ZnS is summarized in Table 16.2.

16.3.1 Melt Growth

The first experiment to melt ZnS in a high pressure furnace was carried out very long time ago.[13] Fisher,[14-17] Medcalf et al.[18] and Addamiano[19] have developed a growth method from the melt under high argon pressure. Ebina et al.[20] have grown ZnS single crystals by the Tamman method. Kozielski et al.[21-23] have grown ZnS crystals, $Zn_{1-x}Cd_xS$ and $ZnS_{1-x}Se_x$ mixed crystals by the high pressure Bridgman method as shown in Fig. 16.3. It was found that various polytypes such as 4H, 6H, 10H, 2H and 3C were obtained as seen in Fig. 16.4. Tm doping in ZnS single crystals was performed by the high pressure Bridgman method and the distribution coefficient of Tm was determined to be $k_0 = 0.09$.[26]

These melt growth studies made it clear that ZnS has many kinds of polytypes and it was found difficult to grow uniform phase single crystals.

16.3.2 Solution Growth

Mita has grown ZnS single crystals from NaCl[27,28] and various inorganic molten salts in a growth apparatus as shown in Fig. 16.5. He found KCl was the most appropriate solvent and could grow needle-like single crystals of diameter 1 mm and length 10 mm.

Cubic ZnS crystals have been grown from halide melts.[29,30] Linares[29] has examined the phase diagram of ZnS-ZnF_2 (Fig. 16.6) and applied this diagram to the growth of

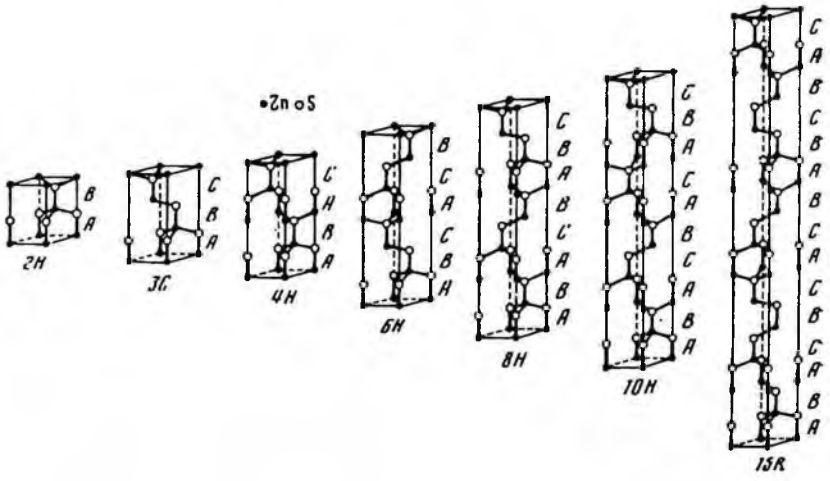

Fig. 16.1 Various polytypes of ZnS (reprinted from Ref. 6 with permission, copyright 1982 Elsevier).

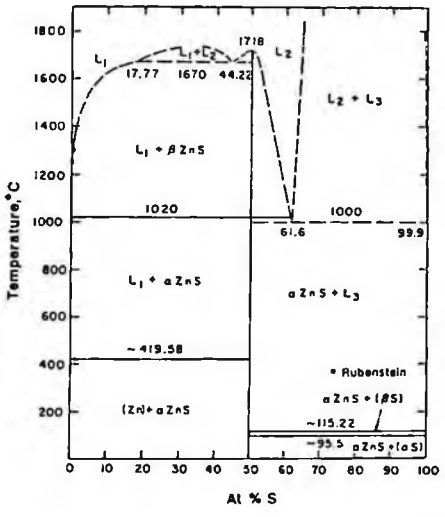

(a)

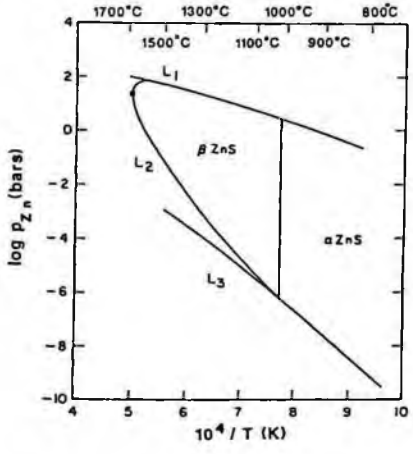

(b)

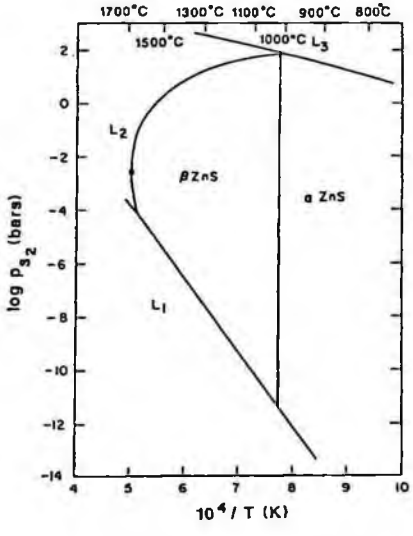

(c)

Fig. 16.2 (a) X-T diagram of ZnS, (b) equilibrium partial pressure of P_{Zn} along the liquidus, (c) equilibrium partial pressure of P_{Te_2} along the liquidus (reprinted from Ref. 12 with permission, copyright 1988 Elsevier).

ZnS from ZnF_2 solvent. Cubic ZnS is stable from 805 °C to at least 1012 °C. Above 1012 °C, cubic and hexagonal and other phases exist. Crystal growth was performed cooling from 1000 °C to 800 °C and cubic single crystals of dimensions 12x6x0.9 mm^3

Table 16.2. Crystal Growth of ZnS

Method	Result	Author	Year	Ref.
VG	Reaction of H_2S with Zn vapor	Lorenz	1891	43
HP-VB	First melt growth of ZnS	Tiede et al.	1920	13
VG	Vaporization under H_2S	Reynolds et al.	1950	44
VG	Sublimation under H_2	Piper et al.	1953	45
VG	Sublimation under H_2 and/or H_2 atmosphere	Kremheller	1955-	46
VG	Growth of crystals of 1-15 g weight	Greene et al.	1960	47
HP-VB	Growth in quartz ampoule covered by graphite crucible	Fisher	1958-1970	14-17
HP-VGF	Growth under various Ar pressures (250-1500 psi)	Medcalf et al.	1958	18
VG	Regrowth of ZnS using polycrystalline ZnS seed	Nishimura	1959	48, 49
HP-VGF	Growth under 150 psi argon atmosphere	Addamiano et al.	1960	19
PVT	Impurity incorporation behavior and heat treatment	Kremheller	1960	50
CVT	Growth of compound semiconductors using I_2 transport reagent	Nitsche	1960-1967	71-73
SG	Growth of needle like crystals from NaCl flux	Mita	1961	27, 28
PVT	Effect of KCl on the structure of grown crystals	Samelson et al.	1961	51
PVT	Self-sealing sublimation method	Piper et al.	1961	52
PVT	Self-sealing method	Indradev	1961	53
CVT	Sublimation growth in H_2S atmosphere	Patek et al.	1961-1962	74-75
SG	Growth of needle like crystals from KCl flux	Mita	1962-1963	27, 28
SG	Growth of 12x6x0.9 mm^3 crystals from ZnF_2 flux	Linares	1962	29
CVT	Growth with HCl as the transport reagent	Jona	1962	76
CVT	Growth with HCl as the transport reagent	Samelson	1962	79
CVT	Growth rate measurement using I_2 as the transport reagent	Jona et al.	1963-1964	77-78
SG	Growth from β-ZnS from ZnF_2 flux	Laudise	1963	30
CVT	Effect of the I_2 reagent content on the morphology of grown crystals	Rumyantsev	1965	80
SG	Solubility in Sn, Cd, Bi. Growth of small crystals	Rubenstein	1966-1968	31-32
PVT	ZnS crystals doped with transition-metals	Indradev et al.	1966	54
HP-VB	Growth at 1850 °C under 50 atm. argon atmosphere	Kozielski	1967	21
HP-VB	Growth of ZnS and ZnCdS and ZnCdSe crystals	Kozielski	1975	22, 23
HP-VB	Growth of ZnS by the Tamman method	Ebina et al.	1967	20
PVT	Growth of $Zn_{1-x}Cd_xS$ by self-sealing Piper-Polish method	Hill et al.	1967	56
SG	Growth from Ga or In melts, 3-5x0.1 mm crystals	Harsey et al.	1967-1968	33-34
SG	Growth from molten halide solutions	Parker et al.	1968	35
SG	Growth of cubic ZnS from $PbCl_2$	Linares	1968	36
PVT	Growth of ZnCdS measuring 15x3x4 mm^3	Indradev et al.	1968	55
CVT	Growth using NH_4Cl and I_2 as the reagent	Lendvey	1971	81

Table 16.2. Crystal Growth of ZnS (continued)

Method	Result	Author	Year	Ref.
CVT	Growth using HCl as the reagent	Ujie et al.	1971	82
PVT	Vertical PVT growth of crystals of several cm^3	Blanconnier et al.	1972	57
HP-VB	Composition analysis after melt growth	Kimura et al.	1973	24
CVT	Growth rate using I_2 as the reagent	Dangel et al.	1973	83
PVT	Theory of growth rate and comparison with the experiment	Tempest et al.	1974	58
PVT	Growth of ZnS_xSe_{1-x} and structural studies	Cutter et al.	1976	59
CVT	Growth rate using I_2 as the reagent	Hartmann	1977	60
PVT/CVT	Comaprison of PVT and CVT	Hartmann	1977	84, 85
HP-VB	Growth ZnCdS and ZnSeS, effect of composition on polytype formation	Kozielski	1975	26
CVT	Growth of ZnS_xSe_{1-x} ($0.2<x<0.8$)	Catano et al.	1976	96
PVT/CVT	Growth of crystals measuring 10x10x5 mm^3	Hartmann	1977	60
SG	Growth fromTe melt	Washiyama et al.	1978	37
PVT	In-situ observation of crystal growth	Shichiri et al.	1978	61
PVT	Modified Piper-Polish method	Russel et al.	1979	62
SG	Growth from molten $PbCl_2$	Nistor et al.	1980	38, 39
PVT	Vertical PVT	Kishida et al.	1980	63
PVT	Growth of 7.5 cm^3 crystals with contactless arrangement using molten tin heating media	Bulakh et al.	1980	64
SG	Growth of plate-like crystals from Te solution	Aoki et al.	1981	40
CVT	Growth of $Zn_{1-x}Cd_xS$ ($x \leqq 0.07$) using I_2 as the reagent	Palosz	1982	86, 87
PVT	Growth of $ZnCd_xS_{1-x}$	Oktik et al.	1983	65
PVT	Growth rate measurement	Kaneko et al.	1984	66
PVT	Growth kinetics and mechanisms	Mochizuki et al.	1985	67, 68
CVT	Growth with I_2 reagent in a vertical furnace	Shouji et al.	1984	88
CVT	Effect of cone angle during growth with I_2 reagent	Yang et al.	1984	89
CVT	Growth with NH_4Cl as the reagent	Matsumoto et al.	1984	90
CVT	Growth of ZnS_xSe_{1-x} and PL measurement	Huang et al.	1986	69
CVT	Growth of large single crystals measuring 10x10x10 mm^3 using I_2 reagent	Kitagawa et al.	1987	91, 92
HP-VB	Process based on HP-VB free of quartz materials	SDS Inc..	1988	25
CVT	Growth with NH_4Cl as the reagent	Noda et al.	1990	93
CVT	Cubic ZnS measuring 1.5 cm^3 using I_2 reagent	Ohno et al.	1990	94
HP-VB	Growth under 100 atm. argon with Tm doping	Boyn et al.	1991	26
SG	Growth from $Sb_{0.4}Te_{0.6}$ alloy solution	Nagano et al.	1991-1992	41, 42
PVT	Growth of mixed crystals of 40-55mm diameter	Korostelin et al.	1996	70

HP-VB: high pressure vertical Bridgman, SG: solution growth, VG: Vapor Growth, PVT: physical vapor transport, CVT: chemical vapor transport

could be obtained. ZnS crystals were grown by the gradient technique in closed transparent silica ampoules. It has been shown that the growth from flux or molten salts yields relatively large crystals.[30]

Rubenstein[31, 32] has measured the solubility of ZnS in tin. Harsey et al.[33, 34] have

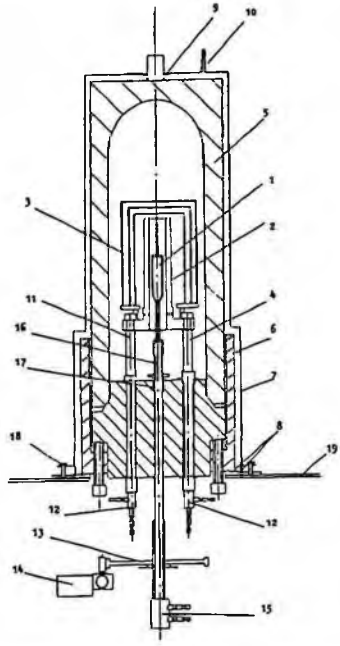

Fig. 16.3 Schematic view of apparatus for ZnS crystal growing: (1) crucible, (2) heater, (3) screens, (4) insulated electrical lead, (5) autoclave, (6) threaded autoclave box, (7) water-cooling jacket, (8) ring gaskets, (9) simmer gasket, (10) water outlet, (11) electrical lead, (12) water inlets, (13) gear wheel, (14) engine with transmission gear, (15) water terminals, (16) sildable rod, (17) rod sealing, (18) cooler set screw, (19) table top (reprinted from Ref. 21 with permission, copyright 1967 Elsevier).

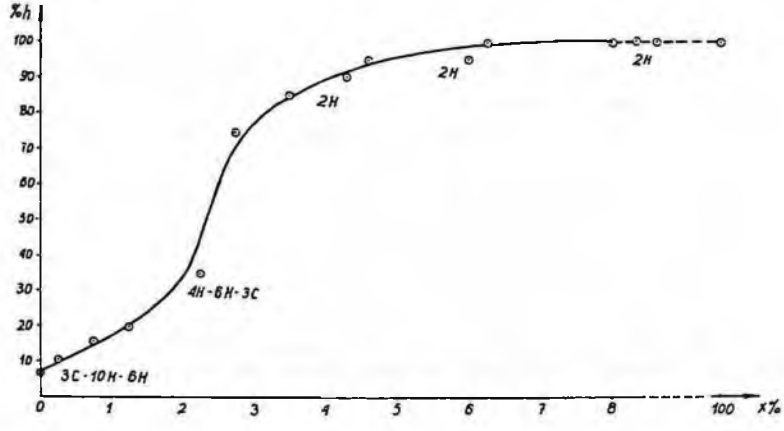

Fig. 16.4 Dependence of average hexagonality on Cd concentration in $Zn_{1-x}Cd_xS$ crystals (reprinted from Ref.23 with permission, copyright 1975 Elsevier).

grown ZnS single crystals from Ga or In solutions. Homogeneous solutions have been prepared at 1000-1200 °C and crystals of 3-5 mm and thickness of 0.1 mm were grown by slow cooling at a rate of 15-20 °C/min.

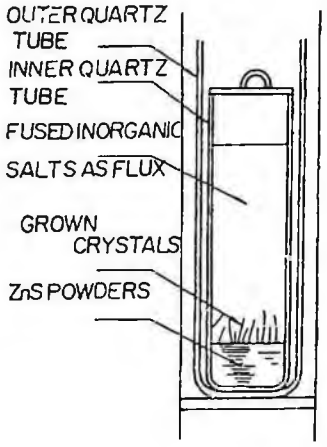

Fig. 16.5 Schematic figure of a solution growth apparatus (from Ref. 28 with permission).

Parker et al.[35] have grown ZnS single crystals from molten halide solutions such as KI, KCl, KI-$ZnCl_2$ and KI-$ZnCl_2$ using an ampoule as shown in Fig. 16.7. The effects of flux compositions, growth temperature and temperature gradient on the morphology of grown crystals have been systematically studied. Cubic ZnS crystals have been grown from halide melts. Linares[36] has grown ZnS single crystals from molten $PbCl_2$ at temperatures from 500 °C to 800 °C.

Washiyama et al.[37] have grown ZnS single crystals from a Te solvent. The solubility of ZnS in Te has been measured and the crystal growth was performed by cooling the

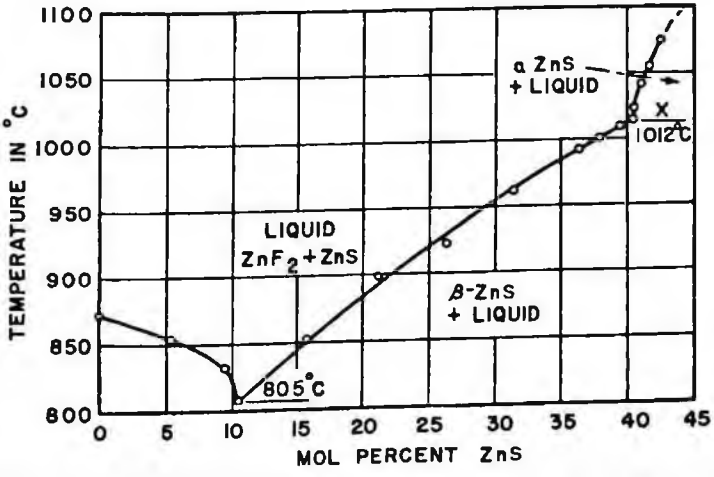

Fig. 16.6 Phase diagram of the system ZnF_2-ZnS.[29]

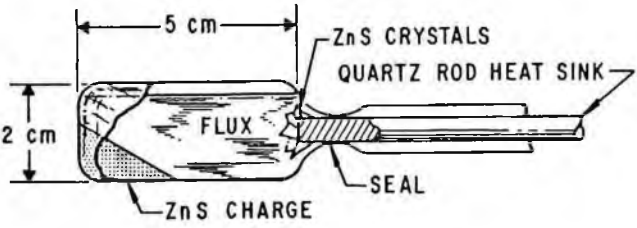

Fig. 16.7 Crystal growth apparatus for a flux growth method (reprinted from Ref. 35 with permission, copyright 1968 Elsevier).

ampoule from 1100-1200 °C to 500-550 °C at a cooling rate of 15-40 °C. Plate-like ZnS single crystals of dimension several mm could be obtained.

Nistor et al.[38, 39] have grown ZnS single crystals from molten $PbCl_2$ by the gradient freezing technique in closed ampoules of transparent silica. The ampoule was suspended in a vertical tube furnace in a temperature gradient of 5 °C/cm with the lowest part of the ampoule kept at 575 °C. Crystals of several mm were grown. They studied the morphology of grown crystals and examined the segregation coefficients of common impurities.[39]

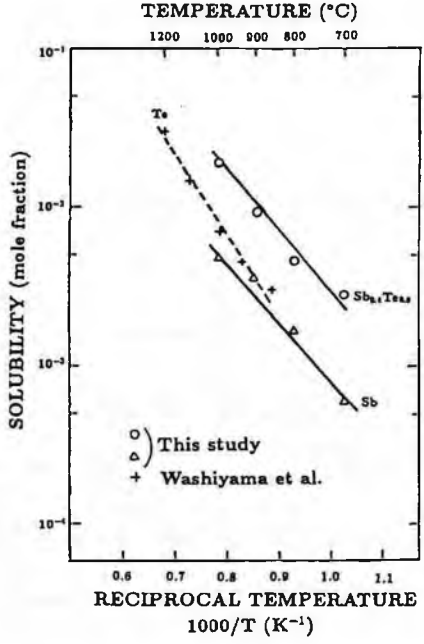

Fig. 16.8 Solubility of ZnS in Te, Sb and $Sb_{0.4}Te_{0.6}$ (from Ref. 41 with permission).

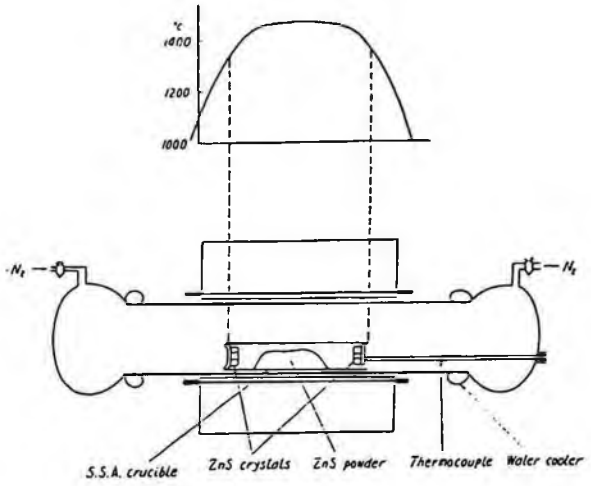

Fig. 16.9 PVT furnace and its temperature distribution (from Ref. 49 with permission).

Nagano et al. have grown ZnS crystals doped with Sb from $Sb_{0.4}S_{0.6}$[41] and ZnS crystals doped with Sb and Te from an $Sb_{0.4}Te_{0.6}$ solution[42] by a temperature difference solution growth method. The solubility is shown in Fig. 16.8, comparing Te and Sb solvents.

16.3.3 Vapor Phase Growth

(1) Physical Vapor Transport (PVT) method

ZnS single crystals have been grown by the vapor phase growth method, mainly by the PVT method and the iodine transport CVT method. In order to grow pure ZnS crystals, PVT methods have been investigated by various authors[43-70] from as early as 1891.

Nishimura[48, 49] has grown ZnS single crystals by the PVT method in a furnace as shown in Fig. 16.9. He examined the effect of growth temperature and the temperature gradient on the morphology and the structure of grown crystals. Samelson and Brophy[51] have grown ZnS single crystals by the PVT method and examined the structure of grown crystals. They found that the addition of KCl at a concentration of 0.5-1.0 mole % was effective in obtaining cubic phase crystals.

Indraev et al.[53-55] have applied a self-sealing vapor phase method (Piper-Polish method, Sec. 2.4.2) for growing ZnS single crystals and $Zn_xCd_{1-x}S$ single crystals. The growth has been performed at 1350 °C under argon, hydrogen sulfide and helium gas atmospheres. ZnS single crystals doped with transition metals have also been grown, using chlorides and sulfides as the dopants. $Zn_xCd_{1-x}S$ single crystals have been grown by the same method and their photovoltaic properties were evaluated.

Hartmann[60] has grown ZnS single crystals by the sublimation method at a charge temperature of 1350 °C and obtained single crystals measuring 5x3x3 mm^3.

Shichiri et al.[61] directly examined crystal growth behavior above and below the transition temperature T_c (1024 °C) using a microscope camera by which crystal growth

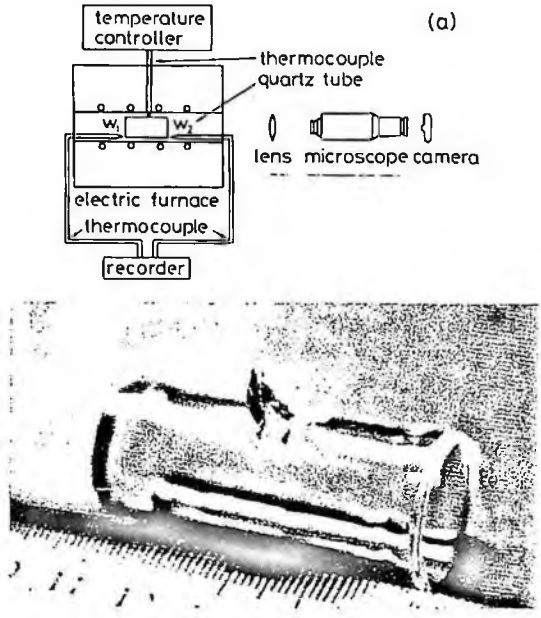

Fig. 16.10 Schematic diagram of (a) apparatus and (b) growth vessel made of quartz (reprinted from Ref. 61 with permission, copyright 1978 Elsevier).

could be observed in-situ in an arrangement as shown in Fig. 16.10.

Russel and Wood[62] examined two PVT methods, a modified Piper-Polish method (Fig. 16.11) and a method using a sealed evacuated capsule. Crystals were grown at about 1600 °C in the former case and mainly wurtzite crystals were obtained. In the latter case, crystals were grown at about 1020 °C, at lower temperatures than the phase

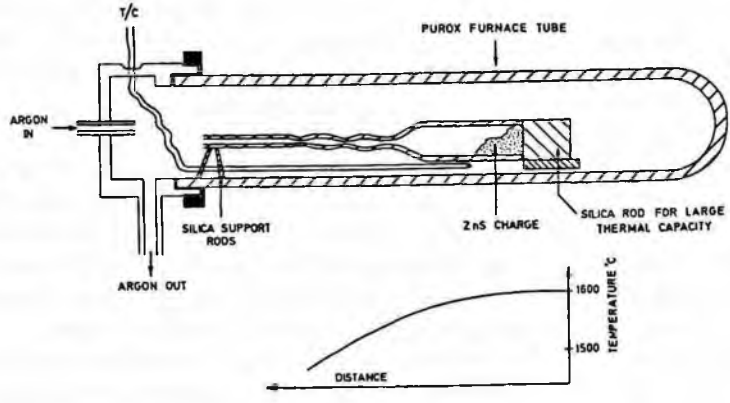

Fig. 16.11 Vapor phase growth of ZnS by a modified Piper-Polish method (reprinted from Ref. 62 with permission, copyright 1979 Elsevier).

transition temperature, and zincblend crystals were obtained.

Kishida et al.[63] have grown ZnS_xSe_{1-x} ($0.89 < x \leqq 1$) mixed crystals by a vertical PVT method and examined their photoluminescence spectra as a function of composition.

Bulakh et al.[64] studied the growth of ZnS on (0001) sapphire, quartz glass and ZnS substrates by the free growth Markov method. They have developed a modified physical vapor transport method, in which the free-growth method invented by Pekar based on the Markov method is used with heating performed by molten tin as explained in Sec. 17.3.3 for ZnSe. This method was used not only for the growth of ZnS single crystals but also $ZnSe_xS_{1-x}$ and ZnSe single crystals. The size of single crystals obtained was up to 7.5 cm^3.

Kaneko and Yumoto[66] measured the growth rate of ZnS and compared the result with a theoretical molecular flux equation. Mochizuke et al.[67,68] studied the sublimation growth of ZnS and ZnS_xSe_{1-x} as a function of the partial pressure of sulphur by using a furnace as shown in Fig. 16.12. The transport rate was determined as shown in Fig.

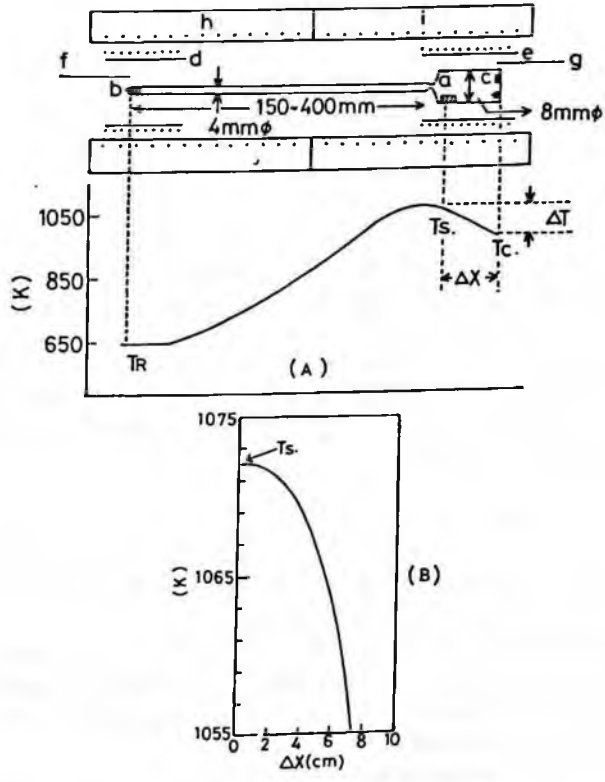

Fig. 16.12 (a) Schematic diagram of (a) furnace and (b) a typical temperature profile (from Ref. 68 with permission).

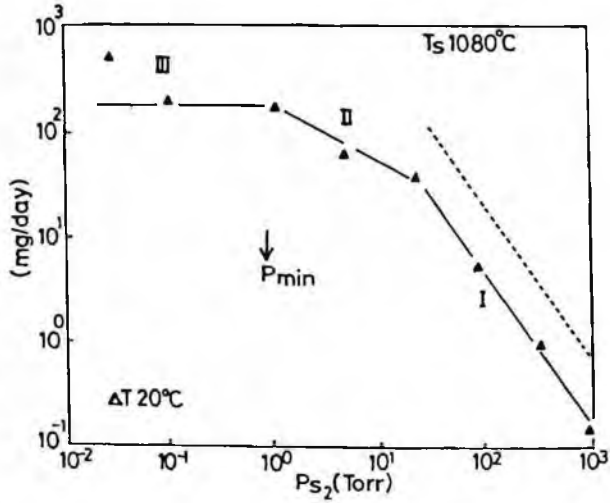

Fig. 16.13 Vapor transport as a function of P_{S_2} (reprinted from Ref. 67 with permission, copyright 1985 Elsevier).

16.13. The vapor transport mechanism and the polarity were discussed as a function of the partial pressure.

(2) Chemical Vapor Transport (CVT) method

Since ZnS has a high melting point with high dissociation pressure and has a phase transition from wurtzite to zincblende, chemical transport methods have been developed since crystal growth can be carried out at temperatures as low as 750-850 °C, even lower than with the physical vapor transport method.

In a closed tube (see the example in Fig. 2.15), ZnS is made to react with I_2 to give a volatile compound ZnI_2 in a high temperature zone, and ZnI_2 is transported to a low temperature zone, where ZnI_2 reacts with sulphur vapor and grown as ZnS single crystals according to the following equation.

$$ZnS + I_2 = ZnI_2 + 1/2S_2 \qquad (16.1)$$

Cl_2 is also used as transport reagent, but since I_2 can be handled as a solid, it is easier to use. The advantages of this method are as follows.

(i) Crystal growth temperature is as low as 750-850 °C, which is much lower than the melting point and is even lower than with the physical transport method.

(ii) Iodine is incorporated in ZnS single crystals and acts as donor for an intense blue emission which is called self activated (SA) emission.

(iii) Cubic single crystals can be obtained.

Crystal growth has been performed by various researchers[71-94] using various reagents such as I_2, HCl, NH_4Cl and H_2S and it is reported that single crystals measuring

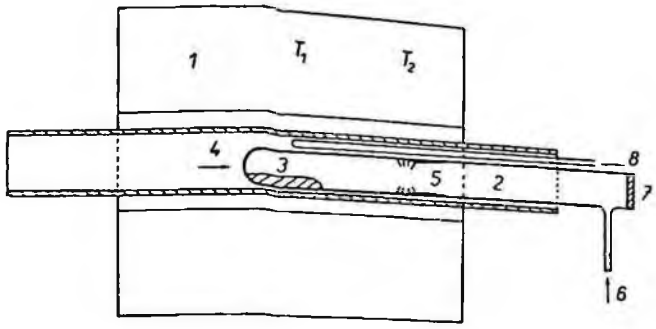

Fig. 16.14 Schematic diagram of experimental arrangement; 1: furnace, 2: silica-glass tube, 3: charge of the original material, 4: sealed end of the tube, 5: growth zone with growing crystals and polycrystalline layer on the walls, 6: control of H_2S pressure in the tube, 7: silica-glass window for observing the growth of crystals, 8: thermocouple (from Ref. 74 with permission).

1-1.5 cm square[91, 92] could be grown.

Nitsche[71-73] has first applied an iodine chemical transport method to the growth of ZnS. Patek et al.[74, 75] have studied the growth of ZnS single crystals using H_2S as the transport reagent in an open tube furnace as shown in Fig. 16.14.

Jona[76] studied the growth of ZnS crystals using HCl as the transport reagent in a simple method as shown in Fig. 16.15. A thermodynamical analysis was done and the transport rate due to the following reaction was measured.

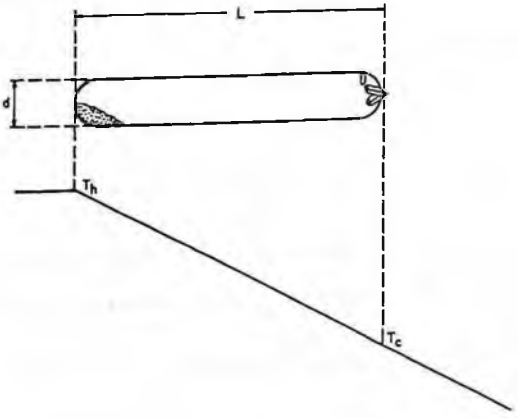

Fig. 16.15 Temperature profile during crystal growth and the appearance of the tube after the growth of ZnS (reprinted from Ref. 76 with permission, copyright 1962 Elsevier).

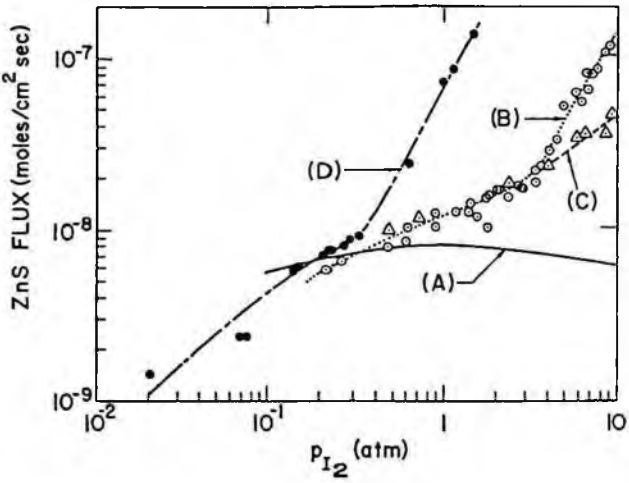

Fig. 16.16 Rate of solid transport in the system ZnS:I as a function of P_{I_2}. Curve A: theoretical solid transport rate calculated from diffusion theory, Curve B-D: experimental results depending on the tube sizes explained in the reference (reprinted from Ref. 78 with permission, copyright 1964 Elsevier)..

$$ZnS + 2\,HCl = ZnCl_2 + H_2S \qquad (16.2)$$

Jona and Mandel[77, 78] have studied the growth of ZnS single crystals by using I_2 as the transport reagent. Cubic single crystals, similar to those obtained in crystal growth from HCl, were obtained. The effect of the iodine pressure on the transport mechanism has been studied and it was found that as the pressure rises, the transport mechanism is at first diffusion-controlled and then becomes convection-controlled as shown in Fig. 16.16.

Samelson[79] has studied the growth of ZnS using H_2S as the transport reagent. The

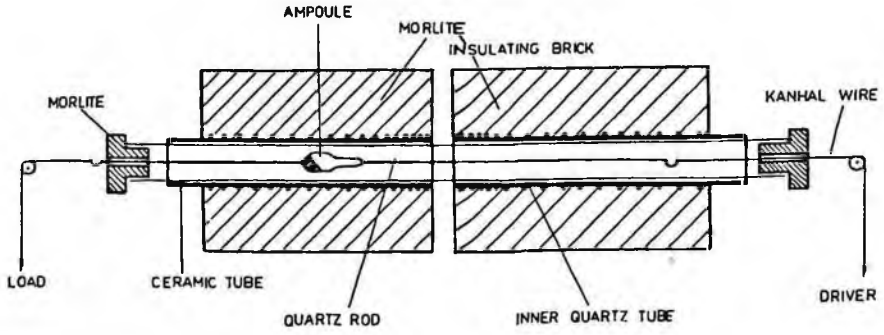

Fig. 16.17 Schematic cross-section of the apparatus used for ZnS single crystal growth (reprinted from Ref. 81 with permission, copyright 1971 Elsevier).

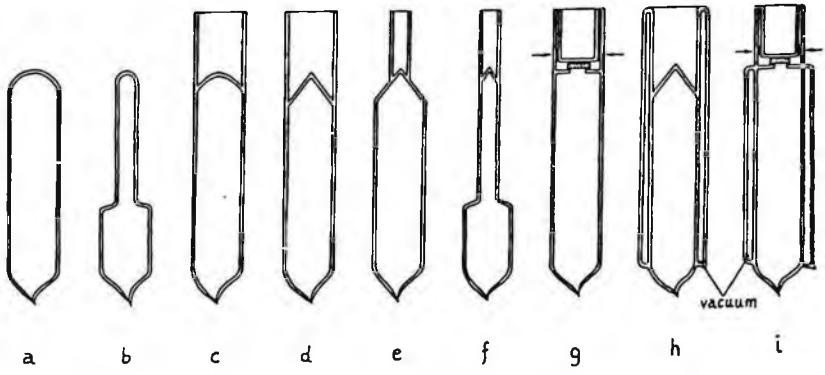

Fig. 16.18 Schematic cross-section of the apparatus used for ZnS single crystal growth (reprinted from Ref. 86 with permission, copyright 1982 Elsevier).

reaction employed is as follows,

$$ZnCl_2 + H_2S = 2HCl + ZnS \qquad (16.3)$$

and the transport rate, the thermodynamics and the growth conditions were discussed.

Lendvay[81] studied the growth of cubic and hexagonal ZnS single crystals using

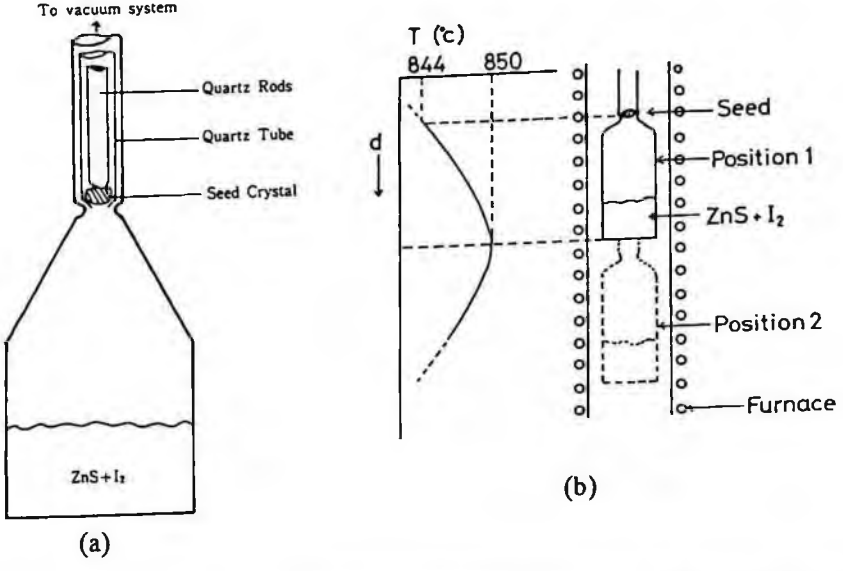

Fig. 16.19 (a) Growth ampoule and (b) the temperature profile and the ampoule position for crystal growth by the CVT method (from Ref. 88 with permission).

transport reagents such as NH_4Cl and I_2. In his experiment, the ampoule was pulled horizontally as shown in Fig. 16.17. Ujiie and Kotera[82] have studied the effect of the transport rate and the hydrogen chloride pressure on the purity of grown cubic ZnS single crystals. Dangel et al.[83] studied the transport rate as a function of tube geometry, temperature gradient, and the concentration of transport reagent for the ZnS:I system.

Hartmman[84, 85] has grown a large single crystals up to 8x8x5 mm^3 with the charge

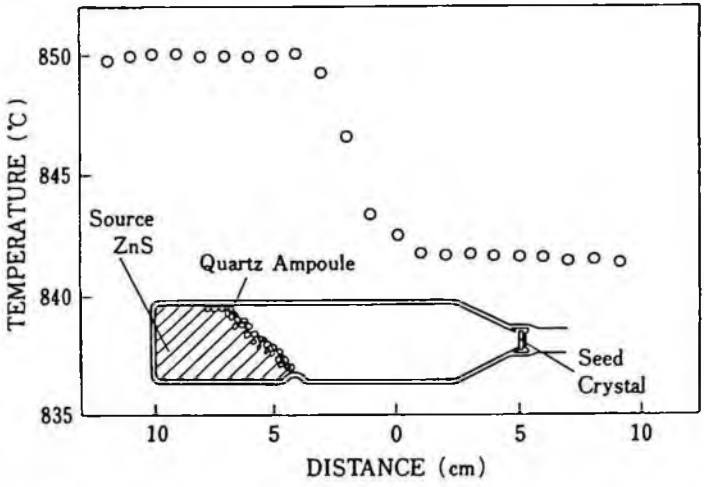

Fig. 16.20 Temperature profile and the growth ampoule for the CVT crystal growth (from Ref. 91 with permission).

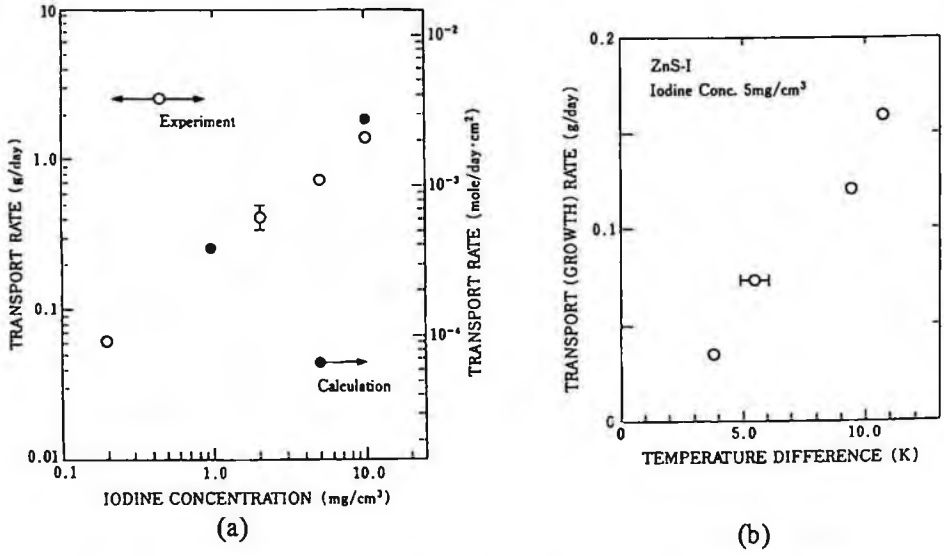

Fig. 16.21 (a) Dependence of the transport rate of ZnS on the iodine concentration and (b) transport rate on the seed crystal as a function of temperature difference (from Ref. 91 with permission).

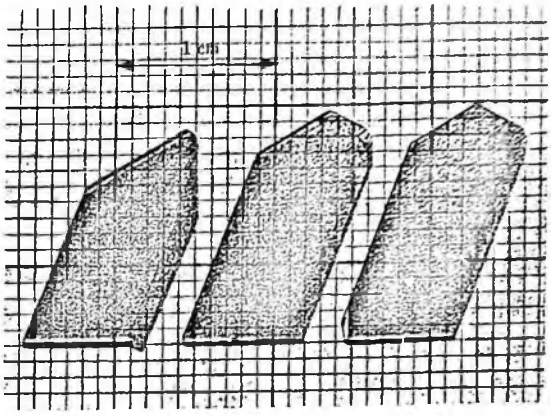

Fig. 16.22 ZnS (111) wafers cut from CVT grown single crystals (from Ref. 91 with permission).

temperature of at 950 °C and a cooling rate of 20-600 °C/hr. Palosz et al.[86,87] studied the dependence of the structure of ZnS on growth conditions for the system of ZnS:I. Nucleation control was achieved by using various shaped ampoules as shown in Fig. 16.18. The growth of $Zn_{1-x}Cd_xS$ ($x \leqq 0.07$) single crystals was also studied by various techniques, such as growth in ampoules of small inner diameter, tapered ampoule and growth on a seed.

Shoji et al.[88] have grown ZnS single crystals by the vertical CVT as shown in Fig. 16.19. Yang et al.[89] used iodine CVT and could grow ZnS single crystals measuring 18x17x9 mm^3.

Crystal growth of ZnS using NH_4Cl as the transport reagent is reported by Matsumoto et al.[90] NH_4Cl dissociates and acts as HCl so that the chemical reaction relevant to the transport is considered to be as follows.

$$ZnS(s) + 2\,HCl(g) = ZnCl_2(g) + H_2S(g) \qquad (16.4)$$

Kitagawa et al.[91,92] have applied the temperature difference constant temperature method as shown in Fig. 16.20 and examined the effect of the temperature difference between the source and the seed (2-10 °C), and of the iodine concentrations (0.02-10 mg/cm^3) on the quality of grown crystals (Fig. 16.21). Large area single crystals could be obtained at higher temperature difference and lower iodine concentrations as shown in Fig. 16.22.

The growth kinetics have been analyzed by Noda et al.,[93] taking diffusion, laminar flow and convective flow into account. The calculation of growth rate based on the diffusive mass transport was performed by Palotz.[95]

Mixed ZnS_xSe_{1-x} ($0.2<x<0.8$) crystals have been grown by the iodine-transported CVT method.[96]

(3) Chemical Vapor Deposition (CVD) method

Polycrystalline ZnS for preparing infrared window materials can be produced by the CVD method from zinc vapor and H_2S gas.[97] The growth rate of the CVD method is about 1-2 μm/min and high purity and dense, homogeneous polycrystalline materials can be obtained.[98] Suzuki et al.[99] has studied the effect of annealing on the electrical properties and MIS type LEDs have been fabricated.

16.3.4 Other Methods

Hydrothermal growth of ZnS, ZnS-H_2O-Na_2S and ZnS-H_2) systems has been reported.[100] ZnS-HgS and ZnS-CdS solid solutions have also been prepared by the hydrothermal synthesis method.[101]

16.4 CHARACTERIZATION

16.4.1 Defects

Ebina et al.[20] have studied the structure of various crystals and found the existence of a large amount of stacking faults. As explained in Sec. 16.2, ZnS has various polytypes. The formation mechanism of polytypes has been studied by Mardix.[102] Steinberger et al.[103] have discussed the formation of stacking faults from dislocation movement.

Various point defects have been studied theoretically and examined by electron spin resonance (ESR) measurement.[104, 105] Kröger[106] has systematically examined the point defects in ZnS and calculated defect concentrations thermodynamically. Ido et al.[107] has calculated thermodynamically the concentrations of various point defects as a function of temperature and dopant concentrations.

16.4.2 Electrical Properties

(1) Mobility and carrier concentrations

Because of the self compensation mechanism (Sec. 4.2.5), ZnS is of n-type conductivity and is difficult to obtain p-type conductive material. The theoretical temperature dependence of electron mobility compared with the experimental Hall mobility is shown in Fig. 16.23.[108] It is also predicted that ZnS crystals grown from a Te solvent are of low resistivity. The energy levels of donors and acceptors of ZnS have been determined[8] as shown in Table 16.3.

Table 16.3 Energy Levels of Donors and Acceptors in ZnS

Impurity	Donor or Acceptor	Energy level from conduction band (eV)	Energy level from valence band (eV)
Ag	A		0.720
Al	D	0.074-0.100	
Cu	A		1.250
In	D	0.400-0.600	
Li	A		0.150
Na	A		0.190

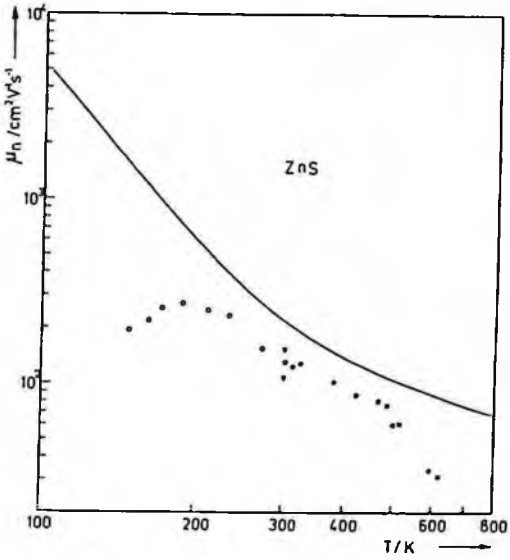

Fig. 16.23 Theoretical electron mobility (solid curve) of pure ZnS compared with experimental Hall mobility data (reprinted from Ref. 108 with permission, copyright 1975 Elsevier).

(2) Heat treatment

The resistivity of ZnS obtained by the iodine CVT method is normally very high because iodine donors are compensated by deep acceptor levels due to impurities and Zn vacancies. In order to reduce the resistivity, heat treatment in the melt of II-group elements with donor impurities such as Al was performed.[3, 109] This heat treatment reduces not only the concentration of zinc vacancies which act as acceptors but also that of copper impurities which act as deep acceptors with energy levels 1.2 eV above the valence band.[110]

Oda et al.[111] showed that low resistive ZnS of about 10 Ω · cm can be reproducibly obtained by heat treatment at 1000 °C in a Zn-Al (typically 15 %Al) melt. It was also pointed out that Cu contamination makes it difficult to obtain low resistive ZnS reproducibly.[112] Heat treatment in Zn-Al, Zn-Ga, Zn-Al-Ga alloy melts at 1000 °C has been studied systematically to determine the appropriate conditions, taking care to reduce the Cu contamination.[112]

16.4.3 Optical Properties

Photoluminescence has been extensively studied in order to clarify the emission mechanism.[113-118] ZnS shows a strong blue light emission which is called Self-Activated (SA) emission. The emission center is believed to be due to complex defects between Zn vacancies with donors such as halogen (I_s^+) or aluminium (Al_{Zn}^{3+}). The blue emission is due to Donor-Acceptor (D-A) pair emission between this SA center and

donors. Blue LEDs can be fabricated using this emission.

ZnS is also promising for LEDs and LDs in the ultraviolet wavelength. For these applications, it is essential to carry out studies of the band edge emission. Fig. 16.24 shows a typical band edge emission spectrum. It was determined that 3.802 eV is the upper line of exciton-polariton and 3.797 eV is the lower line. The emission of 3.789 eV is exciton bound to neutral donor and that at 3.782 eV is the exciton bound to neutral acceptor.[117, 118]

Characterization by Raman scattering,[119, 120] electroluminescence (EL)[121] and cathodoluminescence (CL)[122] has also been performed and their scattering,and luminescence mechanisms have been discussed.

16.5 APPLICATIONS

16.5.1 Light Emitting Diodes (LEDs)

Since p-type ZnS can not be obtained, metal-insulator-semicondcutor (MIS) or metal-semiconductor (MS) structures have been investigated for blue light LEDs.[2, 94, 99, 117, 123-127] For the insulating layer (I layer), various methods have been studied as follows.

(i) Formation of a high resistive surface by heating a low resistive ZnS bulk single crystal
(ii) Deposition of insulating layers such as MgF_2 or NaI
(iii) Deposition of high resistive ZnS
(iv) Ion implantation of S ions
(v) Formation of a ZnS-ZnO mixed crystal layer (pai layer)

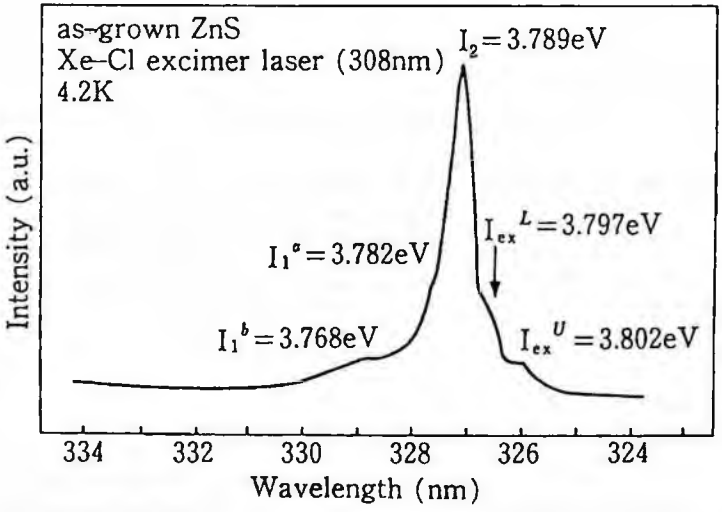

Fig. 16.24 PL edge emission of iodine CVT as grown ZnS crystal.[117]

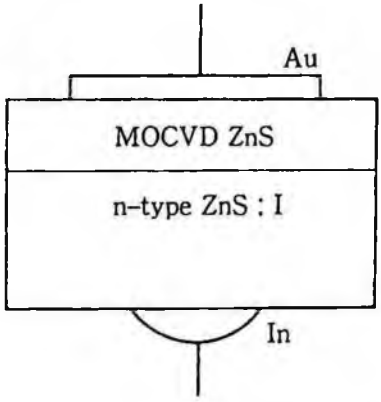

Fig. 16.25 Structure of M S type blue light LED (reprinted from Ref. 126 with permission of Springer Science and Business Media).

(vi) MBE or MOCVD epitaxial layers

It is reported that by using π layers, external quantum efficiency as high as 0.08% could be obtained.

As MOCVD or MBE epitaxial insulating layers, ZnS homo-epitaxial layers show higher efficiency from the viewpoint of their thermal expansion coefficient and lattice matching. An MπS structure with MOVPE ZnS π-layer as shown in Fig. 16.25 has been investigated and the emission at 450 nm due to D-A pairs has been observed.[3] These polycrystalline ZnS materials were used for fabricating LEDs based on the MIS structure.[99]

16.5.2 EL Emitting Devices

ZnS has been extensively studied for EL display material.[128] ZnS thin films are prepared as thin films by vacuum deposition, the three temperature method and sputtering. To form emission centers, transition metals such as Mn and rare earth elements such as Tb are doped. The emission of thin film EL is based on the mechanism in which electrons are accelerated under a strong electric field (1-2x10^6 V/cm) and excite emission centers by impact ionization.

16.5.3 Tunable Lasers

ZnS doped with Cr^{2+}, Co^{2+}, Ni^{2+} is promising for mid-IR tunable lasers.[129, 130] Among various dopants, Cr^{2+} is considered to be most efficient. A laser-pumping experiment was performed using Cr doped ZnS crystals and it was found that the lasing output at 2.35 μm had a slope efficiency of 2 %.

REFERENCES

1. M. Aven and J.Z. Devine, *J. Lumin.* 7 (1973) 195.
2. Y.S. Park and B.K. Shin, in *Electroluminescence*, eds. by J.I. Pankove (Springer-Verlag, Berlin,

1977) p.133.
3. B. Ray, *II-VI Compounds* (Pergamonn, Oxford, 1969).
4. A. Abdel-Kader and F.J. Bryant, *J. Mater. Sci.* **21** (1986) 3227.
5. *Physics and Chemistry of II-VI Compounds*, eds. M. Aven and J.S. Prener (Northe-Holland, Amsterdam, 1967).
6. H. Hartmann, R. Mach and B. Selle, *in Currents Topics in Materials Science, Vol. 9*, ed. E. Kaldis (North-Holland, Amsterdam, 1982) p. 1.
7. W.L. Roth, in *Physics and Chemistry of II-VI Compounds*, eds. M. Aven and J.S. Prener (North-Holland, Amsterdam, 1967) p.118.
8. *Databook of II-VI Compound Semiconductor Crystals* (JEIPA, 1983) (in japanese)
9. *Landolt-Börnstein, Vol. 17 Semiconductors*, ed. O. Madelung (Springer-Verlag, Berlin, 1982) p. 61.
10. A. Addamiano and P.A. Dell, *J. Phys. Chem.* **61** (1957) 1020.
11. EJ. Baars and G. Brandt, *J. Phys. Chem. Solids* **34** (1973) 905.
12. R. C. Sharma and Y.A. Chang, *J. Crystal Growth* **88** (1988) 193.
13. E. Tiede and A. Schleede, *Ber. Deutschen.Chem. Gesellschaft Berlin* **53B** (1920) 1717.
14. A. Fischer, *Z. Natureforschg.* **13a** (1958) 105.
15. A.G. Fischer, *J. Electrochem. Soc.* **106** (1959) 838.
16. A.G. Fisher, *Bull. Am. Phys. Soc.* 6 (1961) **17**.
17. A.G. Fishcer, *J. Electrochem. Soc.* **117** (1970) 41C.
18. W.E. Medcalf and R.H. Fahrig, *J. Electrochem. Soc.* **105** (1958) 719.
19. A. Addamiano and M. Aven, *J. Appl. Phys.* **31** (1960) 36.
20. A. Ebina and T. Takahashi, *J. Appl. Phys.* **38** (1967) 3079.
21. M.J. Kozielski, *J. Crystal Growth* **1** (1967) 293.
22. M.J. Kozielski, *Bull. Acad. Polon. Sci.* **23** (1975) 1315.
23. M.J. Kozielski, *J. Crystal Growth* **30** (1975) 86.
24. H. Kimura and H. Komiya, *J. Crystal Growth* **20** (1973) 283.
25. *Information Bulletin*, San Diego Semicon. Inc. (December, 1988).
26. R. Boyn, M.J. Kozielski and H. Zimmermann, *phys. stat. sol. (a)* **124** (1991) K137.
27. Y. Mita, *J. Phys. Soc. Japan* **16** (1961) 1484.
28. Y. Mita, *J. Phys. Soc. Japan* **17** (1962) 784.
29. R.C. Linares, *Met. Advan. Electron. Mater.* **19** (1962) 329.
30. R.A. Laudise, in *The Art and Science of Growing Crystals*, ed. J.J. Gilman (Wiley, New York, 1963) p. 252.
31. M. Rubenstein, *J. Electrochem. Soc.* **113** (1966) 623.
32. M. Rubensein, *J. Crystal Growth* **3/4** (1968) 309.
33. M. Harsy, G. Gergely, J. Sahcnda, M. Somogyi, P. Sviszt and G. Szigeti, in *II-VI Semiconducting Compounds*, ed. D.G. Thomas (Benjamin, New York, 1967) p.413.
34. M. Harsey, *Mater. Res. Bull.* **3** (1968) 483.
35. S.G. Parker and J.E. Pinnell, *J. Crystal Growth* **3/4** (1968) 490.
36. R.C. Linares, *Trans. AIME* **242** (1968) 441.
37. M. Washiyama, K. Sato and M. Aoki, *Jpn. J. Appl. Phys.* **18** (1979) 869.
38. S.V. Nistor and M.I. Toacsan, *Rev. Roum. Phys.* **25** (1980) 707.
39. L.C. Nistor, S.V. Nistor and M.I. Toacsan, *J. Crystal Growth* **50** (1980) 557.
40. M. Aoki, M. Washiyama, H. Nakamura and K. Sakamoto, *Jpn. J. Appl. Phys.* **21** (1982) Suppl. 21-1, p. 11.
41. M. Nagano, H. Kanie, I. Yoshida, M. Sano and M. Aoki, *Jpn. J. Appl. Phys.* **30** (1991) 1915.
42. M. Nagano, H. Kanie, I. Yoshida, M. Sano and M. Aoki, *Jpn. J. Appl. Phys.* **31** (1992) L446.
43. R. Lorenz, *Chem. Beriche* **24** (1891) 1501.
44. D.C. Reynolds and S.J. Czyzak, *Phys. Rev.* **79** (1950), 543.
45. W.W. Piper and W.L. Roth, *Phys. Rev.* **92** (1953) 503.
46. A. Kremheller, *Sylvannia Technologist* **8** (1955) 11.

47. L.C. Greene, D.C. Reynolds, S.J. Czyzak and W.A. Baker, *J. Chem. Phys.* **29** (1958) 1375.
48. J. Nishimura and J. Tanabe, *J. Phys. Soc. Japan* **14** (1959) 850.
49. J. Nishimura, *Oyo Buturi (Monthly Publ. Jpn. Soc. Appl. Phys.) (in japanese)* **11** (1959) 651.
50. A. Kremheller, *J. Electrochem. Soc.* **107** (1960) 422.
51. H. Samelson and V.A. Brophy, *J. Electrochem. Soc.* **108** (1961) 150.
52. W.W. Piper and S.J. Polish, *J. Appl. Phys.* **32** (1961) 1278.
53. Indradev, *Mater. Res. Bull.* **1** (1966) 173.
54. Indradeva and R.B. Lauer, *Mater. Res. Bull.* **1** (1966) 185.
55. Indradev, L.J. Van Ruyven and F. Williams, *J. Appl. Phys.* **39** (1968) 3344.
56. R. Hill and R.B. Lauer, *Mater. Res. Bull.* **2** (1967) 861.
57. P. Blanconnier and P. Henoc, *J. Crystal Growth* **17** (1972) 218.
58. P.A. Tempest and D.W.G. Ballentyne, *J. Crystal Growth* **21** (1974) 219.
59. J.R. Cutter, G.J. Russell and J. Woods, *J. Crystal Growth* **32** (1976) 179.
60. H. Hartmann, *J. Crystal Growth* **42** (1977) 144.
61. T. Shichiri, T. Aikami and J. Kakinoki, *J. Crystal Growth* **43** (1978) 320.
62. G.J. Russel and J. Woods, *J. Crystal Growth* **47** (1979) 647.
63. S. Kishida, F. Takeda, K. Matsuura and I. Tsurumi, *Res. Rep. Dep. Engineer. Tottori Univ.* **11** (1980) 84.
64. B.M. Bulakh, V.I.Kozlovsky, N.K. Moiseeva, A.S. Nasibov, G.S. Pekar and P.V. Reznikov, *Krist. Tech.* **15** (1980) 995.
65. S. Oktik, G.J. Russel and J. Woods, *J. Crystal Growth* **59** (1982) 414.
66. T. Kaneko and H. Yumoto, *J. Phys. Soc. Japan* **53** (1984) 3884.
67. K. Mochizuki and H. Iwanaga, *J. Crystal Growth* **71** (1985) 459.
68. K. Mochiuki and K. Masumoto, *J. Jpn. Assoc. Crystal Growth* **12** (1985) 293.
69. X. Huang and K. Igaki, *J. Crystal Growth* **78** (1986) 24.
70. Yu.V. Korostelin, V.I. Kozlovsky, A.S. Nasbov and P.V. Shapkin, *J. Crystal Growth* **159** (1996) 181.
71. R. Nitsche, *Phys. Chem. Solids* **17** (1960) 163.
72. R. Nitsche, H.U. Bolsterli and M. Lichensteiger, *J. Phys. Chem. Solids* **21** (1961) 199.3
73. R. Nitsche, in *Crystal Growth*, ed. H.S. Peiser, (Pergamon, Oxford, 1967) p.215.
74. K. Patek, *Czech. J. Phys.* **B11** (1961) 686.
75. K. Patek, M. Skala and L. Souckova, *Czech. J. Phys.* **B12** (1962) 313.
76. F. Jona, *J. Phys. Chem. Solids* **23** (1962) 1719.
77. F. Jona and G. Mandel, *J. Phys. Chem. Solids* **38** (1963) 346.
78. F. Jona and G. Mandel, *J. Phys. Chem. Solids* **25** (1964) 187.
79. H. Samelson, *J. Appl. Phys.* **33** (1962) 1779.
80. Y.M. Rumyantsev, F.A. Kuzetsov and S.A. Stroitlev, *Sov. Phys. Cryst.* **10** (1965) 212.
81. E. Lendvay, *J. Crystal Growth* **10** (1971) 77.
82. S. Ujie and Y. Kotera, *J. Crystal Growth* **10** (1971) 320.
83. P.N. Dangel and B.J. Wuensch, *J. Crystal Growth* **19** (1973) 1.
84. H. Hartmann, *Krist. Tech.* 9 (1974) 743.
85. H. Hartmann, *J. Crystal Growth* **42** (1977) 144.
86. W. Palosz, *J. Crystal Growth* **60** (1982) 57.
87. W. Palosz, M.J. Kozielski and B. Palosz, *J. Crystal Growth* **58** (1982) 185.
88. T. Shoji, K. Mochizuki, S. Fujita and Y. Hiratate, *Bull. Tohoku Inst. Technol.* **5** (1984) 23.
89. B. Yang, S. Feng and Y. Yang, *Luminescence and Display Devices (in chinese)* **6** (1985) 200.
90. M. Matsumoto and G. Shimaoka, *J. Crystal Growth* **79** (1986) 723.
91. M. Kitagawa, Y. Tomomura, S. Yamaue and S. Nakajima, *Sharp Tech. Rep.* **37** (1987) 13.
92. M. Kitagawa, Y. Tomomura, A. Suzuki and S. Nakajima, in *Extended Abstr. 19th Int. Conf. Solid State Dev. Mater.* (Tokyo, 1987) p. 247.
93. K. Noda, N. Matsumoto, S. Otsuka and K. Matsumoto, *J. Electrochem. Soc.* **137** (1990) 1281.

94. T. Ohno, K. Kuritsu and T. Taguchi, *J. Crystal Growth* **99** (1990) 737.
95. W. Palosz, *J. Crystal Growth* **68** (1984) 757.
96. A. Catano and Z.K. Kun, *J. Crystal Growth* **33** (1976) 324.
97. P. Miles, *Opt. Engineer.* **15** (1976) 451.
98. H. Iwata, S. Suzuki and Y. Sasaki, *J. Crystal Growth* **125** (1992) 425.
99. S. Suzuki, S. Kitagawa, H. Iwata and Y. Sasaki, *J. Crystal Growth* **134** (1993) 67.
100. R.A. Laudise and A.A. Ballman, *J. Phys. Chem.* **64** (1960) 688.
101. A. Kremheller, A.K. Levine and G. Gashurov, J. *Electrochem. Soc.* **107** (1960) 12.
102. S. Mardix, *J. Appl. Cryst.* **17** (1984) 328.
103. I.T. Steinberger, I. Kiflawa, Z.H. Kalman and S. Mardix, *Phil. Mag.* **27** (1973) 159.
104. P. Kasai and Y. Otomo, *J. Chem. Phys.* **37** (1962) 1263.
105. J. Schneider, B. Dischler and A. Räuber, *J. Phys. Chem. Solids* **31** (1970) 337.
106. F.A. Kröger, *The Chemistry of Imperfect Crystals 2nd Ed., Vol. 2*, (North-Holland, Amsterdam, 1974) p. 741.
107. T. Ido and Y. Matsushita, *IEICE* **ED88-27** (1988) p. 35.
108. D.L. Rode, in *Semiconductors and Semimetals Vol. 10*, eds. R.K. Willardson and A.C. Beer (Academic Press, New York, 1975) p. 1.
109. M. Aven and H.H. Woodbury, *Appl. Phys. Lett.* **1** (1962) 53.
110. S.S. Devlin, in *Physics and Chemistry of II-VI Compounds*, eds. M. Avena and J.S. Prener (North-Holland, Amsterdam, 1966) p.604.
111. S. Oda and H. Kukimoto, *IEEE Trans. Electron Devices* **ED-24** (1977) 956.
112. A.E. Thomas, G.J. Russell and J. Woods, *J. Crystal Growth* **63** (1983) 265.
113. S. Shionoya, in *Luminescence of Inorganic Solids*, ed. P. Goldberg (Academic Press, New York, 1966) p. 206.
114. K. Sato and M. Aoki, *Jpn. J. Appl. Phys.* **18** (1979) 705.
115. H.-E. Gumlich, *J. Lumin.* **23** (1981) 73.
116. T. Taguchi, T. Yokogawa, S. Fujita, M. Satoh and Y. Inuishi, *J. Crystal Growth* **59** (1982) 317.
117. T. Taguchi, T. Yokogawa and H. Yamashita, *Solid State Commun.* **49** (1984) 551.
118. T. Taguchi, *Oyo Buturi (Monthly Publ. Jpn. Soc. Appl. Phys.) (in japanese)* **54** (1985) 28.
119. H. Kanie, M. Nagano and M. Aoki, *Jpn. J. Appl. Phys.* **30** (1991) 1360.
120. I.V. Akimova, V.I. Kozlovskiy, Yu.V. Korostelin, A.S. Nasibov, A.N. Pechenov, P.V. Renikov, V.I. Reshetov, Ya.K. Skasyrskiy and P.V. Shapkin, p. 195.
121. M.E.Özsan and J. Woods, *J. Phys. D. Appl. Phys.* **10** (1977) 1335.
122. A. Abdel-Kader and H.I. Farag, *J. Mater. Sci.* **23** (1988) 2382.
123. H. Katayama, S. Oda and H. Kukimoto, *Appl. Phys. Lett.* **27** (1975) 697.
124. C. Lawther and J. Woods, *phys. stat. sol. (a)* **50** (1978) 491.
125. A.E. Thomas, J. Woods and Z.V. Hauptman, *J. Phys. D (Appl. Phys.)* **16** (1983) 1123.
126. K. Kurisi and T. Taguchi, in *Electroluminscence*, eds. S. Shionoya and H. Kobayashi, (Springer-Verlag, Berlin, 1989) p. 367.
127. A. Abdel-Kader and F.J. Bryant, *J. Mater. Sci.* **21** (1986) 3227.
128. P. Zalm, *Philips Res. Rep.* **11** (1959) 353.
129. L.D. DeLoach, R.H. Page, G.D. Wilke, S.A. Payne, W.F. Krupke, OSA Proc. Adv. *Solid State Lasers* **24** (1995) p. 127.
130. R.H. Page, K.I. Schaffers, L.D. DeLoach, G.D. Wilke, F.D. Patel, J.B. Tassano, Jr., S.A. Payne, W.F. Krupke, K-T. Chen and A. Burger, *IEEE J. Quan. Electron.* **323** (1997) 609.

17. ZnSe

17.1 INTRODUCTION

ZnSe has a bandgap of 2.7 eV at room temperature and is a promising material for blue light emitting diodes and laser diodes.[1-6] In fact, it has been proved that by the epitaxial growth of ZnSe/GaAs, it is possible to obtain blue-green light emitting diodes and laser diodes.[7-10] In this hetero epitaxial material, significant strain is introduced because of the lattice mismatch and the big difference in thermal expansion coefficients.[11] Furthermore, a layer of Ga_2Se_3 is formed at the ZnSe/GaAs interface.[12] This kind of hetero-epitaxial growth is not appropriate from the viewpoint of device stability. It is therefore desirable to grow high quality ZnSe bulk materials for the substrate to grow epitaxial layers with lattice matching.[13] ZnSe is also promising for laser screens for projection color television sets.[14]

17.2 PHYSICAL PROPERTIES

The physical properties of ZnSe are shown in Table 17.1. These data can be found in various references.[15-19] Since the melting point of ZnSe is as high as 1515 °C and the dissociation pressure is 5 atm., ZnSe is a material which is difficult to grow in single crystals. The vapor pressure of ZnSe is reported in Refs. 20 and 21. The phase diagram of ZnSe has been examined by various researchers.[22-26] Typical ones are shown in Fig. 17.1. ZnSe has a phase transition from wurtzite to zincblende at about 1425 °C,[27] so severe twinning is a problem for the melt growth of ZnSe. The mechanism of this transformation is discussed by various authors.[27-29]

Miscibility between ZnSe and CdTe has been studied by Yim[30] and the wurtzite to zincblende transformation in ZnSe-CdSe was studied by Kulakov and Balyakina.[31] The bandgap and lattice constants of $Zn_{1-x}Mg_xSe$ have been studied by Jobst et al.[32] Self diffusion coefficients have been measured by Woodbery and Hall.[33]

Table 17.1 Physical Properties of ZnSe

Crystal Structure	zincblende
Lattice Constant	5.6687 Å
Density	5.27 g/cm^3
Melting Point	1515 °C
Linear Expansion Coefficient	7.55x10^{-6} /deg
Thermal Conductivity	0.19 W/cm·K
Dielectric Constant	9.1
Refractive index	2.61
Bandgap at Room Temperature	2.71 eV
Optical Transition Type	direct
Electron Mobility at R.T.	530 cm^2/V·sec
Hole Mobility at R.T.	28 cm^2/V·sec

17.3 CRYSTAL GROWTH

In the past, various crystal growth methods have been performed for ZnSe. Even though many methods have been examined, no industrial production method for ZnSe crystal growth has yet been established. ZnSe polycrystals are industrially grown by the CVD method but this method does not allow of single crystal growth. Melt growth has been studied extensively but the twinning problem due to the phase transition is still a large obstacle.

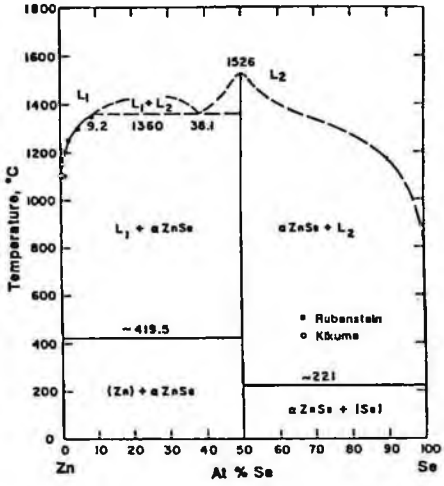

(a)

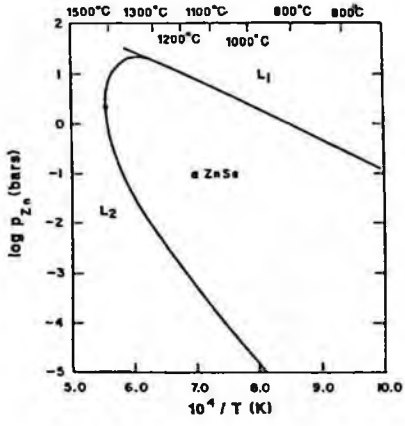

(b)

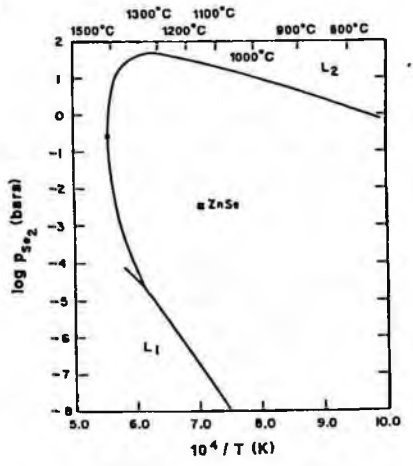

(c)

Fig. 17.1 (a) X-T diagram of ZnSe, (b) equilibrium partial pressure p_{Zn} along the solidus, (c) equilibrium partial pressure P_{Se_2} along the solidus (reprinted from Ref. 24 with permission, copyright 1988 Elsevier).

Good quality single crystals can be grown by low temperature methods such as solution growth and vapor phase growth.

17.3.1 Melt Growth

In the case of ZnSe, melt growth has been performed mainly by high pressure VB or VGF methods. ZnSe has however a phase transition from wurtzite to zincblende at about 1425 °C so that twinning easily take places due to the structural transformation. Various methods of melt growth are summarized in Table 17.2.

(1) Liquid Encapsulated Czochralski (LEC) method

It was long believed that the LEC method was not appropriate for the growth of ZnSe. Hruban et al.[34] have however applied this method to the growth of ZnSe by using B_2O_3 as the encapsulant under a nitrogen gas pressure of 30-40 bars using a commercial high pressure puller (MSR-6). They have shown that ZnSe ingots of 30-65 mm in diameter and 300-800 g in weight could be obtained. It was shown that by increasing the axial temperature gradient, ingots of stable diameter could be obtained as shown in Fig. 17.2.

(2) Zone Melting (ZM) method

Shone et al.[37] have grown undoped and Na-, P- and Mn-doped ZnSe crystals in a vertical furnace under argon pressure of 8 atm. The crucible was heated by a RF heater and the molten zone and the temperature gradient were estimated as 2 cm long and 70 °C/cm, respectively. Polygonization was reduced when the growth rate was less than 8

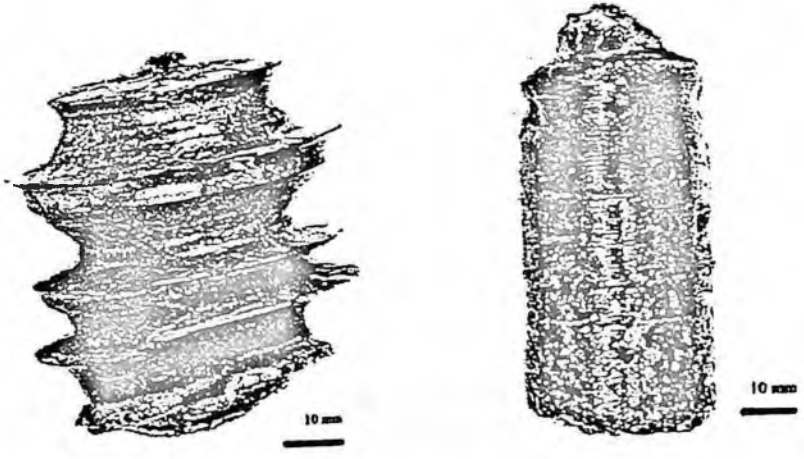

(a) (b)

Fig. 17.2 ZnSe single crystals grown by the LEC method. (a) Isn a low temperature gradient and (b) with diameter control (reprinted from Ref. 34 with permission, copyright 1999 Elsevier).

Table 17.2. Melt Growth of ZnSe

Method	Result	Author	Year	Ref.
HP-VB pressure	Soft-ampoule technique and growth under high	Fisher 1961	1959	38-42
HP-VB	Growth under 120 atm. argon pressure	Tsujimoto et al.	1966	43
ZM	Synthesis of ZnSe and growth by ZM	Libicky	1967	35
HP-VB	Growth under 70 atm. argon pressure, 25ϕ mmx 40 mm crystals	Eguchi et al.	1968	44
HP-VGF	Growth from a stoichiometric melt	Holton et al.	1969	45
HP-VB	High pressure furnace construction	Kozielski	1975	46
HP-VB	Composition analysis after melt growth	Kikuma et al.	1973	47
HP-VB	Crystal growth under argon (10-200 atm.) pressure. 28-36 mm in diameter and 200 mm in length	Kulakov et al.	1976 1981	58-61
HP-VB	Effect of excess Se on the growth rate	Kikuma et al.	1977	48
HP-VB	Low resistivity n-type crystal growth from excess Zn melt	Kikuma et al.	1981 1985	50-53
ZM	Overlap zone-melting for purification	Isshiki et al.	1985	36
SSSR	Self-sealing growth under 5-7 atm. N2 overpressure, growth of 4.5 cm^3 single crystals	Fitzpatrick et al.	1986	74
VB	Growth at 990-1165 °C using closed ampoules	Chang et al.	1987	62
HP-VB pressure	Growth of 25ϕ mmx50 mm crystals under 100 atm.	Terashima 1991	1988-	63-64
HP-VB	Process based on HP-VB free of quartz materials	SDS, Inc.	1988	65
HP-VB	Effect of Zn partial pressure on the melt composition, resistivity and mobility	Kikuma et al.	1989 1991	56-57
ZM	3.5 cm^3 twin-free crystals with Mn-doping	Shone et al.	1989	37
HP-VB	Growth of 25ϕx25 mm crystals with various cone angles under 90 atm. N_2 pressure	Yoshida et al.	1992	66
VB	Double crucible with pBN and Mo. Sealing of the ampoule by Mo welding	Omino et al.	1992	67
HP-VB	Growth of 25 mm diameter crystals with different growth conditions. Reduction of defect densities	Rudolph et al.	1994- 1995	68-70
HP-VB/ HP-VGF	Growth of 25ϕ mmx25 mm crystals with and without B_2O_3 encapsulant	Uehara et al.	1996- 1997	71-72
LEC	Growth of 30-65 mm diameter ingot of 300-800 g with B_2O_3 encapsulation	Hurban et al.	1997	34

VB: Vertical Bridgman, HP-VB: High Pressure VB, VGF: Vertical Gradient Freezing, HP-VGF: High Pressure VGF, ZM: Zone Melting, LEC: Liquid Encapsulated Czochralski, SSSR: Self-Sealing and Self-Releasing

mm/hr. Twin-free crystals of 3.5 cm^3 could be obtained by Mn-doping.

(3) High Pressure Vertical Bridgman (HP-VB) and High Pressure Vertical Gradient Freezing (HP-VGF) methods

This melt growth method has been examined by various researchers in the vertical configurations. Since ZnSe has a high sublimation pressure, a high pressure of inert gas such as Ar was applied during crystal growth.

Fischer[38-42] applied the HP-VB method as shown in Fig. 17.3 for growing ZnSe single crystals. Later, Tsujimoto et al.,[43] Eguchi and Fukai,[44] Holton et al.[45] and

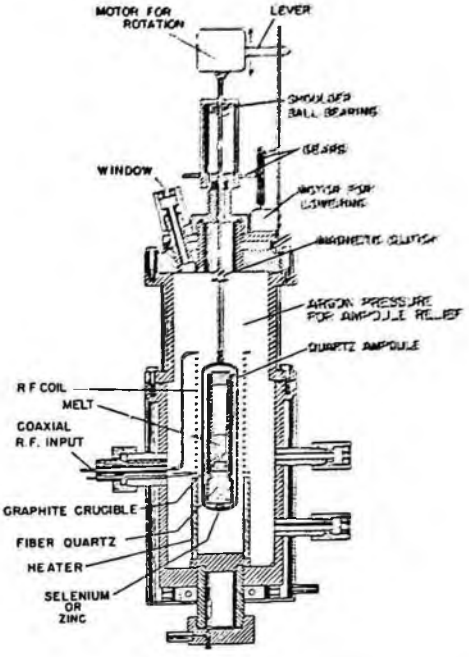

Fig. 17.3 Bridgman growth of ZnSe in a pressure-compensated sealed ampoule in a steel autoclave (reprinted from Ref. 41 with permission of The Electrochemical Society).

Kozielski[46] have grown ZnSe single crystals using HP-VB and HP-VGF methods.

Kikuma et al.[29, 47-57] systematically studied the growth of ZnSe single crystals by the HP-VB method (Fig. 17.4), moving the crucible from outside the furnace by a magnetic coupling mechanism under Ar atmosphere between 55-100 atm. They clarified the effect of growth parameters on the melt composition (Fig. 17.5), and on the electrical and optical properties. Low-resistive n-type ZnSe could be obtained from a melt containing excess Zn.

Kulakov et al.[58-61] have grown ZnSe crystals up to 100 mm in diameter by the Bridgman method under argon pressure of 20 atm. and studied the effect of the temperature gradient and the growth rate on crystal quality.

Chang et al.[62] have grown small ZnSe crystals of 1-15 mm^3, using a closed tube method and the direct reaction of Zn and Se in the ampoule prior to crystal growth in a VGF configuration.

Terashima et al.[63, 64] have grown ZnSe single crystals of diameter 25 mm and length 50 mm by the HP-VB method, using a pressure of 100 atm. and a growth rate of 5-10 mm/hr. Yoshida et al.[66] have grown twin free ZnSe crystals of 25 mm diameter and 25 mm length by the Bridgman method (Fig. 17.6). Purified sintered BN inner and outer crucibles were used and the effect of the growth conditions and the presence of B_2O_3 on twin formation was studied. It was speculated that B_2O_3 which penetrates between the wall of the crucible and the melt will prevent twin formation.

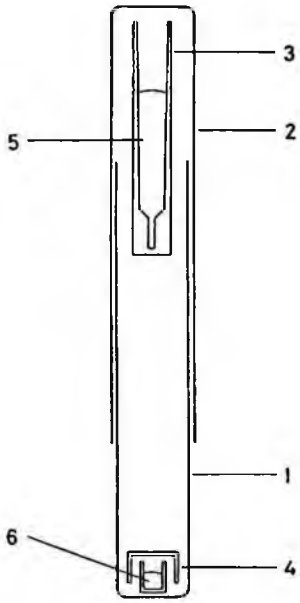

Fig. 17.4 Growth assembly for ZnSe. 1: growth vessel, 2: cap, 3: crucible, 4: reservoir, 5: ZnSe, 6: Zn (reprinted from Ref. 56 with permission, copyright 1989 Elsevier).

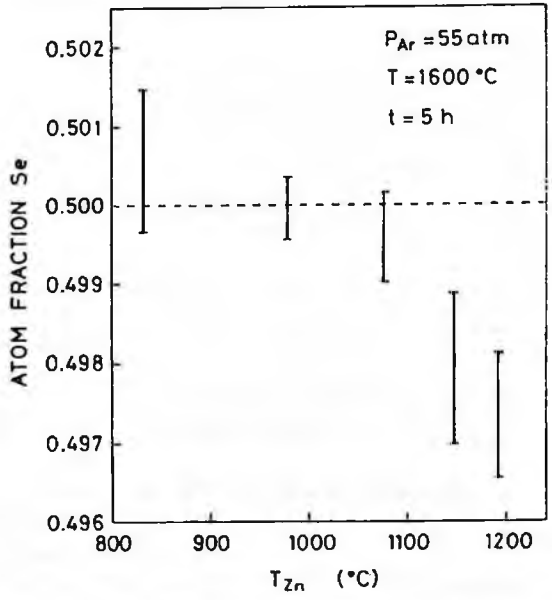

Fig. 17.5 Dependence of the melt composition on the Zn reservoir temperature (reprinted from Ref. 56 with permission, copyright 1989 Elsevier).

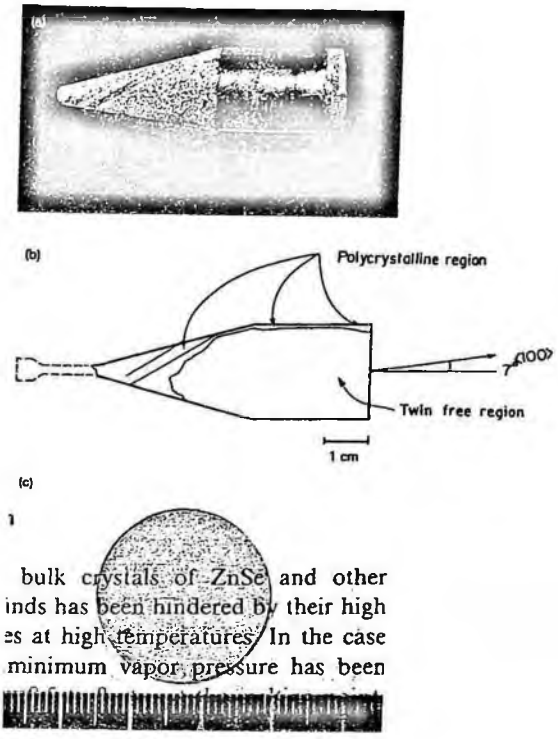

bulk crystals of ZnSe and other
inds has been hindered by their high
es at high temperatures. In the case
minimum vapor pressure has been

Fig. 17.6 (a) Photograph of an as-grown ZnSe ingot, (b) schematic profile of this ingot, (c) typical wafer cut from this ingot (reprinted from Ref. 66 with permission, copyright 1992 Elsevier).

In order to prevent contamination from quartz containers, ampoules made of W or Mo with pBN crucibles welded inside were invented. Omino et al.[67] have developed a double crucible consisting of an inner pyrolytic BN crucible and an outer Mo crucible, the lid of which was sealed by an electron beam welder (Fig. 17.7). Using this crucible, singe crystals could be grown in a vertical Bridgman furnace with a vacuum heating chamber.

Rudolph et al.[68-70] have grown ZnSe crystals of 27 mm diameter using a polycrystalline seed crystal of the same diameter in a furnace as shown in Fig. 17.8. They also studied the relationship between growth velocity and the axial temperature gradient (Fig. 17.9 (a)). They also found that the number of twins is inversely proportional to the number of large-angle grain boundaries (Fig. 17.9(b)).

Uehara et al.[71] and Okada et al.[72] have developed a multiple heater HP-VB furnace with a Zn vapor pressure control system (Fig. 17.10). Using this system, ZnSe single crystals have been grown with B_2O_3 liquid encapsulation as shown in Fig. 17.11.

Lingart et al.[73] have made a simulation analysis of the heat transfer and the temperature distribution for the VB growth of ZnSe.

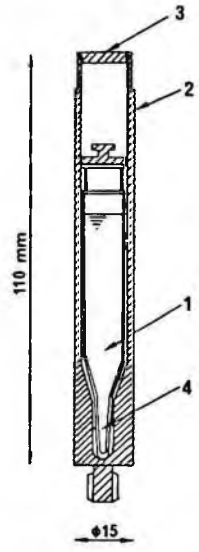

Fig. 17.7 Assembly of the double crucible. 1: pBN inner crucible, 2: Mo outer crucible, 3: lid, 4: capillary (reprinted from Ref. 67 with permission, copyright 1992 Elsevier).

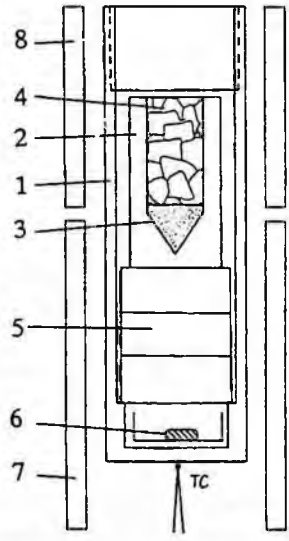

Fig. 17.8 The arrangement of vertical Bridgman growth of ZnSe with a Zn source (reprinted from Ref. 70 with permission, copyright 1995 Elsevier).

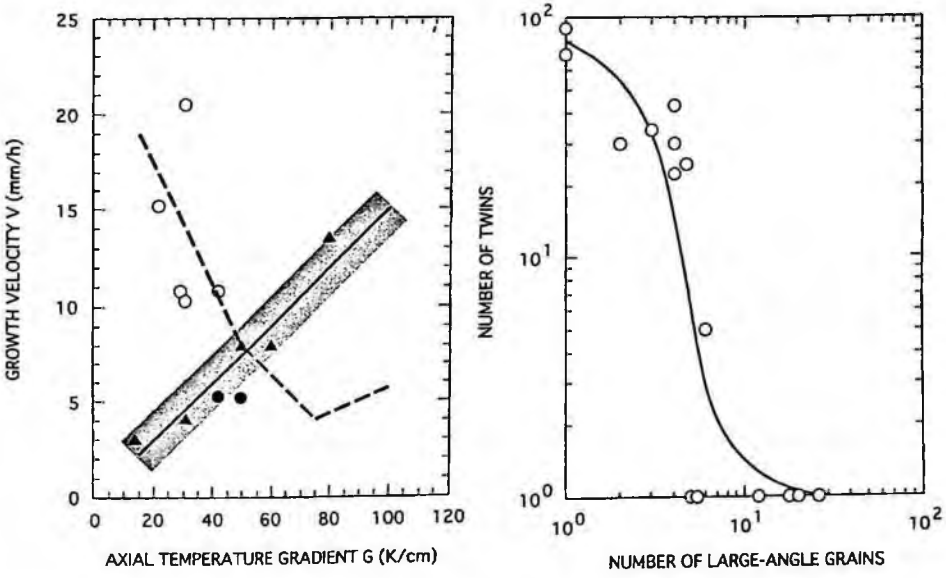

Fig. 17.9 (a) Critical relationship between the growth velocity V and axial temperature gradient G, and (b) dependence of the number of twins on the number of large angle grain boundaries in the cross section (from Ref. 69 with permission).

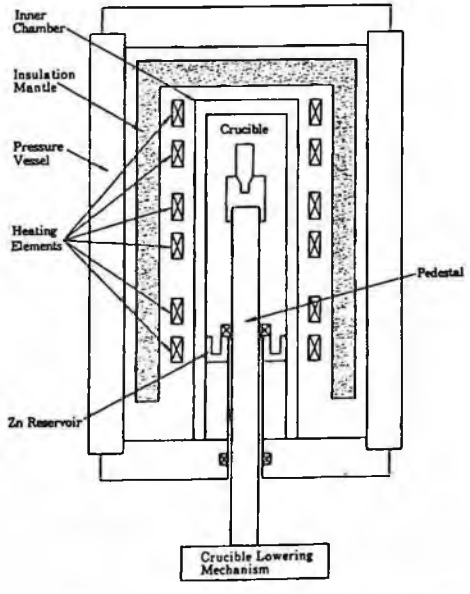

Fig. 17.10 Sectional view of the modified Bridgman furnace (from Ref. 71 with permission).

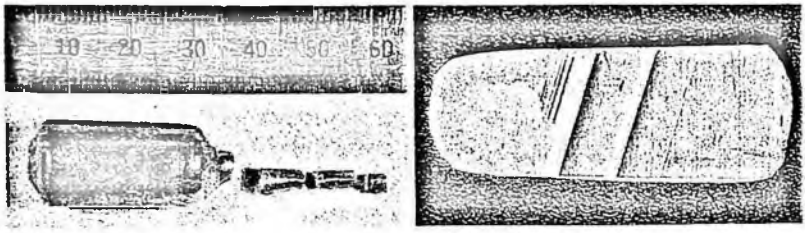

(a) As-grown Crystal (b) Wafer after Polishing and Etching

Fig. 17.11 ZnSe single crystal grown by B_2O_3 liquid encapsulation method (from Ref. 71 with permission)

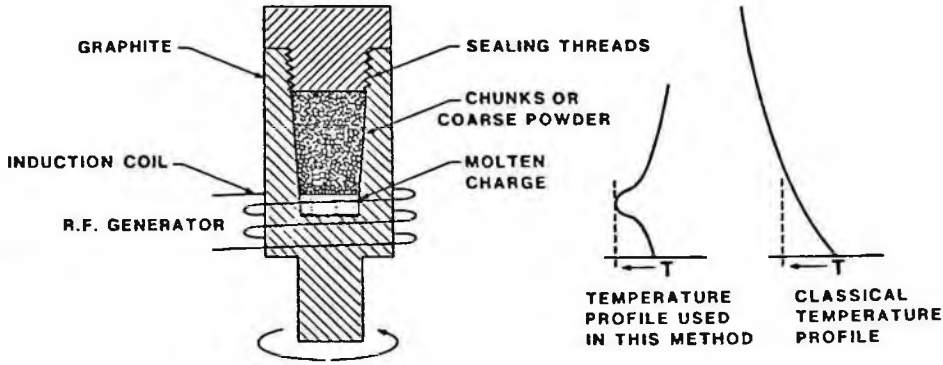

Fig. 17.12 Cross section of the crucible and the temperature profile in the experiment compared with the classical one (reprinted from Ref. 74 with permission, copyright 1986 Elsevier).

(4) Self-Sealing and Self-Releasing (SSSR) method

A low pressure melt growth method, SSSR,[74] which is based on growth in a graphite crucible sealed by the condensed vapor of the constituent II-VI compound is as shown in Fig. 17.12. This method has been applied to the growth of ZnSe and from a boule of 18 mm in average diameter and 35 mm in height, {111} wafers with a single crystal area of 4.5 cm^2 could be obtained.

17.3.2 Solution Growth

In this growth method, ZnSe is grown from various solvents. Since the growth temperature is lower than that for melt growth, the occurrence of twinning due to the phase transition can be avoided. The solubility of ZnSe in these solvents has been studied: In,[75] Ga,75 Bi,[76, 77] Sn,[77] Cd,[77] Zn,[77-79] Te,[80, 81] In-Zn,[79] Se,[82, 83] Sb-Se,[82, 83] As-Se,[82, 83] As-Sb-Se,[82, 83] $Sb_{0.4}Se_{0.6}$,[84] $Sb_{0.4}Te_{0.6}$,[85] as shown in Fig. 17.13. Liquid Phase Epitaxy (LPE)

Table 17.3 Solution Growth of ZnSe

Method	Result	Author	Year	Ref.
SG	Growth by the twin plane reentrant edge mechanism	Faust et al.	1964	89
SG	Solubility of ZnSe in Ga and In	Wagner et al.	1966	75
SG	Solubility of ZnSe in Sn, Bi and Zn	Rubenstein	1966	76,
			1968	77
SG	Growth from Ga and In solutions	Harsey	1968	90
SG	Growth from Te solvent	Washiyama et al.	1979	80, 81
THM	Growth of ZnSe crystals from $PbCl_2$ solvent at low temperatures (800-900 °C)	Triboulet et al.	1982	96
SG	Growth from In-Zn solvent	Kikuma et al.	1980	79
SG	Growth from Se and As-Sb-Se solutions	Aoki et al.	1982	82,
			1983	83
SG	Growth from Sb_2Se_3	Nakamura et al.	1984	84
TDM-CVP	Growth of p-type ZnSe from Se solution under Zn vapor pressure control	Nishizawa et al.	1985	4, 100-103
SG	Growth from Se and/or As solvent	Mochizuki et al.	1987	91
SG	Growth from Te-30%Se solvent	Itoh et al.	1990	92
SG	Growth from Sb_2Se_3-Sb_2Te_3 Se-Te solvents	Araki et al.	1991	85
SG	Growth from Se-Te solvent	Okuno et al.	1992	93, 94
LE-SG	Growth from Se solvent under molten fluoride encapsulation	Unuma et al.	1992	95
THM	Growth of ZnSe crystals from $PbCl_2$ solvent	Dohnke et al.	1997	97
THM	Growth of 10 mm diameter crystal of 30 mm length from SnSe solvent	Dohnke et al.	1999	98
HTSG	Growth from Se solution in a horizontal furnace	Maruyama et al.	2000	99

SG: Solution Growth, LE-SG: Liquid Encapsulated SG, THM: Travelling Heater Method, TDM-CVP: Temperature Difference Method under Vapor Pressure, HTSG: Horizontal Travelling Solvent Growth

of ZnSe has been performed in various solvents, such as Ga-Zn,[86] $CdCl_2$[87] and Te-Se.[88] The growth rate by this method is lower than that by melt growth methods but higher than vapor phase growth methods.

(1) Simple solution growth method

The growth of semiconductors from solution was first performed by Faust and John by the twin-plane reentrant edge mechanism[89] and preliminary work was performed by Rubinson[76, 77] and Harsy et al.[90]

Nakamura et al.[84] found that ZnSe has a very high solubility in $Sb_{0.4}Se_{0.6}$ and tried to grow ZnSe with a thickness of over 30 μm on a {111}B ZnSe substrate by Liquid Phase Epitaxy (LPE).

Mochizuki et al.[91] have grown ZnSe crystals from Se and/or As solvents with and without dopants such as As, Au and Tl. The ampoule sealed with the solvent and the ZnSe source was lowered at a rate of 6 mm/day. After 3-4 weeks, crystals measuring 5x3x2 mm^3 could be obtained. Araki et al.[85] have grown ZnSe crystals from various

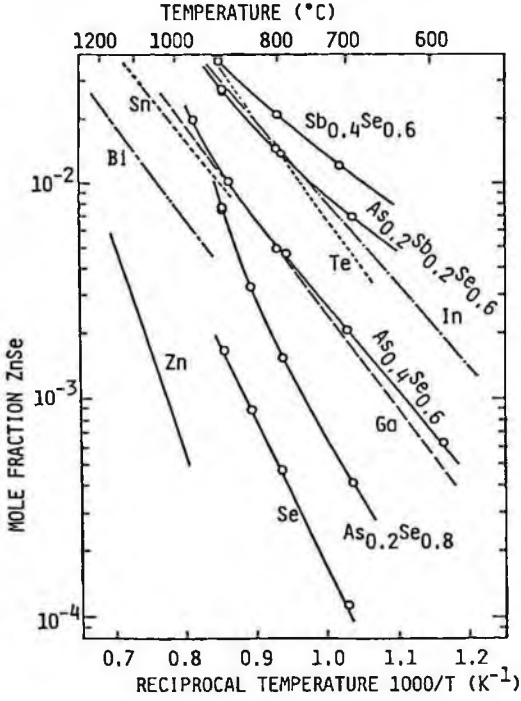

Fig. 17.13 Molar solubilities of ZnSe in various kinds of solvents (from Ref. 84 with permission).

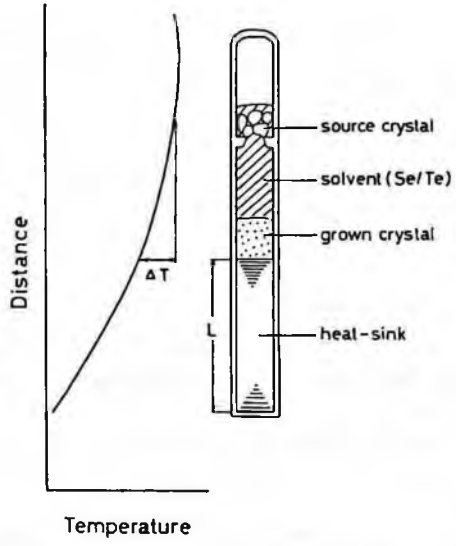

Fig. 17.14 Schematic diagram of the growth crucible and the temperature distribution in the furnace (reprinted from Ref. 93 with permission, copyright 1992 American Institue of Physics).

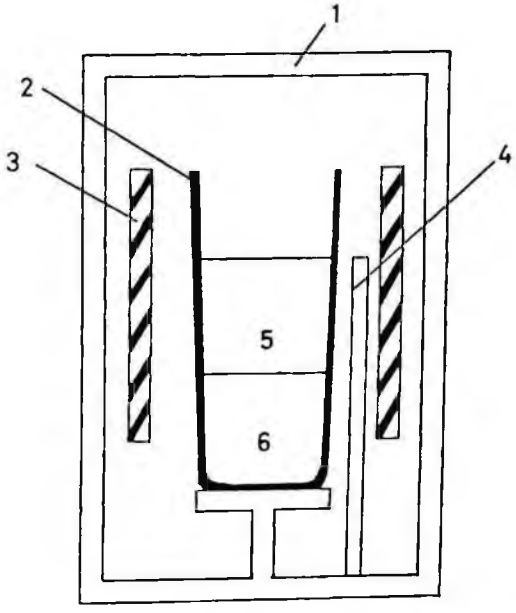

Fig. 17.15 Schematic arrangement of the apparatus for crystal growth of ZnSe with liquid encapsulation. 1: Pressure vessel, 2: pBN crucible, 3: Heater, 4: Thermocouple, 5: Encapsulant, 6: Source (ZnSe+ Se) (from Ref. 95 with permission).

solvents such as Sb_2Se_3, Se-Te, Sb_2Se_3-Sb_2Te_3, Te, Sb_2Te_3. Ito and Kohashi[92] have grown ZnSe crystals from Te and Te-Se solvent. In order to increase the growth rate, it was necessary to suppress the vaporization of the solvent Se.

Okuno et al.[93, 94] have developed a growth method with a Se/Te solvent in which Te is more than 70 mol%. Crystal growth was performed in the arrangement as shown in Fig. 17.14. The role of Te is to increase the growth rate and to reduce the vapor pressure of the solvent. ZnSe crystals could be grown at a temperature as low as 950 °C.

Unuma et al.[95] have reported the growth of ZnSe free from twins from Se solvent. In order to suppress the evaporation of the Se solvent, molten fluorides CaF_2-AlF_2 have been used as the liquid encapsulant under Se overpressure as shown in Fig. 17.15.

(2) Traveling Heater Method (THM)

In order to improve the purity, THM (Sec. 2.3.2) which is one of the solution growth methods, is effective. Triboulet et al.[96] and Donke et al.[97] used $PbCl_2$ as the solvent for growing ZnSe single crystals by the THM.

ZnSe has low solubilities in metal solvents such as Zn, Ga, In, Bi and Sn. This low solubility has made it difficult to grow large crystals by a simple solution growth method. ZnSe has high solubility in halides such as $PbCl_2$, $ZnCl_2$. In Fig. 17.16 (a) the phase diagram of $PbCl_2$-ZnSe is shown.[96] However, these solvents make inclusions and

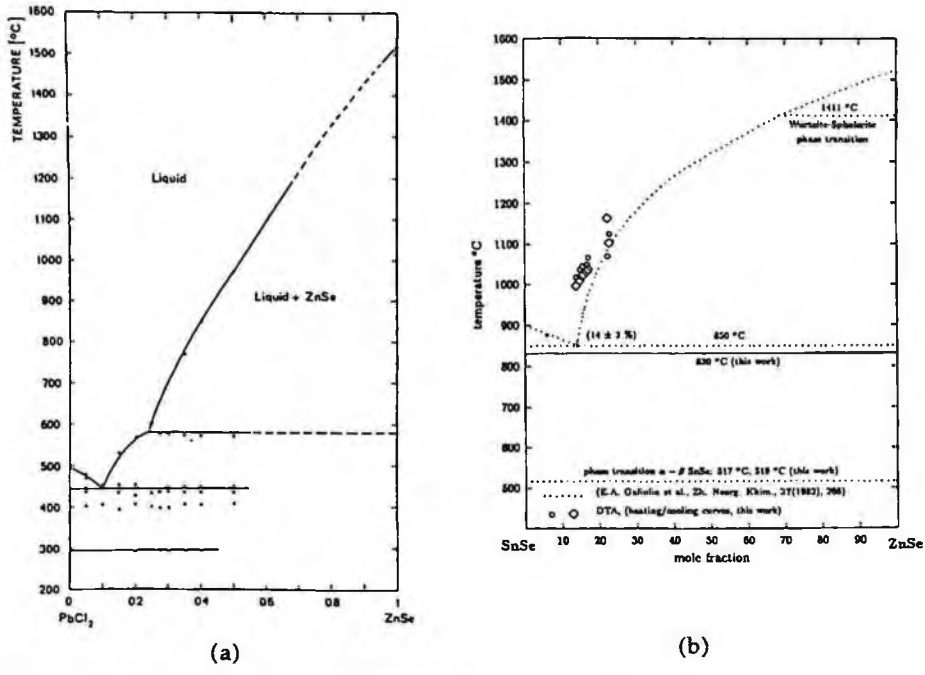

Fig. 17.16 Phase diagrams between solvents and ZnSe. (a) $PbCl_2$-ZnSe (reprinted from Ref. 96 with permission, copyright 1982 Elsevier) and (b) SnSe-ZnSe (reprinted from Ref. 98 with permission, copyright 1999 Elsevier).

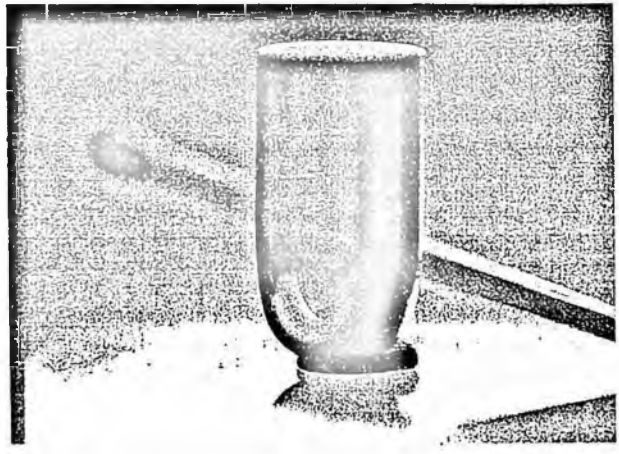

Fig. 17.17 ZnSe crystal grown by THM using SnSe as a solvent(reprinted from Ref. 98 with permission, copyright 1999 Elsevier).

the crystal quality is limited. Donke et al.[98] found that SnSe is a very appropriate solvent because of the high solubility of ZnSe while SnSe has practically no solubility in ZnSe as seen in the phase diagram in Fig. 17.16 (b). They have grown ZnSe crystals from SnSe solvent and succeeded in growing single crystals of 10 mm diameter and 30 mm length (Fig. 17.17) with a good crystal quality evaluated by double-crystal X-ray topography. Maruyama et al.[99] have applied a horizontal traveling solvent growth method to grow ZnSe crystals from Se solution. They found that the crystallinity of grown crystals was 26 arcsec for X-ray rocking curve FWHM with an EPD of 1.4×10^5 cm^{-2}.

(3) Temperature difference method under controlled vapor pressure (TDM-CVP)

The TDM-CVP was invented for the crystal growth of III-V materials by Nishizawa et al. as explained in Sec. 2.3.5. It has been applied to the crystal growth of ZnSe from a Se solution.[4, 100-103] In this method, as shown in Fig. 2.11, Zn pressure is controlled by heating the bottom of the sealed ampoule where the Zn is placed. Se was used as the solvent and the source ZnSe polycrystal was placed on the solution surface and the seed crystal was placed in the bottom of the solution where the temperature difference was set between the top and the bottom of the solution. Crystal growth was performed at 1050 °C while controlling the Zn pressure. As p-type dopant, Li was added to the solution. It was found that p-type ZnSe single crystals could be obtained.[102, 103] Using these p-type ZnSe crystals, the pn junctions which emit bluelight were first achieved.[4] The epitaxial growth of ZnSe on these crystals was also investigated.[104]

17.3.3 Vapor Phase Growth

Since ZnSe has a high sublimation pressure, it is possible to grow single crystals by evaporating ZnSe from the source side at high temperatures to the seed side at lower temperatures. This method has the advantage that pure ZnSe crystals can be grown but the disadvantage is that the growth rate is very slow. In order to improve the low growth rate, a vapor phase growth method using iodine or chlorine as the transport medium has been investigated.

(1) Direct Synthesis (DS) method

The direct synthesis method has been applied to the growth of ZnSe from the constituent element vapors and the structure of the grown crystals analyzed.[105]

(2) Physical Vapor Transport (PVT) method

In an open tube furnace, synthesized ZnSe powders were sublimed to grow crystals under a stream of H_2 by Crucianu and Chistyakow.[106] They obtained dendrite ZnSe crystals. Vohl[107] also applied a similar method. ZnSe powders were heated to 1200 °C under an inert carrier gas such as nitrogen and the vapor of ZnSe was condensed at lower temperatures. Platelet or needle like crystals could be grown but were affected by twinning.

Table 17.4 Physical Vapor Transport Growth of ZnSe

Method	Result	Author	Year Ref.
DS	Analysis of crystal structures	Pashinkin et al.	1960 105
Open tube	Dendrite ZnSe crystals of length 5-6 mm	Crucianu et al.	1960 106
Open tube	ZnSe crystal 25 g in weight	Vohl	1969 107
PVT	Growth by a Piper and Polish method	Aven et al.	1961 108
PVT	Growth kinetics, growth mechanism	Toyama et al.	1969 109
PVT	Growth under partial pressure control	Kiyosawa et al.	1970 110,111
PVT	Growth under partial pressure control	Burr et al.	1971 112
PVT	Vertical PVT with a capillary tube for controlling the vapor pressure in minimum	Blanconnier et al.	1972 113
PVT	Structural characterization of grown crystals	Cutter et al.	1976 114
PVT	Growth of single crystals up to 10x10x5 mm^3	Hartmann	1977 115
PVT	Growth of In-dope ZnSe with n-type conductivity	Papadopoulo et al.	1978 116
PVT	Growth under Zn or Se vapor pressure control	Cutter et al.	1979 117
PVT	Contact free growth on various substrates	Bulakh et al.	1980 118
PVT	Growth using necked ampoules	Takeda et al.	1982 119
PVT	Growth of $(ZnSe)_x(CdTe)_{1-x}$ crystals	Chandrasekharam et al.	1983 120
PVT	Stoichiometry control of $ZnSe_{1-x}S_x$ single crystals	Mochizuki	1982 121
PVT	Growth of $ZnSe_{1-x}S_x$ and PL characterization	Huang et al.	1983 122
PVT	Growth of ZnSe using high-purity source materials refined by overlap zone-melting	Isshiki et al.	1985 123
PVT	Growth of Al-doped ZnSe	Huang et al.	1986 124
PVT	Characterization of crystallographic properties	Koyama et al.	1989 125
PVT	10x4x2 mm^3 with a cold finger attachment	Cheng et al.	1989 126
PVT	50ϕ mmx25 mm crystals and characterization	Cantwell et al.	1992 127
PVT	Growth of $ZnSe_{1-x}S_x$ crystals	Matsushima et al.	1992 128
PVT	Growth with Zn vapor pressure control	Mochizuki et al.	1994 129
PVT	Effect of Zn partial pressure on the crystal quality	Hartmann et al.	1994 130
PVT	In-situ mass flux measurement	Sha et al.	1995 131
PVT	Study of Se precipitates	Chen et al.	1995 132
PVT	Growth of mixed crystals under the same temperature profile	Gratza et al.	1995 133
PVT	Growth of mixed crystals	Korostelin et al.	1996 134
PVT	Mass flux measurement and the effect of partial pressures	Su et al.	1996 135
PVT	In-situ transport rate monitoring	Fujiwara et al.	1996 136
PVT	Growth using semi-open ampoule to give reproducible growth rate	Fujiwara et al.	1996 137
SPVT	Seed crystals grown by solution growth	Kato	1997 138
PVT	Growth of ZnSe and $ZnSe_{1-x}S_x$ single crystals	Mycielski et al.	1997 139
PVT	Growth of ZnSe and ZnSeS of 25 mm diameter	Mycielski et al.	1998 140
SPVT	Growth of <100> and <111> single crystals	Korostelin	1998 141, 142
PVT	Se and Zn vapor pressure control	Tamura et al.	2000 143
PVT	In-situ partial pressure measurement and visual observation of crystal growth	Su et al.	2000 144
PVT	Growth of ZnSe with 18-20 ϕ mmx30 mm	Fang et al.	2000 145
PVT	Effect of seed annealing	Kato et al.	2000 146
PVT	Growth of $SeSe_{1-x}Te_x$ crystals	Su et al.	2000 147
PVT	Seeded growth of ZnS_xZe_{1-x} in H_2 or He	Korostelin et al.	2002 148
PVT	Phosphorus doped ZnSe and its characterization	Sankar et al.	2003 149

DS: Direct Synthesis, PVT: Physical Vapor Transport, SPVT: Seeded PVT

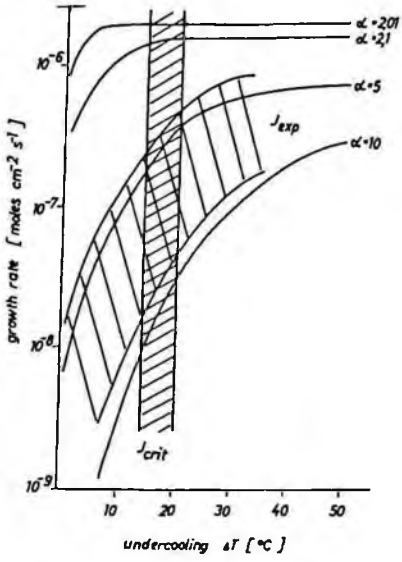

Fig. 17.18 Average growth rate of ZnSe as a function of the undercooling DT (reprinted from Ref. 115 with permission, copyright 1977 Elsevier).

Closed tube or semi-open tube sublimation methods have also been applied for the growth of ZnSe by various researchers.[108-149] Takeda et al.[119] applied the sublimation method in a closed ampoule to ZnSe, in which a necked ampoule was used to control the initial nucleation. The preliminary work on ZnSe crystal growth by the PVT method was performed by various researchers.

Hartmann[115] grew ZnSe single crystals measuring 10x10x5 mm^3 by a PVT method. It was shown that the growth rate is dependent on the undercooling as shown in Fig. 17.18. Hartmann[115] and Papadopoulo[116] pointed out that stoichiometry control during crystal growth is important for growing single crystals. Papadopoulo et al.[116] have grown In doped ZnSe single crystals by a PVT method arranged as shown in Fig. 17.19 and measured their electrical and optical properties. Cutter and Wood[117] have examined theoretically the growth of ZnSe by the PVT method and have grown ZnSe single crystals by controlling the vapor pressure of the constituent.

Bulakh et al.[118] have developed a modified physical vapor transport method, in which the free-growth method invented by Pekar (Fig. 17.20) based on the Markov method was used and molten tin provided the heating as shown in Fig. 17.21 and have grown single crystals up to 7.5 cm^3.

The self-sealing vapor phase growth method has been applied in growing $(ZnSe)_x(CdTe)_{1-x}$ ($0 \leqq x \leqq 1.00$) by Chandrasekharam et al.[120]

Mochizuki[121] has grown $ZnSe_{1-x}S_x$ crystals while controlling the vapor pressure of Se

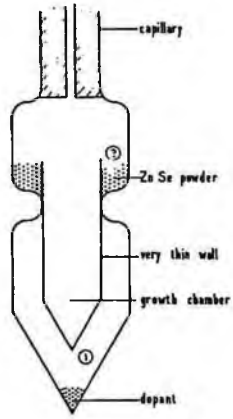

Fig. 17.19 Schematic of the quartz ampoule for a PVT method (reprinted from Ref. 116 with permission, copyright 1978 Elsevier).

and S, and examined the effect of the partial pressure of the constituents on the growth rate and the electrical and optical properties. Isshiki et al.[123] have grown ZnSe crystals, using commercial high purity selenium and zinc purified by vacuum distillation and by overlap zone-melting, and measured photoluminescence to confirm the effect of purification. Huang et al.[122, 124] have grown ZnSe and $ZnSe_{1-x}S_x$ single crystals by the PVT method under Zn partial pressure control and have examined the photoluminescence of grown crystals. Mochizuki et al.[129] have grown ZnSe single crystals by the PVT method under Zn partial pressure control and have examined the photoluminescence of grown crystals.

Koyama et al.[125] have grown ZnSe single crystals by a seeded PVT using a (111)B face seed. Cheng and Anderson[126] have grown ZnSe single crystals by a simple PVT method. A needle-shaped cavity in the cold finger was connected to the ampoule volume which acts as a channel for a seed crystal to be developed.

Cantwell et al.[127] have developed Seeded Physical Vapor Transport (SPVT) method. ZnSe source powders are placed at the center of a quartz ampoule of diameter 50 mm and seed crystals are set at the two ends of the ampoule. Typical crystal dimensions were 50 mm diameter and 25 mm length and the weight was about 190 g. Since seeds are placed at the ends of the ampoule, two crystals with similar dimensions can be grown simultaneously. For growing crystals, the source temperature was set to 1200 °C and the temperature difference between the source and growing crystals was set to less than 100 °C.

Matsushima et al.[128] have grown $ZnSe_{1-x}S_xSe_{1-x}$ crystals ($0.2 \leqq x \leqq 1$) using a necked quartz ampoule. The growth was performed by a modified Piper-Polish method at 1250 °C in a stream of Ar gas at a flow rate of 0.11 /min. About ten ingots of crystals were obtained and the average size of each ingot was 0.5 mm^3. Their photoluminescence spectra were measured as a function of the composition.

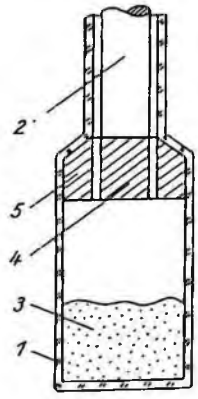

Fig. 17.20 "Free growth in the ampoule with an apex. 1; Quartz ampoule, rod serving as a substrate, 3; charge, 4 and 5; two separated parts of the crystal.[118]

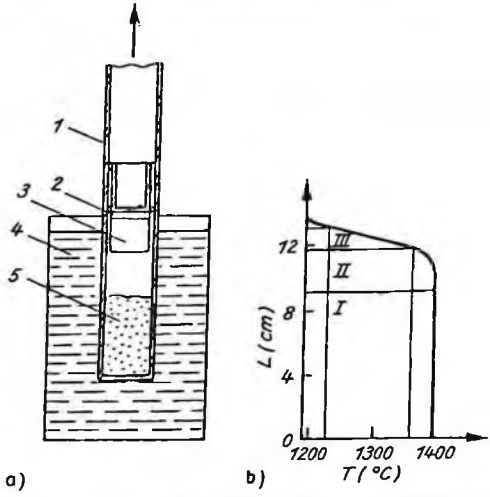

Fig. 17.21 "Free growth" of the crystal with molten tin as a heating medium. (a) Schematic diagram of the growth apparatus; 1: ampoule, 2: substrate, 3: crystal 4: molten tin, 5: charge. (b) Temperature profile along the vertical axis.[118]

Chen et al.[132] have grown ZnSe crystals by a simple PVT method and have examined the precipitation of selenium. Grasza et al.[133] have examined the optimal temperature profile for PVT crystal growth. The conclusion was that an isothermal plateau at the location of the source materials and a temperature hump between the source material and the crystal provided optimal growth conditions. Sha et al.[131] and Su et al.[135] have measured mass flux as a function of temperature by using an optical absorption measurement method.

Fujiwara et al.[136, 137] have studied the transport rate using in-situ monitoring. They have grown ZnSe single crystals by seeded PVT. To grow crystals with highly repro-

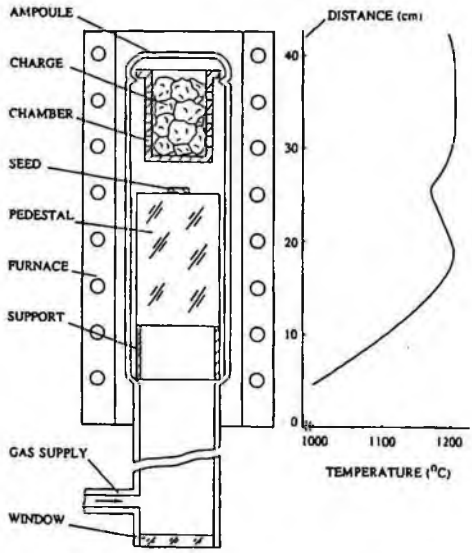

Fig. 17.22 Growth ampoule and temperature profile of the furnace (reprinted from Ref. 141 with permission, copyright 1998 Elsevier).

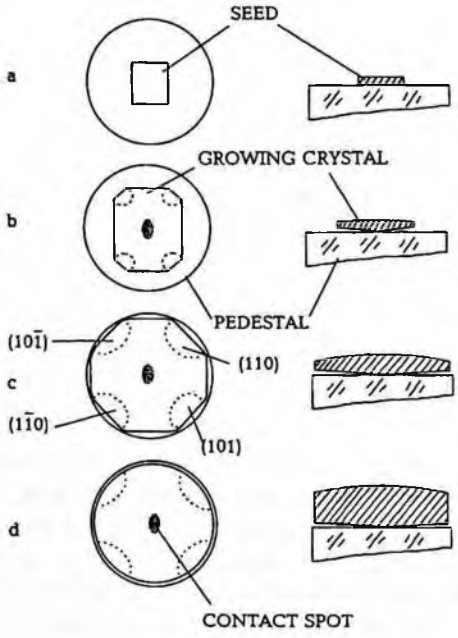

Fig. 17.23 View from the ampoule window (from the left) and cross section along the ampoule axis (from the right) of the grown crystal. (a) Before the growth process, (b) at the stage of radial and normal growth, (c) after finishing tangential growth, (d) after the growth process (reprinted from Ref. 141 with permission, copyright 1998 Elsevier).

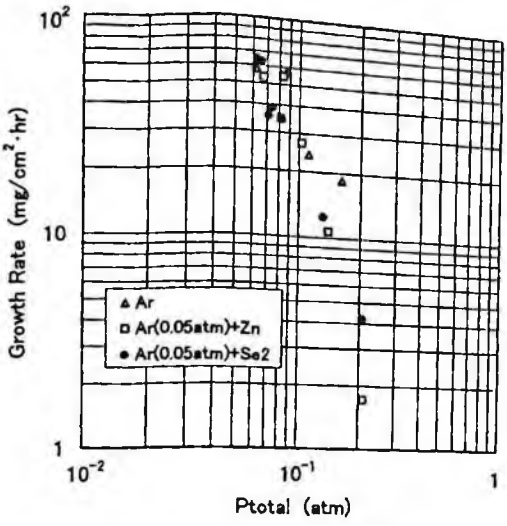

Fig. 17.24 Growth rate as a function of the total pressure (reprinted from Ref. 143 with permission, copyright 2000 Elsevier).

ducible results, a semi-open ampoule was used into which Ar gas was introduced.

Mycielski et al.[139, 140] have grown ZnSe and $ZnSe_{1-x}S_x$ ($x<0.15$) single crystals 25 mm in diameter at 1150 °C by the PVT method, and examined their optical properties.

Korostelin et al.[141, 142] have developed a seeded PVT (SPVT) method in which the seed crystal attachment to the pedestal is improved by the application of a reverse temperature gradient and monitored optically the attachment process as shown in Fig. 17.22 and 17.23. By this method, they have grown ZnSe single crystals with orientations <111> and <100> . Doping by In and Al has been performed at the growth temperatures of 1180-1240 °C. They obtained twin-free 50 mm diameter single crystals with an EPD of $5x10^3$ cm^{-2}. The resistivity was lowered down to 0.05 Ω·cm by annealing in liquid Zn:Al. They also have grown mixed single crystals of 40-55 mm diameter.[149]

Tamura et al.[143] have grown ZnSe in an Ar gas atmosphere by controlling the Zn or Se partial pressure and examined their effect on the growth rate (Fig. 17.24) and the crystal quality (Fig. 17.33). It was found that at an Se_2 partial pressure of $4x10^{-3}$ atm., the best crystal quality was obtained. This is attributed to the stoichiometry of ZnSe achieved at this partial pressure.

Fang et al.[145] have grown ZnSe single crystals of 18-20 mm diameter and 30 mm length by the PVT method at 1100 °C. The EPD was in the range of 1-4 $x10^4$ cm^{-2} and the FWHM of the X-ray rocking curve was 17 arcsec. Su et al.[144] have grown ZnSe single crystals by the seeded PVT method, in which the partial pressure of Se was measured in-situ by optical absorption. Kato and Kikuma[146] have examined the effect of seed

Table 17.5 Chemical Vapor Transport Method and Other Vapor Phase Growth Methods.

Method	Results	Author	Year	Ref.
CVT	Growth using iodine transport reagent	Nitsche	1960 1961	150, 151
CVT	Growth of cubic ZnSe from ZnSe-I_2 system	Kaldis	1965	152-155
CVT	Thermodynamical consideration	Schäfer	1966	156
CVT	Growth from ZnSe-HCl, HBr, and I_2 systems	Paker et al.	1969	157
CVT	Growth with iodine transport reagent	Hartmann	1974-1977	115, 158
CVT	Growth of ZnSe and ZnSSe using I_2	Catano et al.	1976	160
CVT	Growth of ZnSSe crystals up to 24x14x14 mm^3	Fujita et al.	1979	161
CVT	Self nucleation	Poindessault	1979	162
CVT	Low temperature growth	Triboulet et al.	1982	163
STHM	Growth at 900 °C at a rate of 1 mm/hr.	Taguchi et al.	1985	174
CVT	Growth using NH_4Cl as the transport reagent	Matsumoto et al.	1986	164
SCVT	Growth of ZnSe crystals up to 14x14x20 mm^3	Koyama et al.	1988	165-167
CVD	Polycrystalline ZnSe for window materials using ZnSe seed substrates	Goela et al.	1988	173
PVD	ZnSe thick layer growth on GaAs substrates	Sukegawa et al.	1987	176
SSS	Substitution of ZnTe surfaces by ZnSe in Se vapor atmosphere	Seki et al.	1997	177
CVT	Growth of ZnSe crystals 25 mm in diameter using I_2	Fujiwara et al.	1998	168
CVT	Rotational method for growing 25 mm diameter ZnSe single crystals	Fujiwara et al.	1999	169-171
CVT	Growth from Zn-Se-Zn$(NH_4)_3Cl_5$ system	Li et al.	2005	172
STHM	Growth at 1100 °C with undercooling less than 10 °C	Yakimovich et al.	1999	175

CVT: Chemical Vapor Transport, SCVT: Seeded CVT, STHM: Sublimation Travelling Heater Method, SSS: Substrate Surface Substitution

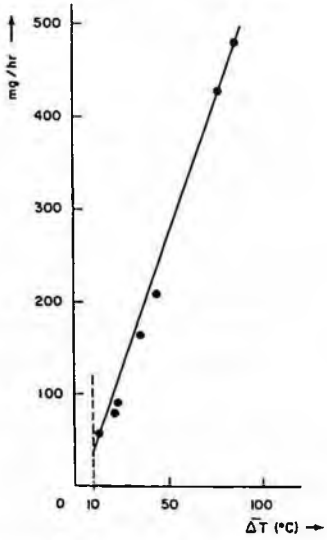

Fig. 17.25 Dependence of the transport rate on the apparent undercooling in the ZnSe-I_2 system (reprinted from Ref. 153 with permission, copyright 1965 Elsevier).

annealing on the quality of grown crystals. ZnSe (111)B was used as the seed crystal, and it was annealed at 1165 °C for 10 hrs prior to crystal growth. It was found that the X-ray rocking curve width was greatly improved by annealing. Su et al.[147] have grown $ZnSe_{1-x}Te_x$ (x = 0.1-0.3) mixed crystals by the vertical and horizontal PVT methods and examined the uniformity of composition. Sankar and Ramachandran[149] have grown undoped ZnSe, P-doped ZnSe and P, Ga-doped ZnSe crystals and have measured their physical properties.

(3) Chemical Vapor Transport (CVT) Method

Physical vapor transport methods can be applicable only for high temperatures up to 1100-1300 °C. To work at lower growth temperatures, chemical vapor transport in which a transport reagent is used, is effective. In the chemical vapor transport method, iodine is often used as the transport reagent. The detail of this method has already been explained in Sec. 2.4.3. The method has been investigated by many researchers.[150-172] This method allows high growth rates, but the incorporation of the transport reagent is difficult to avoid.

Kaldis[153] has grown ZnSe single crystals measuring 20x15x15 mm^3 by seeded CVT. The relationship between the growth rate and the degree of undercooling was investigated as shown in Fig. 17.25 and it was found that ΔT=10 °C is appropriate for a good nucleation on the quartz wall.

Parker and Pinnell[157] have grown ZnSe single crystals with HCl, HBr and I_2 as chemical transport reagents, using a horizontal sealed ampoule as shown in Fig. 17.26. Hartmann1[15, 158] has grown small crystals using I_2 as the transport agent. Catano and Ku[160] have grown ZnSe and $ZnSe_{1-x}S_x$ (x = 0.2-0.8) by the iodine transport seeded CVT method as shown in Fig. 17.27.

Fujita et al.[161] examined the effect of the temperature difference, the ampoule geometry such as the angle at the conical tip and the diameter on single crystal growth, using the growth ampoule shown in Fig. 2.16. It was found that a single crystal measuring 24x14x14 mm^3 could be obtained with a temperature difference of 7 °C in an ampoule with a steep conical tip.

Poindessault[162] has grown ZnSe single crystals by a horizontal self-nucleated CVT method and evaluated their optical and electrical properties. Triboulet et al.[163] have grown ZnSe single crystals by the CVT method. Matsumoto et al.[164] have grown ZnSe and $ZnSe_{1-x}S_x$ single crystals using NH_4Cl as a transport agent.

Koyama et al.[165] have grown ZnSe single crystals by vertical CVT using iodine transport reagent in an ampoule similar to Fig. 17.27 and obtained crystals measuring 14x14x20 mm^3 (Fig. 17.28). They also measured the growth rate as a function of the temperature difference ΔT (Fig. 17.29)

Fujiwara et al.[168-171] have grown 25 mm diameter ZnSe single crystals by the seeded CVT method using iodine as the transport reagent. They optimized the growth temperature, seed orientation and iodine concentration. They further developed a rotational CVT method using a growth ampoule arranged as seen in Fig. 17.30. Fig. 17.31 shows grown crystals as a function of the rotation rate and the iodine density.

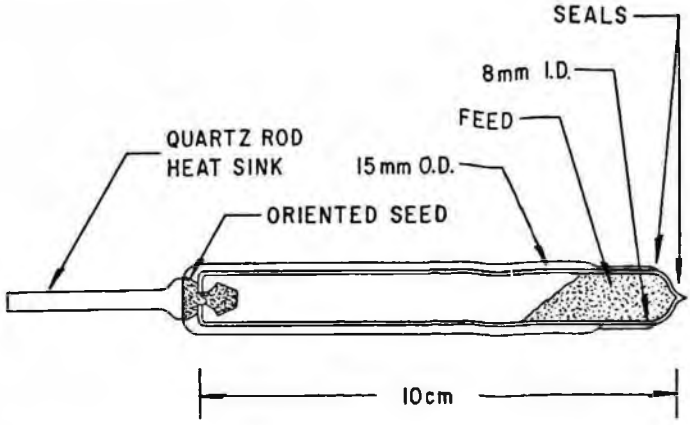

Fig. 17.26 Crystal growth apparatus (from Ref. 157 with permission).

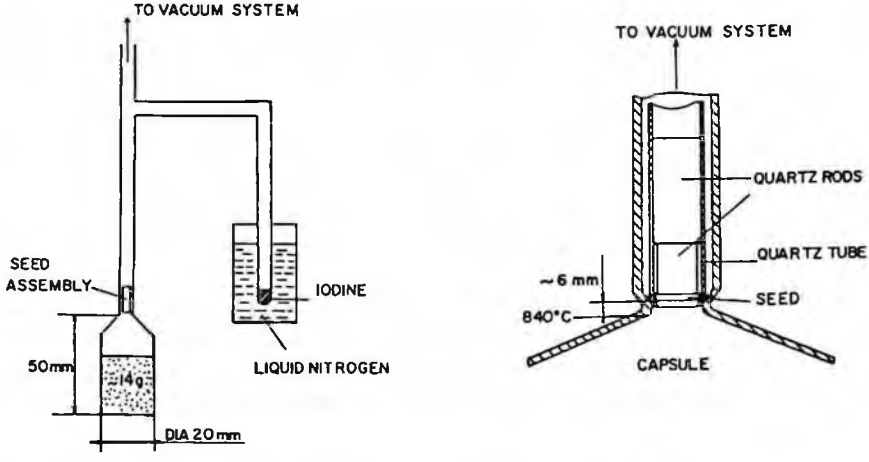

Fig. 17.27 (a) Crystal growth ampoule and side arm, and (b) details of the seed holder assembly (reprinted from Ref. 160 with permission, copyright 1976 Elsevier).

(4) Chemical Vapor Deposition (CVD) method

The subatmospheric CVD method has been developed for fabricating various materials.[173] This method is used industrially to produce infrared optical window materials such as ZnSe, ZnS, CdS, CdTe. It is however limited to producing polycrystalline materials which can be used as the source material for single crystal growth.

(5) Sublimation Travelling Heater Method (STHM)

The STHM (Sec. 2.3.3) has been applied to the growth of ZnSe by Taguchi et al.[174]

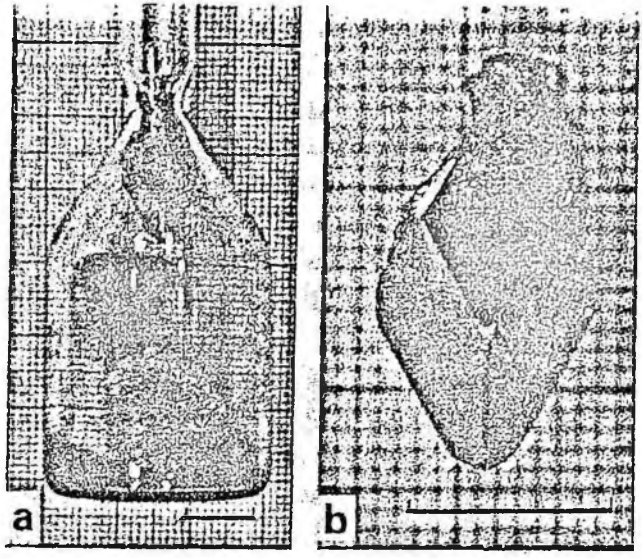

Fig. 17.28 (a) Single crystal with the ampoule, (b) typical as-grown ZnSe single crystal. Markers represent 1 cm. (reprinted from Ref. 165 with permission, copyright 1988 Elsevier)

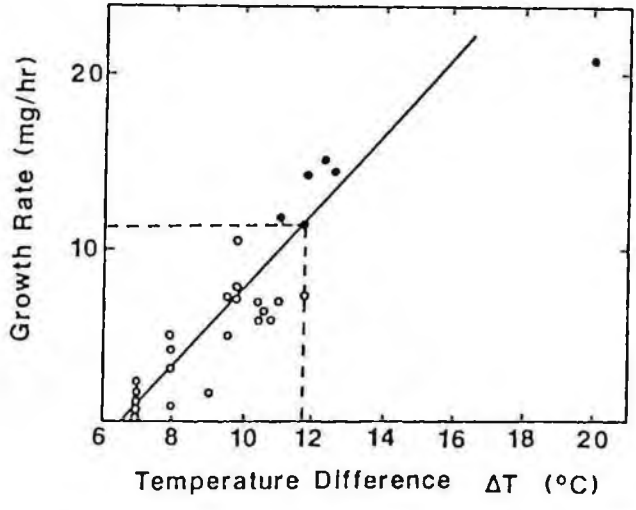

Fig. 17.29 Dependence of the growth rate on the temperature difference ΔT. (●) polycrystals: (○) single crystals. (reprinted from Ref. 165 with permission, copyright 1988 Elsevier)

Crystal growth has been performed at 900 °C with a growth rate of 1 mm/day and photoluminescence properties of the crystals have been evaluated.

Yakimovitch et al.[175] have grown ZnSe single crystals by an unseeded STHM at

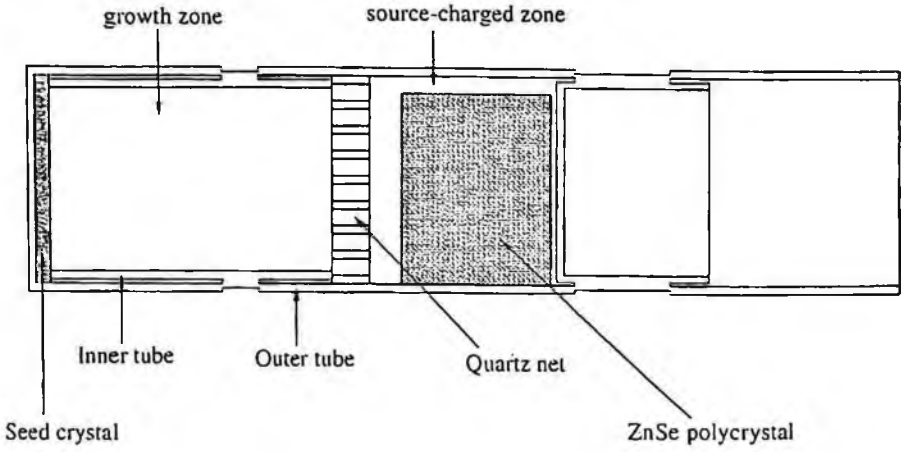

Fig. 17.30 Schematic illustration of growth ampoule (reprinted from Ref. 169 with permission, copyright 2000 Elsevier).

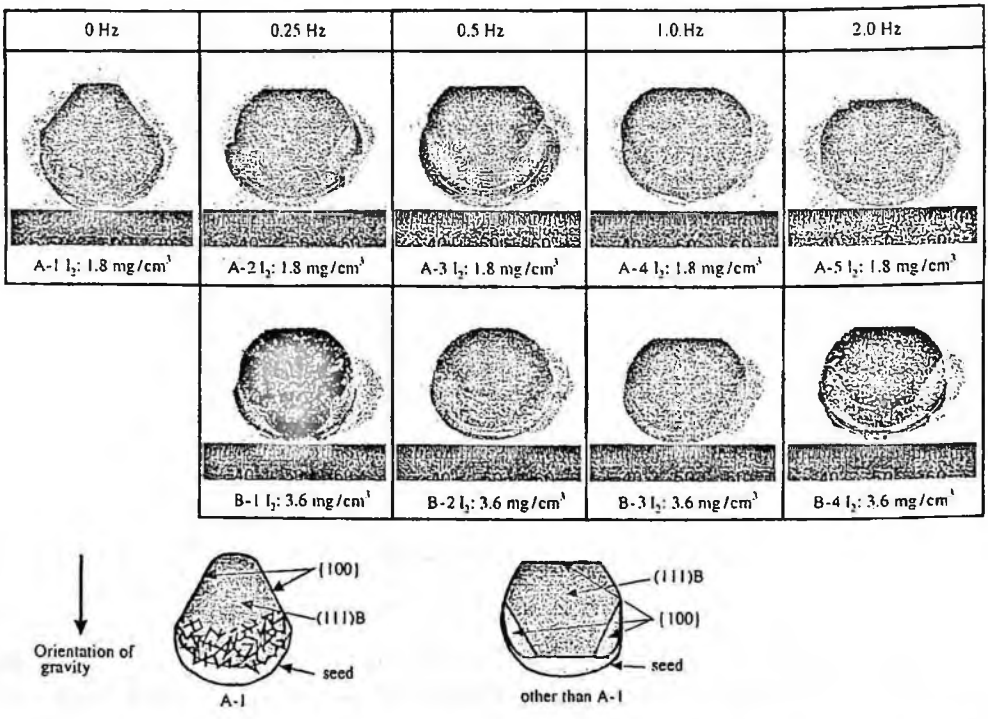

Fig. 17.31 Photographs of grown ZnSe crystals (top and middle rows) and schematic illustrations (bottom row). The direction of gravity during growth of A-1 crystal is indicated by the arrow. (reprinted from Ref. 169 with permission, copyright 2000 Elsevier)

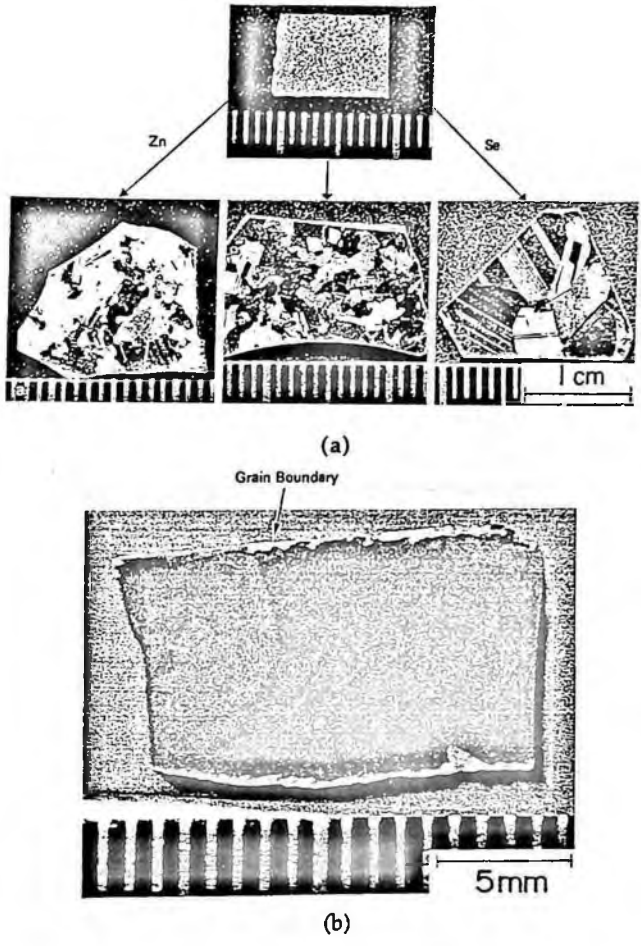

Fig. 17.32 (a) Dependence of the grain growth on the atmosphere at 850°C, and (b) ZnSe crystal of wide single crystal area obtained after two week annealing under a selenium ambient at 1000 °C (reprinted from Ref. 178 with permission, copyright 1990 Elsevier).

1100 °C with undercooling ΔT less than 10 °C. The FWHM of X-ray rocking curve of grown crystals was less than 20 arcsec and the EPD was $5x10^4$ cm^{-2}.

(6) Other methods

Sukegawa et al.[176] have prepared ZnSe substrates with a thickness of about 370 μm by physical vapor deposition (PVD). Thick ZnSe layers were grown on GaAs substrates and GaAs substrates were removed by etching in order to obtain freestanding ZnSe substrates. Seki and Oda[177] have prepared ZnSe materials on ZnTe substrates by solid state substitution of ZnTe by ZnSe under a selenium vapor atmosphere.

Table 17.6 Various etchants for Dislocation Evaluation

Orientation	Etchant	Pit formation	Ref.
(111)A	1-10 % bromine-methanol		184
	7 NH_2SO_4-saturated $K_2Cr_2O_7$	no etch pits	183
	12.5N-NaOH	regular triangular pits	183
	30-50 % NaOH	shallow triangular pits	185, 186, 58, 167
	1N HCl + 1N HNO_3	shallow triangular pits	185
(111)B	7NH_2SO_4-saturated $K_2Cr_2O_7$	regular triangular pits	183
	12.5N-NaOH	shallow triangular pits	183
	30 % NaOH	deep triangular pits	185, 186, 167
	1N HCl + 1N HNO_3	deep triangular pits	185
(110)	30-50 % NaOH	triangular pit	44
(100)	5 -10% bromine-methanol	rectangular pits	126, 127
	30 %NaOH	isosceles triangular pits	185

17.3.4 Solid State Recrystallization

It was found that ZnSe polycrystals show abnormal grain growth and give large grains after heat treatment.[178-180] When ZnSe polycrystals prepared by the CVD method were annealed at 850-1000 °C, large grains could be obtained. Terashima et al. examined the effect of Zn and Se atmospheres and worked out appropriate growth conditions. At 1000 °C under a Se atmosphere, it was found that grains over 1 cm square could be obtained (Fig. 17.32).

17.4 CHARACTERIZATION

17.4.1 Defects

(1) Structures

Kikuma et al.[51, 181] have studied the effect of growth conditions on the formation of microscopic defects such as twins, rodlike grain boundaries, voids, and the wurtzite phase. Terashima et al.[64, 179] have studied the effect of impurities on the grain growth rate. Okuno et al.[182] have estimated the structural perfection by measuring the lattice constant and the X-ray rocking curve FWHM.

(2) Dislocations

Various etchants have been studied to evaluate dislocation densities, as shown in Table 17.6. NaOH solution is frequently used as the EPD etchant, since it can be used for (110) cleaved surfaces so that it is easy to measure the EPD without polishing the sample surface. 30% NaOH solution can also be used for determining the polarity of ZnSe.[189]

Tamaru et al.[143] have studied the effect of the Se vapor pressure on the EPD and X-ray rocking curve width as shown in Fig. 17.33. Korostelin[142] has measured the EPD distribution across (100) wafers as seen in Fig. 17.34.

(3) Native Defects

The formation of native defects in ZnSe has been systematically studied by the analysis

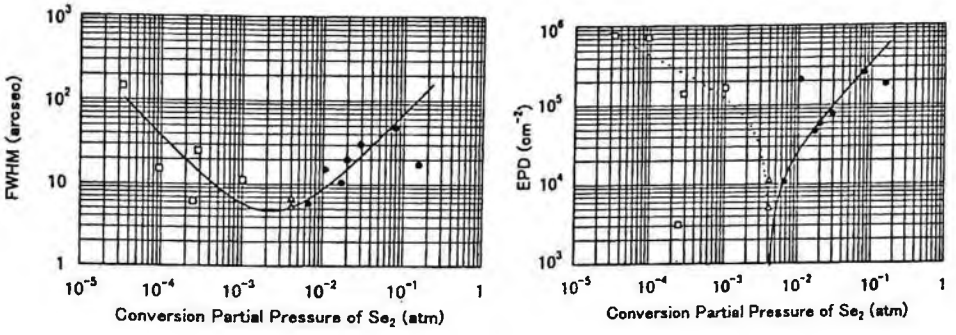

Fig. 17.33 (a) Se_2 partial pressure dependence of the FWHM of the X-ray rocking curve and (b) the etch pit density (reprinted from Ref. 143 with permission, copyright 2000 Elsevier).

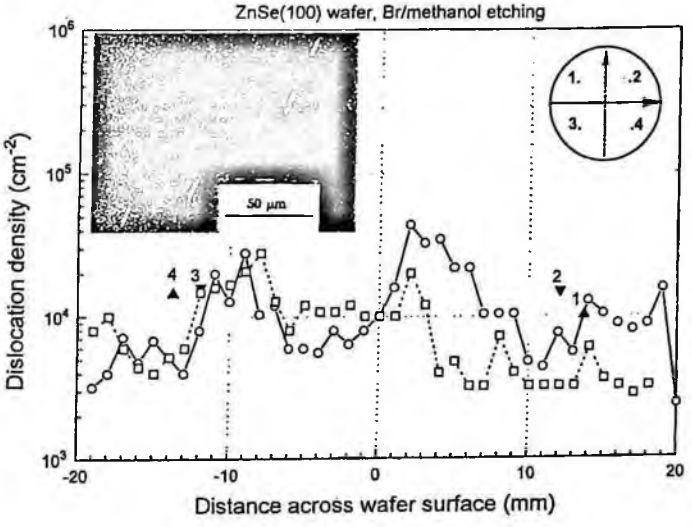

Fig. 17.34 Distribution of etch pit density across the ZnSe (100) wafer surface (reprinted from Ref. 142 with permission, copyright 1999 Elsevier).

of electrical properties and Brouwer plot has been constructed for pure ZnSe and doped ZnSe.[188, 189] It was found that Schottky type defects are predominant for ZnSe. Jansen and Sankey[190] have calculated the formation energy of point defects in ZnTe by an ab-initio pseudo-atomic method and showed the concentration of point defects as a function of stoichiometry as seen in Fig. 17.35.

(4) Deep Levels

Deep levels in various bulk ZnSe preparations have been studied by deep level transient spectroscopy (DLTS)[191-194] and isothermal current transient spectroscopy

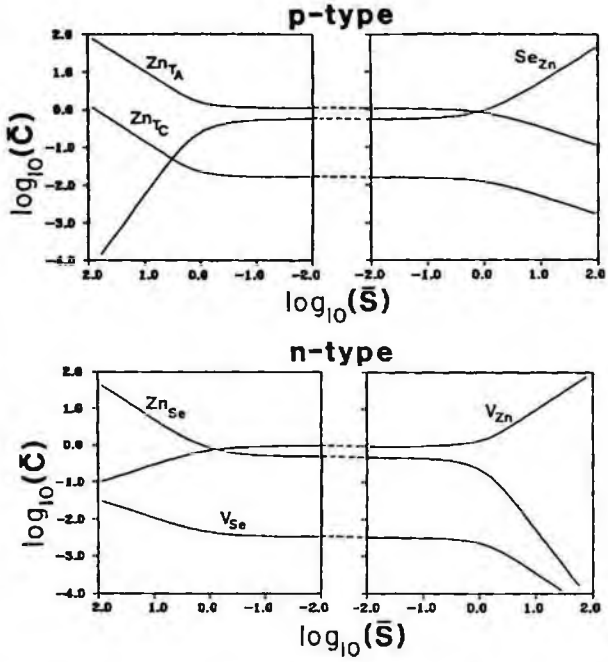

Fig. 17.35 Native defect concentrations as a function of stoichiometry for p-and n-type ZnSe. The right panel is for positive stoichiometry S (excess Zn) and the left panel is for negative stoichiometry S (excess Se) (reprinted from Ref. 190 with permission, copyright 1989 American Physical Society).

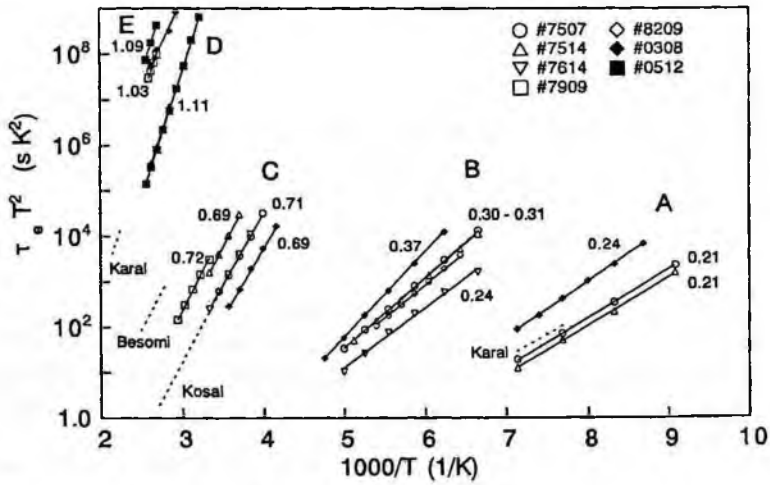

Fig. 17.36 Arrhenius plots of the emission time constants (with T^2 correction) for the five groups of electron traps observed in as-grown ZnSe. Some of the reported data for traps in the literature were replotted by the dotted line. (reprinted from Ref. 195 with permission, copyright 1996 American Institue of Physics)

Table 17.7 Energy Levels of Donors and Acceptors in ZnSe

Impurity	Donor or Acceptor	Energy level from condcution band (eV)	Energy level from valence band (eV)
Ag	A		0.430
Al	D	0.0256-0.0263	
As	A		~0.110
Au	A		~0.550
B	D	0.0256	
Cl	D	0.0262-0.0269	
Cu	A		0.072, 0.650
F	D	0.0288-0.0293	
Ga	D	0.0272-0.0279	
I	A	0.68	
In	D	0.0282-0.0289	
Li	D	0.021-0.0263	
	A		0.66, 0.114
N	A		0.085-0.136
Na	A		0.085-0.128
P	A		0.084, 0.600-0.700

(ICTS).[195] These levels are summarized in Fig. 15.36. There are mainly five electron traps[193, 195] and they are attributed to impurity-Se vacancy complexes, impurities associated with dislocations and extrinsic impurities. Deep levels in ZnS_xSe_{1-x} crystals have also been studied.[191, 196] Grimmeiss et al.[196] have discussed these traps theoretically from the viewpoint of the four center model.

17.4.2 Electrical Properties

(1) Electrical Properties

Because of the self compensation mechanism (Sec. 4.2.5), ZnSe is of n-type conductivity and it is difficult to obtain p-type conductive material. The temperature dependence of electron mobility and carrier concentrations of n-type ZnSe have been measured as seen in Figs. 17. 37 and 17.38.[197] Kikuma et al.[50, 53, 54, 57] have studied the effect of Bridgman growth conditions such as Zn partial pressure on the electrical properties.

Nishizawa et al.[102] have grown p-type ZnSe single crystals by the TDM-CVP method (Sec. 2.3.5). The electrical properties as a function of the Zn vapor pressure have been studied as shown in Figs. 17.39 and it was found that the lowest carrier concentrations are seen with a Zn vapor pressure of 7.2 atm. which is believed to be due to stoichiometry.

In the case of donor doping, donors are compensated by Zn vacancies so that only high resistive materials can be obtained. In order to reduce the resistivity of ZnSe, a Zn dipping procedure has been applied. As grown ZnSe crystals were heat-treated in a Zn melt and it was found that this could reduce the resistivity. This is because amounts of acceptors such as Cu were reduced as were Zn vacancies (V_{Zn}) by incorporation of Zn, thus numbers of acceptors compensating donors were reduced.

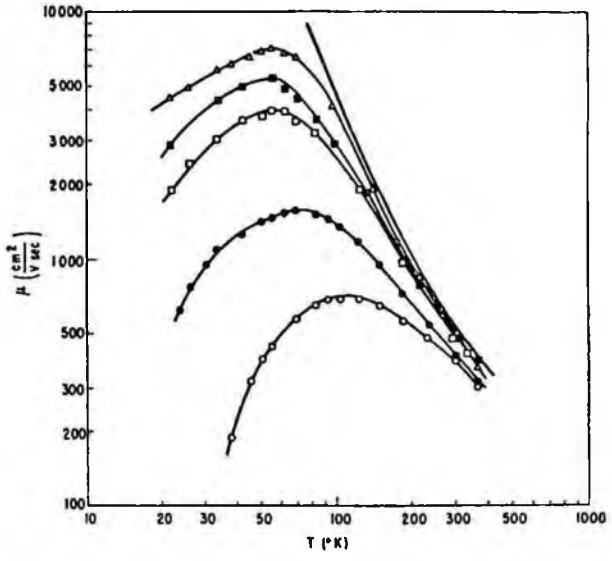

Fig. 17.37 Temperature dependence of Hall mobility of several n-type ZnSe preparations (reprinted from Ref. 197 with permission, copyright 1967 Elsevier)

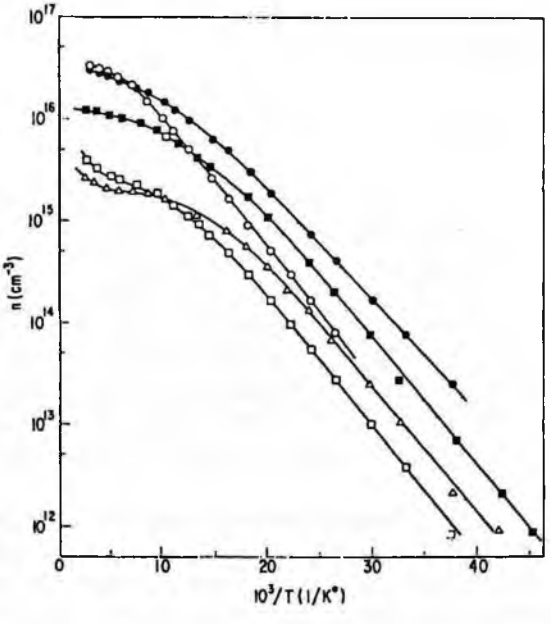

Fig. 17.38 Temperature dependence of carrier concentration of several n-type ZnSe preparations (reprinted from Ref. 197 with permission, copyright 1967 Elsevier).

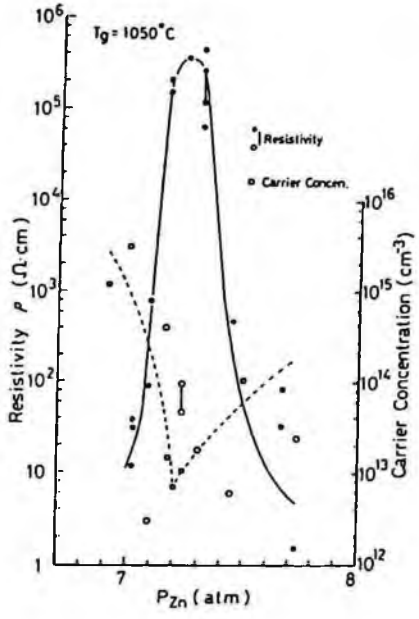

Fig. 17.39 (a) Dependencies of the resistivity and the carrier concentration of as-grown p-type crystals on the applied Zn pressure and (b) temperature dependence of carrier concentration (reprinted from Ref. 102 with permission, copyright 1986 American Institue of Physics).

(2) Doping

Doping of donors and acceptors in ZnSe have been studied by various authors[18, 198-202] and their energy levels were determined[18, 202] as shown in Table 17.7. The ionization

Table 17.8 Assignment of Photoluminescence Peaks

Ex(n=2)		2.8164					
Ex(n=1)		2.8027					
Ex		2.8021					
S band		2.8002					
Donor bound excitons			Al	Cl	Ga	In	F
(D^+, X)	I_{2b}-		2.79828				
			2.79998				
(D^0, X)	I_2		2.79776	2.79766	2.79739	2.79717	2.79694
				2.7959-65		2.7941-5	
			2.7983	2.79836-	2.79823-	2.79803-	
			2.80138	2.80023	2.80151	2.80140	
	I_{0a}	2.79821					
	I_{20}		2.79776	2.79770	2.79751	2.79722	2.79705
Bound exciton complex	I_3		2.79649	2.79531			
			2.79592	2.79496	2.79407		
				2.7959-65		2.7941-45	
	I_{1s}		2.7936				
Acceptor bound excitons							
(A^0, X)	I_1	2.7921(Li), 2.7930(Na)					
V_{Zn}, Cu_{Zn}	I_1^{deep}	2.7826					
		2.7829-2.731					
Y or Yo		2.6					
Q (D-A pair)		2.2					
Deep levels		2.10					
SA (V_{Zn}-Cl_{Se})		1.98					
Cu-red		1.95					

energies of 3d-elements have been studied by Kikoin et al.[203]

(3) Self compensation

As explained in Sec. 4.2.5, it is difficult to obtain p-type conductivity in the case of ZnSe because of the self-compensation mechanism. There are several reports that p-type conductivity had been obtained by annealing in a Zn melt or by stoichiometry control. For epitaxial growth, it has become possible to obtain p-type conductivity reproducibly by nitrogen doping but for bulk crystals, the reproducibility is not yet known.

17.4.3 Optical Properties

Photoluminescence is an effective evaluation method for evaluating purity, the existence of native defects and the crystal perfection. There have been many reports on the photoluminescence of ZnSe.[5, 36, 85, 121-124, 129, 179, 204-219] The assignment of various peaks is as shown in Table. 17.8.

Edge emissions have been studied and assigned by various authors as shown in

Table 17.8. There are free exciton peaks, (D^+,X) and (D^0, X) peaks as I_2 lines, bond exciton complex peaks as I_3 lines, (A^0,X) peaks as I_1 lines and I_1 deep lines. At longer wavelengths than these edge emissions, there are LO replica lines and donor-acceptor (D-A) pair peaks as Q lines, SA lines and others. I_1 deep lines are ascribed to point defects such as V_{Zn} or impurities as Cu_{Zn}.

As shown in Fig. 17.39 (a), as-grown crystals prepared by the sublimation method showed strong free exciton peaks and I1d peaks with phonon replicas, and weak bound exciton peaks of I_2 and I_3 lines. After Zn melt dipping, it was found that I1d peaks due to V_{Zn} disappear and free exciton peaks become stronger. This is explained as the number of Zn vacancies being reduced by Zn melt dipping. The reason why I_2 and I_3 lines become stronger is explained by the reduction of the kinetic energy of excitons.[123, 217]

The effect of the purity of ZnSe crystals on the PL was studied by Isshiki et al.[36] The PL of $ZnSe_xSe_{1-x}$ crystals has been evaluated by Mochizuki[121] and Huang et al.[122] It was found that I_1^{deep} lines weaken as a function of the composition x and this behavior was explained by the increase of phonon coupling. D-A pair emissions of Na-doped ZnSe have been studied by Neumark et al.[211]

Terashima et al.[179] studied the PL of crystals prepared by solid state recrystallization and Araki et al.[85] studied the PL of crystals prepared by solution growth.

17.5 APPLICATIONS

17.5.1 Lasers

Lasers based on ZnSe have been developed mainly by epitaxial growth of ZnSe based quaternary layers by MBE and MOCVD on GaAs substrates. P-type conductivity in spite of the self-compensation mechanism has been achieved by N-doping technologies.[220, 221] Based on this p-type conductivity and a multi-quantum well structure for carrier confinement[222] and Ohmic contact formation, low temperature (77K) blue-green light LDs with a wavelength of 490 nm were first realized for pulsed operation.[8] Following many reports on LDs, finally room temperature CW lasers have been realized by SQW-SCH (single quantum well separate confinement hetero-structure).[9] The lifetime of these LDs was however limited to a few hundred hours[223] and could not be improved. The degradation of LDs was attributed to the dark line defect (DLD) which is the formation of dislocations during lasing.[226] In order to improve this drawback of ZnSe/GaAs LDs, the application of ZnSe substrates has been pursued by various researchers.

17.5.2 Light Emitting Diodes (LEDs)

Blue LEDs were reported using a simple pn structure and ZnSe substrates by various researchers,[1-4, 100, 228-230] applying a p-type conversion process such as annealing under a molten Zn atmosphere.

ZnSe LEDs were then realized using GaAs substrates and MBE epitaxial growth technologies[10, 232-237] developed for blue LDs. As in the case of ZnSe LDs, the study of LEDs on ZnSe substrates has been carried out.[13]

White LEDs based on the blue light emission from a ZnSe based epitaxial structure

and yellow emission from the substrate excited by the blue emission were invented.[238-240] It was found that color temperature can be controlled by the epitaxial composition. The advantage of these white LEDs is in the fact that they do not need fluorescent materials as in the case of GaN based white LEDs.

REFERENCES

1. R.J. Robinson and Z.K. Kun, *Appl. Phys. Lett.* **27** (1975) 74.
2. M. Yamaguchi, A. Yamamoto and M. Kondo, *J. Appl. Phys.* **48** (1977) 196.
3. Y. S. Park and C. R. Gessner, *Appl. Phys. Lett.* **21**(1972) 167.
4. J. Nishizawa, K. Ito, Y. Okuno and F. Sakurai. J. *Appl. Phys.* **57** (1985) 2210.
5. Y. Shirakawa and H. Kukimoto, *J. Appl. Phys.* **51** (1980) 2014.
6. R, N. Bhargava, *J. Crystal Growth* **86** (1988) 873.
7. See the Proceedings of the Fifth Intl. Conf. on II-VI Compounds, Sept. 8-13, (Okayama, Japan, 1991).
8. M.A. Haase, J. Qiu, J.M. DePuydt and H. Cheng, *Appl. Phys. Lett.* **59** (1991) 1272.
9. N. Nakayama, S. Itoh, T. Ohat, K. Nakano, H. Okuyama, M. Ozawa, A. Ishibashi, M. Ikeda and Y. Mori, *Electron. Lett.* **29** (1993) 1448.
10. N. Nakayama, S. Kijima, S. Itoh, T. Ohata, A. Ishibashi and Y. Mori, *Opt. Rev.* **2** (1995) 167.
11. H. Asai and K. Oe, *J. Appl. Phys.* **54** (1983) 2052.
12. J.O Williams, A.C. Wright and H.M. Yates, *J. Crystal Growth* **117** (1992) 441.
13. W.C. Harsch, G. Cantwell and J.F. Schetzina, *phys. stat. sol.* **187** (1995) 467.
14. N.G. Basov, O.V. Bogdankevich, A.S. Nasibov, V.I. Kozlovsky, V.P. Papusha, A.N. Pechenov, Kvantovay *Electronica* **1** (1974) 2521.
15. B. Ray, *II-VI Compounds* (Pergamonn, Oxford, 1969) p.1.
16. *Physics and Chemistry of II-VI Compounnds*, eds. M. Aven and J.S. Prener (North-Holland, Amsterdam, 1967).
17. H. Hartmann, R. Mach and B. Selle, in *Currents Topics in Materials Science, Vol. 9*, ed. E. Kaldis (North-Holland, Amsterdam, 1982), P.1.
18. *Databook of II-VI Compound Semiconductor Crystals (in japanese)* (JEIPA, Tokyo, 1983)
19. *Landolt-Börnstein, Vol. 17 Semiconductors*, ed. O. Madelung (Springer-Verlag, Berlin, 1982) p. 126.
20. K. C. Mills, *Thermodynamic Data for Inorganic Sulfides, Selenides and Tellurides* (Butterworth, London, 1974).
21. W.J. Wosten and M.G. Geers, *J. Phys. Chem.* **66** (1962) 1252.
22. A.G. Fischer, in *Physics and Chemistry of II-VI Compounds*, ed. M.R. Lorenz (North-Holland, Amsterdam, 1967) p. 85.
23. M. R. Lorenz, in *Physics and Chemistry of II-VI Compounds*, eds. M. Aven and J.S. Prener (North Holland, Amsterdam, 1967) p. 73.
24. R. C. Sharma and Y.A. Chang, *J. Crystal Growth* **88** (1988) 193.
25. R.C. Sharma, *J. Crystal Growth* **88** (1988) 839.
26. H. Okada, T. Kawanaka and S. Ohmoto, *J. Crystal Growth* **165** (1996) 31.
27. M.P. Kulakov, V.D. Kulakovskii, I.B. Savchenko and A.V. Fadeev, *Sov. Phys.-Solid State* **18** (1976) 526.
28. P.M. Williams and A.D. Yoffe, *Phil. Mag.* **25** (1972) 247.
29. I. Kikuma and M. Furukoshi, *J. Crystal Growth* **71** (1985) 136.
30. W.M. Yim, J.P. Dismukes, E.J. Stofko and R.J. Ulmer, *phys. stat. sol. (a)* **13** (1972) K57.
31. M.P. Kulakov and I.V. Balyakina, *J. Crystal Growthh* **113** (1991) 653.
32. B. Jobst, D. Hommel, U. Lunz, T. Gerhard and G. Landwehr, *Appl. Phys. Lett.* **69** (1996) 97.
33. H.N. Woodbery and R.B. Hall, *Phys. Rev.* **157** (1967) 157.

34. A. Hruban, W. Dalecki, K. Nowysz, S. Strzelecka and A. Gladki, *J. Crystal Growth* **198/199** (1999) 282.
35. A. Libicky, in *II-VI Semicond. Comp. Inter. Conf.*, ed. D.G. Thomas (Benjamin, New York, 1967) p. 389.
36. M. Isshiki, T. Yoshida, T. Tomizono, S. Satoh and K. Igaki, *J. Crystal Growth* **73** (1985) 221.
37. M. Shone, B. Greenberg and M. Kaczenski, *J. Crystal Growth* **86** (1988) 132.
38. A.G. Fischer, *Z. Naturforsh.* **13a** (1958) 105.
39. A.G. Fischer, *J. Electrochem. Soc.* **106** (1959) 838.
40. A.G. Fischer, *Bull. Am. Phys. Soc.* **6** (1961) 17.
41. A.G. Fischer, *J. Electrochem. Soc.* **117** (1970) 41C.
42. A.G. Fishcer, in *Crystal Growth*, ed. B.R. Pamplin (Pergamon, Oxford, 1980) p. 521.
43. Y. Tsujimoto, Y. Onodera and M. Fukai, *Jpn. J. Appl. Phys.* **5** (1966) 636.
44. O. Eguchi and M. Fukai, *National Tech. Rep. (in japanese)* **14** (1968) 71.
45. W. C. Holton, R. K. Watts and R. D. Stinedurf, *J. Crystal Growth* **6** (1969) 97.
46. M.J. Kozielski, *Bull. Acad. Polon. Sci.* **23** (1975) 1315.
47. H. Kimura and H. Komiya, *J. Crystal Growth* **20** (1973) 283.
48. I. Kikuma and M. Furukoshi, *J. Crystal Growth* **41** (1977) 103.
49. I. Kikuma and M. Furukoshi, *J. Crystal Growth* **50** (1978) 645.
50. I. Kikuma and M. Furukoshi, *Jpn. J. Appl. Phys.* **20** (1981) 2307.
51. I. Kikuma and M. Furukoshi, *J. Crystal Growth* **63** (1983) 410.
52. I. Kikuma, M. Sekine and M. Furukoshi, *J. Crystal Growth* 71(1985) 1321.
53. I. Kikuma and M. Furukoshi, *Jpn. J. Appl. Phys.* **24** (1985) L941.
54. I. Kikuma, A. Kikuchi and M. Furukoshi, *Jpn. J. Appl. Phys.* **29** (1990) L1963.
55. I. Kikuma, M. Sekine and M. Furukoshi, *J. Crystal Growth* **75** (1986) 609.
56. I. Kikuma, A. Kikuchi, M. Yageta, M. Sekine and M. Furukoshi, *J. Crystal Growth* **98** (1989) 302.
57. I. Kikuma, M. Matsuo and T. Komuro, *Jpn. J. Appl. Phys.* **30** (1991) 2718.
58. M.P. Kulakov, V.D. Kulakovskii and A.V. Fadeev, *Izv. Akad. Nauk SSSR, Neorg. Mater.* **12** (1976) 1867.
59. M.P. Kulakov, I.B. Savchenko and A.V. Fadeev, *J. Crystal Growth* **52** (1981) 491.
60. M.P. Kulakov, I.B. Savchenko and A.V. Fadeev, *J. Crystal Growth* **52** (1981) 609.
61. M.P. Kulakov and A.V. Fadeev, *Izv. Akad. Nauk SSSR Neorg. Mater.* **17** (1981) 1565.
62. C. C. Chang, C. C. Wei, Y. K. Su and H. C. Tzeng, *J. Crystal Growth* **84** (1987) 11.
63. K. Terashima, M. Kawachi, H. Yoshida and M. Takena, *Rep. Tech. Group Electron. Mater., IEE Jpn.* **EFM-88-17** (1988) 55.
64. K. Terashima and M. Takena, *J. Crystal Growth* **110** (1991) 623.
65. *Information Bulletin*, San Diego Semicon. Inc. (December, 1988).
66. H. Yoshida, T. Fujii, A. Kamata and Y. Nakata, *J. Crystal Growth* **117** (1992) 75.
67. A. Omino and T. Suzuki, *J. Crystal Growth* **117** (1992) 80.
68. P. Rudolph, K. Umetsu, H.J. Koh and T. Fukuda, *J. Crystal Growth* **143** (1994) 359.
69. P. Rudolph, K. Umetsu, H.J. Koh and T. Fukuda, *Jpn. J. Appl. Phys* **33** (1994) 1991.
70. P. Rudolph, K. Umetsu, H.J. Koh, N. Schafer and T. Fukuda, *Mater. Chem. Phys.* **42** (1995) 237.
71. K. Uehara, Y. Sakashita, H. Okada, T. Kawanaka and S. Ohtomo, *R&D Kobe Steel Engineer. Rep.* **46** (1996) 53.
72. H. Okada, T. Kawanaka and S. Ohmoto, *J. Crystal Growth* **172** (1997) 361.
73. Yu.K. Lingart, S.V. Mukhin and N.A. Tikhonova, *J. Crystal Growth* **108** (1991) 233.
74. B. J. Fitzpatrick, T. F. McGee III and P. M. Harnack, *J. Crystal Growth* **78** (1986) 242.
75. P. Wagner and M.R. Lorenz, *J. Phys. Chem. Solids* 27 (1966) 1749.
76. M. Rubensein, *J. Electrochem. Soc.* **113** (1966) 623.
77. M. Rubensein, *J. Crystal Growth* **3/4** (1968) 309.
78. L. Ozawa and H.N. Hersh, *J. Electrochem. Soc.* **120** (1973) 938.

79. I. Kikuma and M. Furukoshi, *J. Crystal Growth* **50** (1980) 654.
80. M. Washiyama, K. Sato, H. Nakayama and M. Aoki, *Rep. Tech. Group Electron. Mater., IEE Jpn.* **EFM-88-28** (1988) 45. **EFM-78-12** (1978).
81. M. Washiyama, K. Sato and M. Aoki, *Jpn. J. Appl. Phys.* **18** (1979) 869.
82. M. Aoki, M. Washiyama, H. Nakamura and K. Sakamoto, *Jpn. J. Appl. Phys.* **21** (1982) 11.
83. M. Aoki, M. Washiyama and H. Nakamura, in *JARECT Vol. 8, Semicon. Tech.* (1983) p. 1.
84. H. Nakamura, S. Kojima, M. Washiyama and M. Aoki, *Jpn. J. Appl. Phys.* **23** (1984) L617.
85. H. Araki H. Kanie, I. Yoshida, M. Sano and M. Aoki, *Jpn. J. Appl. Phys.* **30** (1991) 1919.
86. S. Fujita, H. Mimoto and T. Noguchi, *J. Crystal Growth* **45** (1978) 281.
87. T. Ido, *J. Crystal Growth* **51** (1981) 304.
88. H. Nakamura, L.Y. Sun, A. Asano, Y. Nakamura, M. Washiyama and M. Aoki, *Jpn. J. Appl. Phys.* **22** (1983) 499.
89. J.M. Faust, Jr. and H.F. John, *J. Phys. Chem. Solids* **25** (1964) 1407.
90. M. Harsey, *Mater. Res. Bull.* **3** (1968) 483.
91. K. Mochizuki, K. Masumoto and H. Iwanaga, *J. Crystal Growth* **84** (1987) 1.
92. K. Itoh and T. Kohashi, *Res. Rep. Ashikaga Univ.* **16** (1990) 49.
93. Y. Okuno, M. Sano, H. Kato and T. Maruyama, *Appl. Phys. Lett.* **60** (1992) 3274.
94. Y. Okuno, H. Kato, T. Maruyama, T. Ikenushi, K. Ishikawa, S. ToKuhashi and K. Tanaka, *Research Report of KAST (Kanagawa Academy of Science and Technology)* (1993).
95. H. Unuma, M. Higuchi, Y. Yamakawa, K. Kodaira, Y. Okano, K. Hoshikawa, T. Fukuda and T. Koyama, *Jpn. J. Appl. Phys.* **31** (1992) L383.
96. R. Triboulet, F. Fargo, R. Legros, H. Lozykowski and G. Didier, *J. Crystal Growth* **59** (1982) 172.
97. I. Dohnke, M. Muhlberg and W. Neumann, *Cryst. Res. Technol.* **32** (1997) 1115.
98. I. Dohnke, M. Muhlberg and W. Neumann, *J. Crystal Growth* **198/199** (1999) 287.
99. K. Maruyama, K. Suto and J. Nishizawa, *J. Crystal Growth* **216** (2000) 113.
100. J. Nishizawa, K. Itoh, Y. Okuno, F. Sakurai, M. Koike, and T. Teshima, in *Proc. IEEE Int. Electron Devices Meeting* (Washington, DC, 1983) p. 311.
101. J. Nishizawa, Y. Okunno and K. Suto, in *Semiconductor Technologies* (Ohmsha and North-Holland, 1986) p. 17.
102. J. Nishizawa, R. Suzuki and Y. Okuno, *J. Appl Phys.* **59** (1986) 2256.
103. J. Nishizawa and K. Suto, *Rep. Tech. Group Electron. Mater., IEE Jpn.* **EFM-88-28** (1988) 45.
104. F. Sakurai, H. Fujishiro, K. Suto and J. Nishizawa, *J. Crystal Growth* **112** (1991) 153.
105. A.S. Pashinkin, G. N. Tischchenko, I. V. Korneeva and B. N. Ryzhenko, *Sov. Phys. Cryst.* **5** (1960) 243.
106. E. Crucianu and D.V. Chistyakow, *Sov. Phys. Cryst.* **5** (1960) 344.
107. P. Vohl, *Mater. Res. Bull.* **4** (1969) 689.
108. M. Aven, D.T.F. Marple and B. Segall, *J. Appl. Phys.* **32** (1961) 2261.
109. M. Toyama and T. Sekiwa, *Jpn. J. Appl. Phys.* **8** (1969) 855.
110. T. Kiyosawa, K. Igaki and N. Ohashi, *J. Jpn. Metal Assoc.* **34** (1970) 1194.
111. T. Kiyosawa, K. Igaki and N. Ohashi, *Trans. Japan Inst. Metals* **13** (1972) 248.
112. K. F. Burr and J. Woods, *J. Crystal Growth* **9** (1971) 183.
113. P. Blanconnier and P. Henoc, *J. Crystal Growth* **17** (1972) 218.
114. J.R. Cutter, G.J. Russell and J. Woods, *J. Crystal Growth***32** (1976) 179.
115. H. Hartmann, *J. Crystal Growth* **42** (1977) 144.
116. A.C. Papadopoulo, A.M. Jean-Lois and J. Charil, *J. Crystal Growth* **44** (1978) 587.
117. J.R. Cutter and J. Woods, *J. Crystal Growth* **47** (1979) 405.
118. B.M. Bulakh, V.I.Kozlovsky, N.K. Moiseeva, A.S. Nasibov, G.S. Pekar and P.V. Reznikov, *Krist. Tech.* **15** (1980) 995.
119. F. Takeda, A. Masuda, S. Kishida, K. Matsuura and I. Tsurumi, *Rep. Fac. Engineer. Tottori Univ.* **13** (1982) 56.

120. P. Chandrsekharam, D. Raja Reddy and B.K. Reddy, *J. Crystal Growth* **63** (1983) 304.
121. K. Mochizuki, *J. Crystal Growth* **58** (1982) 87.
122. X-M. Huang, S. Satoh, K. Mochizuki and K. Igaki, *Jpn. J. Appl. Phys.* **22** (1983) 674.
123. M. Isshiki, T. Yoshida, K. Igaki, W. Uchida and S. Suto, *J. Crystal Growth* **72** (1985) 162.
124. X. M. Huang and K. Igaki, *J. Crystal Growth* **78** (1986) 24.
125. T. Koyama, T. Yoda and K. Yamashita, *J. Crystal Growth* **94** (1989) 1.
126. H. Y. Cheng and E. E. Anderson, *J. Crystal Growth* **96** (1989) 756.
127. G. Cantwell, W. C. Harsch, H. L. Cotal, B. G. Markey, S. W. S. Mckeever and J. E. Thomas, *J. Appl. Phys.* **71** (1992) 2931.
128. Y. Matsushima, K. Yoshino, Y. Yamamoto, S.R. Tiong and M. Hiramatsu, *J. Crystal Growth* **117**(1992) 328.
129. K. Mochizuki, K. Masumoto, T. Yasuda, Y. Segawa and K. Kimoto, *J. Crystal Growth* **135** (1994) 318.
130. H. Hartmann and D. Siche, *J. Crystal Growth* **138** (1994) 260.
131. Y.-G. Sha, C.-H. Su. W. Palosz, M.P. Volz, D.C. Gillies, F.R. Szofran, S.L. Lehoczky, H.-C. Liu and R.F. Brebrick, *J. Crystal Growth* **146** (1995) 42.
132. K.-T. Chen, M.A. George, Y. Zhang, A. Burger, C.-H. Su, Y.-G. Sha, D.C. Gillies and S.L. Lehoczky, *J. Crystal Growth* **147** (1995) 292.
133. K. Grasza, E. Janik, A. Mycielski, J. Bak-Misiuk, *J. Crystal Growth* **146** (1995) 75.
134. Yu.V. Korostelin, V.I. Kozlovsky, A.S. Nasbov and P.V. Shapkin, *J. Crystal Growth* **159** (1996) 181.
135. C.-H. Su, Y.-G. Sha, K. Mazuruk, S.L. Lehoczky, H.-C. Liu, R. Fang and R.F. Brebrick, *J. Crystal Growth*
136. S. Fujiwara, K. Matsumoto and T. Shirakawa, *J. Crystal Growth* **165** (1996) 169.
137. S. Fujiwara, T. Kotani, K. Matsumoto and T. Shirakawa, *J. Crystal Growth* **169** (1996) 660.
138. H. Kato, *Extended Abstr. 44th Spring Meet. Jpn. Soc. Appl. Phys. Related Soc.* (1997) p. 330.
139. A. Mycielski, A. Szadkowski and L. Kowalczyk, *Mater. Sci. Engineer.* **B43** (1997) 108.
140. A. Mycielski, E.Lusakowsaka, A. Szadkowski and L. Kowalczyk, *J. Crystal Growth* **184/185** (1998) 1044.
141. Yu.V. Korostelin, V.I. Kozlovsky, A.S. Nasbov, P.V. Shapkin, S.K. Lee, S.S. Park, J.Y. han and S.H. Lee, *J. Crystal Growth* **184/185** (1998) 1010.
142. Yu.V. Korostelin, V.I. Kozlovsky, A.S. Nasbov and P.V. Shapkin, *J. Crystal Growth* **197** (1999) 449.
143. H. Tamura, K. Suto and J. Nishizawa, *J. Crystal Growth* **209** (2000) 675.
144. C.-H. Su, S. Feth and S.L. Lehoczky, *J. Crystal Growth* **209** (2000) 687.
145. C.S. Fang, Q.T. Gu, J.Q. Wei, Q.W. Pan, W. Shi and J.W. Wang, *J. Crystal Growth* **209** (2000) 542.
146. H. Kato and I. Kikuma, *J. Crystal Growth* **212** (2000) 92.
147. C.-H. Su, Y.-G. Sha, M.P. Volz, P. Carpernter and S.L. Lehoczky, *J. Crystal Growth* **216** (2000) 104.
148. Yu.V. Krostelin and V.I. Kozlovsky, *phys. stat. sol (b)* **229** (2002) 5.
149. N. Sankar and K. Ramachandran, *J. Crystal Growth* **247** (2003) 157.
150. R. Nitsche, *Phys. Chem. Solids* **17** (1960) 163.
151. R. Nitsche, H.U. Bolsterli and M. Lichensteiger, *J. Phys. Chem. Solids* **21** (1961) 199.3
152. E. Kaldis, *J. Phys. Chem. Solids* **26** (1965) 1697.
153. E. Kaldis, *J. Phys. Chem. Solids* **26** (1965) 1701.
154. E. Kaldis, *J. Phys. Chem. Solids* **26** (1965) 1761.
155. E. Kaldis, in *Crystal Growth, Tehory and Techniques, Vol. 1*, ed. C.H.L. Goodman (Plenum, London, 1974) p. 49.
156. V. H. Schäfer and H. Odenbach, *Z. Anorg, Allg. Chem.* **346** (1966) 127.
157. S. G. Parker and J. E. Pinnell, *Trans. AIME* **245** (1969) 451.

158. H. Hartmann, *Krist. Tech.* **9** (1974) 743.
159. M. E. Özan and J. Woods, *J. Phys. D: Appl. Phys.* **10** (1977) 1335.
160. A. Catano and Z.K. Kun, *J. Crystal Growth* **33** (1976) 324.
161. S. Fujita, M. Mimoto, H. Takebe and T. Noguchi, *J. Crystal Growth* **47** (1979) 326.
162. R. Poindessault, *J. Eelectron Mater.* **8** (1979) 619.
163. R. Triboulet, F. Fargo, R. Legros, H. Lozykowski and G. Didier, *J. Crystal Growth* **59** (1982) 172.
164. M. Matsumoto and G. Shimaoka, *J. Crystal Growth* 79 (1986) 723.
165. T. Koyama, T. Yodo, H. Oka, K. Yamashita and T. Yamasaki, *J. Crystal Growth* **72** (1988) 639.
166. T. Koyama, T. Yodo and K. Yamashita, *J. Crystal Growth* **94** (1989) 1.
167. T. Koyama, K. Yamashida and K. Kumata, *J. Crystal Growth* **96** (1989) 217.
168. S. Fujiwara, H. Morishita, T. Kotani, K. Matsumoto and T. Shirakawa, *J. Crystal Growth* **186** (1998) 60.
169. S. Fujiwara, Y. Namikawa and T. Kotani, *J. Crystal Growth* **205** (1999) 43.
170. T. Kotani, S. Fujiwara, T. Hirota, M. Irikura and T. Matsuoka, *SEI Tech. Rev.* **154** (1999) 54.
171. S. Fujiwara, *J. Jpn. Assoc. Crystal Growth* **27** (2000) 61.
172. H. Li, W. Jie and K. Xu, *J. Crystal Growth* **279** (2005) 5.
173. J. S. Goela and R.L. Taylor, *J. Mater. Sci.* **23** (1988) 4331.
174. T. Taguchi, T. Kusao and A. Hiraki, *J. Crystal Growth* 72 (1985) 46.
175. V.N. Yakimovich, V.I. Levchenko, G.P. Yablonski, V.I. Konstantinov, L.I. Postnova and A.A. Kutas, *J. Crystal Growth* **198/199** (1999) 975.
176. T. Sukegawa, F. Kadotsuji, T. Tsujimoto, M. Kaji, M. Kimura and A. Tanaka, *J. Crystal Growth* **174** (1997) 289.
177. Y. Seki and O. Oda, *J. Crystal Growth* **179** (1997) 324.
178. K. Terashima, M. Kawachi and M. Takena, *J. Crystal Growth* **102** (1990) 387.
179. K. Terashima, M. Kawachi and M. Takena, *J. Crystal Growth* **102** (1990) 467.
180. K. Terashima, M. Kawachi and I. Tanigawa, *Oyo Buturi (Monthly Publ. Jpn. Soc. Appl. Phys.) (in japanese)* **61** (1992) 821.
181. I. Kikuma and M. Furukoshi, *J. Crystal Growth* **44** (1978) 467.
182. Y. Okuno, H. Tamura and T. Maruyama, *J. Electron. Mater.* **22** (1993) 685.
183. A. Ebina, K. Asano and T. Takahashi, *Jpn. J. Appl. Phys.* **16** (1977) 1563.
184. A. Sagar, W. Lehmann and J. W. Faust, Jr., *J. Appl. Phys.* **39** (1968) 3556.
185. M. Ohishi and K. Ohmori, *Oyo Buturi (Monthly Publ. Jpn. Soc. Appl. Phys.) (in japanese)* **43** (1974) 1108.
186. T. Koyama, T. Yodo and K. Yamashita, *J. Crystal Growth* **94** (1989) 1.
187. H. Iwanaga, N. Shibata and K. Mochizuki, *J. Crystal Growth* **67** (1984) 97.
188. A.K. Ray and F.A. Kroger, *J. Electrochem. Soc. 125 (1978) 1348.*
189. T. Ido and Y. Matsushita, *IEICE Tech Rep.* **CPM88-18** (1988) p. 35.
190. R.W. Jansen and O.F. Sankey, *Phys. Rev. B* **39** (1989) 3192.
191. Y. Shirakawa and H. Kukimoto, *Solid State Commun.* **34** (1980) 359.
192. D. Verity, F.J. Bryant, C.G. Scott and D. Shaw, *J. Crystal Growth* **59** (1982) 234.
193. M. Karai, K. Kido, H. Naito, K. Kurosawa, M. Okuda, T. Fujino and M. Kitagawa, *phys. stat. sol. (a)* **117** (1990) 515.
194. P. Besomi and B.W. Wessels, *J. Appl. Phys.* **53** (1982) 3076.
195. H. Okada, *J. Appl. Phys.* **80** (1996) 6740.
196. H.G. Grimmeiss, E. Meijer, R. Mach and G.O. Muller, *J. Appl. Phys.* **56** (1984) 2768.
197. S.S. Devlin, in *Physics and Chemistry of II-VI Compounds*, eds. by M. Aven and J.S. Prener, (Northe-Holland, Amsterdam, 1967) p. 551.
198. R.H. Bube and E.L. Lind, *Phys. Rev.* **110** (1958) 1040.
199. Y.S. Park and B.K. Shin, in *Electroluminescence*, eds. by J.I. Pankove (Springer-Verlag, Berlin, 1977) p. 133.

200. D.B. Laks, C.G. Van de Walle, G.F. Neumark and S.T. Pantelides, *Appl. Phys. Lett.* **63** (1993) 1375.
201. D.J. Chadi, *Phys. Rev. Lett.* **72** (1994) 534.
202. M. Prokesch, K. Irmscher, J. Gebauer and R. Krause-Rehberg, *J. Crystal Growth* **214/215** (2000) 988.
203. K.A. Kikoin, I.G. Kurek and S.V. Mel'nichuk, *Sov. Phys. Semicond.* **24** (1990) 371.
204. D.C. Reynolds, L.S. Pedrotti and O.W. Larson, *J. Appl. Phys.* **32** (1961) 2250.
205. T. Taguchi, J. Shirafuji and Y. Inuishi, *phys. stat. sol. (b)* **68** (1975) 727.
206. J.L. Merz, H. Kukimoto, K. Nassau and J.W. Shiever, *Phys. Rev. B* **6** (1972) 545.
207. J.L. Merz, K. Nassau and J.W. Shiever, *Phys. Rev. B* **8** (1973) 1444.
208. P. J. Dean, *Czech. J. Phys.* **B30** (1980) 272.
209. P.J. Dean, D.C. Herbert, C.J. Werkhoven, B.J. Fitzpartrick and R.N. Bhargava, *Phys. Rev. B* **23** (1981) 4888.
210. S. Satoh and K. Igaki, *Jpn. J. Appl. Phys.* **20** (1981) 1889.
211. G. F. Neumark S.P. Herko, T.F. McGee III and B.J. Fitzpatrick, *Phys. Rev. Lett.* **53** (1984) 604.
212. T. Taguchi and T. Yao, *J. Appl. Phys.* **58** (1984) 3002.
213. S. Kishida, K. Matsuura, H. Nobokata, A. Matsuoka and I. Tsurumi, *Solid State Dev.* **164** (1988) 51.
214. D.E. Cooper, J. Bajaj and P.R. Newman, *J. Crystal Growth* 86 (1988) 544.
215. T. Schmidt, G. Daniel and K. Lischka, *J. Crystal Growth* **117** (1992) 748.
216. U.W. Pohl, G.H. Kudlek, A. Klimakow and A. Hoffmann, *J. Crystal Growth* **138** (1994) 385.
217. M. Isshiki, *Trans. IEE Jpn.* **114-C** (1994) 1238.
218. H. Wenisch, M. Fehrer, K. Ohkawa, D. Hommel, M. Prokesch, U. Rinas and H. Hartmann, *J. Appl. Phys.* **82** (1997) 4690.
219. H. Okada, S. Ohmoto, T. Kawanaka and T. Taguchi, *J. Crystal Growth* **182** (1997) 329.
220. K. Ohkawa, T. Kawasawa and T. Mitsuyu, *J. Crystal Growth* **111** (1991) 797.
221. R.M. Park, M.B. Troffer, C.M. Roulean, J.M. DaPuydt and M.A. Hasse, *Appl. Phys. Lett.* **57** (1990) 2127.
222. K. Ichino, Y. kawakami, S. Fujita and S. Fujita, *Oyo Buturi (Monthly Publ. Jpn. Soc. Appl. Phys.) (in japanese)* **61** (1992) 117.
223. E. Kato, H. Noguchi, M. Nagai, H. Okuyama, S. Kijima and A. Ishibashi, *Electron. Lett.* **34** (1998) 282.
224. S. Kijima, H. Okuyama, Y. Sanaka, T. Kobayahsi, A. Tomiya and A. Ishibashi, *Appl. Phys. Lett.* **73** (1998) 235.
225. M. Klude, M. Fehrer and D. Hommel, *phys. stat. sol. (a)* **180** (2000) 21.
226. S. Guha, J.M. DePuydt, M.A. Haase, J. Qiu and H. Cheng, *Appl. Phys. Lett.* **63** (1993) 3107.
227. A. Ishibashi, *J. Crystal Growth* **159** (1996) 555.
228. Y. S. Park, C. R. Gessner and B.K. Shin, *Appl. Phys. Lett.* **21** (1972) 567.
229. A.V. Vasil'ev and A.I. Ryskin, *Sov. Phys.-Solid State* **21** (1979) 613.
230. M. Noguchi, Y. Nemoto, H. Takenoshita, M. Okada and T. Nakau, *IEEE Trans. Electron. Devices* **ED84-90** (1984) 37.
231. K. Akimoto, T. Miyajima and Y. Mori, *Jpn. J. Appl. Phys.* **28** (1989) L528.
232. K. Akimoto, T. Miyajima and Y. Mori, *Jpn. J. Appl. Phys.* **28** (1989) L531.
233. J. Ren, K.A. Boweres, B. Sneed, D.L. Dreifus, J.W. Cook, Jr., J.F. Schetzina and R.M. Kolbas, *Appl. Phys. Lett.* **57** (1990) 1901.
234. D.B. Eason, Z. Yu, W.C. Hughes, C. Boney, J.W. Cook, Jr., J.F. Schetzina, D.R. Black, G. Cantwell and W.C. Harsch, *J. Vac. Sci. Technol.* **B13** (1995) 1566.
235. J. Rennie, Y. Nishikawa, S. Saito, M. Onomura and G. Hatakoshi, *Appl. Phys. Lett.* **68** (1996) 2971.
236. N. Nakayama, *Monthly Display (in japanese)* **June** (1996) 33.
237. W.R. Chen and C.J. Huang, *IEEE Photo. Technol. Lett.* **16** (2004) 1259.
238. H. Matsubara, F. Nakanishi, H. Doi, K. Katayama, A. Saegusa, T. Mitsui, T. Takebe and S.

Nishine, *SEI Tech. Rev.* **155** (1999) 93.
239. K. Katayama, H. Matsubar, F. Nakanishi, T. Nakamura, H. Doi, A. Saegusa, T. Mitsui, T. Matsuoka, M. Irikura, T. Takebe, S. Nishine and T. Shirakawa, *J. Crystal Growth* **214/215** (2000) 1064.
240. T. Nakamura, *40th Meeting*, 162 Comittee, Jpn. Soc. Promo. Sci. (2004) p. 13.

18. ZnTe

18.1 INTRODUCTION

ZnTe is a direct transition compound semiconductor whose bandgap is 2.26 eV which is the same as that of GaP. The bandgap of ZnTe corresponds to the top of the eye sensitivity curve (Fig. 1.15). ZnTe is therefore the best candidate for green LED materials, better than GaP which has the same bandgap as ZnTe but is an indirect transition material. To make green light emitting diodes, the appropriate crystal growth method must be established. The other problem is in the difficulty of p-n control as in the case of other II-VI materials. The conductivity of ZnTe is limited to p-type[1] and there is a need to develop n-type control technology.

18.2 PHYSICAL PROPERTIES

In Table 18.1, the physical properties are summarized. These physical properties are reviewed in Refs. 2-6. The phase diagram of ZnTe has been studied by Kobayashi[7] and Carides and Fisher.[8] The dissociation pressure has been thermodynamically calculated by Jordan and Zupp.[9] In Fig. 18.1, X-T and P-T diagrams which have been calculated by Sharma and Chang[10] are shown. The phase diagram of the ternary compound, $Zn_{1-x}Cd_xTe$ has also been calculated.[11-13]

18.3 CRYSTAL GROWTH

No industrial crystal growth method for ZnTe has yet been fully established. There are several reports on the crystal growth of ZnTe as summarized in Table 18.2. As can be seen from the P-T diagram, since the decomposition pressure of ZnTe is higher than the atmospheric pressure, most crystal growth experiments were limited to solution growth and vapor phase growth.

Table 18.1 Physical Properties of ZnTe

Crystal Structure	zincblende
Lattice Constant	6.1037 Å
Density	5.636 g/cm^3
Melting Point	1295 °C
Linear Expansion Coefficient	8.3x10^{-6} /deg
Thermal Conductivity	0.18 W/K•cm
Dielectric Constant	10.1
Refractive index	2.94
Bandgap at Room Temperature	2.26 eV
Optical Transition Type	direct
Electron Mobility at R.T.	340 cm^2/V•sec
Hole Mobility at R.T.	110 cm^2/V•sec

18.3.1 Melt Growth

(1) Zone Melting (ZM) method

Horizontal zone melting of ZnTe was performed by Zettersrom in unpublished work and was reported in Ref. 14. Horizontal zone melting was conducted under a zinc vapor

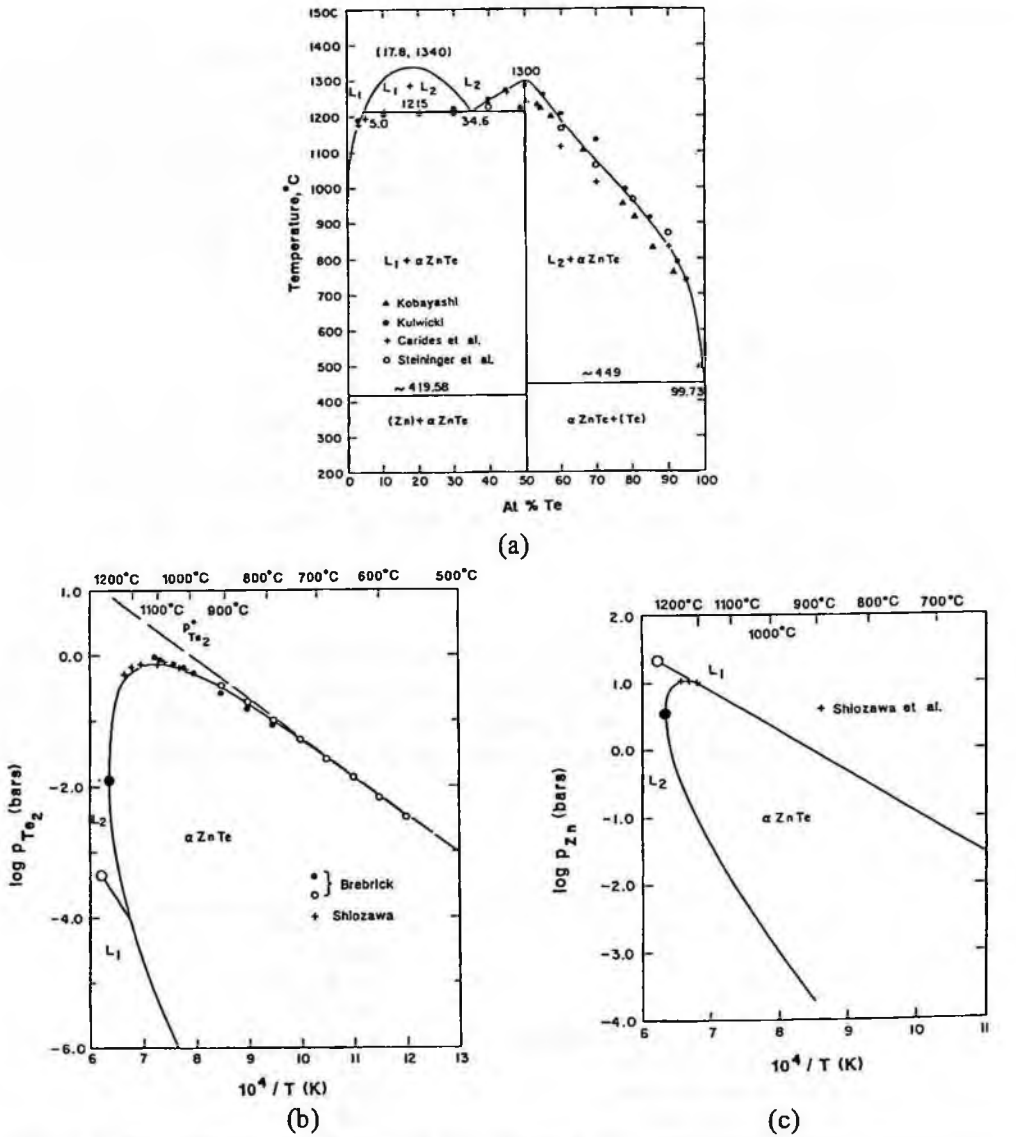

Fig. 18.1 Phase diagram of ZnTe. (a) X-T diagram, (b) equilibrium partial pressure P_{Zn} along the liquidus, (c) equilibrium partial pressure P_{Te_2} along the liquidus. (reprinted from Ref. 10 with permission, copyright 1988 Elsevier)

Table 18.2. Crystal Growth of ZnTe

Method	Result	Author	Year	Ref.
DS	Analysis of crystal structures	Pashinkin et al.	1960	43
HP-VB	Growth of Al-doped ZnTe	Fisher et al.	1964	17
HP-VB	Growth of Al-doped n-type crystals from the Zn-rich melt under high argon pressure	Fisher	1964	18
VGF	Growth with a capillary-tipped ampoule	Fischer	1970	19
ZR	First growth of ZnTe by zone refining	Zetterstrom	1964	14
PVT	Growth under various partial pressure conditions	Albers et al.	1965	47
VPG	Growth of ZnTe from Zn and Te metals	Yamanaka et al.	1965	44
SG	Solubilities of ZnTe in Ga and In	Wager et al.	1966	29
SG	Solubilities of ZnTe in Bi, Sn, Cd, Zn	Rubenstein	1966, 1968	30, 31
PVT	Growth in an ampoule with long capillary tip	De Meis et al.	1967	48
ZR	Temperature gradient 100-160 °C/cm with pulling speed of 6 cm/hr	Libickiy et al.	1967	15
TGSZ	Temperature gradient growth using molten zone	Steiniger et al.	1968	33
VGF	Growth under Zn over pressure	Lynch	1968	21
SG	Growth from Ga or In melts	Harsey	1968	32
PVT	Growth with In by a modified Piper-Polish method	Jordan et al.	1969	49
SG	Growth from Zn and Te solvents	Fuke et al.	1971	34
PVT	Vertical PVT with a capillary tube for controlling the vapor pressure in minimum	Blanconnier et al.	1972	50
HP-VB	Composition analysis after melt growth	Kikuma et al.	1973	22
THM	Growth by THM in In solvent at 900 °C	Bullitt et al.	1974	37
PVT and CVT	Growth of crystals measuring 10x10x5 mm^3	Hartmann	1977	51
ZR	Growth at 1300 °C in 14 mm diameter ampoule	Triboulet	1975	16
THM	Growth from In solvent	Wald	1976	38
CVT	Growth by ZnTe-I_2 and ZnTe-Ge-I_2 systems	Kitamura et al.	1977	58
STHM	Growth at 785-800 °C at a rate of 3 mm/day	Taguchi et al.	1978	66
CVT	Epitaxial growth of ZnTe on GaAs(100) using iodine as the transport reagent	Nishio et al.	1979-1984	59-62
VB	Effect of Zn/Te ratio and growth rate	Ogawa et al.	1982	23
MF-THM	Growth by rotating THM under magnetic field	Takeda et al.	1983	39
VPG	Growth by the horizontal open-tube method	Nishio et al.	1983	45, 46
TDM-CVP	Effect of Zn vapor pressure on resistivity	Maruyama et al.	1988	42
		SDS Inc.	1988	24
Cold THM	Growth directly from Zn and Te source material	Triboulet	1990	40
PVT and THM	Comparison of crystal qualities between PVT and THM using Te solvent	Su et al.	1993	41
SG	Growth from Te solvent with hetero-seeding	Seki et al.	1997	35
PVT	Twin free single crystals by self-seeding PVT EPD of 5x103-104 cm-2, FWHM of 15-25 arcsec	Mysicelski et al.	1998-2000	52-54
VGF	B_2O_3 encapsulated VGF with hetero-seeding	Sato et al.	1999	25
Method	Result	Author	Year	Ref.
SE	Solvent evaporation growth from Te solvent	Sato et al.	1999	36
VGF	80 mm diameter single crystal growth	Sato et al.	2000	26-28
PVT	Seeded vapor phase free growth (SVPEG) of ZnTe single crystals 40-50 mm in diameter	Korostelin et al.	2000	55
CVT	Transport in the ZnT-NH_4Cl system	Il'chuk	2000-2002	63, 64
LEK	Growth of <100>, <110> oriented 80 mm diameter single crystals	Asahi et al.	2003	65

DS: Direct Synthesis, VB: Vertical Bridgman, HP-VB: High-Pressure Vertical Bridgman, VGF: Vertical Gradient Freezing, ZR: Zone Refining, PVT: Physical Vapor Transport, SG: Solution Growth, THM: Traveling Heater Method, CVT: Chemical Vapor Transport, TDM-CVP (Temperature Difference Method under Controlled Vapor Pressure), LEK: Liquid Encapsulated Kyropoulous

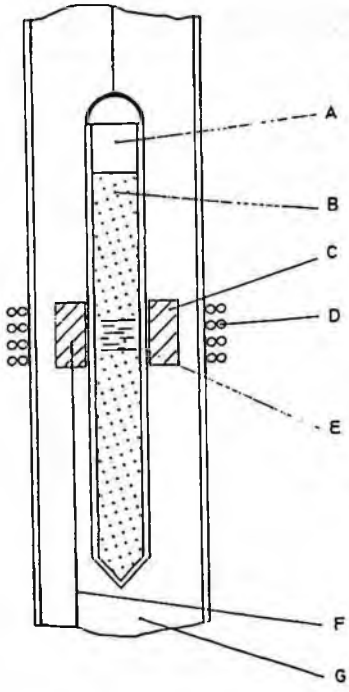

Fig. 18.2 Zone refining assembly, (A) quartz plug, (B) ZnTe, (C) graphite susceptor, (D) rf coil, (E) molten zone, (F) regulation thermocouple, (G) argon (reprinted from Ref. 16 with permission, copyright 1975 Elsevier).

atmosphere.

Libicky[15] first reported the vertical zone refining of ZnTe. ZnTe was set in a graphite crucible and sealed in a quartz ampoule. Zone refining was performed by radio frequency heating. Three passes of zone refining at a rate of 6 cm/h were performed but the grown crystal was not a large one.

Triboulet et al.[16] also examined the possibility of vertical zone refining using a furnace as seen in Fig. 18.2. Since the melting point of ZnTe is ~ 1298 °C, the quartz begins to soften. In order to examine the limitations of quartz as a material for ampoules, semiconductor quality quartz was used for the experiment. The inner ampoule diameter was 14 mm with a wall thickness of 2 mm. The several passes could be carried out without deforming the quartz ampoules at a growth rate of 4 cm/hr. After the last 2.5 cm/hr pass, large single crystals were obtained.

(2) Vertical Bridgman (VB) and Vertical Gradient Freezing (VGF) methods

Fischer[17-20] has grown ZnTe:Al crystals by the high pressure VGF (HP-VGF) method (Fig. 18.3) from a Zn rich melt containing Al under high argon pressure of 30-50 atm. The ampoule temperature was reduced from 1280 °C to 1100 °C and was rapid-quenched in a silicon oil bath. They found that n-type ZnTe could be obtained with a single crystalline region of 5-8 mm. Fischer also applied a capillary-tipped ampoule

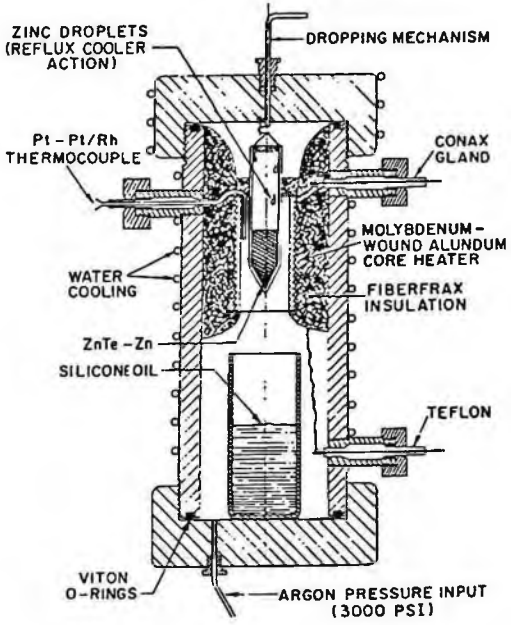

Fig. 18.3 Apparatus for melt-growth and quenching of ZnTe crystals (reprinted from Ref. 18 with permission, copyright 1964 Elsevier).

method in which the excess Te is deposited in the colder region of the capillary extended ampoule.[19,20] Using this method, crystal growth could be performed under atmospheric pressure. Lynch[21] has grown ZnTe crystals 95 mm in diameter and 25 mm in length by the VGF method under Zn vapor pressure control.

Ogawa and Nishio[23] have grown ZnTe crystals by the vertical Bridgmann method at various growing speeds under conventional atmosphere. They obtained crystals of diameter 10 mm and length of about 2-3 cm. At a growth rate of 2.5 mm/day from the melt of Zn/Te = 0.8, comparatively large grains could be obtained. The grown crystal was p-type material with a mobility of 70 $cm^2/V \cdot s$ and with a carrier concentration of 10^{16} cm^{-3}. By doping with phosphorus, low resistivity of ~ 0.50 $\Omega \cdot cm$ was obtained.

Sato et al.[25-28] have developed a high-pressure VGF method (Fig. 18.4) for growing large ZnTe single crystals 80 mm in diameter. Zn and Te are directly synthesized at 650 °C in a pBN crucible with a B_2O_3 encapsulant. ZnTe polycrystals were then heated at a temperature higher than the melting point and gradually frozen with a low temperature gradient in the furnace. By this method, <111> oriented self-seeded ZnTe single crystals of diameter up to 80 mm could be obtained (Fig. 18.5(a)). Since crystals were grown under a low temperature gradient, an average EPD of the order of 2000 cm^{-2} could be obtained as seen in Fig. 18. 5(b).

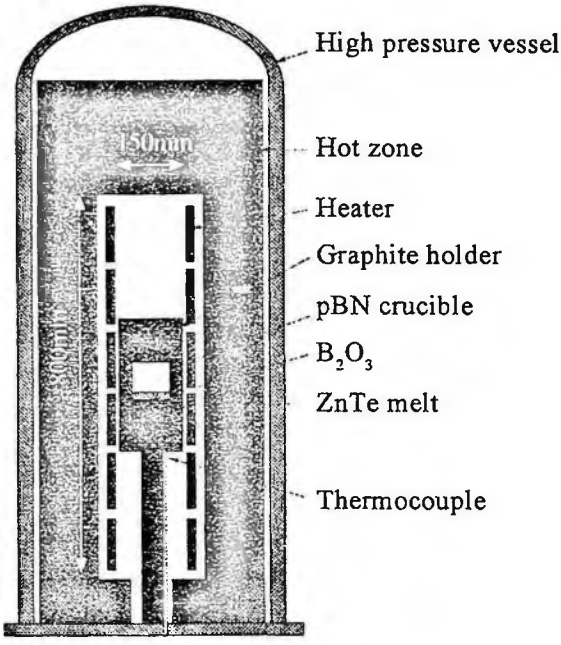

Fig. 18.4 Schematic diagram of high pressure VGF furnace for ZnTe crystal growth (from Ref. 28 with permission).

(3) Liquid Encapsulated Kyropolous (LEK) method

Asahi et al.[65] have developed the LEK method for growing 80 mm diameter <100> and <110> orientated single crystals. They have single crystals 89 mm in diameter and 40 mm in length for these orientations. The dislocation densities were less than 10^4 cm^{-2}.

18.3.2 Solution Growth

(1) Solution Growth (SG) method

Wagner et al.[29] measured the solubility of ZnTe in gallium and indium, and prepared crystal platelets having a size of about 3.5 mm square at a cooling rate of 100 °C/day. Rubenstein determined the solubility of ZnTe in Bi[30] and Sn, Cd, Zn.[31]

Steininger and England[33] have developed a Temperature Gradient Solution Zoning (TGSZ) method (Fig. 18.6) and have grown ZnTe single crystals as shown in Fig. 18.7. Seki et al.[35] have developed a solution growth method using a hetero-seeding technique (Fig. 18.8). Te solvent containing 30 at.% Zn was set in a crucible, at the bottom of which a sapphire substrate is set as a seed crystal. The ampoule was lowered in the furnace under a certain temperature gradient and a ZnTe crystal was grown as shown in Fig. 18.9. It was found that a <001> ZnTe single crystal was grown with the orientation

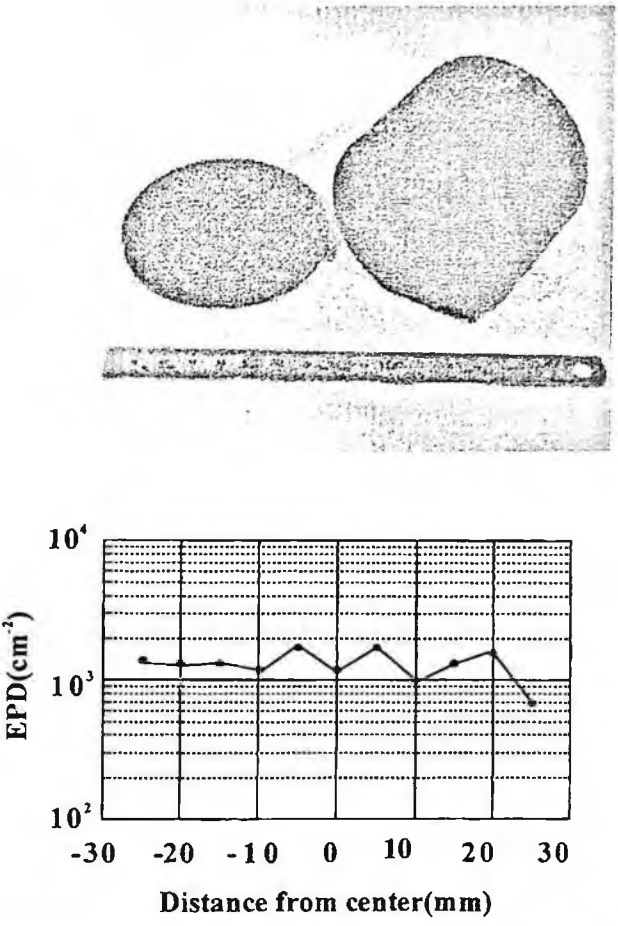

Fig. 18.5 (a) ZnTe single crystal and a sliced wafer grown by the high pressure VGF method and (b) EPD distribution in the grown crystal (from Ref. 27 with permission).

inclined several degrees from the (0001) plane of the sapphire seed crystal. The orientation relationship between the ZnTe single crystal and the sapphire substrate was found to be ZnTe (001) //sapphire (0001) and ZnTe <110> ‖ sapphire <1010> as seen in Fig. 18.10.

Sato et al.[25, 36] has modified the above hetero-seeding method by combining it with the Solvent Evaporation (SE) method. In an ampoule for the hetero-seeding method, a space for solvent condensation is designed. During crystal growth, the tellurium solvent is evaporated so that at the end of the growth, hardly any solvent remains in the graphite crucible. Since no solvent is left after crystal growth, during cooling no cracks can be made which would otherwise be due to the solvent which has a different thermal expansion coefficient to that of grown ZnTe crystals.

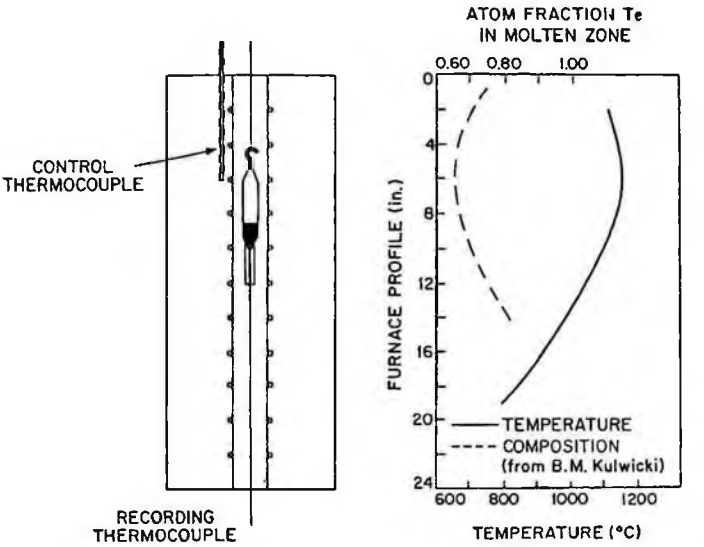

Fig. 18.6 Temperature profile and liquidus composition during TGSZ growth of ZnTe crystals (from Ref. 33 with permission).

Fig. 18.7 Quenched ingot of ZnTe showing molten zone of ZnTe in excess tellurium (from Ref. 33 with permission).

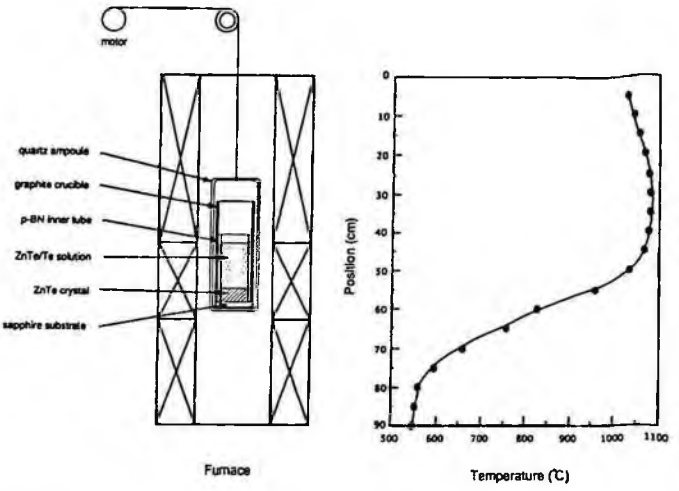

Fig. 18.8 Schematic diagram of the vertical Bridgman furnace with a typical temperature profile (reprinted from Ref. 35 with permission, copyright 1997 Elsevier).

(2) Travelling Heater Method (THM)

Bullitt et al.[37] have grown ZnTe single crystals from an In solvent at 900 °C by the THM method. The grown crystals with an In content of the order of $\sim 6 \times 10^{19}$ cm^{-3} were of high resistivity over 10^{10} Ω·cm. Wald [38] has grown ZnTe crystals from an In solvent and obtained high resistive material. The compensation mechanism has been discussed relative to the formation of point defects.

Triboulet and Didier[16] applied the THM to the growth of ZnTe. ZnTe raw materials were synthesized by the Bridgman method from the mixture of pure Zn and Te with Zn/Te = 40/60. The raw material was set in a 15 mm inner diameter quartz ampoule which was coated with carbon. Crystal growth was performed at 850 and 950 °C with a growth rate of 7 mm/day and the crystals of length 17 cm were grown.

Takeda et al.[39] have grown ZnTe single crystals by the THM combined with an accelerated rotation in a magnetic field. They examined the effect of accelerated rotation in the magnetic field on the stability of the solid-liquid interface and the control of flow in the solution. It was found that accelerated rotation was effective in reducing Te inclusions.

Triboulet et al.[40] developed a modified THM method which they call the Cold Travelling Heater Method (CTHM). In this method, a Cd rod surrounded by Te pieces was used as the source material instead of a CdTe source. Cd and Te source materials were dissolved in the Te solvent molten zone and CdTe crystals were grown from the melt.

(3) Temperature Difference Method under Controlled Vapor Pressure (TDM-CVP)

The TDM-CVP method (Sec. 5.3.5) has been applied to ZnTe.[42] Crystal growth was

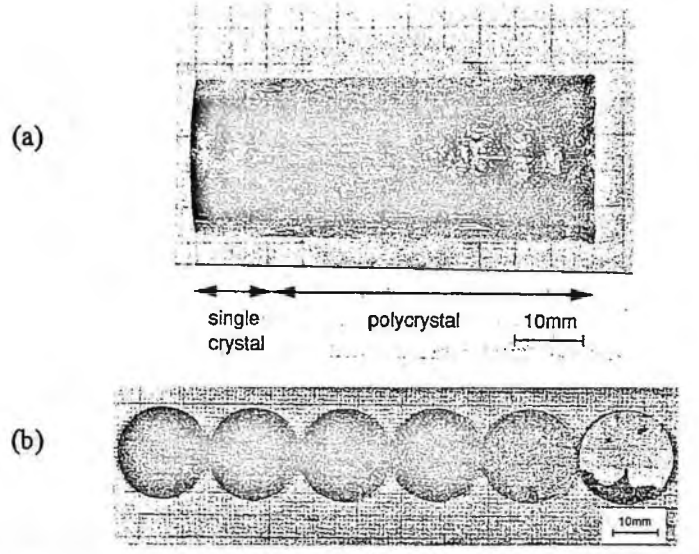

Fig. 18.9 (a) Grown ZnTe crystal and (b) sliced wafers (b) (reprinted from Ref. 35 with permission, copyright 1997 Elsevier).

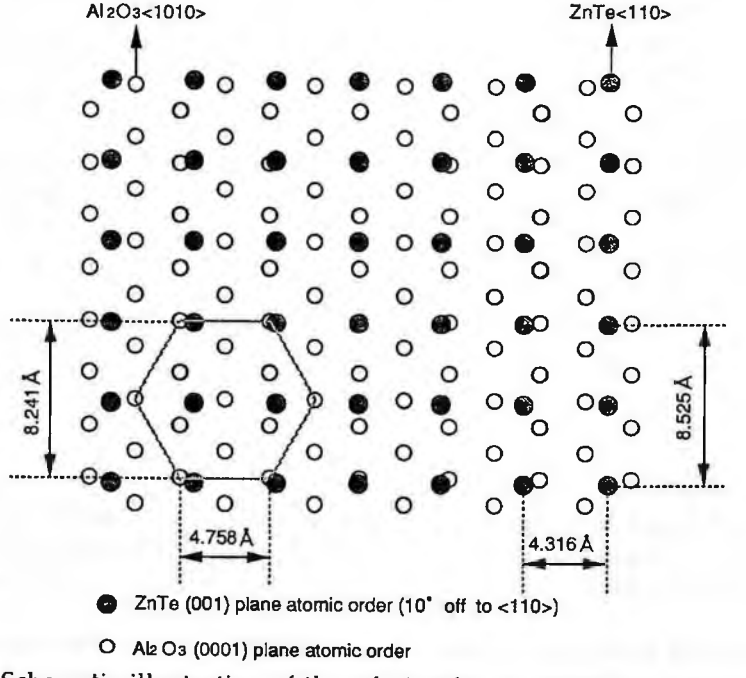

Fig. 18.10 Schematic illustration of the relationship in crystallographic orientations between the grown ZnTe and the (0001) sapphire seeding crystal (reprinted from Ref. 35 with permission, copyright 1997 Elsevier).

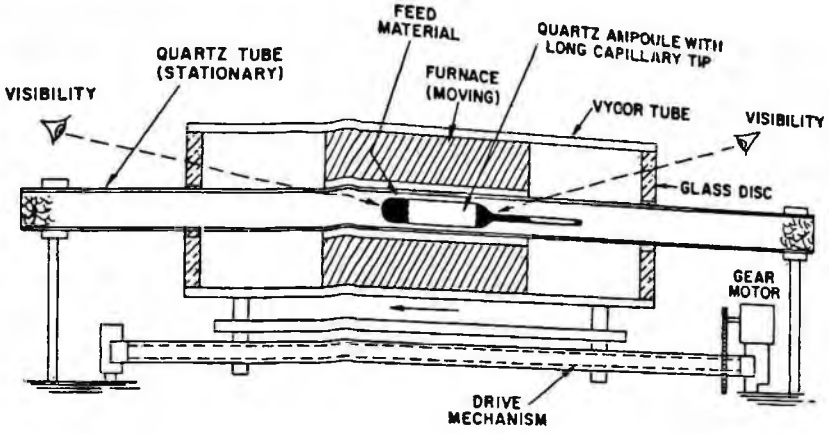

Fig. 18.11 Vapor phase growth in capillary tipped ampoules (reprinted from Ref. 48 with permission, copyright 1967 Elsevier).

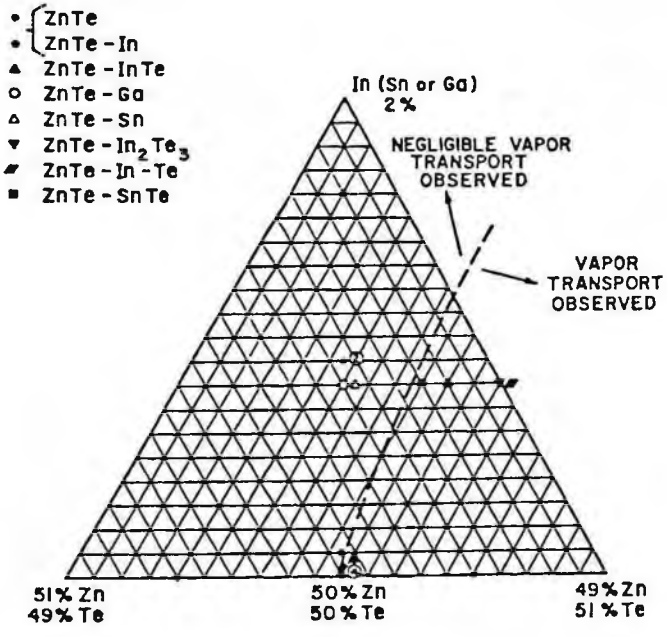

Fig. 18.12 Dependence of vapor transport on charge composition (reprinted from Ref. 49 with permission of The Electrochemical Society).

performed at 950 °C under Zn pressure ranging from 370 to 1,900 Torr. The dependence of the resistivity and the cathodoluminescence spectrum on the Zn pressure was investigated. It was found that the deep level emission in the CL spectrum was greatly reduced under a certain Zn pressure and the resistivity showed a minimum value under the Zn pressure as shown in Fig. 18.20.

18.3.3 Vapor Phase Growth

(1) Direct Synthesis (DS) and open tube growth

Yamanaka and Shiraishi[44] have grown ZnTe small single crystals from Zn and Te metals in a quartz capsule with a pinhole of 0.2-0.8 mm. The grown crystal was 30 mm in length and 10 mm in diameter with single crystals measuring 10x8x5 mm^3. Nishio et al.[45, 46] have applied a horizontal open-tube method to the growth of homo-epitaxial ZnTe crystals in H_2, H_2-I_2 and Ar gas ambients.

(2) Physical Vapor Transport (PVT) method

Albers and Aten[47] have grown ZnTe single crystals while controlling the partial vapor pressure in order to avoid precipitate formation. De Meis and Fishcer[48] have developed a closed tube PVT method as shown in Fig. 18.11. The quartz ampoule is attached with a long capillary tip, the end of which is at room temperature and acts as a cold trap to collect excess volatile materials until the decomposition pressure in the ampoule has reached its minimum.

Jordan and Derick[49] have grown high resistive ZnTe single crystals with In doping by a modification of the Piper-Polish method (Sec. 2.4.3) for suppressing Te precipitates. They have examined the dependence of vapor transport on the charge composi-

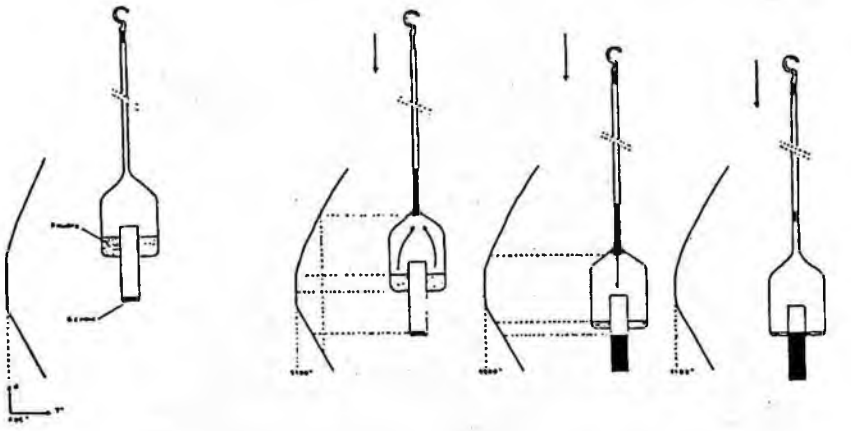

(a) Purification (b) Crystal growth

Fig. 18.13 Successive stages of experimental process of vapor phase growth (reprinted from Ref. 50 with permission, copyright 1972 Elsevier).

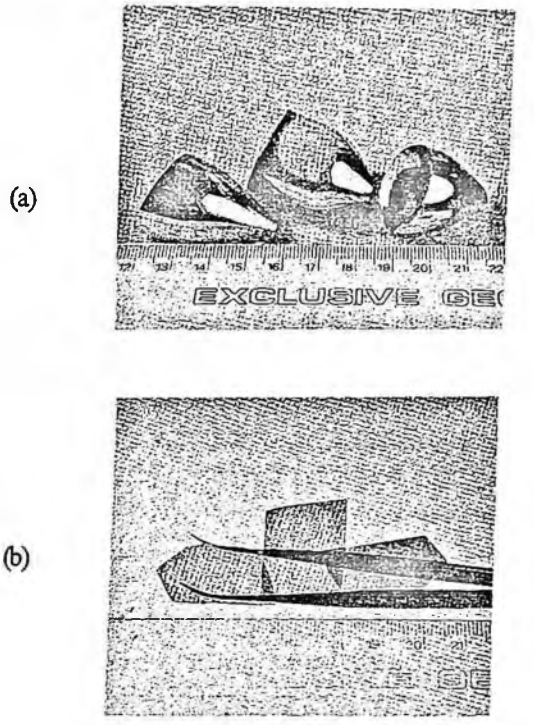

Fig. 18.14 (a) ZnTe single crystals grown by the PVT method and (b) cut substrates (from Ref. 54 with permission).

tion as shown in Fig. 18.12.

Blanconnier and Henec[50] have grown ZnTe single crystals of several cm^3 by a PVT method as seen in Fig. 18.13. In this method, firstly the material is purified as seen in Fig. 18.13(a) and the growth is then performed by lowering the ampoule (Fig. 18.13(b)). The capillary aims to perform the stoichiometry of the charge in order to adjust the pressure to its minimum value. For a given temperature gradient, the transport velocity reaches a maximum. The seed is put in the lowest tube for appropriate nucleation.

Mysicelski et al.[52-54] have developed a PVT method to grow ZnTe and $Cd_{1-x}Zn_xTe$ single crystals 25 mm in diameter and 20-30 mm in length. Typical crystals and substrates are shown in Fig. 18.14. The EPD is around 5 x 10^3-10^4 cm^{-2} and the X-ray rocking curve width 15-25 arcsec.

Korostelin et al.[55] have applied the Seeded Vapor Phase Free Growth (SVPFG) method (Fig. 17.22) to the growth of ZnTe. They have grown 40-50 mm diameter single crystals with EPD of no more than 10^4 cm^{-2} and X-ray rocking curve width of 18-22 arcsec.

Zhou et al.[56] have made a theoretical consideration of the growth of ZnTe by the

PVT method, mainly focusing on the effect of convection on noncongruent transport of species.

(3) Chemical Vapor Transport (CVT) method

Kitamura et al.[58] have examined CVT growth in the ZnTe-I_2 system and ZnTe-Ge-I_2 system. Nishio et al.[59] have grown ZnTe in a closed tube CVT method in the ZnTe-GaAs-I_2 system. Ogawa et al have examined chemical vapor growth in an open tube method with the ZnTe-H_2-I_2 system[60] and in a closed tube method in the ZnTe-I_2 system.[61]

Nishio and Ogawa[62] have made a theoretical study of chemical vapor transport in the ZnTe-I_2 system. Il'chuk et al.[63,64] have examined chemical vapor transport of ZnTe in the ZnTe-NH_4I system theoretically and have done the growth experiment.

(4) Sublimation Traveling Heater Method (STHM)

Taguchi et al.[66] applied the STHM method (Fig. 18.15) in which the vapor phase is used instead of the solution band in the conventional solution THM method. Crystals have been grown with a sublimation temperature of 815 °C and growth temperature ranging

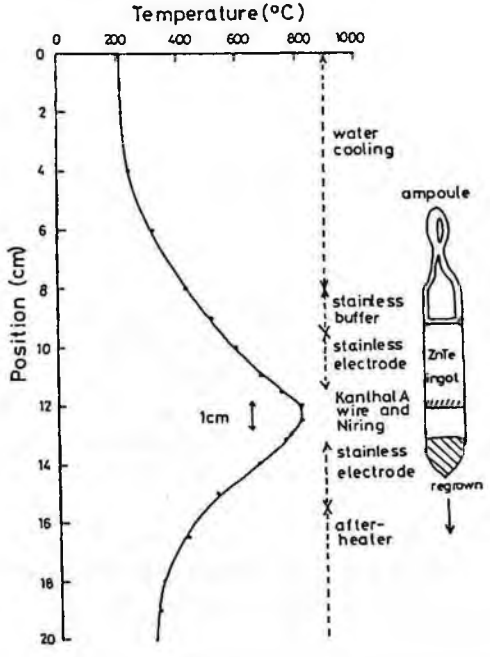

Fig. 18.15 Relative configuration of the temperature profile and the growth ampoule in Sublimation Travelling Heater Method (STHM) (reprinted from Ref. 66 with permission, copyright 1975 Elsevier).

from 785 °C to 800 °C at a growth rate of 3 mm/day. The characteristics of the grown crystals have been evaluated by photoluminescence and the free exciton line at 2.381 eV could be observed.

18.4 CHARACTERIZATION

18.4.1 Purity

Pautrat et al.[67] have examined the behavior of impurities during annealing. ZnTe has Te precipitates as seen from the phase diagram because of the retrograde shape solidus line. They discussed the reaction of impurities and Te precipitates relative to the solid-liquid segregation mechanism. Impurities which dissolved in Te precipitates diffuse to the matrix during annealing.

18.4.2 Defects

(1) Dislocations

For evaluating dislocation densities, hot NaOH (water 1*l* + 20 mol) which reveals dislocations as triangular etch pits as, is mainly used.[23] It is known that the EPD is high when Te precipitates exist as in the case of solution growth from a Te-rich solution.

(2) Twinning

The stacking fault energy of ZnTe has been estimated as explained in Sec. 1.7.2 and it is concluded that it is small, similar to CdTe and ZnSe. Therefore, it is difficult to grow large twin-free single crystals. Large diameter single crystals however can be grown by the HP-VGF as shown in Fig. 18.4, where the temperature fluctuation is greatly reduced as in the case of the growth of InP as explained in Sec. 10.3.3.

(3) Stoichiometry and precipitates

The effect of overpressure on the resistivity was studied by Maruyama et al.[42] as shown in Fig. 18.20 and it was found that under a certain pressure, the resistivity reaches a minimum which will correspond to stoichiometric composition in the crystal.

As with other compound semiconductors, ZnTe also shows Te precipitates which can be revealed by etching (Fig. 18.16). This is due to non-stoichiometry because the congruent point departs from stoichiometry. The behavior of Te precipitates as a function of annealing temperature and Zn overpressure was studied precisely and it was found that Te precipitates can be eliminated with appropriate Zn over pressure control (Fig. 18.17).[68] From these studies, the vapor pressure at which stoichiometric ZnTe can be obtained was determined as

$$P_{Zn}\,(\mathrm{Pa}) = 9.0\times10^{11} \exp(-2.02\ \mathrm{eV}/kT) \qquad (18.1)$$

It was also found that under stoichiometric conditions, high carrier concentrations and good PL spectra without broadband emissions can be achieved without Te precipitates (Fig. 18.22).

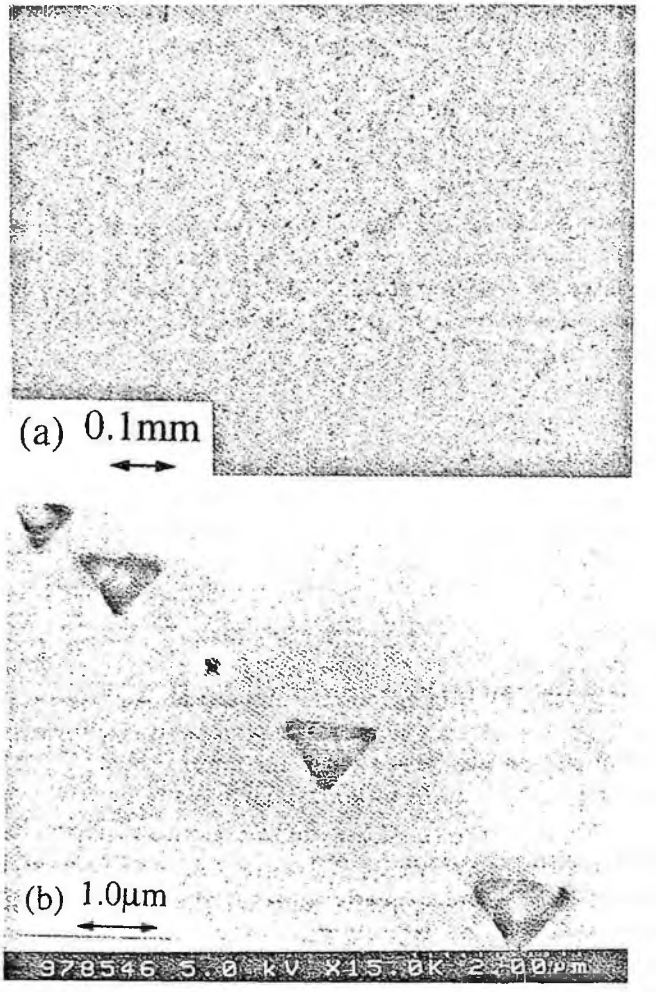

Fig. 18.16 Precipitates revealed as triangular etch pits (reprinted from Ref. 68 with permission, copyright 2000 Elsevier).

(4) Native Defects

Studies on native defects have been made by various authors.[69-73] Berding et al. have calculated the vacancy formation energies as V_{Zn} = 1.20 eV and V_{Te} = 1.12 eV.[69] They also calculated the energies for various defects and impurities.[71]

Jansen and Sankey[72] calculated the formation energy of point defects in ZnTe by an ab initio pseudo-atomic method and showed the concentration of point defects as a

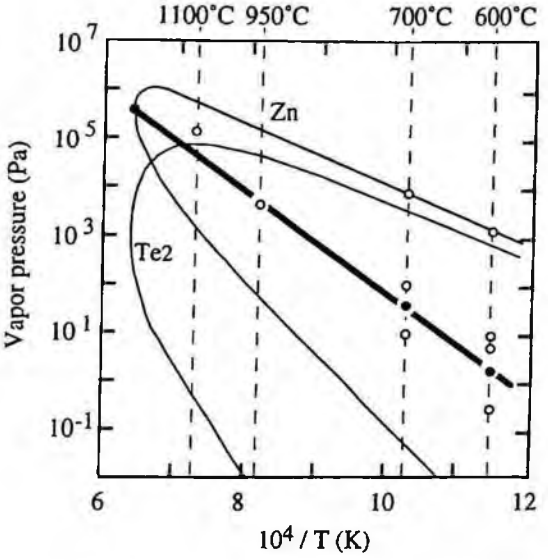

Fig. 18.17 Relationship between annealing temperatures and Zn vapor pressures for controlling the stoichiometric composition of ZnTe(reprinted from Ref. 68 with permission, copyright 2000 Elsevier).

function of stoichiometry as shown in Fig. 18.18. Ionization energies of 3d elements have been calculated by Kikon et al.[73]

Deep levels in p-type ZnTe have been studied by DLTS[74, 75] and three hole traps E_v-0.28 eV, E_v-0.51 eV and E_v-0.59 eV, have been observed. One of them was attributed to the V_{Zn} native acceptor.

18.4.3 Electrical Properties

(1) Resistivity, mobility and carrier concentration

The electrical properties of undoped and doped ZnTe have been evaluated by various authors.[1, 14, 76-78] The dependence of carrier concentrations on the Zn vapor pressure was determined by Thomas and Sadowski[14] as

$$p = 3.73 \times 10^{23} P_{Zn}^{-1/3} \exp(-1.31\ \text{eV}/kT). \qquad (18.1)$$

Smith[1] studied the electrical properties up to 1000 °C under controlled partial vapor pressures of Zn or Te and discussed the role of native defects. Theoretical and experimental Hall mobilities of undoped p-type ZnTe are as shown in Fig. 18.19. Maruyama et al.[42] have prepared ZnTe single crystals under different Zn vapor pressures and found the relationship between the resistivity and the Zn vapor pressure is as shown in Fig. 18.20. They showed that the resistivity reaches a minimum under the stoichiometric condition.

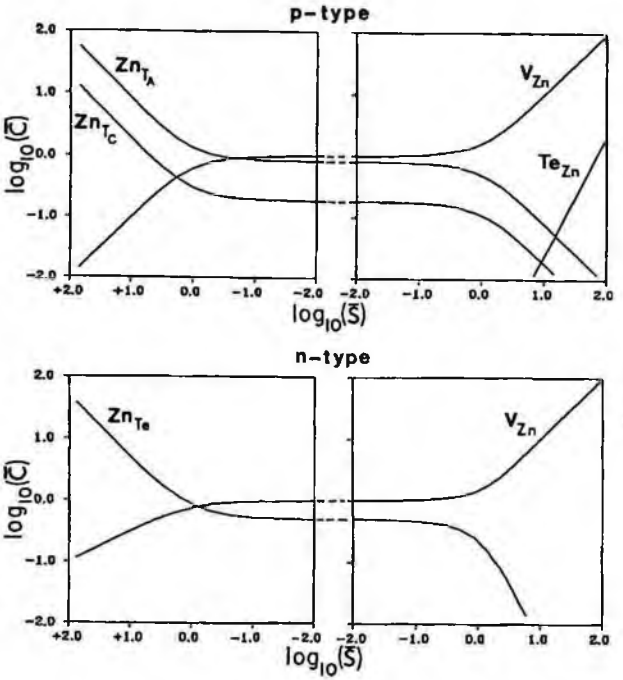

Fig. 18.18 Native defect concentrations as a function of stoichiometry for p- and n-type ZnTe. The upper panel is for positive stoichiometry S (excess Zn) and the lower panel is for negative stoichiometry S (excess Te). (reprinted from Ref. 72 with permission, copyright 1989 American Physical Society)

(2) Doping

The energy levels of donors and acceptors of ZnTe[5, 6] are summarized in Table 18.3. Because of the self compensation mechanism (Sec. 4.2.5), ZnTe is of p-type conductivity and is difficult to obtain n-type conductive material. The reason why p-type ZnTe

Table 18.3 Energy Levels of Donors and Acceptors in ZnTe

Impurity	Donor or Acceptor	Energy level from conduction band (eV)	Energy level from valence band (eV)
Ag	A		0.121
Al	D	0.0185	
As	A		0.079
Au	A		0.277
Cl	D	0.0201	
Li	A		0.0605
Na	A		0.148
P	A		0.0635

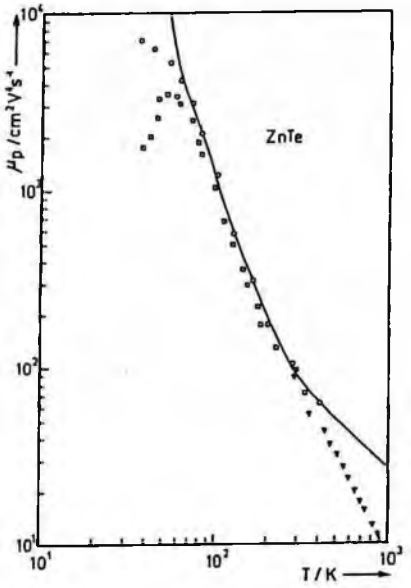

Fig. 18.19 Theoretical hole mobility (solid curve) of pure ZnTe compared with experimental Hall mobility data (from Ref. 78 with permission).

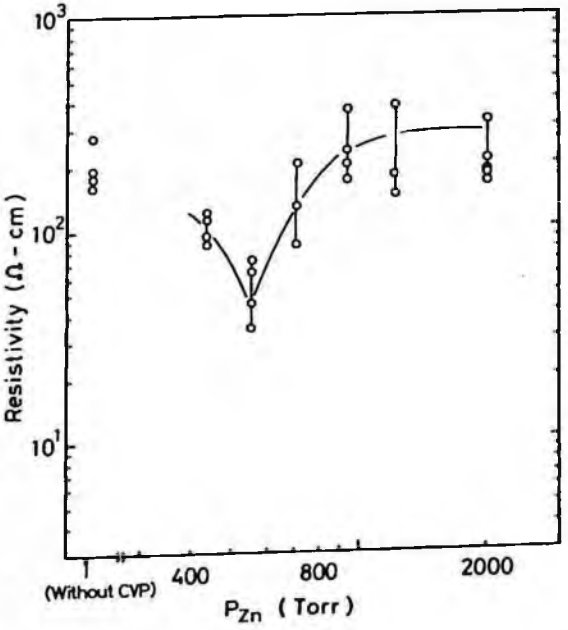

Fig. 18.20 Dependence of resistivity of ZnTe crystal on Zn pressure applied during growth (from Ref. 42 with permission).

can be easily obtained is explained by Dow et al.[79] and Laks et al.[80]

Low resistive p-type ZnTe can be obtained by doping p-type shallow impurities such as phosphorus and arsenic. Shallow acceptor states such as Li, Na, P have been studied by Crowder and Hammer.[81] Aven[82] discussed the Hall mobility and the effect of the interaction between impurities and native defects.

(3) N-type control

N-type conductivity has reportedly been achieved only by quenching Al-doped crystals after crystal growth.[18] Since n-type control of bulk ZnTe is difficult because of self compensation as explained in Sec. 4.2.5, various methods such as epitaxial growth or annealing have been studied. Ogawa et al.[83] achieved Al-doped n-type epitaxial layers by MOCVD and Tao et al.[84] reported Cl-doped n-type epitaxial layers prepared by MBE. Sato et al realized reproducible n-type conversion of p-type ZnTe by Al deposition and annealing.[27]

18.4.4 Optical Properties

The absorption, transmission, reflectivity and fluorescent properties of ZnTe have been studied by various authors.[85-88]

The photoluminescence of ZnTe has been extensively studied on bulk ZnTe and on epitaxial layers by many authors[66, 89-103] and the assignment of PL peaks has been identified as shown in Table 18.4.

Dean et al.[90-92] have studied systematically various acceptor and donor levels in ZnTe and compared the results with all the previous data. Magnea et al.[93] have clarified five substitutional acceptors such as Li_{Zn}, Cu_{Zn}, Na_{Zn}, Ag_{Zn} and Au_{Zn} and identified their ionization energies. The photoluminescence of a high quality ZnTe single crystal grown by HP-VGF is shown in Fig. 18.21.[27] Since fine structures at the emission edge

Table 18.4. Assignment of Photoluminescence Peaks

Lines	Experimental	Theory	Notation
Eg	2.3941		direct energy gap
Iex, n=3	2.392		Free Exciton
Iex, n=2	2.388(2.391)	2.388	Free Exciton
Iex, n=1	2.381	2.38	Free Exciton
ID	2.3774	2.3778	(D^0,X)
Ia(A)	2.375	2.374	(A^0,X)
IA	2.372-2.37		(A^-,X)
IT	2.362	2.36	(D^+,X)
B2	2.339		FB(53meV acceptor)
B3	2.330		FB(Li acceptor)
C2	2.243		DAP(Cu, I)
C3	2.242		DAP(Cu, Cl)
C1	2.235		DAP(Cu, In)
D	1.98		Oxygen isoelectronic trap
F	1.6		Level related with Cl
E	<1.55		Complex between native defects and donors

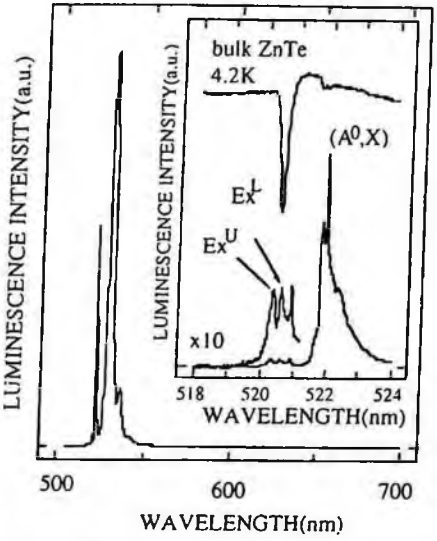

Fig. 18.21 Typical edge emission of high purity bulk ZnTe (from Ref. 27 with permission).

are clearly seen, the grown crystals were found to be of high purity with low defect concentrations.

The photoluminescence spectra as a function of annealing conditions were systematically studied by Uchida et al.[68] as shown in Fig. 18.22. It is seen that under appropriate annealing conditions which may correspond to the stoichiometry, a good PL spectrum without broadband emissions can be obtained.

18.5 APPLICATIONS

18.5.1 Light Emitting Diodes (LEDs) and Laser Diodes (LDs)

Since the bandgap of ZnTe is 2.26 eV, it is promising for pure green LEDs. To achieve these, it will be essential to be able to make p-n junctions. Several trials have been carried out.

Aven and Garwacki[104] have fabricated p-n junctions using $ZnSe_xTe_{1-x}$ single crystals grown by the PVT method. Donnelly et al.[105] and Gu et al.[106] have shown that avalanche MIS diodes can be made and observed the emission of green light. Iodko et al.[107] showed that p-n junctions can be achieved when ZnTe substrates with Al electrodes are annealed with a high power laser.

Sato et al.[26-28] obtained high quality ZnTe single crystals which showed good photoluminescence with high intensity edge emissions without broadband emissions after appropriate annealing.[68] Using these high quality ZnTe single crystals, LEDs have been fabricated by Al diffusion.[28, 108] It was found that good pn junctions can be reproducibly obtained as seen in Fig. 18.23. The realization of a reproducible pn junction is explained by the good crystal quality and Al diffusion from the cathode electrode which

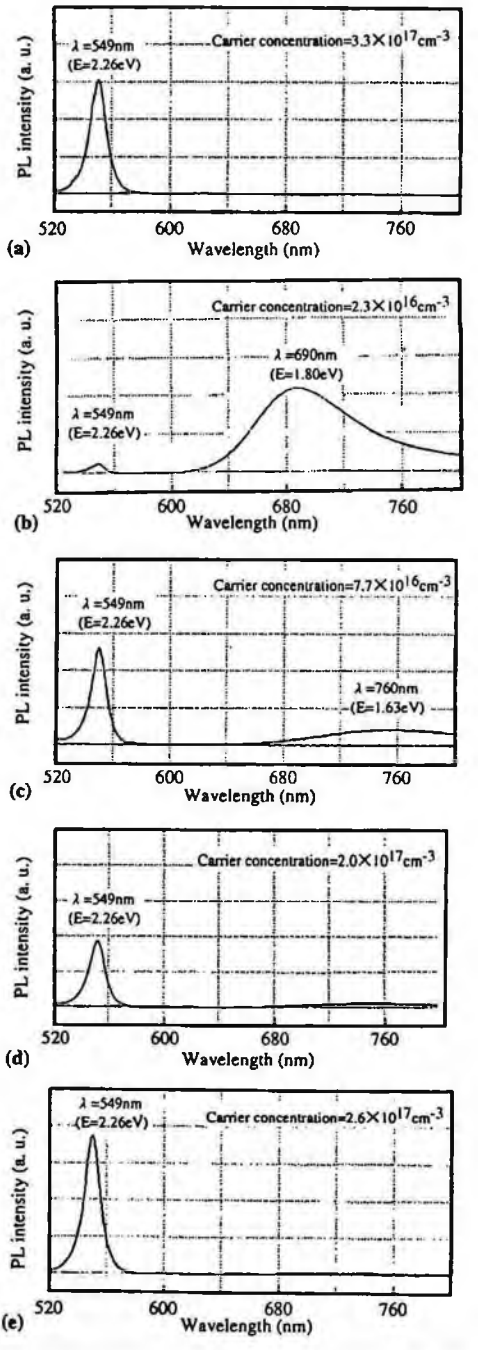

Fig. 18.22 PL spectra as a function of annealing conditions (reprinted from Ref. 68 with permission, copyright 2000 Elsevier).

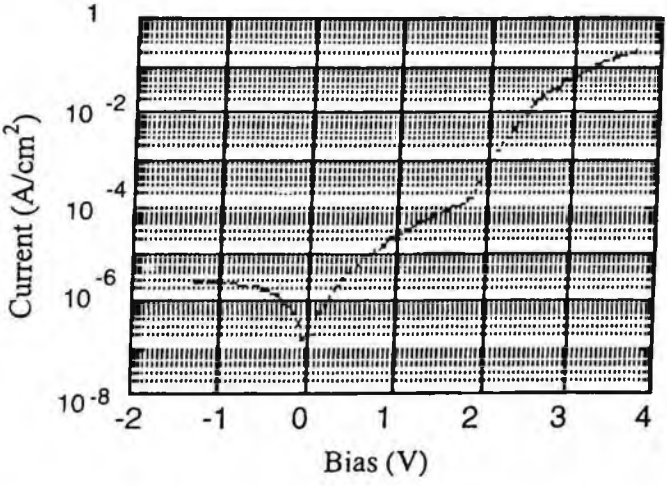

Fig. 18.23 I-V characteristics of p-n junction ZnTe LED structure (from Ref. 27 with permission).

prevents the out-diffusion of Zn atoms and suppresses self-compensation by Zn vacancies. By this process, they showed that pure green LEDs could be made having emission at 557 nm.[27,28]

18.5.2 Electro-Optical EO Conversion Materials

As reviewed by Gunter,[109] materials with high electro-optical coefficients have various applications. ZnTe crystals are now expected to be good in transmitters and transceiver for THz radiation.[110-113]

REFERENCES

1. F.T.J. Smith, *J. Phys. Chem. Solids* **32** (1971) 2201.
2. B. Ray, *II-VI Compounds* (Pergamon, Oxford, 1969) p. 1.
3. *Physics and Chemistry of II-VI Compounnds*, eds. M. Aven and J.S. Prener (North-Holland, Amsterdam, 1967).
4. H. Hartmann, R. Mach and B. Selle, *in Currents Topics in Materials Science, Vol.9*, ed. E. Kaldis (North-Holland, Amsterdam, 1982), P.1.
5. *Databook of II-VI Compound Semiconductor Crystals* (JEIPA, Tokyo, 1983) (in japanese)
6. *Landolt-Börnstein, Vol. 17 Semiconductors*, ed. O. Madelung (Springer-Verlag, Berlin, 1982) p. 157.
7. M. Kobayashi, Intern. *Z. Metallog.* **2** (1912) 65.
8. J. Carides and A. G. Fisher, *Solid State Commun.* **2** (1964) 217.
9. A. G. Jordan and R. R. Zupp, *J. Electrochem. Soc.* **116** (1969) 1265.
10. R. C. Sharma and Y.A. Chang, *J. Crystal Growth* **88** (1988) 193.
11. S. Szapiro, J. *Electron. Mater.* **5** (1976) 223.
12. V.A. Sanitarov and I.P. Kalinkin, *Vide Couches Minces* **209** (1981) 687.
13. L.A. Zabdyr, *J. Electrochem. Soc.* **131** (1984) 2157.
14. D.G. Thomas and E.A. Sadowski, *J. Phys. Chem. Solids* **25** (1964) 395.

15. A. Libicky, in *II-VI Semicond. Comp. Inter. Conf.*, ed. D.G. Thomas (Benjamin, New York, 1967) p. 389.
16. R. Triboulet and G. Didier, *J. Crystal Growth* **28** (1975) 29.
17. A.G. Fisher, *Bull. Am. Phys. Soc.* **6** (1961) 17.
18. A.G. Fischer, J.N. Carides and J. Dresner, *Solid State Commun.* **2** (1964) 157.
19. A.G. Fishcer, *J. Electrochem. Soc.* **117** (1970) 41C.
20. A.G. Fisher, in *Crystal Growth*, ed. by B.R. Pamplin, (Pergamon, New York, 1975) p.521.
21. R. T. Lynch, *J. Crystal Growth* **2** (1968) 106.
22. H. Kimura and H. Komiya, *J. Crystal Growth* **20** (1973) 283.
23. H. Ogawa and M. Nishio, *Rept. Fac. Sci. Engineer. Saga Univ. (in japanese)* **10** (1982) 109.
24. *Information Bulletin*, San Diego Semicon. Inc. (December, 1988).
25. K. Sato, Y. Seki, Y, Matsuda and O. Oda, *J. Crystal Growth* **197** (1999) 413.
26. K. Sato, *J. Jpn. Assoc. Crystal Growth* **27** (2000) 62.
27. K. Sato, O. Oda, T. Inoue, Y. Seki, A. Wakahara, A. Yoshida, S. Kurai, Y. Yamada and T. Taguchi, *phys. stat. sol. (a)* **180** (2000) 267.
28. O. Oda, K. Sato, T. Asahi, A. Arakawa and M. Uchida, *Monthly Dsiplay (in japanese)* **March** (2000) 34.
29. P. Wagner and M.R. Lorenz, *J. Phys. Chem. Solids* **27** (1966) 1749.
30. M. Rubensein, *J. Electrochem. Soc.* **113** (1966) 623.
31. M. Rubensein, *J. Crystal Growth* **3/4** (1968) 309.
32. M. Harsey, *Mater. Res. Bull.* 3(1968) 483.
33. J. Steininger and R. E. England, *Trans. AIME* **242** (1968) 444.
34. S. Fuke, M. Washiyama, K. Otsuka and M. Aoki, *Jpn. J. Appl. Phys.* **10** (1971) 687.
35. Y. Seki, K. Sato and O. Oda, *J. Crystal Growth* **171** (1997) 32.
36. K. Sato, Y. Seki and O. Oda, *Jpn. J. Appl. Phys.* **38** (1999) 5772.
37. J. Bullitt, G. Entine and F.V. Wald, *Mater. Res. Bull.* **9** (1974) 1157.
38. F. V. Wald, *phys. stat. sol. (a)* **38** (1976) 253.
39. F. Takeda, T. Yanagawa, K. Matsuura and I. Tsurumi, *Technol. Res. Rep. IEICE* **SSD82-1647** (1983) p. 1.
40. R. Triboulet, K. P. Van and G. Didier, *J. Crystal Growth***101** (1990) 216.
41. C-H. Su, M.P. Volz, D.C. Gillies, F.R. Szofran, S.L. Lehoczky, M. Dudley, G-D. Yao and W. Zhou, *J. Crystal Growth* **128** (1993) 627.
42. T. Maruyama, T. Kanba and Y. Okuno, *Jpn. J. Appl. Phys.* **27** (1988) 1538.
43. A.S. Pashinkin, G. N. Tischchenko, I. V. Korneeva and B. N. Ryzhenko, *Sov. Phys. Cryst.* **5** (1960) 243.
44. T. Yamanaka and T. Shiraishi, *Jpn. J. Appl. Phys.* **4** (1965) 826.
45. M. Nishio, Y. Nakamura and H. Ogawa, *Jpn. J. Appl. Phys.* **18** (1983) 1101.
46. M. Nishio, Y. Nakamura and H. Ogawa, *Jpn. J. Appl. Phys.* **22** (1983) 1227.
47. W. Albers and A.C. Aten, *Philips Res. Rept.* **20** (1965) 556.
48. W.M. De Meis and G.G. Fischer, *Mater. Res. Bull.* **2** (1967) 465.
49. A. S. Jordan and L. Derick, *J. Electrochem. Soc.* **116** (1969) 1424.
50. P. Blanconnier and P. Henoc, *J. Crystal Growth* **17** (1972) 218.
51. H. Hartmann, *J. Crystal Growth* **42** (1977) 144.
52. A. Mycielski, E.Lusakowsaka, A. Szadkowski and L. Kowalczyk, *J. Crystal Growth* **184/185** (1998) 1044.
53. A. Mycielski, A. Szadkowski, E.Lusakowsaka, L. Kowalczyk, J. Domagala, J. Bak-Misiuk and Z. Wilamowski, *J. Crystal Growth* **197** (1999) 423.
54. A. Micielski and A. Szadkowski, *J. Jpn. Assoc. Crystal Growth* **27** (2000) 64.
55. Yu.V. Korostelin, V.I. Kozlovsky and P.V. Shapkin, *J. Crystal Growth* **214/215** (2000) 870.
56. H. Zhou, A. Zebib, S. Trivedi and W.M.B. Duval, *J. Crystal Growth***167** (1996) 534.
57. H. Hartmann, *Krist. Tech.* **9** (1974) 743.

58. N. Kitamura, M. Kakehi and T. Wada, *Jpn. J. Appl. Phys.* **16** (1977) 1541.
59. M. Nishio, K. Tsuru and H. Ogawa, *Jpn. J. Appl. Phys.* **18** (1979) 1909.
60. H. Ogawa and M. Nishio, *Jpn. J. Appl. Phys.* **20** (1981) 2251.
61. H. Ogawa, M. Nishio and T. Arizumi, *J. Crystal Growth* **52** (1981) 263.
62. M. Nishio and H. Ogawa, *Jpn. J. Appl. Phys.* **23** (1984) 1310.
63. G. Il'chuk, *Inorg. Mater.* **36** (2000) 668.
64. G. Il'chuk, V. Ukrainetz, A. Danylov, V. Masluk, J. Parlag and O. Yaskov, *J. Crystal Growth* **242** (2002) 41.
65. T. Asahi, T. Yabe and K. Sato, *J. Jpn. Assoc. Crystal Growth* **3** (2003) 90.
66. T. Taguchi, S. Fujita and Y. Inuishi, *J. Crystal Growth* **45** (1978) 204.
67. J.L. Pautrat, N. Magnea and J.P. Faurie. *J. Appl. Phys.* **53** (1982) 8668.
68. M. Uchida, Y. Matsuda, T. Asahi, K. Sato and O. Oda, *J. Crystal Growth* **216** (2000) 134.
69. B. Monemar, *Acta Phys. Pol.* **A69** (1986) 733.
70. M.A. Berding, A. Sher and A.-B. Chen, *J. Vac. Sci. Technol.* **A5** (1987) 3009.
71. M.A. Berding, M. van Schifgaarde, A.T. Paxton and A. Sher, *J. Vac. Sci. Technol.* **A8** (1990) 1103.
72. R.W. Jansen and O.F. Sankey, *Phys. Rev. B* **39** (1989) 3192.
73. K.A. Kikon, I.G. Kurek and S.V. Mel'nichuk, *Sov. Phys. Semicond.* **24** (1990) 371.
74. D. Verity, F.J. Bryant, C.G. Scott and O. Shaw, *Solid State Commun.* **46** (1983) 795.
75. D. Verity, F.J. Bryant, C.G. Scott and D. Shaw, *J. Crystal Growth* **59** (1982) 234.
76. M. Aven and B. Segall, *Phys. Rev.* **130** (1963) 81.
77. H. Tubota, *Jpn. J. Appl. Phys.* **2** (1963) 259.
78. D. Kranzer, *phys. stat. sol. (a)* **26** (1974) 11.
79. J.D. Dow, R.-D. Hong, S.K. Klemm, S.Y. Ren, M.-H. Tsai, O.F. Sankey and R.V. Kasowski, *Phys. Rev.* **43** (1991) 4396.
80. D.B. Laks, C.G. Van de Walle, G.F. Neumark and S.T. Pantelides, *Appl. Phys. Lett.* **63** (1993) 1375.
81. B.L. Crowder and W.H. Hammer, *Phys. Rev.* **150** (1966) 150.
82. M. Aven, *J. Appl. Phys.* **38** (1967) 4421.
83. H. Ogawa, G.S. Irfan, H. Nakayama, M. Nishio and A. Yoshida, *Jpn. J. Appl. Phys.* **33** (1994) L980.
84. I.W. Tao, M. Jurkovic and W.I. Wang, *Appl. Phys. Lett.* **64** (1994) 1848.
85. R.E. Nahory and H.Y. Fan, *Phys. Rev.* **136** (1967) 825.
86. S. Narita, H. Harada and K. Nagasaka, *J. Phys. Soc. Jpn.* **22** (1967) 1176.
87. Q. Guo, M. Ikejira, M. Nishio and H. Ogawa, *Solid State Commun.* **100** (1996) 813.
88. J.J. Hopfield, D.G. Thomas and R.T. Lynch, *Phys. Rev. Lett.* **17** (1966) 312.
89. F. J. Bryant and A. T. J. Baker, in *Luminescence in Crystals, Molecules and Solutions*, ed. De. F. Williams (Plenum, New York, 1973) p. 250.
90. P. J. Dean, *J. Lumin.* **18/19** (1975) 755.
91. P. J. Dean, H. Venghaus, J. C. Pfister, B. Scaub and J. Marine, *J. Lumin.* **16** (1978) 363.
92. P. J. Dean, *Czech. J. Phys.* **B30** (1980) 272.
93. N. Magnea, D. Bensahel, J. L. Pautrat and J. C. Pfister, *phys. stat. sol. (b)* **94** (1979) 627.
94. H. Venghaus and P.J. Dean, *Phys. Rev. B* **21** (1980) 1596.
95. N. Killoran and B.C. Cayenett, *Solid State Commun.* **38** (1981) 739.
96. M. Nishio, H. Ogawa, T. Nishinaga and M. Washiyama, *Technol. Res. Rep. ECTC* **SSD85-40** (1985) p.27.
97. M. Nishio, H. Ogawa, T. Nishinaga and M. Washiyama, *Jpn. J. Appl. Phys.* **25** (1986) 1470.
98. F. Takeda, K. Matsuura, S. Kishida, I. Tsurumi and C. Hamaguchi, *Jpn. J. Appl. Phys.* **25** (1986) 910.
99. A. V. Koval, A. V. Simashkevich, K. D. Sushkevich and A. Khel'maui, *Sov. Phys. Semicond.* **22** (1988) 588.
100. K. Wolf, M. Worz, H.P. Wagner, W. Kuhn, A. Naumov and W. Gebhardt, *J. Crystal Growth* **126** (1993) 643.
101. K. Wolf, A. Naumov, T. Reisinger, M. Kastner, H. Stanzl, W. Kuhn and W. Gebhardt, *J. Crystal*

Growth **135** (1994) 113.
102. Y. Biao, M. Azoulay, M.A. George, A. Burger, W.E. Collins, E. Silberman, C.H. Su, M.E. Volz, F.R. Szofran and D.C. Gillies, *J. Crystal Growth* **138** (1994) 219.
103. A.V. Kvit, S.A. Medvedev, Yu.V. Klevkov, V.V. Zaitsev, E.E. Onishchenko, A.V. Klokov, V.S. Bagaev, A.V. Tsikunov, A.V. Perestoronin and M.V. Yakimov, *Phys. Solid Stat.* **40** (1998) 924.
104. M.Aven and W. Garwacki, *J. Appl. Phys.* **38** (1967) 2302.
105. J.P. Donnelly, A.G. Foyt, W.T. Lindley and G.W. Iseler, *Solid-State Electron.* **13** (1970) 755.
106. J. Gu, K. Tonomura, N. Yoshikawa and T. Sakaguchi, *J. Appl. Phys.* **44** (1973) 4692.
107. V.N. Iodko and A.K. Belyaeva, *Mater. Sci. Forum* **182-184** (1995) 353.
108. M. Hanafusa, A. Noda, A. Arakawa, Y. Matsuda, K. Sato and O. Oda, *Appl. Phys. Lett.* **89** (2000) 1989.
109. P. Gunter, *Phys. Rep.* **93** (1982) 199.
110. X.-C. Zhang and X.F. Ma, *Appl. Phys. Lett.* **61** (1992) 2764.
111. A. Nahata, A.S. Weiling and T. Heinz, *Appl. Phys. Lett.* **69** (1996) 2321.
112. Q. Wu and X-C. Zhang, *IEEE J. Select. Top. Quant. Electron.* **2** (1996) 693.
113. Q. Chen, N. Tani, Z. Jiang and X.-C. Zhang, *J. Opt. Soc. Am. B* **18** (2001) 823.

INDEX

This book is concerned with compound semiconductor bulk materials and has been written for students, researchers and engineers in material science and device fabrication. It offers them the elementary and intermediate knowledge of compound semiconductor bulk materials necessary for entering this field. In the first part, the book describes the physical properties, crystal growth technologies, principles of crystal growth, various defects in crystals, characterization techniques and applications. In the second and the third parts, the book reviews various compound semiconductor materials, including important industrial materials and the results of recent research.

ISBN-13 978-981-02-1728-0
ISBN-10 981-02-1728-5

World Scientific
ww.worldscientific.com
23 hc